SUMMARY TECHNICAL REPORT
OF THE
NATIONAL DEFENSE RESEARCH COMMITTEE

Manuscript and illustrations for this volume were prepared for publication by the Summary Reports Group of the Columbia University Division of War Research under contract OEMsr-1131 with the Office of Scientific Research and Development. This volume was printed and bound by the Columbia University Press.

This volume, like the seventy others of the Summary Technical Report of NDRC, has been written, edited, and printed under great pressure. Inevitably there are errors which have slipped past Division readers and proofreaders. There may be errors of fact not known at time of printing. The author has not been able to follow through his writing to the final page proof.

Please report errors to:

JOINT RESEARCH AND DEVELOPMENT BOARD
PROGRAMS DIVISION (STR ERRATA)
WASHINGTON 25, D. C.

A master errata sheet will be compiled from these reports and sent to recipients of the volume. Your help will make this book more useful to other readers and will be of great value in preparing any revisions.

SUMMARY TECHNICAL REPORT OF THE
COMMITTEE ON PROPAGATION, NDRC

VOLUME 2

RADIO WAVE PROPAGATION EXPERIMENTS

OFFICE OF SCIENTIFIC RESEARCH AND DEVELOPMENT
VANNEVAR BUSH, DIRECTOR

NATIONAL DEFENSE RESEARCH COMMITTEE
JAMES B. CONANT, CHAIRMAN

COMMITTEE ON PROPAGATION
CHAS. R. BURROWS, CHAIRMAN

WASHINGTON, D. C., 1946

NATIONAL DEFENSE RESEARCH COMMITTEE

James B. Conant, *Chairman*

Richard C. Tolman, *Vice Chairman*

Roger Adams	Army Representative[1]
Frank B. Jewett	Navy Representative[2]
Karl T. Compton	Commissioner of Patents[3]

Irvin Stewart, *Executive Secretary*

[1]*Army Representatives in order of service:*

Maj. Gen. G. V. Strong
Maj. Gen. R. C. Moore
Maj. Gen. C. C. Williams
Brig. Gen. W. A. Wood, Jr.
Col. L. A. Denson
Col. P. R. Faymonville
Brig. Gen. E. A. Regnier
Col. M. M. Irvine
Col. E. A. Routheau

[2]*Navy Representatives in order of service:*

Rear Adm. H. G. Bowen
Capt. Lybrand P. Smith
Rear Adm. J. A. Furer
Rear Adm. A. H. Van Keuren
Commodore H. A. Schade

[3]*Commissioners of Patents in order of service:*

Conway P. Coe
Casper W. Ooms

NOTES ON THE ORGANIZATION OF NDRC

The duties of the National Defense Research Committee were (1) to recommend to the Director of OSRD suitable projects and research programs on the instrumentalities of warfare, together with contract facilities for carrying out these projects and programs, and (2) to administer the technical and scientific work of the contracts. More specifically, NDRC functioned by initiating research projects on requests from the Army or the Navy, or on requests from an allied government transmitted through the Liaison Office of OSRD, or on its own considered initiative as a result of the experience of its members. Proposals prepared by the Division, Panel, or Committee for research contracts for performance of the work involved in such projects were first reviewed by NDRC, and if approved, recommended to the Director of OSRD. Upon approval of a proposal by the Director, a contract permitting maximum flexibility of scientific effort was arranged. The business aspects of the contract, including such matters as materials, clearances, vouchers, patents, priorities, legal matters, and administration of patent matters were handled by the Executive Secretary of OSRD.

Originally NDRC administered its work through five divisions, each headed by one of the NDRC members. These were:

Division A—Armor and Ordnance
Division B—Bombs, Fuels, Gases, & Chemical Problems
Division C—Communication and Transportation
Division D—Detection, Controls, and Instruments
Division E—Patents and Inventions

In a reorganization in the fall of 1942, twenty-three administrative divisions, panels, or committees were created, each with a chief selected on the basis of his outstanding work in the particular field. The NDRC members then became a reviewing and advisory group to the Director of OSRD. The final organization was as follows:

Division 1—Ballistic Research
Division 2—Effects of Impact and Explosion
Division 3—Rocket Ordnance
Division 4—Ordnance Accessories
Division 5—New Missiles
Division 6—Sub-Surface Warfare
Division 7—Fire Control
Division 8—Explosives
Division 9—Chemistry
Division 10—Absorbents and Aerosols
Division 11—Chemical Engineering
Division 12—Transportation
Division 13—Electrical Communication
Division 14—Radar
Division 15—Radio Coordination
Division 16—Optics and Camouflage
Division 17—Physics
Division 18—War Metallurgy
Division 19—Miscellaneous
Applied Mathematics Panel
Applied Psychology Panel
Committee on Propagation
Tropical Deterioration Administrative Committee

NDRC FOREWORD

As events of the years preceding 1940 revealed more and more clearly the seriousness of the world situation, many scientists in this country came to realize the need of organizing scientific research for service in a national emergency. Recommendations which they made to the White House were given careful and sympathetic attention, and as a result the National Defense Research Committee [NDRC] was formed by Executive Order of the President in the summer of 1940. The members of NDRC, appointed by the President, were instructed to supplement the work of the Army and the Navy in the development of the instrumentalities of war. A year later, upon the establishment of the Office of Scientific Research and Development [OSRD], NDRC became one of its units.

The Summary Technical Report of NDRC is a conscientious effort on the part of NDRC to summarize and evaluate its work and to present it in a useful and permanent form. It comprises some seventy volumes broken into groups corresponding to the NDRC Divisions, Panels, and Committees.

The Summary Technical Report of each Division, Panel, or Committee is an integral survey of the work of that group. The first volume of each group's report contains a summary of the report, stating the problems presented and the philosophy of attacking them, and summarizing the results of the research, development, and training activities undertaken. Some volumes may be "state of the art" treatises covering subjects to which various research groups have contributed information. Others may contain descriptions of devices developed in the laboratories. A master index of all these divisional, panel, and committee reports which together constitute the Summary Technical Report of NDRC is contained in a separate volume, which also includes the index of a microfilm record of pertinent technical laboratory reports and reference material.

Some of the NDRC-sponsored researches which had been declassified by the end of 1945 were of sufficient popular interest that it was found desirable to report them in the form of monographs, such as the series on radar by Division 14 and the monograph on sampling inspection by the Applied Mathematics Panel. Since the material treated in them is not duplicated in the Summary Technical Report of NDRC, the monographs are an important part of the story of these aspects of NDRC research.

In contrast to the information on radar, which is of widespread interest and much of which is released to the public, the research on subsurface warfare is largely classified and is of general interest to a more restricted group. As a consequence, the report of Division 6 is found almost entirely in its Summary Technical Report, which runs to over twenty volumes. The extent of the work of a division cannot therefore be judged solely by the number of volumes devoted to it in the Summary Technical Report of NDRC: account must be taken of the monographs and available reports published elsewhere.

Though the Committee on Propagation had a comparatively short existence, being organized rather late in the war program, its accomplishments were definitely effective. That so many individuals and organizations worked together so harmoniously and contributed so willingly to the Committee's efforts is a tribute to the leadership of the Chairman, Charles R. Burrows. The latest information in this field was gathered from the four corners of the earth, organized, and dispatched to the points where it would aid most in the prosecution of the war.

Much credit must be given, not only to the members of the Committee and its contractors, but also to the many other individuals who gave so generously of their time and effort. This group included a number of our Canadian and British allies. In addition to the assistance given the war effort, a considerable contribution has been made to the knowledge of short-wave transmission and especially to the interrelation of this phenomenon with meteorological conditions. Such information will be most valuable in weather forecasting and in furthering the usefulness of the whole radio field.

Vannevar Bush, Director
Office of Scientific Research and Development

J. B. Conant, Chairman
National Defense Research Committee

FOREWORD

THE SUCCESS of the propagation program was the result of the wholehearted cooperation of many individuals in the various organizations concerned, not only in this country but in England, Canada, New Zealand, and Australia. The magnitude of the research work accomplished was possible only because of the willingness of the workers in many organizations to undertake their parts of the overall program. In fact, the entire program of the Committee on Propagation was carried out without the necessity of the Committee exercising directive authority over any project.

Dr. Hubert Hopkins of the National Physical Laboratory in England and Mr. Donald E. Kerr of the Radiation Laboratory at the Massachusetts Institute of Technology, who were working on this phase of the war effort when the Propagation Committee was formed, were instrumental in giving a good start to its activities. The largest single group working for the Committee was under Mr. Kerr.

The existence of a common program for the United Nations in radio-wave propagation resulted from the splendid cooperation given the Propagation Mission to England by Sir Edward Appleton and his Ultra Short Wave Panel. Later, through the cooperation of Canadian engineers and scientists, Dr. W. R. McKinley of the National Research Council of Canada and Dr. Andrew Thomson of the Air Services Meteorological Division, Department of Transport, Toronto, Canada, undertook to carry on a part of the program originally assigned to the United States. The program was further rounded out by the willingness of the New Zealand Government to undertake an experiment for which their situation was particularly favorable. Dr. F. E. S. Alexander of New Zealand and Dr. Paul A. Anderson of the State College of Washington initiated this work. Needless to say, the labor of the Committee on Propagation could hardly have been effective without the cooperation of the Army and Navy. Maj. Gen. H. M. McClelland personally established Army cooperation, and Lt. Comdr. Ralph A. Krause and Capt. Lloyd Berkner were similarly helpful in organizing Navy liaison and help.

Officers and scientific workers of the U. S. Navy Radio and Sound Laboratory at San Diego, California, altered their program on propagation to fit in with the overall program of the Committee. Capt. David R. Hull, Bureau of Ships, understanding the importance of the technical problems, paved the way for effective cooperation by this laboratory.

Dr. Ralph Bown, Radio and Television Research Director, Bell Telephone Laboratories, integrated the research programs undertaken by Bell Telephone Laboratories for the Committee on Propagation. This joint research program included meteorological measurements on Bell Telephone Laboratories property by meteorologists of the Army Air Forces working with Col. D. N. Yates, Director, and Lt. Col. Harry Wexler of the Weather Wing, Army Air Forces. The accomplishments of the Committee on Propagation are a good example of the effectiveness of cooperation—all parts were essential and none more than the rest.

I want to thank Dr. Karl T. Compton, President of Massachusetts Institute of Technology, who was always willing to discuss problems of the Committee and who helped me to solve many of the more difficult ones, and also, Prof. S. S. Attwood, University of Michigan, whose continual counsel throughout my term of office was in no small way responsible for the success of our activity.

Credit is also due Bell Telephone Laboratories, which made my services available to the Government and paid my salary from August 1943 to September 1945, and to Cornell University, which has allowed me time off with pay to complete the work of the Committee on Propagation since September 1945.

CHAS. R. BURROWS
Chairman, Committee on Propagation

PREFACE

One of the important contributions of the NDRC Committee on Propagation of permanent value is the publication of the technical papers presented at the several Conferences on Propagation, and the publication of documents prepared for the Committee under contract OEMsr-1207 by the Columbia University Wave Propagation Group.

The first Conference was held at the Radiation Laboratory at Massachusetts Institute of Technology in July 1943 prior to the formation of the Committee on Propagation. Those sponsored by the Committee were the 2nd, 3rd and 4th Conferences held, respectively, in New York, February 1944; in Washington, November 1944; and in Washington, May 1945.

The bulk of the material published is taken from the Columbia University reports and from the papers presented at the 3rd and 4th Conferences; the remainder comes from the 2nd conference. By careful selection it has been possible to avoid excessive repetition; and yet on continuing projects, such as transmission studies, it is possible to follow their development over a considerable period of time.

Some of the material has been published in Volume 1 of this series—that dealing with the theoretical aspects of propagation, both standard and nonstandard. In this volume the reader first finds, in Part I, a summarizing review of six transmission experiments carried out in widely separted geographical locations: namely, Massachusetts Bay, San Diego, Arizona, Antigua, West Indies, and Great Britain. The basic objectives here have been to learn the facts concerning transmission and, as far as possible, to correlate them with the transmission theory given in Volume 1 and with the meteorological factors presented in this volume.

In Part II of this volume the subject considered is meteorology: first theory, then equipment, and finally the development of forecasting techniques in which the ultimate goal is the ability to predict radio performance from meteorological measurements made considerably earlier.

In Part III, Chapter 9, on reflection coefficients, presents a certain amount of new material which, however, tends to confirm previous views and further substantiates formulas already available.

In Chapter 10, on dielectric constant, absorption, and scattering, the reader will find a considerable volume of new material. With increasing frequency the absorption by the components of the atmosphere becomes increasingly important while the problems of absorption and scattering, as related to frequency and water droplet size, bear importantly on the ability to track clouds and storms by radar. This problem, storm detection (Chapter II), was interestingly presented by Canadian scientists in the form of a movie of the PPI of a radar tracking snow and thunder storms. The written report must necessarily be less complete.

In Chapter 12, on echoes and targets, the reader will find an interesting treatment of some of the more unusual problems concerning the radar behavior of targets. Volume 2 closes with a consideration of an angle-of-arrival experiment.

Space limitations have made it impossible to include a few reports, but these, together with numerous supporting documents listed in the Columbia University Wave Propagation Group bibliography, have been microfilmed.

Acknowledgment is due to the many authors who have contributed to this series, not only for the material and its oral presentation at the Conferences, but also for their willingness to prepare the material in form for permanent record.

Stephen S. Attwood
Editor

CONTENTS

PART I

TRANSMISSION EXPERIMENTS

Chapter 1

TRANSMISSION EXPERIMENTS OVER MASSACHUSETTS BAY

1.1 MICROWAVE TRANSMISSION IN 1944 — GENERAL DESCRIPTION[a]

THIS PAPER describes the general features of the work on atmospheric refraction undertaken during the summer and fall of 1944; other papers by members of this group will describe specific phases. The results described must be considered strictly tentative. They are the outcome of a hasty survey of a large amount of experimental data which ceased to accumulate only a short time before this report was prepared. Consequently, it has not been possible to do more than abstract the most obvious information.

The principal objectives of the present program were:

1. To study the modification of continental air by the ocean surface and from this study to improve the technique of forecasting modified index curves at low altitudes over water. The reason for the detailed meteorological study is that when beginning this work we believed that the existing ideas of the physical phenomena involved in producing low-level modification were not on a sufficiently sound basis to allow a direct analytical approach.

2. To study experimentally one-way and radar transmission through the range of refraction conditions varying from substandard to trapping. Particular emphasis was to be placed on wavelength dependence, and, when possible, information was to be obtained on vertical coverage patterns under these various refraction conditions.

1.1.1 Radio Program

The radio part of the project employed a combination of one-way and radar apparatus operating over Massachusetts Bay. Two paths were chosen for one-way transmission; one was the 22-mile path[1] from Deer Island (Boston Harbor) to Eastern Point (Gloucester) and the second a 41-mile path farther from the shore line (Eastern Point, Gloucester, to Race Point, Cape Cod; see Figure 1). Over the 22-mile path, transmission was on S band, while on the 41-mile path one-way transmission was on 117 mc and on S, X, and K bands. Radar sets on S and X bands were placed at the transmitter site for the latter path.

On the short path the terminals were placed so as to give approximately grazing incidence, but on the long path the terminals were well below the horizon.

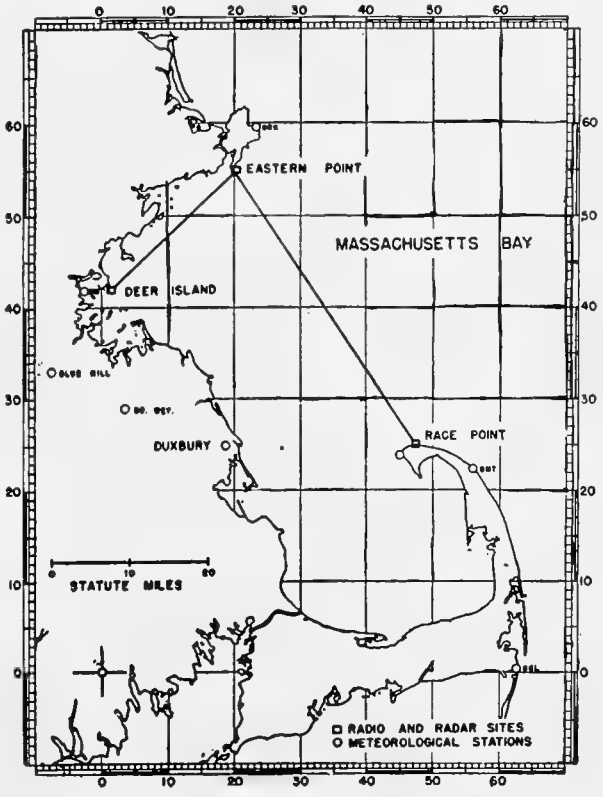

FIGURE 1. Map of the transmission paths.

At the transmitting terminal of the one-way circuit were two radar sets on X and S bands; from this location they could scan the New England coast line to measure signal strength from fixed targets.

Note that the short path is close to the coast line, while the longer path is considerably farther away and is so located that approximately westerly winds undergo appreciable modification by the time they have reached the transmission path.

1.1.2 Transmitters

The transmitter for the short path was located at Deer Island about 120 ft above mean sea level and

[a]By D. E Kerr, Radiation Laboratory, MIT.

supplied approximately 1 w to a paraboloidal antenna 30 in. in diameter.

The transmitter site for the other transmission path and the trucks housing the two radar sets were at Race Point (Provincetown). The radar sets operate on the S and X bands and are approximately 50 ft above mean sea level. They both have antenna diameters of 4 ft and a ratio of transmitted power to minimum detectable power of approximately 167 db. These sets were operated from August 1st through October 20th. The measurements consisted of hourly determination of the strength of echo from four specially selected targets and of recording maximum detection range on fixed targets over water looking up the coast line; in addition, *plan position indicator* [PPI] photographs were taken at hourly intervals. The performance of the radar sets was carefully monitored by appropriate means for determination of transmitted power and minimum detectable received power. All echo signal strengths were measured in absolute values with a signal generator coupled to the system. The records of signal strength from the four selected targets and those of maximum detection range were plotted and returned to the laboratory on a weekly basis.

The tower carrying the one-way transmitting equipment consisted of the bottom half of a 100-ft SCR-271 tower. The house at the foot of the tower served as operations headquarters, while the top house contained the transmitters. The 117-mc antenna was a five-element Yagi array projecting horizontally from the forward corner of the top of the house. The X- and S-band antennas were paraboloids 4 ft in diameter, made of close-spaced grid work designed to reduce wind resistance. The feed for each of these antennas was a dummy-dipole array excited from the open end of a wave guide projecting through the vertex of the paraboloid. The K-band antenna was a paraboloid 2 ft in diameter, illuminated by a small horn. Polarization was horizontal for practically the entire period of the program.

All the microwave antennas were provided with a scheme for rendering them independent of rain. A blast of air from inside the house was injected into the wave guide at the transmitter by means of a blower. This stream of air effectively prevented accumulation of a film of water on the inside of the guide feed.

The transmitter used on 117 mc was one from an SCR-624 VHF (very high frequency) communication set. Its frequency was quartz-crystal controlled, and it delivered approximately 10 w of c-w power into a balanced line connected to the Yagi antenna. The output power of the transmitter was monitored continuously on an Esterline-Angus recording milliammeter.

The S- and X-band transmitters employed pulsed magnetrons operating at a pulse recurrence frequency of 700 c with a pulse length of 1.5 μ sec and a peak power output of approximately 10 kw. The output pulse from the modulator was continually checked by the synchroscopes, and a check was made of the transmitted radio frequency spectrum of the pulses by means of the spectrum analyzer.

Both S- and X-band transmitters were provided with continuously recording monitors operating Esterline-Angus recording milliammeters. Several types of monitor circuits were employed during the course of the program, but the one which proved most satisfactory employed a thermistor bridge coupled by means of wave selector, or directional coupler, to the wave guide between transmitter and antenna. Daily calibrations of the recording thermistor bridge circuits were made, providing a constant check of power output in absolute values. In addition to recording of average power output by frequent checking of spectrum and high-voltage pulse, the cathode current of the magnetrons was also recorded.

The K-band transmitting equipment differed from the S- and X-band equipment only in matters of unessential detail.

1.1.3 Receivers

The receiving terminal of the one-way transmission circuit is located at Eastern Point, Gloucester; the receivers were mounted in a 100-ft tower similar to the one at Provincetown. There were two sets of receivers, one approximately 136 ft above mean sea level in a house at the top of the tower and the other approximately 30 ft above in a house at the bottom of the tower. The receiving antennas are identical with those for the transmitters.

The K-band receiver was a superheterodyne specially constructed for this purpose and put into operation late in the experiment. It had a bandwidth of 14 mc but no *automatic frequency control* [AFC], with the consequence that it required constant attendance to produce a satisfactory record. The receiver for the Deer Island circuit was a narrow-band c-w receiver of the type used in last year's experiments and described in reference 1.

The X- and S-band receivers deserve mention because of their special characteristics, which were developed to meet the requirements of this work. They are provided with AFC circuits arranged to search for a lost signal automatically. Having found the signal, the circuit locks the receiver in tune and continues recording. These receivers have specially designed automatic gain control circuits providing essentially logarithmic response of 70- to 80-db range well spread across the recorder scale. The minimum detectable power for these receivers is approximately 110 db below 1 w for both S band and X band, and the minimum signal required for satisfactory operation of the AFC is approximately 105 db below 1 w. The latter figures are important for this particular setup, since they determine the usefulness of the receivers in studying signal strength near or below that encountered under standard refraction conditions.

The receivers were calibrated daily by means of signal generators coupled permanently to the wave guide between the antenna and the receiver through wave selectors with known fixed coupling losses. Very close check on performance was maintained so that the receivers at all times gave an accurate indication of the absolute value of received signal strength.

The arrangement of S- and K-band receivers in the house on top of the tower was similar to that in the lower house, but the K-band receiver was of a less sensitive type requiring no tuning. There was a 117-mc receiver in the top house but not in the bottom house, and there was no receiver for the Deer Island circuit in the top house.

The outputs of all eight receivers were wired directly into an Esterline-Angus recording milliammeter. With this arrangement one operator was able to keep continuous watch on the performance of all receivers and was required to climb the tower only when major adjustments of the top receivers were necessary.

The Gloucester station was the control station for the radio network formed by all the stations involved in the project. The transmitter station at Provincetown, each of the radar trucks, the fixed meteorological stations, the boat, and one of the airplanes were all equipped to operate radiotelephone on 3.5 mc, thus allowing rapid and efficient exchange of information essential to the operation of all units involved in the program.

1.1.4 Meteorological Program

The meteorological phase of our program consisted of two main parts: (1) meteorological measurements, and (2) forecasting and analysis.

All meteorological measurements were made with varying versions of the psychrograph, earlier models of which are completely described in reference 2. This instrument measures wet and dry bulb temperatures as a function of height, using the electrical resistance thermometer principle. From these measurements the M curve is constructed.

The meteorological soundings were made in the Massachusetts Bay area with psychrographs carried by two aircraft, by captive balloons operating from a boat and from two fixed land stations. The boat operated in the Bay and out to about 100 miles offshore, while the aircraft operated as far as 170 miles offshore. It should be mentioned that aircraft soundings of this type are rather hazardous, since they involve descending to altitudes of approximately 20 ft at large distances from land.

The fixed meteorological stations were located at Duxbury and Race Point. The Duxbury location was chosen to place the sounding station near enough to the shore to obtain a representative sample of the air just leaving the land.

The Race Point meteorological station was located at a position to allow soundings at the water's edge on the westernmost extremity of the top of Cape Cod. The primary purpose of this station was to measure the characteristics of the air after it had been subjected to the influence of the ocean surface between the mainland and the station. This location allowed measurements over a range of wind directions of approximately 180°, but no relevant soundings could be made when the wind had an easterly component, since the air would have had a land trajectory for at least a short period. It was necessary to take all soundings very close to the water's edge to prevent solar heating of the beach from influencing the bottom of the measured M curve. At both Duxbury and Provincetown soundings were taken on a prearranged schedule which, when possible, involved both day and night operation. Soundings, surface wind velocities and hourly observations of sky conditions, etc., were made at both Duxbury and Race Point. The water temperature was also measured at the Provincetown station.

A 60-ft pole was erected at Race Point carrying four anemometers, four psychrographs, and a wind direction indicator. The original scheme involved continuous recording of temperature, humidity, and wind speed at four levels by means of the instruments on the pole, but unfortunately a large sand bar formed

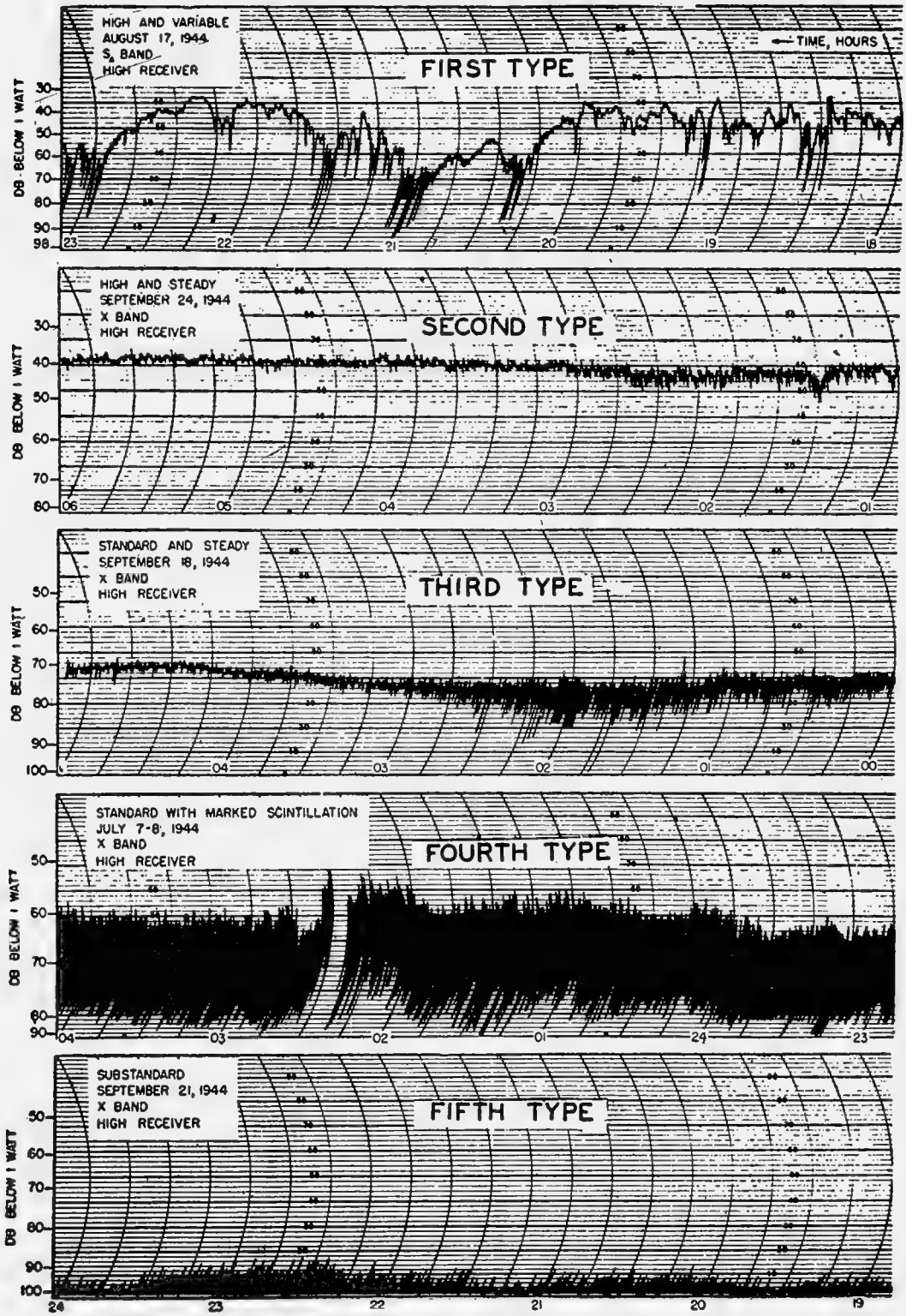

FIGURE 2. Microwave signal types.

in front of the pole soon after it was erected and caused sufficient disturbance of the air in the lowest levels that such measurements were not feasible. The psychrograph, anemometer, and wind direction indicator at the top of the pole continued to be useful, however, and provided the continuous information recorded by the station.

A 50-ft boat, the *Wanderer,* was used for making measurements in Massachusetts Bay. The psychrograph used for measurements from 2- to 48-ft elevation is attached to a cable running between a boom extending outward from the side of the ship and an extension to the top of the mast. A similar psychrograph was used for soundings to higher levels, operating from the winch at the rear of the boat. Further essential meteorological information was provided by the boat in frequent measurements of surface water temperatures in Massachusetts Bay. A direction-finding loop was used to determine position at great distances off shore.

1.2 RADIO AND RADAR TRANSMISSION MEASUREMENTS[b]

The purpose of this paper is to describe the results of a rough preliminary analysis of the transmission experiment. A thorough analysis must await the completion of the meteorological study, since the transmission depends directly upon the meteorological conditions over the path of the radiation. The emphasis here will therefore be mainly on the strictly radio data with only qualitative reference to the meteorological information.

1.2.1 One-Way Transmission

The values of the transmitted powers, antenna gains, and receiver characteristics were chosen so as to make the standard signal level, as computed for the receivers at the top of the tower, well above the minimum detectable level and the minimum level at which the automatic frequency control [AFC] and AFC search are effective. Sufficient compression was used to give a range of about 60 db for useful reception, which had been expected to be enough for the variations due to atmospheric conditions. It turned out, however, that additional range was needed, especially in the direction of greater signal strengths; to accommodate additional received power, attenuators were inserted in the lines. Thus the actual range of values observed is at least 90 db at the microwave frequencies and 40 db at 117 mc.

[b]By Pearl Rubenstein, Radiation Laboratory, MIT.

Signal Types

Figure 2 shows that the types of signal observed at the microwave frequencies (S and X) are not essentially different from those observed in previous tests on a shorter path. The first type is high signal on the average, well above the standard level, with roller fades which may go down to the minimum detectable level and with periods of 2 minutes to an hour or so. These periods are generally shorter at any time on X than on S band. When this type of signal is present on S band it is almost invariably present on X band also and on both paths. It always occurs simultaneously on the high and low receivers at any frequency.

The second type is high and steady. Its level may be anywhere from 5 to about 30 db above the standard, generally higher on X band than on S band. Most of the time this type of signal occurred simultaneously on S and X, but there were some occasions when the S-band signal was of the high and steady type while the X-band signal became of the first type, high with roller fades.

The third kind of signal is about standard and fairly steady. (This may be a limiting case of the high and steady variety.) It does not necessarily occur on both frequencies and on both high and low receivers at the same time.

The fourth type is standard on the average, with scintillation of more than 10 db. The preliminary analysis has not revealed the reasons, or any correlations, for the difference between this and the preceding type; it is certainly nothing obvious, such as wind speed, for example; and it may occur on either frequency when the other is steady.

The fifth type is the "blackout," below standard and variable. This signal type is strongly scintillating. It occurs simultaneously on both frequencies, both paths, and on high and low receivers (except possibly for low X, where the difficulty mentioned above of determining an average value of something very low on the scale is important).

Figure 3 shows the signal types observed at 256 cm. These are distinct from those observed at the microwave frequencies not only in appearance but also in times of occurrence. In general no relation has been found to exist between the types at the two

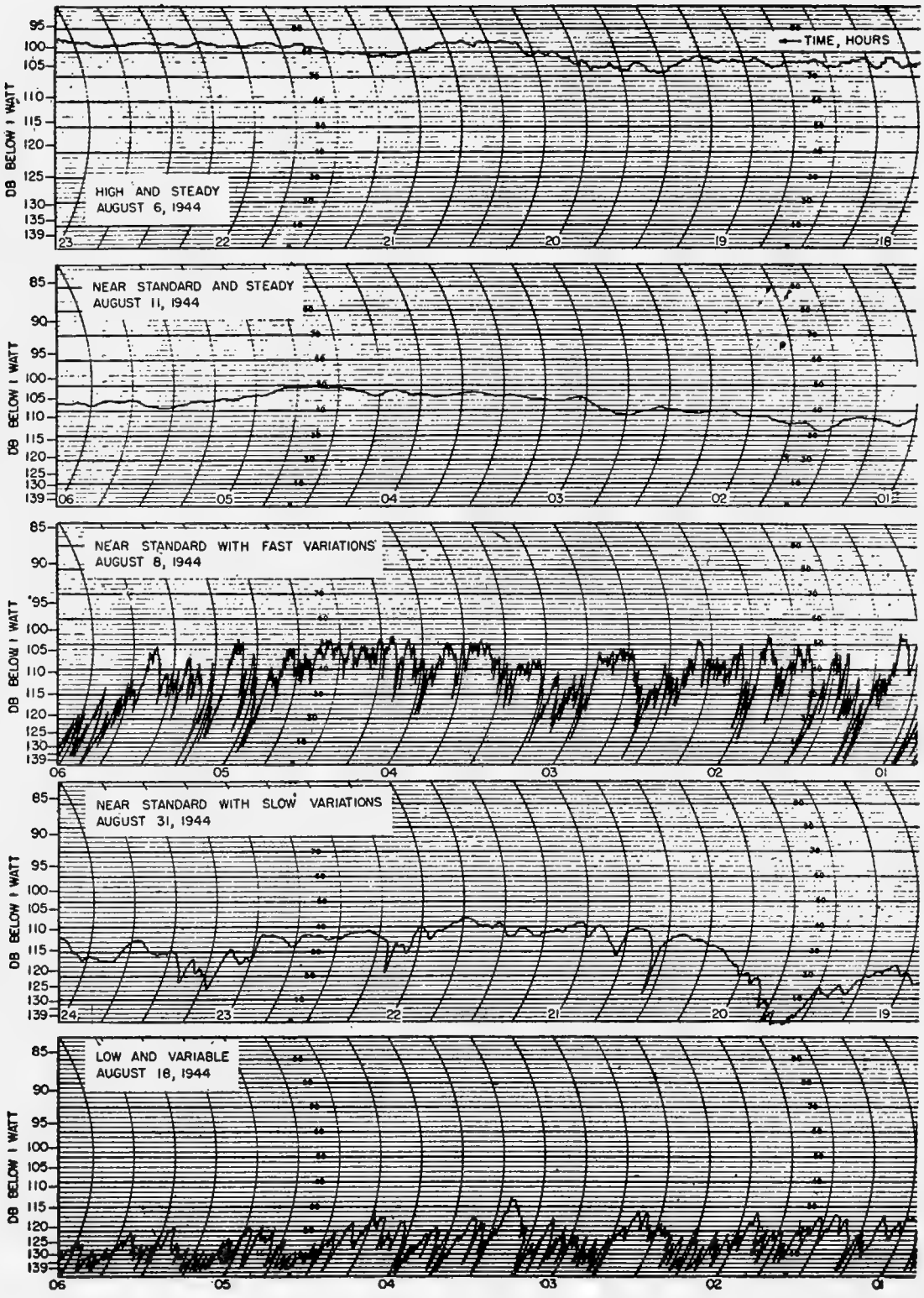

FIGURE 3. Signal types at 256 cm (117 mc).

frequencies although on rare occasions such a relation is indicated; indeed the type may remain constant on one and change on either of the others. Steady signal is most frequent at 256 cm, but the other types shown also occur fairly often. Variations of 30 to 40 db overall take place, and the variations may be fast or slow.

Statistics

A fairly detailed statistical study has been made of the S and X signals at the top level. These were chosen because they were available for the longest periods, and because they gave the most reliable results (because of the receiver characteristics the relation of the standard to the minimum detectable level was most suitable). The other microwave records gave similar results. As for the 256-cm transmission, the most important result was that the signal level was above the minimum detectable very nearly 100 per cent of the time, although fades to this level were fairly frequent. If a choice had to be made of the most reliable frequency for transmission over the circuit, there would be no question in the choice of the longer wavelength.

The statistics available on K band are very similar to those on X band as far as can be determined. Signal levels less than about 20 db above standard cannot be detected on the K band.

The study was made of the average signal level on a weekly basis; it showed marked differences from week to week, depending upon the specific weather situation. For purposes of the statistics a range of values around the standard was included in the standard signal (allowance for scintillation, tides, etc.). This range was taken as ± 5 db on S band and ± 10 db on X band, values determined by inspection of the entire record and thought to give comparable results.

The most interesting result of this analysis was the discovery that standard signal occurs extremely rarely over this path. High signal is most frequent; depending upon the wavelength and the season of the year, substandard and standard signal occur less frequently. In the summer no significant frequency dependence was observed in the statistics. Some typical weeks gave the figures shown in Table 1.

Table 1. Statistics of S- and X-band transmission in summer.

Date	Per cent of time above standard	Per cent of time below standard	Per cent of time standard
July 10–16	63	36	1
Aug. 21–27	97	3	0
Aug. 28–Sept. 3	80	15	5

As the season progressed to the fall, however, several related trends became apparent: (a) the increasing incidence of standard signal, especially on S band; (b) the increasing incidence of high, steady signal, especially on X band, with the level higher above the standard on X than on S; (c) the frequency effect on the incidence of above-standard signal indicated in (b); and (d) the decreasing occurrence of substandard signal. These trends are illustrated in Table 2.

Table 2. Statistics of S- and X-band transmission in the fall.

Date	Per cent of time above standard	Per cent of time below standard	Per cent of time standard*
Sept. 25–Oct. 1	S 58	15	27
	X 80	10	10
Oct. 16–22	S 76	2	22
	X 92	0	8

*By this term is to be understood the percentage time in which the signal is ± 2.5 db of standard on S band and ± 5 db on X band.

No diurnal effect was found in the signal except under some very special circumstances. Not only was no such trend apparent upon visual inspection, but also an analysis of the material by 6-hour intervals confirmed appearances.

Correlations

In addition to the statistical study, another type of analysis has been made to look for correlations between the variations of signal strength with frequency at a given location or with height at a given frequency. Figures 4 to 6 show some typical graphs of such correlations, each point representing average hourly values, for 1 week. Figure 4 shows the variation of the high S- and X-band signal strengths. It is clear that in most cases the two wavelengths change together. This was the predominant behavior throughout the summer. The notable exceptions are those points where X is high and S nearly standard; this is the frequency effect remarked in the discussion of the high and steady signal which became common in the fall. As will be seen later, this occurs with very low modified index inversions, less than 20 ft high.

Figure 5 shows the relation between S-band signal strengths for high and low receivers; the correlation is excellent in practically every case. A similar correlation exists for the high and low X-band signal,

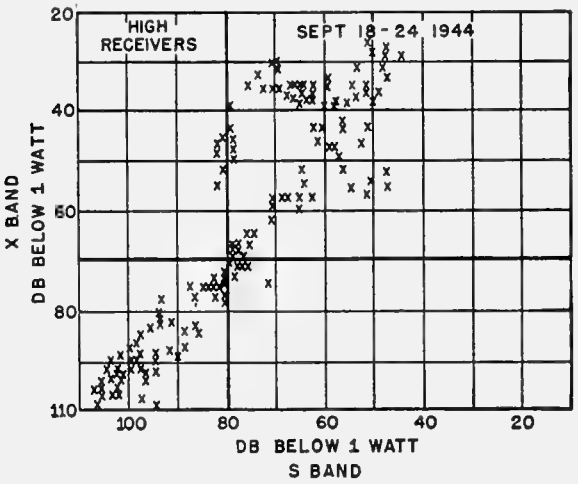

FIGURE 4. Relation between S- and X-band signal strengths.

except for the case of very low signal where the apparent average value of the signal strength on the low receiver is always relatively high. Whether this

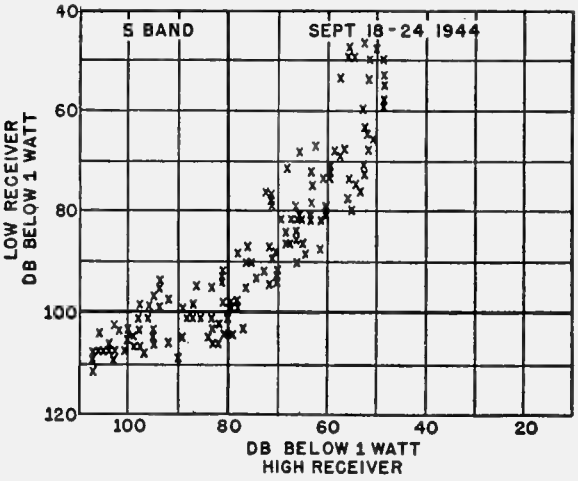

FIGURE 5. Relation between signal strengths at high and low receivers.

is caused by the lack of receiver sensitivity or is a real transmission phenomenon cannot be conclusively decided on the basis of the present information.

Figure 6 shows the relation of signal strengths at 117 mc and S band; the difference between this figure and the preceding two speaks for itself. From the preliminary analysis no consistent correlation has been found between the behavior of the low- and high-frequency transmission.

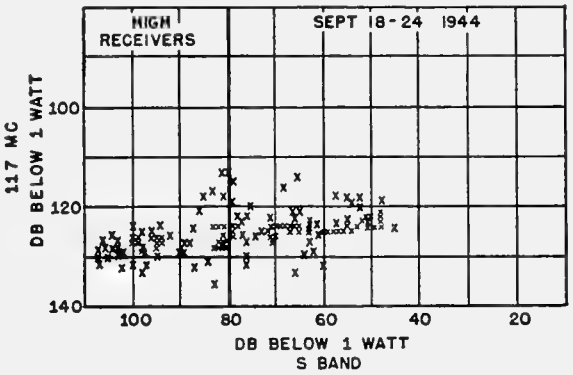

FIGURE 6. Relation between 117-mc and S-band signal strengths.

The variations on the two paths are generally in good agreement although changes in signal type rarely occurred exactly simultaneously; the changes on the short path are always less in magnitude than on the other, as would be expected.

As far as can be determined from the available data the K-band signal correlates quite well in general with that on S and X bands. Only high signal can be observed, of course, with the present equipment.

Relation of Radio Results to Modified Index Curves

Detailed conclusions must await the full analysis of the data. At present certain qualitative conclusions can be drawn:

1. When the surface modified index inversions are present, the microwave signal level is high on the average, and usually the signal has roller-type fades.

2. When the M curve is substandard the signal is low and scintillating. The M curves which are standard all the way down to the surface of the water appear to be very rare, even when the air is colder than the water. The previous results on the short path had tended to discount the importance of the low M inversions which exist over water most of the time, especially with cold air flowing out from the land. The increased sensitivity of the present setup to variations in the M curve, the additional path length, and finally the inclusion of the X-band transmission on the circuit have shown definitely that such low M inversions are far from negligible but will affect S-band communications (or one-way trans-

mission) and both one-way and radar transmission on X band. The signal occurring with these M inversions less than 20 ft high is usually the high, steady type. It is generally not quite so high in average level as that characterized by roller fades found with larger M inversions.

3. The high, steady signal occurring with very low M inversions reveals the only clear-cut cases of frequency diversity between S and X bands. In this case a variety of combinations has been found: nearly standard signal on S band with X-band signal from 10 to 30 db above standard; S band 10 to 15 db above standard with X band 30 or so db above standard; and finally S band about 20 or more db above standard and steady while X band changes to the first signal type: high with fades.

4. One of the most interesting features of the transmission is the fact that at any given location, for a fixed frequency, the increase in field strength is limited; that is, no matter how much the M inversion increases in height or in strength beyond a certain value (which is as yet unspecified) the average value of the signal strength does not continue to increase but rather remains the same within about 10 db. This "saturation" level is of the order of the free space value. (Maximum level goes up to 12 to 15 db above free space but only infrequently.) Consequently, the level reached on a given path appears to be independent of the receiver height (within the height range covered in these measurements), the height-gain effect which exists under standard conditions being essentially eliminated when shore trapping takes place. Under some conditions, especially when the signal is high with fading but has not yet reached the saturation level, the lower of the two receivers has been observed to receive higher signal than the higher one. With stronger signal the values on the two become nearly identical, as has been stated.

These results agree with unpublished calculations made for several values of duct height and M deficit for S band, of the first transmission mode alone, which indicate that the height-gain effect should disappear and the signal approach a certain saturation level. Thereafter, calculations show, the contribution of the first mode decreases, but the observations suggest that perhaps the other modes continue to cause the average level to reach approximately the same value, as duct height and M deficit continue to increase.

It has been found that, with an M inversion over only a portion of the path and a standard curve on at least a small part of it, the signal type may be high with roller fades and the average level high, so that the record is indistinguishable from that which occurs with more uniform conditions.

1.2.2 Radar Transmission

From Race Point, targets were available over water at ranges of 20 to several hundred miles along the coast of Massachusetts and Maine, plus some additional targets inland and whatever shipping was in the vicinity. Of the coastal targets four were chosen for regular observation. These were fairly isolated fixed targets, the echoes from which appeared to be relatively steady in several days' observations, at ranges of 22, 41, 65, and 73 statute miles. Absolute power measurements of the returns of each of these targets (whenever visible) were made hourly by comparison with a signal generator. Each measurement represents the *maximum* value of the signal during a period of 1 to 3 minutes. This differs rather essentially from the hourly averages of the one-way data.

In addition to signal strength measurements, hourly observations were also made of the maximum ranges obtained on surface targets, and *plan position indicator* [PPI] photographs were made which reveal at a glance many interesting features of the radar coverage which are hard to describe briefly in words. The maximum sweep length available on the PPI was 140 miles for the S-band set and 115 miles at X band. Additional range was available on the delayed A-scope sweeps, so that the maximum was 180 miles for most of the period of observations. This was extended to 280 miles for the last week of the test.

In addition a portable K-band radar set was set up near Race Point Light only 17 ft above mean sea level and regular observations of range were made and shipping tracked.

Target Signal Strengths

The strength of the echoes from the four targets, including the nearest one which is ordinarily visible both optically and by radar, varied from below minimum detectable to at least 60 db above for the two nearer targets and about 35 db above for the two more distant targets, at both frequencies. In general the values of the signal strength were higher for the nearer targets, but there were some interesting cases when the more distant targets were visible while the nearer ones were either not seen or were very weak. This may occur at times when the M curve varies

markedly with direction, as happens occasionally when the air trajectory is S or SW or at times of skip distance.

Maximum Ranges

Large variations in the maximum ranges have also been observed at both frequencies, with the upper limit apparently being set only by the length of the sweep: 280 miles on S band and 200 miles on X band. (Note that these radar sets were far from the high-power class.) Lack of fixed targets at ranges between 10 and 25 miles made it impossible to follow in detail the way in which substandard conditions reduced detection range, but there was no question as to the general trend toward reduction of range. The maximum range of the *high sited K-band receiver* [HRK] from its location at the Race Point Light was 46 miles on a land target and about 30 miles on shipping.

It should be borne in mind that our project deals with propagation near and roughly parallel to the coast line. Thus these results are not necessarily applicable to operations perpendicular to the coast with off-shore winds, where the surface M inversions become "washed out."

Statistics

The radar observations include about 1,200 hours of operation. Of these, overall, the X-band ranges were better than "normal" 59 per cent of the time (normal = 29 miles[c]) and the S-band ranges 48 per cent of the time. At both frequencies ranges were below normal 20 per cent of the time. The variations from week to week were great, the maximum values being 95 per cent above normal on X and 75 per cent above normal on S, with about 45 per cent below normal as the lowest value at both frequencies.

Correlations with One-Way Results

A visual comparison of the radar and one-way data suggests fairly good agreement in general between the two. To get a more quantitative evaluation of this agreement, however, correlation diagrams have been drawn.

[c]Unfortunately, in the radar case it is impossible to establish a precise definition of a "standard" range analogous to standard signal in one-way transmission unless detailed information is available on the radar target. In this case we have attempted to determine the detection range on the low hills available as coast line targets, at times when the M curve is standard or very nearly so.

Figure 7 shows such a diagram relating the signal strength of the target at Eastern Point as observed on the X-band system with the signal strength of the

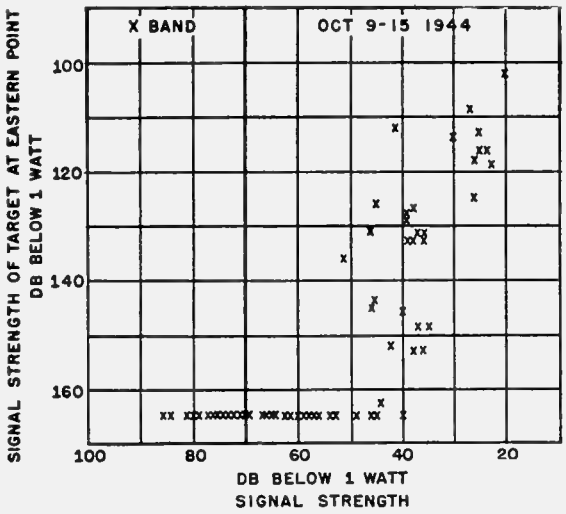

Figure 7. Relation between one-way and radar transmission, Race Point to Eastern Point.

high X-band receiver on the one-way path. As in the previous diagrams, a week has been chosen as the time interval and hourly values are plotted. In this we neglect the difference between the single observation of the radar and the average of an hour's continuous record in the other case. Note also that all radar measurements which give values *equal to or below* the minimum detectable level are plotted *at* the minimum detectable level; thus if a more sensitive receiver had been used, many of these points would have fallen lower in the diagram. The diagram reveals the nature of the relation: the one-way signal strength must rise considerably above the standard value before the target becomes visible. Thereafter, small changes in the one-way signal correspond to much larger changes in the radar echo. As a matter of interest, which may or may not be significant, the values at times fall close to the square law, as they should if the target-reflecting properties remain constant as the atmospheric conditions change.

Figure 8 shows the relation between maximum radar ranges on surface targets and the one-way transmission results. In this case the effects of both substandard and better than standard conditions are noticeable. When the one-way signal strength is below standard, the radar ranges are mainly less than normal; exceptions occur in cases of strong directional effects and S-shaped M curves. As the one-way signal strength

rises above the standard level no appreciable increase in radar range occurs at first. Only when the one-way signal strength has become fairly high do the radar ranges begin to increase. Then the entire gamut of

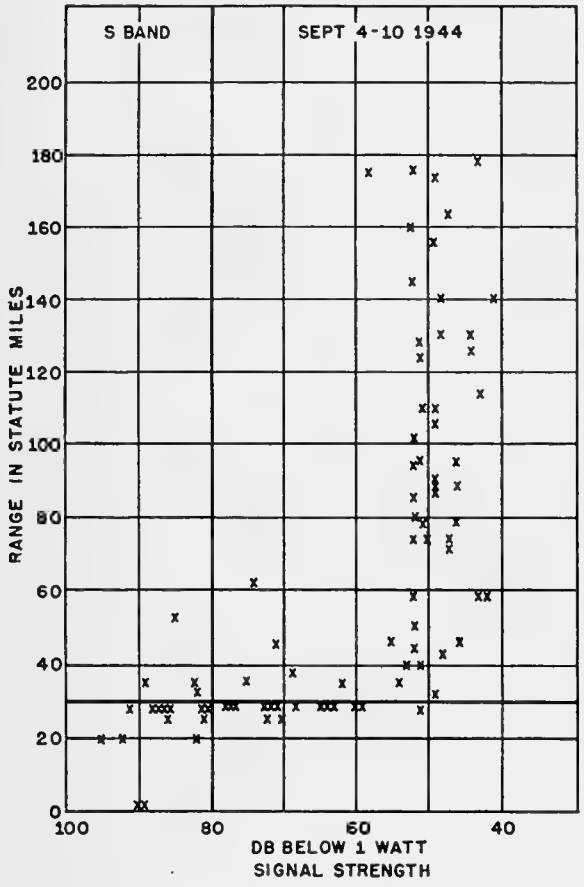

FIGURE 8. Relation between maximum radar ranges and one-way transmission.

long radar ranges, from about 40 to 280 miles, takes place while the one-way signal strength changes only slightly. This is another manifestation of the saturation of the signal at a high value.

SUMMARY

Two major conclusions may be drawn from this preliminary survey:

1. Standard signal is the exception rather than the rule for microwave radiation on this over-water path during the summer and fall. With the high M inversions which occur with warm, dry air over water, signal strengths 30 to 45 db above the standard occur about equally often on both, the upper limit being approximately the free space value, and radar ranges on surface targets are extended to five to ten times their normal values. On the other hand, with the low M inversions (less than 20 ft, say) which occur with air colder than the water, X band is affected more than S. Both may experience increases in signal level of 10 to 30 db above the standard, but the X-band signal is high more often than the S and at any given time usually reaches a higher level. Radar ranges on surface targets are extended by as much as 20 to 25 per cent above normal, and again X band experiences more effect. These increases in signal strength can be of great importance for communications, beacons, or any other application involving one-way transmission of microwaves, such as countermeasure. It should also be remembered whenever secrecy is required.

2. Substandard conditions may be present for several days at a time if the air is warm and moist. The reduction in signal strengths and radar ranges on surface targets which accompanies substandard conditions does not seem to be markedly frequency sensitive. It should be stressed that variations in one-way signal strength of at least 90 db have been observed. The radar ranges have also varied from roughly 10 or 15 miles up to at least 280 miles. These changes are not rare occurrences; deviations from the standard account for the major percentage of the time, especially during warm weather, and at the higher frequencies even during the fall.

1.3 TRANSMISSION CHARACTERISTICS OF AN OVER-WATER PATH[d]

Results were previously reported of some preliminary analyses of one-way radio transmission on a 41-mile over-water path from Provincetown to Gloucester,

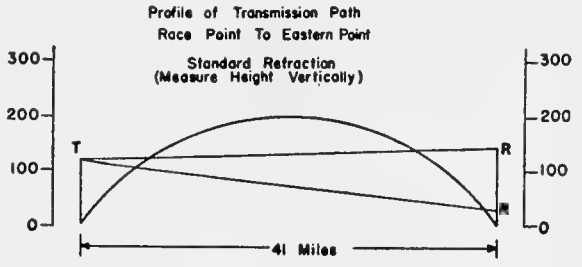

FIGURE 9. Transmission path profiles. (Heights in feet.)

with terminals well below the horizon. S- and X-band radiations were transmitted over the double paths indicated in Figure 9 to both "high" and "low" receivers,

[d]By P. J. Rubenstein and W. T. Fishback, Radiation Laboratory, MIT.

and 117-mc radiation over only the high path. Numerous meteorological surface measurements and low-level soundings were made, and essentially through comparisons with these measurements the following correlations for microwave transmission and surface M curves were obtained.

With positive M deficits, or M inversions, two cases were found.

1. Low ducts, less than 50 ft thick, resulted in a very steady signal at levels well above standard. The increase in signal level took place although the terminals were as much as 100 ft above the top of the M inversion. Such low ducts caused greater increases in the signal level on X band than on S band.

2. High ducts, 100 ft thick or more, resulted in very high signal levels on the average, but with deep fading. The signal level did not continue to increase with increasing duct height but instead "saturated" near the free space level. No frequency diversity between S and X bands was found in this case.

With negative M deficits, or substandard M curves, the signal was always below standard.

In November 1944 no correlations with M curves had been obtained for the 117-mc signal, and a clear lack of correlation with the microwaves had been noted.

A detailed analysis has since been undertaken which is as yet far from complete. This paper describes the method in use and presents some additional results.

In studying the fundamental phenomena of propagation the method employed was to tie the complete representative M curve to the observed transmission results by means of the wave theory. A threefold attack was used:

1. The meteorologists studied each situation in detail to determine a representative M curve and its changes with position and time.

2. Theoretical field strengths were found by putting the representative M curve, or a close approximation to it, back into the wave equation. These theoretical values were then compared with the observations.

3. Empirical correlations were then made between the M curves and the transmission results. This was done because the theory is applicable only to the simplest M curves and to uniform conditions.

This approach was employed in an effort to find parameters in terms of which predictions of range or field strength can be made for operational use. It is not considered a suitable method in itself for use in the field.

The meteorological part of the program has not in general received sufficient attention. Spot measurements at a given time and place do not necessarily give an adequate description of prevailing conditions. A thorough meteorological analysis of the entire period of transmission is therefore under way. For each case the synoptic situation is studied to find the trajectory of the air over the path at the time in question. Radiosondes, surface measurements, winds aloft, measured water temperatures, and all available low-level soundings are studied and the characteristics of the air over the water determined. Then representative low-level soundings are constructed. Such so-called synthetic soundings for the path midpoint are being drawn for 6-hour intervals for each day of operation. In addition, estimates are made of the departures from uniformity over the path and of the times of occurrence of marked changes.

All the radio analysis has been based upon these synthetic soundings and the accompanying discussion. The meteorological analysis is at first made completely independent of the radio data, with minor revisions when necessary after consideration of the transmission data. It is believed that full use of transmission data can be made only through such close cooperation of the persons engaged in both the meteorological and the radio work, not only in the measurements but also in the analysis.

Perhaps the most striking information which has so far resulted from the detailed analysis is the empirical correlation of the 117-mc performance with M curves. Increases in signal level above the standard are found to result from either large surface ducts (200 ft or more thick) or elevated superstandard layers which do not necessarily show overhanging M curves. Such layers occur frequently over Massachusetts Bay, mainly as a result of nocturnal cooling over land. Those which affect the 117-mc transmission occur below about 1,500 ft. Their strength is usually doubtful in view of the lack of accurate information on conditions over land in radiation inversions.

Figure 10 shows the correlation diagrams obtained when, first, all points are included, and second, all cases of elevated superstandard M layers are omitted. (Standard values are —120 db for 117 mc and —80 db for S band.) The first diagram obviously shows no correlation and is the sort of diagram obtained last fall. The second, however, is just what should be expected for the correlation with surface phenomena. The S-band signal rises to the free space value as the duct height goes up to about 100 ft and then "satu-

rates" for higher ducts. The 117-mc signal, however, is affected only by ducts considerably more than 100 ft high. Similarly, only a thin substandard layer is required to affect the S-band signal, but not until the layer is rather thick is the low frequency affected by it.

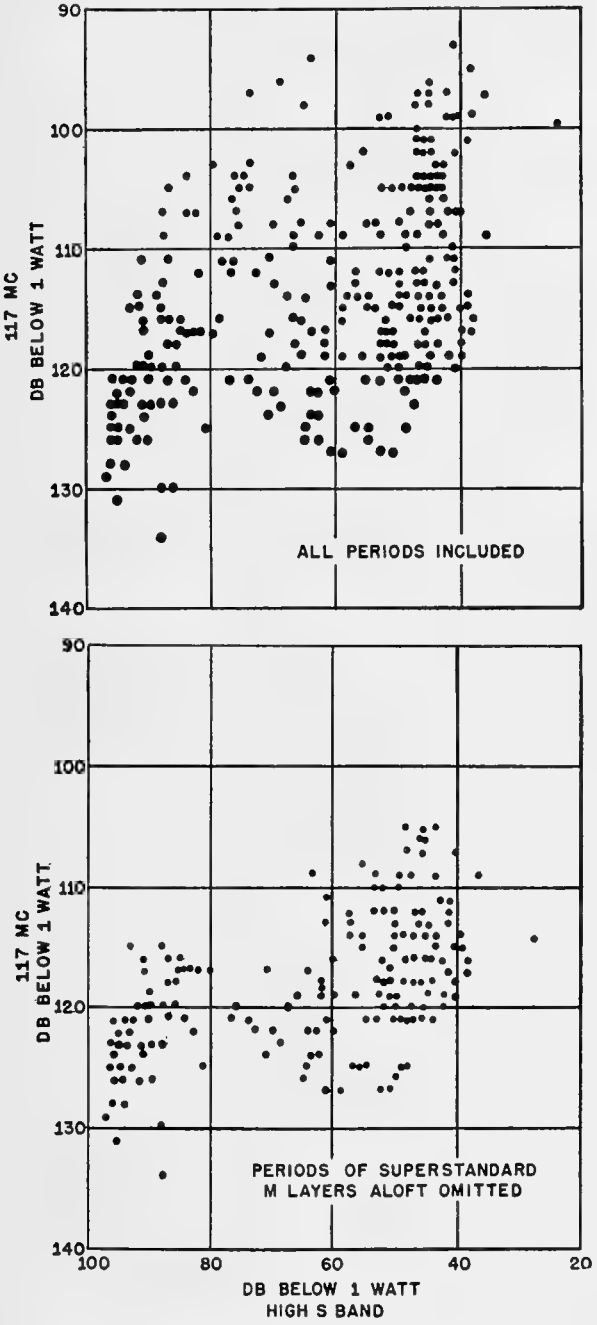

FIGURE 10. Field strengths: 117 mc and S band, July 31 to August 17, 1944.

In the period so far studied (960 hours total) the signal level was above standard 49 per cent of the time, standard 38 per cent of the time, and substandard 13 per cent of the time. Of the superstandard period 46 per cent has been correlated with elevated superstandard M layers, 36 per cent with thick surface ducts, and 4 per cent with situations in which elevated layers and thick surface ducts coexisted. Only 14 per cent of the time remains in doubt, and this includes many periods of exceedingly complex meteorological situations for which the analysis was inconclusive. In addition to correlation of field strengths with M curves, comparisons have been made between measured and theoretical values of field strengths. The theoretical values were calculated on the assumption of bilinear modified index curves, that is, curves made up of two straight-line segments. The M curve is taken to be standard above the joint, and two parameters are used: the height of the joint, or duct thickness, g, and the ratio s of the slope. The straight lines are drawn not in terms of M deficits but to give the best possible fit to the actual M curve. For the range of values of these parameters for which the contribution of the first mode only is of importance the curves of field strength shown in the following two figures are representative.

Figure 11 shows the effect of changing duct height, 0 to 500 ft, on the 117-mc field strength for various values of the slope of the lower segment. The field strength is measured relative to free space value and —33 db is standard. (s = —3 corresponds to a value of dM/dh about —100/100 ft; s = —2 is —30 per 100

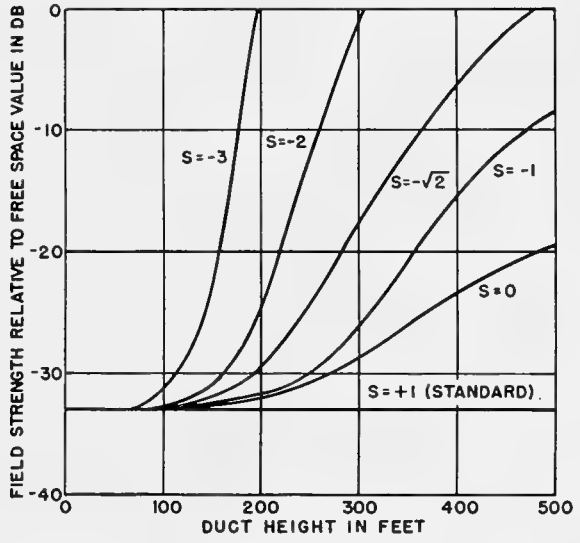

FIGURE 11. Theoretical field strength versus duct height, bilinear index, first mode, 117 mc.

ft, etc.) Note that for the bilinear model, unless the slope of the bottom portion be extreme, the duct height must be of order 200 ft or higher before there is any appreciable effect at this frequency.

Figure 12 is a similar theoretical diagram for the high S-band path. The scale in this case is 0 to 100 ft. At X band the corresponding changes occur over a height range of only about 30 ft. For the low paths

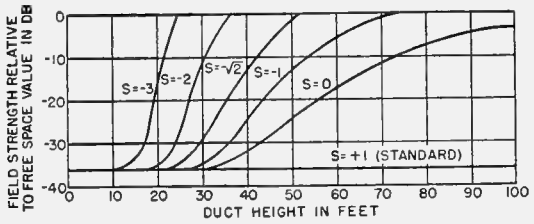

FIGURE 12. Theoretical field strength versus duct height, bilinear index, first mode, high S band.

at any given frequency the curves are similar, but the increases in field strength occur more rapidly, so that the free space value is reached at essentially the same duct height for both high and low paths.

In a few special cases for S and X bands contributions of a number of modes (as many as 18 in one case) have been added in phase. In no case did the calculated field strength reach a value more than 15 db above the free space value, and in most cases it was between —5 and +10 db.

The calculations check well with observations in a qualitative way in spite of the fact that the bilinear curve is not in general a good approximation to the true M curve and that the assumption of a uniform M curve along the entire transmission path is an extreme idealization. They show the order of magnitude of duct heights at which appreciable increases in field strength first occur at a given frequency. They demonstrate also the important fact that the field strength is increased even at considerable heights above the duct. This is so because with a leaky mode the height-gain function does not decrease with height above the duct but instead becomes practically constant over an appreciable range. This is illustrated in Figure 13, where the normalized height-gain function for a leaky case is compared with the standard. The decrease in absolute value of the height gain is compensated by the reduction in the attenuation. It is thus clearly not necessary to put a transmitter inside the low duct in order to take advantage of it; nor does the first mode need to be actually trapped as indicated by ray tracing, but merely less attenuated than the standard.

As to character of the signal, the theory suggests that steady signal is obtained with low ducts because only a single mode is important. With large ducts fading may be caused by interference among many modes which change rapidly in amplitude and phase with small changes in refraction. Even with very large ducts, for terminals well above the duct, steady signal might again be expected because the field strength there would probably again result from a single leaky mode, in this case not the first mode.

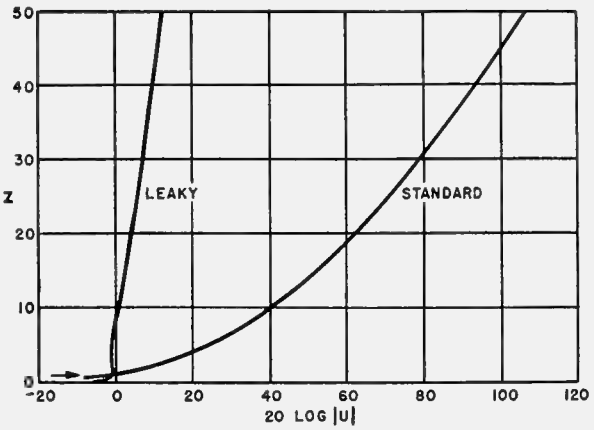

FIGURE 13. Height-gain functions, standard and leaky first modes. (Ordinate: height. Abscissa: gain.)

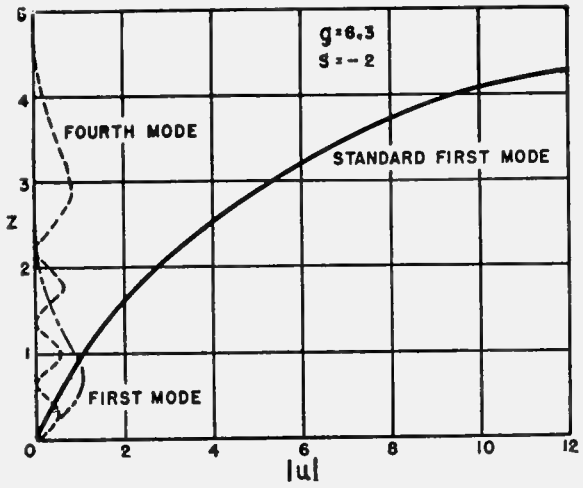

FIGURE 14. Height-gain functions within a duct compared with standard first mode. (Ordinate: height. Abscissa: gain.)

Finally, the calculations agree with observations in showing that even when many modes are strongly trapped, the field strength at a fixed point does not

reach the high value one might expect on the basis of an attenuation proportional to $1/R$ but rather remains near the ordinary free space value. This results from the fact that coincident with the reduction in attenuation which occurs with trapping, there is also an appreciable reduction in the height-gain function within the duct, as shown in Figure 14. The balance of the two countereffects prevents extreme increases in field strengths at all ranges of practical interest for microwaves.

To sum up, the 117-mc transmission is noticeably affected both by thick surface ducts or substandard layers and by elevated superstandard layers up to 1,500 ft altitude, which need not necessarily overhang. The wave theory for elevated layers is not yet sufficiently advanced to permit drawing definite conclusions. As for surface phenomena, an excellent qualitative agreement has been obtained between theoretical and observed results. There has been no indication of a need to revise the formula used for computing the modified index of refraction.

Following presentation of this paper the following data were presented on a similar experiment[3] made on an over-water path between San Pedro and San Diego, California. Transmitting and receiving antennas were at 100-ft elevation, with continuous wave transmission conducted from the San Pedro end of the link simultaneously on 52, 100, and 550 mc. The typical nonstandard condition in this area is produced by dry air aloft subsiding over moist air near the sea surface.

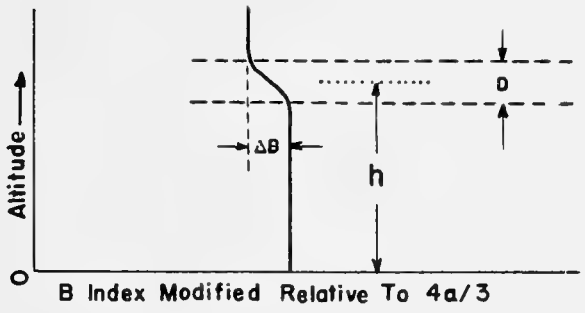

FIGURE 15. Modified index B.

This gives rise to a sharp discontinuity in the index of refraction distribution with altitude at some elevation above the earth.

In analyzing the data from this experiment, the index of refraction modified for $4a/3$, instead of the modified index M, was used. The new modified refractive index, B, thus obtained is shown in Figure 15. The pertinent factors for reflection considerations are as follows: h, the height of the layer above the earth; ΔB, the total change in index through the layer; and D, the thickness of the layer. For moderately high layers, D is much less than h.

Maximum field strength measured during the hour in which a meteorological sounding was taken is plotted against height of the layer above the ocean. The data are segregated into groups for different ranges of change in index of refraction through the layer. Figure 16 shows the data for changes in ΔB between 30 and 40 by means of crosses; for ΔB of 40 to 50 with dots; and for ΔB of 50 to 60 with circles.

If reflections are assumed to take place midway between the transmitters and receivers, the field strength may vary roughly as shown in Figure 16. The height-gain function holds the lower frequency fields down when the layer is low, whereas the added advantage in the reflection coefficient produces relatively stronger fields for the lower frequencies when the layer is high. A complete report will be made soon on the experimental data and its relationship with this consideration.

It was further pointed out that maximum observed field strength need not always coincide with complete trapping. The experimental evidence that for a given frequency the signal strength over a low fixed path first increases as the height of the base of the M inversion increases and then decreases does not necessarily contradict the wave guide theory. When the base is low, transmission is by means of well-excited modes with low attenuation. As the base height increases, the attenuation of some of the modes decreases and the field strength therefore increases. Further increase in base height results in well-locked modes which are more and more difficult to excite. It is then that the most effective mode is one which leaks sufficiently to be excited by a transmitter outside the duct and yet does not leak sufficiently to be strongly attenuated before reaching the receiver. As the height continues to increase, modes which can be excited are all strongly attenuated, and the ones which are only slightly attenuated cannot be excited. Thus signal strength ultimately decreases with increasing height.

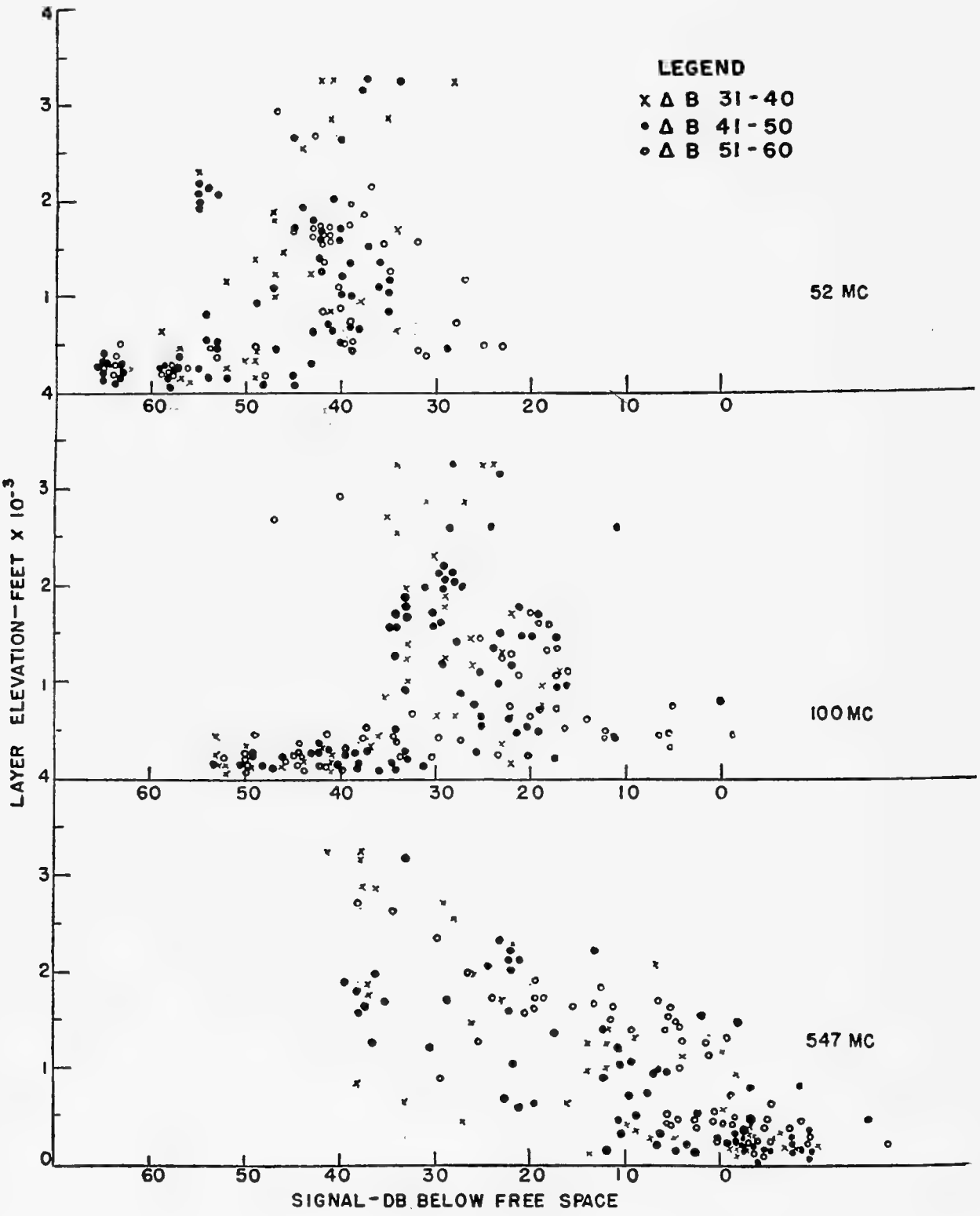

FIGURE 16. Signal versus layer elevation.

Chapter 2

TRANSMISSION EXPERIMENTS NEAR SAN DIEGO

2.1 ONE-WAY TRANSMISSION EXPERIMENTS OVER THE SEA BETWEEN LOS ANGELES AND SAN DIEGO[a]

ONE-WAY TRANSMISSION tests have been made by two methods: over a fixed path and by means of an airplane to sample vertical distribution of field strength. The fixed path is a nonoptical over-water path, 80 nautical miles in length from San Diego to San Pedro near Los Angeles Harbor. No intervening landscape is present at either end of the path. The c-w transmitters are located at the San Pedro end of the path at 100-ft elevation and operate on frequencies of 52, 100, 547, and 3,200 mc. The latter frequency has just recently been added, and insufficient data have been obtained to include in this report. The transmitters are quite conventional, the 52 mc being crystal controlled and the other two being self-excited units in which adequate frequency stability has been obtained by use of high-Q circuits. Monitors, which are read periodically, are provided on each transmitter. The receiver location, at 100-ft elevation, is located on Point Loma, San Diego, near the laboratory. The receivers are of standard construction incorporating a balanced d-c amplifier and Esterline-Angus recorder in the output circuit. Filament and plate voltages are regulated. Detuning effects due to temperature changes are minimized by temperature regulation in the receiver house. Receivers are calibrated at least once each week.

Four receivers have been installed in a PBY-5A plane which is used to sample vertical sections of field strength distribution at various distances up to 130 miles from the transmitters at 100-ft elevation. The frequencies used are 63, 170, 524, and 3,250 mc. Certain precautions were found necessary to insure correct orientation of transmitting antennas on the ground and receiving antennas on the plane. Receiving antennas on the plane are fixed in position, and measurements are taken only with the plane flying toward the transmitters. The plane's orientation is controlled, and the distance from transmitters determined, by utilizing the plane's Type ASE (Admiralty Signal Establishment) radar to home on a beacon located near the transmitters. All four transmitters and transmitting antennas are installed on a single rotating mount. A direction finder system also installed on the rotating assembly and operating on the plane's radar fre-

[a]By L. G. Trolese, U. S. Navy Radio and Sound Laboratory, San Diego, California.

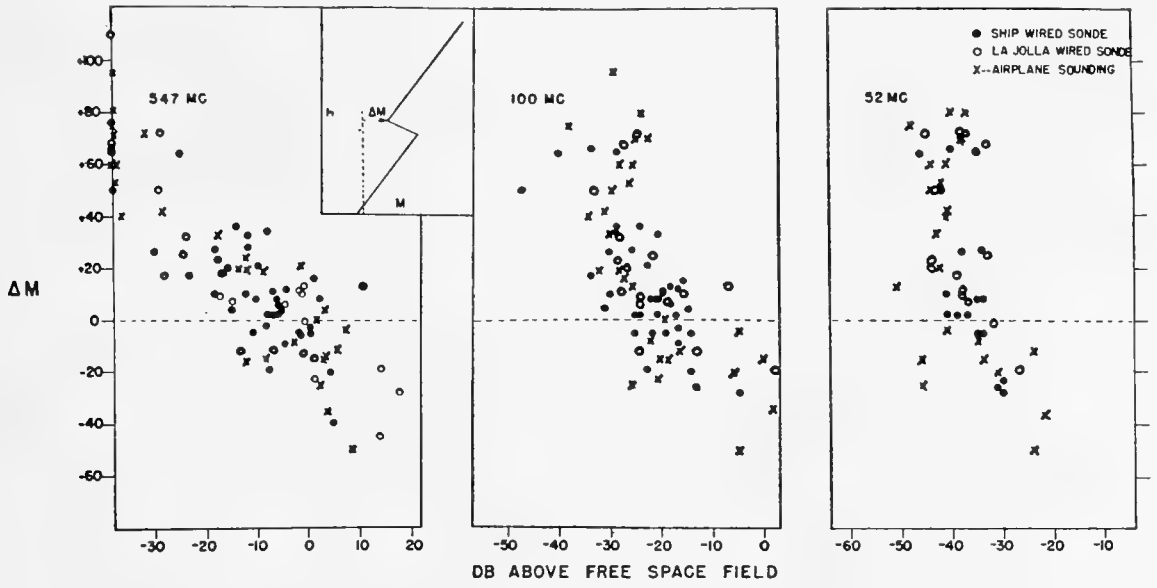

FIGURE 1. Maximum received signal versus atmospheric refraction.

quency is used to check the plane's bearing during flight and keep the transmitting antennas pointed at the plane. Bearing checks have been consistently obtained at ranges up to 130 miles. The d-f bearings agree quite well with those obtained by use of a type FC fire control radar.

2.1.1 One-Way Fixed Link Data

RAY THEORY — GEOMETRIC OPTICS

On the basis of ray theory, when it is assumed implicitly that the energy follows the rays, the modified index criterion for trapping should be expected to agree with experience. Ray tracing theory states that when the modified index at some elevation above a transmitter attains a value equal to or less than its value at the transmitter height trapping can occur.

As a preliminary check on this criterion the maximum field strength observed during the hour in which the meteorological sounding was taken is plotted against ΔM in Figure 1. When the minimum value of M in the refracting stratum is less than its value at the transmitter elevation, ΔM is negative, and the trapping condition is fulfilled. The 52-, 100-, and 547-mc links all show strong fields for large positive ΔM. These data are not compatible with the assumption that the energy follows the rays. The diffracted field is below detection for all the frequencies used on the 80-mile over-water link. This has been confirmed experimentally. On November 5, 1944 a front passed accompanied by heavy rain which dissipated all low-level inversions, and a standard condition resulted. During this period all the signals decreased below detection.

Figure 2 shows the above field strength data plotted against the height of the base of the temperature inversion. (The curves appearing in this figure will be explained later.) Although both the thickness of the inversion layer and the strength of the inversion vary considerably, the correlation of signal strength with the height of the base of the inversion is quite remarkable. The 547-mc signal decreases below detection as the layer heights increase above 3,000 ft; whereas the 100- and 52-mc signals are still relatively strong when the inversion base is above this altitude. These lower frequencies do show a decreasing trend as the layer continues to rise, going completely out, as stated above, when the low-level inversion is washed out.

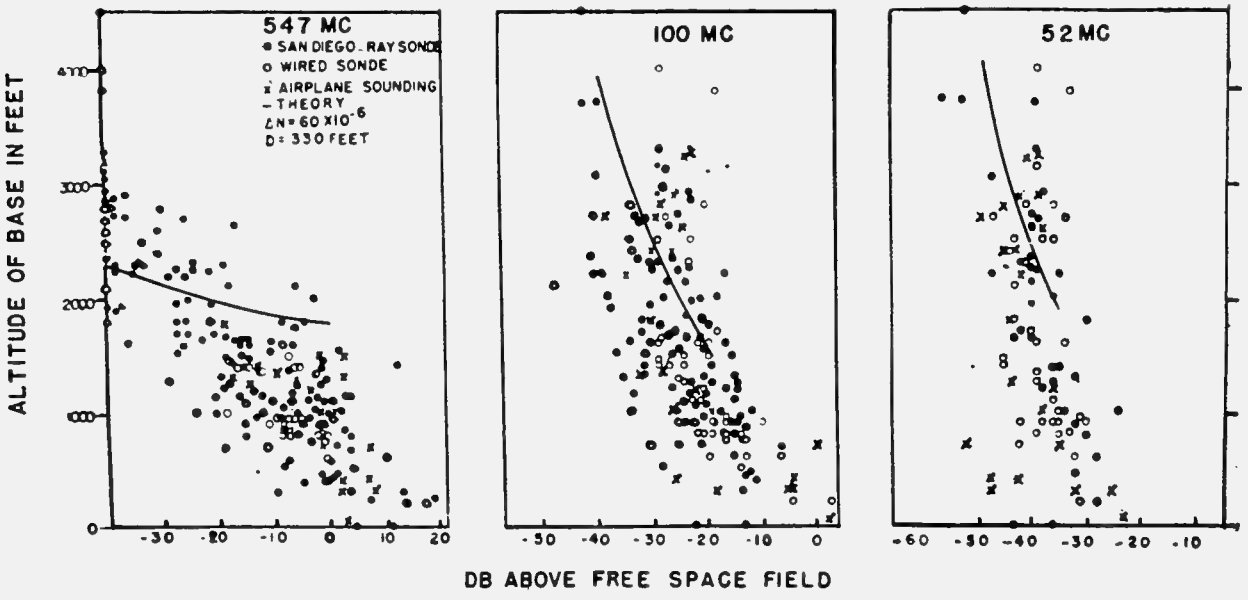

FIGURE 2. Maximum received signal versus altitude of base of temperature inversion.

Figure 3 shows a condensed log of the field strength data taken on the one-way link. Maximum and minimum field strengths during successive 2-hour intervals are plotted, thus showing the general level and fading range for each frequency during a 6-week period. The corresponding elevation of the base of the temperature inversion is shown by the discrete points in the upper part of Figure 3. It is at once apparent that the

signal level is higher for all frequencies when the layer is low and also that the fading range is smaller under these conditions. For a given elevation of the layer the fading range is greater for the higher frequencies.

Figure 4 shows the character of the signal received on the one-way link when the inversion was low and trapping was definitely indicated by the modified index curve. Figure 5 shows the signals under the condition of a high inversion. The time scale is shown along the horizontal at the top of 547-mc tape and at the bottom of the 52-mc record. For the condition of a low layer and strong trapping the level of all the signals is high and the lower frequencies are quite steady. As the elevation of the layer increases the 547-mc signal decreases below detection, the lower frequencies become less steady and the maximum level decreases. Figure 5 in contrast with Figure 4 clearly demonstrates this situation.

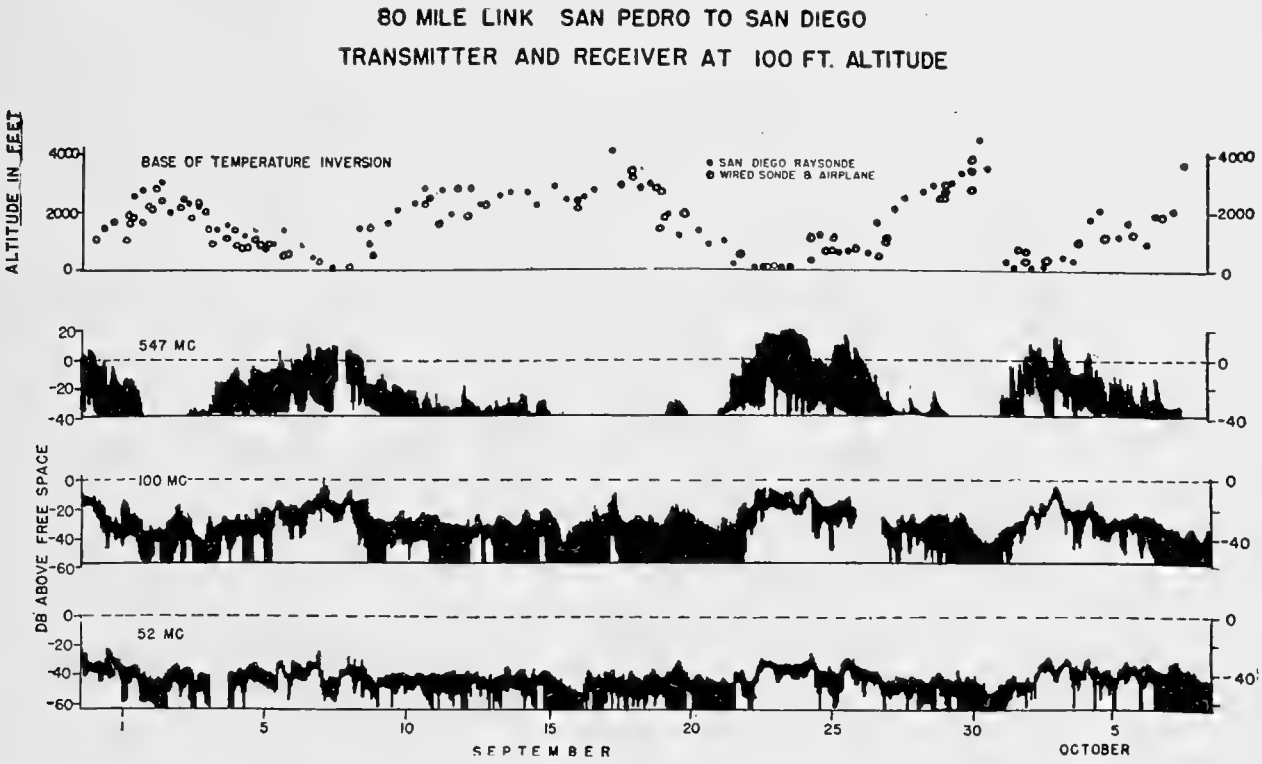

FIGURE 3. Maximum signal and fading range related to height of base of temperature inversion.

WAVE GUIDE THEORY

According to the simple wave guide theory, using the modified index, trapping can occur only when $\Delta M \leqq 0$; and then only when the wavelength is sufficiently small compared with the height of the reflecting layer above the earth. The degree of trapping depends upon the number of modes, or eigenvalues, allowed under the given boundary conditions.

The San Pedro to San Diego continuous transmission link yields data which can be compared with the simple wave guide theory. The 52-mc data are of particular interest, since for this frequency no meteorological data have been taken which would indicate any modes allowed. Yet the field strength has varied over a range of some 30 db, the strongest fields occurring at times of high fields on the 547- and 100-mc links.

Figure 6 shows the variation of the maximum field strength of the 547- and 100-mc frequencies versus the number of modes allowed as calculated from the meteorological data. There is no apparent correlation at either frequency.

REFLECTION THEORY

It has been shown theoretically[1] that reflection from a nonhomogeneous stratum may occur, even when both the index of refraction and its gradient are continuous functions through the layer. The controlling factor, for a given incident angle, is the ratio of the

stratum thickness to wavelength, D/λ. At normal incidence the reflection coefficient is small, even for $D/\lambda \sim 0$; however, such reflections have been observed experimentally.[2] At oblique incidence, for the cases where the index of refraction varies monotonically through the layer, the reflection ratio increases as $D/\lambda \sim 0$. For the modified index type the reflection ratio increases as D/λ decreases, passing through a maximum after which it again decreases.[1]

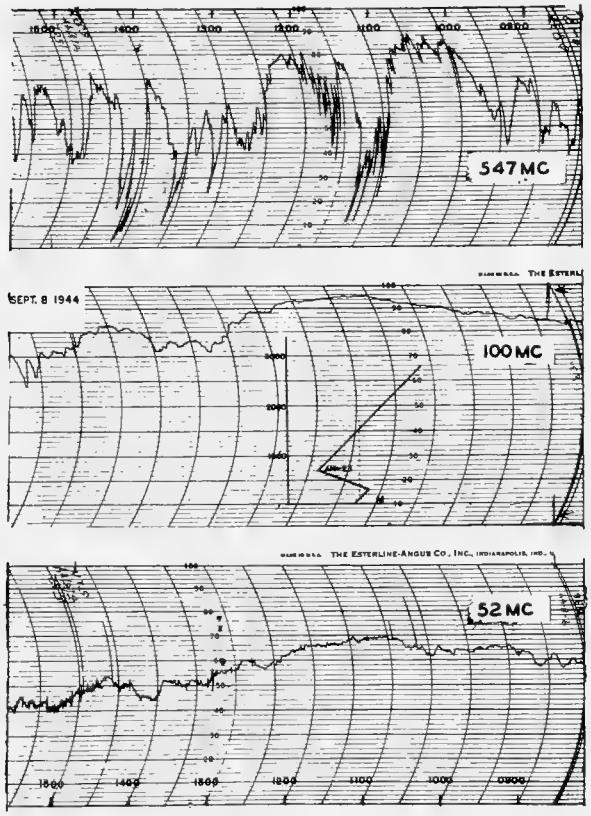

FIGURE 4. Signal types on one-way link for low inversion (trapping).

Figure 7 shows the reflection ratio as a function of D/λ for various angles of incidence, where here the index of refraction is a monotonically decreasing function of height through the layer. The total change in n through the layer is taken to be 60×10^{-6} which is the order of magnitude of the changes noted in this area during the summer season. For a given stratum thickness and height above the earth such that the radiation will be incident upon the layer at angles slightly less than the critical angle, the lower frequencies will be reflected more strongly from the layer. In addition, any deviation of the layer from the horizontal plane will affect the higher frequency radiation more than the lower frequencies. This is manifested by the greater fading range of the 547-mc signal as shown in Figure 3.

Consider the case where the layer is 330 ft thick. Since the angle at which the radiation will be incident upon the layer will depend upon its elevation, it is possible to compare the experimental data with theoretically calculated reflection ratios. In Figure 2, the curves indicate the theoretically predicted variation of field strength as the layer rises. The absolute decibel scale does not apply to the theoretical curves; only the slope is significant. The actual layer thickness and the effective change of the index of refraction through the layer varied around the values used, and so an exact correspondence between theory and experiment should not be expected. However, the agreement is fair. In addition, at any given time the reflecting stratum is a warped surface which changes shape with

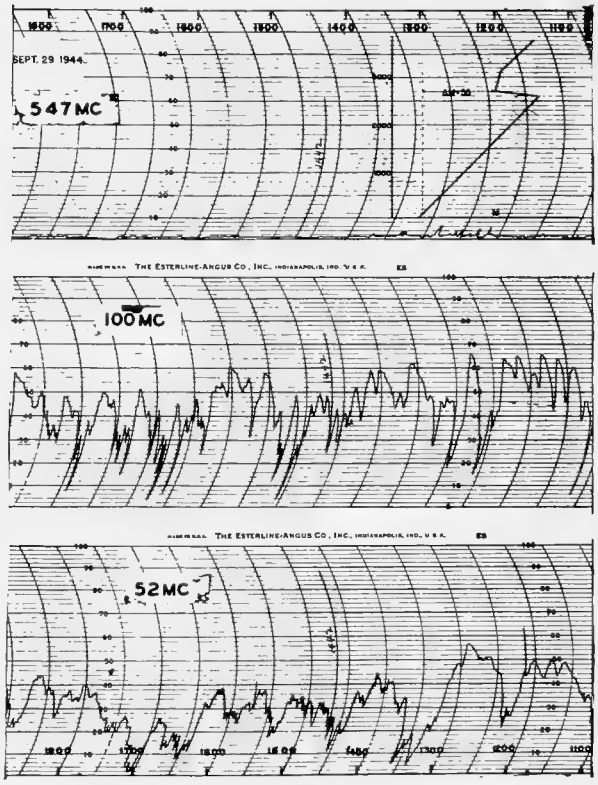

FIGURE 5. Signal types for high inversion. Note the low level of the 547-mc signal.

time. This condition complicates any theoretical treatment of the problem.

The analysis thus far indicates that the variation in

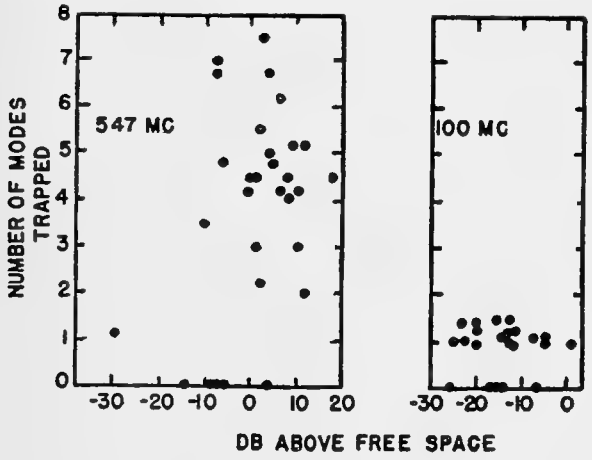

FIGURE 6. Number of modes trapped.

actual index of refraction through the layer has to be used to explain the magnitude of the fields observed on the one-way link. When the layer is thin the longer

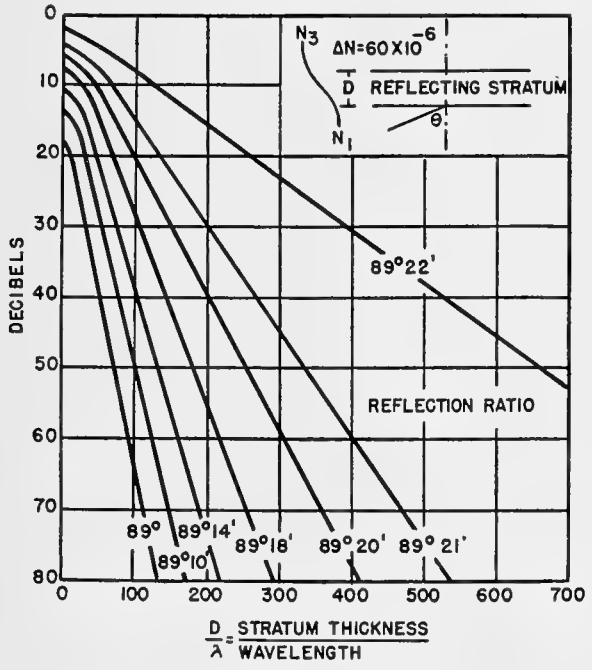

FIGURE 7. Reflection ratio.

wave radiation might be expected to leak more readily through the stratum and thus show less trapping at the greater distances. Actually, the vertical sections of field strength taken in the plane (Figures 8 and 9) show rather large fields above the layer at the longer ranges. This might be interpreted in favor of the modified index over the measured index of refraction. However, on the other hand it could be diffraction due to the low elevation of the layer, or a storage field when the actual index of refraction is used. A study of the attenuation along the path should clear up this last point.

2.1.2 Vertical Field Strength Sections

Two typical sets of field strength data are shown in Figure 8 and in Figure 9. Figure 8 illustrates a case for which there was definite trapping predicted by the modified index criterion. It will be noted that the 63-mc radiation shows little variation in field strength with altitude. In most cases it shows even less variation with time at a given altitude. The higher frequencies show more variation of signal with altitude, and the field strength distribution varies more with time. This variation with time is in complete agreement with the data taken on the San Pedro to San Diego one-way link. The minimum field above the minimum point of the M curve, as predicted by ray theory, is certainly missing at the lower frequencies and rather uncertain at the higher frequencies.

Figure 9 in the following paper shows field strength sections for a day when the reflecting layer was at an elevation of around 3,000 ft. Here the solid line represents the first run and the dotted line the repeat section. The time interval between sections was from an hour to an hour and a half. The sections at about 75 miles from the laboratory show results compatible with the one-way link data. At low elevations the lower frequencies show stronger fields than the higher frequencies. This again is in agreement with reflection theory.

SUMMARY

The modified index of refraction, in conjunction with ray theory, is a poor criterion for trapping. Strong fields are observed well below the horizon when the observed modified index would indicate that no trapping would be taking place. The vertical distribution of field strength for the lower frequencies appears to have little in common with the fields predicted by ray tracing methods where the energy is assumed to follow the rays.

There is no apparent correlation between the experimental data and the simple wave guide analysis.

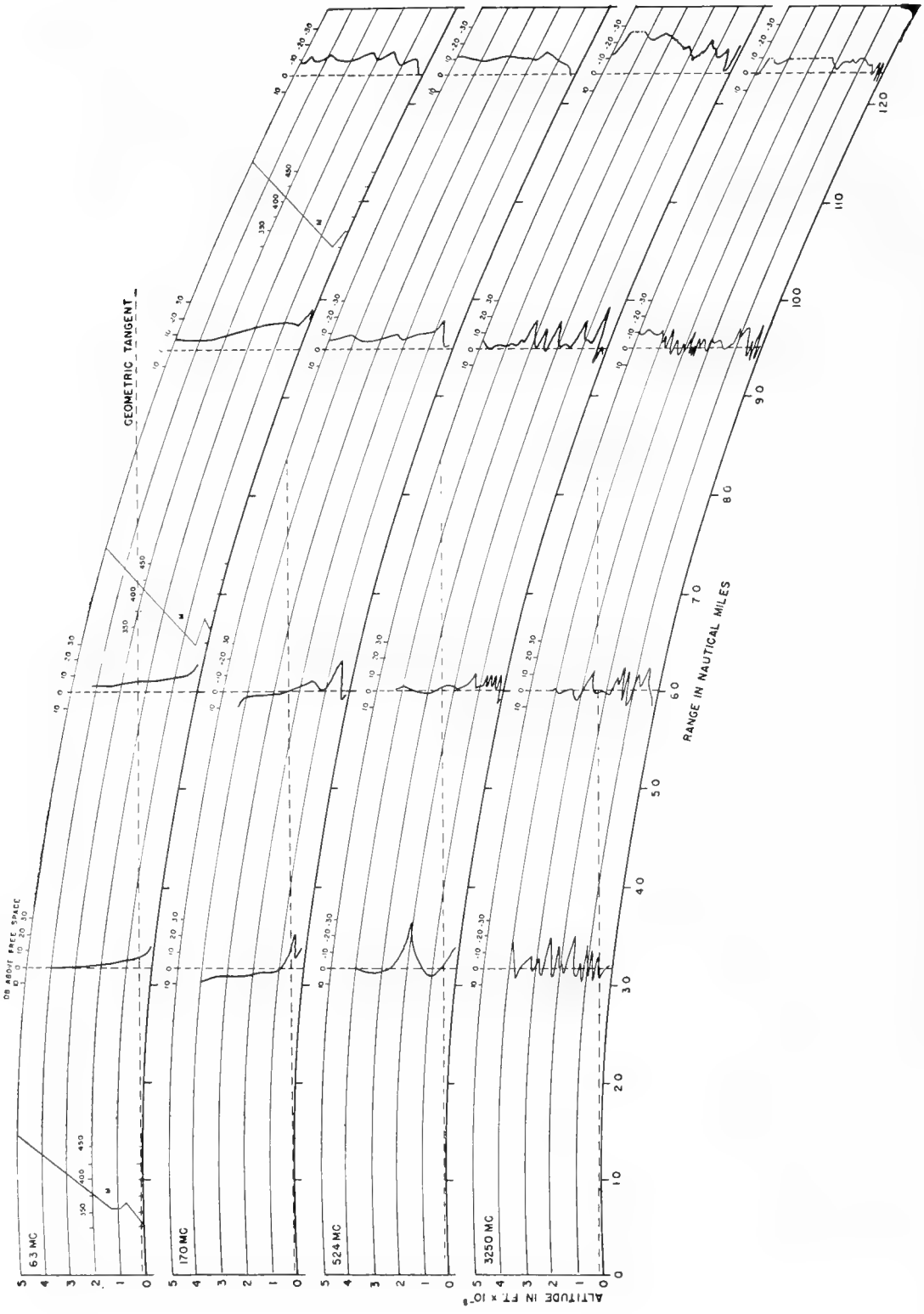

FIGURE 8. Vertical field strength sections. Transmitter at 100-ft elevation. Date: October 2, 1944.

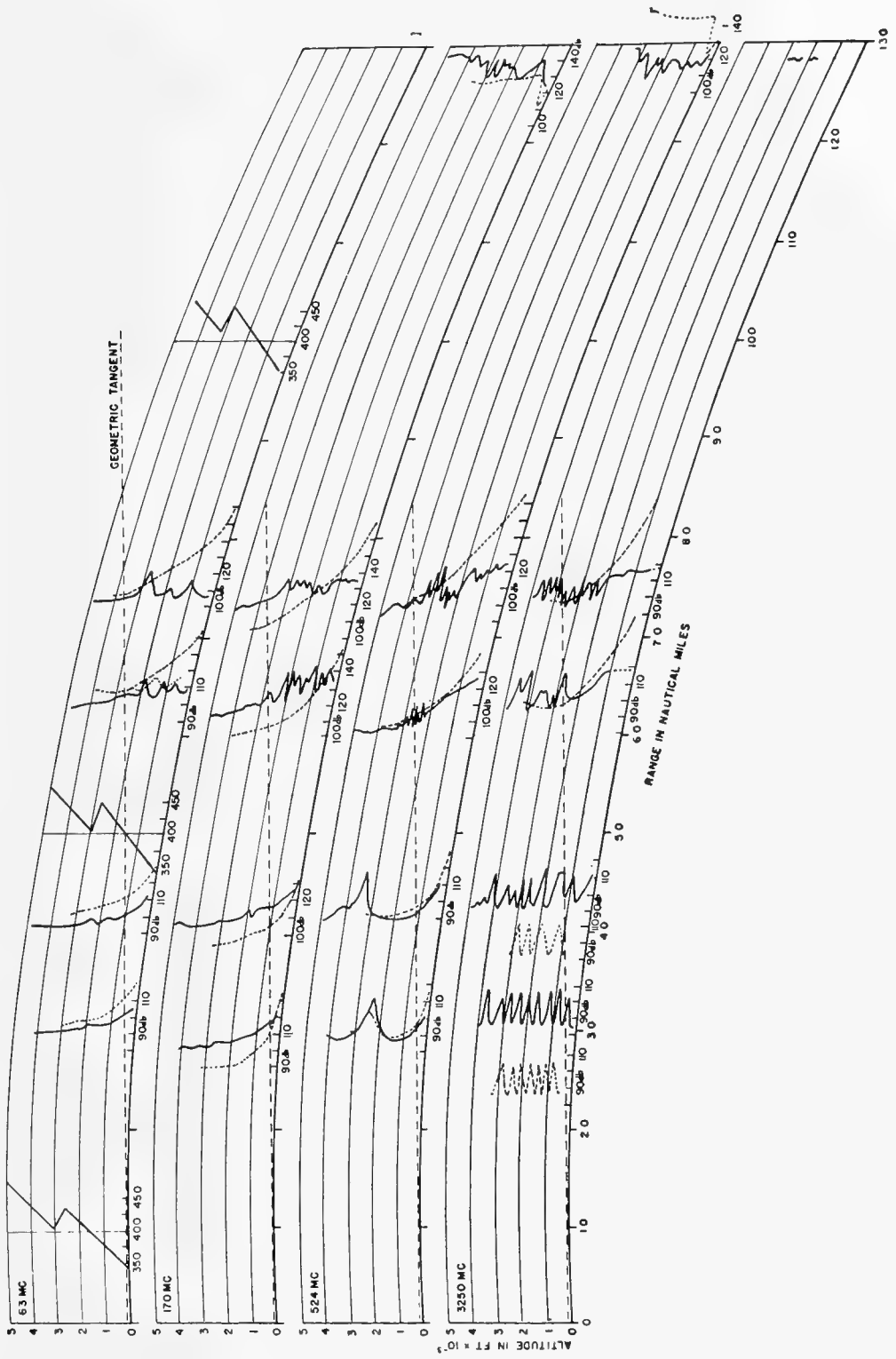

FIGURE 9. Vertical field strength sections. Transmitter at 100-ft elevation. Date: September 29, 1944.

Treating the elevated refracting stratum as a plane reflecting layer seems to agree in general with experience, for the following reasons. (1) The observed frequency sensitivity of the reflecting layer is predicted. (2) The observed fading characteristics of the different frequencies is again in the right direction, the higher the frequency the greater the fading. (3) Strong fields well below the horizon under conditions of high layers cannot be explained on the basis of refraction alone.

2.2 THE CORRELATION OF CALCULATED AND MEASURED FIELD STRENGTHS[b]

Since the time of issue of reference 3, the importance of further experimental check against the calculated patterns has been fully realized.

The field strength cross sections recently obtained by airplane-borne receivers have made possible such a check.

For anything more than a rough qualitative correlation it was soon apparent that quantitative field strength analyses were needed for the actual observed meteorological conditions.

Because of the clearly apparent influence of high level inversion layers on the observed radiation fields, this type of condition was selected. Consider, for example, the M curve at 50-mile range obtained on September 29 reduced to three linear segments as shown in Figure 9.[c] It is clear that the M curves at 10 and 100 miles are not seriously different.

We thus have a condition in which $M - M_0$ decreases by 50 units in a 200-ft interval of altitude attaining the minimum value of +50 at 3,000-ft elevation.

Figure 10 shows the ray diagram constructed for the analysis. The diagonal lines below 4,000 ft represent the positions at which field strengths were measured and calculated.

The actual size of the ray diagrams is 27x40 in. Rays in the region of standard refraction have a 58-in. radius. Through the transition layer the radius is 4 in. The above radii are determined by the vertical and horizontal scaling factors and are approximately one ten millionth of the curvature as given by dM/dh. Note that the downward curvature of the earth and upward curvature of rays in the standard propagation regions are made equal, thus reducing the slopes of the rays and resulting errors inherent with deformed scale graphical methods.

Since the tangent ray (shown with short dashes) intercepts only a small part of the fourth and none of the fifth section of measurements, the analysis methods employed in radar coverage diagrams had to be extended. Specifically, the coverage diagram analysis at NRSL has applied to fields between 85 and 100 db below that at a distance of one meter from the transmitter. This largely excludes consideration of any but interference and trapping zones.

The measurements with which correlation was desired extended to about 30-db weaker fields so that partial reflection and diffraction fields were involved.

Proceeding with the ray tracing analysis, the interference field was calculated at points of intersection of the direct and sea-reflected rays. Path differences were determined using a map measure and a planimeter as explained in reference 4. Ray densities were measured for the direct and reflected components, and the associated fields were added with respect to the phase. The diffraction field below the tangent ray was calculated by Norton's method.

Reflected rays from the layer were introduced as originating at the center of the layer. The reflection coefficients for the angles of incidence were calculated as described in reference 5 for the case of a monotonic transition layer in which the refractive index decreases by 50×10^{-6}. In the terms of field intensity the reflection coefficient values ranged from 0.2 to 0.1 at 63 mc and from 0.01 to 0.003 at 524 mc.

In Figure 9 the calculated normal interference and diffraction fields are shown dotted beside the measured values except at 3,250 mc on which the 30- and 45-mile sections have been displaced for clarity. At 63 mc there is an apparent displacement of about 3 db which is probably associated with the reduction in measurements to the decibels below the field at a distance of 1 m from the transmitter. Note that at 60 miles the interference pattern of the diffraction and partial reflection fields as calculated appears with a phase displacement of about 180 degrees from the observed field. The phase relationship depends, of course, on an assumed value of 90 degree change of phase on reflection.

At 170 mc there is a displacement of about 10 db due to difficulty of reduction in measurements. Introducing a 10-db correction, all values at 170 mc

[b]By F. R. Abbott, U. S. Navy Radio and Sound Laboratory, San Diego, California.

[c]See discussion of Figure 9 in Section 2.1.2.

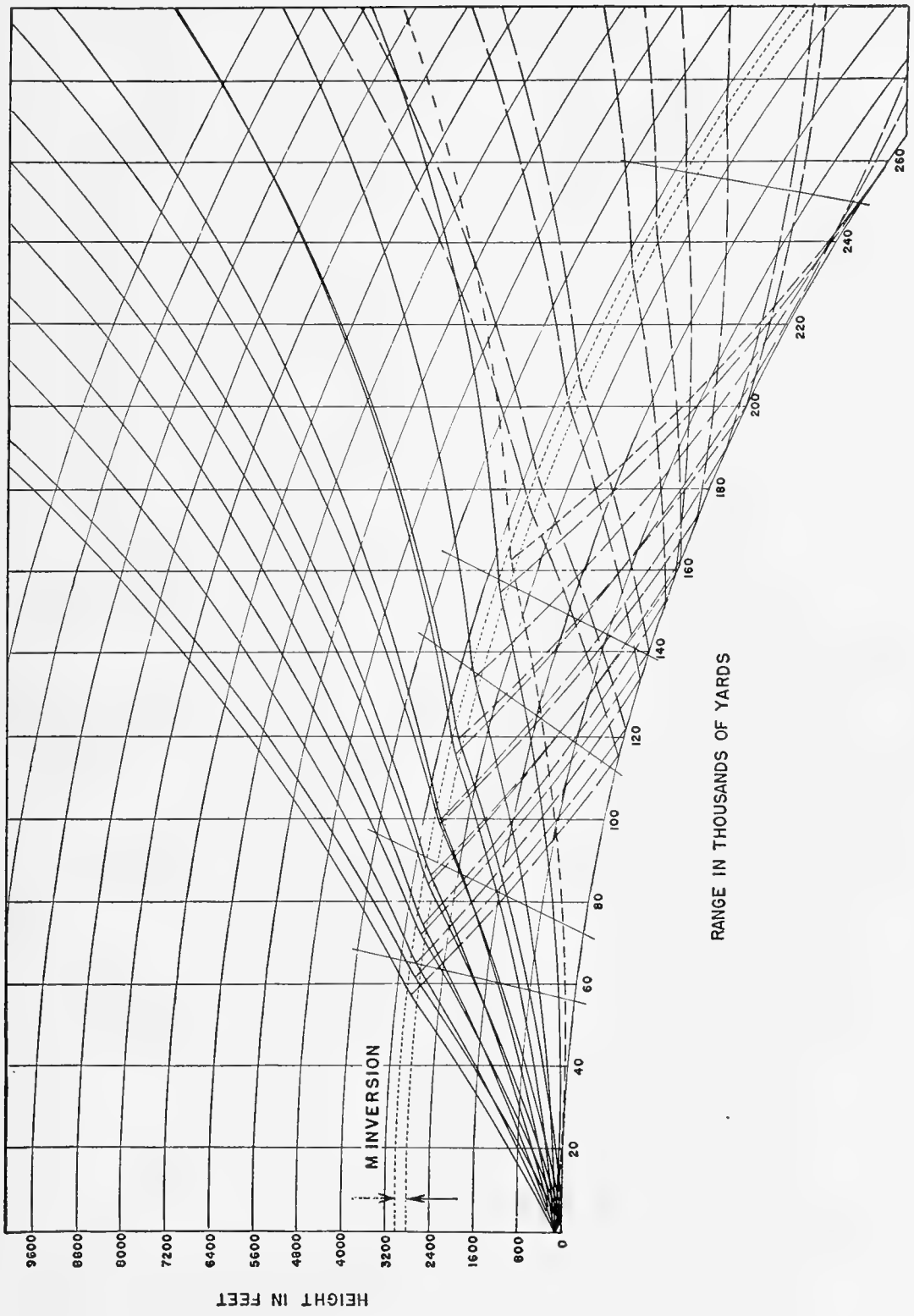

FIGURE 10. Ray diagram 20. *M* curve 30,2,50. Antenna height 100 ft.

agree closely, including the field at 130 miles, due solely to partial reflection. No attempt was made to calculate the detailed variation with altitude.

The agreement between calculated and observed fields at 524 mc is excellent above, but poor below, the tangent ray. At 130 miles 20- to 30-db difference appears. Note that the measured field is about 20 db greater than the 170-mc field at that range. This contradicts the trend of the calculated reflection coefficients which should decrease exponentially with relative thickness of the layer measured in wavelengths. The observed 524-mc fields at 130 miles on some other days of pronounced high-level inversions were well below the 170-mc fields and thus in qualitative agreement with theory. At 3,250 mc there is again good agreement above the tangent ray, but again, in the region below, the observed fields were high though the calculated values became very small.

Thus a preliminary check of analysis versus measurements indicates:

1. Discrepancy of absolute values except where the field at the maximum of a lobe was measured.

2. Excellent agreement as to variation with range and altitude above the geometric tangent as well as in the diffraction-partial reflection zone, except that at 524 mc and 325 mc strong fields were observed below 4,000 ft to 130 miles in contradiction with theory.

Chapter 3

TRANSMISSION EXPERIMENTS IN ARIZONA

3.1 ATMOSPHERIC REFRACTION UNDER CONDITIONS OF A RADIATION INVERSION[a]

An investigation of propagation of high-frequency radio waves under conditions of a nocturnal temperature inversion was made in Arizona over a short period in December 1944. Climatic conditions in this region permitted testing the dependency of refractive index in the lower troposphere on the temperature lapse rate, since the water vapor content was expected to remain relatively constant.

During the day in this area the soil heats rapidly, producing vertical instability and convection mixing near the ground and hence a temperature lapse rate in the lower atmosphere approaching the dry adiabatic rate. After sunset the soil temperature drops rapidly, cooling the layer of air adjacent to the surface and producing a low-level radiation inversion during the night.

It was thought that the progression of this low-level inversion would at times cause the lapse rate of refractive index to vary between slightly positive and zero, which would be the case of greatest interest. If during such a variation of lapse rate field strength observations are made with a receiving antenna which under standard conditions is in the earth shadow region, a test can be made of Hoyle's hypothesis[1] that temperature lapse rate is of greater significance than is now believed. If, for example, the field strength during one-way transmission reaches the value calculated for a flat earth while the modified refractive index lapse rate is still positive, then something must be wrong with either the modified index concept or

[a] By J. B. Smyth, U. S. Na

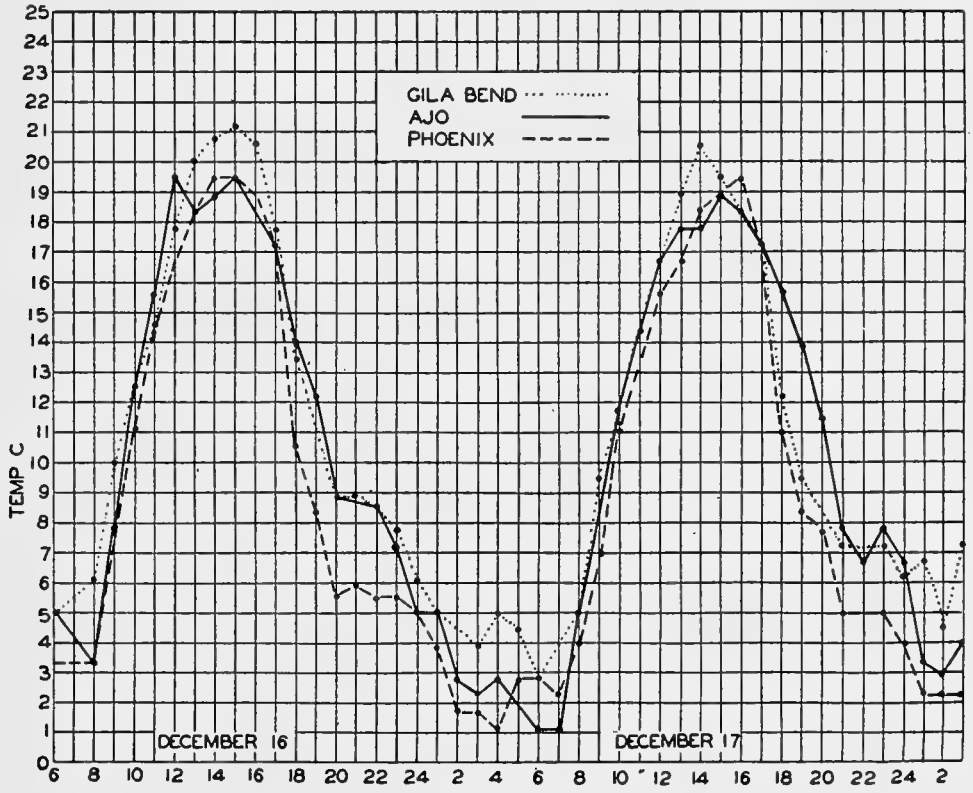

Figure 1. Surface air temperatures at Ajo, Gila Bend, and Phoenix, December 16 to 17, 1944.

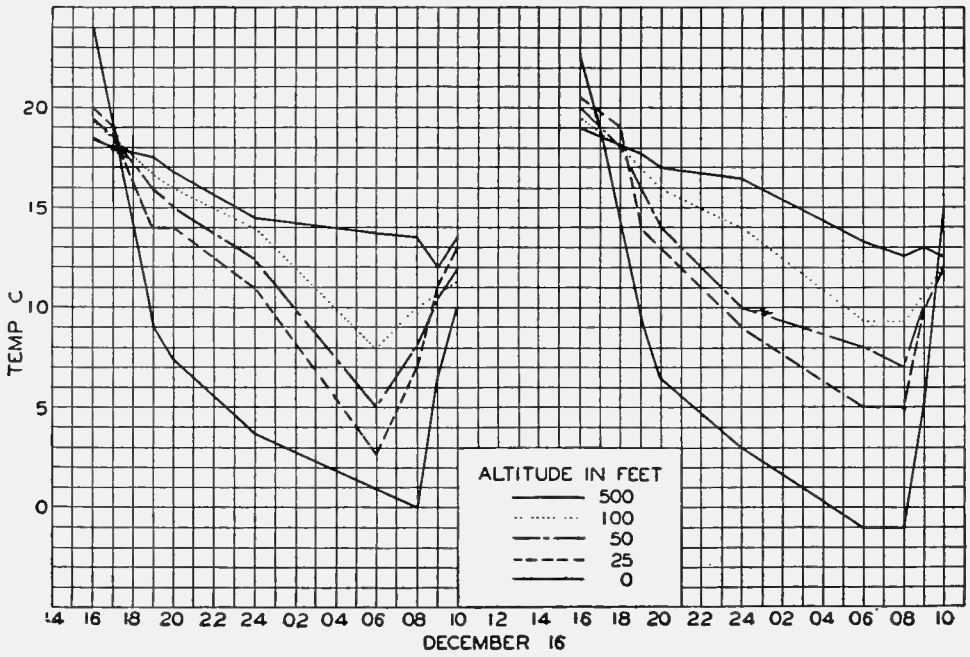

FIGURE 2. Soil and air temperatures at Datelan, December 16 to 17, 1944.

the method of calculating refractive index from meteorological data.

When the modified index lapse rate is relatively constant with altitude, a fairly simple transformation makes the atmosphere nonrefracting and the effective earth radius greater or smaller than the actual radius, and ray tracing should then be valid in the interference field. If no rays reach the receiver, the diffracted field must supply all the energy received.

The propagation path extended from Datelan to Gila Bend, Arizona, a distance of 47 miles over desert terrain. A 3,200-mc transmitter was located on a tower at a height of 53 ft above ground at Datelan, with the receiver 35 ft above the ground in the control tower at the Gila Bend airfield. There is a gentle rise of ground from Datelan to Gila Bend with a total rise in elevation of 402 ft, or about 8.5 ft per mile. The intervening terrain is remarkably uniform, without trees or large irregularities, and there are no buildings except in the immediate vicinity of the transmitter and receiver locations.

Figure 1 shows the diurnal variation of surface air temperature at Ajo, Gila Bend, and Phoenix for December 16 and 17, 1944. These typical data show the uniformity of conditions over that region and the effect of radiation cooling on the air mass near the surface.

Figure 2 shows the variation of the soil temperature with time at Datelan for the same period, as well as temperature changes at 25, 50, 100, and 500 ft above the earth.

The general topography around Gila Bend in conjunction with the diurnal variation in the prevailing surface wind vector shows an interesting condition. Hourly wind vector observations during November and December 1944 showed that by 1900 the prevailing wind was downslope toward the lower elevations. This flow of cold air into the area of the link may be responsible for the overall cooling of the air up to several hundred feet during the night. At present it is not clear how much of this effect should be attributed to radiation and eddy diffusion of heat toward the earth, although on nights with wind speeds from calm to a gentle variable breeze it is difficult to attribute the entire transport of heat to the latter processes.

Some pertinent data are tabulated in Table 1 showing the time at which the signal was first detected and completely lost and the general atmospheric and ground conditions nearest these times. On the afternoon of December 14, the sky was overcast, and the signal was detected about an hour earlier than on the other evenings.

Figure 3 shows the field strength data for a typical day plotted in decibels below free space. The maximum and minimum for half-hour intervals are shown

TABLE 1

Date	Time of sunrise	Signal below detection, time	Cloud condition	Soil temperature	Time of sunset	Signal first detected, time	Cloud condition	Soil temperature
12/13	0653				1655		Few cirrus	1800 13C
12/14	0654	0845	0800 Clear	0800 3.1C	1656	1615	1730 Overcast Altostratus Cirrostratus	2000 9.0C
12/15	0655	0945	0800 Scattered low clouds Scattered middle clouds Scattered altostratus	0800 2.0C	1656	1715	1600 Scattered cirrus	1700 19.4C
12/16	0655	0925	0800 Overcast High cirrus	0900 6.4C	1656	1725	1700 Scattered cirrus	1700 19.3C
12/17	0656	0940	0900 Scattered cirrus	0900 5.3C	1656	1730	Few cirrus	1700 17.9C
12/18	0656	0950	0900 Clear	0900 6.0C	1657	1738	1700 Scattered cirrus and altostratus	2000 8.5C
12/19	0657	0923	0900 Clear	0900 8.8C	1657	1628	1700 Scattered cirrus	1630 20.8C
12/20	1658	0910	0900 Clear	0900 8.7C	1658			

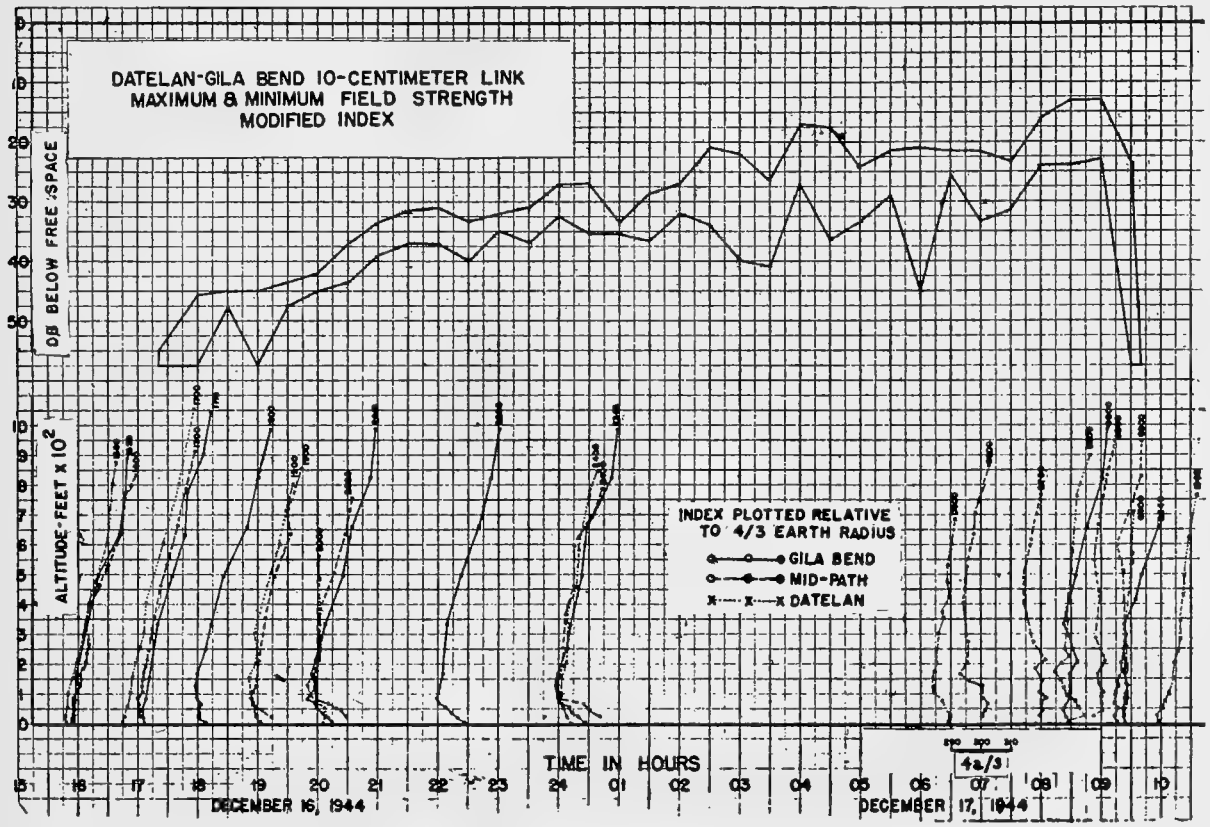

FIGURE 3. Typical field strength and modified index curves, December 16 to 17, 1944.

so that the fading range is apparent. The meteorological data for the period are given in the form of modified refractive index curves relative to a fictitious earth radius of $4a/3$, the time of the sounding being given on each curve.

The diurnal variation in field strength is quite pronounced and regular. The maximum range of fields measured was around 46 db, the maximum field generally occurring at times when the inversion layer was thickest. There is no significant correlation between strong fields and the amount that M decreases at some elevation above the antennas. In fact, at times such as 0900 on December 17 the field strength is quite high and yet M shows little indication of trapping. In most cases strong fields occur at times when the $4a/3$ modification of the index of refraction gradient is near zero or varying slowly with altitude.

The general results of this experiment may be summarized in the following way. Over the desert location a ground-based temperature inversion was found each night due to radiation cooling of the underlying surface. This temperature inversion produced a strong index of refraction gradient in the first few hundred feet above the earth.

The 10-cm nonoptical link showed a marked diurnal variation in field strength in close correlation with the building up and intensification of the temperature inversion. The strongest fields generally accompanied modified index gradients approaching zero in the first few hundred feet above the earth's surface.

The trapping criterion most widely accepted heretofore specifies that, at some elevation above the transmitter and receiver antennas, M should be less than at the antennas. The data herein reported seem to indicate that this criterion is neither necessary nor sufficient to insure strong fields below the optical horizon. The strongest fields observed at 10 cm approached the flat earth value, assuming a reflection value of unity for the earth.[b]

[b]Section 5.4 will be of interest in connection with this chapter.

Chapter 4

TRANSMISSION EXPERIMENTS AT ANTIGUA, WEST INDIES

4.1 PROPAGATION IN S AND X BANDS IN LOW-LEVEL OCEAN DUCTS

4.1.1 General Description[a]

THE EXISTENCE of low-lying ducts over the seas of the world, particularly in the trade wind belt, has been known for the past 2 years. Measurements made by the British and by Washington State College and the Naval Research Laboratory have consistently indicated the presence of ducts ranging in thickness from 20 to 50 ft in regions where the trade wind followed a long over-water trajectory. These ducts are known to vary in intensity and thickness with wind velocity during the trade wind season. It was considered advisable to investigate the possibility that such ducts would permit greatly extended ranges on surface craft and very low-flying aircraft by properly sited radar installations.

Discussion by representatives of the Chief of Naval Operations, NDRC, and the Naval Research Laboratory resulted in organization of a project to make an experimental investigation of meteorological and propagational conditions in an area of the Caribbean theater where such ducts are persistent, with a view to determining their operational usefulness. It was decided that a one-way ship-to-shore transmission path over water would provide the most direct data for analysis, and such a system was set up, using transmitting and receiving equipment provided by the Radiation Laboratory. The transmitters were installed in a patrol craft assigned for the project, there being no larger vessel available, with transmitting antenna heights of 16 and 46 ft.

The site chosen for the receivers at the land-based end of the link was at Judge Bay on the island of Antigua in the Leeward Island group of the British West Indies. Antennas were installed on a tower 50 ft from the water's edge, at heights of 14, 24, 54, and 94 ft, for both S- and X-band receivers.

Antennas for both S- and X-band transmitters were installed on the patrol craft at heights of 16 and 46 ft. These consisted of parabolic reflectors arranged to permit transmission forward or astern, so that transmissions could be made on both the outward and inward legs of the runs. The S-band transmitter peak power output was 42 kw, and its antenna provided a measured gain of 27 db. Output on X band was 31 kw, the antenna providing a measured gain of 29 db. Later in the experiment an S-band antenna was installed at a height above the water of 8 ft. Tests were made with this antenna on two runs. Adequate switching arrangements to permit tests with the different antennas were provided, and power outputs were measured by means of directional couplers and thermistor bridges.

Meteorological measurements from the ship consisted of detailed temperature and relative humidity readings taken on a rigging running from a boom extending out over the water amidship to the yardarm about 46 ft above the water. Low-level sounding equipment of Washington State College design was used for all meteorological measurements. Balloon ascents to heights of 600 ft from the stern of the ship were also made when conditions permitted. Hourly observations of sea temperature, wind, and sling psychrometer readings from the bridge were made. It was impossible to obtain satisfactory soundings on the rigging or by use of balloons and kites when running away from the tower into the wind because of the large amount of water taken over the bow and the resulting salt spray. Shipboard observations during outward runs were therefore confined to the hourly wind velocity, sea temperature, and sling psychrometer readings. On return runs with the wind, balloon and rigging soundings were made. It was necessary to estimate the height above the surface for readings taken below 10 ft because of the severe pitching and rolling motion of this type of ship, and therefore very few such readings were made.

At the receiving end of the radio path, the antennas for S band were 48-in. parabolic dishes with a gain of about 30 db. The X-band antennas were 48-in. dishes cut to 2 ft in the horizontal dimension to broaden the horizontal acceptance angle. This was done to eliminate the effects of minor deviations of the ship from a radial course. These antennas had a measured gain of 35 db. Midway in the experiment an X-band antenna was mounted at the base of the tower at a height of 6 ft, since results up to that

[a] By Lt. R. W. Bauchman, U. S. Naval Research Laboratory.

time indicated the lowest available antenna height on X band gave the strongest signals. All antennas were mounted on swivels to allow alignment on any course over a 40-degree arc and were connected by wave guide and stub-supported coaxial cable.

Two S-band and two X-band receivers feeding stability of the S-band magnetron. The receivers were calibrated with standard test sets before every run and checked upon the completion of each test. Individual calibration curves were then used in plotting the results of each run. Since only two receivers on each band were available, an r-f switching arrange-

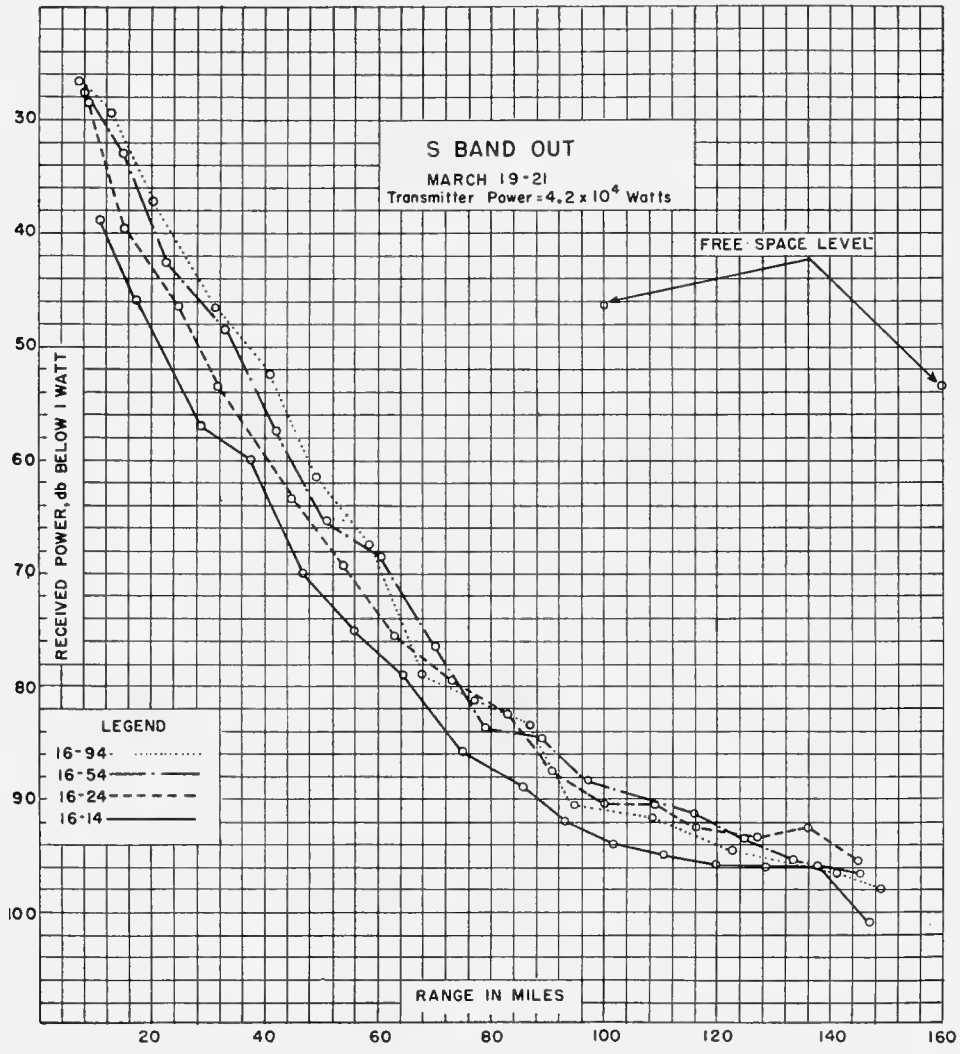

FIGURE 1. S-band run out, March 19 to 21, 1945. Signal strengths of various antenna combinations compared to free space level.

Esterline-Angus recording milliammeters were kindly furnished by the Radiation Laboratory. The S-band receivers had a minimum sensitivity of 110 db below 1 w, while the X-band receivers had a minimum sensitivity of 105 db below 1 w. It was necessary to use automatic frequency control on the X-band receivers, but manual tuning was employed on the S-band receivers because of the greater frequency ment similar to that used on the ship was employed.

Two-way voice communication between the ship and shore station was maintained at all times for coordination of operations. The facilities of an Army radio direction-finding station on the island were available to obtain bearings on the ship.

Meteorological measurements were made at the shore station during operations by means of kite

flights and a guy rigging running from the water's edge to 10 ft above the top of the tower. Detailed soundings in the first 100 ft were then taken by sliding the measuring instruments up and down the rigging. Since the duct conditions important in this investigation were always below 100 ft, only occasional kite soundings (two to three a day) were made to check the higher levels. Most of the data accumulated were taken on the tower rigging where detailed soundings could be made. Wind speeds at the surface and 100 ft levels were recorded hourly. Hygrothermographs were placed at the antenna levels and continuous records taken to determine the diurnal variation of temperature and relative humidity, if any.

A typical procedure was to align the ship at a point about 6 miles off shore (closer ranges were impossible because of reefs lying off the northeastern coast of the island) and commence a run on a prescribed bearing away from the tower. This bearing was predetermined by ship observations of the current wind and sea direction. The receiving antennas were aligned to maximum signal strengths recorded by the receivers and secured in this position by clamping to the deck. The ship operating speed was usually around 10 knots, depending on the current sea conditions. While the ship was moving on the course, antenna changes on the receivers were made every 15 minutes for some runs, while antenna heights on the trans-

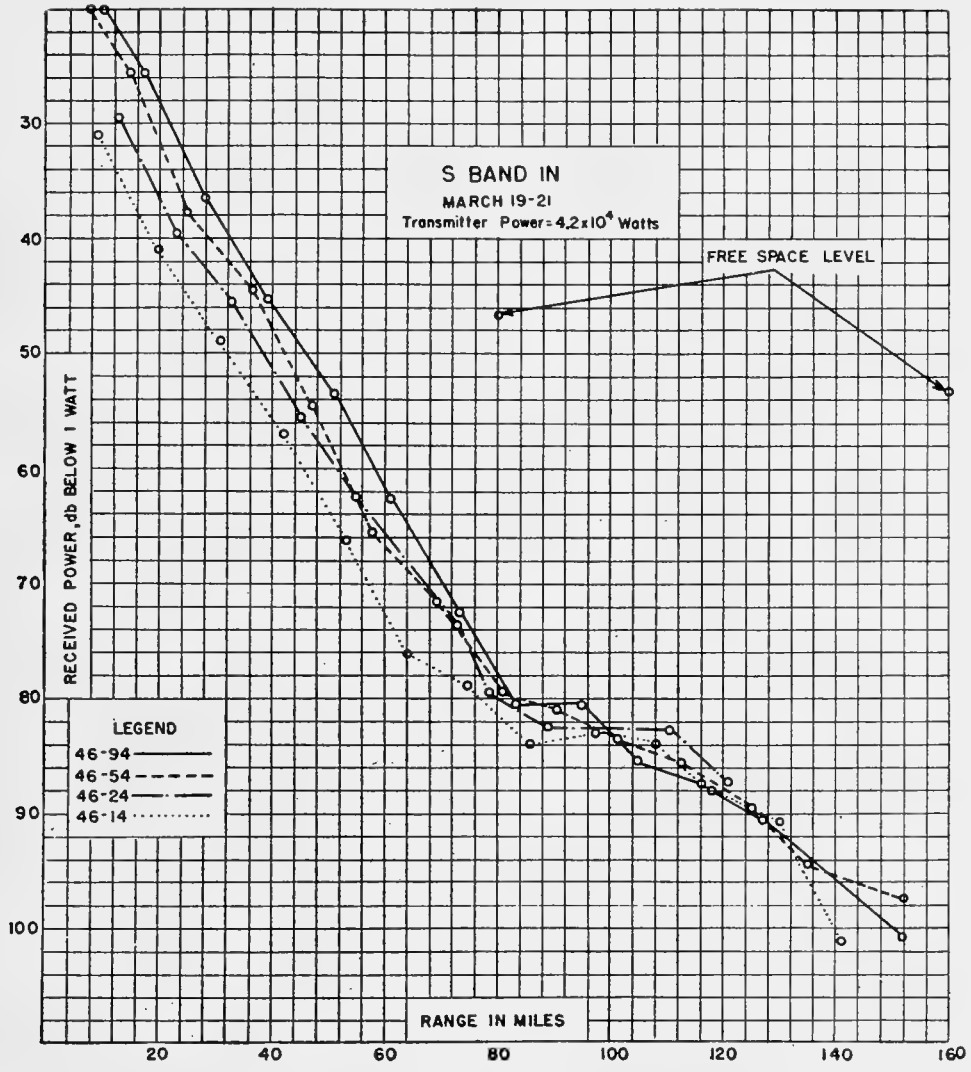

FIGURE 2. S-band run in, March 19 to 21, 1945. Signal strengths of various antenna combinations compared to free space level.

mitting end were changed every 2 hours. After making several runs using this procedure, results showed that there was no discernible diurnal variation of signal strength. Therefore, later runs were made using antenna changes on the transmitting end only at the conclusion of the run out. Periodic changes of the X-band antennas was realigned to give maximum signal return and the change in ship's bearing noted by use of a bearing marker attached to the antenna. This change was then applied to the remaining antennas and the ship's course changed accordingly. Additional checks on the ship's course were obtained

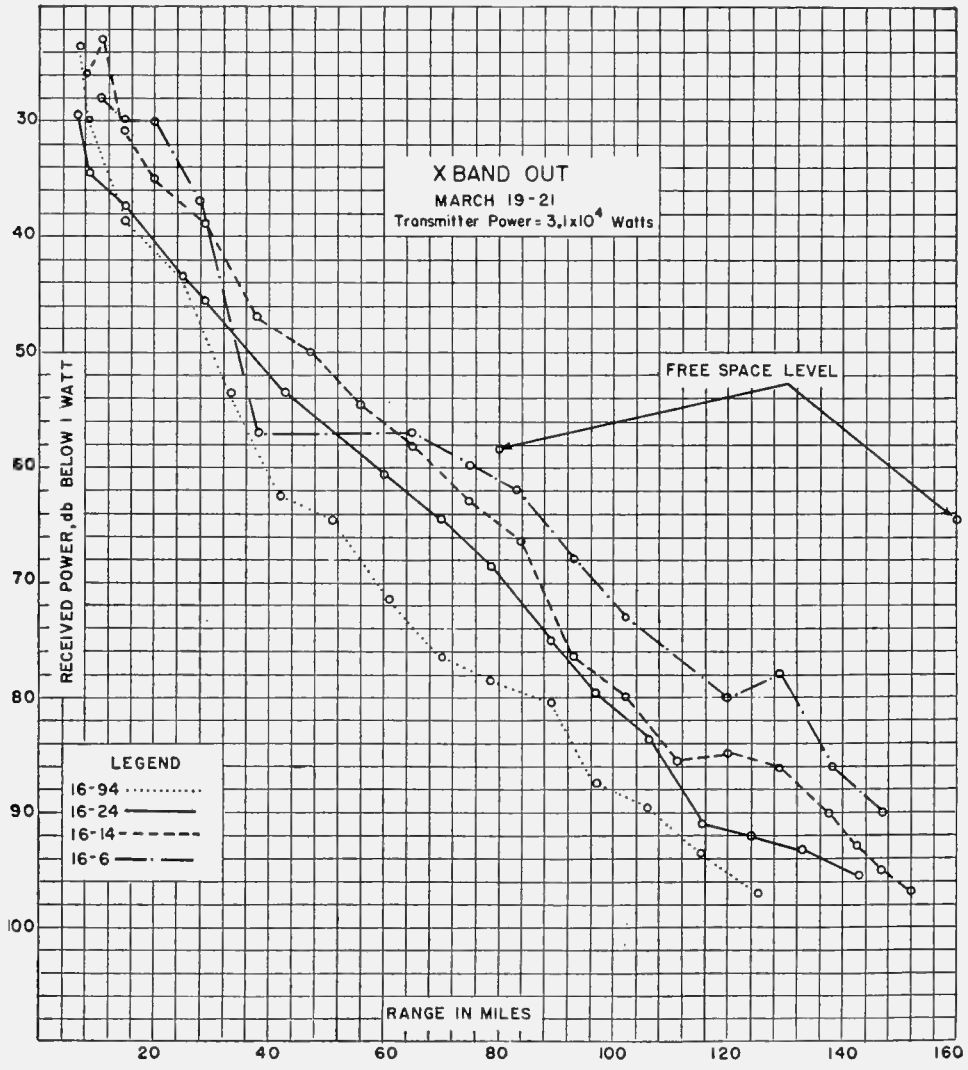

FIGURE 3. X-band run out, March 19 to 21, 1945. Signal strengths of various antenna combinations compared to free space level.

receiving antenna heights were made in order to obtain a complete record of all possible antenna combinations during each run.

One of the main difficulties encountered in this type of operation was keeping the ship on the scheduled course. Deviations from this course were detected by means of sudden drops in signal strength on the X-band receivers. When this occurred, one of the by means of the radio direction-finding station. By using this information, it was possible to detect deviations in the ship's course without losing any part of the record. The ranges of these runs extended up to a maximum of 190 miles. Signals were usually detected out to this range on the lowest X-band combination and the highest S-band combination of transmitting and receiving heights.

Figures 1, 2, 3, and 4 show the plots for one complete run. It is apparent that the lower antenna combinations on X band produced the highest signal level. Signal strengths from higher antenna combinations declined proportionately with height. On S band the reverse appeared to be true, the 46- to 94-ft antenna combination giving the highest average signal level.

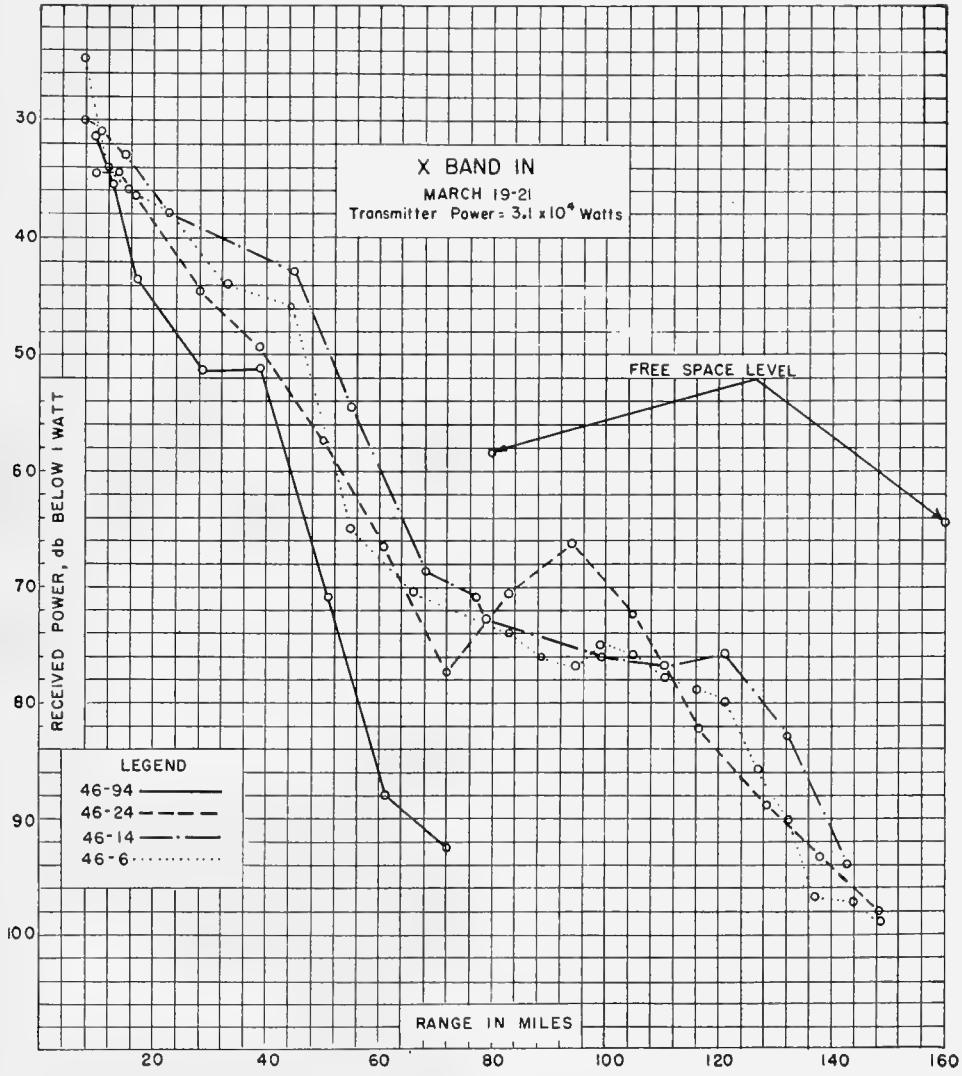

FIGURE 4. X-band run in, March 19 to 21, 1945. Signal strengths of various antenna combinations compared to free space level.

Figure 5 shows a composite presentation of 16-ft transmitting antenna to 14-ft receiving antenna. The average received signal with this antenna combination is 5 to 10 db below the 8- to 6-ft X-band antenna combination.

Figure 6 is a record of all the runs on the 46-ft transmitting and 94-ft receiving antenna combination. This clearly shows that the highest combination available with this setup produced the best results. It can also be seen that the signal level is considerably further below the free space value than is the X-band signal for these ranges.

In order to determine the effect on the signal strength of moving the antenna inland, a mobile unit consisting of an X-band receiver, test set, recorder, and 18-in. parabolic dish were mounted in a truck and operated from a gasoline-driven generator. Measurements during several runs were recorded ¼, ½, and 1 mile inland from the tower. The antenna heights above the sea surface were 25, 50, and 100 ft, respectively. In one instance, the unit was placed behind a

hill with the antenna several feet below the top to see if transmission over the hill was possible. There was a noticeable decrease in signal strength, approximately 13 db, but some signal was still recorded.

Meteorological measurements were taken simultaneously with the inland radio measurements. Kite soundings at several points at increasing distances inland from the water's edge were made, and detailed soundings on a 50-ft windmill tower about ½ mile inland were recorded over a 12-hr period.

Additional meteorological measurements from the ship on the leeward side of the island were made to determine if duct conditions existed in this area. Measurements taken from 2 miles out to approximately 20 miles off shore showed that duct conditions similar to those found on the windward side of the island existed.

During the final phases of the project, an X-band radar was installed at the base of the tower with an antenna height of 6 ft. Measurements of echo strength versus range were made on the PC boat to evaluate the effect of the duct on X-band radar. Antenna heights of the radar were varied from 6 ft to approximately 90 ft by placing the installation on the truck in much the same manner as was done with the receiver in the one-way experiment. This was then set up on sites overlooking the coastline to sea. The heights at which signal strength versus range measurements were made were 6, 15, 50, and 90 ft. The variation in the range of sea clutter for these heights was also observed.

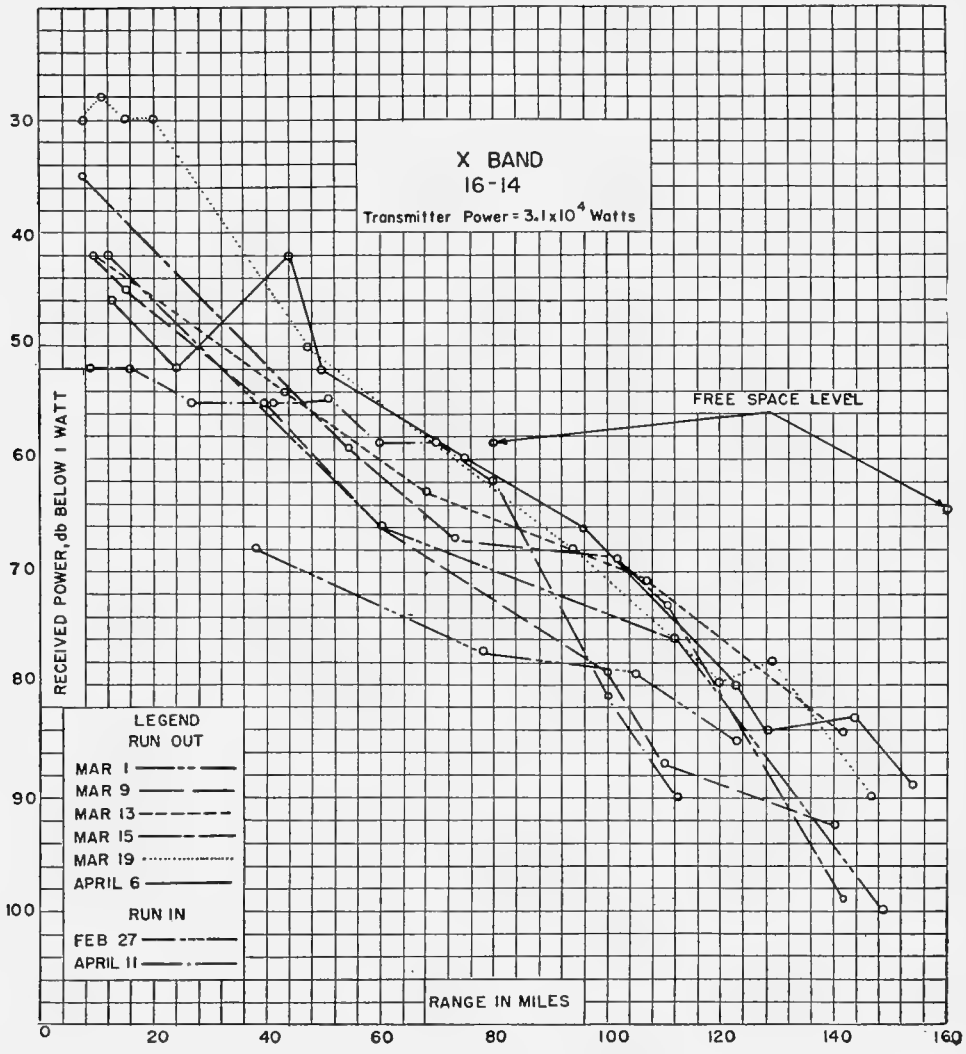

FIGURE 5. X-band runs with 16- to 14-ft antenna combination.

Measurements on the leeward side of the island were also made with this radar with approximate antenna heights of 6, 10, and 75 ft above sea level.

The maximum range obtained using the PC boat as a target with a broadside aspect was 47 miles. This range was observed with the radar antenna at the 6-ft level. The maximum range obtained on the ship from the 90-ft level was 26 miles. Sea clutter was found to vary with the antenna height and wind speed. Maximum return of 15 miles on sea clutter was observed at the 6-ft level with wind speeds of 20 to 30 knots. The maximum range at which sea return was obtained varied proportionately with height up to the 90-ft level. This range was decreased 50 per cent with lower wind speeds of 10 to 15 knots. The most significant radar datum obtained to leeward of the island was the detection of a ship at 45 miles from a 75-ft site.

4.1.2 Meteorological Measurements[b]

The description of the meteorological measurements in connection with the experiment at Antigua is divided into three parts, as follows: first, a brief general description of the West Indian climate; second, a survey of the low-level soundings; and third, a necessarily hurried analysis of the data, with certain tentative conclusions.

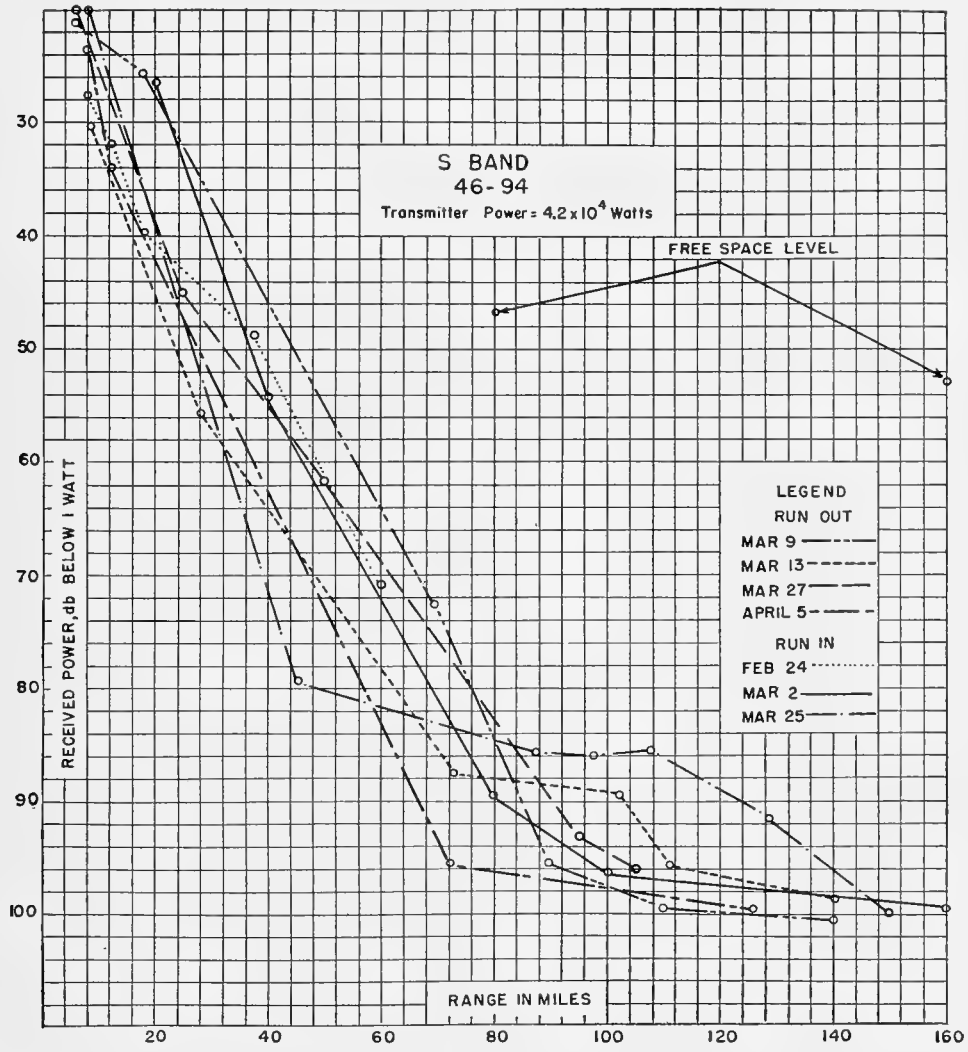

FIGURE 6. S-band runs with 46- to 94-ft antenna combination.

The most noteworthy feature of the climate at Antigua during the late winter is the persistence of

[b]By Lt. W. Binnian, U. S. Naval Research Laboratory.

one type of weather. This weather condition is determined largely by the position and strength of the Bermuda high, a large semipermanent high-pressure area covering much of the Atlantic from 10 to 30 degrees north latitude. The northeast trades blow around and out of the high's southern rim. With a few exceptions during the period of the experiment, the wind direction at Antigua was east-northeast. Once, for a period of 3 days, it went around to north-northeast and on two separate occasions blew from the east. Average daily surface wind speed was 16 knots, with occasional variations between 8 and 27 knots. Representative air temperatures varied between 74 and 78 F, relative humidities between 60 and 80 per cent. The sea water temperature was reasonably constant at 77.5 F, with occasional variations between 76.5 and 78. No significant horizontal gradients of sea temperature were found. Precipitation was wholly

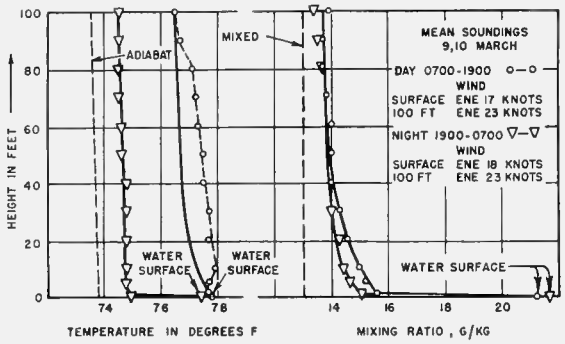

FIGURE 7. Mean temperature and mixing ratio curves, March 9 to 10, 1945.

in the form of showers with a maximum frequency of occurrence around sunrise. Periods of relatively dry weather followed by periods of relatively showery weather and accompanying transitions were experienced. It is felt that these variations were caused by fluctuations in the intensity and position of the Bermuda high or by the trough effects ahead of dissipating cold fronts.

During the entire period of observations, a simple surface duct was found to exist over the water. From the second week in February through the third week in March, and again in the first week of April, duct conditions were essentially constant. This condition, which is called herein the normal condition, is shown in five figures.

Figure 7 shows the average temperature and mixing ratio values for a 2-day period plotted against height. Curves of daytime and nighttime conditions are shown. Soundings were taken every 2 hours. The water surface values are derived from measurements made on the ship. Considerable difficulty was found in obtaining accurate soundings in the daytime due to radiation from the warm land in the case of the tower soundings and the warm ship in the case of ship soundings. As mentioned in Section 4.1, soundings were possible on the ship only when running with

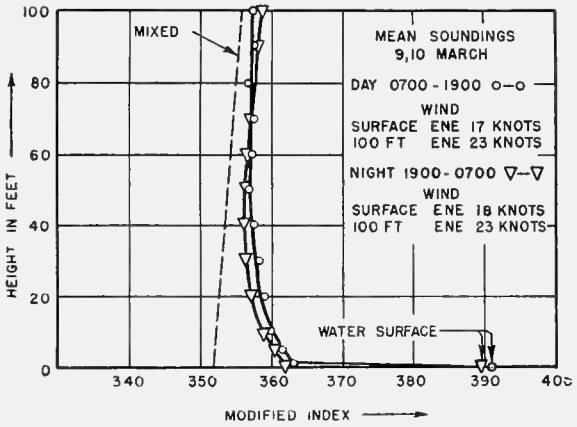

FIGURE 8. Mean modified index curves, March 9 to 10.

the wind. Thus, radiation effects of the ship were maximized, especially in the daytime. However, valuable psychrometer measurements were made on the outbound runs which showed the air to be consistently cooler than the water. On this basis, absolute values

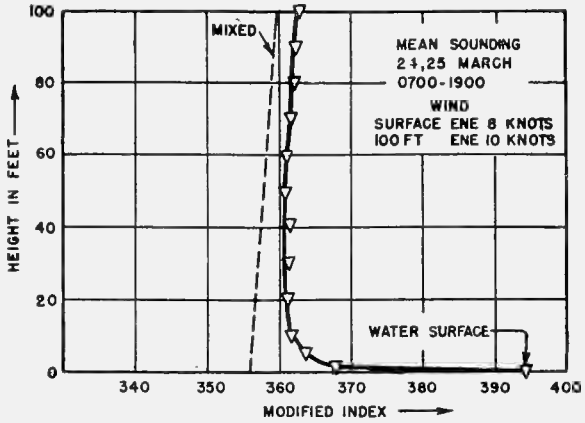

FIGURE 9. Mean sounding during low winds, March 24 to 25.

of temperature in the daytime tower soundings have been arbitrarily adjusted.

Figure 8 is the M curve computed from the temperature and mixing ratio curves just given. The surface duct and the small diurnal change in its properties are readily seen. An interesting point is the existence of a rather sharp discontinuity at the 1-ft level.

Careful independent measurements were made using a number of locations and techniques. All these tests confirmed the failure of the sea surface values to fit to the smooth curve. It appeared possible that propagation results might be more dependent on the M deficit as computed using the 1-ft value than on that computed from the sea temperature. The terms "effective surface values" of temperature, mixing ratio, and M were therefore established, these being defined as the values of these quantities at 1 ft above the water surface. Correspondingly, the *effective* value of M deficit is the difference between the value of M at 1 ft above the sea surface and the lowest value of M for a given sounding, and this effective value should not be

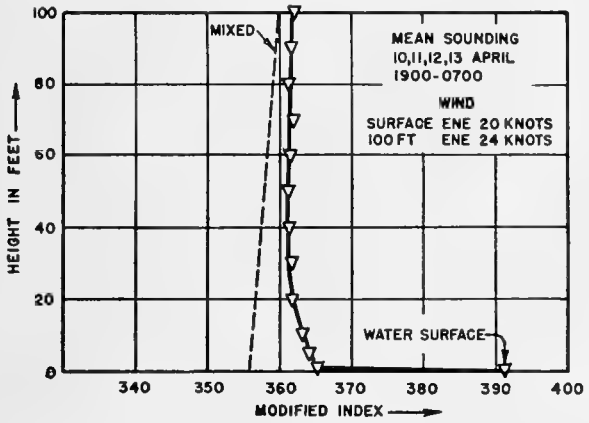

FIGURE 10. Mean sounding during high winds, April 10, 11, 12, 13.

confused with the total M deficit, which may be considerably different. This concept will be employed later in the paper.

Another significant feature of the normal sounding is the fact that, although the minimum value of M is at a height of about 40 ft, the curve does not quite reach the slope corresponding to mixed air in the first 100 ft. Due to the roughness of the few higher soundings obtained, it has been impossible to determine the exact height at which the air becomes mixed. It appears to be between 100 and 200 ft.

The next four soundings show what happened to the duct under abnormal synoptic conditions. The major variations were (a) relatively low winds, (b) relatively high winds, (c) relatively dry air, and (d) relatively moist air.

The figures which follow are mean or representative sample soundings made during each of the conditions described above. All were made on the tower and are chosen as best illustrating the effect on the M curve.

Figure 9 is a mean curve for low winds. It shows a lowering of the top of the duct and a change in slope of that portion of the curve lying between 1 ft and the top of the duct. No marked change is found in the total M deficit.

With wind speeds greater than normal, the duct thickness increased, the effective M deficit decreased,

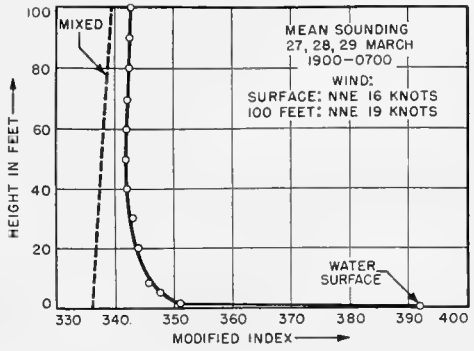

FIGURE 11. Mean soundings during an influx of dry air, March 27, 28, 29.

and the total M deficit also decreased slightly. The average of 4 days' soundings during a windy period is shown in Figure 10.

At one time there was an influx of exceptionally dry air with winds of normal speed. Figure 11 shows the effect on the M curve. The major change is an increase in the total M deficit.

Figure 12 is a sample sounding made during a period when the air was relatively moist. The significant deviation from the normal soundings is the decrease in

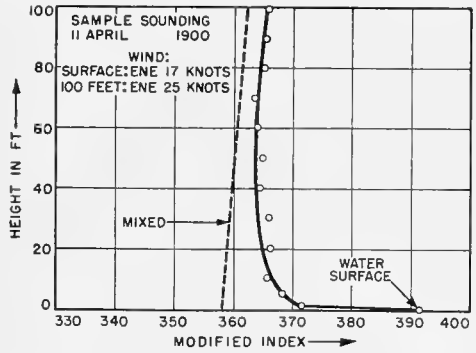

FIGURE 12. Mean soundings during an influx of moist air, March 27, 28, 29.

the total M deficit and the lack of any change in the effective M deficit or in the duct height.

In addition to the shore soundings made at the water's edge, a few soundings were obtained inland, in an effort to determine how far in over the land the duct extended. Unfortunately, most of the data are

sparse and not too reliable. A few good soundings were obtained about 1 mile inland, an example of which is shown in Figure 13. The data were taken during the day and show clearly that no low duct existed at that time. This slide is a composite between a sounding made on a 50-ft windmill and a kite sounding made nearby. The kite was flown to 600 ft and the M curve continued at the slope representing mixed air from 60 ft on up to 600 ft. No night measurements were made.

It was possible to make a few shipboard soundings to leeward of the island, beginning at a distance of 2½ miles and continuing on out to 20 miles. A preliminary study of the results shows no appreciable change over the course and no difference between conditions to lee-

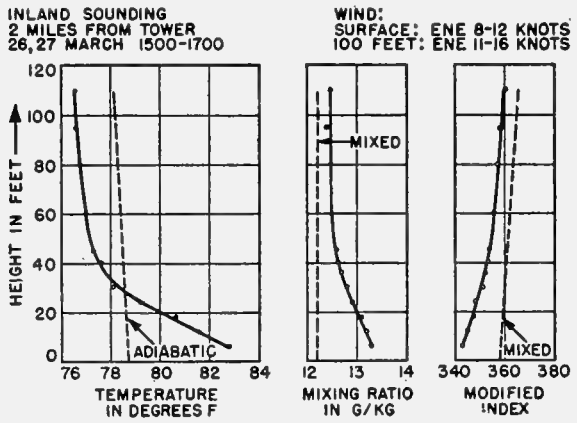

FIGURE 13. Inland soundings, March 26 to 27.

ward and to windward of the island, indicating that the duct is restored very close to shore.

Some plots of certain correlations between wind speed, duct thickness and M deficit follow. The graphs in many cases are composed of very few points and due to the short time available are based on average soundings which have necessarily been smoothed. Figures 14, 15, 16, and 17 are based on the mean tower soundings and mean winds for each run, these being the only smooth data readily available for quick analysis.

Figure 14 shows effective M deficit plotted against wind speed. This portion of the curve seems sensitive to wind speed variation.

Figure 15 shows the effective slope (height of minimum M divided by effective M deficit) plotted against wind speed. Some connection between the two quantities is indicated.

In Figure 16 the height at which M is a minimum is plotted against wind speed. The isopleths of effective M deficit have been sketched in. A few of the points were thrown out in drawing the isopleths. For constant duct height, the effective M deficit apparently first increases with increasing wind speed and then decreases. Unfortunately there are only two points in the low wind region to establish this behavior. It is quite pos-

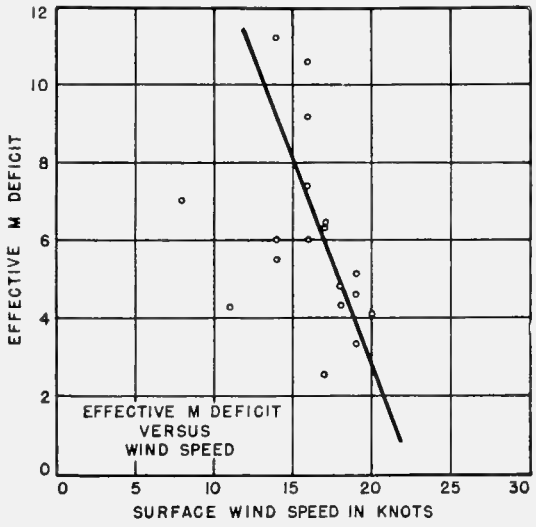

FIGURE 14. M deficit versus wind speed.

sible that the lines should be more nearly horizontal at low wind speeds and then should slope off in the manner shown for winds above 15 knots.

An attempt to plot sea temperature minus air temperature against wind speed showed no correlation.

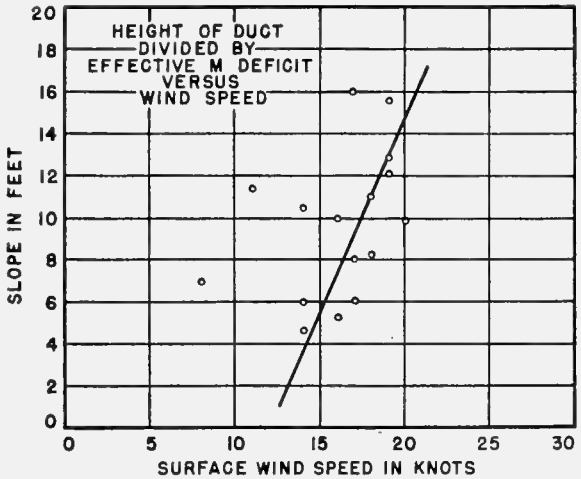

FIGURE 15. Effective M-curve slope versus wind speed.

Plotting mixing ratio based on saturation at sea temperature minus mixing ratio computed from dry and wet bulb temperatures against wind speed also failed to show any correlation.

Figure 17 is a plot of total M deficit versus wind speed, with isopleths of total slope, that is, the duct height divided by the total M deficit. Again, the exact pattern of the isopleths is not definitely determined. With the inclusion of more data in the form of smoothed individual soundings, this chart and the previous ones may prove to be more conclusive. If this is the case, it may then be possible to estimate the values of duct height and effective M deficit simply from single observations of air temperature, air humidity, sea temperature, and wind. Psychrometric observations taken at a height of from 30 to 60 ft above the water would provide the value of M at the top of the duct to ± 1 or 2 M units at the most. An observation of sea temperature leads directly to the sea surface value of M, and the wind speed can be obtained from the ship's anemometer. Thus with the aid of the charts three important points on the M curve can be

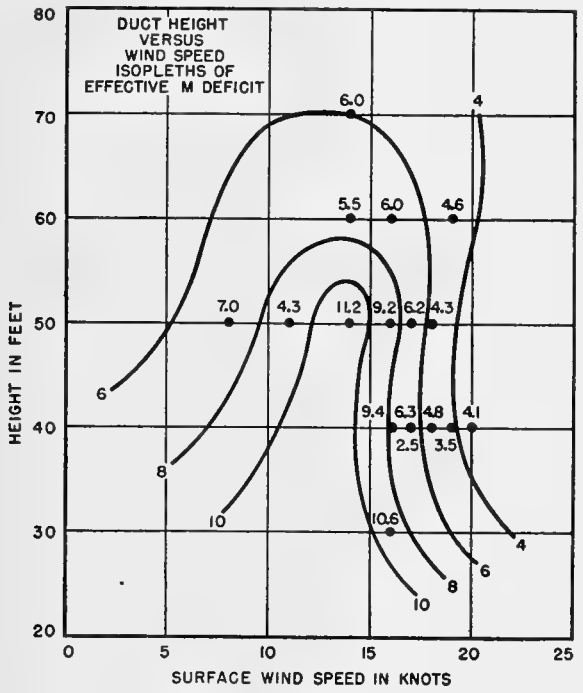

FIGURE 16. Height of M deficit versus wind speed.

obtained, namely, the values of M at the sea surface and at 1 ft and the minimum value of M and its height.

These preliminary results may be summarized as follows:

1. A surface duct between 40 and 50 ft high with a slightly transitional-type layer extending above the duct to between 100 and 150 ft exists most of the time over the water in this area.

2. The duct is destroyed over land in the daytime within about ½ mile of the shore.

3. Islands comparable in size to Antigua have little effect on the duct on the leeward side at a distance greater than 2½ miles off shore.

4. The higher the wind speed the thicker the duct becomes and the less the *effective* M deficit becomes.

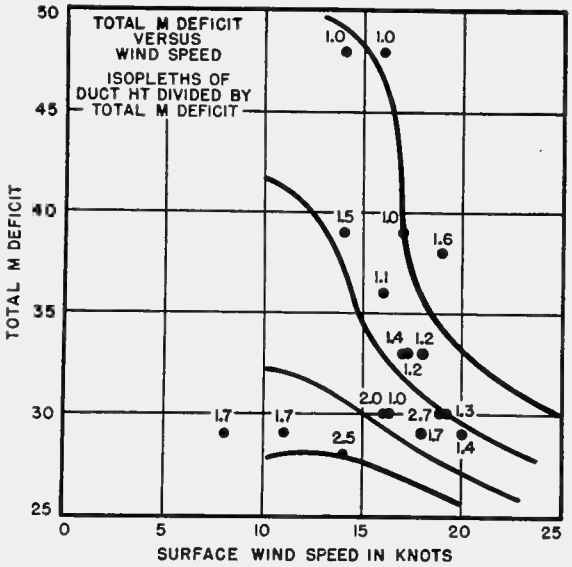

FIGURE 17. Total M deficit versus wind speed.

5. Changes in wind speed have little effect on the total M deficit, which is determined essentially by the temperature and humidity of the air mass as a whole in relation to the surface water temperature.

6. These conditions probably prevail over ocean areas having comparable climates.

4.1.3 Preliminary Results of Radio and Radar Measurements[c]

The main purpose of the experiment was to establish what operational use could be made of low-lying ducts and to confirm observation of the effects of such ducts on radio and radar propagation made in various parts of the world. The data accumulated have been available for study only 2 weeks, and there has been insufficient time for a complete analysis. As a consequence only the highlights of the agreement between experiment and theory have been determined.

Ducts were present all the time, and trapping on both X and S bands, which increased the signals to levels considerably above standard propagation values, was found to exist all the time. The general conclusion

[c]By M. Katzin, U. S. Naval Research Laboratory.

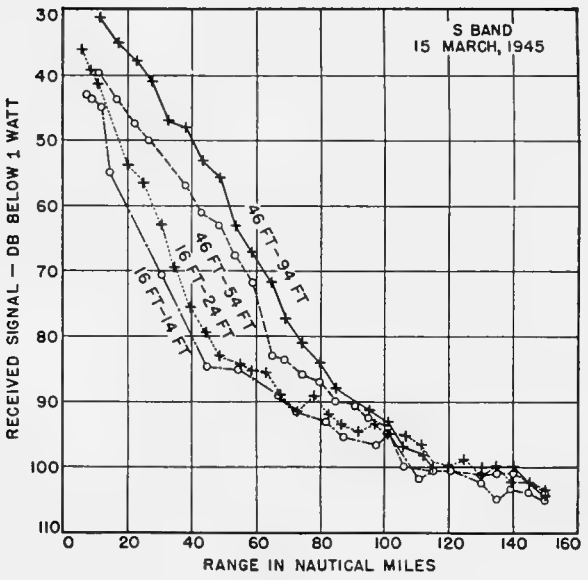

FIGURE 18. Composite S-band run field strengths, March 15.

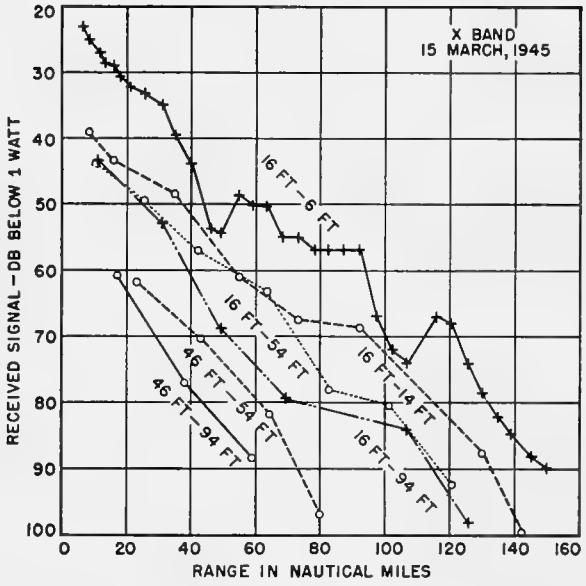

FIGURE 19. Composite X-band run field strengths, March 15.

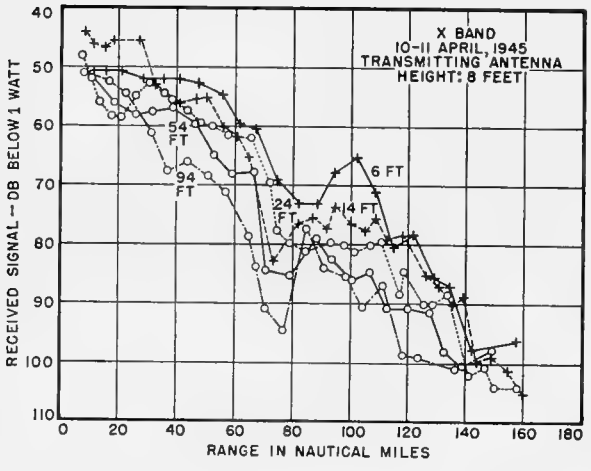

FIGURE 20. Composite X-band run field strengths, April 10 to 11.

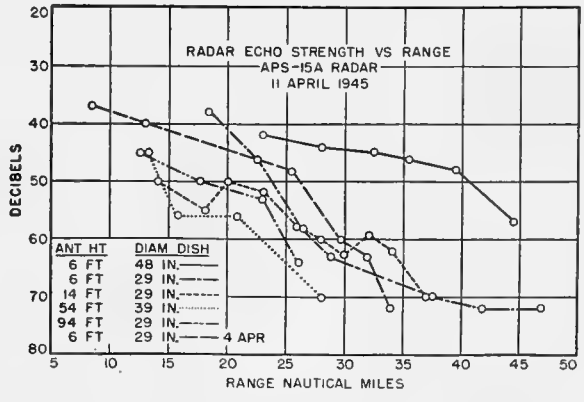

FIGURE 21. Radar echo strength versus range for various antenna heights.

regarding the effect on the two bands was that on S band antennas as high as the experiment would allow gave the highest signal strengths. On X band, on the other hand, the lowest antenna heights which were available usually gave the strongest signals.

Figure 18 is an S-band run made on March 15. It is a composite run containing the results of both the outward and the inward runs. Several of the curves have been omitted for clarity. The highest curve is for a combination of a 46-ft transmitting antenna and 94-ft receiving antenna. The lowest curve is for the two lowest heights, 16 and 14 ft. The slopes of the curves are rather steep for the first 80 miles or so, the signal declining considerably less rapidly thereafter. Also, the variation of the signal with height is shown here to be in the order in the extremes between 25 and 30 db. This interval from 80 to 50 db shows a difference between the two extremes of 30 db. To translate that into a radar situation, double that difference to get a difference of 60 db, showing that on S band the higher antenna combinations would provide considerably better coverage for targets in the order of 100 ft high and with transmitters at the height of about 50 ft. Stated another way, the highest antenna combination would provide coverage beyond that obtainable with the lowest in the order of 30 miles.

There is as yet no reasonable explanation for the extremely slow decrease in signal beyond 80 miles. This feature is very distinctive in the S-band curves. For the X band, it is generally not discernible except on a few runs toward the extreme range portion. The rate of decrease of signal with range in the region inside 80 miles would be exponential if there were a straight line on this figure. Considering it to be so, averaging over a number of runs gives roughly 0.8 db per nautical mile. That decrease is the total amount, the $1/R$ variation not having been extracted from it. Attempts to do so show that the resulting curve does not, in a plot of this sort, fit a straight line as well as the original values themselves, but if the $1/R$ value is taken out of the power relation the average attenuation is then roughly between 0.5 and 0.6 db per nautical mile. In this region (beyond 80 miles), on the other hand, the decrease of signal with range is considerably less, being between 0.15 and 0.2 db per nautical mile. No satisfactory explanation for this behavior has yet been derived.

Figure 19 shows the X-band results for the same period. Antenna heights of 16-ft transmitting and 6-ft receiving produced the highest curve, the lowest curve being obtained on a 46-ft to 94-ft combination. Note that succeedingly higher antenna combinations produced successively lower signal strengths. There is some variation, but when the curves are smoothed to a straight line the attenuation is on the order of 0.33 to 0.5 db per nautical mile. Removing $1/R$ reduces the attenuation to roughly 0.2 db per nautical mile. There is no sharp bend in the curve at about 80 miles, as was the case on the S band. The lowest (16-ft to 6-ft) antenna combination showed more than 35 db greater signal strength than the highest (46-ft to 94-ft) combination. Considering again the radar case, it is found that the higher antenna provides relatively poor coverage compared to the lower. In terms of range for a given signal threshold, the difference in favor of the lower antenna is about 80 miles.

Figure 20 shows an X-band curve obtained during April 10 and 11, when a transmitting antenna height of 8 ft was available. Received signal powers for 6-, 14-, 24-, 54-, and 94-ft receiving antennas are shown. The curves are somewhat scrambled, but the general result is that the lowest antenna again produces the greatest signal, with increasing antenna height producing progressively smaller signals. This was not the case without exception, as can be seen in Figure 4, where the 6- and 14-ft antennas exhibit comparable behavior. In that case the maximum range was obtained on the 14-ft antenna. The average slope in Figure 20 is somewhat less than that shown in Figure 19. Exact averages of all the runs have not yet been worked up.

Figure 21 shows a plot of received signal versus range, made on a 3-cm radar, using a PC boat as a target. The highest curve was obtained with a 6-ft antenna height, using a 48-in. dish to obtain greater gain and range. The other run with 6-ft antenna was made using the regular 29-in. dish. There is a considerable spread in the values of received signal due to the difficulty of measurement. However, the significant thing is that the maximum ranges obtained are in accord with the indications given by the one-way transmission results. Striking an average slope shows the decrease of signal with range to be about 1.0 db for each 1.5 nautical miles.

The important conclusions can be summarized as follows:

1. The surface duct is very persistent.
2. The duct is very effective in extending the ranges

obtainable on both S and X bands, for either one-way or two-way transmission.

3. On S band, the highest combination of transmitting and receiving antennas produces the strongest signal and the greatest range.

4. On X band, the lowest combination of transmitting and receiving antennas produces the strongest signal and the greatest range.

5. Surface ducts in the trade wind regions can be used for communication purposes to a conservative range of 100 miles. Greater ranges are probable but will require further investigation.

6. Rain in the form of squalls does not appreciably affect the received signal.

Chapter 5

TRANSMISSION EXPERIMENTS IN ENGLAND

5.1 BRITISH TRANSMISSION EXPERIMENTS[a]

5.1.1 Introduction

THE BROAD OBJECT of the studies carried out in Great Britain during the past few years has been to establish the characteristic facts of the propagation of centimeter waves (more recently of meter waves also) and especially to determine the relationship between radio performance and meteorological conditions in the lower atmosphere, with forecasting as the ultimate aim.

Although propagation of 10-cm waves to distances much beyond the optical range had been observed under favorable conditions nearly a decade earlier, it was the striking increases in range of decimeter and centimeter wave coastal radars in southern England, observed in the summers of 1940 and 1941 respectively, which led to a concentrated attack on the long-range aspects of the problem. About the same time a need arose for more accurate knowledge of both the short-range "interference" field and the long-range "diffraction" field for certain communication projects, and the radio equipment developed to meet this need formed a nucleus round which the later and more ambitious experiments grew.

The various experimental and theoretical aspects of this work were reviewed in some detail at the meeting of the Ultra Short Wave Propagation Panel under whose auspices the work is being done, in London on October 6, 1944; these reviews have been circulated as listed in references 1 through 15.

Continuous observations have been carried out over a range of optical and nonoptical paths across the Irish Sea on S and X bands and over a single 38-mile land path on S band. These are discussed below. In addition to this work several investigations of more specific propagation problems have been carried out during the summer of 1944.

1. Measurements on two wavelengths in S band, over a 70-mile sea path between a site in South Wales and the summit of Snowdon (3,500 ft). This optical path was studied to obtain data on the probability of missing aircraft on S-band radars under conditions favorable to trapping at low levels over sea.

2. Measurements on a wavelength of about 3½ m over a 90-mile sea path, with heights such that the path length was about twice optical range, to provide quantitative data on the importance of refraction in this waveband.

3. Radar measurements from Llandudno, North Wales, with the Isle of Man and the Irish Coast as the main targets, on S, X, and K bands. The object was to obtain practical data on the relative performance of K band under a variety of meteorological conditions which were studied simultaneously with the radar observations by ship, balloon, and aircraft measurements. Some further reference to the results of (1) and (2) appears below; an interim report on (3) has been circulated.[12]

5.1.2 Irish Sea Measurements

The first plant for simultaneous measurements within and much beyond the optical range on wavelengths of about 9, 6, and 3 cm, using heights of about 100 and 500 ft each site, was made in the latter part of 1941.

The work was planned on an inter-service basis, with equipment provided by Admiralty (developed under Admiralty contract by General Electric Company Research Laboratories from that used in the early communication studies mentioned above) and stations provided and operated by Signals Research and Development Establishment, Ministry of Supply. Arrangements were made for analysis of the data by the National Physical Laboratory, which has also more recently undertaken the development of monitoring equipment. The collaboration of the Meteorological Office was received at an early date, but it was only when the study of the subject had made further progress that the need for detailed low-level meteorological measurements was realized; these have been undertaken by the Naval Meteorological Service, soundings being made in ships and by means of ship-borne balloons. Additional arrangements have recently been made with the Meteorological Office for regular aircraft soundings over the path.

[a]By E. C. S. Megaw, Ultra Short Wave Panel, Ministry of Supply, England.

Some difficulties were encountered early in 1942 in finding sites for the stations which were acceptable from all points of view, and the field work done in that year consisted of several short-period trials over a rather wide variety of land and sea paths. In spite of many limitations, in particular as regards detailed meteorological data, the general conclusions reached in these trials[9] have been largely substantiated by later measurements. Table 1 gives details of the sites finally adopted.

TABLE 1

Station	Height, ft
S. Wales (transmitters)	
A. Garn-Fawr	540
B. Strumble Head	90
N. Wales (receivers)	
C. Rhiw	825
D. Aberdaron	95
Scotland (receivers)	
E. Knockharnahan	375
F. Portpatrick	95

The path length from South Wales (A and B) to North Wales (C and D) is 57 statute miles and that to Scotland (E and F) is 200 statute miles. The path lengths in terms of geometrical optical range for the eight possible paths are shown in Table 2.

TABLE 2. Transmission path lengths.

Path	AC	BC	AD	BD	AE	AF	BE	BF
Distance in units of optical range	0.89	1.21	1.40	2.40	3.82	4.92	5.63	8.45
Distance (miles)	57				200			

In the original scheme all the paths were to be collinear, but this could not be realized with the sites finally adopted; the South Wales to Scotland paths differ by about 17° in bearing from the South Wales to North Wales paths, the bearing of the former being within a fraction of a degree of true north. A scheme for recording data over all paths (though necessarily not continuously) was evolved; each transmitter beam was aimed for half the time along each of the two bearings 17° apart (a 7½-minute period was found the most satisfactory, and a small change in frequency (5 to 10 mc) was made automatically when the beams switched over.

At each frequency the transmitted signal consisted of square pulses, at equal on/off ratio, with a repetition frequency of 1000 c. The "standard" power output in the "on" period was 0.6, 0.3, and 0.15 w for 9, 6, and 3 cm, respectively; the signal records were corrected for any significant departure from these powers. Paraboloid mirrors 48 in. in diameter were used for all transmitters and receivers; these were mounted inside the stations behind large canvas-covered "windows." The increase in mirror gain with frequency more than made up for the reduction in transmitter power, in spite of the less effective utilization of the mirror area. In the receivers the 1,000-c component of the modulation was rectified to operate the recording milliammeters. Provision had been made for monitoring the field radiated from the transmitters and the sensitivity of the receivers, in terms of a standard radiated field. This scheme was brought into operation as the National Physical Laboratory equipment became available; other less complete methods of monitoring the transmitters and checking the receivers had been in operation from the start. (Data for the 5-cm equipment are included here although, as will be noted, it was not used.)

Radiotelephone communication between the North Wales and South Wales stations has been maintained satisfactorily for two periods of several months each using first S- and later X-band equipment, essentially the same as that used for the signal measurements, arranged for duplex operation. A meter-wave system (which gives more continuous service over long nonoptical paths) is now being installed by Admiralty Signal Establishment to link all the stations; it is already operating satisfactorily over the 57-mile path, and a relay link from North Wales to Scotland is being provided.

On S band, operation on all four links across the 57-mile path commenced in November 1943, although the two from Station A (high site) had been running since July. During the preliminary period, up to the beginning of 1944, in which a number of practical difficulties had to be overcome, the radio results were subject to rather more uncertainty than was the case in the earlier measurements where a concentration of experienced personnel was possible for the short periods involved, and detailed analysis of these results has not yet been attempted. One S-band receiver was in operation in Scotland (Station F, low site, 200 miles) from the end of August 1943, but apart from one brief period during September, no signals were received until March 1944, just before the second S-band receiver (Station E, high site) was installed.

On X band all the stations were in operation by July 1944, operation on the 200-mile links having started a month earlier.

After a few months of operation of all 16 links it was realized that the available effort would not be sufficient to cope adequately with the tasks of editing and examining the signal records. Consequently a rather drastic reduction of the centimeter wave program was agreed to for a trial period of 6 months, starting October 1, 1944. For this period the following links were operated continuously (without beam switching): on S band, A to C and D (57 miles) and B to E (200 miles); on X band, A to C and B to D (both 57 miles). (The possibility of a link from B to D on S band with separate equipment was also envisaged.)

It was agreed to postpone operation on 6 cm, but at least one 3½-m link over each of the two path lengths would be added; preliminary measurements on this longer wavelength were already being made. In addition, K-band equipment for at least the optical 57-mile path was to be installed at an early date.

Figure 1 shows a general view of the equipment in one of the stations (D). The X- and S-band receivers are in the center of the picture, with the mirrors and canvas-covered windows behind. The S-band signal generator and monitoring equipment are on the small table beside the S-band receiver. The recorders are mounted on a temporary table (now replaced by the central control desk), extreme right. The empty bay, extreme left, was designed to house the K-band equipment. The meter-wave equipment was mounted in an adjoining room.

In addition to the radio measurements, some study was made of the behavior of a light beam over the 57-mile path during the summer of 1944 in the hope that this might provide useful information on the refraction produced (nearly) by temperature gradient alone. Measurable changes in elevation were sometimes observed by means of a theodolite, but the incidence of adequate visibility was small, and little quantitative information was obtained.

A detailed study of the S-band signal records and meteorological data obtained from February 1944 is being made at the National Physical Laboratory, par-

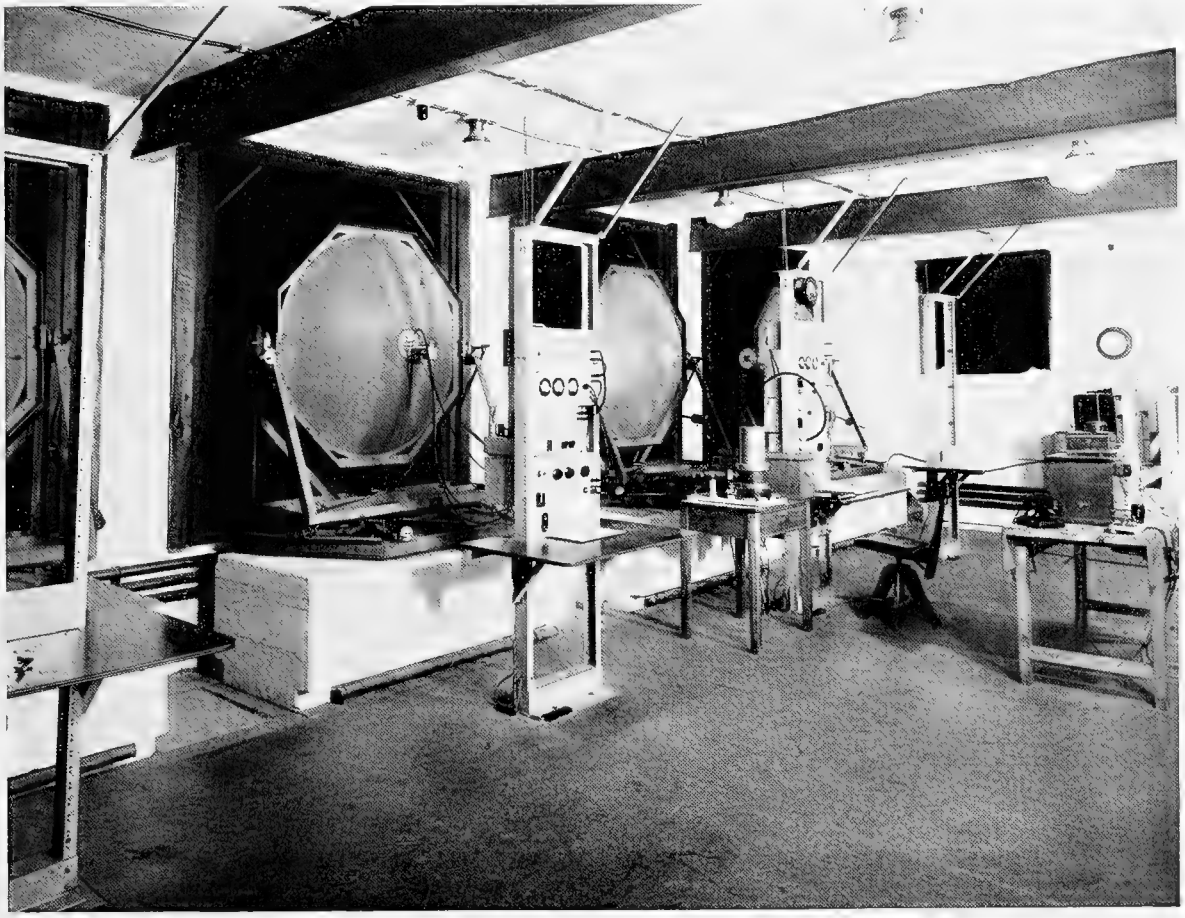

FIGURE 1. General view of the equipment in Aberdaron, North Wales.

ticularly for the 57-mile paths AD and BD.[2] Similar study of the S band and 3½-meter data will follow.

Figure 2 shows a plot of hourly mean signal level for the S-band signal over the links AD and BD for June 1944, with a record of some meteorological factors—fronts, precipitation, and fog—with which comparison has been made.

7. While periods of high level are sometimes characterized by large gradients of water vapor (soundings usually made for the first 200 ft, at one point near the center of the path), no satisfactory correlation has been found between the character of the M curve and the major variations in signal level for the periods which have been studied. In general, as is com-

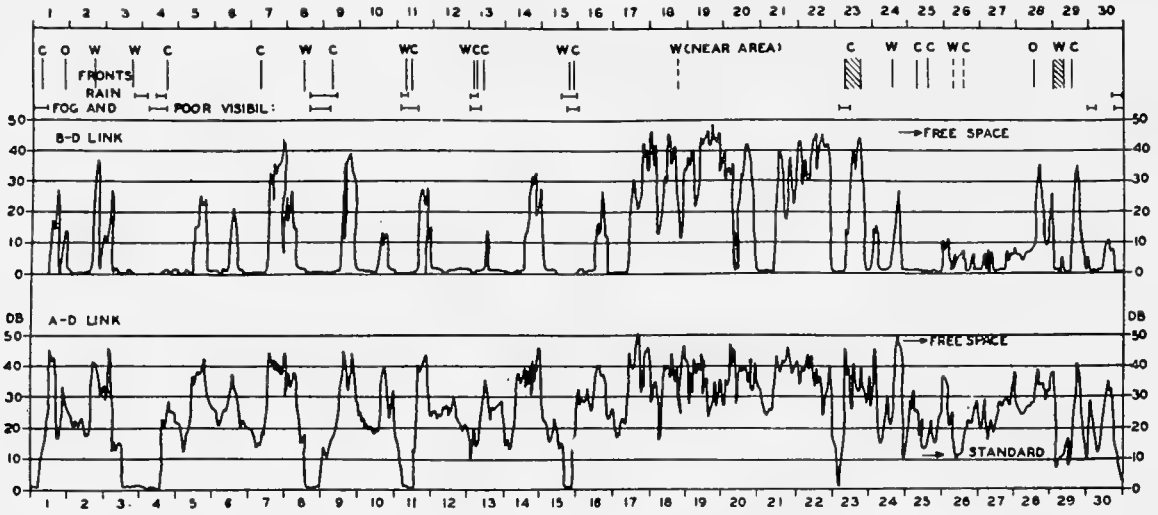

FIGURE 2. Signal strength in decibels above 1 μv receiver input, June 1944, drawn from hourly mean values.

It should be emphasized that analysis of the data obtained during this period has not yet been completed, but the following general conclusions may be drawn:

1. There is general agreement between signal variations for the two paths, though the short-period variations often differ.

2. Signals are obtained over the 200-mile path only when signals over 57-mile path BD exceed about 30 db above 1 μv. But if the latter condition is fulfilled the former does not always follow.

3. There is a marked diurnal variation, when the general level is low or moderate, with high signal in the late afternoon or evening and low level in the early morning.

4. There is evidence for an appreciable seasonal variation with high level for a greater fraction of the time in summer than in winter or spring.

5. Low level occurs commonly in conditions of fog or low visibility (e.g., low level on 174 occasions out of 233 on which fog was recorded between February and June 1944).

6. Low level is usually observed at the passage of fronts (e.g., on 78 occasions out of 106 on which fronts were recorded).

mon experience for similar paths, high levels tend to occur in anticyclonic periods.

The general character of the S-band signal variations for the four 57-mile paths is illustrated by the plots of hourly mean levels for 5 days in August 1944 shown in Figure 3. The range of variation in level increases with the excess of path length over optical range, and there is an obvious similarity between the three nonoptical paths as regards the larger changes in level. This similarity does not extend to the optical path AC, which shows signs of an *inverse* correlation with the major variations of the nonoptical paths. For a standard atmosphere (⅓ earth radius) the receiver on the AC path is near the record maximum of the interference field. For fairly small departures from standard (curvature corresponding to, say, 1.0 to 1.7 times earth radius) the range of variation caused by interference is quite small, about +4 to —7 db relative to free space field; the smallness of the variation is due to the appreciable effect of divergence of the reflected ray in this case.

While other factors beside interference with the reflected ray are almost certainly operative in producing variations over the optical path, slow fading with a range of the order of 10 db is quite common; and

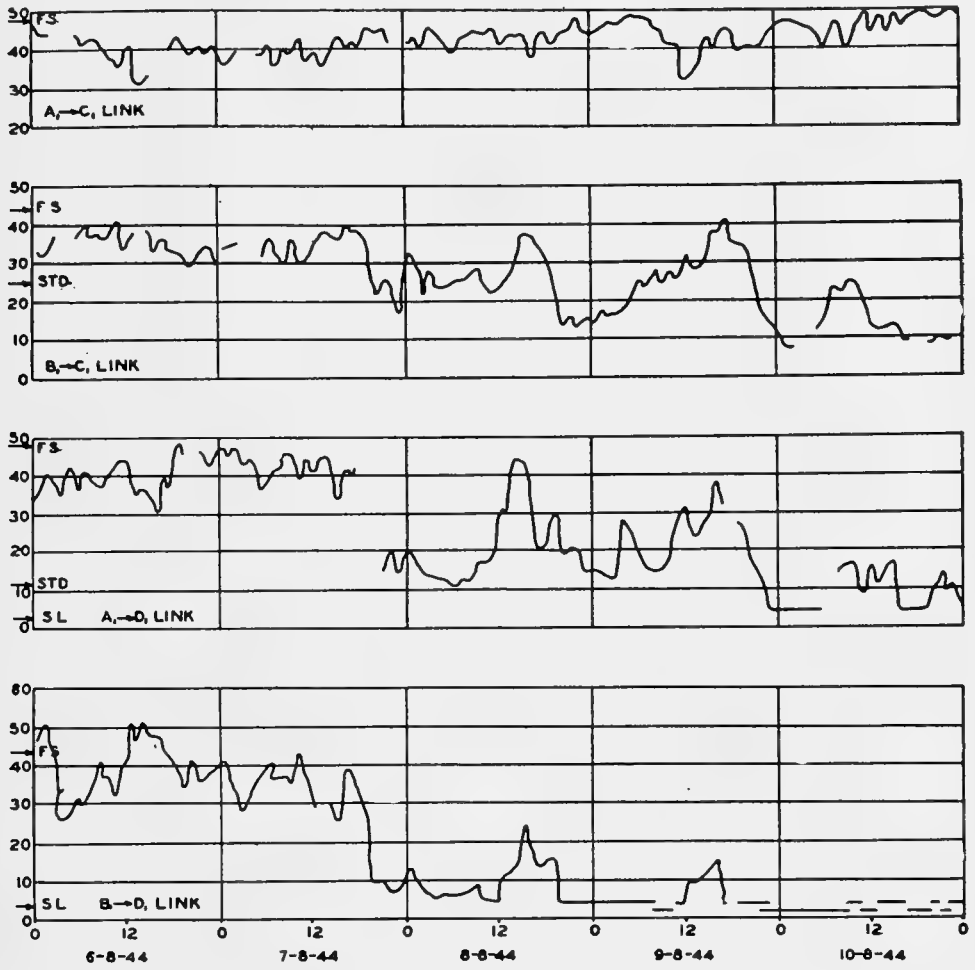

FIGURE 3. Signal strength in decibels above 1 μv receiver input. FS: Free space signal. STD: Standard signal. SL: Sensitivity limit.

a slightly substandard index gradient, which would produce a marked decrease in level for the nonoptical paths, would leave the AC path in the neighborhood of the first interference maximum.

The free space levels (48 db above 1 μv from A, 44 db from B; difference due to different radiated powers at this period; 1½ db estimated atmospheric absorption allowed for) are marked on the plots of Figure 3. For all four paths the highest levels reached are in the neighborhood of the free space value; levels several decibels above free space are occasionally reached during good periods, but they are only rarely maintained for as much as a few hours (e.g., path BD, May 12, 13 and August 5, 6). The long-time average level for path AC should be close to free space level, probably about 2 db above. It is actually about 5 db below for the first half of August 1944 and about 3 db below over a period of several months. While some of this discrepancy may be due to residual experimental error, the fact that it appears to be least during periods of poor transmission between the low stations (e.g., August 10 in Figure 3) may be significant.

For the nonoptical paths BC, AD, and BD the standard level is 20, 37, and 79 db below free space level, respectively, for S band. The corresponding figures for X band are 28, 53, and 113 db. The standard level is shown in Figure 2, and in Figure 3 for paths BC and AD; for path BD it is over 30 db below the receiver threshold. While it is rare, during the summer months, for the level to remain near standard for a large fraction of the time (in February, however, the AD level was within 2 db of standard for about 25 per cent of the time), the minima of the major signal variations usually lie within about ± 5 db of the standard level except (1) during runs

of particularly good weather and (2) during foggy conditions which are likely to be associated with a substandard index gradient. Striking examples of the latter occurred on June 4, 5 (Figure 2) and August 10, 11 (Figure 3). On the last occasion the BC level went about 20 db below standard.

The X-band results for the 57-mile paths are generally similar to those for S band as regards the major variations, but the range of variation is noticeably larger, particularly on paths BC and AD, which are not much longer than optical range; the increase in range of variation for these paths is of the same order as the difference in standard level for the two wavelengths. In general, short-period variations are larger and more rapid for the shorter wavelength.

Figure 4 shows the results for both S and X bands over the 200-mile paths AE (high stations) and BF (low stations) for part of the same period as shown in Figure 3. After allowing for the estimated atmospheric absorption (6 db for S, 16 db for X) the free space levels are similar for the two wavelengths, experimental uncertainty being appreciably greater at X band as regards absolute values. The standard levels are, of course, far below the receiver threshold, actually about 275 db for path AE on S and 490 db for path BF on X.

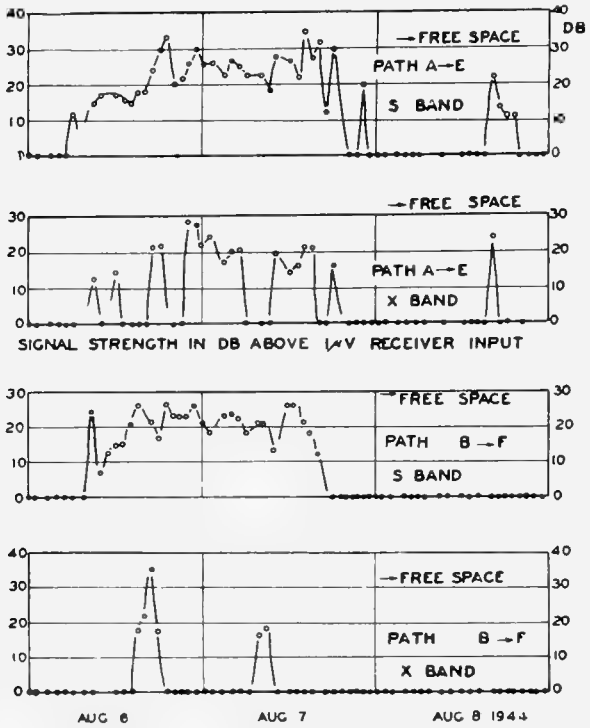

FIGURE 4. Hourly mean values of signal strength on S and X band.

The most striking characteristic of the results is perhaps the similarity in magnitude of the signals both for the two paths and for the two wavelengths. In general, signals are measurable for a greater fraction of the time on the longer wavelength and for the higher sites. (The difference of about 5 db in receiver threshold sensitivity between S and X has only a slight effect on this.) At the peak of good periods the lower sites and shorter wavelengths sometimes reach rather higher levels, as in the case of the 57-mile paths the maximum signal level is frequently comparable with free space; rather rarely it exceeds free space level by something of the order of 10 db. For the 200-mile path the possible error in the estimate of atmospheric absorption is rather more serious, particularly for X band, but it seems improbable that this could alter the general character of the results.

Comparison with the results for the 57-mile BD path in the bottom record of Figure 3 is interesting and is reasonably typical of the extent to which the performance of the long path can be predicted from the performance of the shorter one. It should be emphasized that this was a period of good summer weather apart from the break on August 10–11.

5.1.3 Overland Measurements: Whitwell Hatch to Wembley

A single S-band link has been in continuous operation over this 38-mile path since March 1943. Its terminals, with the transmitter in one of the Admiralty Signal Establishment buildings and the receiver at General Electric Company Research Laboratories, were chosen for operating convenience rather than to meet any special requirements for the path, as an important subsidiary purpose was to provide for controlled long-period tests on equipment developed for use in the less readily accessible stations of the Irish Sea program. Apart from routine checks the equipment normally operates unattended; automatic frequency control at the receiver has been in operation since June 1943. But the receiver is provided with a relay-operated alarm which can be set to operate on an abnormal change of received level in either direction (normally downwards) and this has proved valuable in calling attention to both faults and unusual propagation conditions.

The transmitter is on a hill 725 ft above sea level and the path runs northwards across the Thames valley and the western outskirts of London to the receiver, which is only 170 ft above sea level, in low,

undulating, built-up country. For standard conditions the path is clear except for the last mile where trees and houses form a barrier elevated about ½ degree above the ray path. This introduces a local diffraction loss at the receiver which has been estimated roughly at about 30 db. This estimate is necessarily an uncertain one, both because of the complexity of the real barrier (which is approximated as one or more opaque straight edges) and because of possible seasonal variations.

Seasonal variations in general signal level have been observed with a maximum in late summer of the order of 10 to 15 db higher than the single winter minimum recorded so far. An attempt to explain this variation in terms of changes in the horizontal plane diffraction pattern of part of the barrier with varying opacity of the tree background does not appear to be supported by the results of the past few months (Summer 1944). The mean level for the whole period is, however, close to 30 db below free space (52 db above 1 μv receiver input) and is thus at least of the same order of magnitude as the estimated standard level. The unfortunate effect of this uncertainty regarding standard level is mitigated to a considerable extent by the fact that a land path of this kind gives an easily definable "general" level, which is in fact that obtained under "well-mixed" meteorological conditions.

Further details of the path and a discussion of the results in relation to general meteorological conditions over the path have been given in two National Physical Laboratory reports,[16,17] which cover the first year's operation. A further report is in preparation. The aim here is limited to a general description of the type of results obtained, with examples of some characteristic signal records.

Figure 5 gives a plot of hourly mean level for March 1944 which clearly shows the two main characteristics of the signal: the reasonably constant general level and the regular diurnal cycle which occurs with radiation nights. The period March 21 to 26 is typical of an undisturbed run of clear nights; note the period of marked substandard signal in the early morning of March 27, indicating that condensation near the ground has reduced the water vapor content there sufficiently to make the lapse rate negative. Intermittent rain in bad weather periods usually gives a more variable level than cloudy weather with no precipitation; a small rise in level is often observed with continuous rain (direct effects of rain on the equipment have been carefully guarded against and may be assumed negligible) and a more marked rise with clear skies in daylight following rain. These effects are readily explicable in terms of changes in water vapor distribution.

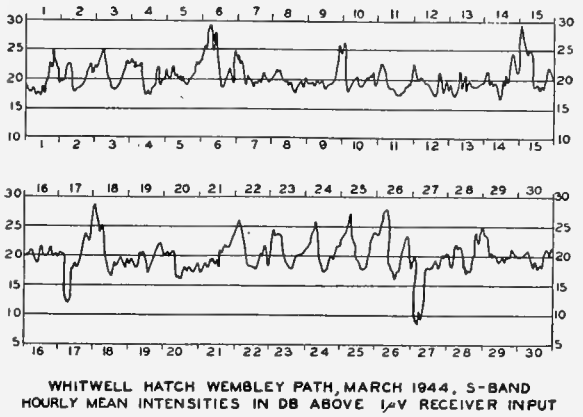

FIGURE 5. Whitwell Hatch to Wembley path, March 1944. S-band hourly mean intensities in decibels above 1 μv receiver input.

The work of the past 6 months (Summer 1944) has shown a definite correlation of high level at night with temperature inversion whether with clear or with variable skies; on the other hand, clear or variable skies with no temperature inversion (e.g., with incoming cold air) show no night peak of signal. In general the increase of level on an initially clear night is arrested by the development of low cloud or of fog. Double maxima are often observed in the night peaks (e.g., March 15 in Figure 5).

The magnitude of the peaks on radiation nights is usually 5 to 10 db; it can occasionally reach 15 to 20 db particularly in summer. It seems very probable from the geometry of the path that earth-reflected rays play little part, at least for moderate degrees of bending. It is therefore reasonable to seek to explain the larger variations as resulting from increasing ray curvature. In terms of the rough estimate mentioned above, a change from standard to "flat earth" conditions would give an increase in level of the order of 10 db, which is a typical figure for the observed rise on an undisturbed radiation night. It is of interest to note that free space level is never reached on this path; the highest instantaneous level reached is 10 to 12 db below free space. In other words complete, or nearly complete, reflection regions do not exist at heights of the order of 1,000 ft or more (required to "clear" the barrier) over this path. This is in line with the observed lack of any effect of high inversion on the signal level.

Figures 6, 7, and 8 show photographs of sections of the original signal records illustrating the main types of signal which are observed. The type of weather involved is shown on the record in each case, also the signal calibration. Figure 9 shows a good example of an effect which is quite often observed, particularly

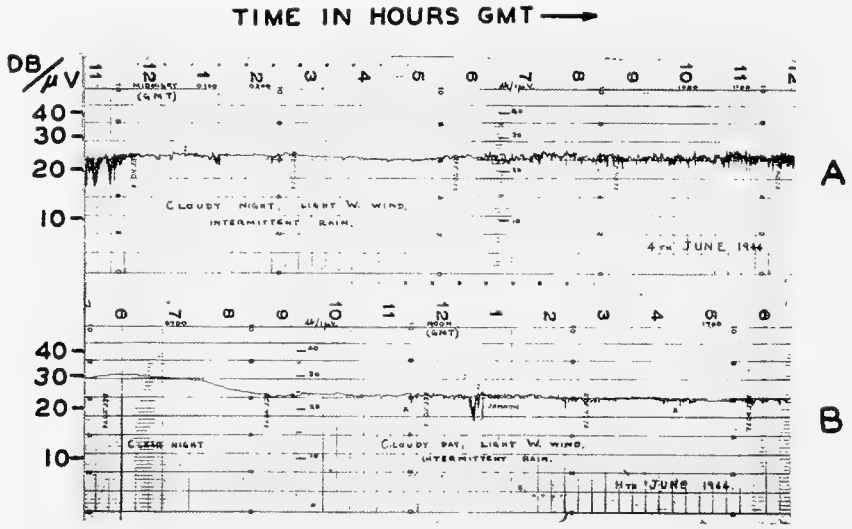

FIGURE 6. Signal records. (A) June 4, 1944 from midnight till noon. Weather cloudy, light W wind, intermittent rain. (B) June 11, 1944, 6 a.m. to 6 p.m. Weather clear in the morning, later cloudy; light W wind, intermittent rain.

in the latter part of radiation nights. It consists in a regular variation showing the characteristic rounded maxima and sharp minima of interference fading. This is in some cases superimposed on a nearly steady high signal (as in Figure 9). In other cases, as in some fog fades, it is superimposed on variations of a different type. It often starts and stops suddenly, completely changing the character of the record while it lasts, and that time ranges from one or two fading cycles to many cycles. This sort of effect has also been observed on other paths, over sea as well as land.

The striking thing about patterns of this sort is that they often correspond to reflection coefficients for the interfering ray which approach unity. In Figure 9 the reflection coefficient calculated from the pattern is about 0.8 at the start, about 0.4 in the middle, and over 0.9 at the end. It is suggested that reflection at small glancing angles from a sharp inversion top provides a possible explanation and that the first part of the pattern in Figure 9 corresponds to an increase in height (the first deep minimum occurring when the inversion top is just above the transmitter) and the latter part to a decrease in height at a different rate. The rates of climb and fall turn out to be about 200 ft per hour and 300 ft per hour respectively. No local soundings are available to check this hypothesis, but the calculated rates of change of height are quite possible.

The general meteorological data for the night (illustrated in Figure 9) are as follows: cloudless, following a fine day; temperature inversion of about 6 F in (approximately) the first 500 ft at 0600 GMT; ground mist about dawn. It is clearly desirable to obtain adequate soundings at periods when this type of effect is observed, especially on account of the widely held view that the index changes which occur at heights of the order involved (about 500 ft above ground level) are inadequate to account for reflection coefficients of the size implied by the pattern observed here.

5.1.4 Difficulties of Existing Theory

In this section a few general characteristics of the radio observations which appear to be at variance with previous theoretical conclusions and which suggest directions in which further work is required will be noted.

1. The most obvious point as far as the Irish Sea data are concerned is the failure of the soundings to provide an adequate guide to the signal variations. The fault may lie in the limited nature of the soundings or in the method of interpreting them, but it is clear that the problem is by no means as simple as was supposed when the soundings were started.

2. The minimum levels obtained (where they are

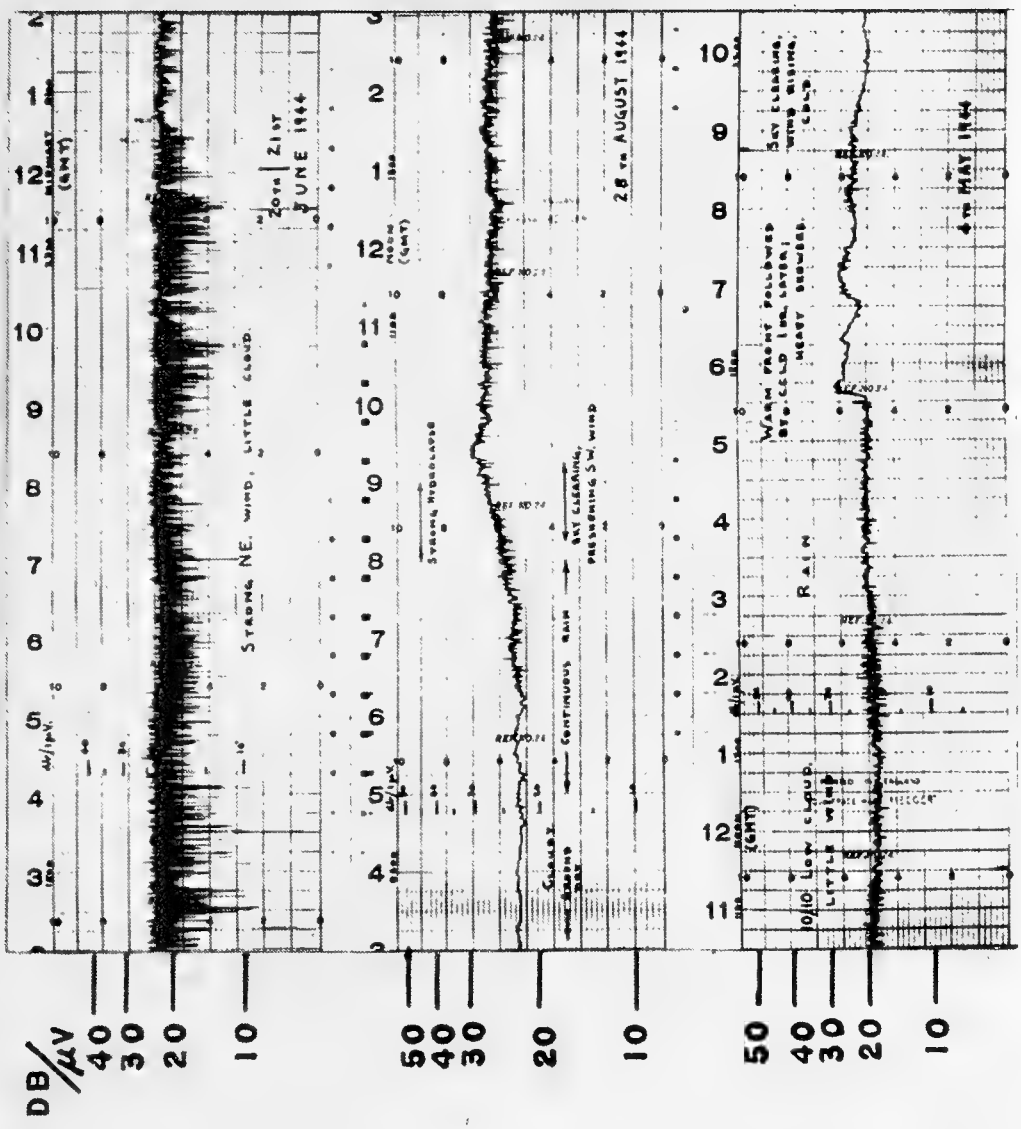

FIGURE 7. Signal records. (C) June 20 to 21, 1944. Strong NE winds, little cloudy. (D) August 28. Cloudy in the early morning changing into continuous rain, then clearing with freshening SW wind. (E) Shows passage of a warm front on May 4, 1944, at 5:30 p.m. followed by a cold front 1 hr later.

high enough to be measured) usually agree tolerably well with the expected values. For the Irish Sea paths, as well as in other measurements, the maximum level rarely goes above that calculated for flat-earth conditions; this level is practically the same as that for free space conditions for all the Irish Sea centimeter links except for paths BF on S band (only) where there is a difference of about 10 db. If complete guiding were a common phenomenon over paths of the lengths actually used, it would appear that levels above free space should occur much oftener and more continuously than is observed. It appears to be a useful working assumption that the level obtained under favorable conditions over nonoptical paths is nearly that calculated for rays with the same curvature as the earth.

3. The fact that the Irish Sea results show that (for centimeter waves) the advantage lies only rarely with the smaller heights and shorter wavelengths suggests that the importance of complete guiding as a criterion for siting stations may have been overemphasized.

4. The good correlation obtained in a number of cases between land-sea temperature difference and signal level suggests that the importance of temperature may be greater than is indicated by existing theory.

5. It appears very difficult to account for the maximum levels reached on the basis of existing theory.

6. The interference patterns of the type discussed above in Section 5.1.3 still await an adequate explanation.

5.2 PROPAGATION WORK IN PROGRESS AT THE NATIONAL PHYSICAL LABORATORY[b]

This report gives a summary of the present position (November 1944) of various investigations being conducted under the auspices of the Ultra Short Wave Propagation Panel of the R.D.F. Applications Committee of the Advisory Council on Scientific Research and Technical Development, Ministry of Supply. The items to which the Radio Division of the National Physical Laboratory is contributing may be listed as follows:

1. Analysis and study of centimeter and meter wave propagation over sea (3-6-9) experiments.

2. Study of properties of water vapor, water, and ice, and the absorption and scattering by these and other substances in the atmosphere.

[b]By W. Ross, British Central Scientific Office.

3. Measurement of reflection coefficient of land at centimeter wavelengths.

4. Study of centimeter wave propagation over land (Whitwell Hatch to Wembley).

The following sections indicate the progress that has been made to date on items 1 and 4. For items 2 and 3, see Sections 10.5 and 9.3.

5.2.1 Analysis and Study of Centimeter and Meter Wave Propagation over Sea (Irish Sea Experiment)

This project utilizes the results of radio transmissions being conducted between two sending stations in South Wales and receiving stations in North Wales and Scotland, jointly by the Admiralty, Ministry of Supply and Air Ministry.

The contribution of the National Physical Laboratory to the installations being used for this investigation has been chiefly connected with the monitoring equipment used at both sending and receiving stations to insure that the radiation from the former and the sensitivity of the latter are maintained constant, so that any variations on the field strength records are known to be due to transmission effects in the atmosphere. The instruments required for the S band are in an advanced state of production, while for the X band the necessary field strength meter for the transmitters has been developed, but some development work is still required on the standard radiator for the receiver calibration. In accordance with a recent agreement as to the limitation of the scope of the investigation, all work on instruments for other wavelength bands has been put in abeyance.

5.2.2 Study of Centimeter Wave Propagation over Land (Whitwell Hatch to Wembley)

A transmitter operating on a wavelength in the S band has been installed at the Admiralty Signal Establishment, Whitwell Hatch, and a continuous recording is being made of the field intensity of the radiation received at the Research Laboratories of the General Electric Company, Wembley, over a land path of 38 miles. Except for some houses and trees within about 5 miles of the receiver, the path is a clear optical one; originally the transmitter was also partially obscured by some trees, removal of the tops of which produced a rise in received field of 10 db. Field strength recording has been in progress over this link since

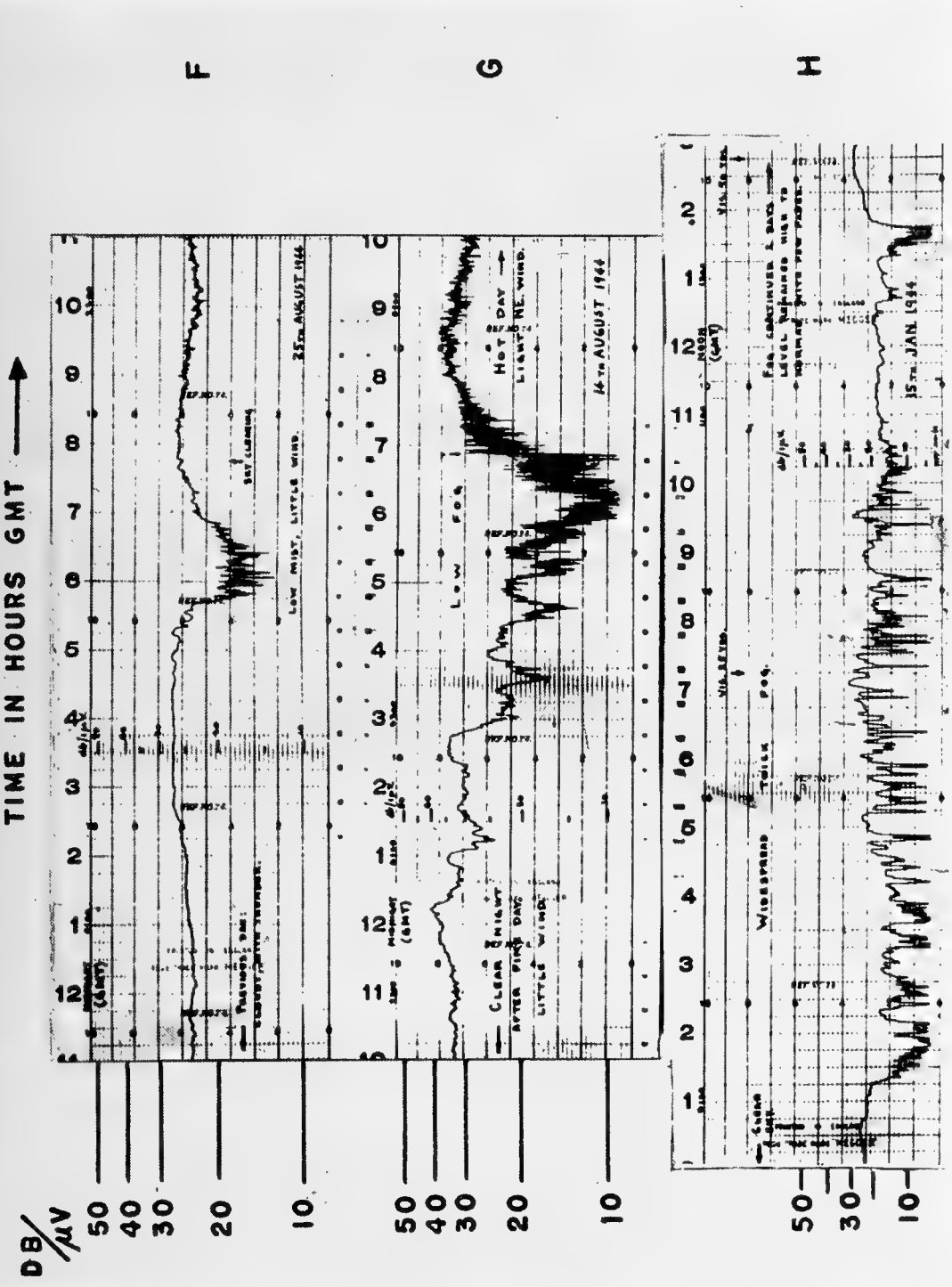

FIGURE 8. Signal records. (F) August 25, 1944, dip in record coincides with low mist. (G) August 14, 1944, shows effect of low fog. (H) January 15, 1944, typical for widespread, thick fog.

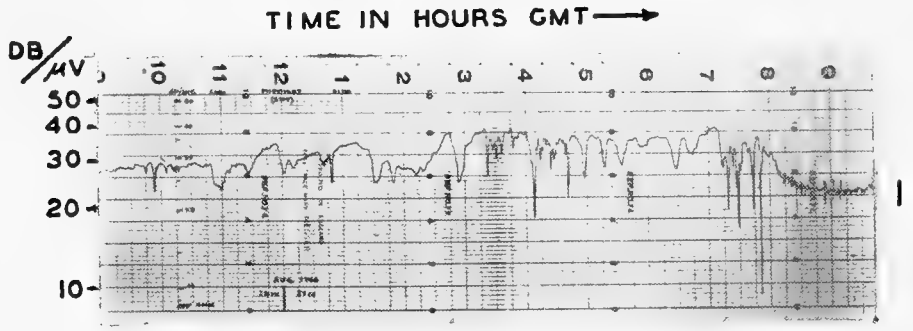

FIGURE 9. Signal record. August 26 to 27, 1944, showing examples of interference fading in radiation nights.

March 1943, and during the intervening 18 months there has been a seasonal variation, with the average daily value in November and December at least 10 db below the value in July and August. Two reports[16,17] have already been issued on the results obtained from an analysis of the records, and a third will be prepared shortly.

Among the main conclusions so far reached are the following. Cloudy weather, either by day or night, tends to produce a signal steady to within about 2 db, while on days of clear and variable skies, the signal exhibits slow (period 5 to 10 minutes) fluctuations of the order of 3 or 4 db, with sharper and more rapid fluctuations superposed. These rapid fluctuations are accentuated by the presence of strong wind. On nights of clear or variable skies with temperature inversions near the ground, the field intensity is from 5 to 10 db above the daytime level and is usually accompanied by variations in the absence of wind. On clear radiation nights, when the wind is too strong to permit the development of a temperature inversion, the peak of signal intensity does not occur. Fog affects the field strength differently according to its depth. A shallow autumn fog causes a sharp decrease in signal strength, while the widespread and more established type of fog experienced in winter may sometimes cause marked interference type of fading with unusually high peak values and at other times may have no apparent effect on the field strength.

The sending and receiving stations on this link are now being equipped with field strength monitoring arrangements to improve the overall accuracy of the radio recording, and a daily statement of the meteorological conditions over the path is being supplied to supplement the ground station records already available. It is contemplated that this link should remain in operation for a further period of 6 to 12 months.

5.3 FADING IN A LINE-OF-SIGHT EXPERIMENT IN ENGLAND[c]

This experiment was carried out between Aberporth, South Wales, and the summit of Mt. Snowdon (3,600 ft). The transmitters were mounted at a height of 120 ft above sea level at Aberporth, the receivers being on Mt. Snowdon. The length of path was about 60 miles as compared with 85 miles optical range.

Two separate radio circuits were used, one on a wavelength of 9 cm and the other on 10 cm. For a standard atmosphere the phase difference between the ray reflected from the sea and the direct ray was about 4.5 radians on 10 cm and about 5 radians on 9 cm, while under "flat earth" conditions the corresponding phase differences were about 12 radians and 13 radians respectively. As the atmospheric conditions varied, an interference pattern was obtained arising from variations in the phase difference. The chief characteristic of the interference pattern was that in a plot of radio signal strength against time the peaks are broad and flat and the minima are sharp and deep. The provision of the two circuits insured that the variations due to alterations in the phase difference could easily be distinguished from variations due to other causes (described below). The reason for this is that the interference minima on one circuit tend to occur at times when the signal strength is high on the other circuit.

The length of time required for the radio signal strength to complete a cycle of the interference pattern was usually about 2 hours. The receivers and transmitters were very carefully calibrated in order to show that the received field strength at interference maximum was equal to twice the free space field. This

[c]By F. Hoyle, Ultra Short Wave Panel, Ministry of Supply, England.

result was established to within an accuracy of ±2 db.

For about 20 per cent of the time (June 1, 1944 to September 30, 1944) the normal interference pattern was replaced by an entirely different form of signal fading. The period of the fading was about 5 minutes, the field strength at maximum was usually between 10 and 12 db above the free space signal, and the peaks of signal were sharp and the minima broad. The latter characteristic is entirely different from interference fading between two rays which must lead to broad peaks and narrow minima; it is more akin to receiver noise or the form of the signal echo received from "window" on radar sets. Thus it would seem plausible to suppose that the signal was the result of a large number of contributions with uncorrelated phases.

The type of fading described in the previous paragraph is especially interesting in view of the very high signal maxima. It was shown that the occurrence of these variations was not associated with the reflection at the surface of the sea. It would appear therefore that atmospheric conditions can exercise a very important effect on the propagation of radio waves over a completely optical path.

5.4 TEMPERATURE EFFECTS ON NONSTANDARD RANGES[d]

Experimental work carried out in the Irish Sea has shown the following three characteristics, all of which are in disagreement with existing theory.

1. It is well known that the present theory requires the contribution of the temperature gradient to be in general small compared with the contribution of the water vapor gradient. In fact if we write

$$\frac{d\mu}{dh} = a\frac{de}{dh} - b\frac{dT}{dh}, \qquad (1)$$

where μ = refractive index,
e = partial pressure of water vapor,
T = temperature in degrees absolute,
h = height coordinate,
a, b are positive constants,

then except in rare cases the present theory requires the $(a)(de/dh)$ term to be large compared with the $(b)(dT/dh)$ term. Thus, since the radio propagation conditions depend on $d\mu/dh$, it is to be expected that a better correlation will exist between the radio signal and the measured value of $(a)(de/dh)$ than between the radio signal strength and the measured value of $(-b)(dT/dh)$. The reverse has, however, been found to be the case; the correlation between the radio signal strength and the measured value of $(a)(de/dh)$ is poor, while the correlation with the measured value of $(-b)(dT/dh)$ is good.

2. A situation similar to that mentioned in (1) has been encountered in attempting to forecast 12 hours ahead for operational radar sets. Table 1 summarizes the results obtained.

Table 1

Forecasting system	No. of cases examined	% of correct forecasts
(de/dh) term	600	56
Continuity method	600	57
(dT/dh) term	150	75

The continuity method of forecasting consists in predicting that tomorrow's conditions will be the same as those observed today. Forecasting from the (dT/dh) term was empirical, it being assumed that a temperature inversion of 1.5 C per 100 ft would give very good propagation conditions, an inversion of 0.75 C per 100 ft would give good conditions, and a temperature lapse would correspond to standard or natural conditions.

3. The value of $d\mu/dh$ calculated from equation (1) using the measured values of de/dh and dT/dh are too small to explain the large signals frequently observed on a wavelength of about 80 mc.

These experimental results enable the following conclusions to be drawn so far as the meteorological conditions around the British Isles are concerned.

1. The radio signal strengths computed from the observed M curve do *not* agree with observation. The method of observing the temperature and water vapor gradients to obtain an M curve is therefore unsatisfactory.

2. A reasonably satisfactory forecasting system can be obtained on the basis of temperature gradient alone. This system is empirical and does not depend on complicated mathematical computations. Accordingly the

[d]By F. Hoyle, Ultra Short Wave Panel, Ministry of Supply, England.

system may be suitable for application under operational conditions.[e]

[e]It has appeared since the November 1944 Propagation Conference that the Propagation Group at San Diego has found a good correlation between the radio data and a simple meteorological parameter based on temperature excess. In the British Isles the temperature excess has to be taken between a height of about 200 ft and sea level, whereas at San Diego the temperature excess has to be taken between a height of about 5,000 ft and sea level. It has also been reported that in the Pacific Area temperature excess is by far the best index for predicting radio propagation conditions. There is some hope, therefore, that it may be possible to work out a method of fairly universal application on the basis of temperature excess.

PART II

METEOROLOGY

Chapter 6

METEOROLOGY—THEORY[a]

6.1 MODIFICATION OF WARM AIR BY A COLD WATER SURFACE[b]

6.1.1 History

TWO OF THE COMMONEST TYPES of M curves which produce nonstandard propagation are the S-shaped curve and the simple trapping curve where M decreases from the surface to 200 ft, say. The S-shaped curve occurs in regions of subsidence, for example, in the extensive subtropical anticyclones. The forecasting of this phenomenon will not be presented in this discussion which is confined to the simple trapping case.

During 1943 the question arose regarding the feasibility of forecasting the change in the temperature and vapor pressure distribution as warm air flows over a cold water surface. Through practice, considerable success had already been obtained in forecasting the M curve a few miles offshore in Boston Harbor. However, it was suggested that a general method be devised whereby the M curve could be predicted for greater distances from the shoreline and for different regions of the world. In order to solve this forecast problem the Boston Harbor soundings were investigated in the light of turbulence theory.

Two factors had to be kept in mind, namely:

1. The Boston Harbor soundings of temperature and vapor pressure were scant. A more serious difficulty was the total absence of data at distances in excess of 15 miles from the land.

2. Since forecasting techniques were the primary aim it was necessary to find a solution which was suitable for field use.

6.1.2 Diffusion Equation

The differential equation for turbulent mass exchange may be written

$$\frac{\partial T}{\partial t} = \frac{\partial}{\partial z}\left(K\,\frac{\partial T}{\partial z}\right). \tag{1}$$

If K, the coefficient of eddy diffusion, is assumed constant, then

$$\frac{T' - T}{T_0 - T_w} = E\left(\frac{z}{\sqrt{4Kt}}\right) - 1, \tag{2}$$

where E = error function, that is,

$$E(\xi) = \frac{2}{\sqrt{\pi}}\int_0^{\xi} e^{-x^2}dx,$$

T' = temperature at a level z over the ocean,
T = initial temperature at z over the land,
T_0 = initial air temperature over land at $z = 0$,
T_w = water temperature,
t = time.

Values of K were then computed from the observational data by evaluating the ratio $(T'—T)/(T_0—T_w)$ for different evaluations and different times. These values were averaged for each level and the results shown in Table 1 were obtained. After plotting K

TABLE 1. Values of K.

Elevation in ft	20	50	100	200	300
K	0.014×10^4	0.07×10^4	0.18×10^4	0.38×10^4	0.67×10^4

against elevation, the approximate linear variation of K was extrapolated to give values of K for elevations up to 700 ft. This level of 700 ft lies well within the limit of 250 m which was indicated by Mildner[1] to be the level where K reaches its maximum.

These values of K were then used to construct Table 2, which gives $(T'—T)/(T_0—T_w)$ for all levels in terms of the time that the air has been over the water. The same values of K were obtained from the analysis of vapor pressure changes; hence the same table can be used to evaluate the ratio $(e'—e)/(e_0—e_w)$. From this table it is a simple matter to reconstruct the M curve at any distance over the ocean, provided the initial state of the air is known. An example of the changes in the M curve are given in Figure 1.

6.1.3 Discussion of Procedure

Summarizing the favorable aspects of this study, it can be stated that:

1. The values of K were almost identical for vapor pressure and temperature changes. This suggests that the data were reliable.

2. The values of K agreed with those of Giblett[2] for wind variations from the surface to 150 ft.

3. This extrapolation method, that is, the error function extrapolation, gives reasonable values after

[a]See also Parts II and III of Chapter 17, Volume 1, Committee on Propagation.

[b]By J. M. Austin, Meteorology Department, MIT.

TABLE 2. Values of $(T' - T)/(T_0 - T_w)$ or $(e' - e)/(e_0 - e_w)$; initially $T_0 > T_w$, $e_0 < e_w$.

Elevation in ft	Time in hours											
	¼	½	¾	1	1½	2	3	4	6	10	15	20
0	1.0	1.0	1.0	1.0	1.0	1.0	1.0	1.0	1.0	1.0	1.0	1.0
20	0.23	0.40	0.49	0.55	0.63	0.67	0.73	0.77	0.81	0.85	0.88	0.89
50	0.17	0.34	0.43	0.50	0.58	0.63	0.69	0.73	0.78	0.83	0.86	0.88
100	0.09	0.23	0.33	0.40	0.49	0.55	0.63	0.67	0.73	0.79	0.83	0.85
150	0.04	0.15	0.24	0.31	0.41	0.48	0.56	0.61	0.67	0.74	0.80	0.82
200	0.02	0.10	0.19	0.25	0.35	0.42	0.51	0.57	0.64	0.71	0.77	0.80
250	0.01	0.08	0.15	0.22	0.31	0.38	0.47	0.54	0.62	0.69	0.75	0.78
300	0.01	0.07	0.14	0.20	0.29	0.36	0.45	0.52	0.60	0.68	0.74	0.77
350	0.01	0.05	0.11	0.17	0.26	0.33	0.43	0.49	0.58	0.67	0.73	0.76
400	0.00	0.04	0.09	0.14	0.23	0.30	0.40	0.46	0.55	0.65	0.70	0.74
450	0.00	0.03	0.07	0.12	0.20	0.27	0.37	0.43	0.53	0.63	0.68	0.72
500	0.00	0.03	0.05	0.10	0.17	0.24	0.34	0.40	0.51	0.61	0.67	0.71
550	0.00	0.02	0.04	0.08	0.15	0.22	0.32	0.38	0.49	0.59	0.65	0.70
600	0.00	0.01	0.03	0.07	0.13	0.20	0.29	0.35	0.46	0.57	0.64	0.69
650	0.00	0.01	0.02	0.06	0.11	0.18	0.27	0.33	0.44	0.55	0.62	0.67
700	0.00	0.00	0.01	0.05	0.10	0.16	0.25	0.31	0.42	0.53	0.61	0.66

All values are negative.

a long period of time. A check was made by comparing Taylor's data off Newfoundland with computed values. This check was quite good.

4. The procedure is simple, and consequently the weather officer could readily calculate the M curve.

However, the entire method may be criticized because:

1. In the integration of the diffusion equation K is assumed constant while in the application of the integrated formula K was found to vary with elevation. The values of K which were used in the final analysis are therefore "effective values."

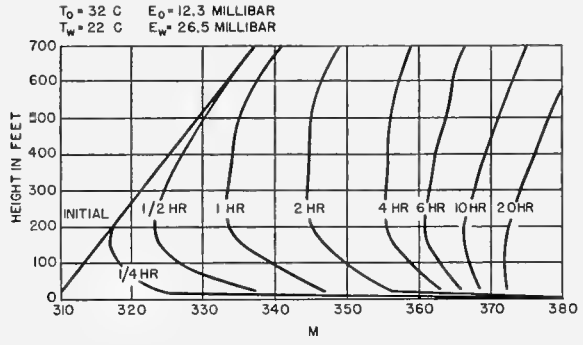

FIGURE 1. Changes in M curves resulting from modification of warm, dry air over cool, moist surface. Zero time corresponds to the coast line; ¼ hr, ½ hr, etc., refer to the time the air has been over water.

2. K has been considered to be independent of the degree of roughness (probably a justifiable assumption over the ocean), the degree of stability, and the wind velocity. These factors were neglected solely because the scant data did not allow a complete analysis of the variation of K.

These "effective values" should give some indication of the true variation of K. They suggest that K varies linearly with elevation except for a quite rapid increase in about the first 30 ft. Consequently it seems reasonable to assume that

$$\frac{\partial T}{\partial t} = \frac{\partial}{\partial z}\left[(pz + q)\frac{\partial T}{\partial z}\right].$$

If $K = pz + q$ then, from the statement that $K(\delta u/\delta z)$ = constant (eddy stress does not vary with height), the velocity variation with elevation is given by

$$u = a \log (z + b) + C.$$

The question now arises: In the laminar layer, is the wind variation with height represented by a logarithmic law?

6.1.4 Previous Investigations

For many years research workers have studied the wind variation near the ground. A few of the conclusions will now be presented.

1. In 1932, Sutton[3] assumed a certain form of the coefficient of correlation between the velocities of the air particles considered at time t and at an interval of time later. This assumption implied that there was a power law for the variation of wind with height.

$$\frac{u}{u_1} = \left(\frac{z}{z_1}\right)^m \qquad m = \frac{n}{2 - n}.$$

2. In 1933, Cardington and Giblett[2] analyzed an extensive series of observations at 4 ft and 143 ft. Of course with only two points the observations could be made to fit either a power law or a logarithmic law. If a power law held, then m is a function of the degree

of stability and wind velocity. If a logarithmic law held, then K is a function of these same quantities.

3. In 1934, Best[4] analyzed data which was measured at seven elevations between 2 cm and 5 m. He concluded that the velocity variation was best represented by a logarithmic function of the form

$$u \backsim \log (z - C)$$

where C is a constant.

Furthermore he found that the power law could be applied only to shallow layers and even then m varies quite considerably with height, wind velocity, and vertical temperature gradient.

4. In 1936, Sutton,[5] who in 1932 suggested the power law variation, definitely favored the logarithmic variation. Furthermore he showed how one could handle the problem of varying stability. Sutton analyzed different sets of data, ranging to 30 m in elevation, to support the logarithmic variation.

5. In 1936, Sverdrup[6] criticized Sutton's logarithmic law and favored a power law in regions of stability. As evidence he introduced Rossby and Montgomery's[7] analysis as well as his own data.

6. In 1937, Sutton[8] quite satisfactorily met Sverdrup's criticism and pointed out that all experimental evidence suggested the logarithmic variation rather than the power law variation.

This represents only a cross section of opinion and perhaps may be summarized as follows:

1. In an indifferent or unstable atmosphere the logarithmic law is generally accepted.

2. In a stable atmosphere there is more support for the logarithmic law than for the power law.

One writer summarized the situation very aptly when he said that all modern mathematical studies on atmospheric turbulence are inexact and depend on certain wide assumptions. An appeal to experiment is therefore essential.

6.1.5 Conclusion

The question now arises, should one assume a power law variation, or is the true wind variation better represented by a logarithmic law? Certainly the experimental evidence tends to favor a logarithmic variation. The advantages and disadvantages of either assumption may be summarized briefly as follows:

1. Power law variation.
   a. m varies with stability, wind velocity, roughness, and elevation.
   b. The mathematical analysis is too complicated for practical use.
2. Logarithmic law variation.
   a. Agrees reasonably well with experimental data.
   b. Agrees with von Kármán's logarithmic law. von Kármán has shown that this law covers an exceedingly wide range of turbulence.
   c. K, like m, varies with stability, wind velocity, roughness, and elevation.
   d. If the logarithmic law holds, K is then a linear function of height. With this relatively simple expression for K it should be much easier to handle the diffusion equation than in the case of a power law variation.
   e. Provided the integration of the diffusion equation is not too complicated, one should be able to reconstruct the temperature and vapor pressure curves. Consequently the exact shape of the M curve can be calculated.

In conclusion it should be borne in mind that theoretical discussion is futile. At best we can only make certain assumptions and derive a result. If this result agrees with observational data then the original assumptions are justified. Furthermore, practical considerations demand that the final solution be simple enough for application in the field.

It seems certain that over a wide range of elevation, say 300 ft, the true wind variation cannot be uniquely defined by one specific logarithmic law or one specific power law. The most desirable procedure may then be an analysis of observations in as simple a manner as possible but yet flexible enough to take care of the most important changes. Consequently it is suggested that experimental data be analyzed on the assumption that K varies linearly with elevation, i.e.,

$$\frac{\partial T}{\partial t} = \frac{\partial}{\partial z}\left(K \frac{\partial T}{\partial z}\right) \quad \text{or} \quad u \frac{\partial T}{\partial x} = \frac{\partial}{\partial z}\left(K \frac{\partial T}{\partial z}\right),$$

where $K = pz + q$, and x is the distance measured horizontally. If accuracy is not seriously affected it is further suggested that approximations be introduced in order to facilitate the application of the results for field use.

6.2 DIFFICULTIES OF LOW-LEVEL DIFFUSION PROBLEMS[c]

The effect of a temperature inversion is largely a secondary one in that by reducing the coefficient of diffusion it favors the formation of large humidity

[c]By Lt. Comdr. F. L. Westwater, Naval Meteorological Service, Royal Navy.

gradients. The coefficient of diffusion K is calculated from the wind profile which is assumed to satisfy a power law of the form $U = Az^m$.

The difficulty arises because m is fixed once and for all before we solve the equation and thus the theory cannot take account of changes in the temperature gradients of a diurnal character in so far as they affect the humidity distribution. At the same time we believe that K is very sensitive to the temperature gradient.

Further, values of m have been used which have no meteorological support. The value $m = 0.5$, for example, implies a wind structure which is absurd if extended up to 100 m and it certainly is invalid near the ground. Chemical warfare technique measures m directly by measuring R, the ratio of the wind at 2 m to the wind at 1 m. Even in the very extreme conditions which prevail over land no value of R exceeding 1.35 is observed. This makes $m = 0.33$. Over the sea, even in a low layer, it is very unlikely that a value of m differing significantly from $\frac{1}{7}$ would be found.

The difficulty is that power laws apply only for very limited ranges of height and can be extended only by using a different power. Their only merit is that they enable the equation of diffusion to be solved; the power law is not a law of nature. A complete solution of the problem would involve a theory giving K as a function of temperature gradient. A start has been made on this for the case of still air which is agitated by thermal turbulence originating from heating on its lowest level. The value of K so calculated is small compared with that for a light wind. It seems likely that the effect of an inversion on K will also be small.

To sum up, radar personnel should be warned that the diffusion theory is at present in a highly unsatisfactory state; any conclusions drawn from it should be treated with the greatest reserve, and some calculations already published are based on assumptions which have no meteorological foundations.

6.3 PRELIMINARY RESULTS OF METEOROLOGICAL MEASUREMENTS IN MASSACHUSETTS BAY[d]

The modification produced in land air when it passes out over water is known to be particularly effective in producing nonstandard microwave propagation. The preliminary results of this study are covered in the present report; they are necessarily incomplete and tentative.

[d]By R. B. Montgomery, Radiation Laboratory, MIT.

6.3.1 Modification of Air Flowing over Water

To begin with, some basic considerations will be presented. Figure 2 shows an airplane sounding in air which is warm and dry relative to the underlying water. Before leaving land the air was vertically homogeneous; that is, potential temperature and specific humidity were constant. This may be seen by comparing the observed temperature and vapor pressure with the broken straight lines drawn for

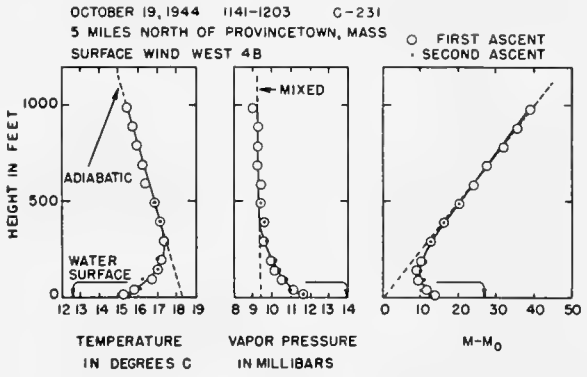

FIGURE 2. Typical airplane sounding, giving temperature and water vapor variation with height.

homogeneous air. The straight line of modified index of refraction M is constructed for homogeneous air; it is close to standard. The air is being modified by loss of heat to the water and by evaporation.

At the common boundary the temperatures of air and water are identical. The vapor pressure also is given by the water temperature; over sea water the vapor pressure is 98 per cent of the saturation value corresponding to the water temperature. It follows that the modified index at the surface is determined by the water temperature alone.

Figure 2 illustrates in a striking manner the similarity in shape of the three curves. The ratio of the change from unmodified value at any height to the change at the surface is the same for all three quantities.

Modification of air over water is due largely to turbulent mixing, which transports heat and water vapor in exactly the same manner (the eddy diffusivity is identical for both). Next to the water boundary there is always a laminar layer, through which heat is transported to the turbulent layer by true conduction while the water vapor is transported by true diffusion; the coefficients for these two related processes happen to be nearly the same, so heat and water vapor are transported vertically to nearly the

same relative degree. The temperature distribution is modified by radiation also, but for an initial period of a few hours this is unimportant compared with the processes just mentioned.

When initially homogeneous air flows over water of constant temperature, a necessary result is therefore that the curves of temperature and water vapor pressure are similar. Furthermore the M curve is similar also, because within the range of any sounding the modified index is approximately a linear function of temperature, vapor pressure, and height.

The extent of similarity revealed in Figure 2 is unusual. Often the three curves have very different shapes. In the latter case the deviation from similarity can be ascribed (1) to lack of homogeneity in the unmodified air, (2) to varying water temperature along the air's trajectory, or (3) to radiation during prolonged over-water modification.

6.3.2 The M Deficit

The distances on the base line from the straight broken line to the arrow are the temperature excess and humidity deficit respectively. There is obviously a corresponding quantity pertaining to index of refraction. The M *deficit* may be defined as the value of the modified index at the water surface less the representative surface value in the unmodified air.

Temperature excess, humidity deficit, and M deficit are related, so any two fully determine the difference between unmodified air and air at the water surface. The two of most direct significance are M deficit and temperature excess. Forecasting is simplified by their use: Temperature excess is necessary in drawing the temperature curve; similarity and M deficit then give the M curve directly. Another advantage in using M deficit is that whether it is positive, zero, or negative determines at once whether the modified air is probably characterized by an M inversion (layer where modified index of refraction decreases upward) by standard, or by substandard M curves, respectively. For instance, the positive M deficit in Figure 2 is a condition necessary for the M inversion to occur.

Specifically, if homogeneous air blows over a water surface of constant temperature and if the M deficit is positive, there is always an M inversion at the water surface. Whether or not this extends sufficiently high to be of importance in the refraction of radio waves depends in part on the magnitude of the M deficit and on the temperature excess.

If homogeneous air blows over a water surface of constant temperature and if the M deficit is zero, the M curve necessarily remains practically standard.

In the case of a negative M deficit a substandard M curve is developed. It should be noted that in this case (as well as in the previous one) the air is losing water vapor by condensation on the water surface. This is simply the reverse of the process with dry air.

6.3.3 Neutral Equilibrium

For simplicity the analysis which follows is limited to cases of positive M deficit. There is then a surface M inversion, the height of which is a convenient quantity to study as a dependent variable. The independent ones are M deficit and temperature excess and, as will be seen, two others.

The first and least complicated case is the one of neutral equilibrium, which corresponds to a temperature excess close to zero, say within 1 C of zero. Since there is no appreciable temperature gradient, the M curve depends only on the moisture distribution. Furthermore this case practically requires a vapor-pressure lapse at the surface, because in the lower part of a homogeneous layer the vapor cannot be saturated (see Figure 3). Hence there is always an M inversion at the surface. Neutral equilibrium is prevalent far from shore.

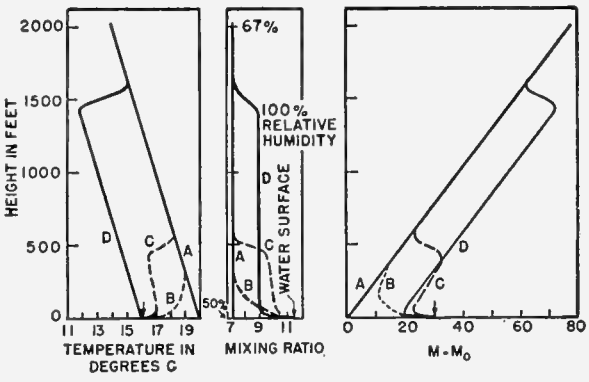

FIGURE 3. Probable course of modification of warm air over water under ideal conditions. A, initial stage. D, final stage.

With neutral equilibrium frictional turbulence is unhindered. Mixing extends to a height roughly proportional to the wind speed; a wind of 20 mph at 100 ft gives mixing up to about 2,000 ft.

The intensity of mixing increases upward rapidly from the surface, so large vertical gradients are confined to the region of relatively little mixing close to the surface. The M inversion probably never extends above 100 ft.

It has been well established that under neutral equilibrium the eddy diffusivity is directly proportional to height within the so-called turbulent boundary layer, which forms the lower tenth of the entire frictional layer mentioned above. In this case wind speed, temperature, and vapor pressure are linear functions of the logarithm of elevation.

While the details are not presented here, it is easily shown that these logarithmic distributions demand that the height of the top of the M inversion be

$$d = \frac{4}{3} a \, \Gamma \Delta M 10^{-6},$$

where a is the radius of the earth, ΔM is the M deficit, and Γ is a meteorological parameter depending on wind speed alone in the case of complete neutral equilibrium. Thus the height of the M inversion is directly proportional to the M deficit with neutral equilibrium.

Published data indicate that the effect of wind speed is not great and give an average value of $\Gamma = 0.08$. This yields $d/\Delta M = 2$ ft. Data obtained during the summer's (1944) project agree with this result.

6.3.4 Unstable Equilibrium

The second case is the one of unstable equilibrium or negative temperature excess. This is similar to neutral equilibrium in that the M deficit is always positive and there is always a surface M inversion.

Instability adds convective mixing to the frictional mixing that would otherwise be present. This convective mixing is especially effective in the central region of the unstable layer and hence confines the large vertical gradients within a still thinner surface layer.

The logarithmic distributions are characteristic of neutral equilibrium only. Consequently, in the unstable cases the height of the M inversion is not simply proportional to M deficit but depends on M deficit in a more complicated manner. In spite of this the proportionality will be assumed as a useful approximation in studying the unstable and stable cases also.

The ratio of height of M inversion to M deficit is definitely less for unstable than for neutral equilibrium. Tentatively it may be said to range between 0.2 ft and 2 ft.

6.3.5 Stable Equilibrium

The last case is the one of stable equilibrium. Stability reduces the mixing with high levels, thus permitting a deeper surface layer of strong gradients to form (as shown in Figure 2). Thus the ratio of height of M inversion to M deficit may be expected to be always greater in stable equilibrium than in neutral equilibrium.

Stability reduces the mixing to such an extent that the air is progressively modified during a long over-water trajectory. It is therefore necessary to introduce a fourth independent variable, length of over-water trajectory, to supplement M deficit, temperature excess, and wind speed.

Under ideal conditions there is reason to believe that the modification would pursue the course sketched in Figure 3. The final state would be an essentially homogeneous layer capped by a temperature inversion at the level already mentioned for the top of the frictionally produced turbulence in neutral equilibrium. The temperature of the layer would follow an adiabatic lapse rate from the water surface to the top. The water vapor would be saturated at the top of the layer, specific humidity being nearly constant throughout the layer except for a strong lapse at the surface. Intermediate stages in the formation of this final state are indicated qualitatively in Figure 3.

It should be noted that the later stages have a transitional or S-shaped M curve and that qualitative theoretical considerations do not reveal which. The initial stage is, however, characterized by simple surface trapping, and it is this stage only for which data are presented below.

The soundings have been studied to determine empirically how the ratio of height of M inversion to M deficit depends on temperature excess, wind speed, and length of trajectory. To eliminate complex M curves the analysis has been limited to cases conforming closely to the following ideal conditions.

1. Initially homogeneous air.
2. Constant surface-water temperature along the air trajectory.
3. Constant wind (wind not changing with time following a parcel).

The ratio of height of M inversion to M deficit is found to increase with length of over-water trajectory quite markedly in the first 10 miles. From 10 miles to 30 miles there is not much further increase. Beyond 30 miles the preliminary analysis reveals no general information.

Figure 4 gives some tentative results based on various sources of information. This includes the cases of neutral and unstable equilibrium in addition to stable equilibrium. Within the stated range of over-

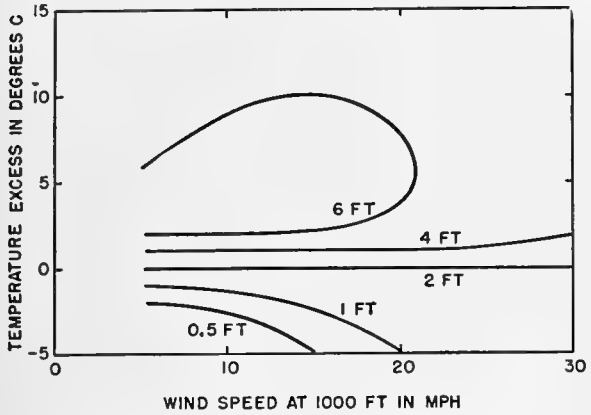

FIGURE 4. Ratio of height of M inversion to M deficit. For positive temperature excess the over-water trajectory is 10 to 30 miles.

water trajectory this diagram gives the height of the M inversion as a function of temperature excess, wind speed, and M deficit. A complete analysis of the observations will yield similar diagrams both more accurate and more detailed. These should prove of definite use in forecasting M curves.

In conclusion, it should be made clear that the work summarized in this report is a group undertaking. A large number of persons, some of them members of Radiation Laboratory Group 42 and other members of the U. S. Army Air Forces, took part in the development and construction of the instruments and in the observing.

6.4 METEOROLOGY OF THE SAN DIEGO TRANSMISSION EXPERIMENTS[e]

During the summer of 1944 a rather intensive experimental propagation program was carried on in San Diego area. The main purpose was to determine the distribution of radiated radio energy in the lower troposphere under the wide range of weather conditions prevailing during this season. A temperature inversion was present from around the first of June through October; the base of the inversion varying from the surface, on a few occasions, up to an altitude of some 4,000 ft. This inversion is characterized by dry superior air subsiding over moist maritime polar air.

6.4.1 Methods of Observation

The field strength data were taken in two ways. A fixed one-way link between San Pedro and San Diego gave continuous records on frequencies of 52, 100, and 547 megacycles, and vertical airplane sections taken at several different distances west of San Diego gave almost instantaneous records of the energy distribution for the same range of frequencies.

The meteorological data were obtained by the use of an airplane and wired sonde; the technique of the latter was described in detail in a previous report.[9] The captive balloon or wired sonde is a modified version of the Washington State College equipment.[10] Daily soundings were taken at the Scripps Pier at La Jolla, 11 miles north of the laboratory. Two 1-week periods of continuous shipboard soundings were made from a YP ship operating in the middle of the San Pedro to San Diego link.

The principal use of the airplane has been in taking vertical field strength sections seaward from the laboratory. During these flights meteorological soundings were made as frequently as possible. The laboratory was fortunate in obtaining from the Washington State College group one of their original sonde units and has adapted this equipment for use in the airplane soundings. The temperature and humidity elements were mounted in an unobstructed aluminum housing approximately 1½ ft above the nose of the PBY-5A airplane.

Since the airplane served the dual purpose of obtaining both meteorological and field strength measurements, all the data were obtained on a fixed course. Field strength sections were made in rapid descents and the meteorological data were obtained in ascents. Navigational difficulties prohibited spiraling for the meteorological data and therefore these soundings covered considerable horizontal distance. Due consideration of this was made in plotting the cross sections.

6.4.2 The San Diego High Inversion

In the summer season San Diego lies within the belt of the subtropical anticyclones, and, with the absence of surface frontal activity, a stagnant circulation exists. Because of the persistence of high-level anticyclonic circulation aloft, pronounced subsidence is maintained throughout this season; 1944, in particular, was characterized by very low humidity above the 2-km level. By subsidence aloft a thermal inversion exists over a large maritime area and thus forms the boundary between the lower maritime polar and the continental tropical or superior air aloft. Variation in height and magnitude of the inversion is the

[e]By Lt. A. P. Stokes, U.S. Navy Radio and Sound Laboratory.

governing factor in daily weather phenomena. There exists a close correlation between the height of the base of the inversion, the pressure at 10,000 ft, and the lapse rate of temperature between the 5,000- and 10,000-ft levels. It is found that with the intensification of the pressure field aloft, the lapse rate of temperature approaches the dry adiabatic condition and thus, under these conditions, indicates increased sub-

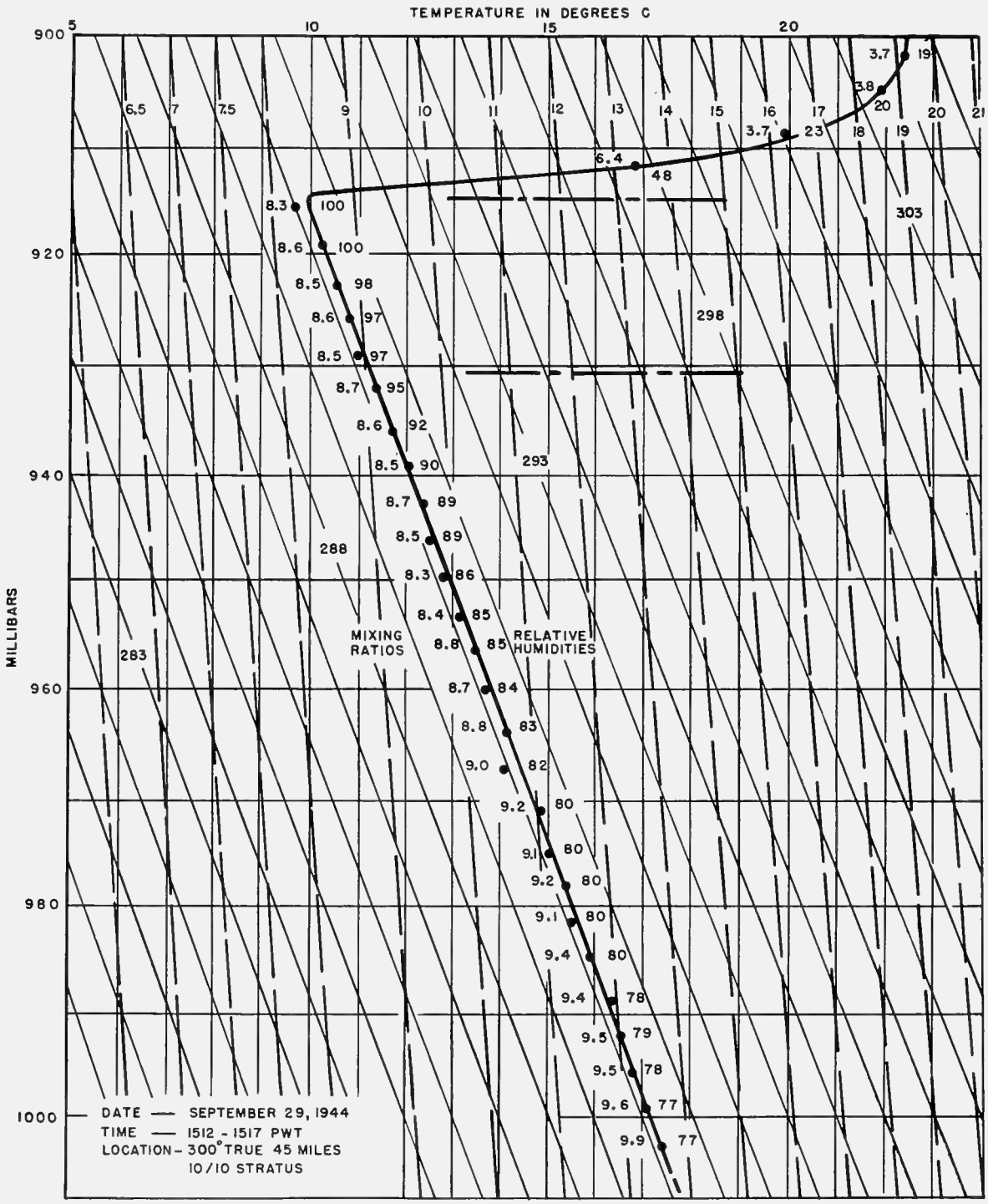

FIGURE 5. Structure of a moderately high inversion near San Diego.

sidence. Consequently the depth of this marine structure is diminished by the lowering of the base of the inversion.

Figure 5 shows the typical structure of a moderately high inversion. Usually the lapse rate of temperature below the base approaches, and in some cases exceeds, the dry adiabatic condition. This vertical mixing insures a homogeneous air mass characterized by the constant vapor pressure in the marine stratum.

Figure 6 shows the typical elevated S type M curve for this condition.

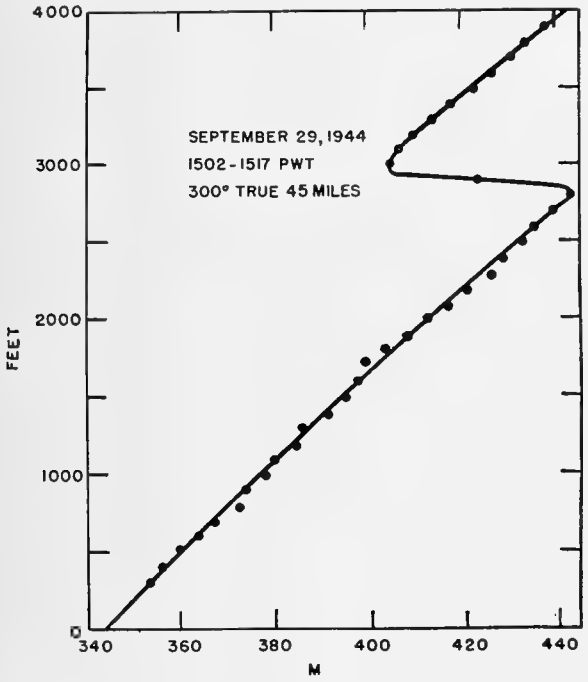

FIGURE 6. M curve corresponding to the inversion shown in Figure 5.

The discontinuity surface between the two distinct air masses exists over a large area. Soundings have been confined within a 130-mile radius of the laboratory, but observations on an FC radar indicate trapping conditions existing between San Diego and Guadalupe Island 225 miles to the southwest.

6.4.3 Shape of the Inversion Surface

Emphasis must be placed on the fact that the discontinuity surface is not horizontal over the area but is at any time a warped surface. Figure 7 shows a series of M curves taken by airplane to the seaward of the laboratory. Both the height of the inversion and gradients in the transitional layer vary greatly

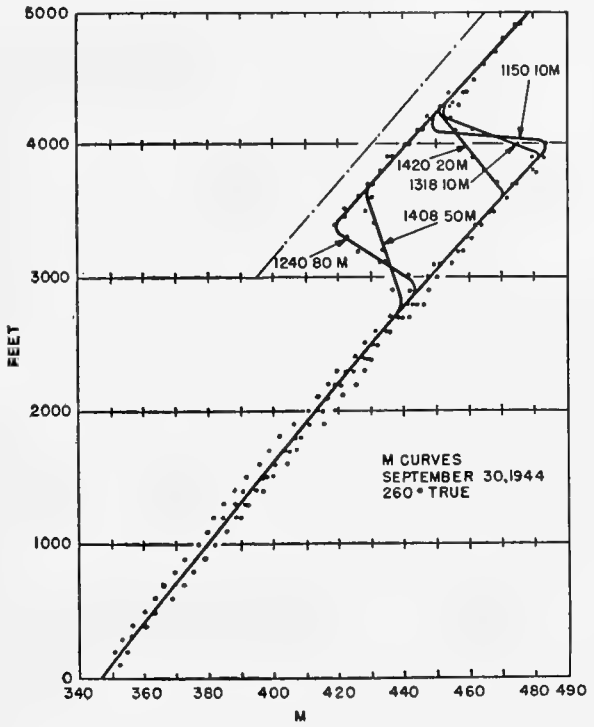

FIGURE 7. M curves at different distances and times.

with distance. Repeated soundings indicate that the apparent slope is not due to large scale lowering during the time interval between observations. The cluster of M values along the mean lapse rate of M in the upper and lower strata indicates the homogeneity of the two air masses along the vector. The possibility of the coexistence of elevated and surface gradients has been considered. No significant surface discontinuities have been detected.

There is a general tendency for the base of the inversion along the shore to have a maximum height at 0800 and a minimum at 1600. Through the exchange of meteorological data between the University of California at Los Angeles and the laboratory this fact is now fairly well established.

Figure 8 is a plot of refractive index from a series of plane soundings. The diagonal lines show the height and distance from the base at which measurements were made. Each line is marked with the time of beginning and ending the flight. The numbers at the ends of the curves are the refractive index $(n-1)$ multiplied by 10^6. The indices are independent of frequency for this range. Again it is noted that conditions vary along the vector.

Figure 9 is a plot of refractive index taken by airplane along the San Diego-San Pedro path, indicat-

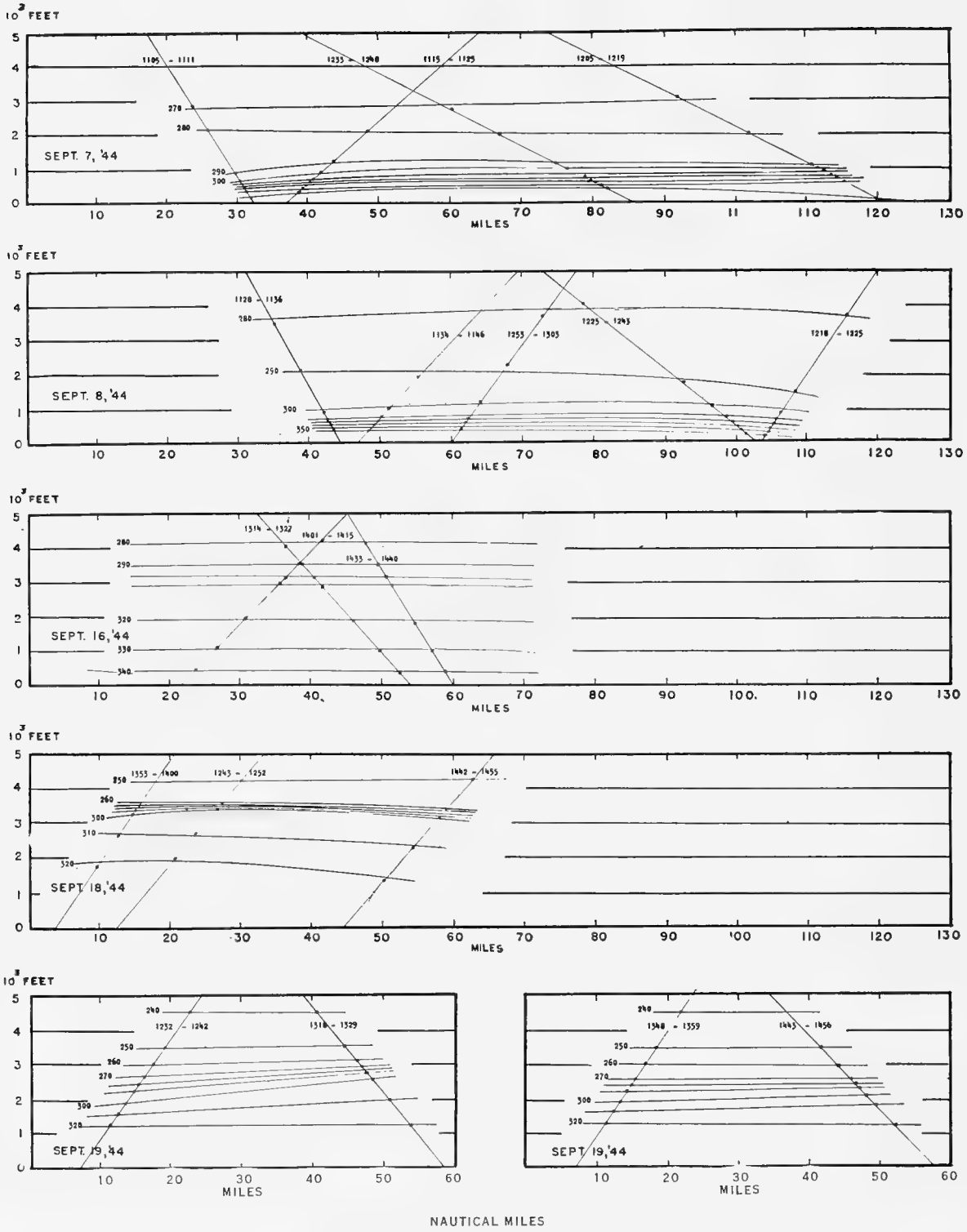

FIGURE 8. Isopleths—refractive index $[(n-1)10^6]$.

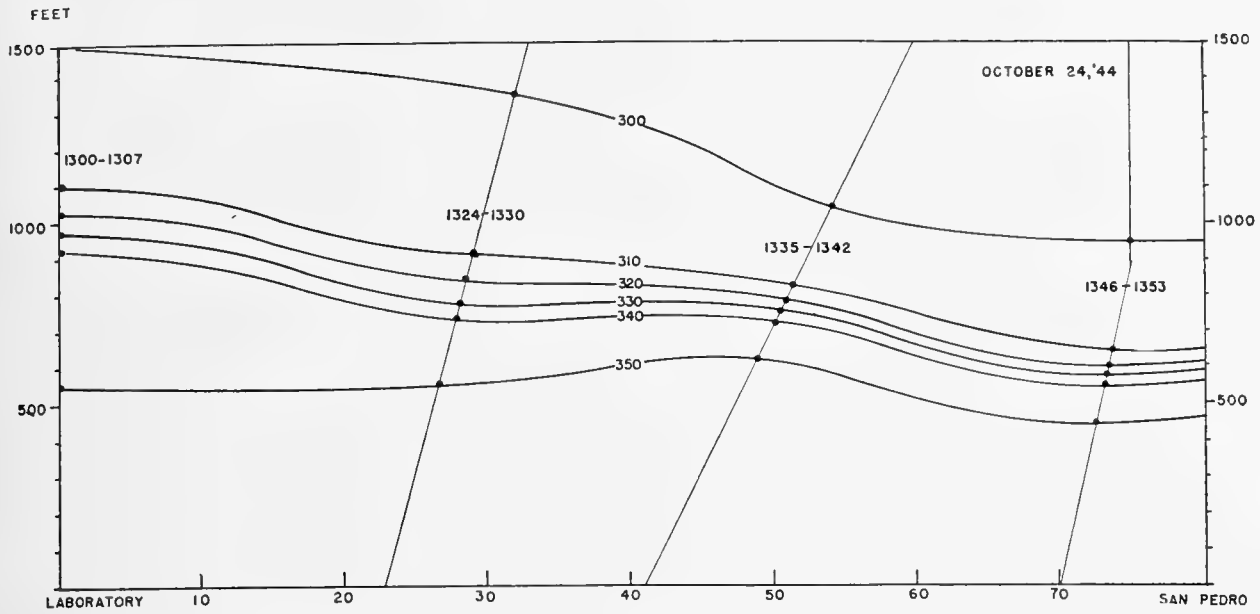

FIGURE 9. Curves of constant refractive index along the San Diego to San Pedro path.

ing the magnitude and height of the strong gradients along the path. The time interval of each sounding is shown on the appropriate section.

Again it must be emphasized that the discontinuity takes the shape of a warped surface, that the gradients vary from point to point, and that the maximum air density change occurs in the region of maximum refractive index gradient. Interface waves in the density discontinuity are possibly superimposed on the already nonuniform structure. These small interface waves are evident by the undulations on the top surface of the stratus cloud deck. The top surface of the cloud deck, which is often present, marks the air mass boundary and is thus a good indicator of the base of the inversion.

It is therefore evident that meteorological observations required for a thorough study of propagation conditions must be as extensive as possible.

6.5 TABLES FOR COMPUTING THE MODIFIED INDEX OF REFRACTION, M[1]

6.5.1 Introduction

The index of refraction of the atmosphere, modified for use on a plane-earth diagram, is a quantity of great importance in the study of radio wave propagation. It is defined by

$$M = \left[(n - 1) + \frac{h}{a}\right] 10^6, \tag{1}$$

where n = ordinary index of refraction,
h = height above sea level (not ground level),
a = radius of the earth.

The equation for n is obtained from Debye's theory of the dielectric constant of gases. In terms of atmospheric quantities, equation (1) assumes the form

$$M = \frac{Ap}{T} - \frac{De}{T} + \frac{Be}{T^2} + Ch, \tag{2}$$

where p = barometric pressure (in millibars)
(1 mm Hg = 1.333 mb),
e = water vapor pressure (mb)
(e is of order of 1% of p),
T = temperature in degrees Kelvin,
$A = 79$, $B = 3.8 \times 10^5$, $C = 0.1570$, $D = 11$,

where h, the height above sea level, is measured in meters.

The constants A, B, and D have been selected to get the best agreement with experimentally determined values of n. The constant C is 10^6 times the reciprocal of the earth's radius in meters. A more detailed explanation of this formula is given under "Constants of the Index of Refraction Formula" in Section 6.5.3.

The formula (2) may be used to calculate M when p, T, and e are known functions of height. Nomograms have been prepared to facilitate such calculations. In this paper tables are presented which permit

[1] By E. R. Wicher, Columbia University Wave Propagation Group.

these calculations to be carried out quickly and accurately. M is a number of the order of 300 to 500. Physically, the important quantity is the slope of M, i.e., dM/dh. This often calls for calculating M at fairly close height intervals, 15 m or even less. The values of M at such heights may differ by only two or three M units. Hence, to obtain even two significant figures for this quantity, the M's must be computed to four significant figures, that is, to tenths of an M unit. It is with a view to this situation that tables were computed.

These tables fall into two groups, depending upon how the moisture in the atmosphere is evaluated. In the first group (Tables 3 to 7) the moisture is given in terms of relative humidity or vapor pressure; in the second (Tables 8 to 11) the mixing ratio is used.

6.5.2 Use of Tables

The following examples explain the mechanics of using these tables. The first two examples use the first group of tables: Tables 3 to 7 inclusive. The quantities H and G which appear in these examples are auxiliary functions which are fully explained in the appendix. Examples III and IV use Tables 8 to 11.

Example I

Relative humidity and temperature given.
p_0[††] = 1,000 (p_0 is pressure at sea level).

h* meters above sea level	t°C	RH%	H[†]	$G\Delta t$[‡]	M_d[§]	M_w[‖]	M_c[¶]	M[**]
20	13	60	275.6	0.0	275.6	41.4	3.1	320.1
70	13	50	274.0	0.0	274.0	34.5	11.0	319.5
120	15	35	270.5	0.0	270.5	27.1	18.8	316.4
450	12	30	262.6	0.0	262.6	19.5	70.7	352.8
1,000	9	20	248.2	0.2	248.4	10.9	157.0	416.3
5,000	—20	20	159.0	7.0	166.0	1.2	785.0	952.2

*Columns for h (meters), t°C, and RH% give the experimentally determined data. (The heights are measured from sea level.)

†Column for H is read from Table 3.

‡$G\Delta t$ is obtained by multiplying values of G given in Table 4 by $\Delta t = t_0 - t$, where t_0 is the air temperature at ground level. Interpolation is unnecessary in this table. This correction may be omitted except where high accuracy is desired.

§M_d is the sum of H and $G\Delta t$. (If $p_0 \neq 1{,}000$ this column should be multiplied by $p_0/1{,}000$ to obtain the true M_d. This, however, is necessary only if p_0 differs appreciably from 1,000 mb, since only the difference of refractive index from its value at the ground is of importance and this difference is not sensitive to moderate changes of p_0.)

‖M_w is obtained from Table 5.

¶M_c is obtained from Table 7 or by multiplying the column for h by 0.1570.

**M is the sum of M_d, M_w and M_c.

††It should be noted that p_0 refers to the barometric pressure at sea level, not ground level. The difference in these quantities may be appreciable

Table 9, which gives pressure as a function of height and temperature, provides a simple method of calculating the sea level pressure from a measurement of the ground level pressure. For example, suppose the elevation of the ground above sea level is 100 m, the temperature is 15 C, and pressure at the ground is 993.0 mb. Table 9 shows for this height and temperature, $p/p_0 = 0.9882$. In this case, $p = 993.0$, and hence

$$p_0 = \frac{p}{0.9882} = \frac{993.0}{0.9882} = 1004.9.$$

Example II

Vapor pressure and temperature given.
$p_0 = 1{,}000$ mb at sea level.

h* meters above sea level	t	e	H[†]	$G\Delta t$[‡]	M_d[§]	f	M_w[‖]	M_c[¶]	M[**]
10	15.0	10.0	274.0	0.0	274.0	4.543	45.4	1.6	321.0
40	15.2	9.8	273.0	0.0	273.0	4.537	44.5	6.3	323.8
75	15.5	9.6	271.5	0.0	271.5	4.527	43.5	11.8	326.8
150	16.0	9.2	268.6	0.0	268.6	4.511	41.5	23.6	333.7
300	15.0	9.0	264.7	0.0	264.7	4.543	40.9	47.1	352.7
1,000	10.0	7.0	247.4	0.3	247.4	4.706	32.9	157.0	437.3

*Columns for h, t, and e are the given data. (The heights are measured from sea level.)

†Column for H is read from Table 3.

‡$G\Delta t$ is obtained by multiplying values of G given in Table 4 by $\Delta t = t_0 - t$, where t_0 = temperature at ground level. Interpolation is unnecessary in this table.

§M_d is the sum of H and $G\Delta t$. [If $p_0 \neq 1{,}000$ this column should be multiplied by $p_0/1{,}000$ to obtain the true M_d. This correction may usually be omitted (see Note §, Example I).]

‖M_w is obtained by taking the product of f, given in Table 6, by e. A slide rule gives sufficiently close results here.

¶M_c is obtained from Table 7 or by multiplying the column for h by 0.1570.

**M is the sum of M_d, M_w, and M_c.

Example III

Mixing ratio w and temperature given.
$p_0 = 1{,}000$ mb at sea level.

h* meters above sea level	t	w	F[†]	p/p_0[‡]	$(p/p_0)F$[§]	M_c[‖]	M[¶]
20	15	9	339.0	0.9976	338.2	3.1	341.3
40	16	8	330.6	0.9953	329.0	6.3	335.3
100	17	7	322.2	0.9882	318.4	15.7	334.1
150	17	7	322.2	0.9824	316.5	23.6	340.1
300	14	6	319.0	0.9650	307.8	47.1	354.9
500	11	4	307.9	0.9420	290.0	78.5	368.5

* Columns for h, t, and w are the assumed data. w is expressed in grams of water vapor per kg dry air.

† F is read directly from Table 8.

‡ p is read from Table 9. In this table $\bar{t}$ means average temperature between ground and height h.

(If $p_0 \neq 1{,}000$ this result should be multiplied by $p_0/1{,}000$. This step may usually be omitted.)

§ $(p/p_0)F$ is the product of the two previous columns.

‖ M_c may be obtained from Table 7 or by multiplication of h by C=0.1570.

¶ M is the sum of $(p/p_0)F$ and M_c.

Example IV

Mixing ratio and temperature given. Simplified method satisfactory for $h \leq 500$ m.**

h* meters above sea level	t	w	F†	u‡	$\frac{h\Delta u}{100}$§	$(n-1)10^6$‖	M_c¶	M
20	15	9	339.0	0.9	0.0	338.1	3.1	341.2
40	16	8	330.6	1.7	0.1	329.0	6.3	335.3
100	17	7	322.2	4.0	0.2	318.4	15.7	334.1
150	17	7	322.2	6.0	0.3	316.5	23.6	340.1
300	14	6	319.0	11.8	0.6	307.8	47.1	354.9
500	11	4	307.9	18.7	1.0	290.2	78.5	368.7

* Columns for h, t, and w are the assumed data. These data are the same as in Example III.

† F is read from Table 8, as before.

‡ u is read from Table 10.

§ Δu is read from Table 11. Δu is then to be multiplied by $h/100$ to give the column $h\Delta u/100$. $\bar{t}$ is the average centigrade temperature from ground to h.

‖ The column $(n-1)10^6$ is given by $F - u + h\Delta u/100$. If the average temperature t is negative, this column is $F - u - (h\Delta u/100)$.

¶ M_c is obtained, as before, from Table 7. M is the sum of $(n-1)10^6$ and M_c.

** This method is not accurate above 500 m. It will be noted, by comparing the results here with those of Example III, that there are occasional differences of 0.1 M units. This is due to rounding off and is not significant.

6.5.3 Procedure Used in Setting up Tables

TABLES 3 TO 7 — RELATIVE HUMIDITY AND TEMPERATURE GIVEN

Equation 2 may be written

$$M = M_d + M_w + M_c, \tag{3}$$

where

$$M_d = \frac{Ap}{T}, \tag{4}$$

$$M_w = fe, \tag{5}$$

$$M_c = Ch, \tag{6}$$

with

$$f = \frac{B}{T^2} - \frac{D}{T}. \tag{7}$$

Tables have been prepared which give the quantities M_d (dry term), M_w (wet term), and M_c (curvature term) separately.

Dry Term. Since equation (4) contains the pressure p, which is not usually measured as a function of height, it is necessary to eliminate direct consideration of p. For this purpose a simplification of the elaborate formula used in the Smithsonian tables for calculating height as a function of pressure is sufficient. This simplification neglects very small pressure effects caused by humidity variations and the change of the acceleration of gravity with height. This problem is discussed more fully in the section on pressure versus height, below. The pressure may then be written

$$p = p_0 \epsilon^{-\alpha h/\bar{T}}, \tag{8}$$

where

p_0 = barometric pressure at sea level,
ϵ = natural logarithmic base,
$\alpha = 0.034163$,

and

$$\bar{T} = \frac{1}{h}\int_0^h T(h)dh. \tag{9}$$

$\bar{T}$ is thus the average temperature from $h = 0$ to the height h. Strictly, $\bar{T}$ should be calculated from equation (9). However, it turns out that p is rather insensitive to $\bar{T}$, and that, except perhaps where high accuracy is desired, it is sufficient to replace equation (9) with

$$\bar{T} = T + \frac{\Delta T}{2}, \tag{10}$$

where $\Delta T = T_0 - T$ and T_0 is the temperature at the surface.

By substituting from equations (8) and (10), equation (4) assumes the form

$$M_d = \frac{Ap_0}{T}\epsilon^{-\alpha h/(T + \Delta T/2)}.$$

For all practical cases,

$$\frac{\Delta T}{2T} \ll 1$$

and hence,

$$M_d = \frac{Ap_0}{T}\epsilon^{-(\alpha h/T)[1-(\Delta T/2T)]}$$

$$= \frac{Ap_0}{T}\epsilon^{-\alpha h/T} \cdot \epsilon^{+(\alpha h \Delta T/2T^2)}.$$

Even at heights as great as 10^4 m it can be seen that the second of these exponentials can be replaced by the first two terms of its expansion. Therefore

$$M_d = \frac{Ap_0}{T}\epsilon^{-\alpha h/T} + \frac{Ap_0 \alpha h}{2T^3}\epsilon^{-\alpha h/T} \cdot \Delta T,$$

or

$$M_d = H(T,h) + G(T,h)\,\Delta T, \tag{11}$$

where

$$H(T,h) = \frac{Ap_0}{T}\epsilon^{-\alpha h/T}$$

and

$$G(T,h) = \frac{Ap_0}{2T^3}\alpha h \epsilon^{-\alpha h/T}. \tag{12}$$

Table 3 gives the quantity $H(T,h)$ as a function of h and t, where

$$t = T - 273$$

is the standard centigrade temperature. In this table, it is assumed that $p_0 = 1{,}000$ mb.

Table 4 gives $G(T,h)$. The term $G\Delta t$ in equation (11) is very small at altitudes less than 500 m and for this range of altitudes may be safely neglected.

Since it is assumed in these tables that $p_0 = 1{,}000$, the value of M_d read from the tables should be multiplied by $p_0/1{,}000$, where p_0 is the actual air pressure at sea level. This step may, however, be eliminated in most cases, particularly as the physically important quantity is not M but differences in M at various heights.

Wet Term. Since

$$e = (\mathrm{RH})e'$$

where RH = relative humidity,

e' = saturation vapor pressure,

and since e' is a function of temperature only, it is possible to prepare a table giving M_w as a function of RH and t. This is Table 5.

A table for f, defined by equation (7), is also included, so that if e is known, M_w can be obtained by simply taking the product fe as indicated by equation (5). Table 6 gives the values of f.

Curvature Term. Table 7 gives the values of the linear term $h/a \times 10^6$, which must be added to obtain the index of refraction modified for use on a "plane earth" diagram.

Error. The discussion of this first group of tables is concluded with some observations on their order of accuracy. Theoretically any errors which arise are due to the expansions used in calculating M_d. At a height as great as 10,000 m, Δt might be, say, 70°. This would give $G\Delta T = 13.3$ for $t = 0$. If the next term had been included the correction would have been only a fraction of this amount. Since at these heights M—1,800, we are safe in saying that the relative error is less than 0.5 per cent, probably much less than this amount. At altitudes of 1,000 m or less the approximation introduces errors too small to be reflected in the fourth significant figure.

Aside from this theoretical error, there are errors in the table due to rounding off in the numerical work. An effort was made to keep this error less than 0.1 M units.

Tables 8 to 11 — Mixing Ratio and Temperature Given

In terms of atmospheric pressure and water vapor pressure, the mixing ratio w is given by

$$w = \frac{623e}{p - e}. \tag{13}$$

Since w involves the pressure p, the scheme used in the first group of tables must be modified. Using equation (13), equation (2) assumes the form

$$M = \frac{p}{p_0} F(T, w) + Ch, \tag{14}$$

where

$$F(T, w) = p_0 \frac{A}{T} + \frac{w}{w + 623}\left(\frac{B}{T^2} - \frac{D}{T}\right). \tag{15}$$

Table 8 gives F for the range of usable values of temperature and mixing ratio. Since F is sensitive to variations in both T and w, the tabulation is made for all integral values of both T and w to avoid laborious interpolation.

Following the procedure used in the discussion of dry term in Section 6.5.3, the pressure p is calculated from equation (8). These results are given in Table 9. In view of the insensitivity of p to $\overline{T}$, the average temperature, it is unnecessary to tabulate p for all values of $\overline{T}$; it is sufficient to tabulate p at 5-degree intervals of $\overline{T}$.

The term Ch has been calculated in connection with the first group of tables and is given in Table 7.

Tables 10 and 11 for Use at Low Altitudes

An objectionable feature of the method given in the preceding section is that it involves taking the product, pF, which makes an application of the tables rather slow. The following method circumvents this difficulty for heights less than 500 m. From equations (1), (8), and (15)

$$(n - 1)\,10^6 = F\epsilon^{-\alpha h/T}. \tag{16}$$

For altitudes of less than 500 m it is safe to suppose that

$$\frac{\alpha h}{\overline{T}} = \frac{\alpha h}{273}\left(1 - \frac{\bar{t}}{273}\right),$$

where $\bar{t}$ is the average centigrade temperature, and that

$$\epsilon^{-\alpha h/\overline{T}} = \epsilon^{-\alpha h/273} \cdot \epsilon^{+\alpha h\bar{t}/(273)^2} = \epsilon^{-\alpha h/273} + \frac{\alpha h\bar{t}}{(273)^2}\epsilon^{-\alpha h/273}. \tag{17}$$

Hence

$$(n - 1)10^6 = F - u + \frac{h\Delta u}{100}, \tag{18}$$

where

$$u = F(1 - \epsilon^{-\alpha h/273}), \tag{19}$$

and

$$\Delta u = \frac{\alpha F\bar{t}}{(273)^2}. \tag{20}$$

Equation (19) is evaluated in Table 10.

Equation (20) is a small correction which must be taken into account when t, the average temperature, differs appreciably from zero. Since this term contributes only 1 per cent to the refractive index in the extreme case of $h = 500$ m, $\overline{t} = 40$, it is sufficient to replace the exponential by its value at the middle of the height range. This approximation does not lead to an error of more than 0.1 M units at these low altitudes.

Pressure versus Height

The differential equation connecting height with pressure may be written

$$\frac{dp}{p} = -\frac{g}{R}\frac{dh}{\overline{T}}, \tag{21}$$

where g = acceleration of gravity,
R = gas constant for air.

Since g is not strictly constant (it varies slightly with height and locality) and since R, to a slight extent, is dependent on the percentage of water vapor in the air and, finally, since T may be an arbitrary function of height, this differential equation cannot be integrated exactly. However, a careful consideration of the order of magnitude of changes in the pressure brought about by the slight changes of g and R leads to the conclusion that such variations may be neglected, particularly as these changes have practically no effect on the slopes of M curves. Picking the best overall values of g and R ($g = 9.80665$ and $R = 287.05$ in the units used in this report) gives $\alpha = g/R = 0.034163$ as the value to be used in equation (8).

The variation of temperature with height cannot, however, be neglected in the integration of equation (21). The integrated form of equation (21) is equation (8), where the approximation

$$\int_0^h \frac{dh}{T} = \frac{h}{\overline{T}} \tag{22}$$

has been made. $\overline{T}$ is the average temperature defined by equation (9) or, more roughly, by equation (10).

An estimate of the order of accuracy of this approximation may be obtained from an examination of the case in which T varies *linearly* with h. Let the reference level temperature be T_0 at $h = 0$ and the temperature at the height h_1 be T_1. Then

$$\frac{h_1}{\overline{T}} = \frac{2h_1}{T_0 + T_1} \tag{23}$$

and, for this linear case

$$\int_0^{h_1} \frac{dh}{T} = \frac{h_1}{T_1 - T_0}\log\frac{T_1}{T_0} = \frac{2h_1}{T_1 - T_0}\left[\frac{T_1 - T_0}{T_1 + T_0} + \frac{1}{3}\left(\frac{T_1 - T_0}{T_1 + T_0}\right)^3 + \cdots\right] \tag{24}$$

by a well-known expansion for the natural logarithm. The first term in the series (24) gives exactly equation (23). Hence, the approximation (22) amounts to dropping the higher-order terms in equation (24). The ratio of the second term to the first is only $\frac{1}{3}[(T_1 - T_0)/(T_1 + T_0)]^2$ or about two parts in 10,000 for the first 2,000 m of the standard atmosphere. This comes out to give an error of about 0.006 mb in the pressure at this height. This is certainly negligible.

For a nonlinear atmosphere the question of the error in equation (22) is chiefly a question of the accuracy in determining T, since any such atmosphere can be broken up into a number of layers in each of which T is linear in h.

Constants of the Index of Refraction Formula

The formula for the ordinary index of refraction, n, which has been used in calculating these tables, is

$$(n - 1)\,10^6 = \frac{Ap}{T} - \frac{De}{T} + \frac{Be}{T^2}, \tag{25}$$

where $A = 79$, $D = 11$, $B = 3.8 \times 10^5$. (26)

The formula given in reference 11, in the units adopted here, is the same as (25) but with

$$A = 78.7, D = 11.2, B = 3.77 \times 10^5. \tag{27}$$

The formula used by Bell Telephone Laboratories (Monograph B-870, 1935) is also (25) but with

$$A = 79.1, D = 10.9, B = 3.81 \times 10^5. \tag{28}$$

The third significant figure in all these constants is questionable. Moreover, the absolute value of n (or M) is not important but only the slopes of M curves. For this purpose it is sufficient if the right form of equation and approximately correct values of the constants are chosen. Hence, in these tables, equations (25) and (26) were adopted.

TABLE 3A. H for t from −30 C (−22 F) to −20 C (−4 F); h to 2,000 m (6,562 ft).
p_0 = 1,000 mb at sea level

h (m) ↓ \ t C →	−30	−29	−28	−27	−26	−25	−24	−23	−22	−21	−20	h (ft)
0	325.1	323.8	322.4	321.1	319.8	318.5	317.3	316.0	314.7	313.5	312.3	0.0
10	324.6	323.3	322.0	320.7	319.4	318.1	316.9	315.6	314.3	313.1	311.9	32.8
20	324.2	322.9	321.5	320.3	319.0	317.7	316.5	315.2	313.9	312.7	311.5	65.6
30	323.7	322.4	321.1	319.8	318.5	317.2	316.0	314.7	313.5	312.2	311.0	98.4
40	323.3	322.0	320.6	319.4	318.1	316.8	315.6	314.3	313.1	311.8	310.6	131.2
50	322.8	321.5	320.2	319.0	317.7	316.4	315.2	313.9	312.7	311.4	310.2	164.0
75	321.7	320.4	319.1	317.9	316.6	315.3	314.1	312.9	311.6	310.4	309.2	248.1
100	320.6	319.3	318.0	316.8	315.5	314.2	313.0	311.8	310.5	309.3	308.1	328.1
150	318.3	317.0	315.8	314.5	313.3	312.0	310.8	309.6	308.4	307.2	306.0	492.1
200	316.1	314.9	313.6	312.4	311.1	309.9	308.7	307.5	306.3	305.1	303.9	656.2
250	313.9	312.7	311.5	310.2	309.0	307.8	306.6	305.4	304.3	303.1	301.9	820.2
300	311.7	310.5	309.3	308.0	306.8	305.6	304.5	303.3	302.2	301.0	299.9	984.3
350	309.5	308.3	307.1	305.9	304.7	303.5	302.4	301.2	300.1	298.9	297.8	1,148.0
400	307.3	306.1	305.0	303.8	302.7	301.5	300.4	299.2	298.1	296.9	295.8	1,312.0
450	305.2	304.0	302.9	301.7	300.6	299.4	298.3	297.2	296.0	294.9	293.8	1,476.0
500	303.0	301.9	300.7	299.6	298.4	297.3	296.2	295.1	294.1	293.0	291.9	1,640.0
600	298.8	297.7	296.6	295.5	294.4	293.3	292.2	291.2	290.1	289.1	288.0	1,969.0
700	294.6	293.5	292.5	291.4	290.4	289.3	288.3	287.2	286.2	285.1	284.1	2,297.0
800	290.5	289.5	288.4	287.4	286.3	285.3	284.3	283.3	282.3	281.3	280.3	2,625.0
900	286.5	285.5	284.5	283.4	282.4	281.4	280.4	279.4	278.5	277.5	276.5	2,953.0
1,000	282.5	281.5	280.5	279.5	278.5	277.5	276.6	275.6	274.7	273.7	272.8	3,281.0
1,500	263.3	262.5	261.6	260.8	259.9	259.1	258.3	257.5	256.6	255.8	255.0	4,921.0
2,000	245.4	244.7	244.0	243.2	242.5	241.8	241.1	240.4	239.7	239.0	238.3	6,562.0
t F → \ h (ft)	−22.0	−20.2	−18.4	−16.6	−14.8	−13.0	−11.2	−9.40	−7.60	−5.80	−4.00	h (ft)

TABLE 3B. H for t from −20 C (−4 F) to −10 C (+14 F); h to 2,000 m (6,562 ft).
p_0 = 1,000 mb at sea level

h (m) ↓ \ t C →	−20	−19	−18	−17	−16	−15	−14	−13	−12	−11	−10	h (ft)
0	312.3	311.0	309.8	308.6	307.4	306.2	305.0	303.8	302.7	301.5	300.4	0.0
10	311.9	310.6	309.4	308.2	307.0	305.8	304.6	303.4	302.3	301.1	300.0	32.8
20	311.5	310.2	309.0	307.8	306.6	305.4	304.2	303.0	301.9	300.7	299.6	65.6
30	311.0	309.8	308.6	307.4	306.2	305.0	303.8	302.7	301.5	300.4	299.2	98.4
40	310.6	309.4	308.2	307.0	305.8	304.6	303.4	302.3	301.1	300.0	298.8	131.2
50	310.2	309.0	307.8	306.6	305.4	304.2	303.0	301.9	300.7	299.6	298.4	164.0
75	309.2	308.0	306.8	305.6	304.4	303.2	302.1	300.9	299.8	298.6	295.5	248.1
100	308.1	306.9	305.7	304.6	303.4	302.2	301.1	299.9	298.8	297.6	296.5	328.1
150	306.0	304.8	303.6	302.5	301.3	300.1	299.0	297.9	296.8	295.7	294.6	492.1
200	303.9	302.8	301.6	300.5	299.3	298.2	297.1	296.0	294.9	293.8	292.7	656.2
250	301.9	300.8	299.6	298.5	297.3	296.2	295.1	294.0	293.0	291.9	290.8	820.2
300	299.9	298.8	297.7	296.5	295.4	294.3	293.2	292.1	291.1	290.0	288.9	984.3
350	297.8	296.7	295.6	294.5	293.4	292.3	291.2	290.2	289.1	288.1	287.0	1,148.0
400	295.8	294.7	293.6	292.6	291.5	290.4	289.4	288.3	287.3	286.2	285.2	1,312.0
450	293.8	292.7	291.7	290.6	289.6	288.5	287.5	286.4	285.4	284.3	283.3	1,476.0
500	291.9	290.8	289.8	288.7	287.7	286.6	285.6	284.6	283.5	282.5	281.5	1,640.0
600	288.0	287.0	285.9	284.9	283.8	282.8	281.8	280.8	279.9	278.9	277.9	1,969.0
700	284.1	283.1	282.1	281.1	280.1	279.1	278.1	277.2	276.2	275.3	274.3	2,297.0
800	280.3	279.3	278.3	277.4	276.4	275.4	274.5	273.5	272.6	271.6	270.7	2,625.0
900	276.5	275.5	274.6	273.7	272.7	271.8	270.9	270.0	269.0	268.1	267.2	2,953.0
1,000	272.8	271.9	271.0	270.0	269.1	268.2	267.3	266.4	265.6	264.7	263.8	3,281.0
1,500	255.0	254.2	253.4	252.6	251.8	251.0	250.2	249.5	248.7	248.0	247.2	4,921.0
2,000	238.3	237.6	237.0	236.3	235.7	235.0	234.3	233.7	233.0	232.4	231.7	6,562.0
t F → \ h (ft)	−4.00	−2.20	−0.40	+1.40	+3.20	+5.00	+6.80	+8.60	+10.4	+12.2	+14.00	h (ft)

TABLE 3C. H for t from −10 C (+14 F) to 0 C (32 F); h to 2,000 m (6,562 ft).

p_0 = 1,000 mb at sea level

h (m) ↓ / t C →	−10	−9	−8	−7	−6	−5	−4	−3	−2	−1	±0	h (ft)
0	300.4	299.2	298.1	297.0	295.9	294.8	293.7	292.6	291.5	290.4	289.4	0.0
10	300.0	298.8	297.7	296.6	295.5	294.4	293.3	292.2	291.1	290.1	289.0	32.8
20	299.6	298.4	297.3	296.2	295.1	294.0	292.9	291.9	290.8	289.7	288.7	65.6
30	299.2	298.1	297.0	295.9	294.8	293.7	292.6	291.5	290.4	289.4	288.3	98.4
40	298.8	297.7	296.6	295.5	294.4	293.3	292.2	291.2	290.1	289.0	288.0	131.2
50	298.4	297.3	296.2	295.1	294.0	292.9	291.8	290.8	289.7	288.7	287.6	164.0
75	295.5	296.3	295.2	294.1	293.0	291.9	290.8	289.8	288.7	287.7	286.6	248.1
100	296.5	295.4	294.3	293.3	292.2	291.1	290.0	289.0	287.9	286.9	285.8	328.1
150	294.6	293.5	292.4	291.4	290.3	289.2	288.2	287.1	286.1	285.0	284.0	492.1
200	292.7	291.6	290.5	289.5	288.4	287.3	286.3	285.3	284.2	283.2	282.2	656.2
250	290.8	289.7	288.7	287.6	286.6	285.5	284.5	283.5	282.5	281.5	280.5	820.2
300	288.9	287.9	286.8	285.8	284.7	283.7	282.7	281.7	280.7	279.7	278.7	984.3
350	287.0	286.0	285.0	283.9	282.9	281.9	280.9	279.9	279.0	278.0	277.0	1,148.0
400	285.2	284.2	283.2	282.1	281.1	280.1	279.1	278.2	277.2	276.3	275.3	1,312.0
450	283.3	282.3	281.3	280.3	279.3	278.3	277.3	276.4	275.4	274.5	273.5	1,476.0
500	281.5	280.5	279.5	278.6	277.6	276.6	275.6	274.7	273.7	272.8	271.8	1,640.0
600	277.9	276.9	276.0	275.0	274.1	273.1	272.2	271.3	270.3	269.4	268.5	1,969.0
700	274.3	273.4	272.4	271.5	270.5	269.6	268.7	267.8	266.9	266.0	265.1	2,297.0
800	270.7	269.8	268.9	268.0	267.1	266.2	265.3	264.4	263.6	262.7	261.8	2,625.0
900	267.2	266.3	265.4	264.6	263.7	262.8	262.0	261.1	260.3	259.4	258.6	2,953.0
1,000	263.8	262.9	262.1	261.2	260.4	259.5	258.7	257.8	257.0	256.1	255.3	3,281.0
1,500	247.2	246.5	245.7	245.0	244.2	243.5	242.8	242.1	241.3	240.6	239.9	4,921.0
2,000	231.7	231.0	230.4	229.7	229.1	228.4	227.8	227.2	226.5	225.9	225.3	6,562.0
	14.0	15.8	17.6	19.4	21.2	23.0	24.8	26.6	28.4	30.2	32.0	h (ft) / t F

TABLE 3D. H for t from 0 C (32 F) to 10 C (50 F); h to 2,000 m (6,562 ft).

p_0 = 1,000 mb at sea level

h (m) ↓ / t C →	±0	1	2	3	4	5	6	7	8	9	10	h (ft)
0	289.4	288.3	287.3	286.2	285.2	284.2	283.2	282.1	281.1	280.1	279.2	0.0
10	289.0	288.0	286.9	285.9	284.8	283.8	282.8	281.8	280.8	279.8	278.9	32.8
20	288.7	287.6	286.6	285.5	284.5	283.5	282.5	281.4	280.5	279.5	278.5	65.6
30	288.3	287.3	286.2	285.2	284.1	283.1	282.1	281.1	280.1	279.1	278.2	98.4
40	288.0	286.9	285.9	284.8	283.8	282.8	281.8	280.7	279.8	278.8	277.8	131.2
50	287.6	286.6	285.5	284.5	283.4	282.4	281.4	280.4	279.5	278.5	277.5	164.0
75	286.6	285.7	284.7	283.6	282.6	281.6	280.6	279.6	278.7	277.7	276.7	248.1
100	285.8	284.8	283.8	282.7	281.7	280.7	279.7	278.7	277.8	276.8	275.8	328.1
150	284.0	283.0	282.0	281.0	280.0	279.0	278.0	277.1	276.1	275.2	274.2	492.1
200	282.2	281.2	280.2	279.3	278.3	277.3	276.3	275.4	274.4	273.5	272.5	656.2
250	280.5	279.5	278.5	277.6	276.6	275.6	274.7	273.7	272.8	271.8	270.9	820.2
300	278.7	277.7	276.8	275.8	274.9	273.9	273.0	272.0	271.1	270.1	269.2	984.3
350	277.0	276.0	275.1	274.1	273.2	272.2	271.3	270.4	269.4	268.5	267.6	1,148.0
400	275.3	274.3	273.4	272.4	271.5	270.5	269.6	268.7	267.8	266.9	266.0	1,312.0
450	273.5	272.6	271.7	270.7	269.8	268.9	268.0	267.1	266.2	265.3	264.4	1,476.0
500	271.8	270.9	270.0	269.0	268.1	267.2	266.3	265.4	264.6	263.7	262.8	1,640.0
600	268.5	267.6	266.7	265.8	264.9	264.0	263.1	262.2	261.4	260.5	259.6	1,969.0
700	265.1	264.2	263.4	262.5	261.7	260.8	259.9	259.1	258.2	257.4	256.5	2,297.0
800	261.8	260.9	260.1	259.2	258.4	257.5	256.7	255.9	255.0	254.2	253.4	2,625.0
900	258.6	257.8	256.9	256.1	255.2	254.4	253.6	252.8	252.0	251.2	250.4	2,953.0
1,000	255.3	254.5	253.7	252.9	252.1	251.3	250.5	249.7	249.0	248.2	247.4	3,281.0
1,500	239.9	239.2	238.5	237.7	237.0	236.3	235.6	234.9	234.3	233.6	232.9	4,921.0
2,000	225.3	224.7	224.1	223.5	222.9	222.3	221.7	221.1	220.5	219.9	219.3	6,562.0
	32.0	33.8	35.6	37.4	39.2	41.0	42.8	44.6	46.4	48.2	50.0	h (ft) / t F

TABLE 3E. H for t from 10 C (50 F) to 20 C (68 F); h to 2,000 m (6,562 ft).

p_0 = 1,000 mb at sea level

h (m) \ t C →	10	11	12	13	14	15	16	17	18	19	20	h (ft)
↓ 0	279.2	278.2	277.2	276.2	275.3	274.3	273.4	272.4	271.5	270.5	269.6	0.0
10	278.9	277.9	276.9	275.9	274.9	274.0	273.1	272.1	271.2	270.2	269.3	32.8
20	278.5	277.5	276.6	275.6	274.6	273.7	272.8	271.8	270.9	269.9	269.0	65.6
30	278.2	277.2	276.2	275.2	274.3	273.3	272.4	271.5	270.5	269.6	268.7	98.4
40	277.8	276.8	275.9	274.9	274.0	273.0	272.1	271.2	270.2	269.3	268.4	131.2
50	277.5	276.5	275.6	274.6	273.7	272.7	271.8	270.9	269.9	269.0	268.1	164.0
75	276.7	275.7	274.8	273.8	272.8	271.9	271.0	270.1	269.1	268.2	267.3	248.1
100	275.8	274.9	273.9	273.0	272.0	271.1	270.2	269.3	268.3	267.4	266.5	328.1
150	274.2	273.3	272.3	271.4	270.4	269.5	268.6	267.7	266.8	265.9	265.0	492.1
200	272.5	271.6	270.7	269.7	268.8	267.9	267.0	266.1	265.2	264.3	263.4	656.2
250	270.9	270.0	269.1	268.1	267.2	266.3	265.4	264.5	263.7	262.8	261.9	820.2
300	269.2	268.3	267.4	266.5	265.6	264.7	263.8	262.9	262.1	261.2	260.3	984.3
350	267.6	266.7	265.8	264.9	264.0	263.1	262.2	261.4	260.5	259.7	258.8	1,148.0
400	266.0	265.1	264.2	263.4	262.5	261.6	260.7	259.9	259.0	258.2	257.3	1,312.0
450	264.4	263.5	262.6	261.8	260.9	260.0	259.2	258.3	257.5	256.6	255.8	1,476.0
500	262.8	261.9	261.1	260.2	259.4	258.5	257.7	256.9	256.0	255.2	254.4	1,640.0
600	259.6	258.8	258.0	257.1	256.3	255.5	254.7	253.9	253.0	252.2	251.4	1,969.0
700	256.5	255.7	254.9	254.0	253.2	252.4	251.6	250.8	250.1	249.3	248.5	2,297.0
800	253.4	252.6	251.8	251.1	250.3	249.5	248.7	247.9	247.2	246.4	245.6	2,625.0
900	250.4	249.6	248.8	248.1	247.3	246.5	245.8	245.0	244.3	243.5	242.8	2,953.0
1,000	247.4	246.6	245.9	245.1	244.4	243.6	242.9	242.1	241.4	240.6	239.9	3,281.0
1,500	232.9	232.2	231.6	230.9	230.3	229.6	228.9	228.3	227.6	227.0	226.3	4,921.0
2,000	219.3	218.7	218.1	217.6	217.0	216.4	215.8	215.2	214.7	214.1	213.5	6,562.0
	50.0	51.8	53.6	55.4	57.2	59.0	60.8	62.6	64.4	66.2	68.0	h (ft) / t F

TABLE 3F. H for t from 20 C (68 F) to 30 C (86 F); h to 2,000 m (6,562 ft).

p_0 = 1,000 mb at sea level

h (m) \ t C →	20	21	22	23	24	25	26	27	28	29	30	h (ft)
↓ 0	269.6	268.7	267.8	266.9	266.0	265.1	264.2	263.3	262.5	261.6	260.7	0.0
10	269.3	268.4	267.5	266.6	265.7	264.8	263.9	263.0	262.2	261.3	260.4	32.8
20	269.0	268.1	267.2	266.3	265.4	264.5	263.6	262.7	261.9	261.0	260.1	65.6
30	268.7	267.8	266.9	266.0	265.1	264.2	263.3	262.5	261.6	260.8	259.9	98.4
40	268.4	267.5	266.6	265.7	264.8	263.9	263.0	262.2	261.3	260.5	259.6	131.2
50	268.1	267.2	266.3	265.4	264.5	263.6	262.7	261.9	261.0	260.2	259.3	164.0
75	267.3	266.4	265.5	264.7	263.8	262.9	262.0	261.2	260.3	259.5	258.6	248.1
100	266.5	265.6	264.7	263.9	263.0	262.1	261.2	260.4	259.5	258.7	257.8	328.1
150	265.0	264.1	263.2	262.4	261.5	260.6	259.7	258.9	258.0	257.2	256.3	492.1
200	263.4	262.5	261.7	260.8	260.0	259.1	258.3	257.4	256.6	255.7	254.9	656.2
250	261.9	261.0	260.2	259.3	258.5	257.6	256.8	256.0	255.1	254.3	253.5	820.2
300	260.3	259.5	258.6	257.8	256.9	256.1	255.3	254.5	253.6	252.8	252.0	984.3
350	258.8	258.0	257.2	256.3	255.5	254.7	253.9	253.1	252.2	251.4	250.6	1,148.0
400	257.3	256.5	255.7	254.8	254.0	253.2	252.4	251.6	250.8	250.0	249.2	1,312.0
450	255.8	255.0	254.2	253.4	252.6	251.8	251.0	250.2	249.4	248.6	247.8	1,476.0
500	254.4	253.6	252.8	251.9	251.1	250.3	249.5	248.7	248.0	247.2	246.4	1,640.0
600	251.4	250.6	249.8	249.1	248.3	247.5	246.7	246.0	245.2	244.5	243.7	1,969.0
700	248.5	247.7	247.0	246.2	245.5	244.7	243.9	243.2	242.4	241.7	240.9	2,297.0
800	245.6	244.9	244.1	243.4	242.6	241.9	241.2	240.5	239.7	239.0	238.3	2,625.0
900	242.8	242.1	241.3	240.6	239.8	239.1	238.4	237.7	237.0	236.3	235.6	2,953.0
1,000	239.9	239.2	238.5	237.8	237.1	236.4	235.7	235.0	234.3	233.6	232.9	3,281.0
1,500	226.3	225.7	225.1	224.4	223.8	223.2	222.6	222.0	221.4	220.8	220.2	4,921.0
2,000	213.5	213.0	212.4	211.9	211.3	210.8	210.3	209.7	209.2	208.6	208.1	6,562.0
	86.0	87.8	89.6	91.4	93.2	95.0	96.8	98.6	100.4	102.2	104.0	h (ft) / t F

TABLE 3G. H for t from 30 C (86 F) to 40 C (104 F); h to 2,000 m (6,562 ft).

p_0 = 1,000 mb at sea level

h (m) \ t C →	30	31	32	33	34	35	36	37	38	39	40	h (ft)
↓ 0	260.7	259.9	259.0	258.2	257.5	256.5	255.7	254.8	254.0	253.2	252.4	0.0
10	260.4	259.6	258.7	257.9	257.2	256.2	255.4	254.5	253.7	252.9	252.1	32.8
20	260.1	259.3	258.4	257.6	256.9	255.9	255.1	254.3	253.4	252.6	251.8	65.6
30	259.9	259.1	258.2	257.4	256.5	255.7	254.9	254.0	253.2	252.4	251.6	98.4
40	259.6	258.8	257.9	257.1	256.2	255.4	254.6	253.8	252.9	252.1	251.3	131.2
50	259.3	258.5	257.6	256.8	255.9	255.1	254.3	253.5	252.6	251.8	251.0	164.0
75	258.6	257.7	256.9	256.0	254.2	254.4	253.6	252.8	251.9	251.1	250.3	248.1
100	257.8	257.0	256.2	255.3	254.5	253.7	252.9	252.1	251.3	250.5	249.7	328.1
150	256.3	255.5	254.7	253.9	253.1	252.3	251.5	250.7	249.9	249.1	248.3	492.1
200	254.9	254.1	253.3	252.5	251.7	250.9	250.1	249.3	248.5	247.7	246.9	656.2
250	253.5	252.7	251.9	251.1	250.3	249.5	248.7	247.9	247.2	246.4	245.6	820.2
300	252.0	251.2	250.4	249.7	248.9	248.1	247.3	246.6	245.8	245.1	244.3	984.3
350	250.6	249.8	249.0	248.3	247.5	246.7	245.9	245.2	244.4	243.7	242.9	1,148.0
400	249.2	248.4	247.7	246.9	246.2	245.4	244.6	243.9	243.1	242.4	241.6	1,312.0
450	247.8	247.0	246.3	245.5	244.8	244.0	243.3	242.5	241.8	241.0	240.3	1,476.0
500	246.4	245.6	244.9	244.1	243.4	242.6	241.9	241.2	240.4	239.7	239.0	1,640.0
600	243.7	242.9	242.2	241.4	240.7	239.9	239.2	238.5	237.8	237.1	236.4	1,969.0
700	240.9	240.2	239.5	238.7	238.0	237.3	236.6	235.9	235.2	234.5	233.8	2,297.0
800	238.3	237.6	236.9	236.1	235.4	234.7	234.0	233.3	232.7	232.0	231.3	2,625.0
900	235.6	234.9	234.2	233.5	232.8	232.1	231.4	230.8	230.1	229.5	228.8	2,953.0
1,000	232.9	232.2	231.6	230.9	230.3	229.6	228.9	228.3	227.6	227.0	226.3	3,281.0
1,500	220.2	219.6	219.0	218.4	217.8	217.2	216.6	216.0	215.5	214.9	214.3	4,921.0
2,000	208.1	207.6	207.1	206.5	206.0	205.5	205.0	204.5	203.9	203.4	202.9	6,562.0
	86.0	87.9	89.6	91.4	93.2	95.0	96.8	98.6	100.4	102.2	104.0	h (ft)
											t F	

TABLE 4. G for h from 50 m (164 ft) to 2,000 m (6,562 ft) and t from −30 C (−22 F) to 40 C (104 F).

h (m) \ t C →	−30	−25	−20	−15	−10	−5	±0	+5	+10	+15	+20	+25	+30	+35	+40	h (ft)
↓ 50	0.00$\bar{5}$	0.004	0.004	0.004	0.004	0.003	0.003	0.003	0.003	0.003	0.003	0.003	0.002	0.002	0.002	164.0
100	0.009	0.009	0.008	0.008	0.007	0.007	0.007	0.006	0.006	0.006	0.005	0.005	0.00$\bar{5}$	0.005	0.004	328.1
150	0.014	0.013	0.012	0.012	0.011	0.010	0.010	0.009	0.009	0.008	0.008	0.008	0.007	0.007	0.006	492.1
200	0.018	0.017	0.016	0.015	0.014	0.014	0.013	0.012	0.012	0.011	0.010	0.010	0.009	0.009	0.009	656.2
250	0.023	0.021	0.020	0.019	0.018	0.017	0.016	0.015	0.014	0.014	0.013	0.012	0.012	0.011	0.011	820.2
300	0.027	0.025	0.024	0.023	0.021	0.020	0.019	0.018	0.017	0.016	0.016	0.015	0.014	0.013	0.013	984.3
350	0.031	0.030	0.028	0.026	0.025	0.023	0.022	0.021	0.020	0.019	0.018	0.017	0.016	0.016	0.015	1,148.0
400	0.036	0.033	0.032	0.030	0.028	0.027	0.025	0.024	0.023	0.022	0.020	0.019	0.019	0.018	0.017	1,312.0
450	0.040	0.037	0.035	0.033	0.031	0.030	0.028	0.027	0.025	0.024	0.023	0.022	0.021	0.020	0.019	1,476.0
500	0.044	0.041	0.039	0.037	0.035	0.033	0.031	0.030	0.028	0.027	0.025	0.024	0.023	0.022	0.021	1,640.0
600	0.052	0.049	0.046	0.044	0.041	0.039	0.037	0.035	0.033	0.032	0.030	0.029	0.027	0.026	0.02$\bar{5}$	1,969.0
700	0.060	0.056	0.053	0.050	0.047	0.045	0.043	0.040	0.038	0.036	0.03$\bar{5}$	0.033	0.031	0.030	0.029	2,297.0
800	0.067	0.063	0.060	0.057	0.053	0.051	0.048	0.046	0.043	0.041	0.039	0.037	0.035	0.034	0.032	2,625.0
900	0.075	0.070	0.066	0.063	0.059	0.056	0.053	0.051	0.048	0.046	0.043	0.041	0.039	0.038	0.036	2,953.0
1,000	0.082	0.077	0.073	0.069	0.065	0.062	0.059	0.056	0.053	0.050	0.048	0.045	0.043	0.041	0.039	3,281.0
1,500	0.114	0.108	0.102	0.097	0.092	0.087	0.082	0.078	0.07$\bar{5}$	0.071	0.068	0.064	0.061	0.059	0.056	4,921.0
2,000	0.142	0.134	0.127	0.121	0.114	0.109	0.103	0.098	0.094	0.089	0.085	0.081	0.077	0.074	0.071	6,562.0
	−22.0	−13.0	−4.0	+5.0	14.0	23.0	32.0	41.0	50.0	59.0	68.0	77.0	86.0	95.0	104.0	t F

TABLE 5. M_w for t from −30 C (−22 F) to 40 C (104 F).

t C	Relative humidity 10	20	30	40	50	60	70	80	90	100	t F
−30	0.2	0.5	0.7	1.0	1.2	1.5	1.7	2.0	2.2	2.453	−22.0
−29	0.3	0.5	0.8	1.1	1.4	1.6	1.9	2.2	2.2	2.700	−20.2
−28	0.3	0.6	0.9	1.2	1.5	1.8	2.1	2.4	2.7	2.967	−18.4
−27	0.3	0.7	1.0	1.3	1.6	2.0	2.3	2.6	2.9	3.261	−16.6
−26	0.4	0.7	1.1	1.4	1.8	2.1	2.5	2.9	3.2	3.580	−14.8
−25	0.4	0.8	1.2	1.6	2.0	2.4	2.7	3.1	3.5	3.925	−13.0
−24	0.4	0.9	1.3	1.7	2.2	2.6	3.0	3.4	3.9	4.301	−11.2
−23	0.5	0.9	1.4	1.9	2.4	2.8	3.3	3.8	4.2	4.708	− 9.4
−22	0.5	1.0	1.5	2.1	2.6	3.1	3.6	4.1	4.6	5.155	− 7.6
−21	0.6	1.1	1.7	2.3	2.8	3.4	3.9	4.5	5.1	5.637	− 5.8
−20	0.6	1.2	1.8	2.5	3.1	3.7	4.3	4.9	5.5	6.130	− 4.0
−19	0.7	1.3	2.0	2.7	3.4	4.0	4.7	5.4	6.1	6.724	− 2.2
−18	0.7	1.5	2.2	2.9	3.7	4.4	5.1	5.8	6.6	7.309	− .4
−17	0.8	1.6	2.4	3.2	4.0	4.8	5.6	6.4	7.2	7.999	+ 1.4
−16	0.9	1.7	2.6	3.5	4.3	5.2	6.1	6.9	7.8	8.678	+ 3.2
−15	0.9	1.9	2.8	3.8	4.7	5.7	6.6	7.6	8.5	9.461	+ 5.0
−14	1.0	2.1	3.1	4.1	5.1	6.2	7.2	8.2	9.3	10.287	+ 6.8
−13	1.1	2.2	3.3	4.5	5.6	6.7	7.8	8.9	10.0	11.157	+ 8.6
−12	1.2	2.4	3.6	4.8	6.1	7.3	8.5	9.7	10.9	12.124	+10.4
−11	1.3	2.6	4.0	5.3	6.6	7.9	9.2	10.5	11.9	13.185	+12.2
−10	1.4	2.9	4.3	5.7	7.1	8.6	10.0	11.4	12.9	14.284	+14.0
− 9	1.5	3.1	4.6	6.2	7.7	9.3	10.8	12.4	13.9	15.472	+15.8
− 8	1.7	3.4	5.0	6.7	8.4	10.1	11.7	13.4	15.1	16.754	+17.6
− 7	1.8	3.6	5.4	7.2	9.1	10.9	12.7	14.5	16.3	18.117	+19.4
− 6	2.0	3.9	5.9	7.8	9.8	11.7	13.7	15.7	17.6	19.568	+21.2
− 5	2.1	4.2	6.3	8.5	10.6	12.7	14.8	16.9	19.0	21.156	+23.0
− 4	2.3	4.6	6.9	9.1	11.4	13.7	16.0	18.3	20.6	22.871	+24.8
− 3	2.5	4.9	7.4	9.9	12.3	14.8	17.3	19.7	22.2	24.670	+26.6
− 2	2.7	5.3	8.0	10.6	13.3	16.0	18.6	21.3	23.9	26.589	+28.4
− 1	2.9	5.7	8.6	11.5	14.3	17.2	20.1	22.9	25.8	28.685	+30.2
± 0	3.1	6.2	9.3	12.4	15.5	18.5	21.6	24.7	27.8	30.911	+32.0
1	3.3	6.6	9.9	13.2	16.5	19.8	23.0	26.3	29.6	32.919	+33.8
2	3.5	7.0	10.5	14.1	17.6	21.1	24.6	28.1	31.6	35.139	+35.6
3	3.8	7.5	11.3	15.0	18.8	22.5	26.3	30.0	33.8	37.509	+37.4
4	4.0	8.0	12.0	16.0	20.0	24.0	28.0	32.0	35.9	39.939	+39.2
5	4.3	8.5	12.8	17.0	21.3	25.5	29.8	34.0	38.3	42.533	+41.0
6	4.5	9.1	13.6	18.1	22.6	27.2	31.7	36.2	40.8	45.280	+42.8
7	4.8	9.6	14.5	19.3	24.1	28.9	33.7	38.5	43.3	48.175	+44.6
8	5.1	10.2	15.4	20.5	25.6	30.7	35.9	41.0	46.1	51.215	+46.4
9	5.4	10.9	16.3	21.8	27.2	32.6	38.1	43.5	49.0	54.394	+48.2
10	5.8	11.6	17.3	23.1	28.9	34.7	40.5	46.2	52.0	57.793	+50.0
11	6.1	12.3	18.4	24.5	30.6	36.8	42.9	49.0	55.1	61.270	+51.8
12	6.5	13.0	19.5	26.0	32.5	39.1	45.6	52.1	58.6	65.094	+53.6
13	6.9	13.8	20.7	27.6	34.5	41.4	48.3	55.2	62.1	69.010	+55.4
14	7.3	14.6	22.0	29.3	36.6	43.9	51.2	58.5	65.9	73.169	+57.2
15	7.8	15.5	23.3	31.0	38.8	46.5	54.3	62.0	69.8	77.505	+59.0
16	8.2	16.4	24.6	32.8	41.0	49.2	57.4	65.6	73.9	82.060	+60.8
17	8.7	17.4	26.0	34.7	43.4	52.1	60.8	69.5	78.1	86.813	+62.6
18	9.2	18.4	27.6	36.7	45.9	55.1	64.3	73.5	82.7	91.866	+64.4
19	9.7	19.4	29.1	38.9	48.6	58.3	68.0	77.7	87.4	97.127	+66.2
20	10.3	20.5	30.8	41.1	51.4	61.6	71.9	82.2	92.4	102.71	+68.0
21	10.8	21.7	32.5	43.4	54.2	65.1	75.9	86.8	97.6	108.46	+69.8
22	11.5	22.9	34.4	45.8	57.3	68.7	80.2	91.6	103.1	114.56	+71.6
23	12.1	24.2	36.3	48.3	60.4	72.5	84.6	96.7	108.8	120.87	+73.4
24	12.8	25.5	38.3	51.0	63.8	76.5	89.3	102.0	114.8	127.53	+75.2
25	13.4	26.9	40.3	53.8	67.2	80.7	94.1	107.6	121.0	134.44	+77.0
26	14.2	28.3	42.5	56.7	70.9	85.0	99.2	113.4	127.6	141.74	+78.8
27	14.9	29.9	44.8	59.8	74.7	89.6	104.6	119.5	134.5	149.39	+80.6
28	15.7	31.5	47.2	62.9	78.7	94.4	110.1	125.9	141.6	157.34	+82.4
29	16.6	33.1	49.7	66.2	82.8	99.4	115.9	132.5	149.1	165.62	+84.2
30	17.4	34.9	52.3	69.7	87.1	104.6	122.0	139.4	156.8	174.27	+86.0
31	18.3	36.7	55.0	73.3	91.7	110.0	128.3	146.7	165.0	183.32	+87.8
32	19.3	38.5	57.8	77.1	96.4	115.6	134.9	154.2	173.5	192.74	+89.6
33	26.3	40.5	60.8	81.0	101.3	121.5	141.8	162.0	182.3	202.56	+91.4
34	21.3	42.6	63.9	85.1	106.4	127.7	149.0	170.3	191.6	212.86	+93.2
35	22.4	44.7	67.1	89.4	111.8	134.1	156.5	178.8	201.2	223.50	+95.0
36	23.5	46.9	70.4	93.9	117.3	140.8	164.2	187.7	211.2	234.63	+96.8
37	24.6	49.2	73.9	98.5	123.1	147.7	172.3	197.0	221.6	246.20	+98.6
38	25.8	51.6	77.5	103.3	129.1	154.9	180.8	206.6	232.4	258.23	+100.4
39	27.1	54.2	81.2	108.3	135.4	162.5	189.6	216.6	243.7	270.80	+102.2
40	28.4	56.8	85.2	113.6	142.0	170.4	198.8	227.2	255.5	283.94	+104.0

TABLE 6. f for t from −30 C (−22 F) to 40 C (104 F).

t C	f	t F	t C	f	t F	t C	f	t F
−30	6.390	−22.0	− 6	5.289	+21.2	+18	4.449	+64.4
−29	6.338	−20.2	− 5	5.250	+23.0	+19	4.419	+66.2
−28	6.286	−18.4	− 4	5.210	+24.8	+20	4.389	+68.0
−27	6.233	−16.6	− 3	5.172	+26.6	+21	4.359	+69.8
−26	6.183	−14.8	− 2	5.133	+28.4	+22	4.330	+71.6
−25	6.134	−13.0	− 1	5.095	+30.2	+23	4.300	+73.4
−24	6.084	−11.2	± 0	5.059	+32.0	+24	4.271	+75.2
−23	6.036	− 9.4	+ 1	5.021	+33.8	+25	4.241	+77.0
−22	5.988	− 7.6	+ 2	4.984	+35.6	+26	4.213	+78.8
−21	5.940	− 5.8	+ 3	4.948	+37.4	+27	4.186	+80.6
−20	5.894	− 4.0	+ 4	4.913	+39.2	+28	4.158	+82.4
−19	5.847	− 2.2	+ 5	4.878	+41.0	+29	4.130	+84.2
−18	5.801	− .4	+ 6	4.843	+42.8	+30	4.102	+86.0
−17	5.755	+ 1.4	+ 7	4.808	+44.6	+31	4.076	+87.8
−16	5.710	+ 3.2	+ 8	4.773	+46.4	+32	4.049	+89.6
−15	5.666	+ 5.0	+ 9	4.738	+48.2	+33	4.022	+91.4
−14	5.622	+ 6.8	+10	4.706	+50.0	+34	3.997	+93.2
−13	5.579	+ 8.6	+11	4.666	+51.8	+35	3.970	+95.0
−12	5.537	+10.4	+12	4.640	+53.6	+36	3.944	+96.8
−11	5.494	+12.2	+13	4.607	+55.4	+37	3.918	+98.6
−10	5.452	+14.0	+14	4.576	+57.2	+38	3.893	+100.4
− 9	5.410	+15.8	+15	4.543	+59.0	+39	3.868	+102.2
− 8	5.370	+17.6	+16	4.511	+60.8	+40	3.844	+104.0
− 7	5.329	+19.4	+17	4.480	+62.6			

TABLE 7. M_c for h from 10 m (32.8 ft) to 2,000 m (6,562 ft).

h(m)	M_c	h(ft)	h(m)	M_c	h(ft)	h(m)	M_c	h(ft)
10	1.6	32.8	280	44.0	918.6	625	98.1	2,051.0
20	3.1	65.6	290	45.5	951.4	650	102.1	2,133.0
30	4.7	98.4	300	47.1	984.3	675	106.0	2,215.0
40	6.3	131.2	310	48.7	1,017.0	700	109.9	2,297.0
50	7.9	164.0	320	50.2	1,050.0	725	113.8	2,379.0
60	9.4	196.9	330	51.8	1,083.0	750	117.8	2,461.0
70	11.0	229.7	340	53.4	1,115.0	775	121.7	2,543.0
80	12.6	262.5	350	55.0	1,148.0	800	125.6	2,625.0
90	14.1	295.3	360	56.5	1,181.0	825	129.5	2,707.0
100	15.7	328.1	370	58.1	1,214.0	850	133.5	2,789.0
110	17.3	360.9	380	59.7	1,247.0	875	137.4	2,871.0
120	18.8	393.7	390	61.2	1,280.0	900	141.3	2,953.0
130	20.4	426.5	400	62.8	1,312.0	925	145.2	3,035.0
140	22.0	459.3	410	64.4	1,345.0	950	149.2	3,117.0
150	23.6	492.1	420	65.9	1,378.0	975	153.1	3,199.0
160	25.1	524.9	430	67.5	1,411.0	1,000	157.0	3,280.0
170	26.7	557.7	440	69.1	1,444.0	1,100	172.7	3,609.0
180	28.3	590.6	450	70.7	1,476.0	1,200	188.4	3,937.0
190	29.8	623.4	460	72.2	1,509.0	1,300	204.1	4,265.0
200	31.4	656.2	470	73.8	1,542.0	1,400	219.8	4,593.0
210	33.0	689.0	480	75.4	1,575.0	1,500	235.5	4,921.0
220	34.5	721.8	490	76.9	1,608.0	1,600	251.2	5,249.0
230	36.1	754.6	500	78.5	1,640.0	1,700	266.9	5,577.0
240	37.7	787.4	525	82.4	1,722.0	1,800	282.6	5,906.0
250	39.3	820.2	550	86.4	1,804.0	1,900	298.3	6,234.0
260	40.8	853.0	575	90.3	1,886.0	2,000	314.0	6,562.0
270	42.4	885.8	600	94.2	1,969.0			

TABLE 8A. $F(t, w)$ for t from −30 C (−22 F) to 40 C (104 F); w from 0 to 12.

t C \ w	0	1	2	3	4	5	6	7	8	9	10	11	12	t F
−30	325.1	335.1												−22.0
−29	323.8	333.9												−20.2
−28	322.4	332.4												−18.4
−27	321.1	331.0												−16.6
−26	319.8	329.7												−14.8
−25	318.5	328.3												−13.0
−24	317.3	327.0												−11.2
−23	316.0	325.6												− 9.4
−22	314.7	324.3												− 7.6
−21	313.5	323.0												− 5.8
−20	312.3	321.7												− 4.0
−19	311.0	320.3												− 2.2
−18	309.8	319.1												− 0.4
−17	308.6	317.8												+ 1.4
−16	307.4	316.5												+ 3.2
−15	306.2	315.9	324.9											+ 5.0
−14	305.0	314.0	322.8											+ 6.8
−13	303.8	312.7	321.6											+ 8.6
−12	302.7	311.6	320.4											+10.4
−11	301.5	310.3	319.0											+12.2
−10	300.4	309.1	317.8											+14.0
− 9	299.2	307.9	316.5											+15.8
− 8	298.1	306.7	315.3											+17.6
− 7	297.0	305.5	314.0	322.5										+19.4
− 6	295.9	304.4	312.8	321.2										+21.2
− 5	294.8	303.2	311.6	319.9										+23.0
− 4	293.7	302.0	310.4	318.7										+24.8
− 3	292.6	300.9	309.1	317.4										+26.6
− 2	291.5	299.7	307.9	316.1	324.2									+28.4
− 1	290.4	298.6	306.7	314.8	322.9									+30.2
± 0	289.4	297.5	305.6	313.6	321.7									+32.0
+ 1	288.3	296.4	304.4	312.4	320.4	328.3								+33.8
+ 2	287.3	295.3	303.3	311.2	319.1	327.0								+35.6
+ 3	286.2	294.1	302.0	309.9	317.8	325.6								+37.4
+ 4	285.2	293.1	300.9	308.8	316.6	324.4	332.0							+39.2
+ 5	284.2	292.0	299.8	307.6	315.4	323.1	330.7							+41.0
+ 6	283.2	291.0	298.7	306.4	314.1	321.7	329.4							+42.8
+ 7	282.1	289.8	297.5	305.2	312.8	320.3	327.9	335.5						+44.6
+ 8	281.1	288.8	296.4	304.0	311.5	319.1	326.6	334.1						+46.4
+ 9	280.1	287.7	295.3	302.8	310.3	317.8	325.3	332.8	340.2					+48.2
+10	279.2	286.8	294.3	301.8	309.2	316.7	324.1	331.6	338.8					+50.0
+11	278.2	285.7	293.2	300.5	307.9	315.3	322.7	330.1	337.3	344.6				+51.8
+12	277.2	284.7	292.1	299.4	306.8	314.1	321.5	328.8	336.0	343.3	350.5			+53.6
+13	276.2	283.6	291.0	298.2	305.6	312.9	320.2	327.4	334.0	341.8	349.0			+55.4
+14	275.3	282.7	290.0	297.2	304.5	311.7	319.0	326.2	333.3	340.5	347.6	354.7		+57.2
+15	274.3	281.6	288.9	296.0	302.3	310.5	317.7	324.9	331.9	339.0	346.1	353.1	360.2	+59.0
+16	273.4	280.7	287.9	295.0	302.2	309.3	316.4	323.5	330.6	337.6	344.7	351.7	358.6	+60.8
+17	272.4	279.6	286.8	293.8	301.0	308.1	315.1	322.2	329.2	336.1	343.2	350.2	357.0	+62.6
+18	271.5	278.7	285.7	292.8	299.9	307.0	313.9	320.9	327.9	334.8	341.8	348.7	355.6	+64.4
+19	270.5	277.6	284.6	291.7	298.7	305.5	312.6	319.6	326.6	333.4	340.3	347.1	354.0	+66.2
+20	269.6	276.7	283.6	290.6	297.6	304.5	311.5	318.4	325.2	332.1	339.0	345.7	352.6	+68.0
+21	268.7	275.7	282.6	289.6	296.5	303.4	310.3	317.2	323.9	330.8	337.5	344.3	351.1	+69.8
+22	267.8	274.8	281.6	288.5	295.5	302.2	309.1	315.9	322.7	329.5	336.2	342.9	349.7	+71.6
+23	266.9	273.8	280.6	287.5	294.4	301.1	307.9	314.7	321.4	328.2	334.8	341.5	348.1	+73.4
+24	266.0	272.9	279.6	286.5	293.3	300.0	306.8	313.4	320.2	326.9	333.5	340.1	346.7	+75.2
+25	265.1	271.9	278.6	285.4	292.2	298.9	305.6	312.2	318.9	325.4	332.1	338.7	345.2	+77.0
+26	264.2	271.0	277.7	284.4	291.0	297.7	304.4	311.0	317.6	324.2	330.8	337.3	343.8	+78.8
+27	263.3	270.0	276.7	283.4	290.0	296.6	303.3	309.8	316.4	322.9	329.5	335.9	342.4	+80.6
+28	262.5	269.2	275.8	282.4	289.0	295.6	302.2	308.7	315.3	321.7	328.2	334.6	341.1	+82.4
+29	261.6	268.3	274.8	281.4	287.9	294.5	300.9	307.5	314.0	320.4	326.9	333.3	339.7	+84.2
+30	260.7	267.3	273.8	280.4	286.8	293.4	299.8	306.3	312.7	319.1	325.5	331.9	338.2	+86.0
+31	259.9	266.5	272.9	279.5	285.9	292.4	298.7	305.2	311.5	318.0	324.3	330.6	336.9	+87.8
+32	259.0	265.5	271.9	278.4	284.8	291.3	297.6	304.0	310.3	316.7	323.0	329.3	335.5	+89.6
+33	258.2	264.7	271.1	277.5	283.8	290.3	296.5	302.9	309.2	315.5	321.7	328.0	334.2	+91.4
+34	257.3	263.8	270.1	276.5	282.8	289.2	295.4	301.7	308.0	314.2	320.4	326.7	332.8	+93.2
+35	256.5	262.9	269.2	275.6	281.8	288.1	294.4	300.7	306.8	313.0	319.2	325.3	331.6	+95.0
+36	255.7	262.1	268.3	274.6	280.9	287.2	293.3	299.5	305.7	311.8	318.0	324.1	330.3	+96.8
+37	254.8	261.1	267.3	273.5	279.8	286.0	292.2	298.3	304.5	310.6	316.7	322.8	328.8	+98.6
+38	254.0	260.3	266.5	272.6	278.8	285.0	291.1	297.2	303.4	309.4	315.5	321.5	327.5	+100.4
+39	253.2	259.4	265.6	271.7	277.9	284.0	290.1	296.2	302.3	308.3	314.3	320.3	326.3	+102.2
+40	252.4	258.5	264.7	270.8	276.9	283.0	289.1	295.1	301.2	307.1	313.1	319.1	325.1	+104.0

TABLE 8B. $F(t, w)$ for t from 15 C (59 F) to 40 C (104 F); w from 12 to 24.

t C \ w	12	13	14	15	16	17	18	19	20	21	22	23	24	w / t F
15	360.2													59.0
16	358.6													60.8
17	357.0	364.0												62.6
18	355.6	362.5	369.2											64.4
19	354.0	360.9	367.6											66.2
20	352.6	359.3	366.1	372.8										68.0
21	351.1	357.8	364.5	371.1	377.9									69.8
22	349.7	356.3	363.0	369.6	376.2	382.8								71.6
23	348.1	354.8	361.5	368.0	374.6	381.1	387.7							73.4
24	346.7	353.3	359.8	366.4	372.9	379.5	385.9	392.4						75.2
25	345.2	351.8	358.3	364.8	371.3	377.7	384.2	390.6	397.0	403.4				77.0
26	343.8	350.3	356.8	363.2	369.7	376.1	382.5	388.9	295.3	401.6	407.9			78.8
27	342.4	348.8	355.3	361.7	368.1	374.5	380.9	387.2	393.5	399.8	406.0	412.3	418.5	80.6
28	341.1	347.5	353.9	360.2	366.7	372.9	379.2	385.6	391.8	398.1	404.3	410.5	416.7	82.4
29	339.7	346.0	352.3	358.7	365.0	371.3	377.6	383.9	390.0	396.2	402.5	408.6	414.7	84.2
30	338.2	344.6	350.8	357.2	363.4	369.6	375.9	382.1	388.3	394.5	400.6	406.8	412.8	86.0
31	336.9	343.2	349.5	355.8	362.0	368.1	374.4	380.5	386.7	392.8	398.9	405.0	411.1	87.8
32	335.5	341.8	348.0	354.1	360.4	366.5	372.7	378.8	384.9	391.1	397.1	403.1	409.2	89.6
33	334.2	340.4	346.6	352.7	359.0	365.0	371.1	377.3	383.3	389.3	395.4	401.4	407.3	91.4
34	332.8	339.0	345.2	351.3	357.4	363.5	369.5	375.6	381.6	387.6	393.7	399.6	405.5	93.2
35	331.6	337.6	343.8	349.8	355.9	362.0	368.0	374.0	380.0	386.0	391.9	397.9	403.8	95.0
36	330.3	336.3	342.4	348.5	354.4	360.4	366.5	372.4	378.3	384.3	390.2	396.1	402.0	96.8
37	328.8	334.9	340.9	346.9	352.9	358.8	364.8	370.8	376.6	382.5	388.5	394.3	400.1	98.6
38	327.5	333.6	339.6	345.5	351.5	357.4	363.3	369.3	375.1	380.9	386.8	392.6	398.4	100.4
39	326.3	332.3	338.2	344.1	350.1	355.9	361.8	367.9	373.5	379.3	385.1	390.9	396.7	102.2
40	325.1	330.9	336.9	342.8	348.6	354.5	360.3	366.5	371.9	377.8	383.5	389.2	394.9	104.0

TABLE 8C. $F(t, w)$ for t from 27 C (80.6 F) to 40 C (104 F); w from 24 to 36.

t C \ w	24	25	26	27	28	29	30	31	32	33	34	35	36	w / t F
27	418.5													80.6
28	416.7	422.9												82.4
29	414.7	421.0	427.1											84.2
30	412.8	418.9	425.2	431.1	437.1									86.0
31	411.1	417.1	423.2	429.2	435.2	441.2	447.2							87.8
32	409.2	415.2	421.2	427.2	433.2	439.2	445.0	451.0	456.8	462.6				89.6
33	407.3	413.4	419.3	425.3	431.1	437.2	443.0	448.8	454.6	460.5	466.4	472.1		91.4
34	405.5	411.5	417.4	423.3	429.2	435.1	440.9	446.7	452.5	458.4	464.1	469.9	475.6	93.2
35	403.8	409.6	415.6	421.4	427.2	433.1	439.9	444.7	450.4	456.2	461.9	467.7	473.4	95.0
36	402.0	407.9	413.7	419.5	425.4	431.1	436.9	442.6	448.3	454.1	459.8	465.5	471.1	96.8
37	400.1	405.9	411.8	417.6	423.3	429.0	434.8	440.5	446.2	451.9	457.5	463.1	468.9	98.6
38	398.4	404.1	410.0	415.7	421.4	427.1	432.9	438.5	444.2	449.8	455.4	461.0	466.7	100.4
39	396.7	402.4	408.1	413.9	419.6	425.3	430.9	436.5	442.1	447.8	453.4	458.9	464.5	102.2
40	394.9	400.7	406.4	412.1	417.7	423.4	429.0	434.6	440.2	445.7	451.3	456.8	462.4	104.0

TABLE 8D. $F(t, w)$ for t from 34 C (93.2 F) to 40 C (104 F); w from 36 to 45.

t C \ w	36	37	38	39	40	41	42	43	44	45	w / t F
34	475.6										93.20
35	473.4	479.1									95.00
36	471.1	476.8	482.4	488.1	493.7						96.80
37	468.9	474.5	480.1	485.6	491.2	496.7	502.2	507.7			98.60
38	466.7	472.3	477.8	483.3	488.9	494.4	499.8	505.3	510.8		100.40
39	464.5	470.0	475.5	481.0	486.6	492.1	497.5	502.9	508.4	513.8	102.20
40	462.4	467.9	473.4	478.9	484.3	489.8	495.2	500.6	506.0	511.4	104.00

TABLE 9. p/p_0 for h from 50 m (164 ft) to 2,000 m (6,562 ft) and $\bar{t}^*$ from −30 C (−22 F) to 40 C (104 F).

h (m) \ t C	−30	−25	−20	−15	−10	− 5	±0	+5	+10	+15	+20	+25	+30	+35	+40	h (ft)
50	0.9930	0.9931	0.9933	0.9934	0.9935	0.9936	0.9938	0.9939	0.9940	0.9941	0.9942	0.9943	0.9944	0.9945	0.9946	164.0
100	0.9860	0.9863	0.9866	0.9869	0.9871	0.9874	0.9876	0.9878	0.9880	0.9882	0.9884	0.9886	0.9888	0.9890	0.9892	328.1
150	0.9791	0.9795	0.9799	0.9802	0.9807	0.9810	0.9814	0.9817	0.9821	0.9823	0.9827	0.9829	0.9832	0.9835	0.9837	492.1
200	0.9723	0.9727	0.9734	0.9738	0.9744	0.9748	0.9753	0.9757	0.9761	0.9766	0.9770	0.9774	0.9777	0.9780	0.9784	656.2
250	0.9655	0.9662	0.9668	0.9674	0.9681	0.9686	0.9692	0.9698	0.9703	0.9707	0.9713	0.9717	0.9722	0.9727	0.9730	820.2
300	0.9587	0.9595	0.9603	0.9610	0.9618	0.9625	0.9632	0.9637	0.9644	0.9650	0.9656	0.9662	0.9667	0.9672	0.9678	984.3
350	0.9519	0.9529	0.9538	0.9547	0.9556	0.9564	0.9572	0.9579	0.9586	0.9593	0.9600	0.9607	0.9613	0.9619	0.9625	1,148.0
400	0.9453	0.9464	0.9474	0.9484	0.9494	0.9503	0.9512	0.9519	0.9529	0.9537	0.9544	0.9551	0.9559	0.9566	0.9572	1,312.0
450	0.9387	0.9399	0.9410	0.9421	0.9432	0.9442	0.9452	0.9462	0.9471	0.9480	0.9489	0.9497	0.9505	0.9513	0.9520	1,476.0
500	0.9321	0.9334	0.9347	0.9359	0.9371	0.9383	0.9394	0.9404	0.9414	0.9424	0.9434	0.9443	0.9452	0.9460	0.9469	1,640.0
600	0.9191	0.9206	0.9222	0.9236	0.9250	0.9263	0.9277	0.9289	0.9301	0.9313	0.9324	0.9335	0.9346	0.9355	0.9366	1,969.0
700	0.9063	0.9081	0.9098	0.9115	0.9131	0.9146	0.9161	0.9176	0.9190	0.9203	0.9216	0.9229	0.9241	0.9253	0.9264	2,297.0
800	0.8936	0.8957	0.8976	0.8995	0.9013	0.9030	0.9047	0.9063	0.9079	0.9095	0.9109	0.9124	0.9138	0.9151	0.9164	2,625.0
900	0.8812	0.8834	0.8856	0.8876	0.8897	0.8916	0.8935	0.8953	0.8971	0.8987	0.9004	0.9019	0.9035	0.9050	0.9064	2,953.0
1,000	0.8688	0.8712	0.8737	0.8760	0.8782	0.8803	0.8824	0.8843	0.8863	0.8881	0.8899	0.8917	0.8934	0.8950	0.8966	3,281.0
1,500	0.8099	0.8133	0.8166	0.8198	0.8230	0.8260	0.8289	0.8317	0.8344	0.8370	0.8395	0.8420	0.8444	0.8467	0.8490	4,921.0
2,000	0.7549	0.7592	0.7633	0.7674	0.7712	0.7749	0.7786	0.7821	0.7855	0.7888	0.7920	0.7951	0.7981	0.8011	0.8039	6,562.0
h (ft) \ t F	−22.0	−13.0	−4.0	+5.0	+14.0	+23.0	+32.0	+41.0	+50.0	+59.0	+68.0	+77.0	+86.0	+95.0	+104.0	h (ft)

*$\bar{t}$ = temperature averaged from the ground to the height h.

TABLE 10A. u for h from 10 m (32.8 ft) to 150 m (492.1 ft); F from 250 to 370. Values to be subtracted from F to obtain $Fp = (n - 1)\ 10^6$.

h (m) \ F	250	260	270	280	290	300	310	320	330	340	350	360	370	h (ft)
10	0.3	0.3	0.3	0.3	0.3	0.4	0.4	0.4	0.4	0.4	0.4	0.4	0.4	32.8
20	0.6	0.7	0.7	0.7	0.7	0.8	0.8	0.8	0.8	0.9	0.9	0.9	0.9	65.6
30	0.9	1.0	1.0	1.0	1.1	1.1	1.1	1.2	1.2	1.3	1.3	1.3	1.4	98.4
40	1.3	1.3	1.4	1.4	1.5	1.5	1.6	1.6	1.7	1.7	1.8	1.8	1.9	131.2
50	1.6	1.6	1.7	1.7	1.8	1.9	1.9	2.0	2.0	2.1	2.2	2.2	2.3	164.0
60	1.9	1.9	2.0	2.1	2.1	2.2	2.3	2.4	2.4	2.5	2.6	2.7	2.7	196.9
70	2.2	2.3	2.3	2.4	2.5	2.6	2.7	2.8	2.9	3.0	3.0	3.1	3.2	229.7
80	2.5	2.6	2.7	2.8	2.9	3.0	3.1	3.2	3.3	3.4	3.5	3.6	3.7	262.5
90	2.8	2.9	3.0	3.1	3.2	3.4	3.5	3.6	3.7	3.8	3.9	4.0	4.1	295.3
100	3.1	3.2	3.3	3.5	3.6	3.7	3.8	4.0	4.1	4.2	4.3	4.5	4.6	328.1
110	3.4	3.5	3.7	3.8	3.9	4.1	4.2	4.4	4.5	4.6	4.8	4.9	5.0	360.9
120	3.7	3.9	4.0	4.2	4.3	4.5	4.6	4.8	4.9	5.1	5.2	5.4	5.5	393.7
130	4.0	4.2	4.3	4.5	4.7	4.8	5.0	5.2	5.3	5.5	5.6	5.8	6.0	426.5
140	4.4	4.5	4.7	4.9	5.0	5.2	5.4	5.6	5.7	5.9	6.1	6.3	6.4	459.3
150	4.7	4.8	5.0	5.2	5.4	5.6	5.8	6.0	6.1	6.3	6.5	6.7	6.9	492.1

TABLE 10B. u for h from 10 m (32.8 ft) to 150 m (492.1 ft); F from 370 to 500. Values to be subtracted from F to obtain $Fp = (n - 1)\ 10^6$.

h (m) \ F	370	380	390	400	410	420	430	440	450	460	470	480	490	500	h (ft)
10	0.4	0.5	0.5	0.5	0.5	0.5	0.5	0.5	0.5	0.6	0.6	0.6	0.6	0.6	32.8
20	0.9	1.0	1.0	1.0	1.0	1.1	1.1	1.1	1.1	1.2	1.2	1.2	1.2	1.3	65.6
30	1.4	1.4	1.4	1.5	1.5	1.6	1.6	1.6	1.7	1.7	1.7	1.8	1.8	1.9	98.4
40	1.9	1.9	2.0	2.0	2.1	2.1	2.2	2.2	2.3	2.3	2.4	2.4	2.5	2.5	131.2
50	2.3	2.4	2.4	2.5	2.5	2.6	2.7	2.7	2.8	2.9	2.9	3.0	3.0	3.1	164.0
60	2.7	2.8	2.9	3.0	3.0	3.1	3.2	3.3	3.3	3.4	3.5	3.6	3.6	3.7	196.9
70	3.2	3.3	3.4	3.5	3.6	3.7	3.7	3.8	3.9	4.0	4.1	4.2	4.3	4.4	229.7
80	3.7	3.8	3.9	4.0	4.1	4.2	4.3	4.4	4.5	4.6	4.7	4.8	4.9	5.0	262.5
90	4.1	4.3	4.4	4.5	4.6	4.7	4.8	4.9	5.0	5.2	5.3	5.4	5.5	5.6	295.3
100	4.6	4.7	4.8	5.0	5.1	5.2	5.3	5.5	5.6	5.7	5.8	6.0	6.1	6.2	328.1
110	5.0	5.2	5.3	5.4	5.6	5.7	5.8	6.0	6.1	6.3	6.4	6.5	6.7	6.8	360.9
120	5.5	5.7	5.8	6.0	6.1	6.3	6.4	6.6	6.7	6.9	7.0	7.2	7.3	7.5	393.7
130	6.0	6.1	6.3	6.4	6.6	6.8	6.9	7.1	7.2	7.4	7.6	7.7	7.9	8.1	426.5
140	6.4	6.6	6.8	7.0	7.1	7.3	7.5	7.7	7.8	8.0	8.2	8.4	8.5	8.7	459.3
150	6.9	7.1	7.3	7.4	7.6	7.8	8.0	8.2	8.4	8.6	8.7	8.9	9.1	9.3	492.1

TABLE 10C. u for h from 150 m (492.1 ft) to 500 m (1,640 ft); F from 250 to 340. Values to be subtracted from F to obtain $Fp = (n - 1)\ 10^6$.

h (m) \ F	250	260	270	280	290	300	310	320	330	340	h (ft)
150	4.7	4.8	5.0	5.2	5.4	5.6	5.8	6.0	6.1	6.3	492.1
175	5.4	5.6	5.9	6.1	6.3	6.5	6.7	6.9	7.2	7.4	574.1
200	6.2	6.4	6.7	6.9	7.2	7.4	7.7	7.9	8.2	8.4	656.2
225	7.0	7.2	7.5	7.8	8.1	8.3	8.6	8.9	9.2	9.5	738.2
250	7.7	8.0	8.3	8.6	8.9	9.2	9.5	9.9	10.2	10.5	820.2
275	8.5	8.8	9.1	9.5	9.8	10.1	10.5	10.8	11.1	11.5	902.2
300	9.2	9.6	9.9	10.3	10.7	11.0	11.4	11.8	12.1	12.5	984.3
325	10.0	10.3	10.7	11.1	11.5	11.9	12.3	12.7	13.1	13.5	1,066.0
350	10.7	11.1	11.6	12.0	12.4	12.8	13.3	13.7	14.1	14.6	1,148.0
375	11.5	11.9	12.4	12.8	13.3	13.7	14.2	14.7	15.1	15.6	1,230.0
400	12.2	12.6	13.2	13.7	14.2	14.6	15.1	15.6	16.1	16.6	1,312.0
425	13.0	13.5	14.0	14.5	15.0	15.5	16.1	16.6	17.1	17.6	1,394.0
450	13.7	14.2	14.8	15.3	15.9	16.4	17.0	17.5	18.1	18.6	1,476.0
475	14.4	15.0	15.6	16.2	16.7	17.3	17.9	18.5	19.0	19.6	1,558.0
500	15.2	15.8	16.4	17.0	17.6	18.2	18.8	19.4	20.0	20.6	1,640.0

TABLE 10D. u for h from 150 m (492.1 ft) to 500 m (1,640 ft); F from 340 to 420. Values to be subtracted from F to obtain $Fp = (n - 1)\ 10^6$.

h (m) \ F	340	350	360	370	380	390	400	410	420	h (ft)
150	6.3	6.5	6.7	6.9	7.1	7.3	7.4	7.6	7.8	492.1
175	7.4	7.6	7.8	8.0	8.2	8.5	8.7	8.9	9.1	574.1
200	8.4	8.6	8.9	9.1	9.4	9.6	9.9	10.1	10.4	656.2
225	9.5	9.7	10.0	10.3	10.6	10.8	11.1	11.4	11.7	738.2
250	10.5	10.8	11.1	11.4	11.7	12.0	12.3	12.6	12.9	820.2
275	11.5	11.8	12.2	12.5	12.8	13.2	13.5	13.9	14.2	902.2
300	12.5	12.9	13.2	13.6	14.0	14.4	14.7	15.1	15.5	984.3
325	13.5	13.9	14.3	14.7	15.1	15.5	15.9	16.3	16.7	1,066.0
350	14.6	15.0	15.4	15.8	16.3	16.7	17.1	17.5	18.0	1,148.0
375	15.6	16.0	16.5	16.9	17.4	17.9	18.3	18.8	19.2	1,230.0
400	16.6	17.1	17.6	18.1	18.5	19.0	19.5	20.0	20.5	1,312.0
425	17.6	18.1	18.6	19.2	19.7	20.2	20.7	21.2	21.8	1,394.0
450	18.6	19.2	19.7	20.3	20.8	21.4	21.9	22.5	23.0	1,476.0
475	19.6	20.2	20.8	21.3	21.9	22.5	23.1	23.7	24.2	1,558.0
500	20.6	21.2	21.8	22.4	23.0	23.6	24.2	24.8	25.5	1,640.0

TABLE 10E. u for h from 150 m (492.1 ft) to 500 m (1,640 ft); F from 420 to 500. Values to be subtracted from F to obtain $Fp = (n - 1)\ 10^6$.

h (m) \ F	420	430	440	450	460	470	480	490	500	h (ft)
150	7.8	8.0	8.2	8.4	8.6	8.7	8.9	9.1	9.3	492.1
175	9.1	9.3	9.5	9.8	10.0	10.2	10.4	10.6	10.9	574.1
200	10.4	10.6	10.9	11.1	11.4	11.6	11.9	12.1	12.4	656.2
225	11.7	12.0	12.2	12.5	12.8	13.1	13.3	13.6	13.9	738.2
250	12.9	13.2	13.6	13.9	14.2	14.5	14.8	15.1	15.4	820.2
275	14.2	14.5	14.9	15.2	15.5	15.9	16.2	16.6	16.9	902.2
300	15.5	15.8	16.2	16.6	16.9	17.3	17.7	18.0	18.4	984.3
325	16.7	17.1	17.5	17.9	18.3	18.7	19.1	19.5	19.9	1,066.0
350	18.0	18.4	18.8	19.3	19.7	20.1	20.5	21.0	21.4	1,148.0
375	19.2	19.7	20.2	20.6	21.1	21.5	22.0	22.4	22.9	1,230.0
400	20.5	21.0	21.5	22.0	22.4	22.9	23.4	23.9	24.4	1,312.0
425	21.8	22.3	22.8	23.3	23.8	24.3	24.9	25.4	25.9	1,394.0
450	23.0	23.6	24.1	24.7	25.2	25.8	26.3	26.9	27.4	1,476.0
475	24.2	24.8	25.4	26.0	26.5	27.1	27.7	28.3	28.9	1,558.0
500	25.5	26.1	26.7	27.3	27.9	28.5	29.1	29.7	30.3	1,640.0

TABLE 11A. Δu for $\bar{t}^* \neq 0$. Values to be multiplied by $h \times 10^{-2}$ and $\left\{\begin{matrix}\text{added to}\\ \text{subtracted from}\end{matrix}\right\}$ u for $\left\{\begin{matrix}\bar{t} < 0\\ \bar{t} > 0\end{matrix}\right\}$.

$\bar{t}$ \ F	250	260	270	280	290	300	310	320	330	340	350	360	370
±10	0.1	0.1	0.1	0.1	0.1	0.1	0.1	0.1	0.1	0.2	0.2	0.2	0.2
±20	0.2	0.2	0.2	0.3	0.3	0.3	0.3	0.3	0.3	0.3	0.3	0.3	0.3
±30	0.3	0.4	0.4	0.4	0.4	0.4	0.4	0.4	0.4	0.5	0.5	0.5	0.5
±40	0.5	0.5	0.5	0.5	0.5	0.5	0.6	0.6	0.6	0.6	0.6	0.7	0.7

*$\bar{t}$ = temperature in degrees centigrade averaged from the ground to the height h.

TABLE 11B. Δu for $\bar{t}^* \neq 0$. Values to be multiplied by $h \times 10^{-2}$ and $\left\{\begin{matrix}\text{added to}\\ \text{subtracted from}\end{matrix}\right\}$ u for $\left\{\begin{matrix}\bar{t} < 0\\ \bar{t} > 0\end{matrix}\right\}$.

$\bar{t}$ \ F	370	380	390	400	410	420	430	440	450	460	470	480	490	500
±10	0.2	0.2	0.2	0.2	0.2	0.2	0.2	0.2	0.2	0.2	0.2	0.2	0.2	0.2
±20	0.3	0.3	0.4	0.4	0.4	0.4	0.4	0.4	0.4	0.4	0.4	0.4	0.4	0.5
±30	0.5	0.5	0.5	0.5	0.6	0.6	0.6	0.6	0.6	0.6	0.6	0.7	0.7	0.7
±40	0.7	0.7	0.7	0.7	0.7	0.8	0.8	0.8	0.8	0.8	0.9	0.9	0.9	0.9

*$\bar{t}$ = temperature in degrees centigrade averaged from the ground to the height h.

TABLE 11C. Δu for $\bar{t}^* \neq 0$. Values to be multiplied by $h \times 10^{-2}$ and $\left\{\begin{matrix}\text{added to}\\ \text{subtracted from}\end{matrix}\right\}$ u for $\left\{\begin{matrix}\bar{t} < 0\\ \bar{t} > 0\end{matrix}\right\}$.

$\bar{t}$ \ F	250	260	270	280	290	300	310	320	330	340
±10	0.1	0.1	0.1	0.1	0.1	0.1	0.1	0.1	0.1	0.1
±20	0.2	0.2	0.2	0.2	0.3	0.3	0.3	0.3	0.3	0.3
±30	0.3	0.3	0.4	0.4	0.4	0.4	0.4	0.4	0.4	0.5
±40	0.4	0.5	0.5	0.5	0.5	0.5	0.5	0.6	0.6	0.6

*$\bar{t}$ = temperature in degrees centigrade averaged from the ground to the height h.

TABLE 11D. Δu for $\bar{t}^* \neq 0$. Values to be multiplied by $h \times 10^{-2}$ and $\left\{\begin{matrix}\text{added to}\\ \text{subtracted from}\end{matrix}\right\}$ u for $\left\{\begin{matrix}\bar{t} < 0\\ \bar{t} > 0\end{matrix}\right\}$.

$\bar{t}$ \ F	340	350	360	370	380	390	400	410	420
±10	0.1	0.2	0.2	0.2	0.2	0.2	0.2	0.2	0.2
±20	0.3	0.3	0.3	0.3	0.3	0.3	0.4	0.4	0.4
±30	0.5	0.5	0.5	0.5	0.5	0.5	0.5	0.5	0.6
±40	0.6	0.6	0.6	0.7	0.7	0.7	0.7	0.7	0.7

*$\bar{t}$ = temperature in degrees centigrade averaged from the ground to the height h.

TABLE 11E. Δu for $\bar{t}^* \neq 0$. Values to be multiplied by $h \times 10^{-2}$ and $\left\{\begin{matrix}\text{added to}\\ \text{subtracted from}\end{matrix}\right\}$ u for $\left\{\begin{matrix}\bar{t} < 0\\ \bar{t} > 0\end{matrix}\right\}$.

$\bar{t}$ \ F	420	430	440	450	460	470	480	490	500
±10	0.2	0.2	0.2	0.2	0.2	0.2	0.2	0.2	0.2
±20	0.4	0.4	0.4	0.4	0.4	0.4	0.4	0.4	0.4
±30	0.6	0.6	0.6	0.6	0.6	0.6	0.6	0.7	0.7
±40	0.7	0.8	0.8	0.8	0.8	0.8	0.8	0.9	0.9

*$\bar{t}$ = temperature in degrees centigrade averaged from the ground to the height h.

6.6 DIURNAL VARIATION OF THE GRADIENT OF MODIFIED M INDEX[g]

The vertical gradient of modified refractive index depends on the vapor pressure and temperature gradients according to the formula[h]

$$\frac{dM}{dz} = \frac{79}{T}\left(\frac{4800 - 0.14T}{T}\right)\frac{de}{dz} - \frac{79}{T^2}\cdot \left(\frac{9600e}{T} + p - 0.14e\right)\frac{dT}{dz} + \left(\frac{1}{21} + \frac{79}{T}\cdot\frac{dp}{dz}\right).$$

Coefficients of vapor pressure and temperature gradients are about 4.5 and 1.5 respectively. The third term gives a positive increase of 4 M units per 100 ft. In this paper[11-14] the diurnal variation of the vertical M gradient will be inferred from the diurnal variation of temperature and humidity gradients.

6.6.1 Temperature Lapse Rates over Land

On clear nights with light winds temperature inversions form in the lower atmosphere. The following characteristics of these inversions are to be noted.

1. The inversion begins as a shallow layer near the ground before sunset, rises sharply after sunset and then more gradually to a maximum height at about sunrise.

2. The temperature difference between two fixed levels in the first 100 ft of the ground is maximum shortly before sunset and oscillates about a slightly lower value the remainder of the night. (See Figure 10.)

Observations at Leafield, England, and Potsdam, Germany, corroborate this. This phenomenon is probably due to the more favorable humidity gradient in the early evening and to the heat of condensation released by dew formation in the later night hours.

Superadiabatic lapse rates characterize the lower atmosphere during clear days. The lapse rates increase sharply from sunrise to 3 or 4 hours after, gradually reach a maximum at about noon, and decrease sharply after the time of the maximum temperature.

6.6.2 Temperature Lapse Rates over the Sea

The air over the sea has a greater diurnal range than the sea itself. Over the Sunda Sea this range has been observed to increase from 0.5 C at the surface to 1.5 C at 500 m. The night lapse rates over the ocean are therefore more unstable than the day lapse rates. Observations of the *Meteor* expedition in equatorial regions revealed a mean inversion of 0.2 C in the first 9 m during the early afternoon, whereas in the early morning a mean lapse of 0.6 C was observed.

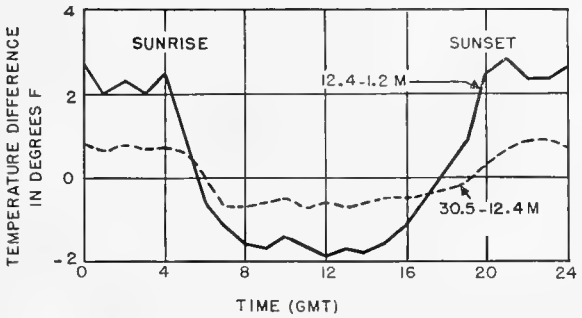

FIGURE 10. Mean temperature variation on clear June days at Leafield, England.

6.6.3 Vertical Vapor Pressure Gradients

At locations where a continuous supply of moisture on the ground is available, vapor pressure gradients follow evaporation processes and are maximum at the time of the maximum temperature at about sunrise. This diurnal course characterizes conditions over the sea, cloudy days over the land, and winter or rainy seasons over the continent.

On clear days over the continent the vertical vapor pressure gradient is minimum at about sunrise, reaches a maximum in midmorning, and lowers to a secondary minimum at the time of the maximum temperature (in desert regions this is the principal maximum shortly after sunset). Evaporation and mixing with drier air aloft govern this course. At night the soil absorbs moisture from the air causing a decrease in vapor pressure gradient.

The seasonal and diurnal variation of vapor pressure gradient is illustrated in Figure 11. Maximum vapor pressure gradients are noted during April, the hottest time of year, and minimum in January. The oceanic type is represented by the curve for July in the rainy season.

6.6.4 Vertical M Gradient

Over the sea both temperature and humidity gradients aid in causing a maximum of trapping during the day and a minimum during the night. The effect, however, is probably small.

Over the continent, a minimum of trapping will exist in midafternoon. Thereafter both temperature

[g]By Raymond Wexler, Camp Evans Signal Laboratory.

[h]Symbols have same meaning as in preceding section, except that h is replaced by z.

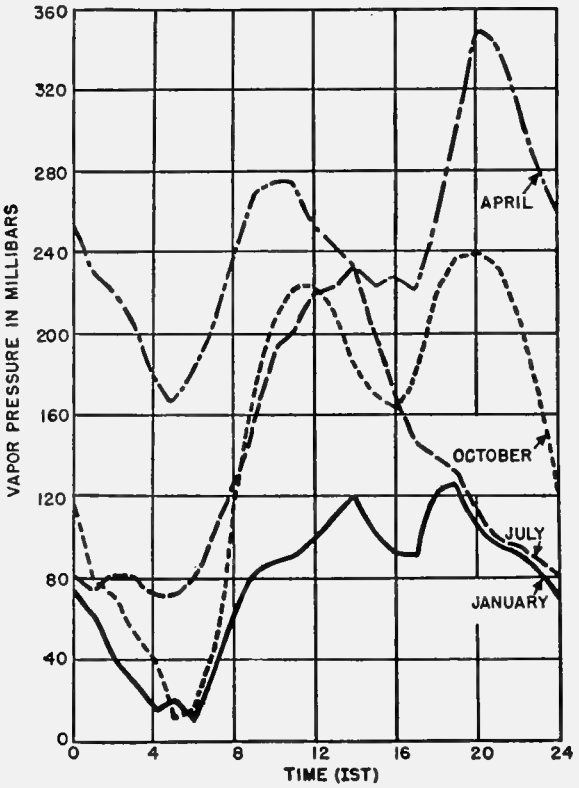

FIGURE 11. Hourly vapor pressure difference, 6 to 46 ft at Calcutta.

and humidity factors will cause a rise in the vertical M gradient to a maximum shortly after sunset. From that time to sunrise a decrease in the M gradient will occur. However, the height of the inversion continues to grow until sunrise, tending to cause an increase in the height of the duct. Whether a maximum or minimum of trapping will occur at sunrise will depend on whether the increase in the height of the inversion balances the decrease in vertical humidity gradient. It is probable that the humidity factor is the more important since the small magnitude of the temperature increase in the upper portions of the inversion will seldom be sufficient to cause a decrease in M with height. After sunrise rising humidity gradients, partially balanced by falling temperature gradients, will cause a small maximum of M gradient at midmorning. Thereafter the M gradient will decrease to the afternoon minimum.

The maximum and minimum decrease of M from 6 ft to 46 ft, based on mean temperature and humidity data at Calcutta, India, are given in Table 12.

In July the morning minimum and afternoon maximum with small amplitude illustrate the oceanic type. The other months illustrate the continental type. According to the table a maximum of trapping in India should occur in April just prior to the rainy season.

TABLE 12. Decrease of M from 6 to 46 ft (Calcutta).

Month	A.M. Min	A.M. Max	P.M. Min	P.M. Max
Jan	1	4	1	6
April	7	9	5	16
July	2	..	..	6
Oct	1	7	3	11

6.7 DETERMINING FLUCTUATIONS IN REFRACTIVE INDEX NEAR LAND OR SEA[1]

In connection with the rapid fluctuation or scintillation frequently observed in microwave reception, questions arise concerning turbulent atmospheric fluctuation at fixed points along the transmission path, particularly fluctuations in refractive index. Rapid measurement of both temperature and humidity so as to give a direct determination of fluctuation in refractive index is difficult. The purpose of this paper is to suggest that in certain cases the measurement of temperature fluctuation alone can give a good indirect estimate of fluctuation in the modified index.

The basic principle underlying this suggestion is that, if two initial kinds of air are mixed in different proportions, for all possible mixtures a fixed relation exists between any two properties conservative for adiabatic changes.

To illustrate this, consider a diagram with potential temperature and specific humidity as coordinates. Two initial kinds of air would be represented by two points on this diagram, and all mixtures of the two kinds would be represented by points on the straight line drawn between the two initial points.

The practical case occurs when one point represents a large homogeneous mass of air, and the other a fixed boundary condition at the ground or water surface. The straight line then represents the mixtures that can occur in the vicinity of the boundary. For these the line shows specific humidity as a function of potential temperature. The relation between potential temperature and potential refractive index could be shown by a similar diagram.

Figure 12 shows some corroboration of this method and also how the method can be applied. This charac-

[1]By R. B. Montgomery, Radiation Laboratory, MIT.

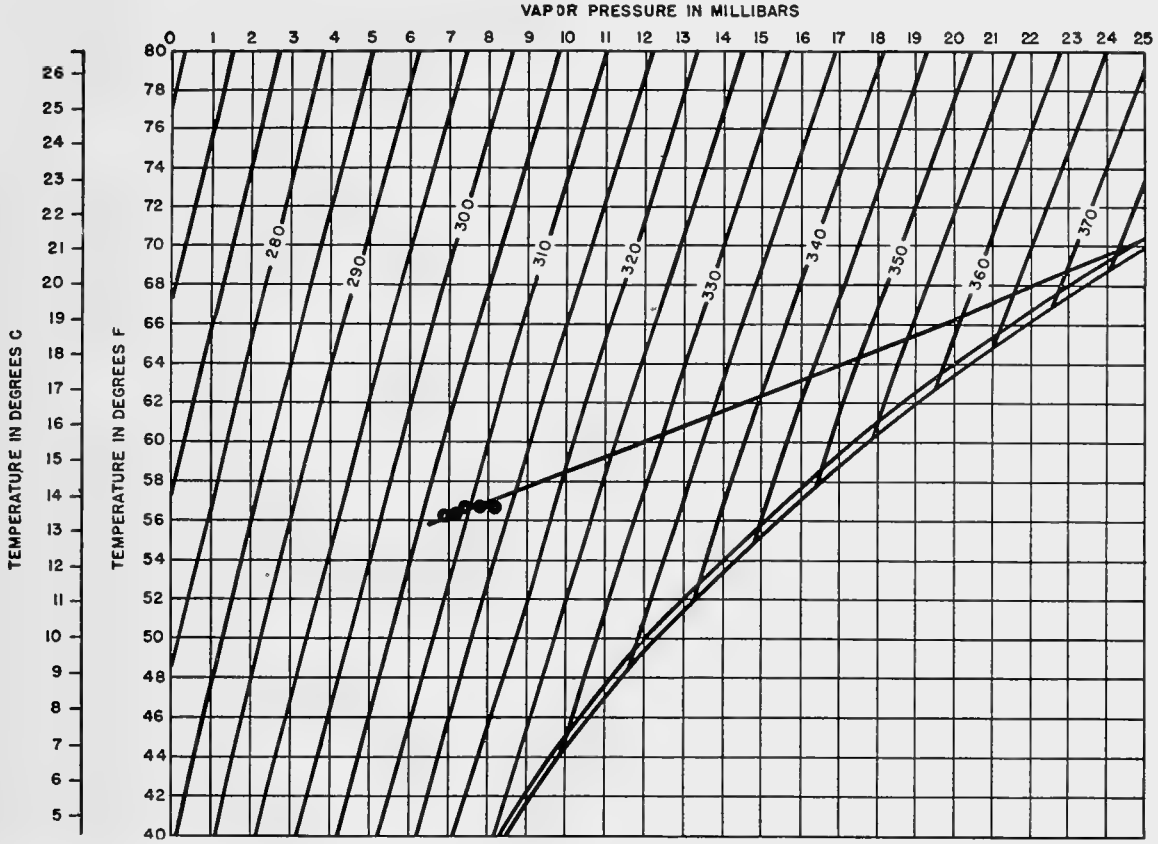

FIGURE 12. Observations on February 24, 1945 at masthead of ship in Gulf Stream, wind 14 knots. Characteristic diagram. Vapor pressure over water is shown by lower bounding curve, over salt water by upper bounding curve. The family of curves gives modified index for 1,000 mb and zero height; or $(n-1)10^6$ for microwaves at 1,000 mb, zero height, where n is refractive index at $h = 0$.

teristic diagram has the same orientation as the Rossby diagram which is in routine meteorological use but with somewhat different coordinates.

The ordinate is temperature and the abscissa is vapor pressure. A pair of curves gives the vapor pressure over fresh water and over sea water. The family of curves gives refractive index at radio frequencies and at a total pressure of 1,000 mb, or $h = 0$.

On the diagram are plotted a few of a long series of determinations made by reading a sling psychrometer at half-minute intervals. These were recently obtained by the Woods Hole Oceanographic Institution at the masthead of a ship crossing the Gulf Stream at a time when the air was much colder than the water. The water temperature was 70 F, fixing the boundary condition. The points lie fairly well on the straight line through the boundary value. They cover a range of 5×10^{-6} in refractive index. Probably a greater range would be indicated by a psychrometer having a more rapid response.

It is seen that, whenever the fluctuation in refractive index at a point in the atmosphere is due to turbulent mixing between a large homogeneous mass of air and air controlled by a fixed boundary condition, the fluctuation may be obtained as follows: Measure the average temperature and humidity at this point and at the boundary, thus determining the relation between refractive index and temperature. Measure the fluctuation of temperature, from which the fluctuation of refractive index may be found from the established relation.

It may be noted that the water temperature less the average air temperature gives a value for the temperature deficit. In the same way one may arrive at a humidity deficit and an M deficit (one million times the deficit of refractive index). Each of these quantities is represented on the diagram by the change from one end to the other of the line. It follows that the suggested method may be stated in terms of the relation that the ratio of temperature fluctuation

to temperature deficit is equal to the ratio of humidity fluctuation to humidity deficit and very nearly equal to the ratio of M fluctuation to M deficit.

6.8 GRAVITATIONAL WAVES AND TEMPERATURE INVERSIONS[j]

It has been noted that the guided propagation of microwaves is often accompanied by deep fades with periods of the order of a few minutes. The suggestion has been made that these fluctuations may be associated with atmospheric wave motion which could make the top of the duct an undulating surface rather than a level one.[16,17] Therefore, it seems desirable to discuss, from a meteorological point of view, the possibility of the existence of such atmospheric waves and the physical characteristics of any which might exist. The purpose of this paper is to review and summarize the meteorological information which is available concerning the subject.

A theoretical consideration of the problem indicates that atmospheric wave motion can occur at any surface in the atmosphere where there is a rapid change in wind velocity with height and a stable stratification of temperature. Such conditions are best fulfilled at temperature inversions, which, it will be noted, usually correspond to a rapid decrease with height of the index of refraction. The wind shear supplies the energy to set up the wave motion, in the same way in which waves are formed at the surface of the ocean. Gravitation acts as a stabilizing or restoring force. Hence, these waves are of a mixed shearing and gravitational type. The waves may be stable or unstable, depending on their wavelength, on the density and wind speed differences between the two media, and on the lapse rates in the two media. For any given values of the density and wind velocity differences and of the lapse rates, there is a critical wavelength below which wave motion is unstable; that is, it disappears into turbulent eddies because of the shearing effect. All wavelengths above this critical value will remain stable because of the gravitational effect. Hence one may speak of the former as "shearing waves" and of the latter as "gravitational waves." It is the stable or gravitational type with which we are concerned.

These considerations hold for wavelengths up to about 500 km. For longer wavelengths the effect of the earth's rotation must be considered. In this paper only the shorter wavelengths where this effect may be neglected will be discussed.

A mathematical analysis of wave motion and determination of the critical wavelengths involves a solution of the equations of motion and continuity and an application of certain boundary conditions. In order to derive the critical wavelengths given below, the following assumptions have been made.

1. The inversion or shearing layer may be regarded as a strict discontinuity between the air above and the air below. This assumption is sufficiently accurate provided the thickness of the layer is small compared to the wavelengths which occur.

2. The velocities associated with the wave motion are small compared with the undisturbed velocities of the air masses above and below the inversion.

3. The height of the inversion above the lower boundary (ground) is equal to or greater than 40 per cent of the wavelength which occurs.

4. There is no friction between the two fluids.

Two cases may be considered. The first is the case where the air masses are assumed to be incompressible and homogeneous. It also holds for two air masses with adiabatic lapse rates. In this case the critical wavelength is given by[18a]

$$\lambda_{\text{crit}} = \frac{2\pi}{(T'-T)g}\,\frac{(U'-U)^2\,T'\,T}{T'+T}\,.$$

In the second case the air masses are compressible and isothermal. For this case the critical wavelength is given by[19]

$$\lambda_{\text{crit}} = \frac{2\pi}{g}\,\frac{(U'-U)^2}{4}\cdot \frac{T'+T}{\sqrt{(T'-T)^2+2\frac{k-1}{kR}\,(T'+T)\,\frac{(U'-U)^2}{4}}}\,.$$

In these two formulas,

T' = temperature in the upper air,
T = temperature in the lower air,
U' = velocity in the upper air,
U = velocity in the lower air,
g = acceleration of gravity,
k = c_p/c_v = 1.405,
R = gas constant for air
= 2.87×10^6 cm^2/sec^2 degree.

In Table 13 the critical wavelengths in meters are tabulated for various values of wind shear and temperature difference. Values for the adiabatic case are

[j]By Lt. R. A. Craig, AAF, Weather Division.

tabulated above values for the isothermal case. For an intermediate lapse rate some intermediate value holds.

TABLE 13. Critical wavelengths in meters for $T = 280°A$.

	ΔU (meters per second)							
ΔT (C)	0	2	4	6	8	10	12	14
0	..	∞	∞	∞	∞	∞	∞	∞
	0	339	677	1016	1354	1693	2031	2370
2	0	180	718	1616	2872	4488	6463	8796
	0	159	493	860	1225	1584	1938	2287
4	0	90	359	808	1436	2244	3231	4398
	0	87	317	632	985	1351	1720	2087
6	0	60	239	539	958	1496	2155	2933
	0	59	226	479	782	1121	1478	1843
8	0	45	180	404	718	1122	1616	2199
	0	44	174	375	634	935	1264	1612
10	0	36	144	323	574	898	1293	1759
	0	36	140	308	529	793	1090	1413
12	0	30	120	269	479	748	1077	1465
	0	30	118	260	451	684	952	1247
14	0	26	103	231	410	641	923	1256
	0	26	101	225	393	600	841	1110

Upper value: incompressible, homogeneous fluids. Lower value: compressible, isothermal fluids.

Thus, for any given inversion, stable wave motion may exist so long as the wavelength is equal to or greater than the listed values and less than about 500 km. There is no theoretical reason to believe that any particular wavelength in this wide range is more apt to occur in nature than any other.

There is, however, some observational evidence to indicate that the wavelengths which occur in the atmosphere are near the lowest possible values which can occur, namely, the critical values tabulated above. Billow clouds have been observed to occur near inversions, and there are some ten cases on record where wavelengths of the billows as well as values for the temperature and wind velocity differences have been observed. In these cases the maximum difference between observed wavelength and critical wavelength was 48 per cent. In only three cases was the difference greater than 15 per cent.[18b]

Other weather phenomena have been observed which indicate stable wave motion in the atmosphere. In 1936, quite regular fluctuations were measured in ceiling height at San Diego on two occasions. The amplitude of the fluctuations averaged 25 to 30 m in the two cases, with periods of about 15 to 20 min over time intervals of 4 or 5 hours.[20] In 1934 at the Blue Hill Observatory in Massachusetts, there occurred wave-like fluctuations in the pressure record, which were analyzed by Haurwitz.[21] In these cases upper-air data were not sufficiently accurate to compute wavelengths quantitatively by means of the critical wavelength formula, but it appeared from approximate values of wind shear and density difference that the critical wavelengths might well be occurring.

If it is desired, then, to predict what wavelengths will occur with a given inversion, the critical values would seem in the light of these observations to give a good estimate of the order of magnitude.

Assuming that these wavelengths are the ones which occur, one can discuss the velocities and periods of the wave motion. For these critical wavelengths, the velocity of the wave motion is the mean of the velocities of the air masses above and below the inversion. Hence the period can be estimated by dividing the wavelength given in the table by this value. As an example, for a mean velocity of 5 m per second, the periods vary from about 6 sec to about 8 min, depending on the wind shear and density difference.

The vertical velocity at the inversion cannot be determined, since an arbitrary constant is involved. However, it can be said that this vertical velocity will be reduced to one-tenth its inversion value at a height d equal to 37 per cent of the wavelength above the inversion. This holds strictly only for the incompressible, homogeneous case but is approximately correct for the other case as well.

It is known, then, from theoretical considerations and some observational material, that wave motion is apt to occur at a layer in the atmosphere where there is a temperature inversion accompanied by wind shear. When such inversions are believed to be of importance in affecting the propagation of radio waves, it should be remembered that there may well be wave motion occurring and that the interface is not necessarily a level surface. It remains to be determined whether this fact will help to explain the observed very high frequency fading. An estimate of wavelength, period, and velocity of the atmospheric wave motion, as given by Table 13, may be of assistance in testing this possibility.

6.9 ANALYSIS OF DUCTS IN THE TRADE WIND REGIONS[k]

This report is an analysis of the frequency and magnitude of low-level and elevated ducts as indicated by meteorological observations over the trade wind areas of the Atlantic and Pacific Oceans. Mete-

[k]By Raymond Wexler, Signal Corps Ground Signal Agency.

orological soundings of the *Meteor* expedition,[22] taken during 1925 to 1927 over the Atlantic Ocean were utilized in analyzing elevated ducts. Climatological data of the Atlantic and Pacific Oceans were employed in study of low-level ducts. A qualitative analysis of 95 soundings of the *Meteor* expedition had previously been made in reference 23.

6.9.1 Elevated Ducts

Trade Wind and Doldrums Areas

A semipermanent high-pressure system is located over the oceans at about 30 degrees of latitude. The northeast trade winds blow from 30°N to about 5°N. Between the equator and 30°S the southeast trade winds prevail. The doldrums, a region of light winds and heavy rainfall, appears between the two wind systems.

Ducts in the Trade Wind Region

In the trade winds a warm, dry subsiding air mass exists over a cool, moist ground layer. The transition zone between the two air masses is characterized by a temperature inversion (increase with height) and a sharp decrease of the water vapor content of the air. It is this transition layer which coincides with the duct, which in this paper is defined as a layer in which the curvature of the path of high-frequency electromagnetic waves exceeds the curvature of the earth. Within these ducts these waves may be trapped, and abnormally long ranges may occur.

As the trade winds blow toward the equator over warmer ocean areas the heating from below causes the duct to rise and to become weaker until finally near the equator the duct disappears and the two air masses become thoroughly mixed.

Height of the Duct Base

The base of the inversion (or duct) increases in elevation equatorward. According to the *Meteor* soundings, taken during March and April, the average elevation of the base of the inversions rose from 700 m at latitudes 15°N to 20°N, to 1,020 m at 10°N to 15°N, and to more than 2,000 m at latitudes 5°N to 10°N. Between the equator and 5°N, no ducts existed to an elevation of 2,500 m.

The elevation of the base of the inversion also increases westward into the Atlantic from the African Coast. At latitudes 15°N to 20°N, its elevation increases from less than 300 m off the African Coast to 1,500 m in mid-Atlantic.

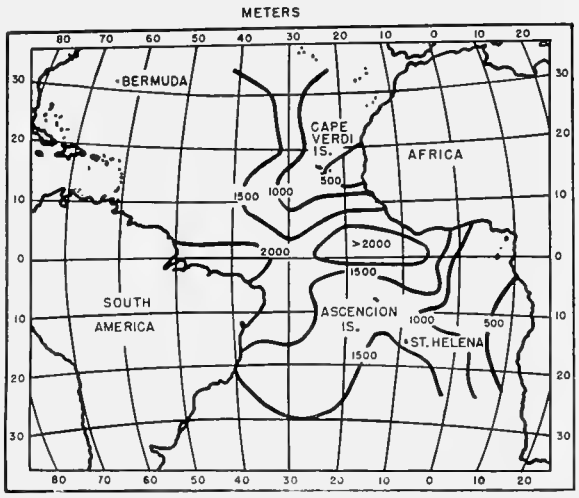

Figure 13. Height of the temperature inversion base over the Atlantic. (After von Ficker.)

Figure 13[24] depicts the height of the temperature inversion base in the Atlantic, based largely on the data from the *Meteor* expedition. South of the equator, soundings were made during the winter season (June to August), while north of the equator the soundings were made chiefly in the spring (March to May). The height of the base of the inversion has a seasonal variation, being greater in winter than in summer.

Figure 14 represents typical *M* curves computed from the soundings of the *Meteor* expedition. Curves A (sounding 182 of the *Meteor* expedition taken just off the African Coast) show a ground-based duct of elevation 140 m on the ascent curve and 90 m on the descent curve. Oceanward, the duct becomes ground-based, S-shaped, as is shown by curves B (sounding 183).

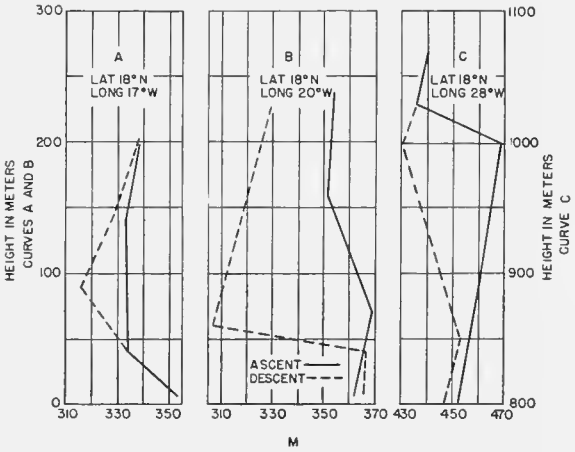

Figure 14. *M* curves, *Meteor* expedition, March 1927.

The descent curve[1] shows a decrease of 59 *M* units in 20 m, corresponding to a ray curvature about 20 times greater than that of the earth's surface. Westward into the Atlantic the inversion base rises to about 1,000 m. (Curve C, sounding 184.)

Frequency of Duct Occurrence

Within the trades proper a duct is practically certain to exist. In Table 14 the percentage of duct occurrence, by latitude according to *Meteor* soundings, is tabulated. The extreme curve (ascent or descent) was utilized in determining the existence of a duct.

Table 14. Frequency of duct occurrence by latitude over the Atlantic Ocean based on the *Meteor* soundings.

Latitude, degrees	Frequency (% of all cases)	No. of cases
20-15N	100	19
15-10N	71	19
10-5N	40	17
5-0N	0	18
0-5S	0	17
5-12S	56	16
12-18S	53	15
18-24S	73	26
24-35S	10	20
35-50S	19	21
50-63S	0	20

It is evident from Table 14 that in the vicinity of the doldrums (5°N to 5°S) the existence of ducts is rare. A maximum frequency occurs between latitudes 15° and 25°. Note that all soundings made between latitudes 15° to 20°N indicated the presence of a duct.

Thickness of Ducts

The average thickness of the duct in the trade wind inversion, according to *Meteor* data, is about 130 m. According to the theory of the dissipation of the ducts near the equator due to heating from below, the thickness should decrease toward the equator. No evidence of such a decrease was found from the *Meteor* soundings, probably because of the large height interval between observations. For this reason too, the figure for average thickness of 130 m is probably too large.

Intensity of Ducts

The decrease of the modified index of refraction within the duct averaged 28 *M* units between latitudes 10° to 20°N, and only 14 *M* units between latitudes 5° and 10°N, indicating a decrease in the intensity of the duct equatorward. The intensity of the duct also decreases oceanward from the coast of Africa.

[1]The ascent and descent curves disagree largely because of the lag of the humidity element in the sounding rig. The curve showing sharper inversion is therefore probably the more accurate.

6.9.2 Surface Ducts

The thickness of surface ducts depends on the wind speed and the magnitude of the vapor pressure difference between the ocean surface and the air at some representative level (say the ship's bridge). It is probable that the wind factor is the more important. Near the west coasts of continents the lowering of the trade wind inversion becomes the most important factor. Duct intensities over the ocean in the Northern Hemisphere, based on climatic charts of the ocean, have been computed by Montgomery and Burgoyne.[25]

Wind Speed

According to observations taken in the Pacific north of New Guinea and northeast of Saipan, ducts were less than 10 ft in depth at wind speeds of one knot and were 40 to 60 ft at wind speeds of 10 to 20 knots.[26] According to climatic charts of the ocean (6), the average wind speed in the trade winds is maximum in summer at 15° to 20°N and in winter at 10° to 15°N. In the Southern Hemisphere maximums are at 10° to 15°S in summer (December to February) and at 5° to 10°S in winter. These latitudes in the respective seasons should also coincide with the maximum thickness of surface ducts.

Vapor Pressure Difference

As the air flows toward the equator over continually warmer water surfaces moisture is being supplied to the air by evaporation from the water surface. Nearer the equator the increased rainfall decreases the water vapor pressure difference between the ocean surface and the air above. According to climatic charts[27] the maximum vapor pressure difference between ocean surface and the air above in the trade exists at about latitudes 20° in summer (in both hemispheres) and at latitudes 10° to 15° in winter. This effect should also contribute to the existence of a maximum duct height in the trade winds at about 20° latitude in summer, 15° in spring and fall, and 10° in winter.

Surface Ducts near the Western Coasts of Continents

All soundings of the *Meteor* expedition within 300 miles of the coast of Africa showed intense ground-

based ducts or S-shaped ground-based ducts. These ground-based ducts are also a common occurrence on the west coast of the United States. At San Diego the average height of the inversion base is near 1,000 ft during the summer.[28] The height of the duct base has a diurnal variation, being maximum in the morning at about 0800 local time and minimum at about 1600. The diurnal variations are governed by land and sea breeze phenomena.

6.9.3 Experimental Evidence

During 1944, aircraft traffic to and from Ascension Island at 8°S in the Atlantic was tracked by two 105-mc radars sited 2,500 and 1,700 ft above mean sea level. The following observed phenomena were reported verbally.

1. Ranges were greater during the dry season than during the wet season.

2. Ranges westward (270°) were greater than to the northeast (40°), and greater northeastward than to the north (10°).

The decrease in duct intensity equatorward described herein is commensurate with observation (2), in which ranges are reported to be less toward the equator than along a parallel of latitude.

6.9.4 Conclusions

1. Over the trade wind areas of the oceans both elevated and surface ducts often exist.

2. The elevated duct is of maximum intensity and frequency at 15° to 20° of latitude. It decreases in intensity and frequency equatorward, disappearing in the doldrums.

3. The surface duct, dependent largely on wind speed, is of maximum depth at about latitude 20° in summer, 15° in spring and fall, and 10° in winter.

4. Near the western coasts of continents the elevated duct lowers into an intense ground-based duct.

Chapter 7

METEOROLOGICAL EQUIPMENT FOR SHORT WAVE

7.1 METEOROLOGICAL EQUIPMENT FOR PROPAGATION STUDIES[a]

7.1.1 Outline of Problem

EXPERIENCE GAINED during the last 2 years with radar, especially microwave radar, and with experimental microwave communication equipment has shown that the electromagnetic radiation field produced by a transmitter is subject to large variations depending on the weather. These variations are caused by *refraction* and so are related to variations of dielectric constant in the atmosphere. Pressure, temperature, and humidity determine the dielectric constant (refractive index).

It has been found that above a certain height variable with season and geographical location but rarely exceeding 1,500 m above ground, atmospheric refraction is reasonably constant. In the lower levels and especially in the lowest hundred meters of the atmosphere, temperature and moisture conditions strongly affect the radiation field and thereby influence the operation of radar and other short and microwave equipment. In order to evaluate this effect in quantitative terms, the temperature and moisture distribution in the lowest layers must be determined with as high a degree of accuracy as is compatible with speed, ease of operation, and other practical limitations.

A number of methods have been tried during the past 2 years which range from measurements with ordinary radiosonde equipment to the use of a psychrometer on the steps of a fire ladder. Two facts have appeared rather clearly: First, hairs are not suitable for moisture measurements of this type on account of their great sluggishness (except perhaps for stationary use on towers), since the time of adaptation of a hair to appreciable changes in humidity is of the order of 3 to 5 minutes. Secondly, it has been found that ordinary radiosondes are not usually appropriate because the readings obtained from them normally are taken about 100 m apart in vertical distance and for this particular problem a more detailed knowledge of the temperature and moisture distribution is necessary. With a clock-driven radiosonde this can be remedied by loading the sonde down by means of a ballast (water or sand) which slows down the ascent of the instrument in the lower levels. If the ballast is made to run out gradually, the full lift of the balloon may be restored at any given level. This method cannot be applied to the U. S. Weather Bureau radiosonde in which temperature and moisture data are sent out by a mechanism in which electric contacts are closed by a pressure cell at predetermined levels (see, however, Section 7.1.8, below).

On the whole it has been found more advisable to develop new or improved instruments or to adapt special instruments for a low-level sounding technique rather than to rely on the existing facilities for aerological measurements. The methods developed so far involve the use of planes and dirigibles as well as captive balloons and kites. For the lowest strata, specially built towers and ship installations have come into use.

7.1.2 Wet and Dry Bulb Methods

The use of humidity data for radio propagation problems involves new features in instrumental technique because the main effects of strong refraction are found under approximately calm weather conditions. Therefore, when wet and dry bulb methods for humidity measurements are used, particular care must be taken to insure satisfactory aeration of the wet bulb. As a rule, an air speed of about 3 m per second (about 6.5 mph) is considered adequate ventilation for the wet bulb. In a plane, dirigible, or kite the necessary aeration is automatically provided. But on a tower or when carried by a captive balloon, artificial aeration will frequently be necessary. It has been claimed,[b] however, that if a wet bulb electrical resistor is used in conjunction with a captive balloon adequate aeration can be provided by giving the balloon cable a few violent jerks of about 5-ft amplitude.

An ordinary sling psychrometer held out of the window of a flying plane and aerated by the slip stream has been found to give fairly reliable results, provided the wet bulb is kept properly moistened. This method has been used with good success for preliminary research work. It may be presumed that the use of a

[a] By W. M. Elsasser, Columbia University Wave Propagation Group.

[b] Data, courtesy of U.S. Navy Radio and Sound Laboratory, unpublished.

rather slow-flying plane is essential, in order to keep the dynamic temperature correction small and also in order to insure a not too excessive rate of evaporation.

Thermocouples, thermopiles, and temperature-sensitive resistors frequently are used as temperature responsive elements in place of actual wet and dry bulb thermometers. They are incorporated in specially designed electrical bridge circuits in which the temperatures are read on either indicating or recording meters.

7.1.3 Temperature and Humidity Resistance Elements

TEMPERATURE

Temperature-sensitive resistors are satisfactory both with regard to accuracy and the absence of lag. The British have used platinum resistance thermometers very successfully in stationary installations. In the United States electrolytic or ceramic resistance elements are commonly used. The latter can be made to change their resistance several fold over a relatively narrow temperature interval. Their accuracy is therefore limited, not so much by the accuracy of the current measurement as by their intrinsic stability after calibration, proper radiation shielding, etc.

The electrolytic element developed for the Bureau of Standards radiosonde[1,2] has a time-lag constant (time required to attain the fraction $(1—e^{-1}) = 0.63$ of the total change) of 8 sec at an airspeed of 3 m per second, of 14 sec at an airspeed of 1 m per second, and of 40 sec in still air.

Recently the ceramic Sanborn element[c] has come into use; it has about the same lag characteristics as the electrolytic element but is practically free from aging. The following time-lag constants have been measured:[4] 8 sec at an airspeed of 3 m per second and 12 sec at an airspeed of 1 m per second. Another source reports 20 sec at an airspeed of 5 m per second (this value seems too large in comparison with the others) and 42 sec in still air. (See footnote b, pg. 97.)

MOISTURE

The Bureau of Standards resistance element as well as the Gregory humidiometer (a British development) uses a dilute solution of lithium chloride.

In the Bureau of Standards element the lithium chloride film is deposited on the surface of a thin cylinder on which there is a bifilar winding of two thin wires. The stability and aging characteristics of this element are described in the literature.[1,3] An average actual accuracy of 5 per cent relative humidity is claimed for the ordinary radiosonde when used under routine conditions. Higher accuracy (1 per cent RH) is claimed, at least at temperatures above freezing, when used with captive balloon equipment,[5a] partially because the current is frequently reversed to cut down polarization effects and partially because the calibration can be more closely watched. Tests[3] show that at an airspeed of 2.5 m per second the time lag constant is 3 sec at 24 C and 11 sec at 0 C.

The Gregory humidiometer[d,e] uses a lithium chloride solution soaked in a clean cotton cloth. The resistance of the element changes from over 100,000 ohms at 30 per cent RH to as little as 50 ohms at 100 per cent RH. It undergoes pronounced aging during the first several days and then remains sensibly constant for a number of weeks. The instrument is in an experimental stage and is at present being tried out at the Rye towers in Sussex (see Section 7.1.6, below).

7.1.4 Circuit Design for Resistor Elements

Thermocouples or thermopiles are commonly used in a conventional bridge circuit. In connection with the electrolytic and ceramic type of resistance elements, circuits have recently been developed that include certain features novel in the technique of atmospheric measurements.

In the equipment developed by Washington State College[5a] the standard radiosonde temperature element was originally used, but in a more recent type they have combined the Sanborn temperature element and the radiosonde electrolytic humidity element. The electric equipment (Figure 1) consists of a dry cell with potentiometer supplying about ½ volt, two double-pivot microammeters, one in series with each of the elements, and a 6-volt d-c motor. The relay reverses the current through the elements at a rate of 50 cycles (100 reversals) per minute while maintaining constant polarity at the meters. The current is smoothed by large condensers in parallel with the meters. The commutation eliminates polarization of the electrolytic elements and greatly increases their accuracy and useful life. The commutation period is so selected that it is long enough to prevent inductive and capacitative interaction between the two circuits

[c]Manufactured by Paul H. Sanborn, 2602 Riverview Drive, Parkersburg, W. Va.

[d]Information supplied to the U. S. Propagation Mission to England.

[e]Instruments made by Negretti and Zamba, Ltd., London.

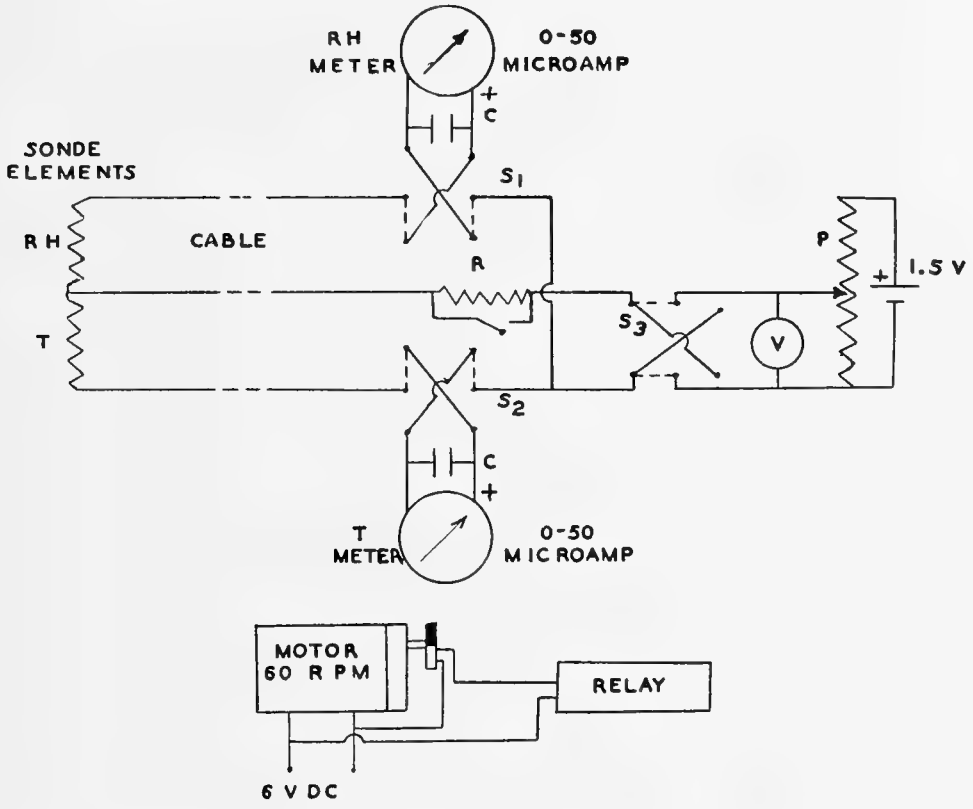

FIGURE 1. Wired sonde circuit.

The potentiometer P applies a constant voltage (0.36 v at low and 0.18 v at high RH) to both of the independent circuits of the sonde proper. The currents, determined by the resistances of the relative humidity and temperature elements respectively, are read on the RH meter and T meter. S_3 commutates these currents at half-second intervals; S_1 and S_2, actuated simultaneously with S_3, maintain constant polarity at the meters. The 1,000-μf condensers CC smooth the currents through the meters. $S_1S_2S_3$ are contained in the pile-up of a single relay which is actuated by a miniature worm-geared motor as shown. The 10,000-ohm protective resistance R is shorted out during measurement. Connections to the ground end of the cable are made through slip rings (not shown) mounted on the cable reel. All components, excepting the sonde, cable, and 6-v storage battery, are housed in a single case 20x9x7 in.

but is short enough to allow of smoothing the currents through the meters.

The circuit illustrated in Figure 2 has been developed by the Propagation Group at the Radiation Laboratory, MIT.[4] The apparatus includes two Sanborn resistance elements, one of them surrounded by a moistened wick. The current flowing through the resistors originally was fed into an amplifier which drove a recording milliammeter. However, after a number of amplifiers had been tried, the simple scheme shown in Figure 2 was adopted and, at the time of the writing of this report, is being used for all measurements made by the Radiation Laboratory, those from planes as well as those from captive balloons which will be described later.

The dry and wet elements are placed in the circuit alternately by means of a hand-operated switch. The device can be calibrated by means of a set of fixed precision resistors and the balance of the bridge is checked before each flight. An advantage of this method is the possibility of using a commercial d-c recorder (0 to 1 ma) immediately at the plate terminals of the amplifier tube. This is particularly favorable for use in airplanes and dirigibles.

It is well known that the ordinary thermocouple is not readily adapted to recording purposes. Only at stationary installations such as towers, where multijunction thermopiles can be used, is it possible to record the indication of the sensitive galvanometers required.

7.1.5 Anemometers

Wind measurements are of importance in connection with off-shore winds at coasts which give rise to pronounced refraction of short and microwaves. The ordinary commercial anemometers become quite un-

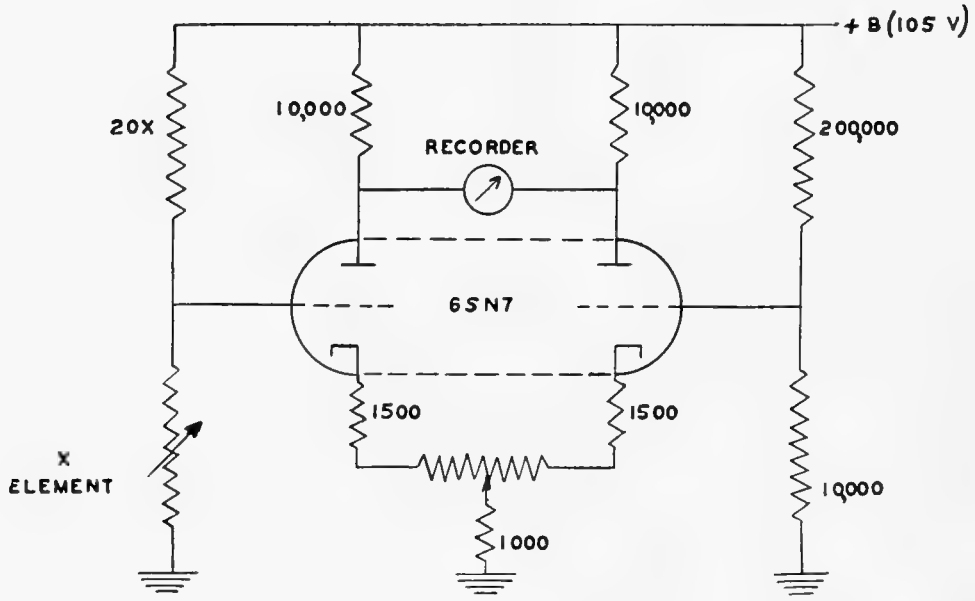

FIGURE 2. Schematic circuit of electronic amplifier.

The resistance of the thermal element, *X*, controls the bias of one triode of the double triode, 6SN7, which acts as a vacuum tube voltmeter to compare the resistance of the thermal element with a standard resistance. A 1-ma recording meter is placed between the two plates. The resistance in the grid circuits is so chosen as to place 10 v across the thermal element at the lowest temperature of each range. This voltage decreases as the temperature rises. The zero is set by means of a 100-ohm potentiometer in the cathode circuit. Calibration of the amplifier is obtained by switching a series of precision resistors in steps of 1,000 ohms into the circuit in place of the thermal element. A range of roughly 25 C for full scale is used, and changes of 0.25 C can be measured. Sufficient overlapping is provided so that both wet and dry bulbs can record on a single setting.

The stability is such that with a change in line voltage between 95 and 120 v there is no readable change in the meter deflection at 0 (when the tubes are balanced) or at full scale reading. When tubes are replaced there is, at worst, a change of 1 per cent of full scale deflection tapering to no deflection at 0.

reliable at very low wind speeds (of the order of ½ m per second) and may stop completely. A special anemometer for low wind speeds[6] has been designed by the British Chemical Warfare Service and is used as a regular piece of field equipment by its units. In the United States a highly sensitive anemometer has been developed at the California Institute of Technology.[7] This instrument records wind speeds from 0.5 to perhaps 30 mph. It has the conventional three cups rotating on a vertical axis. Each rotation is registered on a counter by magnetically operated electrical contacts. For higher wind velocities the counter may be switched to record only every hundred rotations. The apparatus is delicate and is critical in its behavior toward certain adjustments.

7.1.6 Semipermanent Installations

TOWERS

Two major installations of towers are at present in existence in England. They are the Porton towers and the Rye towers. The Porton towers on the Salisbury Plain form part of the extensive meteorological equipment of the British Chemical Warfare Service and have been in use for a considerable number of years.[8] Continuous records of dry and wet bulb temperatures at heights of 4, 23, and 56 ft above the ground are made. The elements used are platinum resistance thermometers connected into bridge circuits and are artificially aerated. The recording mechanism is located near the bottom of the tower.

A similar set has recently been installed on the Rye towers in Sussex which form part of a CH radar system. Temperature and relative humidity are recorded for heights of 4, 50, 155, and 360 ft above ground. The resistance thermometers are similar to those at Porton, but the moisture measurements are made with the Gregory humidiometer described above.

In a large research project on microwave refraction carried on in the summer of 1944 by the Propagation Group at the Radiation Laboratory, a mast was erected at one terminal of the path. Wet and dry bulb temperatures are recorded continuously with the device described in Section 7.1.4 at heights of 4, 16, 36, and 55 ft above the sea surface, these heights varying somewhat with the tide. The measuring elements are located in one end of a horizontal piece of tubing 3 ft

long, and in the other end, close to the pole, an aeration fan is mounted. Wind velocity records are made by means of Stewart anemometers.

Ships

The Royal Navy has detailed three yachts for atmospheric measurements on an experimental microwave transmission path over the Irish Sea. They are provided with dry and wet thermocouples at altitudes of 5, 10, 40, and 50 ft above sea level. The former two are mounted on hinged beams outboard, while the latter two are on a mast in the forward part of the ship. The thermocouples are copper-constantan, and there are two in series for the temperature measurement with the cold junctions placed in a Dewar flask filled with melting paraldehyde (maintaining a temperature of 50 F). There are two pairs of dry and wet junctions connected in series which measure the wet bulb depression. The galvanometer is in the ship's cabin. Aeration is provided by the ship's movement, and when measurements are made the ship sails into the wind to minimize the effects of the discharge from the smokestack.

In the project at the Radiation Laboratory just referred to measurements are also being made from the mast of a boat. The 48-ft mast is provided with a 6-ft cross arm and a motor-aerated housing containing the elements can be raised from the bottom of the mast to the end of the cross arm, giving continuous information over the height of its travel.

Measurements carried out on shipboard by means of captive balloons or kites will be discussed in Section 7.1.8.

7.1.7 Measurements on Board Planes and Dirigibles

As has been mentioned before, a sling psychrometer held out of the window of a flying plane will give reasonably accurate results if some elementary precautions are taken to insure proper moistening of the wick.

The two types of instruments described in Section 7.1.4 have been adapted for use with airplanes. In the Radiation Laboratory instruments the two elements are mounted diagonally in a piece of Bakelite tubing about 1½ in. in diameter, the dry element in front of the wet element, relative to the wind stream. In the earlier airplane measurements water was blown over the moist element and a reading made when the recorder showed equilibrium to be reached. Now capillary action is used throughout, the water being supplied from a small vessel underneath the Bakelite tube. This instrument has been tested in a wind tunnel with wind speeds up to 145 mph. The dynamic pressure effect increases the reading by 0.4 C at the cruising speed of the plane (100 mph). This value was checked, both in the plane itself and in a wind tunnel.

The Washington State College [WSC] instrument has been adapted for airplane measurements and has been used on several types of planes during tests in Panama.[5b] The elements were housed in a single-walled cylinder of aluminum, about 1.75 in. in diameter, covered on the forward end with a cone. A small circular opening (⅜ in. in diameter) made by cutting off the end of the cone reduced the velocity of the air across the elements to about one twenty-second of the plane's speed. Comparison of a plane sounding and a balloon sounding in the same region at the same altitude and time gave identical results within reasonable experimental error.

With airplane measurements the determination of the plane's altitude becomes an important task. In the experimental flights at the Radiation Laboratory the altimeter of the plane itself was used. According to the experience obtained in Panama it is desirable to have an additional altimeter placed directly before the operator in order to facilitate rapid and accurate altitude determinations. The nominal accuracy of an airplane altimeter is about 20 ft. Over sea it may be possible to determine the absolute altitude of the plane with about the same degree of accuracy, but over land less accuracy is to be expected.

Measurements from a dirigible (blimp) have been carried out by Radiation Laboratory. The instrument is suspended on a cable about 100 ft below the ship.

7.1.8 Captive Balloon Sondes and Kites

Radio Transmission Type

Two different methods have been tried in connection with balloons and kites. When first used in practice an ordinary radiosonde was attached to the balloon (kite) and the results were recorded on the ground by radio in the usual way. This method was used in an experimental investigation carried out under the auspices of the AAF Board, Orlando, Fla.[9] Although by the nature of the instrument the measurements are spaced 200 to 300 ft apart, a rough survey of the temperature and moisture distribution sufficient for some operational purposes was gained in this way.

The record on the ground was taken by means of a standard U. S. Army radiosonde receiver.

It was pointed out in this report[9] that it might be advantageous to use a combination of two radiosondes in tandem, such that in one instrument the contacts are connected to the temperature device, in the other to the humidity element. It would then be possible to obtain simultaneous temperature and moisture readings at the same elevation, instead of alternating ones, as is the case when only one instrument is used. This would, however, require the use of two receivers at the ground with two slightly different carrier frequencies.

Another adaptation of the standard Weather Bureau radiosonde was made by WSC.[5a] The ground installation was similar to that used by the Weather Bureau in its full radiosonde measurements, but the standard radiosonde was modified by replacing the pressure- (altitude-) actuated switch by a clock-driven commutator. The results obtained were quite satisfactory, and the technique may be appropriate at stations where standard radiosonde equipment is available.

Wired Transmission Type

The other captive balloon or kite instruments are of the wired type with galvanometers or recorders at the ground. They may be classified as light and heavy types. The light instrument merely carries temperature and humidity elements aloft which together with the radiation shield do not weigh more than a few ounces. To this is added the weight of the cable or string carrying the connecting wires. The heavy instrument carries its own aeration equipment in the form of a fan driven by a small electric motor. The fan and the heavier construction of the frame required to accommodate it increase the weight of the airborne unit to several pounds. In addition there must be at least one more lead on the cable to supply power to the fan.

The first captive balloon instrument was built in England about 2 years ago.[10] The balloon is anchored by an electric cable and the instrument is provided with a fan. The overall weight of the instrument without cable is about 8 lb. Its main part is a piece of polythene tubing in the shape of an inverted Y with the fan placed on top of the tubing while the two legs of the Y contain the dry and wet thermopiles. The latter are four-junction copper-constantan combinations. The cold junctions are enclosed in a small Dewar flask filled with melting ice which is located about 10 in. below the Y piece.

The cable of this instrument has five leads, three for the thermocouples and two for the fan (2 to 4 volts of direct current); the instrument is suspended from the balloon proper by means of a 100-ft string which minimizes the influence of irregular motions of the balloon upon the instrument. The ground equipment consists of potentiometers and a spot galvanometer with a switch to alternate between the dry and wet couples.

The light type of balloon or kite sounding equipment was first developed by WSC.[5a,5b] The temperature and humidity elements are surrounded by a double-walled aluminum radiation shield, and the whole airborne assembly weighs only a few ounces. Originally the standard Weather Bureau temperature element was used; now they use the Sanborn element together with the Bureau of Standards humidity elements in the circuit shown in Figure 1.

The sounding procedure used with this instrument consists in letting the balloon go rapidly up to a maximum altitude chosen so high that moisture and temperature variations with height are comparatively slow. The characteristic features of the atmospheric stratification lie below this level. A rough survey of this stratification is made during the ascent. The instrument is then reeled in and is stopped at a number of predetermined levels, long enough to let the elements reach equilibrium with the surrounding air. The levels chosen are spaced at height intervals small enough so that the readings taken reveal the atmosphere structure accurately. It has been found that rapid lowering of the sonde between readings will provide sufficient aeration of the elements to give quite accurate readings even in completely calm weather.

The balloon sonde of the Navy Radio and Sound Laboratory uses a dry and a wet Sanborn resistor surrounded by a double-walled aluminum radiation shield. Often wind aeration is found to be sufficient for the wet bulb element, but in calm air the instrument is aerated before readings by giving the cable a series of rapid jerks of about 5-ft amplitude. The ground equipment consists of a 0 to 50 microammeter which can be connected to the dry element, the wet element, and a standard resistor in turn by means of a double-pole triple-throw switch. Voltage is supplied by a dry cell and potentiometer.

The captive balloon sondes used by Radiation Laboratory[4] employ dry and wet Sanborn resistors mounted diagonally in a piece of Bakelite tubing surrounded by an aluminum radiation shield. The circuit and am-

plifier have been described in Section 7.1.4. In the lightweight wind-aerated instrument the piece of Bakelite tubing containing the resistors is horizontal. Owing to the shape of the aluminum shield it will take up an orientation in the wind such that the air strikes the dry element before the wet element. More frequently, however, they use a heavier, fan-aerated instrument in which the Bakelite tubing is vertical and the fan is placed on top of the assembly. This instrument has been extensively used in the recent experiments at the New England coast; either it was attached to a barrage balloon (35-lb lift), or in calm weather to a large Neoprene balloon (see Section 7.1.8). The latter type of balloon was also used to make ascents from a boat in light and moderate winds.

Recently, a type of captive balloon equipment has been developed commercially[11] which uses the standard United States radiosonde recording equipment as the ground component. The airborne component consists of an audio relaxation oscillator with the measuring element connected in the grid circuit. Changes in the measured temperature or relative humidity alter the frequency developed by the oscillator. By means of a special attachment on the ground the balloon sonde is used in connection with the regular radiosonde receiving and recording equipment. The airborne component includes dry cells for the operation of the oscillator and the weight of the airborne unit is about 2 lb.

Cable and Balloon Technique

The cable which connects the measuring elements aloft to meters on the ground is one of the most critical parts of the wired sonde. The earliest British instrument[10] used a cable obtained by stranding together thin, insulated, flexible copper cables; the weight is about 2½ lb per 100 ft. Similar cables were used for a while by Radiation Laboratory; later on they changed to the types of cable to be described presently.

WSC developed a cable technique[5a,5b] in which the pull of the balloon or kite is taken up by a strength member such as strong linen twine. Fishline, breaking strength 64 lb, was originally used.[5a] Three No. 30 enameled copper wires are wound around the strength member with a pitch of several inches. After being made up the cable was passed under thinned airplane dope to cement it together and make it waterproof. The weight of this cable is about 1 lb per 1,000 ft.

Later developments in this cable resulted in three types that have survived accelerated tests equivalent to 1 year's exposure to salt spray without developing serious leakage.[5b]

Type A consists of a braided Fiberglas strength member (nominal strength 80 lb), three No. 30 Formex-insulated copper wires, and a braided nylon sheath impregnated with vinyl plastic.[f]

Type B has an enameled stainless steel strength member (nominal strength 40 lb) and three Formex conductors within an impregnated nylon sheath.[g]

Type C is similar to Type A but has a 180-lb test Fiberglas strength member; it is used with large kites.[f]

These cables are wound around the drum of an ordinary winch, and the conductors are connected to the ground equipment by means of slip rings mounted on the winch.

It has been found advantageous, especially for the heavier instruments, to suspend the instrument from the balloon on a 100-ft fishline; this line acts as a buffer in protecting the instruments from sudden jerks of the balloon.

Neoprene balloons[h] are recommended in preference to rubber latex balloons. They have a much longer useful life than rubber balloons and give warning before breaking by becoming misshapen. The 300-g N-4 balloon is used in connection with the WSC instrument.[5b] The N-700 balloon has been used by Radiation Laboratory for the fan-aerated instrument. Barrage balloons (lift 35 lb) were also successfully used in winds slightly in excess of those that permit the use of lighter balloons.

The light type of balloon becomes unmanageable in winds above about 6 to 8 miles per hour. A two-reel technique has been developed[5b] to extend the use of balloons to somewhat higher wind speeds (from 6 to 10 mph). The pull of the balloon is taken up by a separate fishline, the reel of the fishline being placed windward relative to the reel of the cable (Figure 3).

In wind speeds above about 8 mph kites are used in place of balloons. A small folding kite[i], standard for "Gibson Girl" emergency radio equipment, is easy to handle and requires only a light cable, but its ceiling is limited to about 400 ft. This type of kite has been used successfully for soundings from boats.

A heavier, 7-ft kite[j] is well adapted to land-based soundings. It flies at a high angle (55° to 60°) and can be put up at minimum wind speeds. At the high relative wind speeds encountered in ship-based sound-

[f]Supplied by International Braid Co., Providence, R. I.
[g]Supplied by Boston Insulated Wire and Cable Co., Boston, Mass.
[h]Supplied by the Dewey and Almy Co., Cambridge, Mass.
[i]Supplied by Hoffman Radio Co., Los Angeles, Calif.
[j]Supplied by F. C. Seyfang, Atlantic City, N. J.

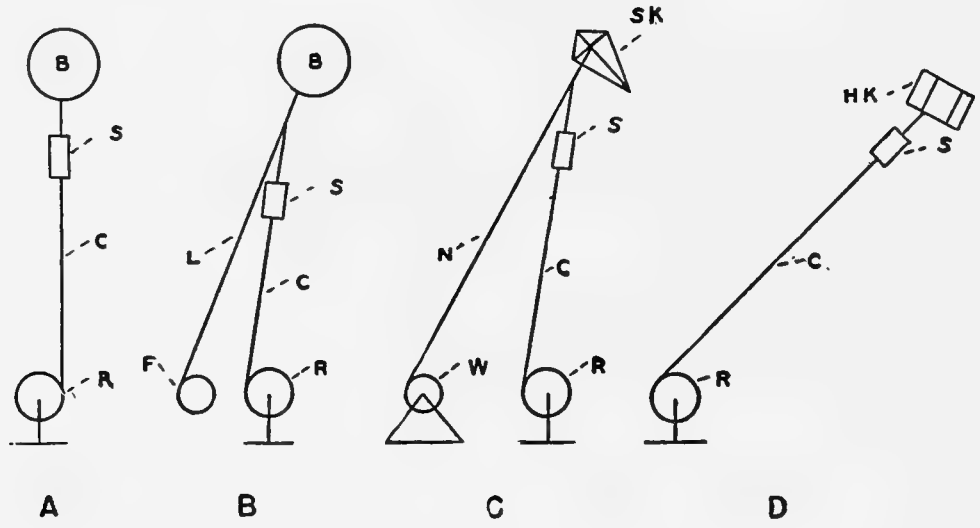

FIGURE 3. Sounding techniques for use at the wind speed ranges indicated. [5b]

Temperature and humidity elements mounted within the radiation shield *S* are connected through the 3-conductor cable *C* with slip rings on the cable reel *R*. The meter box (not shown) is connected to the brushes of *R*. *B*: 300-g Neoprene balloon. *L*: light fishline. *F*: fishline reel. *SK*: Seyfang 7-ft kite. *N*: nylon kite line. *W*: kite winch. *HK*: Hoffman single cell box kite. Arrangement (D) is suitable for sounding from moving ships; its ceiling is limited to about 400 ft by the small lift of this kite.

ings the pull of this kite is excessive and launching correspondingly difficult.

Sounding techniques are shown schematically in Figure 3. For the kite a braided, waterproof nylon line, breaking strength 150 lb. is recommended. For ship-based soundings or conditions where sudden high stresses are likely, a 300-lb test nylon line may be used.

There seems to be no difficulty in measuring the altitude of the captive balloon or kite.[5a] The length of line paid out is determined either by counting the turns of the reel or by means of markers attached to the cable at regular intervals; if the line is off the vertical, its mean inclination can be measured with sufficient accuracy by a simple hand inclinometer.

7.2 AUTOMATIC RECORDING OF METEOROLOGICAL SOUNDINGS[k]

A means has been developed for making automatic recordings on a Leeds and Northrup Speedomax or Friez Cycloray recorder of low-level meteorological soundings of temperature and humidity. The design of the equipment has been restricted in the sense that the standard Weather Bureau-Army-Navy electrolytic hygrometer and negative resistance temperature units must be utilized; all recordings must be made on the existing automatic radiosonde recorders just named.

[k]By E. Dillon Smith, U. S. Weather Bureau, Washington, D. C.

General Design Considerations

The existing standardized electrolytic hygrometer strip polarizes when direct current is placed on its terminals. However, if a reversed direct current is placed on the terminals of the strip, this polarization tendency is neutralized. This would seem to indicate the desirability of placing a low-frequency alternating current on its terminals in lieu of the direct current commutation principle which generally has been used in existing low-level meteorological sounding equipment.

The frequency of the alternating current to be placed on the strip will in general be controlled by the reactance of the low-level sounding cable. In view of this limitation a frequency of approximately 10 c has been used.

The temperature resistor operates equally well on either direct or alternating current; therefore, it requires no equipment design considerations.

Electrical Characteristics of Elements

Present practice makes the "lock-in" for the temperature and humidity elements through a resistor in series with the elements. However, this technique introduces errors in the readings both above and below that for the lock-in point. Effectively, the slopes of the calibration curves are altered, affecting the readings on the indicators. In view of this situation, it is fundamental that voltages should be measured across

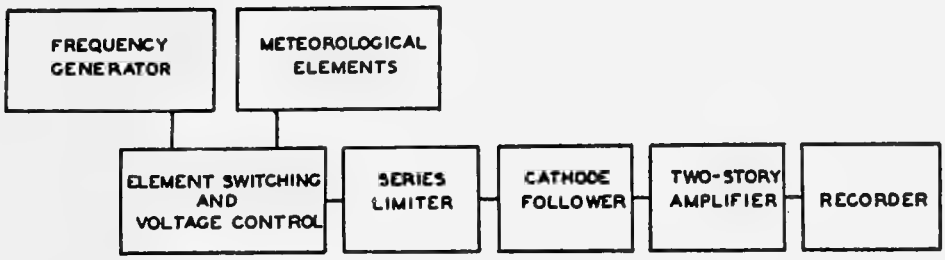

FIGURE 4. Basic components of amplifier-recorder.

the hygrometer or temperature elements. Any lock-in device must be inherent in the equipment as remote from the voltage appearing across the elements. This principle has been incorporated in the design of the equipment.

Since the electrolytic hygrometer element can be designed so that it will not polarize under direct currents approaching 100 μa, it appears desirable to design the recording equipment for possible adaptation to this type of element. In other words, the amplifiers must be capable of handling direct currents as well as alternating currents.

CABLE ERROR

If the standard temperature and hygrometer curves are used originally for calibrating the recorder, it is important to note that the cable resistance will introduce a positive error. For average Southwest Pacific climate and sounding heights up to about 3,000 ft, the positive temperature error is roughly 1.5 F while the positive hygrometric error is about 5 per cent RH.

These errors, unfortunately, cannot be compensated without complete recorder calibration at the outset or by mathematically adjusting the standard calibration curves. Thus, since the cable is a fixed resistance, the standard curve can be recomputed to allow for any fixed cable resistance, with the result that no error will be introduced into the recorder.

In consideration of the above requirements, it will be necessary, in adapting the standard U. S. Weather Bureau electric hygrometer and temperature elements, to provide (1) a means of developing a stable low-frequency voltage across the elements, (2) to switch from one element to another in measuring the voltages across these elements, (3) to amplify such voltages, (4) to provide a means of controlling the sensitivity and range of the recorder, and (5) to supply the output of the amplifier to a 0 to 500 microammeter automatic recorder.

ELECTRONIC AMPLIFIERS

The basic components of the amplifier-recorder are shown in Figure 4. The frequency generator operates at 10 c and is composed of three units, (1) a phase-shift oscillator, (2) a paraphase amplifier, and (3) a controllable push-pull output amplifier.

The amplifier-recorder unit is composed of (1) a series limiter, (2) a cathode follower, and (3) a two-story amplifier, as shown in Figure 5. For the sake of simplicity, the automatic switching device that changes the current from hygrometer to temperature element has been shown schematically. The switching takes place at any rate between approximately 1.0 to 0.1 c; this rate is not critical.

Since the amplifier must be able to handle either direct or alternating current, the balanced two-story

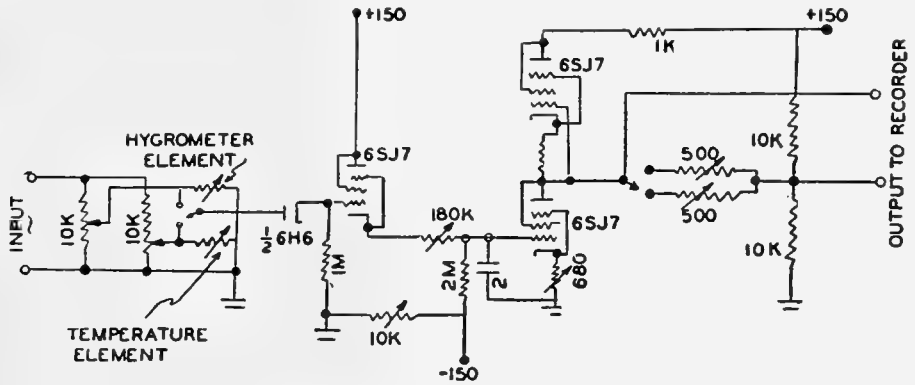

FIGURE 5. Automatic recorder circuit.

amplifier has been constructed, wherein the top tube is the plate load for the lower tube of the two-story amplifier. The output of this amplifier is approximately equal to one-half the amplification factor of the tube.

As shown in Figure 5, this amplifier is fed by a cathode follower which has impressed upon it from the series limiter only the positive peaks of the a-c voltage drop across the hygrometer or temperature element. The voltage across the elements can be as low as ¼ to ½ v, depending upon the sensitivity adjustment of the amplifier. It will operate with voltages as high as 30 to 60 v across the elements.

Reducing Amplifier Output to Ground

The amplifier output is at one-half the positive voltage of the plate supply above ground. However, this output can be reduced to ground by the introduction of a cathode follower or more simply by three series sections of a resistor and glow tube connected in series. The output of the two-story amplifier is fed into the junction between the first and second sections while the output is taken from the junction of the second and third sections, where the first section is connected to the positive plate supply and the third section connects to a negative potential equal to one-half the positive voltage. It is not necessary to make this addition to the present equipment.

Recorder Accuracy

It is possible to measure temperatures to less than ¼ of a degree Fahrenheit and humidities to less than ½ of 1 per cent. However, this accuracy is not necessarily required for low-level atmospheric soundings and construction of M curves.

Conclusion

Direct automatic recording of low-level temperature and hygrometer readings is suggested. The method is especially adaptable for fixed or shipboard station operation.

Chapter 8

METEOROLOGY—FORECASTING

8.1 FORECASTING TEMPERATURE AND MOISTURE DISTRIBUTION OVER MASSACHUSETTS BAY [a]

BEFORE GOING into a description of the forecast program and results it will be profitable to describe the method used in coordinating the observations.

8.1.1 Meteorological Observations

Soundings were made according to two major plans. The first was in conjunction with the radio path. According to that plan, airplane soundings were made once or twice a day at two or three points along the transmission path. The boat would take either mast or balloon soundings along the path while measurements at Race Point Light (Provincetown) would continue at 2- to 4-hour intervals during most of the day and sometimes at night. The Race Point Station had the advantage of being well away from land (for all but easterly winds) and soundings there would thus represent the condition of the air over a large portion of the path. The soundings just described were made primarily for correlation with the signal strength measurements.

The second plan was to obtain soundings in successive steps in air moving off the coast as that air became more and more modified by the cool ocean surface. For this reason, days during which the air was westerly or nearly so were set aside for this type of measurement. The Duxbury soundings gave a representation of the structure of the air before it left the land. One airplane made soundings at about 2, 7, and 25 miles offshore. The times of take-off were staggered to allow the first airplane to complete its third ascent before the second plane would begin its first sounding.

The boat played a vital role in such a plan. It ran along the line of the air trajectory for as long as was practicable to take water temperature measurements and mast soundings, usually an 8- to 10-hour period.

The Race Point Meteorological Station was coordinated into this general plan by having it take continual balloon soundings at, say, 2-hour intervals both before and after the airplane ascents. The purpose of these soundings was both to fit in as an extra sounding in the general plan and also to yield some information as to amounts of change of the meteorological conditions with time. Also, in general, the times of soundings at Race Point Station were scheduled about 1 hour later than those at the overland station to give the air sufficient time to travel from one to the other.

8.1.2 Forecast Program

A forecast program was begun during July and continued to October 10, 1944, in order to try out existing methods of forecasting and to help develop new techniques. A more natural step would have been to analyze the data taken during the summer and then to put that analysis into the form of forecast procedures, as was done at the end of the 1943 Boston Harbor transmission experiment. However, since speed was essential it was decided to initiate a forecast program simultaneous with the observations. The very act of forecasting tended to focus attention on the important weather factors, at the same time giving invaluable help in planning the day-to-day observations.

The type of forecast made was different from the usual form. It consisted of a "space forecast" rather than the usual time forecast. That is, knowing the conditions at one point at a given time the problem was one of finding the conditions at another location at the same time. It involves the entire problem of modification of an air mass by a water surface.

The forecasts were in the form of curves of temperature and moisture, from which the modified index curve was computed. A time and a location in Massachusetts Bay were selected at which it had been determined previously that a sounding would be made. Almost invariably airplane observations were chosen to use as verifications because those soundings were at sufficient altitudes so that both the modified and the unmodified air were sampled. The forecasts were made from the surface to 1,000 ft, whereas the airplane soundings started from about 20 ft and continued to 1,000 ft. For verification, the forecast and the sounding were plotted on the same graph.

[a] By I. Katz, Radiation Laboratory, Lt. J. R. Gerhardt, Lt. W. E. Gordon, Army Air Forces, and P. W. Kenworthy, U. S. Weather Bureau, Boston, Mass.

8.1.3 Army Analysis and Forecasts

The program of the Army forecasters included the forecasting of transmission and radar ranges; the approach to this problem was empirical. The basis of the program was again the analysis of the first 6 weeks' data, this time including the signal strength measurements which have been described. Signal strengths were divided into four ranges qualitatively described as low, standard, high, and very high, corresponding to M curves of the types substandard, standard, superstandard, and trapping. This analysis did not consider variations in the M curve over the path but rather related signal to the prevailing type of curve. On this basis, then, a transmission forecast for a 24-hour period involved the forecasting of prevailing M curves over the transmission path for appropriate time intervals. The length of these time intervals was determined by the rapidity with which the weather factors affecting the M distribution were changing. Specifically, a 24-hour transmission forecast involved two M-curve forecasts plus forecasts of temperature and dew point trends. These forecasts were supplemented frequently with M-curve forecasts for times of minimum or maximum propagation conditions. These meteorological data could then be translated qualitatively into values and trends of signal strength. This information was presented in the form of a graph of signal strength versus time.

8.1.4 How the Forecast Is Made

The forecast in general involves two determinations: one, of the initial conditions of the air before it leaves land; and two, the modifications of the air by the water surface. A study of the synoptic situation and the low-level circulation reveals the location of the point where the air in question leaves the land. The synoptic situation shows the general flow pattern; local winds from the surface to 2,000 ft indicate the specific pattern over the area under consideration.

The initial temperature and moisture distributions are determined by studying the local hourly teletype sequences and radiosonde observations. The modification of the air is determined by considering the relation of the surface water temperature to the representative air temperature and dew point, the over-water travel, and the rate of modification.

Time forecasts were also made by the Army forecasters. They involved straight meteorological forecasts of the initial conditions to which were applied the space forecast technique just described.

Example. This is a forecast made by the Weather Bureau. The synoptic weather map on the morning of July 26 indicated a rather weak flow of modified continental polar air moving in an easterly direction from the mainland of eastern Massachusetts out over the waters of Massachusetts Bay. The temperature of this air was potentially more than 21 C and under sunshine was developing surface temperatures near the shore line of more than 21 C by 0800. The forecast was for 1000 about 5 miles southeast of Eastern Point, Massachusetts. The temperature over land about a half-hour before this was expected to be about 24 C, and the air flow as indicated by winds aloft was such as to allow the air warmed to about this figure to be out over this position within a half-hour. The lapse rate over land would be approaching the dry adiabatic by this time; so, as a guide, a lapse rate amounting to about 3 C per 1,000 ft was projected to 1,000 ft starting from 24 C at the surface. A value for the sea water temperature of 17 C was predicted from recent observations made in the Bay. Using past experience, one then assumed a water modification up to about 300 ft, and the T curve was constructed starting from the surface value of 17 C, showing a sharp inversion at first and a gradual inversion until it met the guiding line representing the air from the land. The radio observation made at MIT about midnight, July 25 to 26, was considered to be a fairly good check of the properties of the air mass involved. A surface temperature of between 21 and 22 C was indicated.

In forecasting the moisture curve, a value at the surface corresponding to the water temperature was made the base of the curve. Over-land dew points were initially predicted to be about 13.5 C, which would give a vapor pressure value of between 15 and 16 mb at the top of the water modification zone. An examination of the raobs, both MIT and Portland, show mixing ratios of about 10.5 g per kg between 500 and 1,000 ft, which corresponds to 15 or 16 mb. This makes a good check on the prevailing initial dew points. The raob at Albany indicated that air which was a little drier was moving in from the west so that a slight decrease in the vapor pressure was forecast between 500 and 1,000 ft. (This part of the forecast did not prove to be correct, since, as the verification of the forecast in the figure shows, the moisture value remained fairly uniform from 400 up to 1,000 ft.) Another curve was drawn similar to the T curve to connect the surface vapor pressure value with that value at

the top of the water modification zone, and from there to 1,000 ft a gradual decrease was forecast on the basis of the conclusions regarding the advection of a little dry air indicated by the midnight Albany sounding.

The verification shown by the broken line in Figure 1 turned out rather well in this instance. The computed and verified M curve proved to possess almost identical slopes throughout with the top of

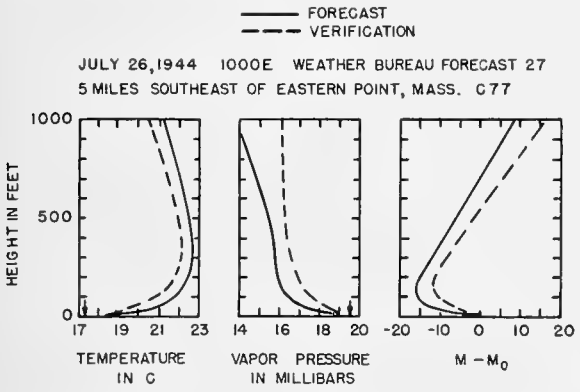

FIGURE 1. Space forecast of M curves.

the M inversion in both very close to 150 ft. This was one of the better forecasts. It can be seen that actual values of temperature and vapor pressure between forecast and verification might vary by several degrees, but as long as they have the same slopes at the same elevation they will produce M curves reasonably close to one another.

Conclusions. It is felt that the method of forecasting used was a marked improvement over the technique employed previously. It is potentially capable of dealing with the low-level modification problem in the case where the intial air is stratified as well as the one in which the initial air is homogeneous before it passes out to sea.

8.2 RADAR PROPAGATION FORECASTING[b]

This is a report of results obtained by an AAF board project investigating radar propagation forecasting, which was started as two distinct programs in September 1944. The first part of the project was carried out at the Radiation Laboratory with facilities used by Group 42 during over-water transmission measurements in the summer of that year. During that time, with the invaluable assistance of Group 42, a forecasting system was developed for the over-water case, the results of which are presented in Section 8.1.[c] These reports gave preliminary results of the MIT program and the recommended forecasting procedures. The second part of the propagation forecasting program was set up at Orlando, Florida, to study particularly the *over-land* forecasting phase and to investigate some of the operational uses of such forecasts.

With this in mind, AAF Board Project H3767, "The Determination of the Practicability of Forecasting Meteorological Effects on Radar Propagation," was initiated late in 1945 with the following specific objectives:

1. To determine the practicability of forecasting those low-level meteorological conditions which affect radar propagation.
2. To determine the accuracy with which radar propagation forecasts can be made from the corresponding meteorological conditions.
3. To determine the operational uses of such forecasts.
4. To determine the optimum meteorological observation site with relation to the site of the radar employing the forecasts.
5. To determine the suitability of available low-level sounding equipment.

It was originally planned to study the over-land and over-water problems simultaneously, but because of the lack of a coastal radar site until the last month of the program the project was divided into two phases: (1) the general study of the over-land propagation variations in an attempt to devise a suitable forecasting procedure and (2) an evaluation of the results obtained from both the over-water and over-land methods, with possible tactical applications under field conditions at the site of a powerful coastal radar.

Figure 2 is a map of central Florida giving in detail specific facilities used throughout the project. Headquarters was established at the Weather Central, Orlando, where complete weather information, forecasts, and analyses were available. The meteorological data used throughout the project consisted of surface and upper air observations for the general central Florida area.

Detailed synoptic maps of Florida were drawn covering periods of 6 hours each to determine wind patterns and representative land temperatures and dew points; piballs[d] for Orlando, Sebring, and Tampa were plotted up to 2,000 ft to determine trajectories and

[b]By Lt. J. R. Gerhardt and Lt. W. E. Gordon, AAF Board.

[c]Elaborated in references 1 to 3.

[d]A small balloon with standard rate of rise released for tracking by a theodolite for estimation of upper-air winds.

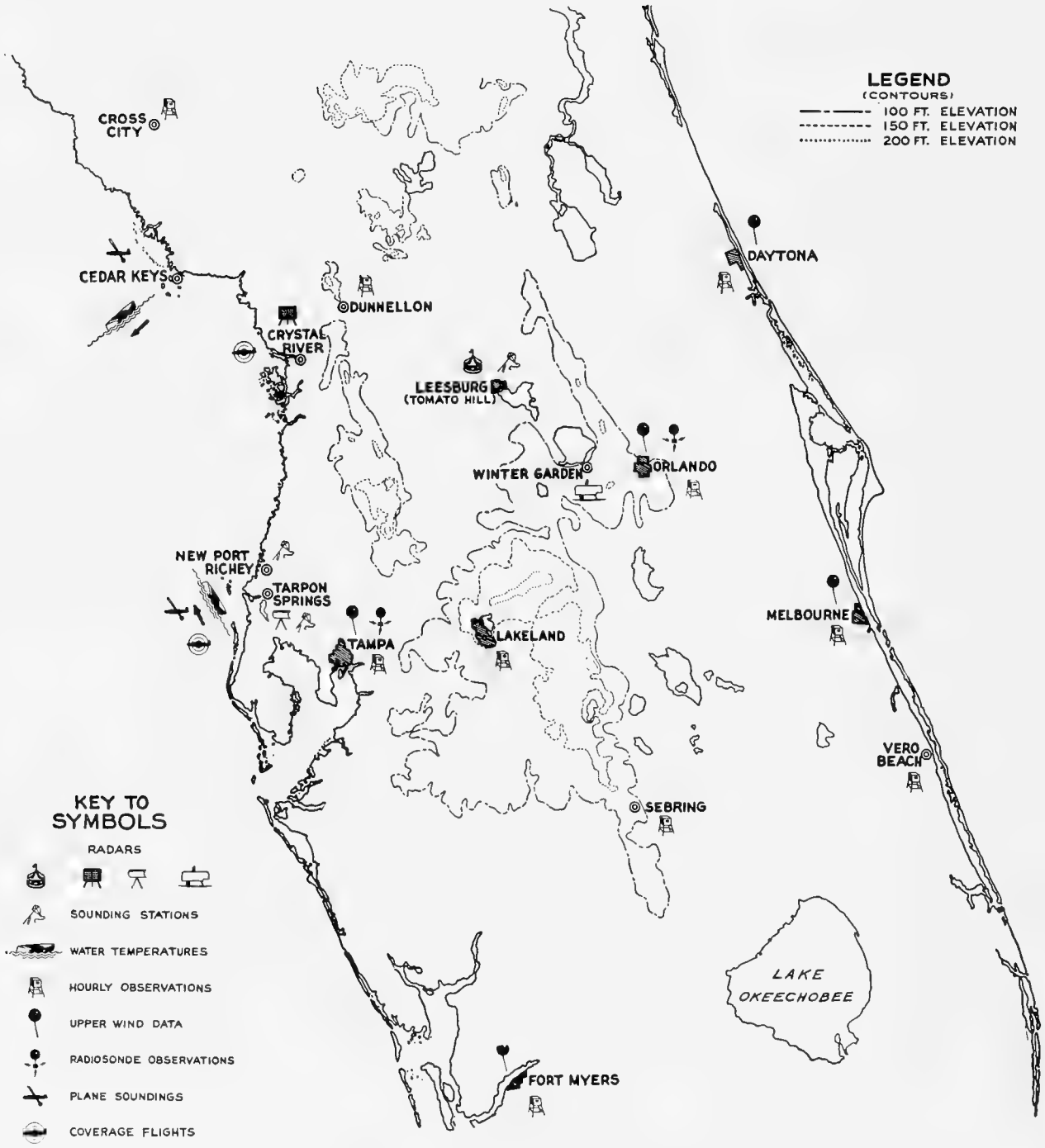

FIGURE 2. Map of central Florida with locations of weather and radar installations used in Project 3767.

wind speeds above surface levels, while the Orlando, Tampa, Tallahassee, and Jacksonville raobs were studied to correlate subsidence and radiation effects with radar propagation variations.

During the first phase of the project, sounding stations were established at Leesburg and New Port Richey using both the Washington State College wired sonde and the MIT psychrograph. Radar data were taken from the S-band V beam and the P-band SCR-588 at Tomato Hill, only a few miles from the

Leesburg sounding site, the SCR-584 at Winter Garden, and the P-band SCR-271 at Crystal River during their operating hours. The Tarpon Springs program employed a medium early warning and an SCR-615 radar, both on S band, located on the Gulf coast, and the Crystal River SCR-271 and Winter Garden SCR-584. The sounding station was located within a half mile of the Tarpon Springs radar site. During the entire program sea surface temperatures were measured several times weekly at either the Cedar Keys or Anclote Crash Boat bases out to a distance of about 20 miles at 2- to 4-mile intervals.

Low-level soundings were made during the entire project primarily as an aid in interpreting radar performance and in determining representative air values and secondarily in an attempt to evaluate the operational suitability of the available sounding equipment. Results of the latter portion of the work will be presented later in this report. Ground-based soundings were made by means of various combinations of 350- and 700-g balloons, 7-ft Seyfang kites, and a small barrage balloon.

The sounding stations were originally located so as to be as representative as possible of interior and coastal areas, although it was found later that, without the additional mobility of airborne measurements, individual ground-based soundings were likely to be too strongly influenced by local topographic effects to be completely reliable. Because of clearance requirements, the ground-based soundings were restricted to 600 ft, although it was determined that 1,000 ft would be a much safer limit, with occasional measurements up to 3,000 ft considered desirable. Soundings were taken before dawn at 1000 Eastern War Time, after sunset, and at 2300 EWT to obtain sufficient data on the effects of radiation and other meteorological phenomena. As far as specific sounding procedures are concerned, both the small balloons and kites gave satisfactory results, although for most of the wind speeds encountered in this area the 7-ft kite was too small for efficient operation. No limiting surface wind speed can be given as a dividing line between kite and balloon operation, since it has been found that occasionally even in surface calms strong velocity gradients exist immediately above the surface layer. Although it is realized that a barrage balloon is not a standard item of equipment for sounding measurements, it is unreservedly recommended and whenever available should be used for simplicity and reliability of sounding procedure.

The method employed in this project for the radar verification of superrefraction was to record *plan position indicator* [PPI] scope appearance of ground clutter return. The oscilloscope screen was assumed segmented into eight 45° sectors, and the maximum range on a ground target in each sector was noted hourly during periods of operation. In an attempt at correlating the radar performance with the existing meteorological conditions, a classification system was devised in which each distinguishable propagation condition was assigned a single number. After collecting observations for some time from each unit the data were examined, and an average of the normal pattern was chosen as the standard, or class 1, type of propagation. Averages of reported increased ranges in various sectors were calculated, while the azimuthal variations due to shadow effects of surrounding terrain, coast line and obstructions were considered. The consistency with which various increased range averages were attained determined the number of classes of propagation assumed for each unit. On the assumption that the meteorologist could forecast and correlate M-curve types corresponding with four types of propagation, four such propagation classes were chosen for the S-band V beam and the P-band SCR-271 at Crystal River. Figures 3 and 4 show the four classes of propagation as defined for the SCR-271 at Crystal River. The class 4 picture definitely shows the Florida coast-line detail painted in. Observations from most of the other units, however, were classed only as 1 (standard) and 2 (nonstandard) propagation because of the radar shadows of certain topographical features near their sites. Due possibly to the peninsular situation of Florida, it was impracticable to forecast accurately four different classes of propagation, but forecasting on a basis of two classes, standard and nonstandard, can and should be done.

During the first part of the over-land program an attempt was made to forecast the specific M curves as shown by the Leesburg and New Port Richey sounding stations and to correlate these curves with the two to four propagation classes outlined for each radar unit. However, because of the wide variation of surface terrain (sand, swamps, lakes, forests) in this general area, no single sounding was necessarily representative of the entire air mass, since subsidence and radiation effects almost certainly varied considerably over the different kinds of terrain surrounding the sounding locations. On this basis, then, rather

than attempting to forecast a hypothetical representative M curve, a series of correlations was made relating the general synoptic situation directly to the radar performance. Using this method, the actual over-land forecasting results showed that, while approximately 80 to 85 per cent of the total operating hours could be correctly forecast as either standard or nonstandard propogation periods, only some 50 per cent of the nonstandard hours could be forecast correctly. This is only a little better than climatology, and more work remains to be done on the over-land forecasts of propagation variations.

In addition to the ground clutter verification of superrefraction, several low-level coverage flights were made from Leesburg to Crystal River and some 80 miles out into the Gulf at an altitude of 100 ft, retturning at 1,000 ft to check coverage above duct levels. Only a very few flights were made during periods of extended propagation, but during these periods, while interference from extended ground clutter prevented detection of the plane over land, extended ranges were recorded for the VHF (very high frequency) air-to-ground communication contact.

In a further attempt to investigate some of the operational possibilities of trapping conditions at low and intermediate altitudes, measurements were taken of maximum ranges on the airborne X-band APQ/13 radar during routine flights. However, as the ranges observed were very erratic, no conclusions could be drawn. In this respect it should be stated that while excellent cooperation was obtained in getting various radar and aircraft observations, the project had a low priority and as a consequence could not fully investigate many of the more important operational possibilities which would have required extensive use of radar and aircraft facilities.

The over-water forecasting program at Tarpon Springs was set up to compare the results of forecasts made under field conditions of limited meteorological data with those made using all available meteorological information given in the forecasting system presented in reference 3. This system was based primarily on the over-water modification studies presented at the last conference, where duct height d was related to the wind speed at 1,000 ft, the distance of over-water travel, and the M deficit, which is the difference between the M value at some reference level, in this case the sea surface, and the M value of the unmodified air reduced to sea level. In general, no attempt was made to forecast the specific lapse rates

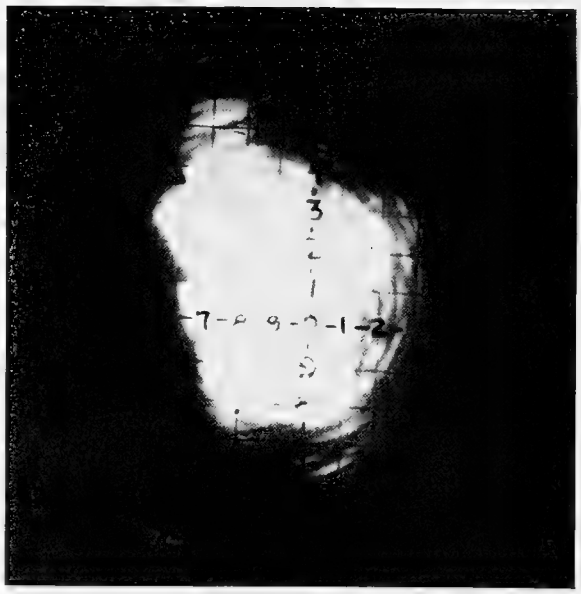

FIGURE 3A. Typical Class 1 pattern, P-band SCR-271, Crystal River. Grid squares are approximately 5 miles on a side.

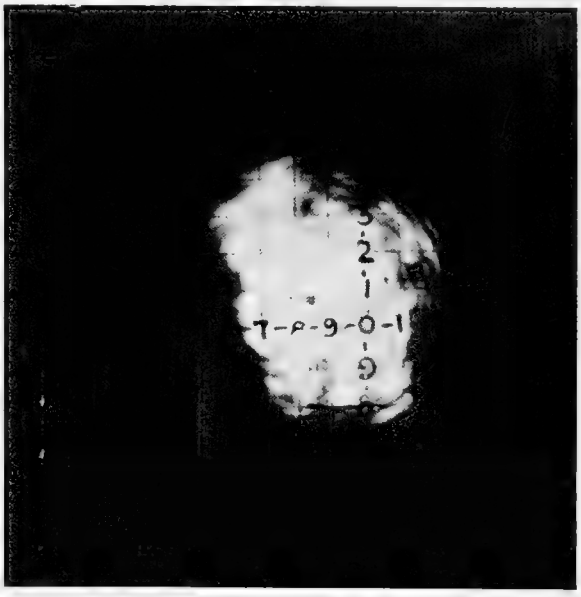

FIGURE 3B. Typical Class 2 pattern, P-band SCR-271, Crystal River.

and M curves corresponding to the current meteorological situation. With uniform weather conditions existing over water, there was assumed a 100 per cent correlation betwen the M curve and the corresponding radar performance, so that it was merely necessary to determine the representative d and ΔM of the air mass to obtain the complete propagation forecast.

FIGURE 4A. Class 3 pattern, SCR-271, Crystal River. Coast line well painted in.

FIGURE 4B. Typical Class 4 pattern, SCR-271, Crystal River

As it was impracticable to establish a permanent target in the Gulf of Mexico beyond the radar horizon, the existence of superrefraction was generally assumed when there was extended appearance of coast-line clutter. It is realized that such an effect may not be representative of open water conditions because of the possibility of local sea breezes giving rise to the necessary temperature and moisture gradients for trapping. However, on this basis, 18 out of 20 forecasts correctly verified the presence or absence of extended coast-line clutter to within 1 to 2 hours of the total duration. With extended echoes existing during 55 per cent of the test days over the coastline, this accuracy is considerably greater than could be arrived at by any purely statistical procedure. It should be stated here that these forecasts proved to be particularly valuable to the radar personnel, since certain engineering tests in progress on the radars made an accurate evaluation of the effects of superrefraction on the radar set performance necessary during the calibration flights.

As an additional check on the existence of superrefraction over water, forecasts were made of the ranges for S-band radars and VHF communication on low-level coverage flights into the Gulf. Of a total of ten flights, six were made during periods of extended coast-line return, three of which were correctly forecast as giving superrefraction on S-band radar and two as giving increased ranges on VHF communication. Although this is not so accurate as the forecast of surface effects, a large error may have been introduced by the fact that the forecasted duct heights were of the same order of magnitude as the lowest levels attained by the plane in its flight over the Gulf. All the over-water flights showed normal horizon ranges at 1,000- to 3,000-ft levels on the return legs.

In another attempt to determine the vertical coverage patterns resulting from low-level nonstandard propagation, several free balloon flights were made. Standard weather service reflectors were attached to the balloons, which were released from Army crash boats at distances of 20 and 60 miles from the coast. Possibly because of lack of radar efficiency, only the balloons released at 20 miles were picked up by the coastal radar. Although no nonstandard conditions were observed during the releases, the method seems suitable for making vertical coverage measurements.

Radar and weather data for the period January 1 to March 15 were tabulated and analyzed during the month of March. The primary data consisted of S-band radar reports from Winter Garden and Leesburg and low-level soundings from Leesburg, supplemented by the synoptic charts and radiosonde observations supplied by the 26th Weather Region.

The analysis resulted not in a system of forecasting such as that developed for over-water use but rather

in a series of clues to be used as an aid to over-land forecasting in Florida. Since the clues are closely related to the topography and peninsular situation of Florida and to the season of the year, they are not directly applicable to other locations in their present form. However, they suggest that investigation of these points at other locations would quickly yield useful correlations. Some examples of these relations follow.

1. Of the 600 ft low-level sounding standard curves, 90 per cent gave standard ranges.

2. During early morning hours:
   a. Surface winds of 10 mph or more produced standard propagation always; winds of 5 to 9 mph produced superrefraction 20 per cent of the time; 2 to 4 mph showed superrefraction 60 per cent of the time; and calm winds produced superrefraction almost always.
   b. Similarly, the 1,000-ft winds of 30 mph or more produced standard, while 1,000-ft winds of 10 mph or less almost always produced superrefraction.
   c. Superrefraction occurred with clear skies except on two occasions, one with broken high clouds, the other with broken middle clouds, never with low clouds.
   d. High-pressure centers within 700 miles and with gradients of 1 mb per 100 miles or less produced superrefraction.
   e. Ground fog patches were observed during periods of class 4 propagation, with two exceptions.

3. Simple surface ducts of 70 ft and ΔM_{50} (reference level 50 ft) of 4 or more and elevated S curves with ducts above 200 ft and ΔM_{50} of 6 or more produced class 3 or 4 propagation with possibly one exception.

4. Large ΔM's observed by radiosonde between 1,000 and 3,000 ft showed no correlation with S-band propagation but did show fair correlation with superrefraction on P band. Superrefraction on both S and P band showed good correlation with large ΔM's observed below 1,000 ft.

5. The height of the temperature inversion increased with increasing 1,000 ft wind speeds up to 10 or 12 mph, then decreased slowly with further increase in wind.

6. Substandard propagation conditions were never observed over land, either on the radar or the soundings.

A series of low-level soundings taken at hourly intervals throughout the night were related to corresponding radar ranges. The soundings were made at Leesburg; the radar data were taken at Tomato Hill (2 miles west of the sounding site) and at Winter Garden (25 miles southeast of the sounding site).

The general weather situation for the night of March 5 to 6 shows maritime tropical air pouring up over Florida around the western end of the Bermuda high, giving clear skies and southerly winds of 10 mph at 1,000 ft and 2,000 ft at 2000 EWT,[e] increasing to 20 and 25 mph respectively by midnight, and to 23 and 35 mph by 0400. Figure 5 shows the PPI scopes

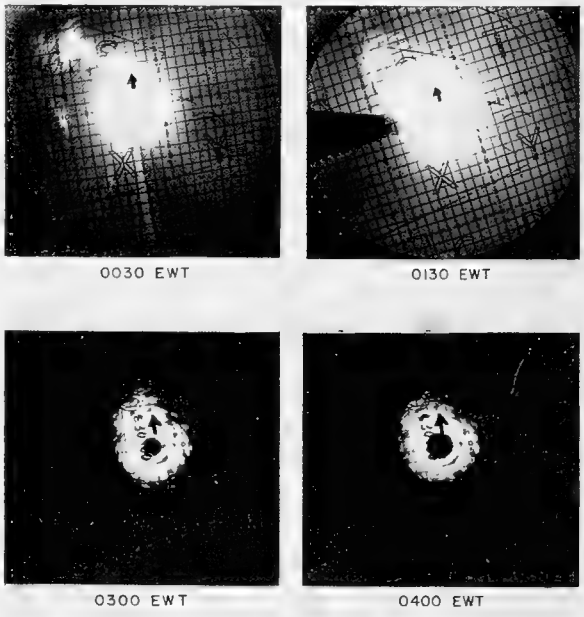

FIGURE 5. SCR-588, Leesburg, night of March 5 to 6, 1945.

of the P-band SCR-588. The arrows point north; the small grid squares are 5 miles on a side. Before midnight, propagation was standard, as illustrated by the 0400 frame. The ranges built up rapidly, reaching 65 miles and decreased slowly between midnight and 0400. (Radar shadows of surrounding topographical features account for the uneven distribution of range increase.)

Figure 6 shows the progression on the S-band SCR-584. The bold line points north, the range markers are at 10,000-yd intervals. (The sounding site is roughly 315° at 45,000 yd.) From 1900 to 2200 propagation

[e]All times to follow are Eastern War Time.

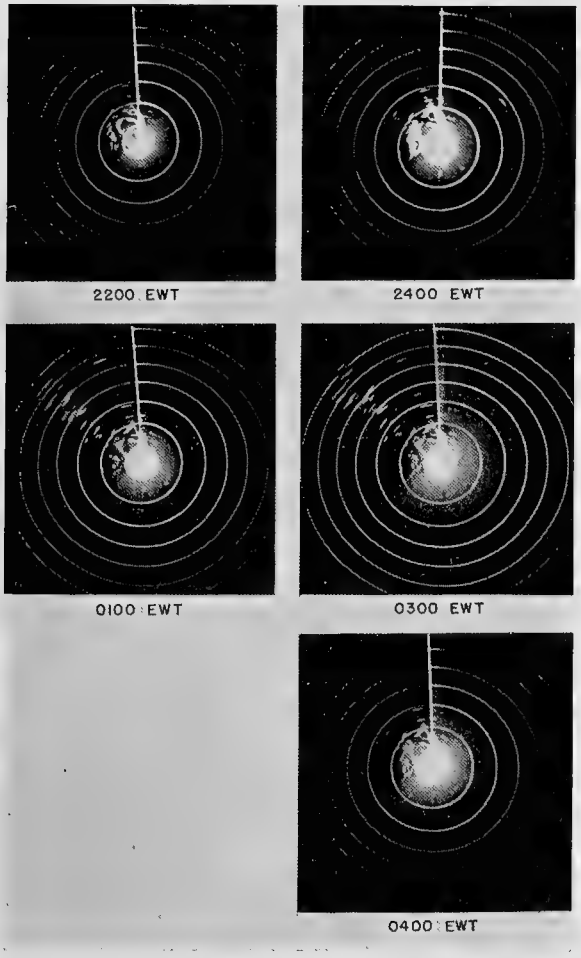

FIGURE 6. SCR-584, Winter Garden, night of March 5 to 6, 1945. Superstandard propagation occurs to the northwest at 0100 and 0300 EWT. At 0400 EWT the pattern is again standard. The line on the PPI indicates true north.

went from standard to above standard and returned to standard. After midnight ranges built up rapidly and held until after 0300, when they began a gradual return to standard, reaching that condition shortly after 0400.

The M curve measured at 1900 was standard, followed by those illustrated in Figure 7. Unfortunately, no soundings were taken between 2035 and 0008, and consequently the evolution of the elevated S from the surface duct is not shown. We know that the surface wind decreased from 4 mph at 2000 to calm at midnight, while the 1,000-ft wind increased from 10 to 20 mph. The duct height and ΔM value were approximately constant from midnight to 0200, after which the curve gradually approached standard.

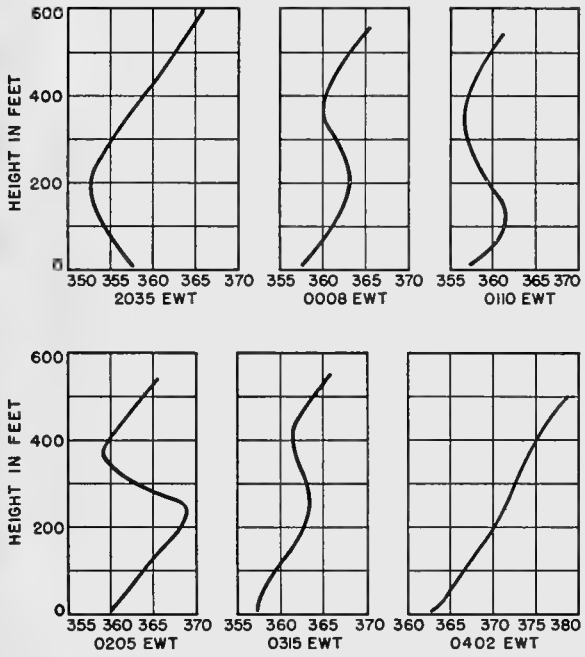

FIGURE 7. M curves for night of March 5 to 6, 1945, based on soundings at Leesburg AAF.

Table 1 summarizes the weather and radar variations. It should be pointed out that the antenna height for the P-band SCR-588 was 140 ft above the sounding site, for the S-band SCR-584 the same height as the sounding site. Thus at 2100 we have a 200-ft surface duct trapping the SCR-584, but not trapping the

TABLE 1. Radar-weather tabulation, March 5–6.

	Time (EWT)												
	19	20	21	22	23	00	01	02	03	04	05	06	07
SCR-584 ground range* (S-band)	1	2	2	1	1	1	2	2	2	1	1	1	1
SCR-588 ground range (P-band)	..	..	1	..	..	2	2	3	2	1	1	1	1
M-curve type†	S	D	D	..	..	L	G	L	L	S	T_a	S	S
Duct height (ft)	..	200	200	..	..	370	350	380	400	..	450	..	..
ΔM	..	14	14	..	..	14	14	14	11	..	6	..	..
Surface wind (mph)	5	4	4	..	..	0	1	3	5	6	6	5	7

*Ground range: 1, standard; 2, 3, 4, degrees of superrefraction.

†M-curve types: S, standard; D, duct (simple surface trapping); G, ground-based S curve; L, elevated S curve; T_a, transitional aloft.

SCR-588 (duct height 60 ft above the antenna), while from midnight to 0300 an elevated duct of the order of 380 ft traps both sets (duct height some 250 ft above the SCR-588 antenna). By 0400 the winds became strong enough to wipe out the stratified layers and mix the air, giving standard conditions. At 0500 a trace of a transitional condition aloft appears in the sounding but is not sufficient to extend the range.

During the months of January and February data were collected on S-band V beam at Tomato Hill during 47 days. Of these days' observations 37 per cent showed nonstandard conditions. During the same period the SCR-271 at Crystal River showed at least slight increases in ranges on 72 per cent of the days' observations which were recorded, although only 17 per cent attained the strength of class 3.

The longest ground range observed on the S-band set at Tomato Hill was 200 miles on the morning of January 25, while the longest ground range observed on the SCR-271 at Crystal River was 140 miles on the morning of February 17. Both these ranges were the maximum permitted by the radar presentation.

During the month of April at Tarpon Springs, 65 per cent of 24 days' observations showed nonstandard conditions, with 46 per cent giving surface return at greater than 80 miles, indicating strong superrefraction. The longest range recorded was the coast-line effect out to 220 miles.

To determine suitable low-level airborne sounding equipment, the psychrometer equipment ML-313/AM, the WSC wired sonde, and sling psychrometer ML-24A were mounted in aircraft L-4 (cruising speed 55 mph) and compared with the MIT psychrograph carried by a barrage balloon.

From considerations of the forecasting method an accuracy of ± 0.2 C in wet and dry bulb temperatures and a lag coefficient less than 45 sec are desirable. The accuracy of the MIT psychrograph is ± 0.2 C in temperatures, with a lag coefficient of the order of 15 sec.

These data were gathered during hours of daylight and are spread rather evenly between 0900 and 1700. The MIT psychrograph was held at a fixed point in space where a conservative estimate of the fluctuations of temperature was 0.3 C. The airborne instruments integrate the measurements for a given level, hence a spread in the data is reasonably indicated and the statistical value of sigma may be considered representative of the accuracy of the test instrument.

The procedure for each test instrument involved making five to ten regular low-level soundings supplemented by a series of passes at a fixed level. Necessary ground checks were carefully made using forced ventilation, and standard corrections for airborne instruments were applied.

Psychrometer equipment ML-313/AM, consisting of a wet and dry bulb thermometer in a streamline housing, was mounted as far back in the cabin of the L-4 as was practical. Since the L-4 is a single engine plane it was expected that the engine heat and propellor blast would influence the readings. The data are as follows:

Dry bulb	
Number of pairs of readings:	174
Average difference:	— 0.06 C
67% of the points agree to within	0.20 C
Wet bulb	
Number of pairs of readings:	156
Average difference:	+ 0.08 C
67% of the points agree to within	0.14 C

The ML-313 was, in addition, mounted on aircraft L-5 (single-engined, cruising speed 100 mph). The data are similar to those given above. The data indicate that, despite the expected influences of propeller blast and engine heat, the equipment is suitable for low-level soundings for propagation work.

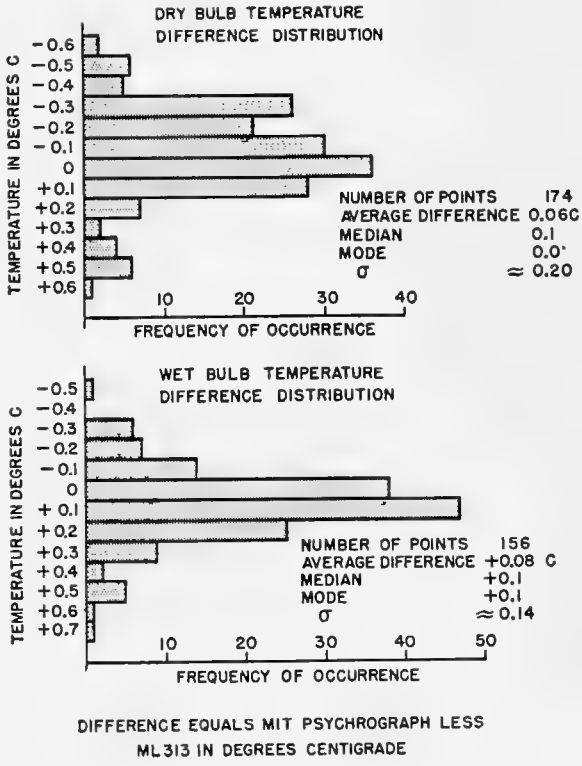

FIGURE 8. Instrument comparison. MIT psychrograph and psychrometer ML 313/AM on Aircraft L-4.

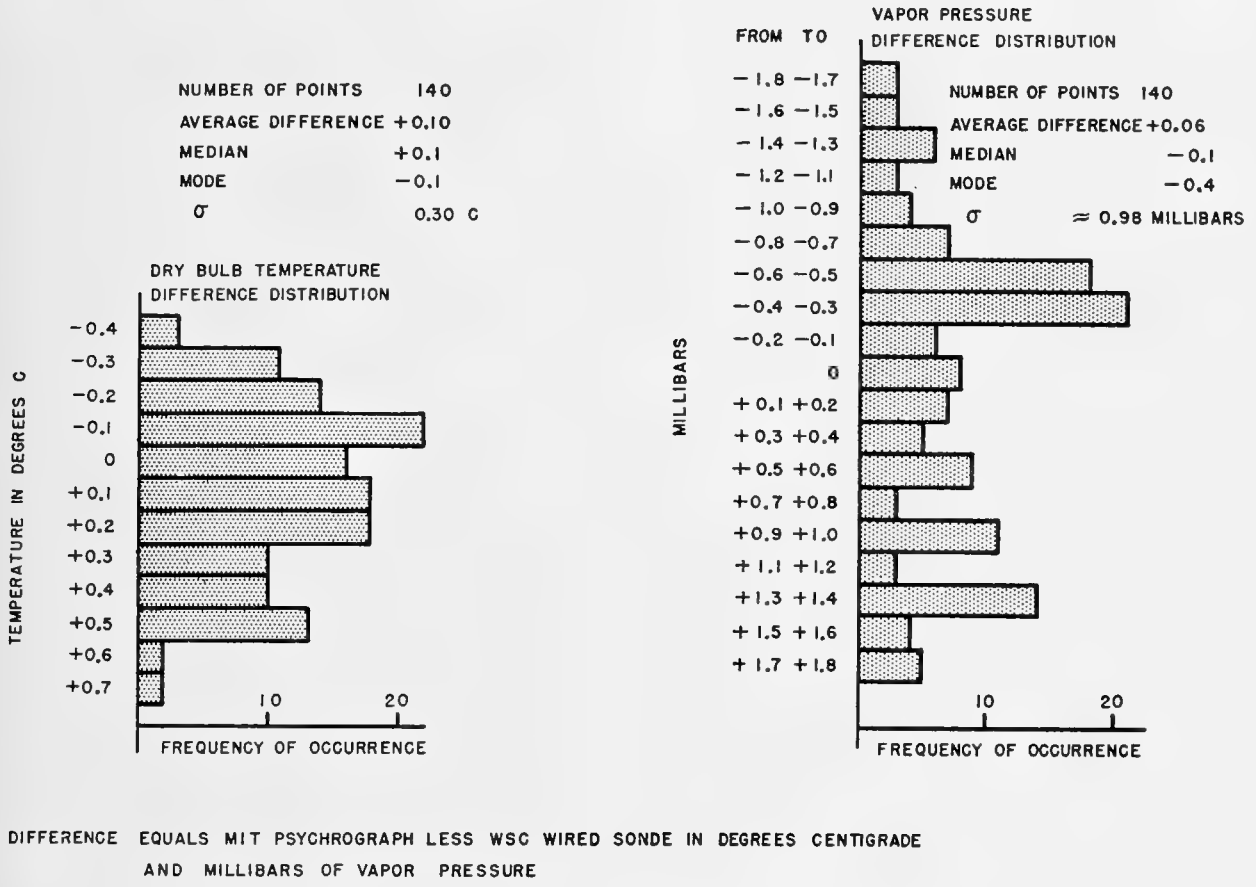

FIGURE 9. Instrument comparison. MIT psychrograph and WSC wired sonde on Aircraft L-4.

The WSC wired sonde was mounted on the strut of the L-4 some 5 ft away from the cabin of the plane. The comparison data follow:

Dry bulb	
Number of pairs of readings:	140
Average difference:	+ 0.10 C
67% of the points agree to within	0.30 C
Vapor pressure	
Number of pairs of readings:	140
Average difference:	+ 0.06 mb
67% of the points agree to within	0.98 mb

The differences in moisture readings are rather larger than desirable.

The sling psychrometer ML-24A was tested similarly but was considered unsuitable because of lack of protection from radiation.

Of the ground-based sounding equipment used during the program, the MIT psychrograph consistently gave excellent results. The WSC wired sonde is capable of good results, but several mechanical difficulties render it unsuitable for field use by the services in its present form. It is expected that these difficulties will be ironed out in a revision of the wired sonde.

The following statements are the personal opinions of the authors and do not represent the official opinion of the Army Air Forces Board.

1. There is a military need for a propagation forecasting service. If a radar set is to be used most efficiently, its full capabilities and limitations (including the effects of weather) must be known.

2. Propagation forecasts over water using the method described in reference 3 are sufficiently accurate for operational purposes. It is recommended that further experimental study of long over-water propagation and vertical coverage be carried on.

3. Propagation forecasts over land are not sufficiently accurate for operation uses. Further study of the over-land forecasting problem is indicated.

4. For maximum operational employment of the forecasts, the forecaster should be located at the radar site. Communication with a class A weather station, a ground-based low-level sounding station at the radar

site, and supplementary airborne soundings are required.

5. Psychrometer equipment ML-313/AM mounted on a slow, single-engined aircraft is suitable for low-level airborne soundings for propagation forecasting work.

8.3 APPLICATION OF FORECASTING TECHNIQUES AND CLIMATOLOGY[f]

8.3.1 Introduction

PURPOSES OF THE REPORT

1. To make available, primarily to radar and meteorological officers, information on the principal meteorological factors which have an important effect on radio and radar performance.

2. To indicate how suitable utilization of certain of these meteorological factors can lead to improved efficiency and increased exploitation of radio and radar devices:

a. With respect to variable adjustments applied to daily routine operations (such as the supplementary use of scouting planes when the coverage of early warning radars is anticipated to be poor, etc.).

b. With respect to longer-range planning in establishing radio and radar stations (optimum choice of sites, most desirable frequencies to use, etc.).

MATERIAL COVERED IN THE REPORT

Radio-Meteorology. Since most of the basic information which has been obtained by various research groups and in military and naval operations involving radar is familiar to the reader or is adequately covered in other reports,[4-7] the essential points with reference to the effect of meteorological factors have been extracted and are here presented in condensed form. The primary emphasis is on the phenomena associated with nonstandard propagation, i.e., on the conditions under which radar ranges are unusually large or unusually small. Related elements—temperature, humidity, the variation of each of these with height, M curves, ducts, etc.—are defined, and the role they play in the effectiveness of radar performance is discussed briefly.

Specific Relationships between Meteorological Elements and Radar Performance. Of the several investigations carried out on this subject, mostly in connection with the prediction of trapping effects and consequently of radar ranges, one which has met with as much success as any and is fairly similar in essence to some of the others is presented here. It was developed in a study of the modification that air undergoes in passing over water and is designed to predict the formation and subsequent structure of surface ducts which are formed along coast lines and over oceanic areas.

From observations of the representative surface temperature and humidity of the air, the sea temperature, and the wind direction and velocity, this method indicates whether a surface duct is to be expected and the height to which it is likely to extend. Practical application of the method can therefore be of direct assistance in anticipating radar performance for short periods in advance or for regions where detailed meteorological observations may be limited. Enough particulars, together with charts and nomograms, are given to enable one with meteorological training to apply these prediction techniques and thus facilitate daily or hourly adjustments to make optimum use of radar equipment.

Computed Climatological Information on Surface Ducts. To obtain a broad picture of the variation in radio and radar ranges likely to be encountered in the western Pacific region, average duct widths (height from the base to the top of the duct) have been computed. These computations are based on the relationships between meteorological elements and radar performance mentioned above and utilize climatological data consisting of monthly averages of air temperature, humidity and sea temperature, and monthly frequencies of winds with specified direction and speed.

The area covered includes the Japanese islands, the coasts of Korea, Manchuria, and China, the northern Philippines, the Marianas, the Bonins, and the Ryukyu Islands—approximately 10° to 50°N latitude and 120° to 150° E longitude. The computations indicate the percentage of time surface ducts of various widths may be expected at different times of the year and at different locations within the region. This information is summarized in tabular form. The results are not intended to represent an accurately detailed picture but do give a sufficiently close approximation of average conditions influencing certain aspects of radio and radar performance so that they may be used as a guide in long-term operational planning.

[f] By A. T. Waterman, Jr., and C. Harrison Dwight, Columbia University Wave Propagation Group.

8.3.2

Radio-Meteorology

Evidences of Nonstandard Propagation

Since the start of the war, cases of very long radio ranges and radar coverages, together with extreme variations of these quantities, have become well known to personnel working at microwave frequencies. Such phenomena, when due to influences acting on the propagated electromagnetic waves and not to freak behavior in set performance, have been classed under the term nonstandard propagation. It has been found that nonstandard propagation (such as is illustrated by the behavior of microwaves when they are constrained to follow a path of such curvature that the rays remain close to the surface of the earth and hence reach otherwise inaccessible targets—a phenomenon frequently referred to as trapping) is directly associated with certain conditions that occur in the lower levels of the atmosphere (normally below 5,000 ft) which have been given the name of ducts. Detailed analyses of the structure of ducts have been presented adequately in the previously mentioned reports. Hence the paragraphs immediately following give only a brief and somewhat simplified description of the meteorological elements associated with ducts.

Meteorological Conditions Associated with Ducts

Remarks on Pressure, Temperature, and Humidity. The meteorological situations in which trapping of microwaves occurs involve certain types of stratification in the lower levels of the atmosphere. The amount of stratification is dependent on the vertical distributions of pressure, temperature, and humidity.

Although the atmospheric pressure at any particular elevation and, to a lesser extent, the rate at which pressure decreases with altitude may vary from one time to another, these variations are relatively unimportant as far as their direct influence on propagation is concerned and so may be neglected in practical considerations.

On the other hand, temperature and its change with altitude do have an immediate bearing on duct formation. Under more or less average conditions throughout the troposphere, the temperature decreases with increasing altitude and the term "temperature lapse rate" is defined as the rate of decrease of temperature with height (and consequently is usually expressed in degrees Fahrenheit per 1,000 ft or degrees centigrade per kilometer). For reference purposes a "standard" lapse rate has been taken as 3.47 F per 1,000 ft. (Further details of the National Advisory Committee on Aeronautics standard atmosphere are given in the Appendix on page 130.) Under certain conditions the temperature throughout a layer of the atmosphere may *increase* with height, in which case a temperature inversion (Figure 10) is said to exist.

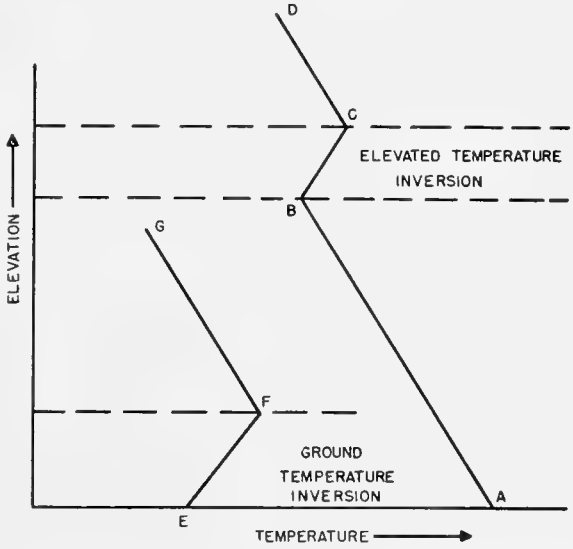

Figure 10. Vertical variation of temperature showing a ground inversion EF and an elevated inversion BC. The slopes of the portions FG, AB, and CD denote standard conditions, a decrease of temperature with elevation.

In general the lapse rate of temperature is important in meteorology because of its relationship to the vertical *stability* of the atmosphere, that is, to the feasibility with which vertical air currents can develop. It turns out that, except within clouds or regions of active precipitation, the stability conditions can be closely evaluated from a knowledge of the actual lapse rate relative to the "dry adiabatic" lapse rate (approximately 5.5 F per 1,000 ft). If the actual lapse rate is larger than the dry adiabatic, i.e., if the temperature decreases at a rate greater than 5.5 F per 1,000 ft in elevation, any vertical currents which develop will tend to exaggerate in intensity, and a condition of unstable equilibrium (Figure 11A) will exist. Conversely, if the actual lapse rate is less than the dry adiabatic or, especially, if a temperature inversion is present, the development of vertical currents will be hindered and the air will tend to become horizontally stratified. This is the case of stable equilibrium (Figure 11C). The in-between case, in which the actual temperature lapse rate is the same as the dry adiabatic, is that of neutral equilibrium (Figure 11B).

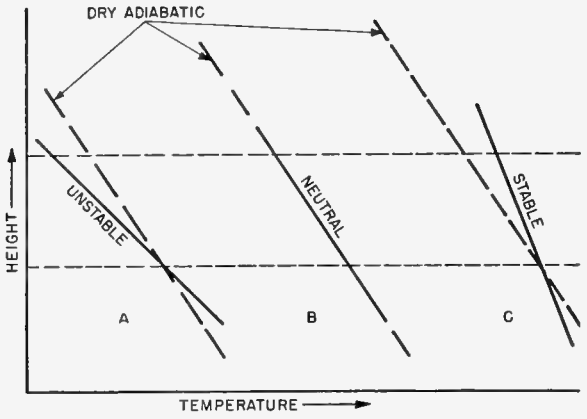

FIGURE 11. Temperature-height curves for the cases of (A) unstable air, (B) neutral air, and (C) stable air. The dry adiabatic (lapse rate) is indicated for comparison.

In addition to the direct relationship which these stability conditions bear toward the trapping of microwaves, which will be described presently, there is also an indirect relationship caused by the modification that air undergoes when it moves over a sea or land surface with properties (temperature and moisture) different from those of the air itself. For example, air moving over land, the temperature of which is *higher* than that of the air, will be heated in its lowest layers by contact with the ground and thus tend to become *unstable*. This leads to vertical currents which will carry the modifying influences to appreciable heights in the air. On the other hand, air moving over a surface cool in relation to the air will be cooled by contact with the ground, tend to develop *stable* characteristics, damp out vertical currents, and so confine the modifying influences to very low layers.

The distribution of moisture with altitude, in its direct influence on nonstandard propagation, has an even more pronounced effect than that of temperature. As a means of describing the moisture content of the air, any one of several concepts may be used: dew point, wet bulb temperature, relative humidity, absolute humidity, specific humidity, and mixing ratio, all of which are defined in the Appendix. Except when evaporation or condensation is taking place (as in the case of clouds, rain, dew, etc.), the moisture content of the air has little effect on the temperature structure and therefore is not a major influence on stability conditions in so far as they are connected with the formation of ducts. What is of direct importance is the vertical distribution of humidity itself and the manner in which this distribution is affected by modifying influences. As an example of the latter, the case of warm and relatively dry air moving over a humid surface, such as dense vegetation or the ocean, might be mentioned. In this case, evaporation of water into the lower layers of the air leads to a greater decrease in moisture with altitude than was originally present in the air.

Other modifying influences, of course, affect both the vertical distribution of temperature and humidity and the stability conditions of the air. Some of these are subsidence (the gradual sinking of large layers of air leading to increased stability and decreased relative moisture content), radiation, and turbulent mixing. These are merely mentioned here in view of the fact that their various interactions at times may become quite complicated, hence requiring that proper interpretation be made by one trained or experienced in meteorology.

Refractive Index. The manner in which pressure, temperature, and humidity directly influence trapping depends on the phenomenon of refraction or the bending of rays as they pass through media with different dielectric properties or through a medium with variable dielectric properties. The velocity of electromagnetic waves through any particular medium such as the air depends on a quantity known as the refractive index of that medium. When the refractive index varies throughout the medium, as is usually the case in the atmosphere, the resulting variation in wave velocity leads to a bending of the rays. For example, the refractive index of the atmosphere often decreases with height, in which case rays are bent downward toward the surface of the earth, so that instead of traveling in straight lines they tend to follow to a certain extent the curvature of the earth. The amount of bending depends on the manner in which the refractive index varies with height. Under the proper conditions it is possible for rays to be bent to such a degree that they are confined to one layer of the atmosphere. This phenomenon, the trapping of radio waves, is usually associated with only the microwave frequencies and is limited to those rays which leave the transmitter at an angle with the horizontal of less than 1 degree, and therefore to only the lowest lobe in a radar coverage diagram.

For the atmospheric refraction to be strong enough to cause trapping of microwaves it is necessary that the refractive index of the atmosphere decrease with altitude at a sufficiently rapid rate. For convenience in dealing with problems of nonstandard propagation, a quantity known as the modified refractive index has

been defined and is usually denoted by the letter M. It depends on pressure, temperature, humidity, and height and can be readily calculated from the proper nomograms[8] or from tables,[9] or directly from the formula.[8]

When values of M are computed for various elevations from measurements of the pressure, temperature, and humidity at those elevations, a graph can be made of the value of M plotted against height. This M curve gives directly a graphical representation of the structure of the atmosphere with reference to the existence of ducts. A decrease of M with elevation is called an M inversion, since under standard conditions M increases with altitude, and indicates the existence of a duct. This, then, is the criterion for the meteorological conditions necessary for the trapping of radio waves. The top of the duct is taken to be that level at which M reaches a minimum (as in Figure 15) and the base of the duct the level at which a vertical projection from the value of M at the top of the duct intersects the lower portion of the M curve (as in Figure 16) or the ground (as in Figure 17). The term "duct width" is used to refer to the thickness of the duct, i.e., the vertical distance between the top and the base.

The vertical distribution (a) of temperature and (b) of humidity may each contribute to the formation of an M inversion, in the following ways.

1. A strong temperature inversion tends to lead to duct formation.

2. A rapid decrease of humidity with altitude tends to lead to duct formation.

If the first of these is predominant the duct is said to be dry, and if the latter is predominant the duct is said to be wet. Often both factors are operative together; that is, in the M inversion there is both an increase in temperature with altitude and a decrease in humidity with altitude, the duct being more sensitive to the effect of the humidity distribution than to that of the temperature distribution.

Types of M Curves. For purposes of clarification, the various types of M curves that may exist can be classified as follows:

1. *Standard type* (Figure 12). In a standard atmosphere M increases linearly with altitude at a rate of 3.6 M units per 100 ft (0.118 M unit per m). Radio and radar waves are bent slightly downward, the paths of the rays actually having a radius of curvature about four times that of the earth; but no trapping occurs. Standard conditions, in their effect on propagation, hardly differ at all from those of neutral and unstable

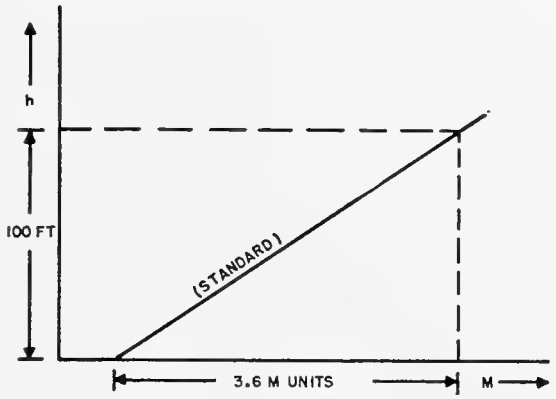

FIGURE 12. Standard type of M curve.

equilibrium (except in special cases as mentioned later) and so are frequently found in well-mixed air, as is likely to occur on sunny afternoons and in areas of turbulence.

2. *Transitional type* (Figure 13). In the lower levels M is constant with elevation. Correspondingly, rays are bent downward more than in the standard case but not so strongly as in a duct, i.e., the rays are not actually trapped. Being literally a transitional case,

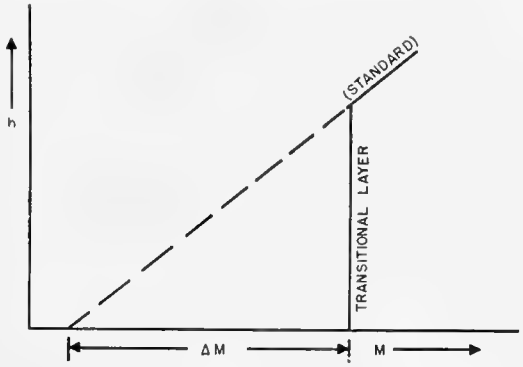

FIGURE 13. Transitional type of M curve.

this type of M curve is likely to occur during the formation or dissolution of a duct, or when the meteorological factors tending to cause a duct are incompletely operative. The M deficit (ΔM, defined in Section 8.3.3), is indicated in the figure.

3. *Substandard type* (Figure 14). In the lower levels M increases *more than* 3.6 M units per 100 ft, which corresponds to rays being bent downward only very slightly or, in some cases, actually upward from the line of sight, thus giving shorter maximum ranges on surface and low-flying targets. There is no trapping. Depending to some extent upon the elevation of the transmitter, the field strength in the substandard

region may be reduced considerably below normal, even to the point of producing radar and communication "blackout." The M deficit is negative with this type of curve. Associated meteorological conditions are usually those in which warm, moist air passes over a

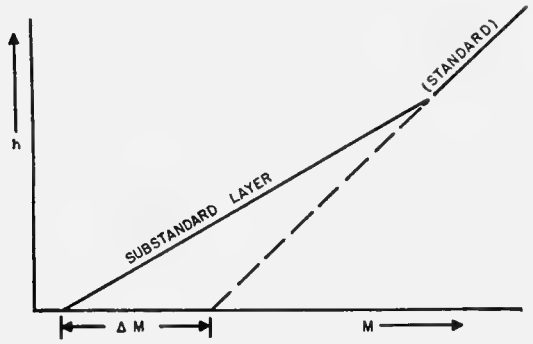

FIGURE 14. Substandard type of M curve.

relatively cool land or sea surface, quite frequently in connection with the formation of surface fog.

4. *Simple surface trapping* (Figure 15). The M curve has a negative slope in the inversion layer which comes down to the land or water surface. The duct is of the ground-based type, and its width is the height of the upper boundary of the inversion layer. Rays which are propagated at an angle of 1 degree or less with the horizontal may be trapped within the duct. As a consequence, radio and radar ranges may be exceedingly large. Simple surface trapping occurs quite frequently over the oceans—particularly where warm, dry air from over land flows out over a cooler sea surface—along coast lines with an afternoon sea breeze, and occasionally over land with radiational cooling at night.

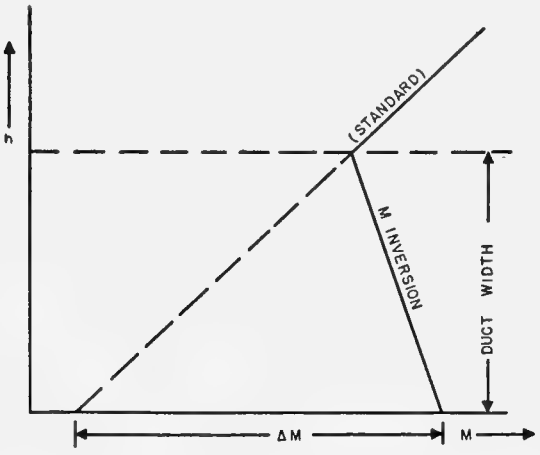

FIGURE 15. Simple surface trapping.

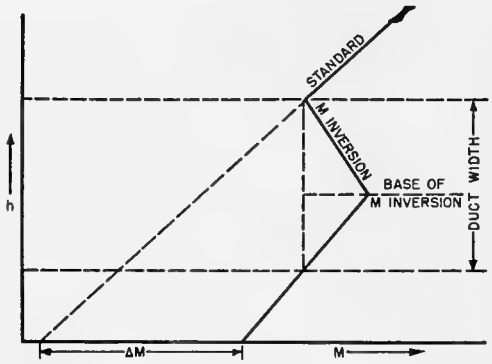

FIGURE 16. Elevated S-shaped type.

5. *Elevated S-shaped type* (Figure 16). The inversion layer has a width given by the difference in elevation of the end points of the negative portion of the M curve, but the width of the duct extends downward to the level where the vertical projection of the upper minimum of the M curve intersects the latter. Trapping occurs when the transmitter is at an elevation which places it within (or close to) the duct and is most pronounced when the transmitter is at the elevation of the base of the M inversion. This type of duct may be brought about by subsidence or as the result of a Föhn wind blowing off shore from mountains paralleling a coast. Examples of elevated S-shaped M curves are observed off the southern California coast and off the east coasts of Japan and New Guinea (see Section 8.3.5).

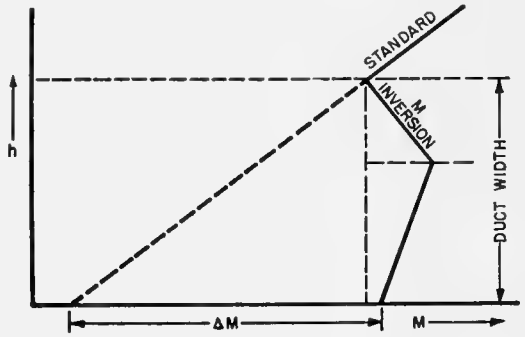

FIGURE 17. Ground-based S-shaped type.

6. *Ground-based S-shaped type* (Figure 17). When the conditions which could produce type 5 (Figure 16) exist down to the surface of the earth or to the sea, this type of duct may occur. It usually has a width considerably greater than that found in the simple trapping case (type 4, Figure 15).

That it is possible for ducts of two types to occur simultaneously has been shown from observations off

the east coast of New Guinea when a Föhn wind flows out over a sea breeze, the latter producing simple surface trapping (Figure 18). (See Section 8.3.5.)

Factors Affecting the Extent of Trapping. The principal factors which determine the extent of trapping are:

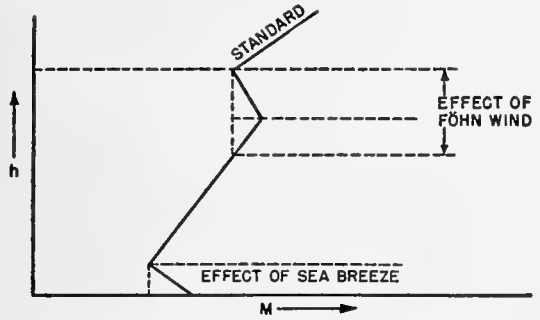

FIGURE 18. Combination of types 4 and 5. (See Figures 15 and 16.)

1. The amount by which M decreases through the M inversion.
2. The duct width, for the wider the duct the more energy will be trapped.
3. The elevation of the transmitter with respect to the duct, the trapping being most complete when the transmitter is at the base of the M inversion.
4. The angle at which the rays are propagated from the transmitter; the smaller the angle made with the top of the duct, the greater the range.
5. The frequency of the propagated waves; in general, the higher the frequency, the greater the extent of trapping.

8.3.3 Specific Relationships Between Meteorological Elements and Radar Performance

Research on Forecasting of Radio and Radar Ranges

Army Air Force Board Project. Realizing the important and direct effects of temperature and humidity distributions on microwave propagation, several projects have been undertaken in the attempt to develop a systematic method of forecasting the meteorological conditions leading to nonstandard propagation. Of these methods, one which has met with a considerable degree of success is described below. The methodology, developed by the Army Air Force Board working in conjunction with the Radiation Laboratory at MIT,[3] is designed to predict the formation of surface ducts over water. Its fundamental concepts are quite similar to those used in other methods of radio and radar forecasting.[10]

General Procedure. In essence the method consists of an analysis of the modification that air undergoes in the lower 1,000 ft as it moves from a large land mass out over the ocean. The study was carried out in the vicinity of Cape Cod, but indications are that the numerical factors entering into the procedure are much more generally applicable. In the modification of the air moving over the sea, the following assumptions are made.

1. The air initially (before moving off the land mass) is well mixed, i.e., it exhibits conditions close to neutral equilibrium (see Figure 11).
2. The stability conditions of the air as it moves out over water are determined by its initial temperature (over land) relative to that of the sea surface.
3. The modified air at the sea surface acquires the same temperature as the sea.
4. In the modified air at the sea surface the moisture content becomes that corresponding to saturation at the sea surface temperature, except for a correction owing to the salinity of the sea.
5. The resulting M curve is determined by the quantities:
   a. Temperature excess.[g]
   b. M deficit.[g]
   c. Wind speed and direction.
   d. Distance of over-sea travel (in some cases).

Thus the method attempts to relate duct formation to a limited number of easily determined meteorological factors. It involves a simplified consideration of the upward diffusion of heat and moisture. It turns out, however, that the simplified assumptions yield results which in practical application are of sufficient accuracy to be of definite use in forecasting the existence of nonstandard conditions. It should also be mentioned that, although the method is designed primarily for situations in which air over land moves out over the sea, it can also be satisfactorily applied to situations in which the air has a purely over-sea trajectory.

The particular steps to be taken in carrying out the procedure follow.

Method of Determining Duct Width

Observation of Initial Conditions. The necessary meteorological measurements to be taken should be

[g]These terms are defined on page 124.

as representative as possible, i.e., uninfluenced by purely local effects. Measurements are:

1. Surface air temperature (of the unmodified air over land, in the case of air moving off a land mass);
2. Surface air humidity (also of the unmodified air which can be expressed in terms of relative humidity, specific humidity, dew point, wet bulb temperature, or vapor pressure);
3. Sea surface temperature;
4. Wind speed and direction (preferably at 1,000 ft-elevation); and sometimes
5. Distance from land (of primary importance only in the case of stability conditions, when the air is warmer than the sea surface).

All these data may, of course, be profitably supplemented by aerological soundings, weather maps, and any other pertinent information available.

Modification of Air by Sea Surface. As a qualitative description of the modification that the air undergoes in moving over water, three cases may be distinguished, namely:

1. *Neutral equilibrium* (resulting when the initial surface air temperature is the same as the sea temperature). The temperature structure of the air remains unchanged; however, since the air is usually not completely saturated, moisture is supplied to the lower layers by evaporation from the sea surface, in this way causing a greater decrease of humidity with height, which tends to establish an M distribution such that the modified refractive index is either constant or decreasing with height. In the case in which the air is initially completely saturated no modification takes place.

2. *Unstable equilibrium* (resulting when the initial surface air temperature is less than the sea surface temperature). In this case the moisture content of the air is always less than that corresponding to saturation at the sea surface temperature, so that the lower layers of air suffer an increase in humidity as well as in temperature. Owing to the greater sensitivity of M to humidity than to temperature this tends to bring about a decrease of M with height in a layer of air adjacent to the sea surface, while the unstable conditions give rise to vertical mixing which keeps the M distribution close to standard above this layer so that the duct is confined to lower levels than in the case of neutral equilibrium.

3. *Stable equilibrium* (resulting when the initial surface air temperature is greater than the sea surface temperature). If, in addition, the air is initially quite dry, i.e., has a moisture content less than that corresponding to saturation at the sea surface temperature, then the resulting rapid decrease of moisture with height plus the stable temperature distribution leads to a tendency to surface duct formation. On the other hand, if the initial moisture content of the air is relatively large, moisture may be condensed out of the surface layers of air thus tending to give rise to an increase in humidity with elevation which when sufficiently marked may counteract the effect of the stable temperature distribution and so prevent the formation of a duct or even produce substandard conditions. In either case, the stable structure of the air tends to hinder vertical mixing so that modification from the surface upward proceeds slowly and hence is highly dependent on the distance traveled by the air over the water.

Necessary Calculations. To determine quantitatively the possibilities of duct formation, the following items can be readily calculated from any particular observed set of initial conditions.

1. *Temperature excess,* which is merely the representative surface air temperature (before modification) minus the sea surface temperature.

2. *M deficit,* defined as the value of M corresponding to the sea surface temperature minus the value of M determined from the representative surface air temperature and humidity (before modification); values of M can be ascertained from nomograms,[h] tables,[i] or directly from the formula.[j] In the case of M corresponding to the sea temperature, a 98 per cent saturation is assumed; the 2 per cent vapor pressure correction is subtracted to take into account the salinity of the sea water.

3. *Ratio of duct width to M deficit,* determined from the chart in Figure 19 for a given temperature excess and wind speed as measured at the 1,000-ft level.

4. *Duct width,* found by multiplying the above ratio (3) by the M deficit.

Applicability of the Method. Since the procedure is designed to take into account only the surface modification of air over water, its application is restricted to the prediction of the first four types of M curves described in Section 8.3.2: standard, substandard, simple surface trapping, and transitional. The causes

[h]Nomograms are included and explained in the Appendix.

[i]Tables for computing M can be found in references 8 and 9.

[j]The formula expressing M in terms of pressure, temperature, humidity, and elevation is given in the Appendix.

of S-shaped M curves are not considered in this method. Standard conditions can be presumed to occur when the calculations indicate a duct width of zero, which is the case when the M deficit is zero. If the M deficit is *negative*, then the calculated duct width will be negative, and substandard conditions are to be inferred. A *positive* M deficit indicates duct formation (simple surface trapping), and the calculations of the duct width given an estimate of the height to which the duct extends. If this height is small, conditions may be inferred to correspond to the transitional case. Once the duct width is calculated, a complete picture of the distribution of M with height can be approximated as indicated in Figure 15 by assuming that standard conditions prevail above the duct and that the M deficit (ΔM) is the difference between the actual M value at the sea surface and the M value that would exist at the sea surface if the standard conditions were extended down to the surface.

The method is not applicable to conditions over land.

In the case of air with a purely sea trajectory, it turns out that the procedure is closely valid if, in place of the air temperature and humidity measurements made over land, these measurements are taken in the air at a slight elevation above the sea surface, for example, at bridge level on a large ship.

In practical application results will be most reliable when the assumptions listed under "General Procedure" are satisfied. However, this does not mean that the method is useless under other circumstances. Figure 19, which is the crux of the method, is largely empirical and is based on relationships which have been observed to hold under various meteorological conditions. Consequently, reasonably accurate results are not limited to only a few idealized situations.

It should be mentioned also that use of the method in a literal manner can be improved upon if the calculated results are modified by the judgment of someone trained or experienced in meteorology. Complicating factors such as variations in the initial stability conditions, variability of the sea surface temperature, effects of convergence, divergence, and subsidence, and presence of fronts can best be taken into account by one familiar with their effects.

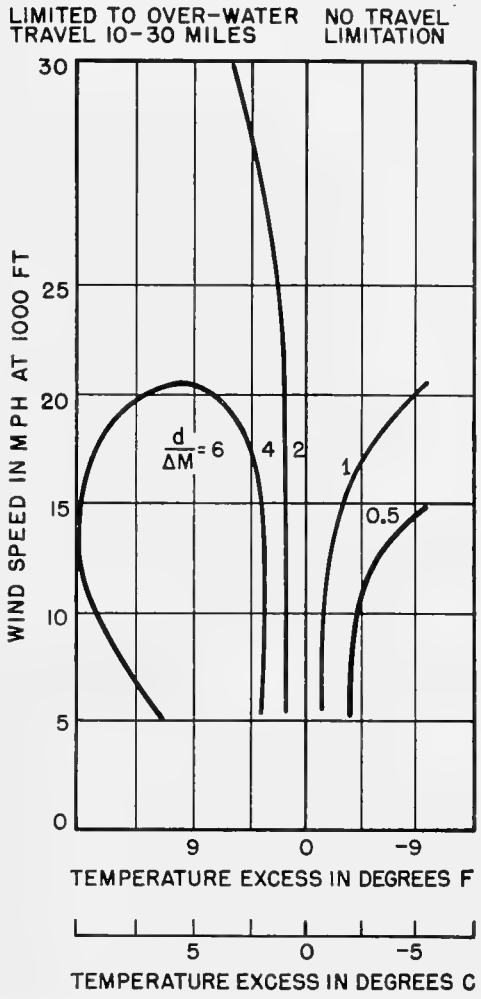

FIGURE 19. Graphs showing the value of the ratio of duct width d to the M deficit, ΔM for values of temperature excess and wind speed at the 1,000-ft level. (Typical values are given in Table 2.)

QUALITATIVE PREDICTION OF RADAR RANGES

The method described above gives a means of estimating surface duct formation, whereas what is needed is a knowledge of the effect of the duct on radio propagation. It is impossible to make a blanket statement giving the exact range that will be obtained with any particular duct width, since the range depends on the power of the radio or radar set (also on the character of the target, in the case of radar), as well as on the factors listed in Section 8.3.2. However, some numerical estimates of trapping effects can be made.

Dependence on Duct Width, Frequency, and Elevation of Site. An approximate expression relating the maximum wavelength that can be trapped by surface ducts is given by

$$\lambda_{max} = 0.076d\sqrt{\Delta M - 0.036d},$$

in which λ_{max} is the maximum wavelength in centimeters, d is the duct width in feet, and ΔM is the M deficit in M units. Table 2 is developed from this formula and indicates, for given values of ΔM and d,

the wavelength above which trapping will not occur. A rough generalization can be made by stating that, when the wavelength of the radiation is around 3 cm, duct widths of 20 ft or more will be sufficient to cause simple surface trapping, and, when the wavelength is around 10 cm, duct widths of at least 40 or 50 ft will be sufficient, provided in each case that the transmitter is located within the duct. Thus, for a particular radar frequency and location, an estimation of duct width becomes a critical factor in anticipating whether an appreciable amount of trapping will occur and consequently whether radar ranges will be appreciably larger than under standard conditions.

Table 2. Values of the maximum wavelength (in cm) for which waves can be trapped in a surface duct for given values of M deficit (ΔM) and duct width (d).

	ΔM (M units)					
d(ft)	2	5	10	15	20	25
10	0.97	1.63	2.36	2.90	3.36	3.78
20	1.72	3.14	4.62	5.75	6.67	7.49
30	2.19	4.52	6.80	8.50	9.93	11.1
40	2.28	5.74	8.88	11.2	13.1	14.7
50	1.69	6.80	10.9	13.8	16.2	18.3
60	..	7.65	12.8	16.3	19.2	21.8
70	..	8.35	14.5	18.8	22.2	25.2
80	..	8.82	16.2	21.2	25.2	28.6

Dependence on Extraneous Factors. Meteorological conditions other than ducts often have important effects on propagation. Surface fog frequently causes substandard conditions. Rain and clouds may attenuate the propagated energy and effectively decrease the range. Heavy rain and sometimes cumulo nimbus clouds cause radar echoes.

Operational Use and Limitations

The restrictions surrounding the possible utilization of this prediction technique have been covered earlier in this section, where it is indicated in what respects applicability is limited. Subject to these limitations, the method can be employed to advantage. Short-term predictions (a day or so ahead) of duct formation and radar range can aid in estimating the coverage of a particular radar set. Information of this nature should lead to the more efficient use of radar facilities.

8.3.4 Computed Climatological Information on Surface Ducts

Purpose of This Information

Inasmuch as the present report is designed to aid radar and meteorological officers in the Pacific theater of war, it has been thought expedient to include climatological information on that area which gives an indication of the occurrence of surface ducts. For this purpose, computations have been carried out, using the methodology presented in Section 8.3.3, to yield the following:

1. Estimation of the per cent of time surface ducts of certain widths are likely to occur at various times of the year and at various places in the western Pacific theater.

2. Estimation of the variation in duct width with the time of year, geographical location, etc.

3. Estimation, from (1) and (2) above, of the amount of trapping to be expected for specified radio frequencies and specified elevations of sites.

Regions Chosen for Study

The area chosen for investigation was that bounded approximately by 10° and 50° N latitude and by 120° and 150° E longitude. These regions include the Japanese islands, the coasts of Korea, Manchuria, and China, northern Philippines, the Marianas, the Bonins, and the Ryukyu Islands. The computations were carried out for representatively selected 5x5 degree sectors or "squares." The results for several regions in this area are summarized and are given below.

Sources of Climatological Data

The charts and atlases used in compiling the data can be found in references 11 to 15.

Method of Computation

The procedures described in Section 8.3.3 were applied as follows:

1. A determination of the monthly mean temperature excess was made for each 5x5 degree square for each month (1) by taking the difference between the mean temperature of the air over the sea and the mean sea surface temperature, and (2) by taking the difference between the mean temperature of the air at a land station (when the given square was near a coast) and the mean sea surface temperature.

2. A determination of the monthly mean M deficit[k] was made for each square for each month using the

[k]These calculations do not represent exactly the correct mean value of the M deficit, since M is not a linear function of the temperature and humidity, and so the value of M computed from mean temperature and humidity data is not quite the same as the mean of all M's computed from individual temperatures and humidities. A cursory evaluation of this error has indicated that the values computed are if anything conservative, i.e., that the actual mean M deficits are probably larger than those computed.

nomograms and taking the data for (1) the mean temperature and wet bulb depression of the air over the sea and the mean sea temperature, and (2) the mean temperature and relative humidity of the air at a land station (when the given square was near a coast) and the mean sea temperature.

3. For each square for each month note was made of the various surface wind velocity ranges that occurred with each wind direction (eight points of the compass) and the percentage of time the wind lay within each velocity range.[1]

4. In terms of the mean temperature excess and mean M deficit, the corresponding duct width was computed for each wind velocity range, and, knowing the percentage of time that winds of each magnitude occurred, it was possible to compute the percentage of time that ducts of various widths would occur, both for each wind direction (on an eight point compass) and for the overall picture regardless of wind direction.

Results of Computations

The results were summarized by lumping individual squares showing similar characteristics into nine regions within the whole area. In each region data for the individual months were lumped together on the basis of similarity to divide the year into three or four parts (these varying according to region). Then for each group of months in each region were listed those results which were considered to be the most important, namely,

1. The range in duct widths, giving an indication of the variability at any one place at any one time of year.

2. The percentage of time that ducts characterized by widths greater than 40 ft occur and, following this, the most prevalent wind direction associated with ducts of these widths, as well as the minimum wind velocity necessary to establish them.

3. The percentage of time that ducts characterized by widths from 20 to 40 ft occur, similarly followed by the associated prevailing wind direction and the minimum required wind velocity.

4. The percentage of time that ducts do not occur or have a width less than 20 ft.

Figure 20 contains these summarized results. The numerical listings in the figure make no claim toward being exact, as is evident in view of the remarks made in Section 8.3.3 on the applicability and limitations of the method, in addition to the slightly erroneous computations of the monthly mean M deficit and the use of the surface winds instead of those at 1,000 ft. (The effect of the latter two errors is mainly to cause the calculated duct widths to tend toward the conservative side.) In Figure 20, for purposes of consistency throughout the area, only the calculations based on air temperature and humidity records over the sea were used [i.e., only (1) under "Method of Computation"]. The difference between these calculations and those based on land station data is primarily that temperature excesses and M deficits are larger in the latter case (this again tends to make the tabulated results conservative).

Other deficiencies of the method which might be cited are the neglect to take into account the occurrence of fog or rain (which tends to create substandard or standard conditions) and the omission of the influence of local effects such as the topography along coast lines (see Section 8.3.5). In some cases the period of record was fairly short, so that the data used in the calculations were not always completely representative. Lastly, the ranges of duct widths were calculated on the assumption that there was a variation of wind speed only, not allowing for possible variation in temperature excess and M deficit.

In spite of these shortcomings, the calculated results show regional and seasonal trends consistent both with what might be expected on the basis of qualitative physical reasoning and also with a limited number of actual observations taken in the Pacific (see Section 8.3.5). In conclusion we may safely state that the results represent to a reasonable approximation the average conditions of surface duct width and variability.

Use of Computed Results

Since the computations are based on climatological data and are limited in exactness, they do not have forecasting value in the sense of indicating specifically what trapping conditions will be on any particular day. They serve merely to indicate in a general way the average conditions that might be expected over a period of time. For example, the percentage of time that duct widths in excess of 40 ft occur gives an estimate of the fraction of time that properly sited S- or X-band radars would be able to take advantage of extremely large ranges; the percentage of time that duct widths from 20 to 40 ft occur indicates that portion

[1]This led to a slight error, inasmuch as the wind at 1,000 ft should have been used in place of the surface wind (data were available only for the latter). This error in most cases resulted in calculated duct widths of slightly less magnitude than would have been obtained if the 1,000-ft wind had been used.

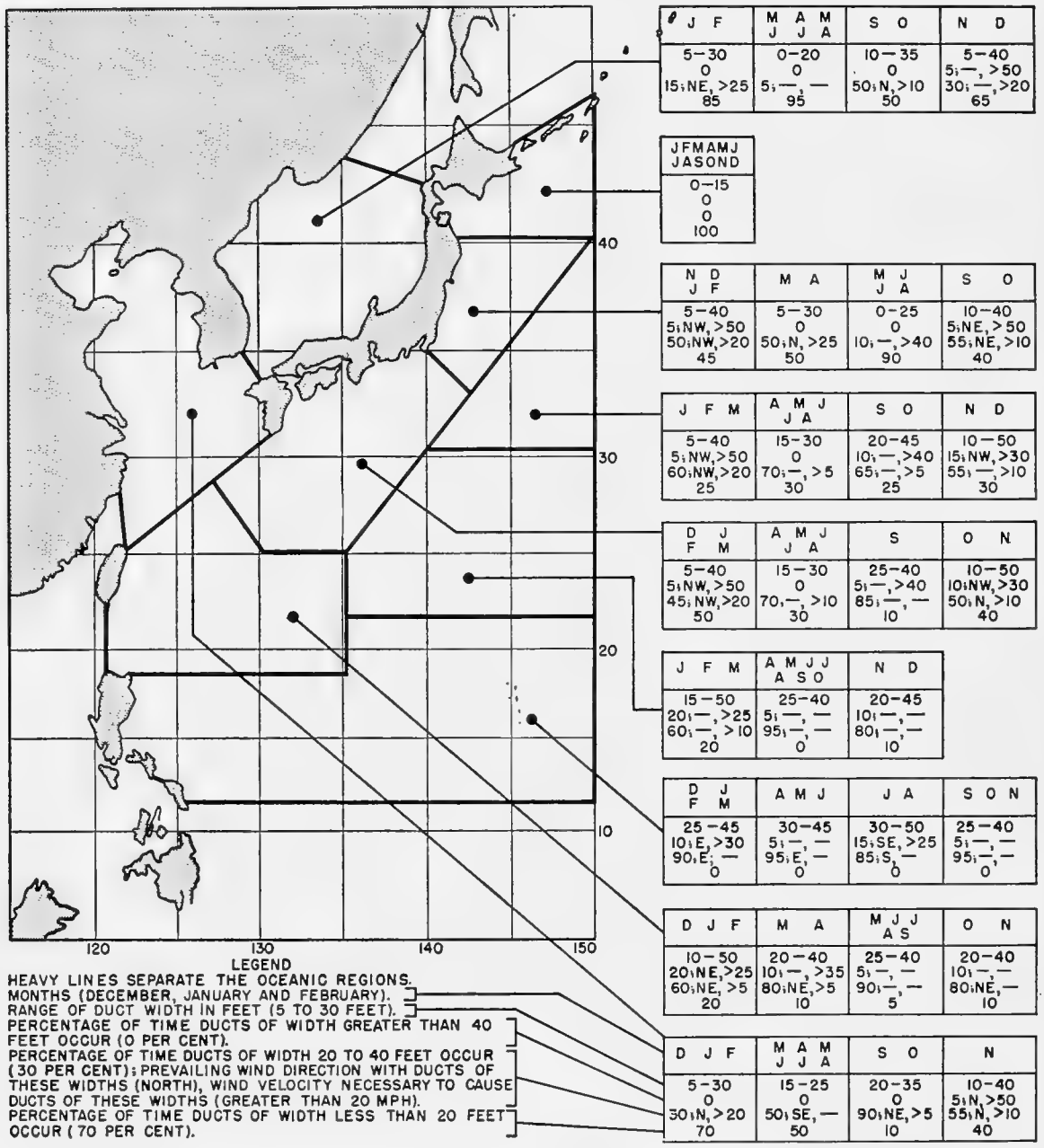

J F	M A M J J A	S O	N D
5–30 0 15; NE, >25 85	0–20 0 5; —, — 95	10–35 0 50; N, >10 50	5–40 5; —, >50 30; —, >20 65

JFMAMJ JASOND
0–15 0 0 100

N D J F	M A	M J J A	S O
5–40 5; NW, >50 50; NW, >20 45	5–30 0 50; N, >25 50	0–25 0 10; —, >40 90	10–40 5; NE, >50 55; NE, >10 40

J F M	A M J J A	S O	N D
5–40 5; NW, >50 60; NW, >20 25	15–30 0 70; —, >5 30	20–45 10; —, >40 65; —, >5 25	10–50 15; NW, >30 55; —, >10 30

D J F M	A M J J A	S	O N
5–40 5; NW, >50 45; NW, >20 50	15–30 0 70; —, >10 30	25–40 5; —, >40 85; —, — 10	10–50 10; NW, >30 50; N, >10 40

J F M	A M J J A S O	N D
15–50 20; —, >25 60; —, >10 20	25–40 5; —, — 95; —, — 0	20–45 10; —, — 80; —, — 10

D J F M	A M J	J A	S O N
25–45 10; E, >30 90; E; — 0	30–45 5; —, — 95; E, — 0	30–50 15; SE, >25 85; S, — 0	25–40 5; —, — 95; —, — 0

D J F	M A	M J J A S	O N
10–50 20; NE, >25 60; NE, >5 20	20–40 10; —, >35 80; NE, >5 10	25–40 5; —, — 90; —, — 5	20–40 10; —, — 80; NE, — 10

D J F	M A M J J A	S O	N
5–30 0 30; N, >20 70	15–25 0 50; SE, — 50	20–35 0 90; NE, >5 10	10–40 5; N, >50 55; N, >10 40

FIGURE 20. Summarized results of climatological duct with calculations.

of the time in which X-band radars would be needed to benefit from surface duct conditions; the percentage of time that no ducts (or exceedingly small ducts) occur points out limitations in the utilization of simple surface trapping. Inasmuch as the transmitter should be located within the duct (if the maximum benefit is to be received from trapping conditions), these factors indicate preferable elevations of the transmitter. In general, the information given in Figure 20 can be helpful in relatively long-range planning procedures, in deciding on the most effective type of radar set, the optimum frequency to use, and the most advantageous elevations at which to establish sites, etc., for operations to be conducted during a particular season of the year and in a particular region.

8.3.5 Direct Indications of Nonstandard Conditions in the Western Pacific

General Conclusions

Evidences of superrefraction have frequently been found at Guadalcanal and in the general vicinity of New Guinea and New Zealand. Data obtained on the radio-meteorology of the western Pacific in the region from New Guinea to Saipan, from soundings made there in 1944 and 1945,[16-18] indicate the following conditions in both the equatorial and trade wind belts of the Pacific.

1. Unmodified winds of long sea trajectory produce ducts which attain sufficient height and intensity to trap microwaves in the 3,000- to 10,000-mc range.

2. At the relatively low wind speeds characteristic of the equatorial belt (4 to 10 knots), the duct height increases with wind speed from about 20 to about 40 ft. X-, and possibly S-, band radars with properly placed antennas may be expected to show marked increase in range on surface craft and on aircraft flying within the duct.

3. At the higher wind speeds typical of the trade wind belt (10 to 20 knots), ducts 50 to 60 ft wide occur regularly. Properly sited S-, as well as X-, band radars may be expected to show marked and persistent increases of range on surface targets. The persistence of the duct in these regions suggests its use in microwave communications.

4. Unless modified by passage over nearby land masses, the atmosphere is approximately *standard* from 60 to 1,000 ft.

5. The results are so similar to earlier measurements taken in the Caribbean on northeast trade wind air of long sea trajectory as to warrant the conclusion that this type of duct formation is general, at least in tropical and subtropical regions, throughout the world.

6. From the experimental results around Saipan and the Marianas it is concluded that the coverage of radars operated at frequencies much lower than 3,000 mc will probably not be affected by the oceanic ducts.

7. The coverage of microwave radars (3,000 mc and higher) which are sited above 100 ft may not be affected by low-level conditions.

8. If coverage on surface craft or ultra-low-flying aircraft beyond the range of existing facilities is required and if prevailing wind speeds exceed 10 knots, S-band radars sited 10 to 30 ft above sea level may give better results than high-sited ones.

9. X-band radars sited at 10 to 20 ft should be useful down to wind speeds of the order of 6 knots.

10. In microwave communication links, the use of low-sited antennas may increase range beyond that attainable by siting at the highest available altitudes. (From the standpoint of water vapor attenuation and duct utilization, X-band frequency appears to be the optimum for this purpose.)

11. From a series of ship-based kite soundings taken northeast of Saipan in the two distinct weather regimes, (1) a typical fair weather period, with steady 10- to 20-knot trades blowing and (2) a stormy period with variable 4- to 15-knot southerly winds and frequent rain squalls, it has been found that *all* soundings yield simple surface trapping curves exclusively, the average duct widths being respectively (1) 44 ft and (2) 37 ft.

12. Although measurements were not taken under the conditions mentioned in paragraph 11 (2) above, soundings immediately after the squalls showed the usual duct. (Sea surface temperatures were constant at 84 to 85 F. Close to the surface the temperature lapse rate was superadiabatic, but it was dry adiabatic above 100 ft.)

Observations upon Ducts other than Simple Surface Trapping

Although the emphasis in this report is placed upon simple surface trapping, nonstandard propagation is found under other distributions of atmospheric moisture and temperature. Elevated inversions are found up to around 5,000 ft, due to subsidence in anticyclones over the Pacific[7]; the western and the southern portions of this area usually exhibit the higher elevations. Illustrative of one of the other factors in nonstandard propagation is the Föhn wind which often produces an elevated S-shaped duct and frequently is superimposed upon a sea breeze. Figure 21, plotted from data taken in the vicinity of the

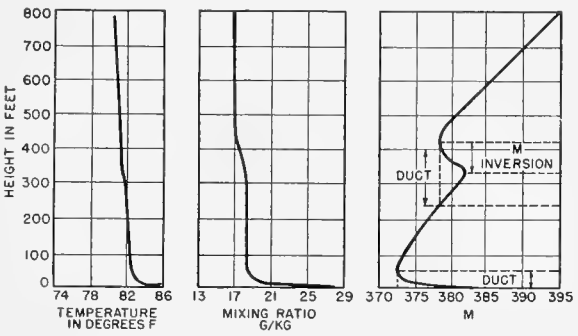

Figure 21. Data from Geelvink Bay, New Guinea, showing surface duct as well as elevated S-shaped duct due to Föhn effect from 10,000-ft mountains 100 to 150 miles to windward (SW).

New Guinea coast,[18] indicates the occurrence of an elevated S-shaped curve, below which is found simple surface trapping or the usual trade wind surface inversion. While the existence of conditions favorable to such effects off the coasts of Japan may be assumed, on account of the lofty mountains, there are no data available on this point. The only information on

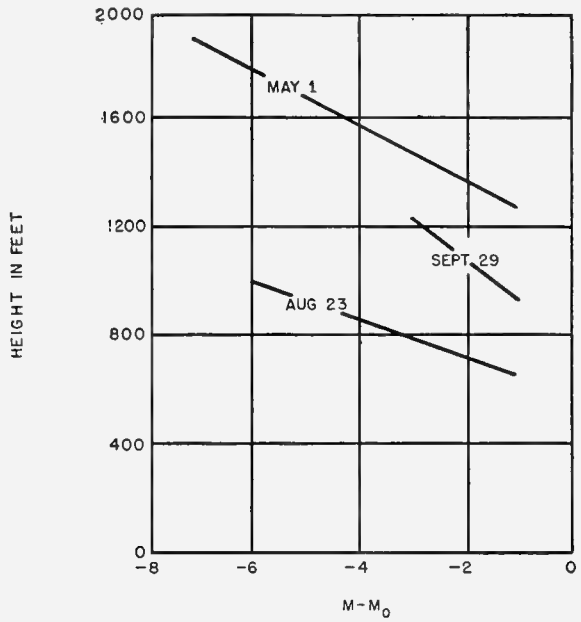

FIGURE 22. M deficits calculated from soundings made at Tateno, Honshu, 1928.

trapping in the Japanese area has been obtained from a study of soundings made in 1928 at Tateno,[19] on the east coast of Honshu, some fifty miles from Tokyo. The data, plotted in Figure 22, shows three cases of an M inversion. The numerical quantities are given in Table 3.

TABLE 3. Aerological soundings at Tateno, Honshu, in 1928, together with computed duct widths and the magnitude of the M deficit.

Date	Elevation of duct top (ft)	Elevation of duct base (ft)	Duct width (ft)	Magnitude of M deficit
May 1	1,900	1,300	600	−6
August 23	1,000	650	350	−5
September 29	1,250	950	300	−2

NOTE ON ATTU AND THE ALEUTIANS[20,21]

Fixed echoes have been obtained at abnormally long ranges (100 to 150 miles). The "Battle of the Pips" was an illustration of pronounced superrefraction. The latter has been observed on at least four occasions by operators of airborne radars returning to Attu from missions over the Kuriles, when VHF radar beacons have returned signals to planes at 5,000 ft and 300 to 350 miles, or about three times the horizon line distance. Meteorological data on duct conditions during the cycle of the Aleutian seasons are needed (up to 1,000 ft).

APPENDIX

STANDARD ATMOSPHERE

Definition. The National Advisory Committee on Aeronautics [NACA] defines the "standard atmosphere" as that which exhibits:

1. A sea level pressure of 1,013 mb (= 760 mm of mercury = 29.92 in. of mercury).

2. A sea level temperature of 15 C (= 59 F) which decreases at a rate of 6.5 C per km (= 3.47 F per 1,000 ft) in the lower atmosphere; and in addition the moisture content may be specified as follows:

3. A relative humidity of 60 per cent, which corresponds to a water vapor pressure of approximately 10 mb at sea level and to a rate of decrease in the lower atmosphere of about 1 mb per 1,000 ft.

Properties. The following table for the standard atmosphere indicates the variation with height of (a) temperature, (b) pressure, (c) water vapor pressure for 60 per cent relative humidity, (d) a quantity containing the index of refraction, n, and (e) the modified refractive index, M.

Altitude Meters	Altitude Feet	Temperature C	Temperature F	Pressure (mb)	Water vapor pressure for 60% RH (mb)	$(n-1)\times 10^6$	M
0	0	15.0	59.0	1,013	10.2	322	322
150	492.1	14.0	57.2	995	9.6	316	339
300	984.3	13.0	55.4	977	9.0	309	357
500	1,640.4	11.7	53.1	955	8.3	300	379
1,000	3,280.8	8.5	47.3	894	6.7	281	438
1,500	4,921.2	5.2	41.4	845	5.3	266	501

RADIO METEOROLOGY TERMS

Index of Refraction. This can be defined for any particular medium as the ratio of the velocity of electromagnetic waves in a vacuum to their velocity in the medium. The relationship indicating the amount of bending or change in direction that occurs as electromagnetic radiation crosses a boundary between two media with different refractive indices is given by Snell's law:

$$n_1 \cos \alpha_1 = n_2 \cos \alpha_2$$

in which n_1 is the refractive index of the first medium,

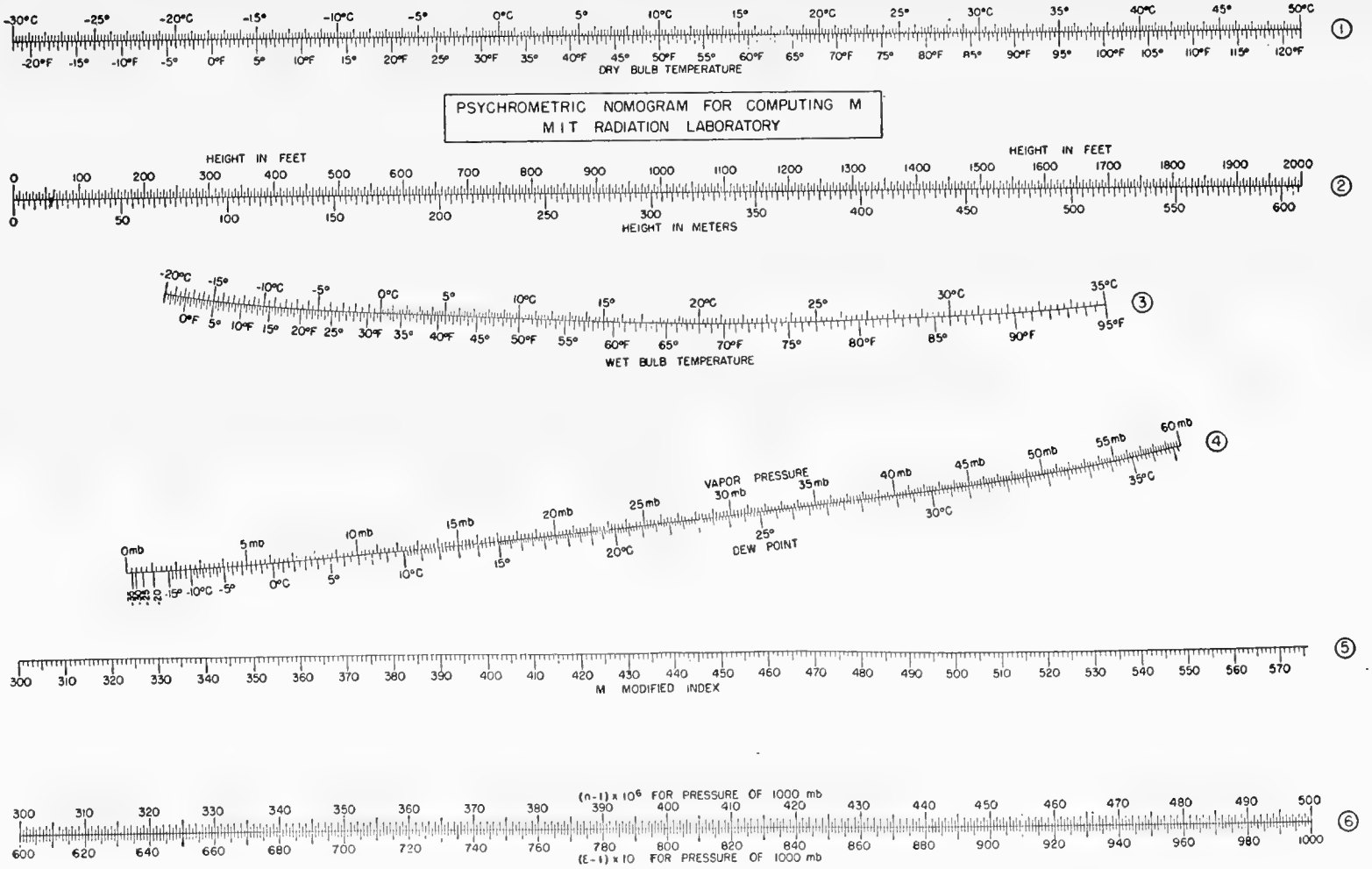

FIGURE 23. Psychrometric nomogram.

n_2 that of the second medium, α_1 the angle which the ray in leaving the first medium makes with the boundary, and α_2 the angle which the ray in penetrating the second medium makes with the boundary. In the case of the atmosphere (one medium with a variable refractive index) this expression can be modified to relate the gradual bending of a ray to the manner in which the refractive index varies. The value of the refractive index, n, at any particular point in the atmosphere can be determined from measurements of pressure, temperature, and humidity by substitution in the formula,

$$n = 1 + \frac{79}{T}\left(p + \frac{4800e}{T}\right) 10^{-6} ,$$

or, expressed differently,

$$(n - 1)\, 10^6 = \frac{79}{T}\left(p + \frac{4800e}{T}\right),$$

in which the temperature, T, is measured in °K, and the atmospheric pressure, p, and vapor pressure, e, in millibars.

Modified Refractive Index. It is considered more convenient, in problems of radio propagation, to define a slightly different quantity M, which is related to the index of refraction by

$$M = \left(n + \frac{h}{a} - 1\right) 10^6 ,$$

in which n is the index of refraction, a is the radius of the earth (21×10^6 ft) and h is the height above the surface of the earth (measured in the same units as a). In terms of pressure, temperature, humidity, and height, M is given by

$$M = \frac{79}{T}\left(p + \frac{4800e}{T}\right) + \frac{h}{a} 10^6 ,$$

in which the units of measurement used are the same as above. The rate at which M increases with altitude is given by

$$\frac{dM}{dh} = \left(\frac{dn}{dh} + \frac{1}{a}\right) 10^6 ,$$

which in the standard atmosphere is

$$\frac{dM}{dh} = -0.039 + 0.157$$
$$= 0.118\, M \text{ unit per meter}$$
$$= 0.036\, M \text{ unit per foot.}$$

Psychrometric Nomogram. Radiation Laboratory (MIT) has developed a nomogram with which to compute the modified index of refraction from the necessary meteorological parameters. This chart is known as the psychrometric nomogram. (See p. 131.)

Meteorological Terms

Absolute Humidity. The mass of water vapor present in a unit volume of air is known as the absolute humidity of the air. It is another way of expressing the water vapor density.

Specific Humidity. The specific humidity of moist air is the ratio of the weight of water vapor mixed with the air to the weight of the moist air. If p is the barometric pressure and e is the partial pressure of the water vapor, then the specific humidity is given by

$$q = 622\, \frac{e}{p - 0.377e} \text{ g per kg} .$$

Mixing Ratio. The ratio of the mass of water vapor mixed with unit mass of perfectly dry air is known as the mixing ratio and may be expressed as

$$w = 622\, \frac{e}{p - e} \text{ g per kg} .$$

Relative Humidity. The ratio of the actual water vapor pressure to the saturation vapor pressure at the same temperature is known as the relative humidity of moist air. If e and e_s are the respective vapor pressures, then (in per cent) the relative humidity is expressed as

$$\text{RH} = \frac{e}{e_s} \times 100 .$$

Wet Bulb Temperature. The lowest temperature to which a wetted ventilated thermometer can be brought by evaporation is called the wet bulb temperature. It is not strictly an air temperature.

Air Mass. An extensive body of air which approximates horizontal homogeneity is known as an air mass. The four principal types are illustrated by the accompanying table.

Source region	Moisture classification	Thermal classification	Name	Symbol
Land	Dry	Hot	Tropical continental	cT
		Cold	Polar continental	cP
Oceanic	Wet	Hot	Tropical maritime	mT
		Cold	Polar maritime	mP

Front. The surface of separation between dissimilar air masses is known as a frontal surface. On a surface weather map a "front" is the intersection of this surface with the surface of the earth.

Dry Adiabatic Lapse Rate. When dry air ascends so as to expand adiabatically, it is said to cool at the

dry adiabatic lapse rate (5.5 F per 1,000 ft or 1 C per 100 m). There must be no condensation or evaporation of associated water vapor during the process.

Subsidence. An extensive sinking process, resulting in dynamically heated air and an increase in stability, most frequently observed in anticyclones, is known as subsidence.

Instructions for Use of Nomogram

This nomogram (Figure 23) may be used to compute M when temperature is expressed in degrees Fahrenheit or centigrade, humidity in terms of wet bulb (degrees Fahrenheit or degrees centigrade), dew point (degrees centigrade), or vapor pressure (millibars), and height in feet or meters. Place a straightedge so as to align the temperature on scale 1 with the wet bulb temperature on scale 3 (or with the dew point or vapor pressure on scale 4). The point at which the straightedge intersects scale 6 indicates the value of the modified index uncorrected for height. Pivot the straightedge at this point (on scale 6) so that it crosses scale 2 at the desired height. Then read the value of M where the straightedge crosses scale 5.

PART III

MISCELLANEOUS EXPERIMENTS

Chapter 9

REFLECTION COEFFICIENTS

9.1 REFLECTION COEFFICIENT MEASUREMENTS AT THE RADIATION LABORATORY[a]

DURING THE LATTER PART of 1943 the S-band reflection coefficient measurements begun in the spring and reported at the July 1943 conference have been carried on, and work of a similar nature has been started to determine X-band values. The interference pattern was observed by recording field strength as a function of distance with both receiver and transmitter heights held constant. One end of the path was ground-based, while the other end was carried in an airplane which flew over sea toward the land station at a constant altitude and bearing. A one-way c-w path was used, the transmitters, receivers, and recorders being identical to those used previously. The time constant of the receiver and recorder was 0.3 sec, corresponding to 0.01 mile for the usual air speeds used.

When appreciable specular reflection was obtained, a regular succession of maxima and minima were observed on the record. The product of the divergence factor and reflection coefficient was found by determining the ratio of electric field strength at adjacent maxima and minima. The geometrical expression for the divergence factor was assumed correct and all variations were lumped in the experimental value of the reflection coefficient. It was required that a record give a check on the positions of maxima and minima for standard refraction and that the maxima obey the $1/R^2$ law (power) before the record would be worked up.

Flights over land made in 1943 at Orlando, Florida, Riverhead, Long Island, and Cambridge, Massachusetts, fail to show a regular interference pattern. There is a more or less erratic variation of field intensity with distance, but the magnitude of the variation is generally small, and the records obey the $1/R^2$ law. It is believed that the terrain is rough enough to scatter all incident radiation of microwaves and that specular reflection will therefore not be observed. There is considerable evidence, however, that if a microwave transmitter is placed at a fairly low height over terrain as smooth as an airport runway, specular reflection will be observed.

Observations over sea made late in 1943 on S band with horizontal polarization have not agreed with earlier results. A correlation has been found between wind (and presumably wave) direction with respect to the path and the magnitude of the reflection coefficient. The correlation suggests that low values observed are due to back scattering. Figure 1 shows lines drawn as a means of the values observed on the 4 days when exceptionally good flights were made during the winter. On November 25, the wind was blowing across

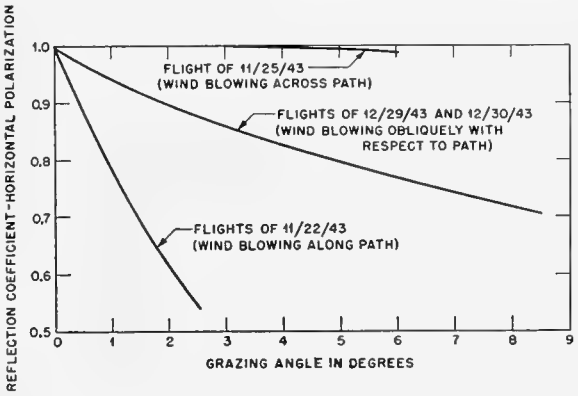

FIGURE 1. Reflection coefficient, horizontal polarization, versus grazing angle. Sea water. Wavelength—S-band.

the path, and high values of the reflection coefficient were observed. On November 22, the wind was blowing along the path, and low values were observed. On December 29 and 30, the wind was blowing obliquely with respect to the path and intermediate values were observed. While the values on any given flight lie fairly close to the lines, there is a considerable amount of scatter. This scatter is now believed to be real and supports the results obtained by the British.

Figure 2 shows the results obtained this winter on S band with vertical polarization. The values observed fall about the theoretical curve. If any correlation with wind direction exists, it is masked by the variation within a single flight.

Equipment difficulties have just been overcome and work is getting under way to determine X-band values. One flight made on horizontal polarization

[a]By W. J. Fishback, Radiation Laboratory, MIT.

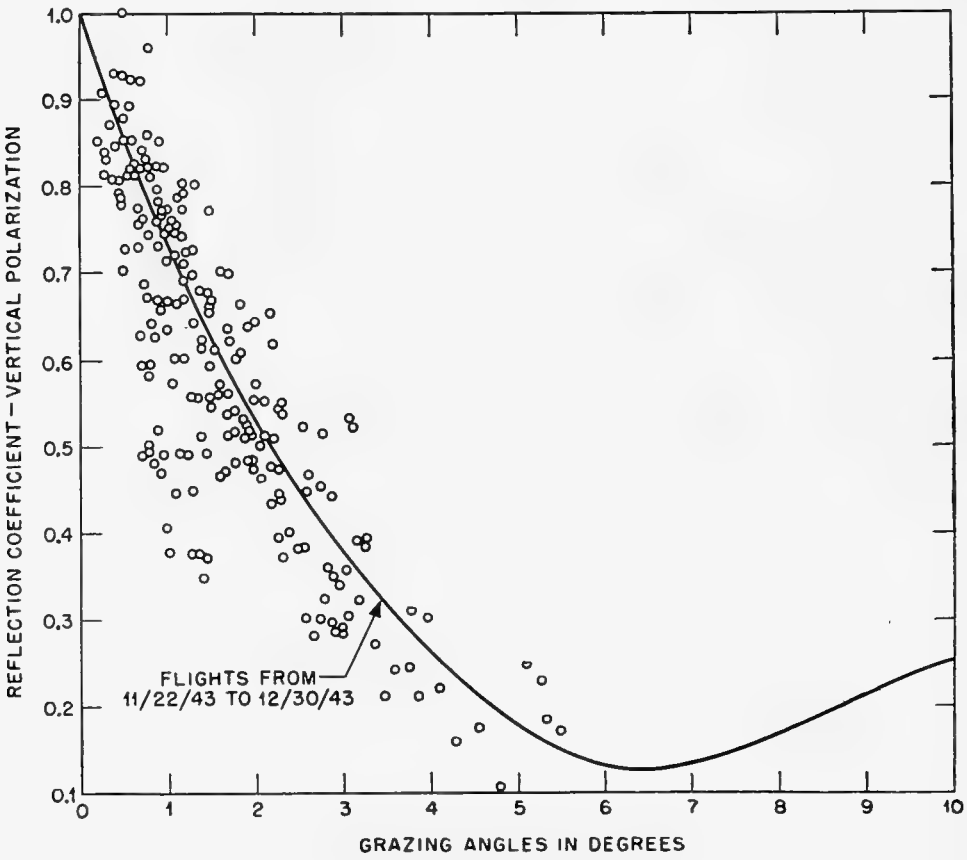

FIGURE 2. Reflection coefficient, vertical polarization, versus grazing angle. Sea water. Wavelength—S band.

shows values greater than 0.9 up to 3 degrees. On three flights made with vertical polarization the points have fallen just slightly above the theoretical curve.

It is planned to carry on simultaneous measurements of X- and S-band values to determine the values to be expected on X band and to prove or disprove the correlation suggested above.

9.2 EARTH CONSTANTS IN THE MICROWAVE RANGE[b]

9.2.1 Reflection Coefficients

In writing a summary of the latest results, it was thought that the following grouping of the data would be useful.

1. Determination of the electrical constants of the ground, sea, and fresh water.
2. Study of ground and sea reflections under conditions encountered in actual operations.
3. Irregular reflections or scattering.

[b]By L. Goldstein, Columbia University Wave Propagation Group.

Electrical Constants of the Ground, Sea, and Fresh Water

To obtain reliable data on the reflection coefficient, dielectric constant, and conductivity of the ground and also of fresh and sea water, a series of radio experiments were performed[1-3] which gave results that compared fairly well with those obtained in laboratory experiments. The experimental conditions were relatively well defined and the physical characteristics of the ground or water derived from these experiments appear to be highly reliable. The wavelengths of the radiation used in these experiments lie in the S band at 9 and 10 cm.

In the experiments with 9-cm waves,[1,2] the nature of the reflecting surface was prepared beforehand and its humidity, occasionally, well controlled. Similarly, with vegetation on the ground, the reflection could be measured with different heights of the turf which was grown on the grounds reserved for the measurements.

The conditions of the ground in the experiments with 10-cm waves were somewhat less well defined.

However, the experimental setup was portable in this case, which proved to be advantageous.

It seems desirable to give first the results obtained under the best-defined conditions[1,2] (9 cm) for a variety of grounds and compare those with the results of the 10-cm waves obtained under less well-defined conditions.[3] The latter results are given always in graphical form.

The grazing angle interval (0° to about 30°) explored with the 10-cm waves was quite large, and a graphical representation of the results is well justified. At 9 cm only three or at most four angles of incidence were investigated.

The schematic representation of the experimental setup is given in Figure 3. If ρ denotes the ratio of

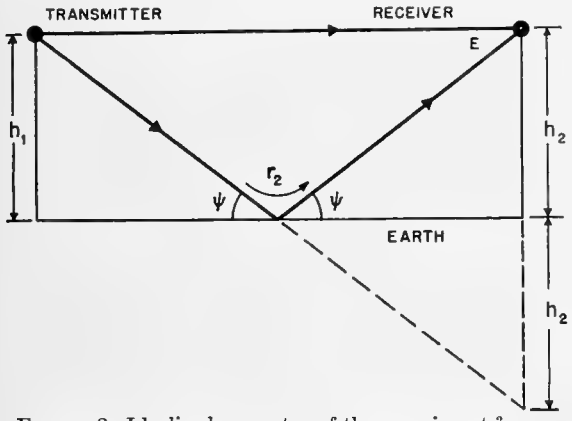

FIGURE 3. Idealized geometry of the experiment.[3]

the amplitude of the reflected wave to that of the incident wave in the vicinity of the reflecting surface, then at the position of the receiver the total field received in case of reinforcement is

$$E_{\max} = E + k\rho E.$$

E is the field strength of the direct wave and k is a correction factor taking into account the directivity of the transmitter and receiver as well as the increased path length of the reflected ray as compared to that of the direct ray. In case of phase opposition

$$E_{\min} = E - k\rho E.$$

These lead to

$$\rho' = k\rho = \frac{(E_{\max} / E_{\min}) - 1}{(E_{\max} / E_{\min}) + 1}.$$

Throughout the work at 10 cm this corrected reflection coefficient ($k\rho$) or ρ' has been investigated. Presumably k is nearly unity so that $\rho' = \rho$.

Very Dry Sandy Ground. Table 1, for 9 cm, refers to very dry ground. In order to obtain a precise value of the complex dielectric constant of this very dry sandy ground its absorption coefficient was measured directly. The measurement was made by interposing a filled container between transmitter and receiver.

TABLE 1. Reflection coefficients of very dry sandy ground for $\lambda = 9$ cm.[1,2]

Grazing angle degrees	Vertical polarization		Horizontal polarization	
	Calculated	Observed	Calculated	Observed
22	0.18	0.20	0.48	0.47
36.5	0.015	0.03	0.33	0.33
46.5	0.08	0.09	0.26	0.27

The container, a wooden trough, had ¼ in. plate glass ends, 18 in. square, one of which was movable, thus allowing a test of the absorber up to a thickness of 12 in. The most suitable values of ϵ_r (real part of the complex dielectric constant ϵ_c) and conductivity σ or $\epsilon_i = 60\ \sigma\lambda$ (imaginary part of the complex dielectric constant) which fit the reflection and absorption coefficient data were found to be $\epsilon_r = 2$, $\sigma = 0.033$ mho per meter, $\epsilon_i = 0.18$.

It should be mentioned here that the calculated reflection coefficients were obtained by using the generalized Fresnel formulas for reflection of electromagnetic waves by plane dielectric surfaces. The incident waves travel in vacuum (or air) and fall on the plane surface of a dielectric at the grazing angle ψ. The complex dielectric constant ϵ_c is

$$\epsilon_c = \epsilon_r - j\epsilon_i,$$
$$= \epsilon_r - j\,60\,\sigma\lambda,$$

where ϵ_r is the real part of the dielectric constant and $\epsilon_i = 60\sigma\lambda$ is its imaginary part. σ is the conductivity of the dielectric medium in mhos per m, and λ is the wavelength, in vacuum, of the incident radiation. The generalized Fresnel formulas, for horizontally and vertically polarized waves, respectively, are

$$\rho_h e^{-j\phi_h} = \frac{\sin\psi - (\epsilon_c - \cos^2\psi)^{\frac{1}{2}}}{\sin\Psi + (\epsilon_c - \cos^2\psi)^{\frac{1}{2}}} \quad \text{(horizontal)}$$

$$\rho_v e^{-j\phi_v} = \frac{\epsilon_c \sin\Psi - (\epsilon_c - \cos^2\psi)^{\frac{1}{2}}}{\epsilon_c \sin\Psi + (\epsilon_c - \cos^2\psi)^{\frac{1}{2}}} \quad \text{(vertical)},$$

where ρ denotes the magnitude of the complex reflection coefficient and ψ is the angle of lag of the reflected component behind the incident component of the electric field.

The results at 10 cm and for dry sand are given in Figure 4. The theoretical curves given on the

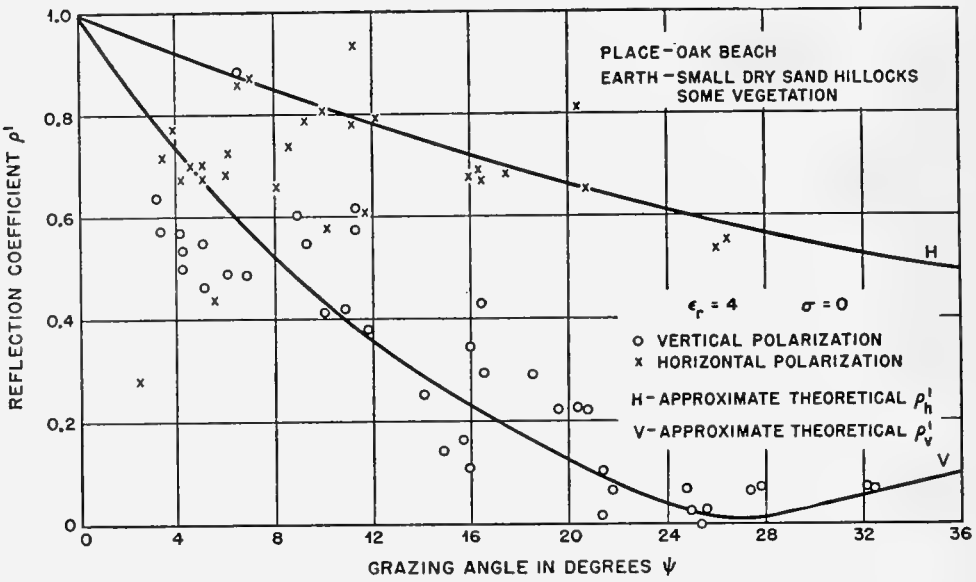

FIGURE 4. Reflection coefficient ρ' versus ψ. $\lambda = 10$ cm. d=225, 100, 75 ft.

graph do not necessarily represent the best fit. These curves were computed for $\epsilon_r = 4$ and $\sigma = 0$ (perfect dielectric). The experimental Brewster angle turns out to be around 23° (grazing angle).

The experimental results for clay-sand soil are given in Figure 5. The theoretical curves are the same as those given in the preceding case, that is, for $\epsilon_r = 4$ and $\sigma = 0$. It will be noted that the fit with the experimental values is less satisfactory in this case. The author attributes the discrepancy between the observed and computed values of the reflection coefficient, in part, to the quality of the soil which consisted of lumps of about a half wavelength diameter. In general the roughness of the ground contributes considerably to scattering. It is rather to be expected that a theoretical curve representing specular reflection coefficients from a smooth surface should not fit well the experimental data referring to such a rough ground.

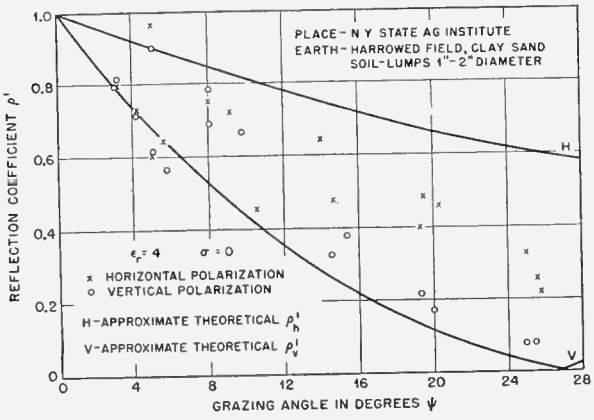

FIGURE 5. Reflection coefficient ρ' versus ψ. $\lambda = 10$ cm. d=100, 300 ft.

Saturated Ground. Table 2 represents the results obtained at 9 cm for the reflection coefficient of saturated ground.

The most suitable values of ϵ_r and σ or ϵ_i to fit both reflection and absorption measurements are $\epsilon_r = 24$, $\sigma = 0.66$ mhos per meter, and $\epsilon_i = 3.56$.

Tests carried out at 10 cm on ground of somewhat similar type (tidal flat and moist sand) are given in

TABLE 2. Reflection coefficients of saturated ground. $\lambda = 9$ cm.[1,2]

Grazing angle degrees	Vertical polarization				Horizontal polarization			
	Calculated		Observed		Calculated		Observed	
	$\epsilon_r = 24$ $\sigma = 0.66$	$\epsilon_r = 25$ $\sigma = 0$	Heavy rain	Watered by hose	$\epsilon_r = 24$ $\sigma = 0.66$	$\epsilon_r = 25$ $\sigma = 0$	Heavy rain	Watered by hose
22	0.31	0.31	0.28	0.32	0.85	0.86	0.90	.0.86
36.5	0.50	0.50	0.50	0.50	0.78	0.79	....	0.78
46.5	0.57	0.57	0.58	0.58	0.74	0.75	0.72	0.74

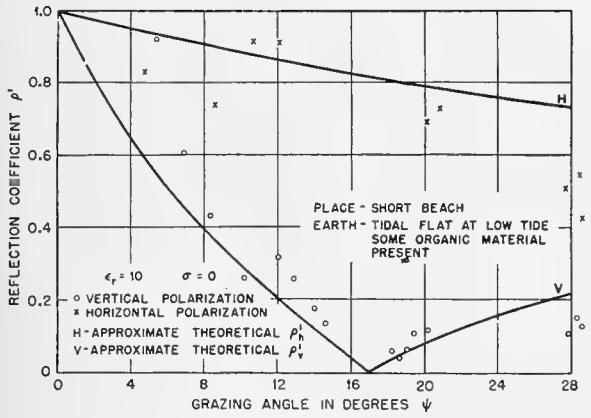

FIGURE 6. Reflection coefficient ρ' versus ψ. $\lambda = 10$ cm. d = 90 ft.

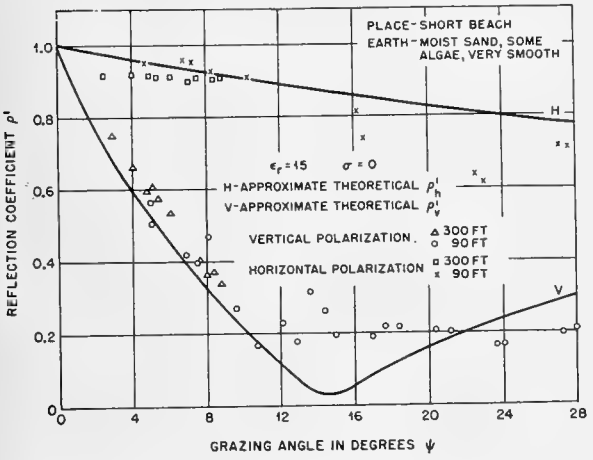

FIGURE 7. Reflection coefficient ρ' versus ψ. $\lambda = 10$ cm. d = 300, 90 ft.

Figures 6 and 7. The theoretical curves in Figure 6 correspond to a perfect dielectric ($\sigma = 0$) with $\epsilon_r = 10$. Since the conductivity of the soil is not zero, the true value of the reflection coefficient for vertical polarization cannot be zero at the Brewster angle. The data seem to confirm this point.

The data of Figure 7 refer to moist and very smooth beach sand. It is thought that these observations are the most reliable so far as self-consistency is concerned. Again the computed curves refer to a perfect dielectric with $\epsilon_r = 15$.

An important difference between the measurements at 9 cm at a fixed location and those made at 10 cm with the portable setup consists of the fact that at 9 cm direct absorption measurements could be performed in addition to measurements of the reflection coefficent. The electrical constants could thus be determined at 9 cm without ambiguity.

Fresh Water and 4% Salt Solution (or Sea Water). (1) *Tap water.* Table 3 gives the results on the reflection coefficients of tap water (temperature not given).

TABLE 3. Reflection coefficients of tap water. $\lambda = 9$ cm.[1,2]

Grazing angle degrees	Vertical polarization		Horizontal polarization	
	Calculated	Observed	Calculated	Observed
20	0.51	0.51	0.92	0.90
35	0.69	0.67	0.88	0.88
45.5	0.73	0.70	0.85	0.83

The values of ϵ_r and ϵ_i which best represent both the reflection and absorption data are $\epsilon_r = 80$, $\sigma = 2.2$ mhos per m, and $\epsilon_i = 11.9$.

2. *Fresh water pond.* The results on 10-cm waves are collected in Figure 8.[3] These data refer to a fresh water pond and the theoretical curve corresponds to a smooth and perfect dielectric surface with $\epsilon_r = 80$. The curves do not fit too well at the smaller grazing angles. If the conductivity were taken into account,

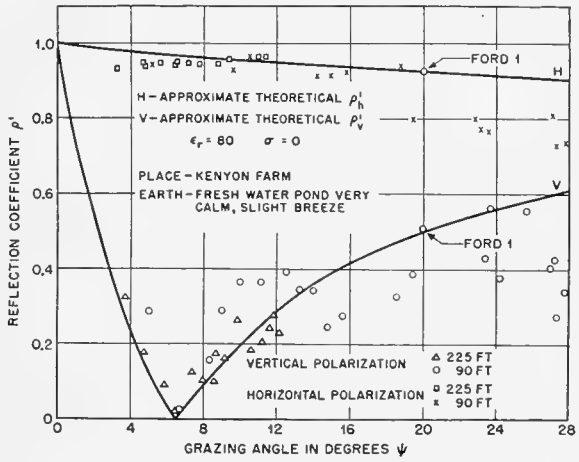

FIGURE 8. Reflection coefficient ρ' versus ψ. $\lambda = 10$ cm. d = 90, 225 ft. Fresh water pond.

presumably a better fit might be achieved. Two points, marked Ford,[1,2] taken from Table 3 were included for comparison.

3. *Salt solution.* In order to simulate sea water a 4 per cent salt solution was used for the determination of the reflection coefficient. At 9 cm the best fit was obtained with $\epsilon_r = 80$, $\sigma = 6.1$ mhos per m, and $\epsilon_i = 33$.

4. *Sea water.* Figure 9 gives the results obtained at 10 cm. The computed curves drawn to fit the data correspond to $\epsilon_r = 69$, $\sigma = 6.5$ mhos per m, $\epsilon_i = 39$. It appears that the data can be fitted with the com-

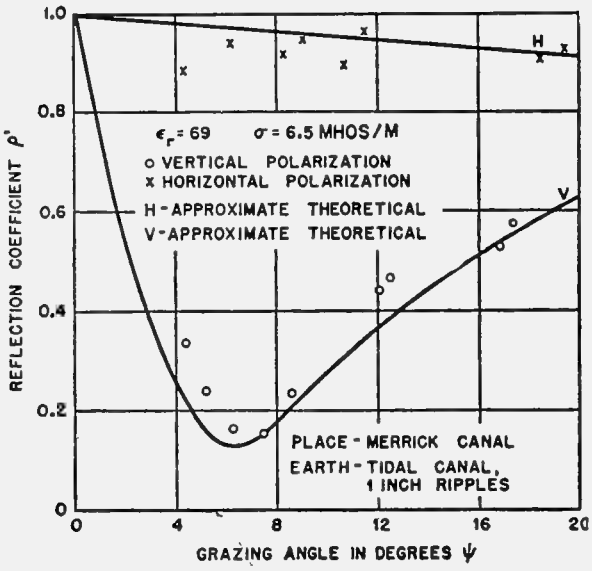

FIGURE 9. Reflection coefficient ρ' versus ψ. $\lambda = 10$ cm. d = 130 ft. Sea water (tidal canal).

puted curves as long as the ripples on the tidal canal are of small amplitude (about 1 in.).

Figure 10, which also refers to sea reflection, corresponds to ripples which had an amplitude of about 2 in., and here the observed reflection coefficients for vertical polarization fall well below the computed curve at the larger values of grazing angle. Probably the choice of the dielectric constants used in the computations may account for at least a part of the discrepancy.

Grass-Covered Ground. The following results obtained at the experimental grounds[1,2] with 9-cm waves refer to various types of grass-covered earth.

The results obtained with the portable 10-cm set appear on Figures 11, 12, 13, and 14. These graphs show clearly the influence of vegetation on the reflection coefficient. Consult Table 5 for corresponding results at 9 cm.

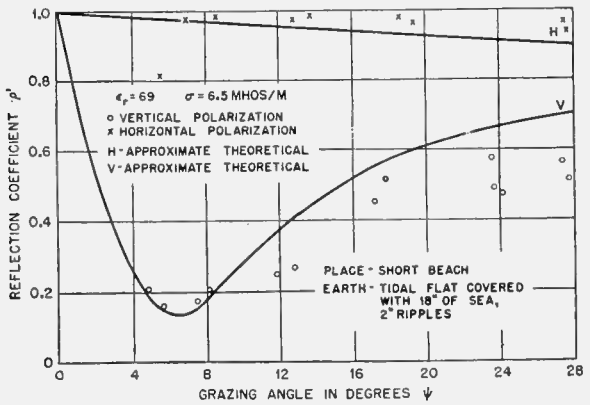

FIGURE 10. Reflection coefficient ρ' versus ψ. $\lambda = 10$ cm. d = 90 ft. Sea water.

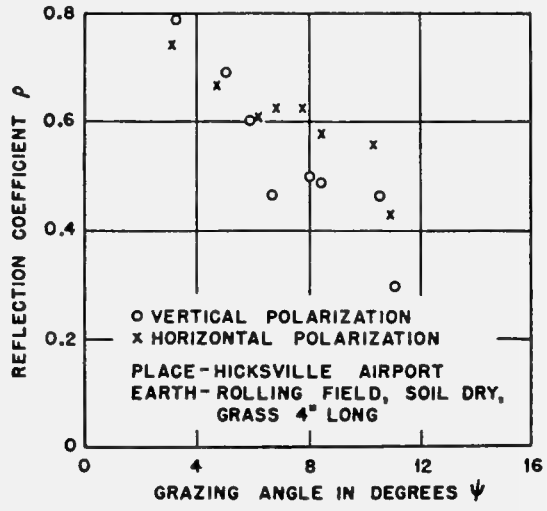

FIGURE 11. Reflection coefficient ρ versus ψ. $\lambda = 10$ cm. d = 225 ft. Grass covered ground.

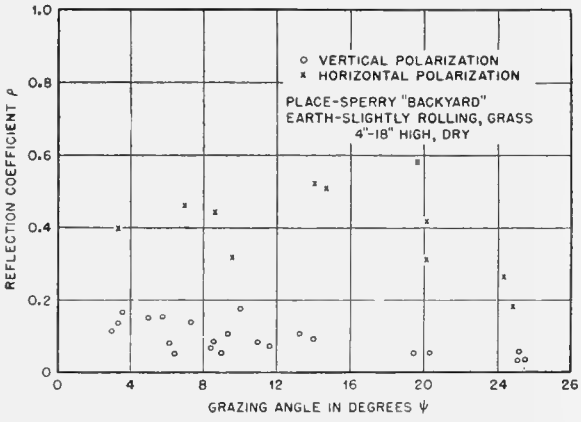

FIGURE 12. Reflection coefficient ρ versus ψ. $\lambda = 10$ cm. d = 100, 225 ft. Grass covered ground.

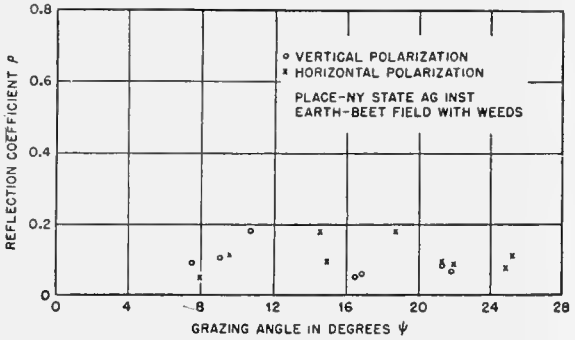

FIGURE 13. Reflection coefficient ρ versus ψ. $\lambda = 10$ cm. d = 100 ft. Beet field with weeds.

TABLE 4. Reflection coefficient of level, grass-covered ground. $\lambda = 9$ cm. Grazing angle 10°.

Ground conditions	Vertical polarization Calculated	Observed	Assumed constants ϵ_r	σ mhos/m	Horizontal polarization Calculated	Observed
Grass cut very short and rolled dry. (No rain for at least 7 days.)	0.47	0.46	3	0.055	0.79	0.79
Cut very short and rolled wet. (Several hours of rain on previous night.)	0.36	0.37	6	0.11	0.86	0.86
Grass about 1 in. high, wet. (Same day as previous test.)	0.36	0.51	6	0.11	0.86	0.83

TABLE 5. Magnitudes ρ_v and ρ_h, observed values. $\lambda = 9$ cm.[1,2]

Appearance of ground	Height of vegetation, cm	Grazing angle 22° v	h	36.5° v	h	56.5° v	h
Bare	0	0.32	0.86	0.50	0.78	0.58	0.74
True leaves beginning to form, ground visible	3–4	0.40	0.50	0.44	0.55	0.47	0.56
Dense clumps, ground showing in places	9–12	0.18	0.65	0.23	0.58	0.33	0.49
Ground almost obscured	20–25	0.06	0.32	0.10	0.39	0.17	0.41
Ground completely obscured	35–45	0.04	0.19	0.05	0.26	0.11	0.28

TABLE 6. Reflection coefficient of rough ground. $\lambda = 9$ cm.[1,2]

Grazing angle, degrees	Vertical polarization Level estimated	Long grass	Short grass	Bare	Horizontal polarization Level estimated	Long grass	Short grass	Bare
22	0.20	0.08	0.20	0.23	0.82	0.12	0.74	0.81
36.5	0.40	0.06	0.17	0.27	0.73	0.12	0.43	0.50
46.5	0.48	0.06	0.16	0.26	0.68	0.03	0.36	0.46

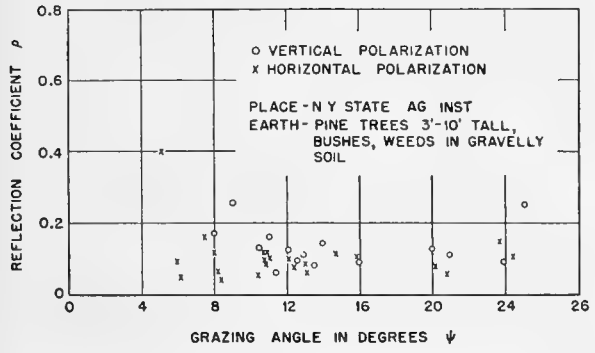

FIGURE 14. Reflection coefficient ρ versus ψ. $\lambda = 10$ cm. d = 102, 200 ft. Trees, bushes, weeds in gravelly soil.

Since, however, the data of Table 5 refer to wet vegetation-covered ground, they cannot be compared directly with the results at 10 cm since these seem to correspond to dry vegetation.

Table 6 gives the data obtained at 9 cm for unmown meadow land having an average variation in ground level of about 7 cm. The ground was covered with a dense layer of grass about 30 cm high. The reflection coefficient of this surface was measured, then remeasured with the grass mown as short as the roughness of the ground permitted. The turf was next removed, some of the irregularities of the ground were eliminated, and the reflection coefficient of the surface so prepared was measured again. The results of these measurements are to be found in Table 6. The *estimated* reflection coefficient of level ground of the same moisture content is also included here.

Finally, the results on the electrical constants of different kinds of grounds for 9-cm waves have been collected in Table 7.

TABLE 7. Electrical constants of the ground. $\lambda = 9$ cm.[1,2]

Medium	ϵ_r	σ mhos/m	ϵ_i	Attenuation factor db/m
Very dry sandy loam	2	0.033	0.178	36
Saturated sandy loam	24	0.666	3.54	220
Tap water	80	2.22	12.0	380
4% solution of coarse salt	80	6.11	33.0	1100
Dry turf	3	0.055 (est)	0.30	50 (calc)
Wet turf	6	0.11 (est)	0.60	80 (calc)

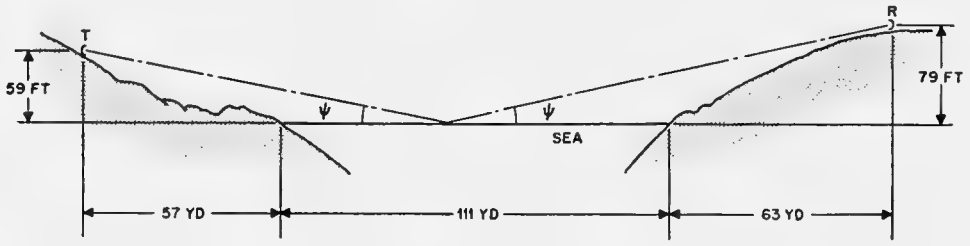

FIGURE 15. Cross section of Porth Gain Bay (Wales) in vertical plane through transmitter and receiver.

It is seen that in the previous experiments[1,2] no attempt was made at finding the phase angle shift at reflection. At 10 cm[3] such an attempt was made. However, the distances involved here could not be measured more accurately than a small fraction of a half wavelength, or 5 cm. Therefore, these experiments are not to be considered, as the author himself points out, as giving quantitative information on the phase angle shift at reflection and they will not be discussed here.

9.2.2 Summary of Experimental Investigations on Reflection

Here the results of certain additional reports of experiments on microwave reflection by either sea or land performed under more nearly operational conditions are summarized.[4-7]

In one series of experiments[4] performed by British workers, at 9.3 cm, the transmitter was located on the shore and could be placed at two heights, 35 and 130

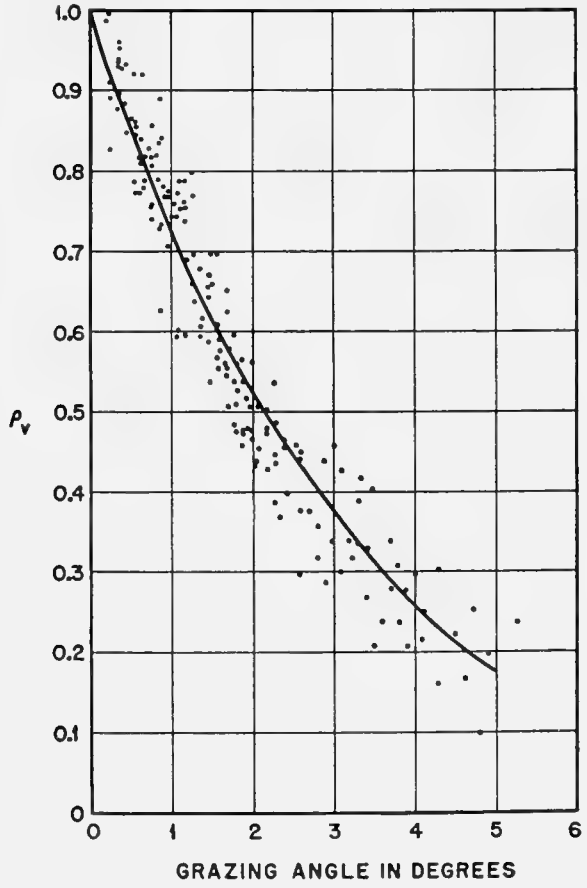

FIGURE 16. Sea reflection coefficient ρ_v versus grazing angle ψ at 10 cm. Vertical polarization.

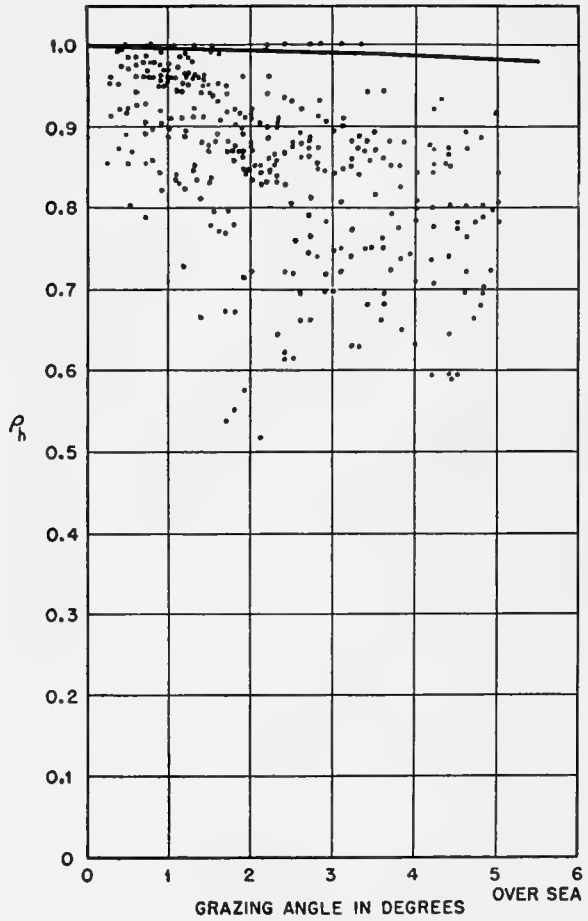

FIGURE 17. Sea reflection coefficient ρ_h versus grazing angle ψ at 10 cm. Horizontal polarization.

ft. The receiver was placed on a ship at a constant height of about 33 ft. The field strength of the radiation was measured as a function of the distance from the transmitter. This distance varied between 3,500 and 42,000 yd. The observed values of the field strengths correspond well with calculations based on electromagnetic theory.

In a second series of experiments[5] both the transmitter and receiver were stationary. The topography of the location and the experimental setup are represented schematically in Figure 15. The main conclusion drawn from these experiments was that even for a calm sea (vertical amplitude of the waves less than 8 in.) the mean amplitude of the reflected vertically polarized beam was only about half the steady amplitude of the direct wave. The amplitude of the reflected wave, however, occasionally rises to greater values than that of the direct wave, but this lasts only for short lengths of time of the order of 0.5 sec.

In the case of the reflection of horizontally polarized radiation at the surface of a smooth sea it is known that even for grazing angles as large as 10° the amplitude of the reflected wave is very nearly equal to that of the direct wave. The irregularities of the sea, however, reduce the amplitude of the reflected wave. This reduction is due to scattering, i.e., to nonspecular reflection of the radiation by the irregularities of the sea surface. It is recalled here that the surface irregularities will play an important role as soon as they are larger than λ/ψ, λ being the wavelength and ψ the grazing angle in radians.

The Radiation Laboratory workers,[6,7] used an airplane as the carrier of the receiver flying toward the transmitter. For 10- and 3.2-cm waves the latest results are given in Figures 16, 17, 18, and 19. These show that theory and experiment check satisfactorily for vertical polarization, but for horizontal polariza-

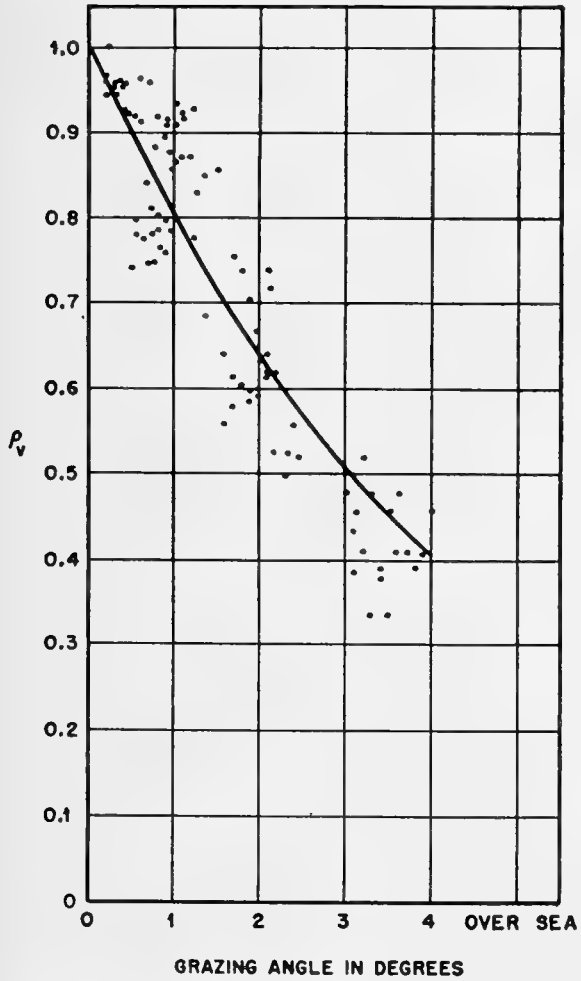

FIGURE 18. Sea reflection coefficient ρ_v versus grazing angle ψ at 3.2 cm. Vertical polarization.

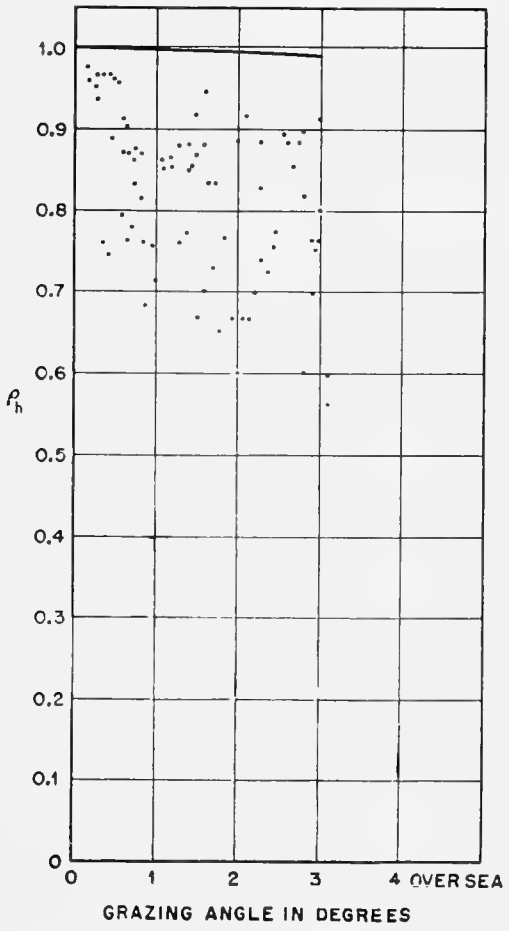

FIGURE 19. Sea reflection coefficient ρ_h versus grazing angle ψ at 3.2 cm. Horizontal polarization.

tion the experimental values of reflection coefficient generally fall well below the theoretical values based on the assumption of a smooth sea. Whereas over sea a regular interference pattern existed, over land (Orlando, Florida) no specular reflection was observed. The lobe structure was absent in the observations over land.

Another experiment[8] carried out over land was performed using X-band waves between Beer's Hill and Deal, New Jersey. The reflection coefficient of the ground is expected to change with the seasons on account of seasonal vegetation changes on the path. One series of measurements lead to reflection coefficients of 0.17 and 0.20 for horizontally and vertically polarized radiation respectively.

9.2.3 Specular Reflection and Scattering

Ordinarily neither the sea nor the land are ideally smooth, and one would expect always nonspecular reflections which tend to perturb the interference pattern of the direct and reflected rays from a smooth surface.

It has been pointed out[9] that the condition which has to be fulfilled for specular reflection to occur is that the grazing angle ψ be such that $\sin \psi \leqq \lambda/g$, where g is the wavelength of the sea waves. Clearly this is a kind of limiting condition and assumes the perfect regularity of the sea waves. It is seen that the above condition expresses the fact that the smaller the grazing angle, the smaller are the apparent irregularities of the sea and, if these apparent irregularities are much closer than the wavelength of the incident radiation, it is to be expected that specular reflection should predominate.

A direct consequence of this condition is that the echoes from a target, that is, a ship, will not be drowned by the clutter from the sea waves for large distances between the target and observer. Whereas at closer distances (large grazing angles) the echo from the target might be drowned by the irregular reflection, i.e., scattering from the sea. To this effect, a report is quoted in which it is stated that ships could only be detected beyond a certain distance from the shore.

It is also thought[10] that the discrepancies observed between the theoretically predicted and measured sea reflection coefficients (horizontal polarization) could be attributed to scattering. The irregular reflections have the effect of decreasing considerably the ratio of the successive maxima and minima of the interference pattern developed. The discrepancies referred to are those discussed by the Radiation Laboratory workers.[7] In this connection, Eckersley mentions some experiments by Hoyle on sea reflections in which no correlation could be observed on the voltage registered by two aerials a few inches apart. This tends also to suggest the existence of scattering from the sea.

In another series of transmission experiments[10] it was observed that the contrast between maxima and minima was poor. Here the experiments were carried out at 200 mc over sea at a distance of 100 miles between an airplane and a ground station. The divergence of the observed from the calculated values of reflection increases as the grazing angle increases. This seems to be in agreement with the results according to which the sea surface may be considered as formed by a number of corrugations which, for small grazing angles, appear to be so close together that the reflection is mostly specular.

As to the frequency variation of scattering one would expect more and more scattering with increasing frequency.

The effect of uneven ground on the reflection coefficient was investigated by the British workers already mentioned.[1,2] The reflecting ground consisted of an artificially prepared series of uniform ridges, placed along, across, and at 45° to, the direction of propagation. These ridges simulated waves, and their wavelength D lay between 0.6 and 1.2 m, whereas the double amplitude h varied between 5 and 15 cm, and the wavelength of the radiation used was 9 cm.

Tables 8 and 9 give the reflection coefficients of the uneven ground when the direction of propagation is at 45° with the ridge and along or across the ridge system. The tables also give an estimation of the reflection coefficient of level ground of the same moisture content as that under test.

The results given in these tables show how a relatively small irregularity in the ground surface is sufficient to prevent regular reflection. The reflection coefficient becomes erratic when it has fallen below a value of about 0.1. The values given for level ground refer only very approximately to the state of the ground in the ridged condition. Since the measurements extended over several days, those relative to level ground may not correspond necessarily to the same degree of moisture as those referring to the ridged ground. The level reflection coefficients in the two preceding tables differ from each other because those of Table 8 refer to drier ground than those of Table 9.

TABLE 8. Reflection coefficient of ground ridged at 45° with the direction of transmission. $\lambda = 9$ cm.[1,2]

Grazing angle, degrees	Vertical polarization				Horizontal polarization			
	Level estimate	$D = 60$ cm $h = 14$ cm	$D = 120$ cm $h = 10$ cm	$D = 120$ cm $h = 5$ cm	Level estimate	$D = 60$ cm $h = 14$ cm	$D = 120$ cm $h = 10$ cm	$D = 120$ cm $h = 5$ cm
22	0.08	0.07	0.09	0.13	0.65	0.14	0.18	0.30
36.5	0.13	0.04	0.05	0.07	0.51	0.04	0.06	0.16
46.5	0.22	0.04	0.04	0.04	0.45	0.07	0.06	0.10

TABLE 9. Reflection coefficient of ground ridged along or across the direction of transmission. $\lambda = 9$ cm.

Grazing angle, degrees	Vertical polarization				Horizontal polarization			
		Along	Across			Along	Across	
	Level estimate	$D = 60$ cm $h = 14$ cm	$D = 60$ cm $h = 16$ cm	$D = 120$ cm $h = 12$ cm	Level estimate	$D = 60$ cm $h = 14$ cm	$D = 60$ cm $h = 16$ cm	$D = 120$ cm $h = 12$ cm
12	0.23	0.20	0.10	0.30	0.86	0.4	0.2	0.4
22	0.06	0.03	0.05	0.12	0.76	0.07	0.10	0.18
36.5	0.28	0.03	0.02	0.06	0.64	0.10	0.12	0.16
46.5	0.36	0.04	0.08	0.08	0.58	0.04	0.08	0.14

9.3 MEASUREMENTS OF THE REFLECTION COEFFICIENT OF LAND AT CENTIMETER WAVELENGTHS, CARRIED OUT AT NATIONAL PHYSICAL LABORATORY[c]

Experiments have been made on the reflection and absorption of radio waves in the S-band of wavelengths by workers in the National Physical Laboratory in England. The reflection coefficient has been measured at angles of incidence to the vertical, of 80°, 68°, 54°, and 44° on level ground, fresh water, sea water, uneven ground, ground covered with vegetation, and ground covered with ½ in. mesh wire netting. The absorption in soil, fresh water, sea water, and ½ in. mesh wire netting has also been measured by a laboratory method. An interim report[1] gave some of the salient results obtained on ground reflection.

The main conclusions which have been drawn from the results obtained are given below.

1. Specular reflection can be obtained only from a very level surface, with little or no vegetation on it. The electrical constants of such surfaces are given in Table 10, from which the coefficient of specular reflection can be deduced for the angle of incidence and state of polarization concerned.

[c]By W. Ross, British Central Scientific Office, Washington, D. C.

2. The reflection coefficient decreases with uneven ground and is reduced to a value of about 0.2 by inequalities of level of about one wavelength. This conclusion is based mainly on a series of experiments in which the ground was raked into a series of ridges resembling waves, which could be either in, across, or at an angle to, the direction of transmission. Similar results were obtained when a large sheet of wire netting was similarly disposed in a series of waves.

3. Vegetation reduces the reflection coefficient, in general, and when about 2 ft high causes a reduction in reflection coefficient to a value of about 0.2. An interesting exception was found when level ground was covered with vegetation less than half a wavelength high (about 1½ in.) when the reflection coefficient with vertical polarization increased slightly with high angles of incidence over that obtained with level ground.

TABLE 10

Nature of surface	Dielectric constant	Conductivity mhos / m
Bare sandy loam, very dry	2	3×10^{-2}
Bare sandy loam, saturated with water	24	6×10^{-1}
Turf with grass very short (cricket wicket), dry	3	5×10^{-2}
Turf with grass very short (cricket wicket), wet	6	1×10^{-1}
Fresh water	80	2
Sea water (4% salt solution)	80	5

Chapter 10

DIELECTRIC CONSTANT, ABSORPTION AND SCATTERING

10.1 ABSORPTION AND SCATTERING OF MICROWAVES BY THE ATMOSPHERE[a]

THE PRESENT REPORT deals with the absorption of microwaves in the 0.2- to 100-cm wavelength range, by the atmospheric gases and by floating or falling water drops like clouds, fog, and rain of maximum drop diameter 0.55 cm.

The theory of absorption and scattering of waves by spherical particles is briefly reviewed. The results are applied to water drops.

For small drops, the attenuation, which depends only upon the amount of liquid water per unit volume and is independent of the drop size, is 0.28, 0.049, and 0.0045 db per kilometer for each gram of liquid water per cubic meter of air for the K, X, and S bands, respectively. Since the concentration of liquid water in clouds does not seem to exceed 1 g per cubic meter of air, the above values represent upper limits. These values refer to water droplets at temperatures around 18 C. The attenuation increases with decreasing temperature of the water drops.

While the attenuation does not depend upon the total rate of rainfall, it is possible to calculate the maximum values to be expected for any precipitation rate. These are 0.16, 0.45, 0.005, 0.001, and 0.0006 db per kilometer for each millimeter precipitation per hour at 1.25, 3, 5, 8, and 10 cm, respectively. These theoretical maximum values of attenuation compare fairly well with the values observed and are for water drops at 18 C.

In the wavelength range mentioned it is shown that, with the exception of the biggest drops and shortest waves, the wave energy converted into heat inside the drops is much larger than the scattered energy.

The radar absorption coefficient, defined as the fraction of the incident power scattered backward per unit layer thickness of the echoing medium, has been computed for different rains. This allows the estimation of the power received in radar observations of storm clouds and rains. The theoretical predictions seem to be consistent here also with the results of the few recent radar studies which tend to show that echoes are due mainly to water drops of the dimensions occurring in rains.

[a]By L. Goldstein, Columbia University Wave Propagation Group.

In the introduction a résumé is given of the status of microwave absorption by atmospheric oxygen and water vapor. With the exception of the resonance region of oxygen (resonance wavelength around 0.5 cm), this absorption turns out to be of only very limited practical importance for waves longer than about 3 to 5 cm.

10.1.1 Introduction

The present report is intended to review the status of microwave propagation through rain, clouds, and fog. In order, however, to convey a precise idea of the total atmospheric absorption, we shall include here some of the most important numerical results recently obtained on the absorption of microwaves by atmospheric gases, like oxygen and water vapor.[1-7]

First of all, in medium- and low-altitude fair-weather clouds and fogs, with the possible exception of heavy sea fogs, the attenuation is of negligible importance for longer waves. It may become important at shorter waves. For instance, in the K band the attenuation[b] is 0.28 db per kilometer for each gram of liquid water per cubic meter of air. The X- and S-band waves are attenuated, respectively, 0.049 and 0.0045 db/km/g/m^3. Since in these clouds and ordinary fogs the liquid water concentration does not seem to exceed 1 g/m^3, these values are very likely upper limits. Actually, by halving these numbers one would be nearer the true values, inasmuch as liquid water contents reported in clouds[8,9] varies between 0.15 and 0.50 g/m^3. An interesting and simplifying feature of cloud and fog absorption is the fact that the smallness of their water drops, as compared with the wavelength, makes the attenuation independent of the drop sizes. The cloud and fog attenuation depends linearly on the liquid water concentration of the atmosphere, and in the microwave region it decreases monotonically with increasing wavelength.

In rains or rain clouds the attenuation does not depend directly on the total rate of rainfall, a variable so familiar to meteorologists. It is, nevertheless, possible to give upper limits to the attenuation per unit precipitation rate. These are as follows: 0.16, 0.45, 0.005, 0.001, and 0.0006 db per kilometer for each mil-

[b]The attenuation values given in this report are always for one-way transmission.

limeter per hour rate of rainfall, at 1.25-, 3-, 5-, 8-, and 10-cm wavelengths, respectively. The drops forming these rains were supposed to be at temperatures near 18 C. By increasing the preceding values by about 30 per cent one would very likely take care of raindrops at lower temperatures, since the absorption increases with decreasing temperature of the drops.

In the computation of attenuation for rains it was assumed that ideal conditions prevailed throughout the rains under consideration. By this was meant that the same sample of rain falling, say, over an area of 1 sq m would be found anywhere inside the area covered by the rain. Such ideal rains seem to be rather simple theoretical models. Considerable fluctuations in the rate of rainfall over relatively short distances (1 km or less) have been reported.[10] These spatial irregularities of rains exclude any simple interpretation of the experimental data on rain attenuations. The computed values of attenuation are based on a few data on drop size distributions[11] in rains.

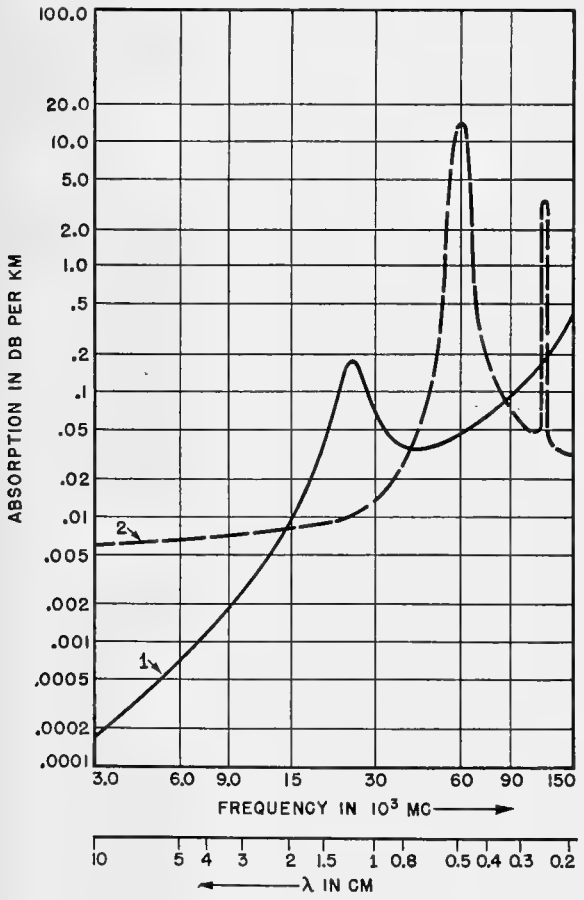

FIGURE 1. Oxygen and water vapor absorption versus wavelength. (1) Absorption due to water vapor in an atmosphere at 76-cm pressure containing 1 per cent water molecules, or 7.5 g per cu m. The water resonance line is assumed to be at 24,000 mc, and its half-width at half maximum (line breadth) is 3,000 mc. (2) Absorption due to oxygen in an atmosphere at 76-cm pressure, whose resonance band at $60 \cdot 10^3$ mc is supposed to have a line breadth of 600 mc.

In Figure 1,[2] the individual oxygen and water vapor attenuation curves have been plotted in the 0.2- to 10-cm wavelength range, using the most acceptable data available on the position of line centers and line widths. Any change in the water vapor content from the one adopted for this graph (7.5 g/m^3 of air or 6.2 g per kilogram of air) or the total pressure can be taken rapidly into account in computing the combined oxygen and water vapor attenuations, since the attenuation values are proportional to the partial pressures of oxygen and water vapor. For practical purposes the effect of atmospheric temperature variations can be neglected.

In Figure 2 is plotted the total (oxygen plus water vapor) attenuation (curve 1) in an atmosphere at 76-cm pressure with the same water vapor content as the water curve of Figure 1. Curves 2, 3, and 4 are rain attenuation curves computed for a moderate rain (rate of rainfall 6mm per hour), a heavy rain (22mm per hour), and an excessive rain of cloud burst proportion (43 mm per hour). The corresponding drop size distributions were given by Best.[11]

In any rain the resulting total attenuation is the sum of the gaseous (oxygen plus water vapor) and corpuscle or liquid drop attenuation values.

It is thus seen that for waves of 3 cm or shorter the rain attenuation may become prohibitive, whereas the gaseous attenuation loses its practical importance at waves longer than about 2 cm. The attenuation of rain computed in this report extends from 5 cm toward longer waves. In the region $\lambda = 1.25 - 5$ cm, only two attenuation values are available,[12] at 1.25 and 3 cm respectively. The dashed portions of the rain attenuation curves are thus extrapolations drawn through the two computed points. The shape of these extrapolated portions of the curves, in view of the decreasing trend of the computed dielectric absorption values with the wavelength,[13] seems to suggest that the rain attenuation might level off or even decrease for waves shorter than 1 cm. However, without a closer investigation of the raindrop absorption in this wavelength region, no precise statement can be made on this subject.

As regards the normal atmospheric absorption of microwaves, it may be mentioned that the oxygen ab-

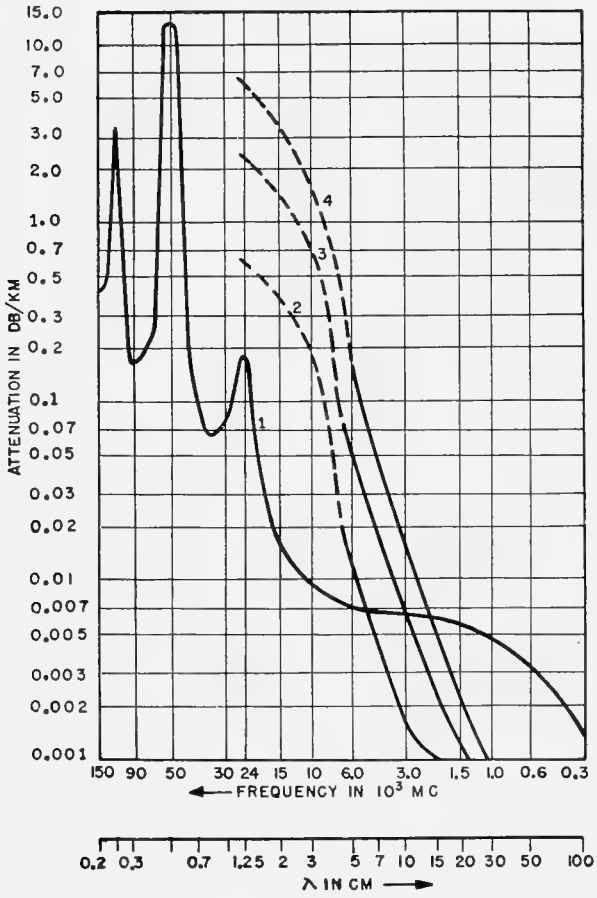

FIGURE 2. Atmospheric attenuation for one-way transmission. (1) Oxygen and water vapor (total p=76 cm Hg, t=20 C, water vapor=7.5 g per cu m). (Van Vleck). (2) Moderate rain (6 mm per hr) of known drop size distribution. (3) Heavy rain (22 mm per hr). (4) Rain of cloudburst proportion (43 mm per hr).

sorption is due to the paramagnetic character of this gas. It is through the interaction of the magnetic field strength with the magnetic dipole moment of the oxygen molecule that microwaves are absorbed by this gas. In the microwave region the oxygen molecule has a resonance line at $\lambda = 0.25$ cm and a band near 0.5 cm, while water vapor seems to have a resonance line around 1.25 cm and interacts with the radiation field through its electric dipole moment. The whole subject has been discussed exhaustively.[1,2]

The study of the scattering of microwaves by raindrops shows that the radar observations of rainclouds can be explained satisfactorily if the scattering is attributed to spherical particles of dimensions similar to those of raindrops, even though no rain reaches the ground. Recent experimental work[14,15] has helped considerably in clearing up the apparent inconsistency which previously existed in this subject.

On the whole, taking into consideration the irregularities of the precipitation forms in space, it may be said that theory provides a fairly good picture of microwave propagation through a cloudy, foggy, or rainy atmosphere.

The major object of the present paper is to report the theoretical and experimental work done on attenuation of microwaves by liquid or solid water particles falling through the atmosphere, as well as clouds and fog, which are water and ice particles in suspension.

Theoretical work has thus far been concerned with the problem of a plane electromagnetic wave scattered and absorbed by a single spherical or spheroidal particle, first studied in detail by Mie[16] for other purposes.

The application of the results of Mie to very short radio waves propagated through rain, clouds, and fog, i.e., through a swarm of spherical water droplets, was made by Ryde.[12,17] The present report is, in part, an extension of his work using more detailed meteorological data on rains.

A compact and elegant presentation of the problem of absorption and scattering of a plane wave by a sphere is given by Stratton.[18a] The method followed by him was first used by Lord Rayleigh.[19] In the following section a brief review of this method will be given.

10.1.2 Scattering and Absorption of Radio Waves by Spherical Particles

Let the center of a sphere of radius a be the origin of a rectangular coordinate system and suppose a plane wave to be propagated along the positive z axis and to fall on the sphere (Figure 3). The sphere of permeability μ_1 (henrys per meter) and complex inductive capacity ϵ_1 (farads per meter) is embedded in a medium of permeability μ_2 and inductive capacity ϵ_2. The plane wave is supposed to be polarized parallel to the x axis.

The electric and magnetic field strengths $\mathbf{E}_i$, $\mathbf{H}_i$ of the incident wave (subscript i) are expanded into spherical wave functions.[18a] The reason for this expansion lies in the boundary conditions and will appear clearly below.

$$\mathbf{E}_i = \mathbf{E}_x = \mathbf{a}_x E_0 e^{-jk_2 z + j\omega t},$$
$$\mathbf{H}_i = \mathbf{H}_y = \frac{1}{\eta_2} \mathbf{a}_y E_0 e^{-jk_2 z + j\omega t}, \tag{1}$$

where

$$k = (\mu\epsilon\omega^2 - j\mu\sigma\omega)^{\frac{1}{2}} \tag{2}$$

is the complex wave number of the medium (here $k_2 = 2\pi/\lambda$, λ being the wavelength referred to air or

free space), the square root is so taken that the imaginary part is negative, and η is the intrinsic impedance of the medium, or

$$\eta = \frac{\mu\omega}{k}, \quad \eta_2 = \sqrt{\frac{\mu_2}{\epsilon_2}} = 377 \text{ ohms.} \tag{3}$$

The conductivity σ is expressed in mhos per meter; the frequency ω, in radians per second; $\mathbf{a}_x$, $\mathbf{a}_y$, and $\mathbf{a}_z$ are unit vectors pointing in the positive x, y, and z directions, respectively.

The plane wave vectors[c] $\mathbf{a}_x e^{-jk_z z}$ and $\mathbf{a}_y e^{-jk_z z}$ will now be expanded into spherical wave vectors[18a] at a point of spherical polar coordinates (r,θ,ϕ). It is readily recalled that

$$\begin{aligned} x &= r\sin\theta\cos\phi, \\ y &= r\sin\theta\sin\phi, \\ z &= r\cos\theta, \end{aligned} \tag{4}$$

with

$$0 \leq \theta \leq \pi \text{ and } 0 \leq \phi \leq 2\pi .$$

These spherical vector waves will be denoted by **m** and **n**. They form complete orthogonal sets whose members are defined by the following equations:

$$\begin{aligned} \mathbf{m}_{0n}^{(\alpha)} &= \frac{1}{\sin\theta} z_n^{(\alpha)}(kr)\, P_n^1(\cos\theta)\cos\phi\, \mathbf{i}_2 \\ &\quad - z_n^{(\alpha)}(kr)\frac{dP_n^1}{d\theta}\sin\phi\, \mathbf{i}_3, \\ \mathbf{m}_{en}^{(\alpha)} &= -\frac{1}{\sin\theta} z_n^{(\alpha)}(kr)\, P_n^1(\cos\theta)\sin\phi\, \mathbf{i}_2 \\ &\quad - z_n^{(\alpha)}(kr)\frac{dP_n^1}{d\theta}\cos\phi\, \mathbf{i}_3, \end{aligned} \tag{5}$$

$$\begin{aligned} \mathbf{n}_{0n}^{(\alpha)} &= n(n+1)\frac{z_n^{(\alpha)}(kr)}{kr} P_n^1(\cos\theta)\sin\phi\, \mathbf{i}_1 \\ &\quad + \frac{1}{kr}\frac{\partial}{\partial r}[rz_n^{(\alpha)}(kr)]\frac{dP_n^1}{d\theta}\sin\phi\, \mathbf{i}_2 \\ &\quad + \frac{1}{kr\sin\theta}\frac{\partial}{\partial r}[rz_n^{(\alpha)}(kr)]P_n^1(\cos\theta)\cos\phi\, \mathbf{i}_3, \\ \mathbf{n}_{en}^{(\alpha)} &= n(n+1)\frac{z_n^{(\alpha)}(kr)}{kr} P_n^1(\cos\theta)\cos\phi\, \mathbf{i}_1 \\ &\quad + \frac{1}{kr}\frac{\partial}{\partial r}[rz_n^{(\alpha)}(kr)]\frac{dP_n^1}{d\theta}\cos\phi\, \mathbf{i}_2 \\ &\quad - \frac{1}{kr\sin\theta}\frac{\partial}{\partial r}[rz_n^{(\alpha)}(kr)]P_n^1(\cos\theta)\sin\phi\, \mathbf{i}_3. \end{aligned} \tag{6}$$

[c] Henceforth the time factor $e^{+j\omega t}$ will be omitted, as it does not play a direct role in what follows.

Here, $P_n^1(x)$ is the first associated Legendre polynomial of the first kind; $\mathbf{i}_1$, $\mathbf{i}_2$, and $\mathbf{i}_3$ are unit vectors drawn in the increasing r, θ, and ϕ directions at the point (r,θ,ϕ) on the sphere of radius r (Figure 3). The vectors $\mathbf{i}_2$ and $\mathbf{i}_3$ are tangent to the sphere along

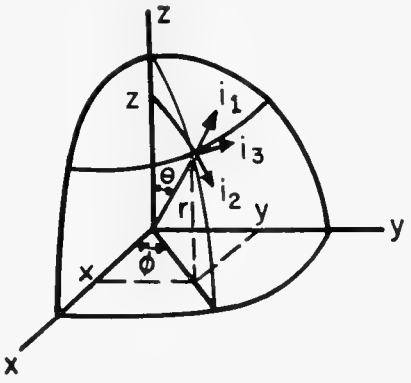

FIGURE 3. Spherical coordinates.

a meridian and a parallel circle respectively. The superscript α takes on two values. In the expressions for the incident wave and the transmitted wave inside the scattering sphere, it has the value 1, while its value is 3 in the expressions for the scattered wave.

Explicitly,

$$\begin{aligned} z_n^{(1)}(x) &= (\pi/2x)^{\frac{1}{2}} J_{n+\frac{1}{2}}(x), \\ z_n^{(3)}(x) &= (\pi/2x)^{\frac{1}{2}} H_{n+\frac{1}{2}}^{(2)}(x). \end{aligned} \tag{7}$$

$J_{n+\frac{1}{2}}(x)$ is the Bessel function of the first kind and half integer order, while $H_{n+\frac{1}{2}}^{(2)}(x)$ is the Hankel function of the second kind and half integer order.

The expanded field strengths of the incident wave are then

$$\begin{aligned} \mathbf{E}_i &= E_0 \sum_{n=1}^{\infty} (-j)^n \frac{2n+1}{n(n+1)} (\mathbf{m}_{0n}^{(1)} + j\mathbf{n}_{en}^{(1)}), \\ \mathbf{H}_i &= -\frac{E_0}{\eta_2} \sum_{n=1}^{\infty} (-j)^n \frac{2n+1}{n(n+1)} (\mathbf{m}_{en}^{(1)} - j\mathbf{n}_{0n}^{(1)}). \end{aligned} \tag{8}$$

It is seen that the nth expansion coefficient of $\mathbf{E}_i$ into the **m** waves is $(-j)^n[(2n+1)/n(n+1)]$, whereas the corresponding expansion coefficient into the **n** waves is $(-)^n \cdot j^{n+1}[(2n+1)/n(n+1)]$, etc.

The radiation field induced by the incident radiation is composed of the transmitted radiation field $(\mathbf{E}_t, \mathbf{H}_t)$ and the scattered radiation $(\mathbf{E}_s, \mathbf{H}_s)$ which, at large distances (r) from the scattering sphere, behaves as a divergent spherical wave, whose amplitude vanishes as $1/r$.

The scattered and transmitted steady-state fields

will now be expanded, in analogy with the incident field $(\mathbf{E}_i, \mathbf{H}_i)$. Thus,

$$\mathbf{E}_s = E_0 \sum_{n=1}^{\infty} (-j)^n \frac{2n+1}{n(n+1)} (a_n^s \, \mathbf{m}_{0n}^{(3)} + j b_n^s \, \mathbf{n}_{en}^{(3)}),$$
$$\mathbf{H}_s = -\frac{E_0}{\eta_2} \sum_{n=1}^{\infty} (-j)^n \frac{2n+1}{n(n+1)} (b_n^s \, \mathbf{m}_{en}^{(3)} - j a_n^s \, \mathbf{n}_{0n}^{(3)}), \tag{9}$$

valid at distances $r > a$, i.e., outside the sphere in medium 2. Clearly in equations (6) and (7), in the expressions of $\mathbf{m}$ and $\mathbf{n}$, k_2 replaces k according to equations (5) and (6).

Inside the sphere (complex wave number k_1, intrinsic impedance η_1), the transmitted field is expanded in the following way:

$$\mathbf{E}_t = E_0 \sum_{n=1}^{\infty} (-j)^n \frac{2n+1}{n(n+1)} (a_n^t \, \mathbf{m}_{0n}^{(1)} + j b_n^t \, \mathbf{n}_{en}^{(1)}),$$
$$\mathbf{H}_t = -\frac{E_0}{\eta_1} \sum_{n=1}^{\infty} (-j)^n \frac{2n+1}{n(n+1)} (b_n^t \, \mathbf{m}_{en}^{(1)} - j a_n^t \, \mathbf{n}_{0n}^{(1)}). \tag{10}$$

The final determination of the scattered and transmitted fields is thus reduced to finding the coefficients (or amplitudes) a_n^s, b_n^s, and a_n^t, b_n^t.

The preceding formulas permit one to write down rapidly the polar components of the different field strengths $(\mathbf{E}_i, \mathbf{H}_i)$, $(\mathbf{E}_s, \mathbf{H}_s)$, and $(\mathbf{E}_t, \mathbf{H}_t)$. The boundary conditions at the surface of the sphere demand the continuity of the tangential components of the total field outside the sphere and the transmitted field. If we denote these tangential components by subscripts θ or ϕ, the boundary conditions take on the following form:

$$E_\theta^i + E_\theta^s = E_\theta^t, H_\theta^i + H^s = H_\theta^t, r = a. \tag{11}$$

These lead to the following systems of equations for the determination of the coefficients (a_n^s, b_n^s) and (a_n^t, b_n^t):

$$a_n^t \, z_n^{(1)}(N\rho) - a_n^s \, z_n^{(3)}(\rho) = z_n^{(1)}(\rho). \tag{12}$$

$$\mu_2 a_n^t \frac{d}{d(N\rho)} [N\rho \, z_n^{(3)}(N\rho)] - \mu_1 a_n^s \frac{d}{d\rho} [\rho z_n^{(3)}(\rho)] = \mu_1 \frac{d}{d\rho} [\rho z_n^{(1)}(\rho)],$$
$$\mu_2 N b_n^t \, z_n^{(1)}(N\rho) - \mu_1 b_n^s \, z_n^{(3)}(\rho) = \mu_1 z_n^{(1)}(\rho),$$
$$b_n^t \frac{d}{d(N\rho)} [N\rho \, z_n^{(1)}(N\rho)] - N b_n^s \frac{d}{d\rho} [\rho z_n^{(3)}(\rho)] = N \frac{d}{d\rho} [\rho z_n^{(1)}(\rho)], \tag{13}$$

where $N = k_1/k_2$, $\rho = k_2 a$ and the $z_n^{(1)}(x)$ and $z_n^{(3)}(x)$ are the spherical Bessel functions defined in equation (7). Elimination of a_n^t from the first pair and that of b_n^t from the second pair of these equations leads to

$$a_n^s = -\frac{\mu_1 z_n^{(1)}(N\rho) [\rho z_n^{(1)}(\rho)]' - \mu_2 z_n^{(1)}(\rho) [N\rho z_n^{(1)}(N\rho)]'}{\mu_1 z_n^{(1)}(N\rho) [\rho z_n^{(3)}(\rho)]' - \mu_2 z_n^{(3)}(\rho) [N\rho z_n^{(1)}(N\rho)]'},$$
$$b_n^s = -\frac{\mu_1 z_n^{(1)}(\rho) [N\rho z_n^{(1)}(N\rho)]' - \mu_2 N^2 z_n^{(1)}(N\rho) [\rho z_n^{(1)}(\rho)]'}{\mu_1 z_n^{(3)}(\rho) [N\rho z_n^{(1)}(N\rho)]' - \mu_2 N^2 z_n^{(1)}(N\rho) [\rho z_n^{(3)}(\rho)]'}. \tag{14}$$

The primes at the square brackets stand for differentiation with respect to the argument of the Bessel function inside the brackets. Similarly, eliminating a_n^s and b_n^s, respectively, one would get a_n^t and b_n^t appearing in the field strengths inside the sphere.

For the computation of either the scattered or absorbed radiation, one needs to know the field strengths at a large distance r from the center of the sphere, i.e., for $r \gg a$, or $k_2 r \gg k_2 a$. It is important to notice in this connection that the coefficients a_n and b_n become small for $n > k_2 a$, and the summation over n may then be limited to the integer $n \sim k_2 a$. At great distances r, $k_2 r > n$; in other words, the order n of the terms of importance is less than the argument $(k_2 r)$ of the spherical Bessel functions. Under these conditions the asymptotic expressions of these functions can be used. These are given by[18a]

$$z_n^{(1)}(kr) \cong \frac{1}{kr} \cos\left(kr - \frac{n+1}{2}\pi\right),$$
$$z_n^{(3)}(kr) \cong \frac{1}{kr} e^{-j(kr - \frac{n+1}{2}\pi)}. \tag{15}$$

From these asymptotic expressions one sees that the radial components of the scattered field strengths can be practically neglected; they decrease with r as $1/r^2$, in contrast with the θ and ϕ components which decrease as $1/r$. This means that for large r, the field is transverse to the direction of propagation (radiation zone). Hence,

$$E_r^s = H_r^s = 0, r \gg a, \tag{16}$$

and with $\sigma_2 = 0$

$$E_\theta^s = \eta_2 H_\phi^s = \left(\frac{j}{kr}\right) E_0 e^{-jkr} \sum_{n=1}^{\infty} \frac{2n+1}{n(n+1)} \cdot \left(a_n^s \frac{P_n^1}{\sin\theta} + b_n^s \frac{dP_n^1}{d\theta}\right) \cos\phi,$$
$$E_\phi^s = -\eta_2 H_\theta^s = -\left(\frac{j}{kr}\right) E_0 e^{-jkr} \sum_{n=1}^{\infty} \frac{2n+1}{n(n+1)} \cdot \left(a_n^s \frac{dP_n^1}{d\theta} + b_n^s \frac{P_n^1}{\sin\theta}\right) \sin\phi. \tag{17}$$

Since the resultant field at any point outside the sphere is obtained by superposition of the incident and scattered or reflected fields, one has

$$\mathbf{E} = \mathbf{E}_i + \mathbf{E}_s; \ \mathbf{H} = \mathbf{H}_i + \mathbf{H}_s . \tag{18}$$

In view of equation (16), the complex Poynting vector associated with this resultant field is radial, so that

$$S_c = \tfrac{1}{2}\,(E_\theta H_\phi^* - E_\phi H_\theta^*), \tag{19}$$

where an asterisk denotes the complex conjugate. Using equation (18) one gets

$$S_c = \tfrac{1}{2}\,(E_\theta^i H_\phi^{i*} - E_\phi^i H_\theta^{i*}) + \tfrac{1}{2}\,(E_\theta^s H_\phi^{s*} - E_\phi^s H_\theta^{s*}) + \tfrac{1}{2}(E_\theta^i H_\phi^{s*} + E_\theta^s H_\phi^{i*} - E_\phi^i H_\theta^{s*} - E_\phi^s H_\theta^{i*}). \tag{20}$$

The first term on the right-hand side is the rate of flow of energy in the incident wave and the second term is the rate of flow in the scattered wave. The total scattered power is then

$$P_s = \tfrac{1}{2}\,\mathrm{Re}\int_0^{2\pi}\int_0 (E_\theta^s H_\phi^{s*} - E_\phi^s H_\theta^{s*})\, r^2 \sin\theta d\theta d\phi, \tag{21}$$

where Re denotes "Real part of . . ." and the integral is extended over the surface of a large sphere of radius r. In our case, using equations (16) and (17), one gets

$$P_s = \frac{1}{2\eta_2}\mathrm{Re}\int_0^{2\pi}\int_0^{\pi} (|\,E_\theta^s\,|^2 + |\,E_\phi^s\,|^2)\, r^2 \sin\theta d\theta d\phi. \tag{22}$$

In the case of an absorbing sphere, the net flow of energy across a closed surface around the sphere is absorbed energy flow, and it is directed inward. One may thus write that this absorbed energy, which disappears in the form of heat, is

$$P_{ab} = \mathrm{Re}\int_0^{2\pi}\int_0^{\pi} (-S_c)\, r^2 \sin\theta d\theta d\phi. \tag{23}$$

Since the integral of the incident flow across a closed surface is zero, equation (23) in connection with equation (21) leads to the definition of the rate of flow of total energy or the power subtracted from the beam, i.e., $(P_{ab} + P_s)$, as an integral over a closed surface of the third term on the right-hand side of the radial component S_c of the Poynting vector, equation (19). Thus

$$P_t = P_{ab} + P_s = \tfrac{1}{2}\,(-\mathrm{Re})\int_0^{2\pi}\int_0^{\pi} (E_\theta^i H_\phi^{s*} + E_\theta^s H_\phi^{i*} - E_\phi^i H_\theta^{s*} - E_\phi^s H_\theta^{i*})\, r^2 \sin\theta d\theta d\phi. \tag{24}$$

Substituting equations (16) and (17) into equation (24) and remembering that the ϕ integration leads to a factor π and that the integrals over products of the associated Legendre polynomials $P_n^1(x)$ are different from zero only in the following combination of these products appearing in equations (22) and (24),

$$\int_0^{\pi}\left[\left(\frac{P_n^1}{\sin\theta}\right)^2 + \left(\frac{dP_n^1}{d\theta}\right)^2\right]\sin\theta d\theta = \frac{2}{2n+1}\,[n\,(n+1)]^2\,,$$

one finds,

$$P_s = \frac{\pi E_0^2}{k_2^2\,\eta_2}\sum_{n=1}^{\infty}(2n+1)\,(|\,a_n^s\,|^2 + |\,b_n^s\,|^2)\,, \tag{25}$$

and

$$P_t = \frac{\pi E_0^2}{k_2^2\,\eta_2}(-\mathrm{Re})\sum_{n=1}^{\infty}(2n+1)\,(a_n^s + b_n^s)\,. \tag{26}$$

We shall also need the fraction of the power scattered backwards by the sphere, i.e., in the direction $\theta = \pi$, per unit solid angle. One thus obtains, with $d\omega = \sin\theta d\theta d\phi$,

$$\left(\frac{dP_s}{d\omega}\right)_{\theta=\pi} = \frac{E_0^2}{8k_2^2\,\eta_2}\,\mathrm{Re}\sum_{n=1}^{\infty}\sum_{m=1}^{\infty}(-)^{n+m}(2n+1)\cdot(2m+1)\,(a_n^s - b_n^s)\,(a_m^{s*} - b_m^{s*}), \tag{27}$$

as a simple calculation shows, starting from equation (22).

It has already been mentioned in connection with the definition of the complex wave number, equation (2), of a homogeneous and isotropic medium that its imaginary part is chosen to be negative. We shall write

$$jk = \alpha + j\beta, \tag{28}$$

where β is the phase constant and α the attenuation constant; both are real. The explicit expressions of β and α in terms of the characteristic electromagnetic properties of the medium, namely, inductive capacity ϵ, permeability μ and conductivity σ for the given frequency $\omega/2\pi$ are the following:[18a]

$$\beta = \omega\left[\frac{\mu\epsilon}{2}\left(\sqrt{1 + \frac{\sigma^2}{\epsilon^2\omega^2}} + 1\right)\right]^{\frac{1}{2}}, \tag{29}$$

$$\alpha = \omega\left[\frac{\mu\epsilon}{2}\left(\sqrt{1 + \frac{\sigma^2}{\epsilon^2\omega^2}} - 1\right)\right]^{\frac{1}{2}}. \tag{30}$$

With equation (28) the field strength, electric or magnetic, in a plane wave propagated in such a medium along, say, the z axis, is, omitting the time factor, of the form:

$$\mathbf{F} = \mathbf{F}_0\, e^{-j\beta z - \alpha z},$$

$\mathbf{F}_0$ being an amplitude vector directed along either one of the two remaining coordinate axes. The attenuation

factor α simply means that in this medium an advance of the wave through a distance of $1/\alpha$ meter is accompanied by a decrease in the field strengths in the ratio of $1:e = 0.368$, or the power per unit area (Poynting vector) decreases in the same ratio over half that distance or $1/2\alpha$ meter.

In the mks system, the attenuation factor is then α nepers per meter, whereas the power absorption coefficient is 20α ($\log_{10}e$) decibels per meter $= 8.686\alpha$ db per meter.

Our problem is the study of propagation in a medium which is neither homogeneous nor isotropic, inasmuch as it consists of a suspension of water droplets in the atmosphere. It can be proved that in such a medium the attenuation factor is the sum of all the different partial attenuation factors due to different physical phenomena.

The particle attenuation factor will still be denoted by α. More appropriately we might call α the average particle attenuation factor. It may be defined as

$$\alpha = \frac{1}{2} N Q_t \text{ neper per unit length,} \qquad (31)$$

where N is the average number of water drops per unit volume and Q_t the total cross section of one droplet. The absorption effect of one spherical water drop is given by Q_t which is the ratio of the power P_t removed by the drop from the beam falling on it to the incident power per unit area. Provided the effect of all the drops be linearly additive, equation (31) will express their average attenuation effect. The incident power density is the complex Poynting vector of the beam

$$S_{c,z} = \frac{E_0^2}{2\eta_2} \cdot \qquad (32)$$

Therefore, with equations (3) and (26),

$$Q_t = \frac{\lambda^2}{2\pi} (-\mathrm{Re}) \sum_{n=1}^{\infty} (2n+1)\,(a_n^s + b_n^s), \qquad (33)^{d}$$

where $\lambda = 2\pi/k_2$ is the wavelength of the radiation in air or free space. Similarly the cross section for scattering is, with equation (25),

$$Q_s = \frac{\lambda^2}{2\pi} \sum_{n=1}^{\infty} (2n+1)\,(|a_n^s|^2 + |b_n^s|^2). \qquad (34)$$

The differential cross section for back scattering (or radar cross section) is then, with equations (27) and (32),

$$\left(\frac{dQ_s}{d_w}\right)\theta = \pi = \sigma(\pi) = \left(\frac{\lambda}{4\pi}\right)^2 \mathrm{Re} \sum_{n=1}^{\infty} \sum_{m=1}^{\infty} (-)^{n+m} (2n+1) \cdot (2m+1)\,[a_n^s a_m^{s*} + b_n^s b_m^{s*} - 2a_n^s b_m^{s*}]. \qquad (35)$$

These are the formulas on which the computations of attenuation have been based. They are certainly correct in the wavelength region 1 cm to 100 cm with which the present study is mainly concerned, and they correctly take into account the linear dimensions of the scattering and absorbing particles. According to Brillouin[20] these formulas have to be modified in the limit $\lambda \ll a$, in which case for perfect reflection they lead to a scattering cross section $2\pi a^2$, double of the expected geometrical cross section. Since the modifications mentioned do not play any role for $\lambda \geq 3a/10$, which condition will always be satisfied in the present report, they will not be discussed here.

10.1.3 The Scattering Amplitudes[e] a_n^s and b_n^s

The scattered fields ($\mathbf{E}_s$, $\mathbf{H}_s$) outside the sphere and the transmitted fields ($\mathbf{E}_t$, $\mathbf{H}_t$) inside are due to forced oscillations of the sphere caused by the incident field ($\mathbf{E}_i$, $\mathbf{H}_i$). The fields ($\mathbf{E}_s$, $\mathbf{H}_s$) and ($\mathbf{E}_t$, $\mathbf{H}_t$) given by equations (7) and (8) can be regarded as due to electric and magnetic 2^n-poles ($n = 1$ corresponds to dipoles, $n = 2$ to quadrupoles, etc.) induced in the substance of the spherical particle. In the steady state these poles oscillate with the frequency of the incident radiation field. When this frequency approaches a characteristic frequency of the free vibrations of the electric or magnetic 2^n-poles of the sphere, resonance will occur. It can, indeed, be shown that the amplitudes a_n are associated with vibrations of magnetic poles and the b_n's with vibrations of electric poles. The characteristic frequencies of the free vibrations of magnetic poles of a sphere are determined by a condition which annuls the denominator of a_n, those of electric poles by a condition which annuls the denominator of b_n, given by equation (14).[18b] The characteristic frequencies of the free vibrations are, however, complex in contrast with the

[d]The minus sign is missing in the presentation in reference 18a; see formulas (26) and (29) on page 569. This leads to the incorrect result, for nonabsorbing spheres, that the scattering cross section Q_s reduces in this case to the negative of the total cross section Q_t. Clearly Q_s reduces to $+Q_t$.

[e]Since henceforth we will deal only with the scattering coefficients a_n^s, b_n^s, we will omit the superscript s.

real frequency of constraint of the radiation field falling on a sphere, as in the present case. The denominators of the amplitudes a_n and b_n, although reduced, can never become zero, and there are no difficulties caused by resonance.

A glance at the formulas (14) shows the complexity of the amplitudes a_n and b_n. An exact computation of these coefficients is out of the question on account of the lack of tables of Bessel and Hankel functions of complex argument in the range needed here. They reduce to simple expressions in the limit when the parameter $\rho = 2\pi a/\lambda \ll 1$. In the present work we shall be mostly interested in the cases where $\rho < 1$ or $\rho \ll 1$. In these cases a series expansion of the amplitudes in ascending powers of the parameter ρ can be used. With the expansions of the spherical Bessel and Hankel functions

$$z_n^{(1)}(\rho) = 2^n \rho^n \sum_{m=0}^{\infty} \frac{(-)^m (n+m)!}{m!\,(2n+2m+1)!}\,\rho^{2m},$$

$$z_n^{(3)}(\rho) = 2^n \rho^n \sum_{m=0}^{\infty} \frac{(-)^m (n+m)!}{m!\,(2n+2m+1)!}\,\rho^{2m} + \frac{j}{2^2\,\rho^{n+1}} \sum_{m=0}^{n} \frac{(2n-2m)!}{m!\,(n-m)!}\,\rho^{2m}$$

used in equation (14), one is lead to the following amplitudes, keeping the first few terms of the expansions and assuming $\mu_1 = \mu_2$, i.e., the equality of the permeabilities of the medium and the sphere:

$$a_n = -j2^{2n}\left(\frac{n!}{(2n+1)!}\right)^2 \frac{N^2-1}{2n+3}\,\rho^{2n+3} \cdot \left[1 + \rho^2\left(\frac{N^2-1}{2n+1} - \frac{N^2+1}{2(2n+5)}\right) + \cdots\right], \quad (36)$$

$$b_n = -j2^{2n}\left(\frac{n!}{(2n+1)!}\right)^2 \frac{(2n+1)(n+1)(N^2-1)}{nN^2+n+1} \cdot \rho^{2n+1} \cdot \left[1 + \rho^2 \frac{(2n+1)[(2n-1)N^2 - n - 1]}{(2n+3)(2n-1)(nN^2+n+1)} + \cdots\right]. \quad (37)$$

From these expressions one derives at once the explicit formulas representing the induced magnetic dipole (a_1), electric dipole (b_1), and electric quadrupole (b_2) amplitudes. One has, then, neglecting powers of ρ higher than the sixth,

$$a_1 = \frac{-j}{45}(N^2-1)\rho^5,$$

$$b_1 = \frac{-2j}{3}\,\frac{N^2-1}{N^2+2}\,\rho^3\left(1 - \frac{3}{5}\,\frac{N^2-2}{N^2+2}\,\rho^2 - \frac{2j}{3}\,\frac{N^2-1}{N^2+2}\,\rho^3\right), \quad (38)^{\dagger}$$

and

$$b_2 = \frac{-j}{15}\,\frac{N^2-1}{2N^2+3}\,\rho^5.$$

It would appear interesting to present the relationships connecting the amplitudes of the electric and magnetic poles a_n and b_n with those appearing in the treatment of Mie which was used by Ryde.[17] The magnetic and electric amplitudes in Mie's notation are respectively p_n and a_n, and the relationships in question are the following:

$$p_n^{\text{Mie}} = (-)^n j\,(2n+1)\,a_n,$$

$$a_n^{\text{Mie}} = (-)^{n+1} j\,(2n+1)\,b_n. \quad (39)$$

Finally the formulas (38) can be transformed so as to have the real and imaginary parts of the amplitudes separated easily. The refractive index N of the spheres is connected with their complex dielectric constant by

$$\epsilon_c = N^2 = \epsilon_r - j\epsilon_i, \quad (40)$$

or with

$$N = n\,(1 - j\chi), \quad (41)$$

the complex index of refraction, one has

$$\epsilon_r = n^2\,(1-\chi^2);\ \epsilon_i = 2n^2\chi. \quad (42)$$

[†]Some misprints and slight errors in the expressions for these amplitudes may be noted in reference 18a. On page 571 in the formula (35) and in the denominator of the coefficient of ρ^2, read $(2n+2)$ instead of $(2n+1)$. In the formula (36) the minus sign on the right-hand side is missing. In reference 18a, b_1^r and b_2^r have the wrong sign and the ρ^5 term in b_1^r is incomplete. It is recalled that $+i$ has been replaced throughout this report by $-j$.

Using equation (40) in the amplitudes (38) one gets

$$a_1 = \frac{1}{45}\left[-\epsilon_i - j(\epsilon_r - 1)\right]\rho^5,$$

$$\operatorname{Re} b_1 = \frac{-2\epsilon_i}{(\epsilon_r+2)^2+\epsilon_i^2}\rho^3 - \frac{2}{5}\cdot$$

$$\epsilon_i \frac{\left[(\epsilon_r+2)(7\epsilon_r-10)+7\epsilon_i^2\right]}{\left[(\epsilon_r+2)^2+\epsilon_i^2\right]^2}\rho^5 - \frac{4}{9}\cdot$$

$$\frac{(\epsilon_r-1)^2(\epsilon_r+2)^2+\epsilon_i^2\left[2(\epsilon_r-1)(\epsilon_r+2)-9\right]+\epsilon_i^4}{\left[(\epsilon_r+2)^2+\epsilon_i^2\right]^2}\rho^6,$$

$$\operatorname{Im} b_1 = -\frac{2}{3}\frac{(\epsilon_r-1)(\epsilon_r+2)+\epsilon_i^2}{(\epsilon_r+2)^2+\epsilon_i^2}\rho^3 - \frac{2}{5}\cdot$$

$$\frac{(\epsilon_r-1)(\epsilon_r-2)(\epsilon_r+2)^2+\epsilon_i^2\left[2(\epsilon_r+1)^2-(3\epsilon_r+20)\right]+\epsilon_i^4}{\left[(\epsilon_r+2)^2+\epsilon_i^2\right]^2}\cdot$$

$$\rho^5 + \frac{8}{3}\frac{\epsilon_i\left[(\epsilon_r-1)(\epsilon_r+2)+\epsilon_i^2\right]}{\left[(\epsilon_r+2)^2+\epsilon_i^2\right]^2}\rho^6,$$

$$b_2 = \frac{1}{3}\frac{-\epsilon_i-(j/5)\left[(\epsilon_r-1)(2\epsilon_r+3)+2\epsilon_i^2\right]}{(2\epsilon_r+3)^2+4\epsilon_i^2}\rho^5. \tag{43}$$

These amplitudes are the same as those found by Ryde.[g] They allow the computation of attenuation and back scattering with a certain approximation. The results thus obtained are the more accurate, the smaller the parameter $\rho = 2\pi a/\lambda$.

In the computation of the amplitudes a_n and b_n we have used the same values of the real and imaginary parts of the dielectric constant of water ϵ_r and ϵ_i as the ones used by Ryde. These were obtained by using the Clarendon Laboratory values for ϵ_r and ϵ_i for waves of 1.26-cm wavelength[21] and determining with them the transition wavelength λ_0 in the Debye[13] formulas

$$\epsilon_r = \epsilon_{\infty p} + \frac{\epsilon_\infty - \epsilon_{\infty p}}{1+\left(\frac{\lambda_0}{\lambda}\right)^2}, \quad \epsilon_i = \frac{\lambda_0}{\lambda}(\epsilon_r - \epsilon_{\infty p}), \tag{44}$$

$$\epsilon_{\infty p}^{\frac{1}{2}} = 1.33, \ \epsilon_\infty = 81, \ \lambda_0 = 1.59 \text{ cm}.$$

The values of ϵ_r computed with these formulas happen to be in fair agreement with the experimental values obtained by a large group of independent workers.[17,22] There seems to be a regrettable situation concerning the values of ϵ_i, and no serious studies have been made on the temperature and frequency variation of this quantity, so fundamental for the microwave region. A beginning in this direction has been undertaken by the Radiation Laboratory.[23] In Figure 4 we have drawn the curves $\epsilon_r(\lambda)$ and $\epsilon_i(\lambda)$ in the range 1 to 11 cm, and Table 1 gives the values of the dielectric constant used in this work in the wavelength interval 1 to 100 cm.

It is interesting to consider here the temperature variation of ϵ_c. Recent measurements made in the

[g] In his first report Ryde[17] gave incorrectly the coefficients of ρ^5 in both the real and imaginary parts of b_1. The coefficient of ρ^5 in the real part was corrected in the second report. In comparing the b_1's with the amplitudes given by Ryde, the relations (38) have to be taken into account.

TABLE 1. Values of the dielectric constant of water at $t \backsim 18$C, used in this work.*

λ, cm	ϵ_r	$\epsilon_i = 60\sigma\lambda$	σ mhos/m
1	24.2	35.6	5.93×10
1.26	32.5	38.6	5.11×10
1.62	43.3	39.5	4.13×10
2	50.6	38.5	3.20×10
2.5	58.2	35.9	2.39×10
3.0	63.6	32.7	1.81×10
4.0	70.3	27.2	1.13×10
5	73.8	22.7	7.56
6	76.0	19.3	5.36
8	78.0	15.1	3.15
10	79.0	12.3	2.05
15	81	8.40	9.33×10^{-1}
20	81	6.30	5.25×10^{-1}
30	81	4.20	2.33×10^{-1}
50	81	2.52	8.40×10^{-2}
75	81	1.68	3.73×10^{-2}
100	81	1.26	2.10×10^{-2}

*The computations of the attenuation and scattering effects are all based on this table and refer therefore always to temperatures of about 18C, unless stated otherwise.

TABLE 2. Temperature variation of the dielectric constant of water (K band).

	Degrees C	ϵ_r	ϵ_i
Water	3	27	27
	25	35	23
	60	44	14
Ice	−15	3.3	0.011

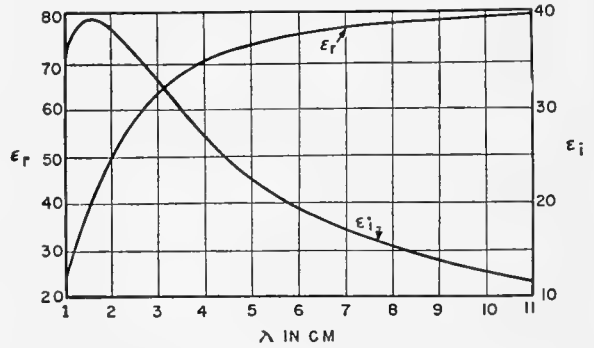

FIGURE 4. Dielectric constant of water ($t \backsim 18$C) $\epsilon_c = \epsilon_r - j\epsilon_i$.

Radiation Laboratory in the K band[23] gave the results shown in Table 2.

As might have been expected, the dielectric absorption ϵ_i increases with decreasing temperature.

With the above values of ϵ_r and ϵ_i the computation of the amplitudes a_n and b_n is straightforward. The amplitudes a_n and b_n have the form

$$a_n = \sum_{l=2n+3}^{\infty} (\alpha_n^{(l)} + j\bar{\alpha}_n^{(l)})\, \rho^l, \tag{45}$$

$$b_n = \sum_{l=2n+1}^{\infty} (\beta_n^{(l)} + j\bar{\beta}_n^{(l)})\, \rho^l. \tag{46}$$

Thus we let $\alpha_1^{(5)}$ denote the real part of the coefficient of ρ^5 in a_1 and $\bar{\alpha}_1^{(5)}$ its imaginary part. Similarly, $\beta_1^{(3)}$, $\bar{\beta}_1^{(3)}$ are the real and imaginary parts of the coefficient of ρ^3 in b_1, etc.

As equation (43) shows $\alpha_1^{(5)}$ and $\bar{\alpha}_1^{(5)}$ are directly proportional to $(-\epsilon_i)$ and $(\epsilon_r - 1)$ respectively. As the wavelength increases, $\alpha_1^{(5)}$ changes approximately from -0.9 to -0.03 after passing through a shallow minimum on account of the variation of ϵ_i. In the same interval $\bar{\alpha}_1^{(5)}$ increases from about 0.5 to 1.8.

$\beta_1^{(3)}$ turns out to be practically negligible, in comparison with $\bar{\beta}_1^{(3)}$, which is almost constant in this wavelength range. $\beta_1^{(5)}$ and $\bar{\beta}_1^{(5)}$ behave similarly. With $\beta_1^{(6)}$ and $\bar{\beta}_1^{(6)}$ the roles are inverted.

Finally $\beta_2^{(5)}$ and $\bar{\beta}_2^{(5)}$ both vary in the range under consideration.

As a rule, those coefficients of the powers of ρ ($= \pi D/\lambda$) (D = diameter of the sphere) which do not contain terms in ϵ_r and powers of ϵ_r separately in the numerator, but only the products $\epsilon_r\, \epsilon_i$, and powers of ϵ_i, are considerably smaller than those which do contain ϵ_r and its powers separately.

10.1.4 The Attenuation of Radio Waves by Spherical Raindrops[h]

The knowledge of the coefficients a_n and b_n allows finally the computation of the absorption cross section for any spherical water drops of given diameter D at those temperatures where the amplitudes can be computed.

The absorption coefficient becomes, with the cross section found above, [equations (33) and (43)],

$$\alpha = 0.4343 \times 10^6 \frac{N\lambda^2}{2\pi} (-\mathrm{Re}) \sum_{n=1}^{n=\infty} (2n+1)\,(a_n + b_n)$$

db per kilometer. (47)

In our approximation for the amplitudes, we may write

$$\alpha = 0.4343 \times 10^6 \frac{3\pi NV}{\lambda} (c_1 + c_2\rho^2 + c_3\rho^3 + \cdots)$$

db per kilometer (48)

where N is the number of spherical drops, each of volume V per cubic centimeter, λ is the wavelength in centimeters of the incident radiation. The parameter ρ is, as above, $\pi D/\lambda$, D being the diameter in centimeters of a drop, and the coefficients c_1, c_2, c_3, $\cdots$ are the following functions of the wavelength, the temperature of the drops being taken as a constant ($t \sim 18$ C),

$$c_1 = \frac{6\epsilon_i}{(\epsilon_r+2)^2 + \epsilon_i^2},$$

$$c_2 = \frac{\epsilon_i}{15} + \frac{5}{3}\frac{\epsilon_i}{(2\epsilon_r+3)^2+4\epsilon_i^2} + \frac{6}{5}\frac{\epsilon_i[(\epsilon_r+2)(7\epsilon_r-10)+7\epsilon_i^2]}{[(\epsilon_r+2)^2+\epsilon_i^2]^2},$$

$$c_3 = \frac{4}{3}\frac{(\epsilon_r-1)^2(\epsilon_r+2)^2+\epsilon_i^2[2(\epsilon_r-1)(\epsilon_r+2)-9]+\epsilon_i^4}{[(\epsilon_r+2)^2+\epsilon_i^2]}. \tag{49}$$

It is possible to give the attenuation formula another simple form by noticing that NV is the total volume of water per cubic centimeter in the form of drops or $10^6\, NV$ is the total volume of water per cubic meter. Since the density of water is 1 g per cubic centimeter, numerically, the quantity $10^6\, NV$ is the mass m of liquid water per cubic meter, in air. The transformed attenuation formula becomes finally

$$\alpha = 4.092 \frac{m}{\lambda} (c_1 + c_2\rho^2 + c_3\rho^3 + \cdots) \text{ db per kilometer.} \tag{50}$$

It is seen that when $\rho = \pi D/\lambda \ll 1$ so that all the terms in the expansion in equation (50) are small in comparison with c_1, the attenuation factor reduces to

$$\alpha_{\rho<<1} = \frac{4.092\, mc_1}{\lambda} = \frac{24.55}{\lambda}\frac{m\epsilon_i}{(\epsilon_r+2)^2+\epsilon_i^2}$$

db per kilometer. (51)

Hence, when the diameter of the water drops is very small in comparison with the wavelength of the incident radiation, the attenuation does not depend on the

[h]The attenuation values given in this report refer always to one-way transmission and are additive to the free space attenuation.

size of the drops but only on the total mass of liquid water per unit volume contained in the air. It is interesting to find, for a given wavelength, the largest diameter for which the approximation (51) can still be used in practice. If it is practical to use (51), (as in reference 12), for

$$c_2\rho^2 \leq \frac{c_1}{10}, \tag{52}$$

then in order that (51) shall represent the attenuation factor within 10 per cent, the diameter of the spheres must (for given λ), be equal to or less than D_c with

$$D_c = \frac{\lambda}{10}\left(\frac{c_1}{c_2}\right)^{\frac{1}{2}} \text{ cm}. \tag{53}$$

In Table 3 appear the values of c_1, c_2, and D_c in the wavelength range 1 to 100 cm. The values of c_3 are not included, since this coefficient turns out to be practically constant, in this range, increasing from the value of 1.224 for $\lambda = 1$ cm to 1.239 for $\lambda = 100$ cm.

It is evident that for values of ρ which are not too small, equation (48) or (50) has to be used. When ρ is sufficiently close to unity these series cease to give any good values of the absorption cross section Q_t or the attenuation factor α. In the K and X bands, Ryde and Ryde[12] have, therefore, computed the attenuation factors exactly. These computations were included (without being checked) in Tables 4 and 5, where Q_t and α have been computed for a series of drops ranging

TABLE 3

λ, cm	c_1	c_2	D_c cm
1	0.109	2.53	0.0656
1.1	0.0994	2.60	0.0680
1.26	0.0862	2.69	0.0713
1.5	0.0730	2.73	0.0774
2	0.0543	2.64	0.0906
3	0.0365	2.23	0.121
4	0.0273	1.85	0.154
5	0.0217	1.54	0.187
6	0.0179	1.31	0.222
8	0.0137	1.01	0.293
10	0.0110	0.835	0.363
15	0.00724	0.570	0.534
20	0.00541	0.427	0.712
25	0.00437	0.342	0.892
30	0.00364	0.285	1.07
50	0.00219	0.171	1.78
75	0.00146	0.114	2.68
100	0.00109	0.085	3.57

TABLE 4. Absorption cross section Q_t (cm^2) of water drops with diameter D (cm).

λ, cm \ D, cm	0.05	0.10	0.15	0.20	0.25	0.30	0.35	0.40	0.45	0.50	0.55
1.25	$6.19\,10^{-5}$	$9.60\,10^{-4}$	$5.66\,10^{-3}$	$1.89\,10^{-2}$	$5.04\,10^{-2}$	$1.13\,10^{-1}$	$2.15\,10^{-1}$	$3.66\,10^{-1}$	$5.66\,10^{-1}$	$7.62\,10^{-1}$	1.01
3	$9.19\,10^{-6}$	$1.52\,10^{-4}$	$1.30\,10^{-3}$	$5.53\,10^{-3}$	$1.63\,10^{-2}$	$3.73\,10^{-2}$	$6.65\,10^{-2}$	$1.08\,10^{-1}$	$1.52\,10^{-1}$	$2.15\,10^{-1}$	$2.72\,10^{-1}$
5	$2.84\,10^{-6}$	$2.75\,10^{-5}$	$1.20\,10^{-4}$	$3.79\,10^{-4}$	$9.85\,10^{-4}$	$2.24\,10^{-3}$	$4.59\,10^{-3}$	$8.68\,10^{-3}$	$1.54\,10^{-2}$	$2.59\,10^{-2}$	$4.18\,10^{-2}$
8	$1.09\,10^{-6}$	$9.49\,10^{-6}$	$3.65\,10^{-5}$	$1.02\,10^{-4}$	$2.40\,10^{-4}$	$4.98\,10^{-4}$	$9.63\,10^{-4}$	$1.74\,10^{-3}$	$2.97\,10^{-3}$	$4.85\,10^{-3}$	$7.63\,10^{-3}$
10	$6.90\,10^{-7}$	$5.84\,10^{-6}$	$2.16\,10^{-5}$	$5.76\,10^{-5}$	$1.46\,10^{-4}$	$2.59\,10^{-4}$	$4.81\,10^{-4}$	$8.44\,10^{-4}$	$1.40\,10^{-3}$	$2.25\,10^{-3}$	$3.47\,10^{-3}$
15	$2.98\,10^{-7}$	$2.45\,10^{-6}$	$8.66\,10^{-6}$	$2.18\,10^{-5}$	$4.59\,10^{-5}$	$8.65\,10^{-5}$	$1.51\,10^{-4}$	$2.51\,10^{-4}$	$3.98\,10^{-4}$	$6.10\,10^{-4}$	$9.06\,10^{-4}$
20	$1.67\,10^{-7}$	$1.36\,10^{-6}$	$4.71\,10^{-6}$	$1.15\,10^{-5}$	$2.36\,10^{-5}$	$4.31\,10^{-5}$	$7.29\,10^{-5}$	$1.17\,10^{-4}$	$1.78\,10^{-4}$	$2.66\,10^{-4}$	$3.85\,10^{-4}$
30	$7.36\,10^{-8}$	$5.93\,10^{-7}$	$2.02\,10^{-6}$	$4.88\,10^{-6}$	$9.74\,10^{-6}$	$1.73\,10^{-5}$	$2.83\,10^{-5}$	$4.38\,10^{-5}$	$6.48\,10^{-5}$	$9.29\,10^{-5}$	$1.30\,10^{-4}$
50	$2.67\,10^{-8}$	$2.14\,10^{-7}$	$7.27\,10^{-7}$	$1.73\,10^{-6}$	$3.41\,10^{-6}$	$5.96\,10^{-6}$	$9.57\,10^{-6}$	$1.45\,10^{-5}$	$2.09\,10^{-5}$	$2.93\,10^{-5}$	$3.97\,10^{-5}$
75	$1.19\,10^{-8}$	$9.44\,10^{-8}$	$3.21\,10^{-7}$	$7.63\,10^{-7}$	$1.49\,10^{-6}$	$2.60\,10^{-6}$	$4.15\,10^{-6}$	$6.23\,10^{-6}$	$8.94\,10^{-6}$	$1.24\,10^{-5}$	$1.66\,10^{-5}$
100	$6.77\,10^{-9}$	$5.41\,10^{-8}$	$1.83\,10^{-7}$	$4.34\,10^{-7}$	$8.50\,10^{-7}$	$1.47\,10^{-6}$	$2.35\,10^{-6}$	$3.51\,10^{-6}$	$5.02\,10^{-6}$	$6.92\,10^{-6}$	$9.27\,10^{-6}$

TABLE 5. Attenuation α/N (db/km) in fictitious rains with a concentration of one drop per cubic centimeter of D cm diameter.

λ, cm \ D, cm	0.05	0.10	0.15	0.20	0.25	0.30	0.35	0.40	0.45	0.50	0.55
1.25	2.69 10	$4.17\,10^{2}$	$2.46\,10^{3}$	$8.23\,10^{3}$	$2.19\,10^{4}$	$4.90\,10^{4}$	$9.33\,10^{4}$	$1.59\,10^{5}$	$2.46\,10^{5}$	$3.31\,10^{5}$	$4.37\,10^{5}$
3	3.99	6.61 10	$5.63\,10^{2}$	$2.40\,10^{3}$	$7.08\,10^{3}$	$1.62\,10^{4}$	$2.89\,10^{4}$	$4.68\,10^{4}$	$6.61\,10^{4}$	$9.33\,10^{4}$	$1.18\,10^{5}$
5	1.23	1.19 10	5.22 10	$1.65\,10^{2}$	$4.28\,10^{2}$	$9.72\,10^{2}$	$1.99\,10^{3}$	$3.77\,10^{3}$	$6.69\,10^{3}$	$1.13\,10^{4}$	$1.81\,10^{4}$
8	$4.73\,10^{-1}$	4.12	1.59 10	4.43 10	1.04 10^{2}	$2.16\,10^{2}$	$4.18\,10^{2}$	$7.54\,10^{2}$	$1.29\,10^{3}$	$2.10\,10^{3}$	$3.31\,10^{3}$
10	$2.99\,10^{-1}$	2.54	9.37	2.5 10	6.35 10	$1.12\,10^{2}$	$2.09\,10^{2}$	$3.66\,10^{2}$	$6.09\,10^{2}$	$9.76\,10^{2}$	$1.51\,10^{3}$
15	$1.30\,10^{-1}$	1.07	3.76	9.47	1.93 10	3.76 10	6.58 10	1.09 10^{2}	$1.73\,10^{2}$	$2.65\,10^{2}$	$3.93\,10^{2}$
20	$7.26\,10^{-2}$	$5.89\,10^{-1}$	2.04	5.02	1.03 10	1.87 10	3.17 10	5.07 10	7.73 10	1.15 10^{2}	$1.67\,10^{2}$
30	$3.20\,10^{-2}$	$2.57\,10^{-1}$	$8.79\,10^{-1}$	2.12	4.23	7.50	1.23 10	1.90 10	2.82 10	4.04 10	5.63 10
50	$1.16\,10^{-2}$	$9.29\,10^{-2}$	$3.16\,10^{-1}$	$7.53\,10^{-1}$	1.48	2.59	4.16	6.29	9.10	1.27 10	1.72 10
75	$5.16\,10^{-3}$	$4.12\,10^{-2}$	$1.39\,10^{-1}$	$3.31\,10^{-1}$	$6.49\,10^{-1}$	1.13	1.80	2.70	3.88	5.37	7.21
100	$2.94\,10^{-3}$	$2.35\,10^{-2}$	$7.93\,10^{-2}$	$1.89\,10^{-1}$	$3.69\,10^{-1}$	$6.40\,10^{-1}$	1.02	1.53	2.18	3.01	4.03

in diameter from 0.05 to 0.55 cm. For wavelengths $\lambda \geq 5$ cm, the three-term series expansion (48) was used. It is expected that at these shorter waves, where the critical diameters are smaller than the drop diameters mentioned, the cross sections and attenuation factors given in the tables will be but fair approximations of the exact values of these quantities.

The range of values of ρ covered by these tables extends from about $\rho = 0.0016$ to $\rho = 1.4$. In Figures 5 and 6 two families of curves are drawn giving $Q_t\,(\lambda)_D$ and $\alpha(\lambda)_D/N$, the diameter of the drops being kept constant, and $Q_t(D)_\lambda$ and $\alpha(D)_\lambda/N$, the wavelength of the radiation being kept constant. Since our computations cover the range from $\lambda = 5$ cm, we have extended our curves on Figure 5 so as to cover the K and X bands, using the values of the cross sections and attenuations given in these bands by Ryde and Ryde. Their data are represented again in the upper curves of Figure 6.

We are now prepared to apply these results to meteorological phenomena and shall, for this purpose, give a summary of typical data on clouds, fogs, and rains to be used in this work.

10.1.5 Typical Data on Clouds, Fogs, and Rains

To compute the attenuation due to the different forms of condensation demands a knowledge of the

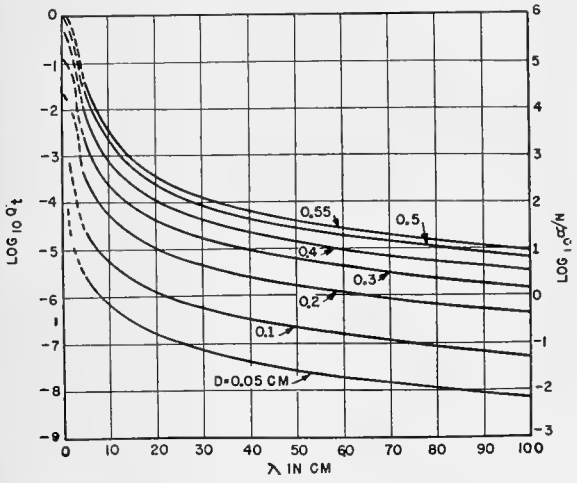

FIGURE 5. Absorption cross section, Q_t, and attenuation constant, α, of spherical water drops as a function of the wavelength. The abscissa gives the wavelength, λ, in centimeters. The right-hand ordinate scale gives $\log_{10}(\alpha/N)$, where α/N, the attenuation constant in a rain with 1 drop per cu cm, is expressed in decibels per kilometer. The numbers on the curves give the diameter, D, of the drops in centimeters. The left-hand ordinate scale gives $\log_{10} Q_t$ with Q_t being expressed in square centimeters.

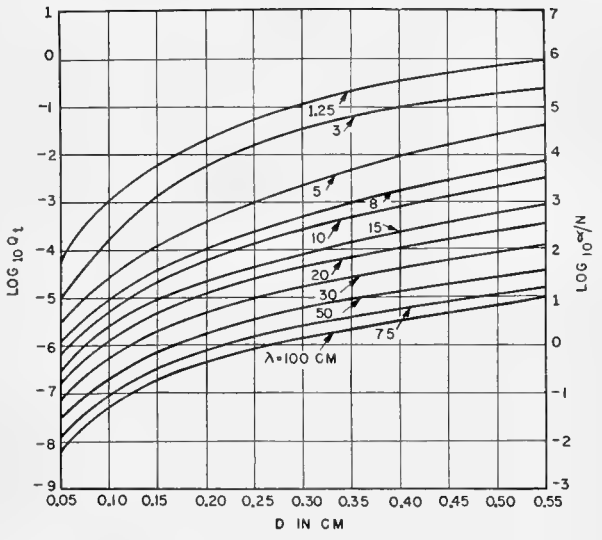

FIGURE 6. Absorption cross section, Q_t, and attenuation constant, α, of spherical water drops as a function of the drop diameter. The abscissa gives the drop diameter, D, in centimeters. The right-hand ordinate scale gives $\log_{10}(\alpha/N)$, where α/N, the attenuation constant in a rain with 1 drop per cu cm, is expressed in decibels per kilometer. The numbers on the curves give the wavelength, λ, of the incident radiation in centimeters. The left-hand ordinate scale gives $\log_{10} Q_t$, with Q_t being expressed in square centimeters.

water drop size distributions and their volume concentration. Indeed, if such a form of condensation contains N_k droplets per cubic centimeter having a diameter of k cm, with k varying from, say, 0 to s, then the attenuation factor due to this form will be the sum of the attenuation factors associated with each of the different drop groups with diameter of $1, 2, \cdots, \cdots, \cdots, n, \cdots, s$ cm. In other words,

$$\alpha_{\text{total}} = \sum_{k=0}^{s} \alpha_k = 0.4343 \times 10^6 \sum_{k=0}^{s} N_k Q_{t,k} \quad \text{db per kilometer,} \qquad (54)$$

according to equation (31), where N_k is the number per cubic centimeter of the drops k, and $Q_{t,k}$ is the total absorption cross section in square centimeters of one spherical water drop of diameter k cm.

It was shown above that theory allows a precise computation of the cross sections Q_t, provided the dielectric constant of water is given at the temperature of the drops. The concentration of N_k is a purely meteorological datum and must be obtained experimentally. As far as as the writer is aware, data on drop concentrations and drop size distributions are extremely scarce, and it appears that no systematic researches have as yet been undertaken for the purpose of obtaining such data.

Recently, observations were made available on drop size distributions in clouds of different types.[8,9] The main results of interest to the attenuation problem are that in clouds of different altitudes the diameter of the drops does not seem to exceed 0.02 cm. The liquid water content of the clouds examined by Mazur[9] varied between about 0.15 and 0.50 g/m^3. The results of Diem[8] are, on the whole, similar.

Some data on ice clouds are included in Best's memoranda.[11]

Data on fogs are extremely meager. The diameter of fog droplets appears to be of the same order of magnitude as those of liquid water clouds.[24,25] Humphreys, in his table of precipitation values, gives 0.006 g/m^3 as the liquid water content in fog.

The data on rains used in this report are those from reference 11. For additional data recently collected see reference 26.

The most important set of data which is directly usable in this work is contained in Table 6. In the last row of this table p is the precipitation rate or rate of rainfall, expressed in millimeters per hour, and results directly from the total volume of water falling per square meter per second, since $p = 36 \times 10^{-4} V$, where V is expressed in cubic millimeters per square meter per second.

Rains 1 and 2 refer, according to Best,[11] to a rain looking very ordinary, falling over a large area. Type 3 is a rain with breaks and sunshine. Type 4 corresponds to the beginning of a short rainfall like a thundershower. Type 5 refers to a sudden rain from a small cloud, associated with a calm, sultry atmosphere. Type 6 was a violent rain like a cloudburst with some hail. Types 7, 8, an 9 are for the heaviest period and the period of stopping of a continuous fall which at times took the form of a cloudburst. The preceding characteristics of the rains in Table 6 are quotations from the paper of Best.

These data on drop size distributions are the only data available to the writer. Clearly the rate of rainfall cannot be correlated from these data to any drop size distribution. A priori, it seems unlikely that a strict correlation between drop size distribution and rate of rainfall should exist. To a rain of given drop size distribution corresponds necessarily a determined rate of rainfall, but the reverse is not true, since a given rate of rainfall might be obtained with a large variety of drop size distribution.[10] In other words, the drop size distribution is the only physical characteristic of a rain as far as attenuation and back scattering (echo) of radiowaves are concerned.

In any one location, even the drop size distribution of a rain is but an instantaneous characteristic of that rain. No data are available concerning the fluctuations in time of drop size distribution.

The space distribution of raindrops is another problem on which too few data are available. According to Kerr and Rado,[10] K-band rain absorption experiments over a relatively short path (~4km) have shown that the simultaneous rates of rainfall at three points of such a path were almost invariably appreciably different. The rates were measured at the location of the transmitter, the receiver, and at a point in between. Needless to say, under such circumstances the possibility of a quantitative interpretation of the experimental data on attenuation is almost excluded.

Table 6. Drop size distributions in rains.

	Number of drops/m^2/sec in nine different types of rain								
D, cm	1	2	3	4	5	6	7	8	9
0.05	1,000	1,600	129	60	...	100	514	679	7
0.10	200	120	100	280	50	1,300	423	524	233
0.15	140	60	73	160	50	500	359	347	113
0.20	140	200	100	20	150	200	138	295	46
0.25	...	...	29	20	0	0	156	205	7
0.30	...	...	57	...	200	0	138	81	0
0.35	...	...	...	...	0	0	0	28	32
0.40	...	...	...	...	50	0	0	20	39
0.45	...	...	...	...	...	200	101	...	0
0.50	...	...	...	...	...	...	...	...	25
Total No. of drops	1,480	1,980	488	540	500	2,300	1,840	2,180	500
Total volume mm^3/m^2/sec	1,005	1,112	1,656	681.2	5,258	11,970	9,535	6,298	4,236
p mm/hr	3.6	4.0	6.0	2.46	18.9	43.1	34.3	22.6	15.2

It may be mentioned here that the earlier attenuation experiments on 1-cm waves by Robertson and his collaborators[27] as well as those of Mueller[3] on K/2 band were made over a shorter path (about 400 meters) and the rate of rainfall was measured only at one place, roughly in the middle of the path. Since the path length of the Oxford workers[28] was 2 km, there was ample room for possible fluctuations in the rate of precipitation. The K-band radar transmission studies by the Bell Telephone Laboratory workers were made over longer paths,[29] and here, too, a situation somewhat similar to those reported by the Radiation Laboratory workers might have existed, as the authors duly noticed it.

The meteorological irregularities which thus seem to be inherent in precipitation data eliminate the possibility of a quantitative theory of attenuation and back scattering of radiowaves by rains or other precipitation forms. Although the data contained in Table 7 are used extensively in this report, the results thus obtained should be regarded as semiquantitative indications rather than rigorous theoretical predictions.

Given the number of raindrops of known dimensions falling over a certain area in a given time and given also the terminal velocity of the drops, the spatial concentration of raindrops can be derived at once. In Figure 7 the terminal velocity curve is drawn

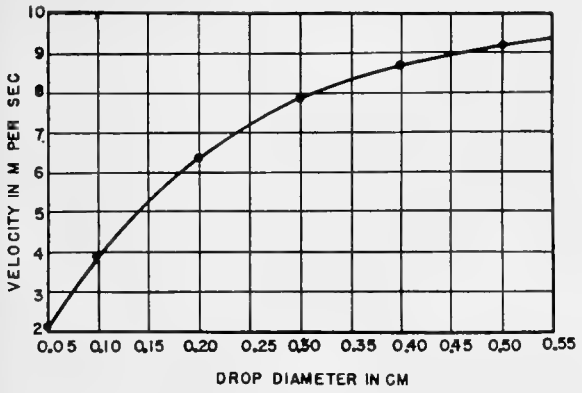

FIGURE 7. Terminal velocity of raindrops (experimental).

as a function of drop diameter. These velocities were measured at Porton and are quoted in Best's paper.[11]

From Table 6 we may obtain data for Table 7, giving raindrop concentration N_k of drops with diameter $k=D$ cm. These concentrations, as are the data included in Table 6, may be regarded as characteristic for rains of the indicated precipitation rate, but they are not necessarily typical for those rains. Also given is the liquid water content of the atmosphere associated with the rains of Table 6 and its graphical representation in Figure 8. The curve drawn on this graph should not, however, be considered as representing any functional relationship between the liquid

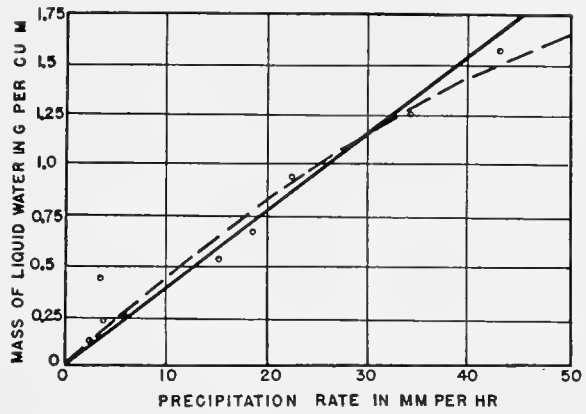

FIGURE 8. Computed liquid water distribution (cm^3/m^3 or g/m^3) based on experimental drop size distributions in different rains. The slope of the straight line approximation is 0.038 $g/m^3/mm/hr$.

water concentration of the rainy atmosphere and the rate of rainfall. It can indeed easily be proved that the liquid water concentration associated with a rain depends only on the fractional precipitation rates of the different drop groups. It does not depend directly on the total rate of rainfall. Any rain of given total precipitation rate can be built up by a number of drop size distributions which determine different liquid water concentrations in the atmosphere. This means that it is *theoretically* incorrect to draw a graph entitled "Liquid Water Concentration versus Rate of Rainfall", as is frequently done. A curve so drawn can however be of considerable practical value when rough concentrations corresponding to given rates of rainfall are desired.

It can be seen that the resulting liquid water distributions are in fair agreement with those reported by Humphreys in his table of precipitation values[25] already mentioned. It may be added here that aloft and in certain parts of rain clouds, where considerable updraft exists, the drop concentrations may be expected to be larger than those derived from Table 6.

These data will now be used in the computation of attenuation and back scattering by the different precipitation forms, assuming always ideal conditions and leaving aside the above-mentioned irregularities

TABLE 7. Number of raindrops per cubic meter in rains of different precipitation rates.

	Distribution								
	A	B	C	D	E	F	G	H	I
	p, mm/hr								
D, cm	2.46	3.6	4.0	6.0	15.2	18.7	22.6	34.3	43.1
0.05	28.5	476	752	61.4	3.33	.....	323	245	47.6
0.10	71.8	512	30.8	25.6	59.7	12.8	134	108	333
0.15	31	27	11.4	14	21.5	9.52	66	68.4	95.2
0.20	3.13	22	31.2	15.6	7.2	23.4	46.1	21.6	31.2
0.25	2.76	...	...	4.0	0.96	0	28.3	21.5	0
0.30	...	...	...	7.2	0	25.3	10.2	17.6	0
0.35	...	...	...	...	3.83	0	3.35	0	0
0.40	...	...	...	...	4.48	5.75	2.3	0	0
0.45	...	...	...	...	0	...	...	11.3	22.5
0.50	...	...	...	...	2.71	...	...	...	...
Liquid water g/m³	0.130	0.439	0.217	0.242	0.521	0.673	0.930	1.25	1.55

in space. For reasons stated above, theoretical results are significant only with regard to orders of magnitude.

10.1.6 Attenuation by Idealized Precipitation Forms

The data included in the preceding section show, first of all, that in clouds and fogs the attenuation can be given rigorously. Indeed, Table 3 indicates that the critical diameter even for waves of 1-cm wavelength is over 0.06 cm. Since we have seen that in clouds and fogs the drop diameters never exceed 0.02 cm, it appears that formula (51) is applicable, and the attenuation of all waves of wavelength $\lambda \geq 1$ cm is independent of the size of the drops. Furthermore, taking $m = 1$ g per cubic meter in formula (51) one probably obtains an upper limit for the attenuation of these waves.[1] In Figure 9 the attenuation is plotted down to $\lambda = 0.2$ cm. The dielectric constant of water has been computed in this range by using the Debye formula for wavelengths $\lambda > 1$ cm. Clearly the attenuation in fogs and clouds even in the region $\lambda \sim 1$ cm is not of great importance except for long ranges and radar observations. The attenuation becomes negligible for waves with $\lambda \geq 10$ cm.

Table 3 also shows that the attenuation becomes practically independent of the drop size distribution for wavelengths equal to or larger than about 20 cm. In the 5- to 20-cm range the three-term formula (48) or (50) in connection with (54) will represent fairly well the attenuation in different rains, with increased accuracy at longer wavelengths. Below $\lambda = 5$ cm this formula is inapplicable, but there Ryde

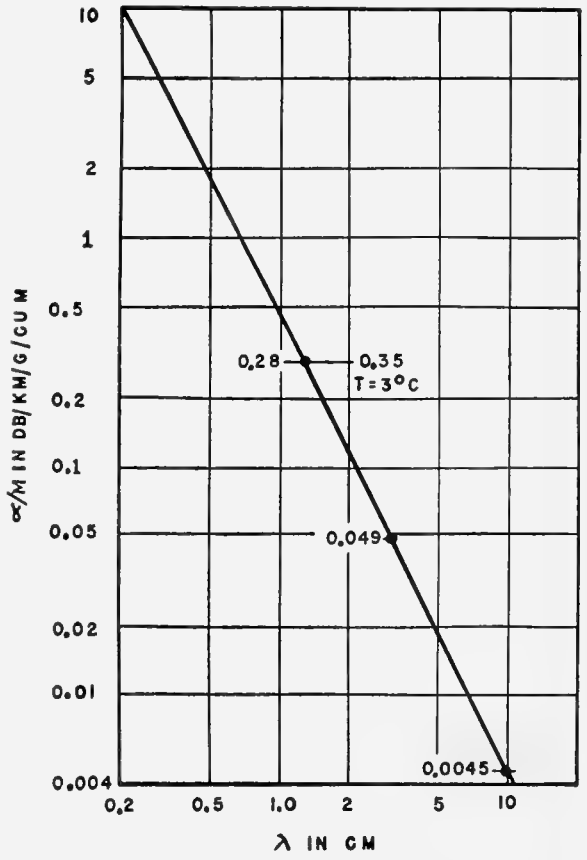

FIGURE 9. Attenuation factor in liquid clouds and fogs. $t = 18$ C.

[1] Attention may be called to the absence of data on the liquid water distributions in heavy sea fogs.

and Ryde's[12] exact attenuation values are available. The attenuation formula in a rain, as given by equation (54), can be transformed easily to another form. If p_k denotes the partial precipitation rate of the drops of k cm diameter in a given rain of total precipitation rate p, then clearly,

$$p = \sum_{k=0}^{s} p_k, \tag{55}$$

s being the diameter of the largest drops in this rain. Now

$$p_k = 3.6 \times 10^6 V_k v_k N_k \text{ mm per hour}, \tag{56}$$

where V_k is the volume of a raindrop of k cm diameter, v_k is its terminal velocity in meters per second and N_k is their number per cubic centimeter. The attenuation of a rain of total precipitation rate p is, then, according to equation (54),

$$\alpha_{\lambda,p} = \sum_{k=0}^{s} \alpha_\lambda(p_k) = \frac{0.4343}{3.6} \sum_{k=0}^{s} \frac{p_k Q_{t,k}}{V_k v_k} \text{ db per kilometer}, \tag{57}$$

after substituting N_k from equation (56) into (54).

For a given wavelength λ, the ratio $Q_{t,k}/V_k v_k$ is a constant characteristic of drops whose diameter is k cm. This ratio will be denoted by q_k. The attenuation formula then becomes, finally,

$$\alpha_p = 0.126 \sum_{k=0}^{s} p_k q_k, \tag{58}$$

which shows that the attenuation in rains of a total precipitation rate of p mm per hr depends linearly on the individual precipitation rates p_k of all the drop groups k which build up this rain. The attenuation does not depend directly on the total precipitation rate p. The points representing the experimental observations in the coordinate plane (α,p) should cover a certain region of this plane, but no single curve $\alpha(p)$ exists, since there is no direct relationship between α and p. A curve drawn in this plane is significant only in so far as it permits one to predict a possible attenuation value in any rain of given precipitation rate or vice versa.

It is, however, possible to draw in the (α,p) coordinate plane a straight line which, at a given wavelength, will represent the theoretical upper limit for the attenuation. Indeed, using Table 6 for the attenuation in fictitious rains with a distribution of one drop per cubic centimeter, and Table 9, giving the precipitation associated with the same fictitious rains, one may compute the ratio α_k/p_k for any such rain formed by a single group of drops of diameter k cm and the precipitation rate p_k of the same rain. This ratio for a given wavelength λ of the radiation varies with k, the diameter of the drops, and in the diameter range 0 to 0.55 cm this ratio takes on an optimum value for a certain diameter D. This, then, is the slope of the straight line in the (α,p) plane which determines the theoretical upper limit α_{max} of the attenuation in any rain of total rainfall p.

TABLE 8. Precipitation rates p/N in fictitious rains with a concentration of one drop per cubic centimeter.

Drop diameter D, cm	p/N mm/hr
0.05	4.99×10^2
0.10	7.34×10^3
0.15	3.34×10^4
0.20	9.6×10^4
0.25	2.14×10^5
0.30	4.08×10^5
0.35	6.76×10^5
0.40	1.05×10^6
0.45	1.54×10^6
0.50	2.17×10^6
0.55	2.92×10^6

The different steps taken in computing the total attenuation equation (58) in a rain of total rate of fall of p mm per hour appear in Figure 10 where the drop size distribution and the partial attenuations due to the different drop groups of a 22.6-mm per

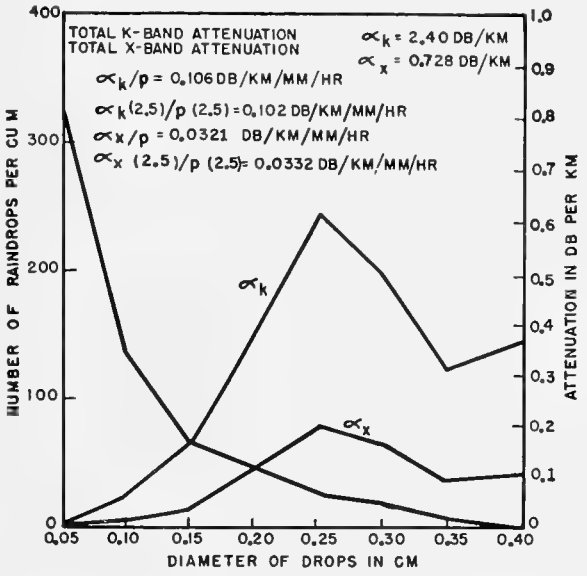

FIGURE 10. Drop size distribution and attenuation in a 22.6-mm per hr rain. Unlabeled curve represents N_k values; number of raindrops per cu m = N_k.

TABLE 9. Attenuation in rains of known drop size distribution and rate of fall (db/km).

mm/hr	λ, cm 1.25	3	5	8	10	15	20	30	50	75	100	Distribution
2.46	$1.93\,10^{-1}$	$4.92\,10^{-2}$	$4.24\,10^{-3}$	$1.23\,10^{-3}$	$7.34\,10^{-4}$	$2.80\,10^{-4}$	$1.52\,10^{-4}$	$6.49\,10^{-5}$	$2.33\,10^{-5}$	$1.03\,10^{-5}$	$5.85\,10^{-6}$	A
4.0	$3.18\,10^{-1}$	$8.63\,10^{-2}$	$7.11\,10^{-3}$	$2.04\,10^{-3}$	$1.19\,10^{-3}$	$4.69\,10^{-4}$	$2.53\,10^{-4}$	$1.08\,10^{-4}$	$3.88\,10^{-5}$	$1.72\,10^{-5}$	$9.75\,10^{-6}$	C
6.0	$6.15\,10^{-1}$	$1.92\,10^{-1}$	$1.25\,10^{-2}$	$3.02\,10^{-3}$	$1.67\,10^{-3}$	$5.84\,10^{-4}$	$3.02\,10^{-4}$	$1.25\,10^{-4}$	$4.34\,10^{-5}$	$1.93\,10^{-5}$	$1.09\,10^{-5}$	D
15.2	2.12	$6.13\,10^{-1}$	$5.91\,10^{-2}$	$1.17\,10^{-2}$	$5.68\,10^{-3}$	$1.69\,10^{-3}$	$7.85\,10^{-4}$	$2.95\,10^{-4}$	$9.23\,10^{-5}$	$4.15\,10^{-5}$	$2.35\,10^{-5}$	E
18.7	2.37	$8.01\,10^{-1}$	$5.13\,10^{-2}$	$1.10\,10^{-2}$	$6.46\,10^{-3}$	$1.85\,10^{-3}$	$9.09\,10^{-4}$	$3.60\,10^{-4}$	$1.20\,10^{-4}$	$5.36\,10^{-5}$	$3.03\,10^{-5}$	F
22.6	2.40	$7.28\,10^{-1}$	$5.29\,10^{-2}$	$1.21\,10^{-2}$	$6.96\,10^{-3}$	$2.27\,10^{-3}$	$1.17\,10^{-3}$	$4.81\,10^{-4}$	$1.66\,10^{-4}$	$7.41\,10^{-5}$	$4.19\,10^{-5}$	G
34.3	4.51	1.28	$1.12\,10^{-1}$	$2.32\,10^{-2}$	$1.17\,10^{-2}$	$3.64\,10^{-3}$	$1.75\,10^{-3}$	$6.83\,10^{-4}$	$2.24\,10^{-4}$	$9.95\,10^{-5}$	$5.63\,10^{-5}$	H
43.1	6.17	1.64	$1.65\,10^{-1}$	$3.33\,10^{-2}$	$1.62\,10^{-2}$	$4.96\,10^{-3}$	$2.29\,10^{-3}$	$8.71\,10^{-4}$	$2.78\,10^{-4}$	$1.23\,10^{-4}$	$6.98\,10^{-5}$	I

hour rain are plotted. It is seen that the numerous smaller drops hardly contribute to the attenuation, which is caused mostly by the fewer larger drops and has a maximum around the 2.5-mm drops.

In Table 9 is given the total attenuation (decibels per kilometer) in the wavelength range 1.25 to 100 cm in different rains of precipitation rates ranging from 2.46 to 43.1 mm per hour corresponding to given distributions. In Figure 11 are plotted some curves showing, for a few rains, the variation of the total attenuation factor as a function of the wavelength. The dashed portions of these curves join the points previously computed,[12] the calculations starting at $\lambda = 5$ cm.

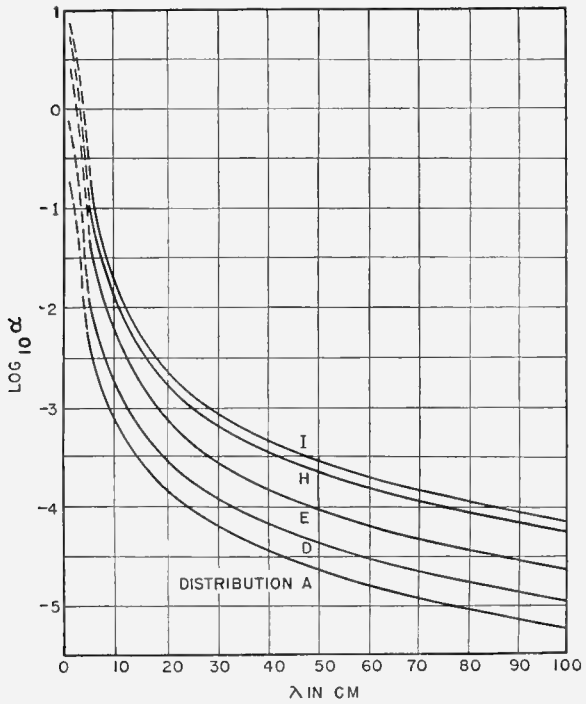

FIGURE 11. Attenuation in rains of known drop size distribution as a function of the wavelength. The abscissa gives the wavelength, λ, in centimeters. The ordinate scale gives $\log_{10} \alpha$, where the attenuation constant, α, is expressed in decibels per kilometer. The letters on the curves refer to the drop size distributions given in Table 7.

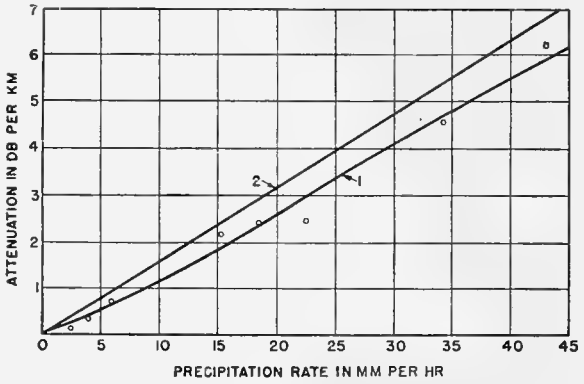

FIGURE 12. (1) Computed K-band attenuation based on experimental drop size distributions. (2) Theoretical upper limit. $\alpha/p = 0.16$ db/km/mm/hr. $t = 18$ C.

Figures 12, 13, and 14 represent, at three typical wavelengths, the total attenuations in different rains. The results of the calculation are represented by the points indicated on these figures, and the smooth curve passing through these points serves to illustrate the

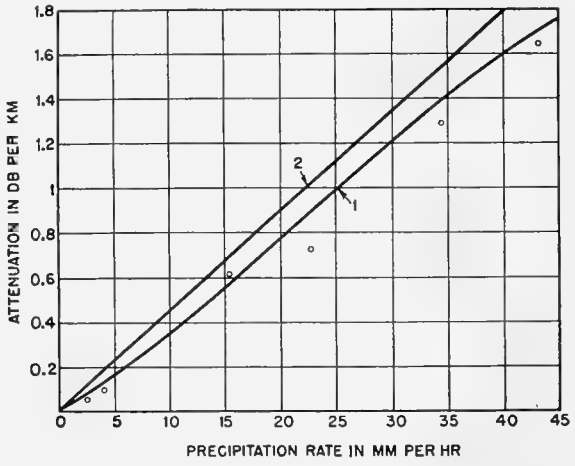

FIGURE 13. (1) Computed X-band attenuation based on experimental drop size distributions. (2) Theoretical upper limit. $\alpha/p = 0.045$ db/km/mm/hr. $t = 18$ C

procedure usually followed by the experimental workers, as we have already mentioned. It is evident that these curves have little, if any, direct physical significance. Similarly the curves of Figure 11 associated with different rains merely indicate the trend of variation of α as a function of the wavelength, since no single curve of this type can characterize a rain of given total precipitation rate of p mm per hour.

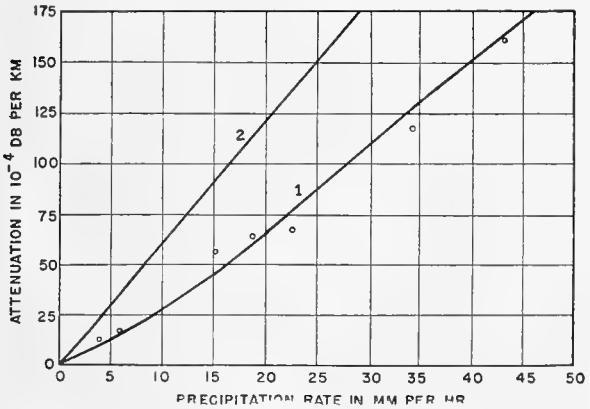

FIGURE 14. (1) Computed S-band attenuations based on experimental drop size distributions in different rains. (2) Theoretical upper limit of α/p, attenuation per unit rate of precipitation, is 6.10^{-4}db/km/mm/hr. $t = 18$ C.

Table 9 shows that the attenuation is of no practical importance for S band and longer waves even with the heaviest rains or cloudbursts. This result is summarized in Table 10 (the theoretical upper limits of the attenuations per unit precipitation rate).

TABLE 10. Theoretical upper limits of attenuation per unit precipitation rate ($t \sim 18$ C).

λ, cm	$(\alpha/p)_{max}$ db/km/mm/hr
1.25	1.6×10^{-1}
3	4.5×10^{-2}
5	5.0×10^{-3}
8	1.0×10^{-3}
10	6.0×10^{-4}
15	3.0×10^{-4}
20	1.4×10^{-4}
30	6.4×10^{-5}

These values in Table 10 correspond to raindrop temperatures of about 18 C. At lower temperatures the values of (α/p) included in this table might be increased about 25 to 30 per cent.

The results of the different workers in the field are summarized in Table 11.

It will be seen that the above values of α/p compare favorably with the theoretical values.[j] The difficulties in the interpretation of the experimental data as mentioned already should be kept in mind when comparing the experimental values with the theoretical predictions.

[j]The same seems to be true of S-band wavelengths where rough attenuation measurements are available in "solid" storm clouds.[31]

TABLE 11. Experimental values of the attenuation per unit precipitation rate.

λ, cm	(α/p) db/km/mm/hr	Authority
0.62	0.37	Mueller[3]
0.96	0.15	Adam *et al*[28]
1.089	0.2	Robertson[27]
1.25	0.19	Southworth *et al*[29]
	0.09—0.40	Rado[10]
3.2	0.032—0.042	King and Robertson[30]

As remarked by Ryde and Ryde,[12] the attenuation by hailstones and snow should be appreciably smaller than that due to raindrops, the dielectric constant of ice being considerably smaller than that of liquid water.

A final remark may be made concerning the theoretical results given here. It has been assumed throughout the preceding discussion that the raindrops are spherical. This is likely to be the case with practically all the drop groups existing in rains, with the exception of the biggest drops, which may undergo deformations. Presumably the effects of small deformations are not of great importance.

10.1.7 The Scattering of Microwaves by Spherical Raindrops

The cross section for scattering of electromagnetic waves by spherical particles is given for any direction by equation (34). Using the approximate expressions of the amplitudes as given by equations (38) and (43) and the notation $\alpha_1^{(5)}$, $\bar{\alpha}_1^{(5)}$, $\beta_1^{(3)}$, $\bar{\beta}_1^{(3)}$ representing the real and imaginary coefficients of ρ^5 in a_1^r, of ρ^3 in b_1^r, etc., as indicated above, we get the following expression for the total scattering cross section:

$$Q_s = \frac{\lambda^2}{2\pi}\rho^6\Big\{3\,|\,\beta_1^{(3)}\,|^2 + 6\,[\beta_1^{(3)}\beta_1^{(5)} + \bar{\beta}_1^{(3)}\bar{\beta}_1^{(5)}]\,\rho^2 + 6\,[\beta_1^{(3)}\beta_1^{(6)} + \bar{\beta}_1^{(3)}\bar{\beta}_1^{(6)}]\,\rho^3 + \{3\,[\,|\,\alpha_1^{(5)}\,|^2 + |\,\beta_1^{(5)}\,|^2] + 5\,|\,\beta_2^{(5)}\,|^2\}\rho^4 + 6\,[\beta_1^{(5)}\beta_1^{(6)} + \bar{\beta}_1^{(5)}\bar{\beta}_1^{(6)}]\,\rho^5 + 3\,|\,\beta_1^{(6)}\,|^2\rho^6 + \cdots\Big\}\ \text{cm}^2. \tag{59}$$

Here, for instance,

$$|\,\beta_1^{(3)}\,| = [\beta_1^{(3)}]^2 + [\bar{\beta}_1^{(3)}]^2;\ |\,\alpha_1^{(5)}\,|^2 = (\alpha_1^{(5)})^2 + (\bar{\alpha}_1^{(5)})^2, \text{ etc.}$$

For values of $\rho \ll 1$ and when the terms in ρ^2 and higher powers can be neglected in the braces, the total cross section for scattering reduces, using the explicit expressions of $\beta_1^{(3)}$ and $\bar{\beta}_1^{(3)}$, to

$$Q_{s,\,\rho<<1} = \frac{128\pi^5 a^6}{3\lambda^4} \cdot \frac{(\epsilon_r-1)^2(\epsilon_r+2)^2+\epsilon_i^2[2(\epsilon_r-1)(\epsilon_r+2)+9]+\epsilon_i^4}{[(\epsilon_r+2)^2+\epsilon_i^2]^2} \text{ cm}^2. \tag{60}$$

When the dielectric absorption vanishes, i.e., $\epsilon_i \longrightarrow 0$, this reduces further to

$$Q_{s,\,\rho<<1,\,\epsilon_i\longrightarrow 0} = \frac{128\pi^5 a^6}{3\lambda^4}\left(\frac{n^2-1}{n^2+2}\right)^2 \text{ cm}^2, \tag{61}$$

which is the well-known Rayleigh scattering cross section, since $\epsilon_r = n^2$ in this case.

In Table 12 are given the scattering cross sections computed within the range of ρ, 0.00157 to 0.576, or in the drop diameter range 0.05 to 0.55 cm and wavelength range 3 to 100 cm. Needless to say, the actual cross sections for scattering at the larger ρ values are always larger than the Rayleigh cross sections [equation (60)]. For $\rho < 0.10$ the scattering cross sections are, within a few per cent, given by the first Rayleigh term (60) of equation (59). However, in the present case of absorbing spherical drops, the parametric representation (59) of the cross section is not of much practical interest since some of the coefficients of the powers of ρ are strongly dependent on the wavelength. The cross section is not a unique function of $\rho = (\pi D/\lambda)$ but is a complicated function of λ and D, and the series representation is valid only in describing the dependence on the diameter D of the drops, the wavelength being kept constant. In Figures 15 and 16 two families of curves have been plotted representing Q_s as a function of the diameter D of the raindrops at constant wavelength and as a function of the wavelength at constant diameter, respectively.

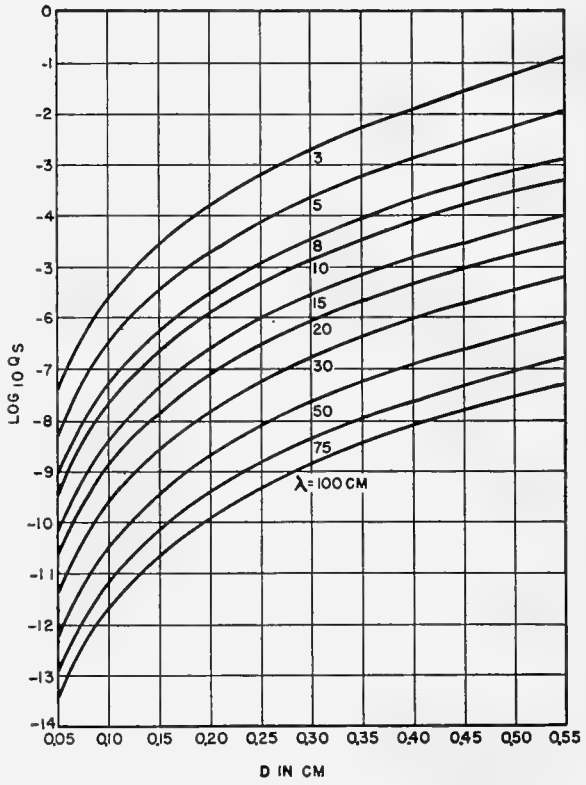

FIGURE 15. Scattering cross section, Q_s, of spherical water drops as a function of the drop diameter. The abscissa gives the drop diameter, D, in centimeters. The ordinate scale gives $\log_{10} Q_s$, the scattering cross section Q_s being expressed in square centimeters. The numbers on the curves indicate the wavelength, λ, of the incident radiation in centimeters.

The knowledge of the total scattering cross section Q_s and the total cross section Q_t allows at once the computation of the absolute probabilities ω_s for electromagnetic waves falling on spherical water drops to be

TABLE 12. Total scattering cross section Q_s (cm²) of spherical water drops of D cm diameter.

	D, cm										
λ, cm	0.05	0.10	0.15	0.20	0.25	0.30	0.35	0.40	0.45	0.50	0.55
3	$3.62\,10^{-8}$	$2.35\,10^{-6}$	$2.74\,10^{-5}$	$1.58\,10^{-4}$	$6.06\,10^{-4}$	$1.98\,10^{-3}$	$5.36\,10^{-3}$	$1.31\,10^{-2}$	$2.96\,10^{-2}$	$6.36\,10^{-2}$	$1.31\,10^{-1}$
5	$4.70\,10^{-9}$	$3.04\,10^{-7}$	$3.51\,10^{-6}$	$1.97\,10^{-5}$	$7.56\,10^{-5}$	$2.32\,10^{-4}$	$5.97\,10^{-4}$	$1.36\,10^{-3}$	$2.86\,10^{-3}$	$5.61\,10^{-3}$	$1.04\,10^{-2}$
8	$7.23\,10^{-10}$	$4.64\,10^{-8}$	$5.35\,10^{-7}$	$2.98\,10^{-6}$	$1.14\,10^{-5}$	$3.44\,10^{-5}$	$8.72\,10^{-5}$	$1.96\,10^{-4}$	$4.01\,10^{-4}$	$7.65\,10^{-4}$	$1.37\,10^{-3}$
10	$2.93\,10^{-10}$	$1.88\,10^{-8}$	$2.15\,10^{-7}$	$1.21\,10^{-6}$	$4.62\,10^{-6}$	$1.38\,10^{-5}$	$3.50\,10^{-5}$	$7.85\,10^{-5}$	$1.59\,10^{-4}$	$3.01\,10^{-4}$	$5.41\,10^{-4}$
15	$5.80\,10^{-11}$	$3.75\,10^{-9}$	$4.33\,10^{-8}$	$2.43\,10^{-7}$	$9.03\,10^{-7}$	$2.70\,10^{-6}$	$6.80\,10^{-6}$	$1.52\,10^{-5}$	$3.10\,10^{-5}$	$5.87\,10^{-5}$	$1.04\,10^{-4}$
20	$1.83\,10^{-11}$	$1.17\,10^{-9}$	$1.35\,10^{-8}$	$7.51\,10^{-8}$	$2.86\,10^{-7}$	$8.53\,10^{-7}$	$2.16\,10^{-6}$	$4.81\,10^{-6}$	$9.74\,10^{-6}$	$1.83\,10^{-5}$	$3.25\,10^{-5}$
30	$3.62\,10^{-12}$	$2.32\,10^{-10}$	$2.66\,10^{-9}$	$1.49\,10^{-8}$	$5.66\,10^{-8}$	$1.69\,10^{-7}$	$4.11\,10^{-7}$	$9.51\,10^{-7}$	$1.92\,10^{-6}$	$3.62\,10^{-6}$	$6.43\,10^{-6}$
50	$4.65\,10^{-13}$	$2.99\,10^{-11}$	$3.44\,10^{-10}$	$1.91\,10^{-9}$	$7.29\,10^{-9}$	$2.18\,10^{-8}$	$5.51\,10^{-8}$	$1.22\,10^{-7}$	$2.48\,10^{-7}$	$4.65\,10^{-7}$	$8.27\,10^{-7}$
75	$9.22\,10^{-14}$	$5.91\,10^{-12}$	$6.79\,10^{-11}$	$3.78\,10^{-10}$	$1.44\,10^{-9}$	$4.31\,10^{-9}$	$1.08\,10^{-8}$	$2.42\,10^{-8}$	$4.91\,10^{-8}$	$9.22\,10^{-8}$	$1.63\,10^{-7}$
100	$2.93\,10^{-14}$	$1.88\,10^{-12}$	$2.15\,10^{-11}$	$1.20\,10^{-10}$	$4.56\,10^{-10}$	$1.37\,10^{-9}$	$3.45\,10^{-9}$	$7.64\,10^{-9}$	$1.56\,10^{-8}$	$2.93\,10^{-8}$	$5.20\,10^{-8}$

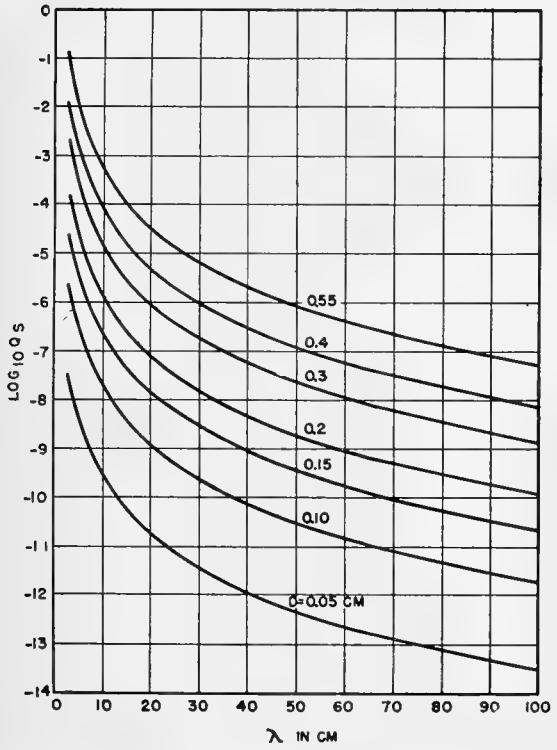

FIGURE 16. Scattering cross section, Q_s, of spherical water drops as a function of the wavelength. The abscissa gives the wavelength, λ, of the incident radiation in centimeters. The ordinate scale gives $\log_{10} Q_s$, the cross section Q_s being expressed in square centimeters. The numbers of the curves indicate the drop diameter, D, in centimeters.

scattered in any direction and the absolute probabilities $\tilde{\omega}_{abs}$ for being absorbed by the drops, the absorbed energy being then transformed into heat in the drops (true absorption). Indeed, this probability ω_s of the waves being scattered in any direction is equal to the ratio of the scattering cross section Q_s to the cross section Q_t which is associated with all the possible eventualities, here only two, namely, scattering and true absorption. Hence,

$$\tilde{\omega}_s = \frac{Q_s}{Q_t} \tag{62}$$

and, consequently, the probability of true absorption is

$$\tilde{\omega}_{abs} = 1 - \tilde{\omega}_s. \tag{63}$$

In Table 13 are given the probabilities $\tilde{\omega}_s$ in the drop diameter range 0.05 to 0.55 cm and wavelength range 3 to 100 cm. A glance at this table shows that with the exception of the shortest wavelengths and largest drops the probability of the waves being truly absorbed is always much larger than that of their being scattered. The smaller the drops the greater the chance of absorption, since, according to the cross-section formulas, for small drops Q_s is proportional to D^6/λ^4 (Rayleigh's law) whereas $Q_t \sim Q_{abs}$ is proportional to D^3/λ and in our case the drop diameter D is always smaller than the wavelength λ of the radiation.

10.1.8 Back Scattering (Echoes)

Whereas the attenuation of microwaves is of interest to both communication and radar, back scattering is of importance to radar only. The importance of the echo phenomena is twofold. On the one hand, it is of operational interest to distinguish between atmospheric echoes of the waves and their reflection from other targets in the atmosphere. On the other hand, the observation of these phenomena has led to the recognition of its meteorological value in helping to map the storm topography of the atmosphere (storm detection) around the position of the observer and at ranges limited only by the characteristics of the radar set used.[14,31-33]

The echo intensities may be computed from formula (35) for the differential cross section of drops $\sigma(\pi)$ for back scattering (scattering angle π).

TABLE 13. Probability of scattering $\tilde{\omega}_s$ by spherical water drops of D cm diameter.

	λ, cm									
D, cm	3	5	8	10	15	20	30	50	75	100
0.05	$3.94\ 10^{-3}$	$1.64\ 10^{-3}$	$6.63\ 10^{-4}$	$4.25\ 10^{-4}$	$1.94\ 10^{-4}$	$1.09\ 10^{-4}$	$4.92\ 10^{-5}$	$1.74\ 10^{-5}$	$7.74\ 10^{-6}$	$4.33\ 10^{-6}$
0.10	$1.54\ 10^{-2}$	$1.09\ 10^{-2}$	$4.89\ 10^{-3}$	$3.22\ 10^{-3}$	$1.53\ 10^{-3}$	$8.60\ 10^{-4}$	$3.91\ 10^{-4}$	$1.40\ 10^{-4}$	$6.33\ 10^{-5}$	$3.47\ 10^{-5}$
0.15	$2.11\ 10^{-2}$	$2.90\ 10^{-2}$	$1.47\ 10^{-2}$	$9.96\ 10^{-3}$	$5.00\ 10^{-3}$	$2.87\ 10^{-3}$	$1.32\ 10^{-3}$	$4.73\ 10^{-4}$	$2.11\ 10^{-4}$	$1.17\ 10^{-4}$
0.20	$2.86\ 10^{-2}$	$5.15\ 10^{-2}$	$2.91\ 10^{-2}$	$2.10\ 10^{-2}$	$1.11\ 10^{-2}$	$6.51\ 10^{-3}$	$3.05\ 10^{-3}$	$1.10\ 10^{-3}$	$3.95\ 10^{-4}$	$2.76\ 10^{-4}$
0.25	$3.72\ 10^{-2}$	$7.60\ 10^{-2}$	$4.75\ 10^{-2}$	$3.16\ 10^{-2}$	$1.97\ 10^{-2}$	$1.21\ 10^{-2}$	$5.81\ 10^{-3}$	$2.14\ 10^{-3}$	$9.66\ 10^{-4}$	$5.37\ 10^{-4}$
0.30	$5.31\ 10^{-2}$	$1.03\ 10^{-1}$	$6.91\ 10^{-2}$	$5.33\ 10^{-2}$	$3.12\ 10^{-2}$	$1.75\ 10^{-2}$	$9.77\ 10^{-3}$	$3.66\ 10^{-3}$	$1.61\ 10^{-3}$	$9.32\ 10^{-4}$
0.35	$8.06\ 10^{-2}$	$1.29\ 10^{-1}$	$9.06\ 10^{-2}$	$7.28\ 10^{-2}$	$4.50\ 10^{-2}$	$2.96\ 10^{-2}$	$1.45\ 10^{-2}$	$5.76\ 10^{-3}$	$2.60\ 10^{-3}$	$1.47\ 10^{-3}$
0.40	$1.21\ 10^{-1}$	$1.54\ 10^{-1}$	$1.13\ 10^{-1}$	$9.31\ 10^{-2}$	$6.66\ 10^{-2}$	$4.11\ 10^{-2}$	$2.17\ 10^{-2}$	$8.42\ 10^{-3}$	$3.88\ 10^{-3}$	$2.18\ 10^{-3}$
0.45	$1.95\ 10^{-1}$	$1.84\ 10^{-1}$	$1.35\ 10^{-1}$	$1.14\ 10^{-1}$	$7.79\ 10^{-2}$	$5.47\ 10^{-2}$	$2.96\ 10^{-2}$	$1.19\ 10^{-2}$	$5.50\ 10^{-3}$	$3.11\ 10^{-3}$
0.50	$2.96\ 10^{-1}$	$2.17\ 10^{-1}$	$1.58\ 10^{-1}$	$1.34\ 10^{-1}$	$9.63\ 10^{-2}$	$6.88\ 10^{-2}$	$3.90\ 10^{-2}$	$1.59\ 10^{-2}$	$7.43\ 10^{-3}$	$4.23\ 10^{-3}$
0.55	$4.82\ 10^{-1}$	$2.49\ 10^{-1}$	$1.80\ 10^{-1}$	$1.56\ 10^{-1}$	$1.15\ 10^{-1}$	$8.44\ 10^{-2}$	$4.95\ 10^{-2}$	$2.08\ 10^{-2}$	$9.82\ 10^{-3}$	$5.61\ 10^{-3}$

According to equation (22), the power scattered by a spherical particle per unit solid angle at a point (r,θ,ϕ) is

$$\left(\frac{dP_s}{d\omega}\right)_{\theta,\phi} = \frac{1}{2\eta_2} \cdot [\,|E_\theta^s|^2 + |E_\phi^s|^2]\, r^2. \qquad (64)$$

Using equations (16) and (17), we obtain, remembering that the incident power per unit area is $(1/2\eta_2)\, E_0^2$, the following expression for the differential scattering cross section:

$$\left(\frac{dQ_s}{d\omega}\right)_{\theta,\phi} = \sigma(\theta,\phi)$$

$$= \left(\frac{\lambda}{2\pi}\right)^2 \mathrm{Re} \sum_{n=1}^{n=\infty} \sum_{m=1}^{m=\infty} \frac{(2n+1)(2m+1)}{n(n+1)\, m(m+1)} \cdot$$

$$\left[a_n a_m^* \left(\frac{P_n^1 P_m^1}{\sin^2\theta} \cos^2\phi + \frac{dP_n^1}{d\theta}\frac{dP_m^1}{d\theta} \sin^2\phi \right) \right.$$

$$+ b_n b_m^* \left(\frac{P_n^1 P_m^1}{\sin^2\theta} \sin^2\phi + \frac{dP_n^1}{d\theta}\frac{dP_m^1}{d\theta} \cos^2\phi \right)$$

$$\left. + 2a_n b_m^* \left(\frac{P_n^1}{\sin\theta}\frac{dP_m^1}{d\theta} \cos^2\phi + \frac{P_m^1}{\sin\theta}\frac{dP_n^1}{d\theta} \sin^2\phi \right) \right] \mathrm{cm}^2. \qquad (65)^k$$

Or, limiting ourselves to the approximation where only the electric dipole (b_1), electric quadrupole (b_2), and magnetic dipole (a_1) are effective, we find, using the explicit expressions of the associated Legendre polynomials,

$$\left(\frac{dQ_s}{d\omega}\right)_{\theta,\phi} = \sigma(\theta,\phi)$$

$$= \left(\frac{\lambda}{4\pi}\right)^2 \cdot$$

$$\mathrm{Re}\Big[9|b_1|^2 (\sin^2\phi + \cos^2\theta\cos^2\phi) + 9|a_1|^2(\cos^2\phi + \cos^2\theta\sin^2\phi)$$

$$+ 25|b_2|^2 (\cos^2\theta\sin^2\phi + \cos^2(2\theta)\cos^2\phi)$$

$$+ 18 a_1 b_1^* \cos\theta + 30 b_1 b_2^* \cos\theta(\sin^2\phi + \cos(2\theta)\cos^2\phi)$$

$$+ 30 a_1 b_2^* (\cos^2\theta\sin^2\phi + \cos(2\theta)\cos^2\phi) \Big]\ \mathrm{cm}^2. \qquad (66)$$

Here the first term inside the brackets represents the contribution of the electric dipole, the second is the magnetic dipole term, the third is the electric quadrupole term, and the three others correspond to interference terms between these three poles.

In the optical case it is known that the larger the parameter $\rho = \pi D/\lambda$, i.e., the nearer the wavelength is to the diameter of the scattering sphere, the more the radiation is scattered forward than backward. A study of equation (66) for water drops of 1-cm diameter shows that for spheres of this size it is only when $\lambda \geq 15$ cm or $\rho \leq 0.2$ that the back-scattered intensity is about the same as the forward-scattered intensity. For such ρ values only the dipole term in equation (66) remains of practical importance.

Suppose that we adopt a ρ value of 0.2 as a rough indication of what happens in the case of actual raindrops, the diameter of which is less than about 0.55 cm. It is then seen that for radar purposes the use of longer waves is favored, as far as the amount of back-scattered power is concerned, viz., in those cases where the greatest amount of back scattering from water drops is of operational importance. This will clearly occur in radar meteorology. However, when it is desirable to limit as much as possible the back scattering from rain or rainclouds, one might make use of this forward-backward scattering dissymmetry, which is the more pronounced the shorter the wavelength as compared with the diameter of the raindrops. This dissymmetry might, however, be counterbalanced by a rapid increase in the attenuation as well as a general decrease in the intensity of scattering.

The differential cross section for back scattering results from equation (66) by taking $\theta = \pi$ there. Using the explicit expressions (43) of the amplitudes a_1, b_1, and b_2, one obtains for this back scattering (or radar cross section)

$$\sigma(\pi) = \left(\frac{\lambda}{4\pi}\right)^2 \rho^6 (A_0 + A_2\rho^2 + A_3\rho^3 + A_4\rho^4 + A_5\rho^5 + A_6\rho^6 + \cdots)\ \mathrm{cm}^2, \qquad (67)$$

with the following coefficients A^n, using the notation defined by equations (45), (46), and (59):

$$A_0 = 9|\beta_1^{(3)}|^2,$$

$$A_2 = 18\,[\beta_1^{(3)}\beta_1^{(5)}\bar{\beta}_1^{(3)}\bar{\beta}_1^{(5)} - \alpha_1^{(5)}\beta_1^{(3)} - \bar{\alpha}_1^{(5)}\bar{\beta}_1^{(3)}] - 30\,[\beta_1^{(3)}\beta_2^{(5)} + \bar{\beta}_1^{(3)}\bar{\beta}_2^{(5)}],$$

$$A_3 = 18\,[\beta_1^{(3)}\beta_1^{(6)} + \bar{\beta}_1^{(3)}\bar{\beta}_1^{(6)}], \qquad (68)$$

$$A_4 = 9\,[|\alpha_1^{(5)}|^2 + |\beta_1^{(5)}|^2] - 18\,[\alpha_1^{(5)}\beta_1^{(5)} + \bar{\alpha}_1^{(5)}\bar{\beta}_1^{(5)}] - 30\,[\beta_1^{(5)}\beta_2^{(5)} + \bar{\beta}_1^{(5)}\bar{\beta}_2^{(5)} - \alpha_1^{(5)}\beta_2^{(5)} - \bar{\alpha}_1^{(5)}\bar{\beta}_2^{(5)}] + 25|\beta_2^{(5)}|^2,$$

$$A_5 = 18\,[\beta_1^{(5)}\beta_1^{(6)} + \bar{\beta}_1^{(5)}\bar{\beta}_1^{(6)} - \alpha_1^{(5)}\beta_1^{(6)} - \bar{\alpha}_1^{(5)}\bar{\beta}_1^{(6)}] - 30\,[\beta_1^{(6)}\beta_2^{(5)} + \bar{\beta}_1^{(6)}\bar{\beta}_2^{(5)}],$$

$$A_6 = 9|\beta_1^{(6)}|^2.$$

The radar cross-section formula (67) is the same as that given by Ryde.[17] Again $\sigma(\pi)$ is not a function

[k] With $\theta = \pi$ this reduces to equation (27) of the radar cross section.

of ρ only since the coefficients of the successive powers of ρ in the expansion (67) depend on the wavelength. The computed echo cross sections $\sigma(\pi)$ for spherical water drops with diameters in the range 0.05 to 0.55 cm and the wavelength range 3 to 100 cm are given in Table 14.[l] These cross sections reduce practically to the Rayleigh type, i.e., the series (67) reduces to its first term for the smaller drops at any wavelength and for any drops for wavelengths larger than about 15 cm. Since the Rayleigh term predominates in $\sigma(\pi)$, with the exception of the larger drops and smaller wavelengths, the trends of variation of $\sigma(\pi)$ with either the diameter, at constant wavelength, or the wavelength, at constant diameter, are similar to those of Q_s, the total scattering cross section. A graphical representation of the data of Table 14 is thus of no particular interest; they appear implicitly in Figures 15 and 16.

In order to compute the radar attenuation factor α associated with echo phenomena occurring with rain of known drop size distribution, we have but to use equation (31) and hence obtain for N_k drops of k cm diameter per cm^3,

$$\alpha_{\pi,k} = \frac{1}{2} N_k \sigma_k(\pi) \text{ neper/cm}, \qquad (69)^m$$

and for a given distribution of particles

$$\alpha_\pi = \sum_{k=0}^{s} \alpha_{\pi,k} = \frac{1}{2} \sum_{k=0}^{s} N_k \sigma_k(\pi) \text{ neper/cm}. \qquad (70)$$

Using the radar cross section of Table 14 and the drop size distributions in different rains as given in Table 7, we have computed α_π, the attenuation factor due to back scattering in the wavelength range 3 to 100 cm. The results of these calculations are included in Table 15 and in Figure 17. The variation of α_π is represented as a function of the wavelength of the incident radiation in different rains of given drop size distribution and precipitation rate. As already emphasized in connection with the study of the attenuation, these curves are characteristic, probably, of those rains, but they are not unique, since a given rain of known precipitation rate might very likely be built up from a variety of drop size distributions.

Since the absorption coefficient ($2\alpha_\pi$) for back scattering represents also the fraction of the incident power

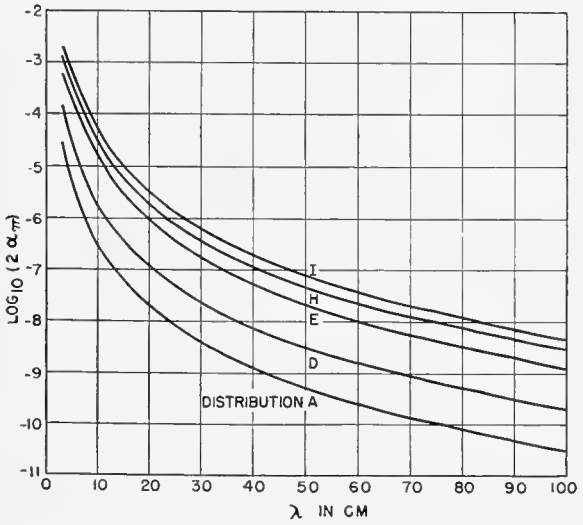

FIGURE 17. Absorption coefficient, $2\alpha_\pi$, due to back scattering (echo) as a function of the wavelength in different rains. The abscissa gives the wavelength, λ, in centimeters. The ordinate scale gives $\log_{10}(2\alpha_\pi)$, the absorption coefficient $2\alpha_\pi$ being expressed in km^{-1}. The letters on the curves refer to the drop size distributions listed in Table 7.

[l]For the shorter waves and large drops the cross sections given are merely orders of magnitude, as the convergence of equation (67) is too slow in that case; in fact, it is even slower than the expression for Q_s.

[m]The coherent portion of the scattering is neglected here on account of the assumed random distribution of the scatterers. See, nevertheless, a recent note by F. Hoyle.[34]

TABLE 14. Back scattering cross section $\sigma(\pi)$ (cm^2) of spherical water drops of D cm diameter.

D, cm	λ, cm: 3	5	8	10	15	20	30	50	75	100
0.05	$4.25\ 10^{-9}$	$5.55\ 10^{-10}$	$8.63\ 10^{-11}$	$3.50\ 10^{-11}$	$6.96\ 10^{-12}$	$2.18\ 10^{-12}$	$4.32\ 10^{-13}$	$5.60\ 10^{-14}$	$1.11\ 10^{-14}$	$3.50\ 10^{-15}$
0.10	$2.64\ 10^{-7}$	$3.52\ 10^{-8}$	$5.47\ 10^{-9}$	$2.24\ 10^{-9}$	$4.44\ 10^{-10}$	$1.40\ 10^{-10}$	$2.77\ 10^{-11}$	$3.59\ 10^{-12}$	$7.09\ 10^{-13}$	$2.24\ 10^{-13}$
0.15	$2.88\ 10^{-6}$	$3.97\ 10^{-7}$	$6.28\ 10^{-8}$	$2.54\ 10^{-8}$	$5.10\ 10^{-9}$	$1.60\ 10^{-9}$	$3.18\ 10^{-10}$	$4.12\ 10^{-11}$	$8.14\ 10^{-12}$	$2.57\ 10^{-12}$
0.20	$1.48\ 10^{-5}$	$2.15\ 10^{-6}$	$3.45\ 10^{-7}$	$1.42\ 10^{-7}$	$2.84\ 10^{-8}$	$8.94\ 10^{-9}$	$1.77\ 10^{-9}$	$2.29\ 10^{-10}$	$4.52\ 10^{-11}$	$1.43\ 10^{-11}$
0.25	$5.02\ 10^{-5}$	$7.42\ 10^{-6}$	$1.30\ 10^{-6}$	$5.34\ 10^{-7}$	$1.07\ 10^{-7}$	$3.42\ 10^{-8}$	$6.73\ 10^{-9}$	$8.72\ 10^{-10}$	$1.72\ 10^{-10}$	$5.45\ 10^{-11}$
0.30	$1.34\ 10^{-4}$	$2.25\ 10^{-5}$	$3.80\ 10^{-6}$	$1.57\ 10^{-6}$	$3.19\ 10^{-7}$	$1.20\ 10^{-7}$	$2.02\ 10^{-8}$	$2.62\ 10^{-9}$	$5.17\ 10^{-10}$	$1.64\ 10^{-10}$
0.35	$2.48\ 10^{-4}$	$5.40\ 10^{-5}$	$9.37\ 10^{-6}$	$3.91\ 10^{-6}$	$8.01\ 10^{-7}$	$2.58\ 10^{-7}$	$5.04\ 10^{-8}$	$6.53\ 10^{-9}$	$1.29\ 10^{-9}$	$4.08\ 10^{-10}$
0.40	$5.04\ 10^{-4}$	$1.12\ 10^{-4}$	$2.03\ 10^{-5}$	$8.55\ 10^{-6}$	$1.77\ 10^{-6}$	$5.75\ 10^{-7}$	$1.13\ 10^{-7}$	$1.46\ 10^{-8}$	$2.88\ 10^{-9}$	$9.13\ 10^{-10}$
0.45	$7.76\ 10^{-4}$	$2.12\ 10^{-4}$	$3.99\ 10^{-5}$	$1.70\ 10^{-5}$	$3.55\ 10^{-6}$	$1.16\ 10^{-6}$	$2.32\ 10^{-7}$	$3.00\ 10^{-8}$	$5.92\ 10^{-9}$	$1.87\ 10^{-9}$
0.50	$9.91\ 10^{-4}$	$3.65\ 10^{-4}$	$7.30\ 10^{-5}$	$3.14\ 10^{-5}$	$6.63\ 10^{-6}$	$2.18\ 10^{-6}$	$4.32\ 10^{-7}$	$5.60\ 10^{-8}$	$1.11\ 10^{-8}$	$3.50\ 10^{-9}$
0.55	$5.95\ 10^{-4}$	$5.82\ 10^{-4}$	$1.24\ 10^{-4}$	$5.44\ 10^{-5}$	$1.16\ 10^{-5}$	$3.87\ 10^{-6}$	$7.70\ 10^{-7}$	$9.98\ 10^{-8}$	$1.97\ 10^{-8}$	$6.24\ 10^{-9}$

TABLE 15. Absorption coefficient due to back scattering (echo) $2\alpha_\pi$ km^{-1} in rains of known drop size distribution and rate of fall.

	λ, cm										
mm/hr	3	5	8	10	15	20	30	50	75	100	Distribution
2.46	$2.94\,10^{-5}$	$4.21\,10^{-6}$	$7.01\,10^{-7}$	$2.86\,10^{-7}$	$5.74\,10^{-8}$	$1.82\,10^{-8}$	$3.60\,10^{-9}$	$4.66\,10^{-10}$	$9.20\,10^{-11}$	$2.91\,10^{-11}$	A
4.0	$5.06\,10^{-5}$	$7.31\,10^{-6}$	$1.17\,10^{-6}$	$4.81\,10^{-7}$	$9.63\,10^{-8}$	$3.03\,10^{-8}$	$5.99\,10^{-9}$	$7.76\,10^{-10}$	$1.53\,10^{-10}$	$4.85\,10^{-11}$	C
6.0	$1.44\,10^{-4}$	$2.32\,10^{-5}$	$3.90\,10^{-6}$	$1.61\,10^{-6}$	$3.25\,10^{-7}$	$1.17\,10^{-7}$	$2.31\,10^{-8}$	$2.99\,10^{-9}$	$5.91\,10^{-10}$	$1.87\,10^{-10}$	D
15.2	$6.12\,10^{-4}$	$1.73\,10^{-4}$	$3.30\,10^{-5}$	$1.41\,10^{-5}$	$2.94\,10^{-6}$	$7.62\,10^{-7}$	$1.50\,10^{-7}$	$1.94\,10^{-8}$	$3.83\,10^{-9}$	$1.21\,10^{-9}$	E
18.7	$6.67\,10^{-4}$	$1.27\,10^{-4}$	$2.22\,10^{-5}$	$9.25\,10^{-6}$	$1.90\,10^{-6}$	$6.51\,10^{-7}$	$1.28\,10^{-7}$	$1.66\,10^{-8}$	$3.28\,10^{-9}$	$1.04\,10^{-9}$	F
22.6	$5.69\,10^{-4}$	$1.01\,10^{-4}$	$1.74\,10^{-5}$	$7.24\,10^{-6}$	$1.47\,10^{-6}$	$4.91\,10^{-7}$	$9.70\,10^{-8}$	$1.26\,10^{-8}$	$2.49\,10^{-9}$	$7.88\,10^{-10}$	G
34.3	$1.28\,10^{-3}$	$3.02\,10^{-4}$	$5.58\,10^{-5}$	$2.36\,10^{-5}$	$4.90\,10^{-6}$	$1.63\,10^{-6}$	$3.22\,10^{-7}$	$4.17\,10^{-8}$	$8.24\,10^{-9}$	$2.61\,10^{-9}$	H
43.1	$1.83\,10^{-3}$	$4.89\,10^{-4}$	$9.16\,10^{-5}$	$3.90\,10^{-5}$	$8.14\,10^{-6}$	$2.66\,10^{-6}$	$5.26\,10^{-7}$	$6.82\,10^{-8}$	$1.35\,10^{-8}$	$4.26\,10^{-9}$	I

back scattered per unit thickness of the scattering medium, Tables 14 and 15 allow the computation and estimation of the echo power to be expected in radar observations under given conditions. The difficulties which seemed to exist earlier are cleared up by assuming that in those clouds which give rise to echoes precipitation actually occurs, even though no rain reaches the ground.[35] This is substantiated to some extent by recent work[15] which succeeded in verifying Rayleigh's law by observing cloud echoes simultaneously with both S- and X-band radar sets. Further proof was added by the Canadian group,[14] whose exhaustive study in the S band clearly showed the role of raindrops in cloud echo phenomena. In fact, these workers stated that there was no record of an echo without rain.

It is interesting to extract from Table 15 the fraction of the incident power back-scattered from different rains of 1-km depth expressed in decibels. As just mentioned, the power back-scattered by a thickness Δx is

$$\Delta P_\pi = -2\alpha_\pi P_i \Delta x, \tag{71}$$

and the fraction of the incident power P_i scattered backward by a layer $\Delta x = 1$ km is then $10 \log_{10} \Delta P_\pi / P_i$ db or $(10 \log_{10} 2\alpha_\pi)$ db $(2\alpha_\pi)$ is given in Table 15. The results are included in Table 16.

With Table 16 and the known sensitivity of a radar set, the maximum free space distance from the set at which these rains are observable can be computed at

TABLE 16. Power scattered backward by a layer of 1 km of rain in different rains (decibels).

Distribution	p, mm/hr	λ, cm 3	5	8	10	15	20	30	50
A	2.46	−45	−54	−61	−65	−72	−77	−84	−93
D	6.0	−38	−46	−54	−58	−65	−69	−76	−85
E	15.2	−32	−37	−45	−48	−55	−61	−68	−77
H	34.3	−29	−35	−42	−46	−53	−58	−65	−74
I	43.1	−27	−33	−40	−44	−51	−56	−63	−71

once. The peak power received by a radar set from Volume 3, Chapters 2 and 9, is

$$P_2 = P_1 G_1 G_2 \frac{S_\pi}{4\pi d^2} \left(\frac{3\lambda}{8\pi d}\right)^2$$

where P_1 is the transmitted power (peak power),

G_1 and G_2 are respectively the transmitter and receiver antenna gains relative to a doublet,

d is the distance of the set from the echoing rain drops, and

S_π is the back scattering cross section.

The beam usually intersects the rain boundary and therefore it can be assumed that S_π is made up of the combination of all the drops included in the echoing volume. This volume may be taken as a spherical shell of thickness Δd whose base is a spherical segment of area

$$2\pi d^2 (1 - \cos\theta),$$

2θ being approximately the half-power beam width of the set.

The rain echo cross section is then

$$S_\pi = 2\pi d^2 (1 - \cos\theta) \left[\Delta d \sum N_i \sigma_i(\pi)\right].$$

Here the summation extends over all the different drop groups forming the rain and $\sigma_i(\pi)$ is the differential cross section for back scattering in the direction π with the direction of propagation of the initial beam. It should be remembered that $\sigma_i(\pi)$ is the cross section per unit solid angle. Hence, the received peak power,

$$P_2 = \frac{P_1 G_1 G_2}{4} \left(\frac{3\lambda}{8\pi d}\right)^2 \theta^2 \left[\Delta d \sum N_i \sigma_i(\pi)\right]$$

for small θ (θ in radians). The quantity $[\Sigma N_i \sigma_i(\pi) \Delta d]$ is tabulated in Table 16 for $\Delta d = 1$ km and the different rains of Table 7. It is thus clear that the knowledge of the set characteristics permits at once the computation of the received power echoed by a rain falling at a certain distance r from the set provided

the assumption is made that the echoing rain layer is 1 km thick. This is clearly arbitrary but is likely to give the right order of magnitude.

There has been discussed in a rather unorthodox way[12] the effect of the absorption on the back scattering of radiation taking into account also the finite pulse length of the radiation source.

These results seem to be consistent with the meager quantitative information available in this field. This fact would tend to classify the atmospheric radar echoes as back scattering phenomena due to water drops of precipitation size. It may further be re-emphasized that theory provides an adequate explanation for scattering and absorption of electromagnetic waves passing through different clouds or precipitation forms. The limitations imposed on the theoretical results are due essentially to irregularities inherent in the meteorological elements.

10.1.9 Summary

The present report gives a detailed review of the theoretical and experimental status of microwave atmospheric absorption. This absorption is due to the gases of the atmosphere, oxygen, and water vapor, on the one hand, and to the swarms of floating or falling water drops, clouds, fog, rain, and snow, on the other.

The status of the gaseous absorption of the atmosphere is reviewed briefly in Section 10.1.1. Figure 1 gives the oxygen and water vapor attenuation curves in the 0.2 to 10-cm wavelength range. The water vapor attenuation is given for a vapor content of 7.5 g/m^3 of air, or 6.2 g per kilogram of air. In the equatorial belt, 15° S to 15° N, at sea level, the attenuation due to the atmospheric gases is approximately constant. It is about 0.18 and 0.008 db per kilometer for 1.25- and 3-cm waves respectively. In the tropical region the seasonal variation of these attenuations is quite large.

Figure 2 helps to give a clear picture of the atmospheric absorption due to oxygen and water vapor simultaneously with the absorption in rains of different types. It is seen that in the wavelength range 1 to 5 cm the rain attenuation is more important than the gaseous atmospheric attenuation. The latter predominates at waves shorter than 1 cm and longer than about 5 cm, losing entirely its practical importance at these longer waves.

The theory of absorption and scattering of electromagnetic waves by dielectric spheres (see Section 10.1.2) is briefly presented following the Rayleigh method as developed by Stratton.

The contribution of a swarm of spherical water drops of the same size, floating or falling in the atmosphere, to the average field strength attenuation factor is given by

$$\alpha = \frac{1}{2} N Q_t \text{ neper per unit length,}$$

where N is the average concentration of the drops, and Q_t their total cross section. This total cross section is the ratio of the power removed from the incident beam by one drop, through scattering and internal absorption to the power density of the incident beam. Similar definitions hold for the scattering cross section, absorption cross section and differential cross section for back scattering or radar cross section. The total cross section Q_t has the following form:

$$Q_t = \frac{\lambda^2}{2\pi} (-\mathrm{Re}) \sum_{n=1}^{n=\infty} (2n+1)\,(a_n+b_n),$$

where λ denotes the wavelengths in free space of the incident radiation and a_n and b_n, ($n = 1,2,3,\cdots$) form an infinite set of scattering amplitudes or coefficients associated with magnetic and electric poles of increasing order induced in the water drop by the field strengths of the radiation. Thus a_1 is associated with a magnetic dipole, b_1 with an electric dipole, b_2 with an electric quadrupole, etc.

Section 10.1.3 is devoted to the study of the amplitudes a_n and b_n. These are complicated functions of the wavelength λ, diameter D, or radius a of the drops, as well as the complex refractive index N or dielectric constant ϵ_c of water. Approximate expressions of the amplitudes can be derived by expanding them in series of ascending powers of the parameter $\rho = \pi D/\lambda$ for $\rho < 1$. Retaining only terms up to ρ^6, we found the following expressions of the first amplitudes,

$$a_1 = -\frac{j}{45}(N^2-1)\,\rho^5,$$

$$b_1 = -\frac{2j}{3}\frac{N^2-1}{N^2+2}\rho^3\left(1+\frac{3}{5}\frac{N^2-2}{N^2+2}\rho^2-\frac{2j}{3}\frac{N^2-1}{N^2+2}\rho^3\right),$$

$$b_2 = -\frac{j}{15}\frac{N^2-1}{2N^2+3}\rho^5,$$

where N is the complex refractive index of water with respect to free space and $N^2 = \epsilon_c = (\epsilon_r - j\epsilon_i)$ is its complex dielectric constant. The numerical computation of these amplitudes requires knowledge of the dielectric constant of water in the desired wavelength and temperature range. Whereas experimental

data on the real part of the dielectric constant of water are relatively abundant in the microwave region and around 18 C, data on the imaginary part or the conductivity are very scarce. The Debye theory has, therefore, been used to compute the dielectric constant of water in the microwave region, and the theoretical results seem to be supported by the new experimental data (see Table 1). Recent data in the K band on the temperature variation of the dielectric constant of water are given in Table 2. The graphical representation of both real and imaginary parts of the dielectric constant in the wavelength range 1 to 11 cm appears on Figure 4. The numerical values of a_1, b_1, and b_2 are discussed briefly at the end of this section.

The attenuation factor (see Section 10.1.4) is here computed to the approximation of taking into account the amplitudes a_1, b_1, and b_2. Clearly, inasmuch as these amplitudes are expressed in the form of series in ascending powers of the parameter $\rho = \pi D/\lambda$, the attenuation factor takes on a similar form. One gets

$$\alpha = \frac{3\pi}{20}\frac{m}{\lambda}(c_1+c_2\rho^2+c_3\rho^3+\cdots) \text{ neper per unit length,}$$

where m is the mass of liquid water in the form of drops per unit volume of the atmosphere, λ is the wavelength of the radiation in free space, and c_1, c_2, c_3, etc. are dimensionless coefficients depending on the wavelength implicitly through the dielectric constant of the substance of the sphere. For values of ρ small compared with unity, i.e., for waves long compared with the diameter of the drops, for which the terms in ρ^2, ρ^3, . . . can be neglected, the attenuation factor reduces to one term,

$$\alpha_{\rho<<1} = \frac{3\pi}{20}\frac{mc_1}{\lambda}$$

$$= \frac{9\pi}{10}\frac{m}{\lambda}\frac{\epsilon_i}{(\epsilon_r+2)^2+\epsilon_i^2} \text{ neper per unit length.}$$

This shows that for small drops or longer waves the attenuation factor becomes independent of the drop size and depends only on the amount of liquid water per unit volume present in the atmosphere. Table 3 contains (in the 1- to 100-cm wavelength range) the values of the coefficients c_1, c_2, c_3. It also gives the critical drop diameters below which, for a given λ, the one term attenuation formula holds within 10 per cent accuracy. A few values of D_c are the following:

λ, cm	1	1.26	3	5	10	15
D_c, cm	6.56×10^{-2}	7.13×10^{-2}	1.21×10^{-1}	1.87×10^{-1}	3.63×10^{-1}	5.34×10^{-1}

Table 4 gives the total cross section of spherical water drops in the diameter range 0.05 to 0.55 cm and wavelength range 1.25 to 100 cm. Table 5 gives attenuation values in decibels per kilometer. Figures 5 and 6 represent in graphical form the variation of the absorption cross section and attenuation factor (1) at constant drop diameter, as a function of the wavelength, and (2) at constant wavelength, as a function of the drop diameter, respectively.

These results are directly applicable to any precipitation forms of which drop size distribution and average drop concentration have been determined.

Meteorological data necessary to the computation of the attenuation factor of different precipitation forms have been collected in Section 10.1.5. Data on drop concentrations and drop size distributions are extremely scarce.

In liquid water clouds of different altitudes and in fogs, observations indicate that the drop diameters do not exceed 0.02 cm. In low and medium altitude good weather clouds the liquid water concentration varies between 0.15 and 0.50 g per cubic meter, and a concentration of 1 g/m^3 is very likely an extreme upper limit. In fogs, with the possible exception of heavy sea fogs, the liquid water concentration seems to be considerably smaller.

The data on drop size distribution in rains used in this work are given in Table 6, and, in a different form, directly applicable to the computation of the attenuation factor, in Table 7. These data indicate that the precipitation rate does not determine the drop size distribution of a rain, inasmuch as a rain of given precipitation rate can be built up with different drop size distributions. It does not seem, therefore, that the precipitation rate can play the role of a true physical variable in the attenuation law of rains.

Attention is also called to observed irregularities in the precipitation rate over relatively small distances (about 1 km), which makes it difficult to interpret the experimental data on radio wave attenuations even in terms of this apparent variable of total precipitation rate. These and other meteorological irregularities seem to eliminate the possibility of a quantitative theory of attenuation or back scattering of radio waves by rain or other precipitation forms. Clearly, the experimental study of these as yet chaotic meteorological features might disclose certain trends which could be advantageously incorporated in the theory of attenuation of a stormy atmosphere.

Figure 7 gives the empirical relationship between the terminal velocity of raindrops and their diameter.

The measurements cover practically the whole range of drops which reach the ground in rains, or from 0.05 to 0.55 cm. The terminal velocity of these drops varies between 2 and 9 m per second approximately. Figure 8 represents another empirical relationship between the liquid water concentration of the rainy atmosphere and the rate of rainfall. A rough linear approximation to the apparent empirical curve leads to a water content 0.038 g/m^3 for each millimeter per hour precipitation rate. But, strictly speaking, there cannot be an analytical connection between the liquid water concentration and the rate of rainfall. Inasmuch as the same rate of rainfall can be achieved by a number of different drop size distributions, therefore, to a single value of the abscissa — the precipitation rate — there may be associated a series of ordinate values or liquid water concentrations. The curves of Figure 8 are, therefore, of interest only because they are helpful in predicting very roughly liquid water concentrations in different rains.

The subject of Section 10.1.6 is the computation of the attenuation in different precipitation forms, no account being taken of the inherent irregularities.

Since the size of the drops in fogs and fair weather clouds are small compared with even the shortest wavelength (1.25 cm) considered in this report, the one term attenuation formula holds rigorously. Figure 9 represents the attenuation curve in decibels per kilometer in clouds and fogs for a liquid water concentration of 1 g/m^3 which, as mentioned above, is an upper limit.

A few attenuation values may be given as follows:

λ, cm	1.25	3	5	10
α/m db/km/gm/m^3	0.28	0.049	0.018	0.0045

Even for 1.25-cm waves the attenuation would become important only at long ranges for radar observations. For waves of length $\lambda > 3$ cm the attenuation in fair weather clouds and fogs is of no practical importance.

Table 3, on the critical diameter of water drops, shows that the attenuation becomes practically independent of the drop size distribution in rains for wavelengths longer than about 15 or 20 cm, inasmuch as raindrops whose diameter is larger than 0.55 cm or 0.6 cm do not reach low altitudes. In the 5- to 20-cm wavelength range the three-term attenuation formula will represent fairly well the attenuation in different rains. At wavelengths smaller than 5 cm exact computations of the amplitudes a_n, b_n are necessary.

It is shown that in any rain the attenuation depends linearly on the partial precipitation rates of the different drop groups making up this rain, but it does not depend directly on the total rate of rainfall.

Figure 10 purports to show the connection between the drop size distribution in a given rain and the partial or fractional attenuation values in the K and X bands of the different drop groups making up this rain. It is seen that the numerous small drops do not, for practical purposes, contribute to the attenuation, which is due mainly to the bigger drops.

Table 9 contains attenuation values of different rains of known drop size distribution and rate of rainfall. Figure 11 is a graphical representation of these results. It will be seen that at the shorter waves the attenuation may become important in heavy rains.

Figures 12, 13, and 14 are graphical representations of certain results included in Table 9 at K-, X-, and S-band wavelengths, respectively. The attenuation values corresponding to the points in these graphs have been computed for the rains of Table 9, and we have drawn a curve through the computed points. Accordingly, the plot of attenuation as a function of total precipitation is a mass plot. That is, for any given total precipitation the attenuation will have different values, depending upon the distribution of the drop size for the rain in question. Figures 12, 13, and 14 represent mass plots of the meager data available for K, X, and S bands, respectively, together with the limiting curve that would result if all the drops were of the size that gives maximum attenuation. Tables 10 and 11 contain, respectively, the theoretically predicted upper limits of attenuation for water drops around 18°C and the experimental attenuation per unit rate of precipitation. In view of the difficulties in the interpretation of the experimental data, it may be said that there is fair agreement between the observed and predicted attenuation values in rains.

The attenuation due to hailstones and snow should be considerably smaller than that caused by rain. The reason for this difference is due to the small dielectric absorption of ice as compared with the dielectric absorption of liquid water.

Section 10.1.7 deals with the total scattering (in the whole solid angle) of microwaves by spherical water drops. The scattering cross-section formula is given in a series of ascending powers of $\rho = \pi D/\lambda$, the first term of the series being ρ^6. For small

values of ρ, the cross section reduces to the first term of this series, which, when the dielectric absorption is negligible, reduces to the Rayleigh scattering cross section. Table 12 includes the results of the numerical computations and Figures 15 and 16 are their graphical representation.

The knowledge of the total cross section and scattering cross section allows the computation of the absolute probabilities $\tilde{\omega}_s$ for the waves to be scattered in any direction or to be absorbed internally by spherical water drops. The scattering probabilities are given in Table 13. The probabilities for internal absorption are complementary to these, i.e., they are equal to $(1 - \tilde{\omega}_s)$. It is thus seen that, with the exception of the shortest waves and the biggest raindrops, the probability of the waves being absorbed internally, the absorbed wave energy heating the drops, is much larger than the probability of their being scattered in any direction.

In Section 10.1.8 the differential scattering cross section in a chosen direction is first derived rapidly and then is given explicitly so as to show clearly the contributions of the induced electric dipole, electric quadrupole, magnetic dipole, and their interference terms. Attention is here called to the already well-known fact that in the optical spectrum region dissymmetry appears in the angular distribution of the scattered radiation. That is to say, the larger the parameter ρ or the nearer the drop diameter to the wavelength, the greater the power scattered in the direction of the propagation in comparison with that scattered backward or at 180° to the direction of propagation.

The back-scattering cross section or radar cross section of water drops is given in the form of a series in ascending powers of the parameter ρ. Table 14 contains the results of numerical computations of these radar cross sections for water drops in the diameter range 0.05 to 0.55 cm and wavelength range 3 to 100 cm.

The radar cross section allows the determination of a radar attenuation constant. The radar absorption coefficient, or the double of the attenuation constant, is the fraction of the incident power scattered backward by a layer of unit thickness of the echoing medium. Table 15 contains the numerical values of this radar absorption coefficient in different rains of known drop size distribution, and Figure 17 is its graphical representation. Table 16 is a somewhat modified form of Table 15, in so far as it gives in decibels the fraction of the incident power scattered backward by a 1-km layer of different rains. The theoretically predicted back scattering seems to be in fair agreement with the rather few experimental data on the power received in radar observations of rains or rain clouds.

In conclusion it may be stated that, in view of the scarcity of meteorological data and the irregularities inherent in meteorological phenomena, the theory provides a satisfactory picture of the propagation of microwaves through a variety of precipitation forms present in the atmosphere.

10.2 K-BAND ABSORPTION — EXPERIMENTAL[a]

Our knowledge of the attenuation of K-band radiation in the normal atmosphere is based upon the theory outlined by Van Vleck and upon a number of experiments, some of which were undertaken to obtain data needed in the theory, others of which were attempts to measure directly absorption by the atmosphere.

The width of the rotational lines of water vapor in the infrared has recently been measured in work at the University of Michigan. The width of the oxygen lines responsible for the strong absorption at 0.5 cm and the rather small effect at K band are inferred from experiments at the Radiation Laboratory. The absorption in oxygen was measured directly at several wavelengths in the neighborhood of 0.5 to 0.6 cm. The gas was contained in a wave guide about 6 m long. This guide could be evacuated and then filled with gas to any desired pressure between zero and roughly 1,000 mm Hg. The radiation was obtained as the second harmonic generated in a crystal rectifier fed by a K-band oscillator. The source was amplitude modulated at audio frequency, and the signal was detected by a second crystal at the far end of the wave-guide path. The attenuation in the gas was determined by comparing the signal received with the guide evacuated to that received with gas present in the guide. The absorption of pure oxygen, at various pressures, as well as that of controlled mixtures of oxygen and other gases, was measured. The results confirm the predictions of the theory in a very convincing manner and suggest a value of the line width lying between 0.05 and 0.02 cm^{-1}.

Direct measurements of atmospheric absorption at K band have been made by a group at the Radia-

[a]By E. M. Purcell, Radiation Laboratory, MIT.

tion Laboratory using a K-band radar set in an airplane. For this purpose, the set was provided with fixed attenuators which could be switched in or out of the system. Both r-f and i-f attenuators carefully calibrated were used. The experiment consisted in flying a straight level course away from a known target and determining the maximum range to which the target could be seen with and without attenuation in the system. The maximum ranges involved were of the order of 30 miles. From the results a value for the attenuation in the atmosphere can be calculated, assuming free space propagation, and this value in turn correlated with the meteorological data. The latter were obtained from radio-sonde flights at MIT.

After making allowance for the rather small oxygen effect, the results are best represented by a figure of 0.02 db per nautical mile for 1 g/m^3 of water vapor. In several of the flights the target was an accurately made 4-ft corner reflector. This provides an independent upper limit to the attenuation, since all system parameters (antenna gain, S/N, etc.) were known, and one can calculate how far the corner should have been seen with any supposed amount of atmospheric attenuation. The upper limit estimated in this way is about 0.04 db per nautical mile for 1 g/m^3 of water vapor.

An entirely different method for measuring attenuation in the atmosphere has been developed at Radiation Laboratory. It is possible to measure the apparent radiation temperature of any matched r-f load, including an antenna, with great precision ($\sim$ 1 C). In the case of an antenna, the temperature measured is the temperature of whatever the antenna is looking at, that is, the temperature of whatever would absorb the energy emitted from the antenna if the antenna were transmitting. When the antenna is pointed at the sky, the temperature measured is some mixture of the temperature of outer space and the temperature of the air, the influence of the latter being determined in a direct and simple manner by the absorption coefficient of the air layer. From measurements of the apparent temperature of the sky at various elevation angles, the total absorption in decibels for a vertical path through the entire atmosphere can be deduced. The data which have been collected in this manner show good internal consistency; assuming that the MIT radio-sonde data give the total water vapor in the atmosphere correctly, a value of 0.04 db per nautical mile for 1 g/m^3 is obtained for the water vapor attenuation. This is larger than the other value quoted above. The reason for the discrepancy is not yet known.

10.3 ABSORPTION OF K-BAND RADIATION BY WATER VAPOR[o]

An experiment to determine the location and shape of the water vapor absorption line in the K-band region of the electromagnetic spectrum is in progress. The experiment consists in the measurement of the change in Q of a large copper box when water vapor is introduced. From this change in Q the loss by absorption in the water vapor can be determined and hence the attenuation of K-band radiation in water vapor.

The experimental setup consists of an approximately cubical (but irregular in terms of λ) copper box of 15.8 cu m volume. Energy from a pulsed magnetron is fed into this box through a wave guide which terminates in a matched horn facing a rotating copper fan placed in the roof of the box. The purpose of this fan is to stir up the standing wave pattern in the box. Throughout the interior of the box are placed strings of Chromel-constantan thermocouple junctions sealed in 707 glass tubing. Alternate junctions are coated with a mixture of polystyrene and iron powder. In all, there is a total of 220 painted or "hot" junctions in the box. Provision is made for introducing water vapor into the box and for circulating the air. The temperature is maintained at 45 C during all runs, and the pressure is atmospheric (760 $\pm$ 15 mm, depending on conditions). An aperture of area 400 sq cm which may be opened or shut by means of a sliding copper door is located in one side of the box. Radiation entering the box is absorbed by the walls, by the paraphernalia in the box, by the gas, by the apertures (if any), and by the thermocouple junctions. The coated thermocouple junctions absorb more energy than the uncoated junctions and a net emf is produced. A single junction would give an emf proportional to the value of the square of the electrical field at its position, but the reading would be very sensitive to the location of the couple and, even if this were held fixed, would be sensitive to small deformations of the walls. The large number of the couples actually used averages the value of the square of the electric field, $\mathbf{E}^2$, over the entire box, and the fan previously mentioned assists in this averaging. The Q of the box and its contents is, for constant magnetron power output, proportional to $\mathbf{E}^2$ and thus to the emf of the thermocouples.

Since the couple emf is also proportional to the power output of the magnetron, changes in the output power will show up in the results in the same way as

[o]By J. M. B. Kellogg, Columbia University Radiation Laboratory.

changes in Q. Original difficulties arising from this cause, which were encountered because of variation in the a-c line voltage and the modulator voltage, have been largely eliminated by the use of stabilizing transformers and a magnetron load current stabilizing circuit. Furthermore, a method of taking data was devised which only required the power output to be maintained constant for a few minutes at a time.

The Q of the water vapor, Q_V, is given by

$$\frac{1}{Q_V} = K\gamma\lambda \,, \tag{72}$$

where γ is the attenuation in db per nautical mile, λ is in centimeters, and K is a constant. In order to obtain absolute values of the attenuation, it is necessary to introduce into the system a known Q in terms of which the other Q's may be evaluated. For this purpose, the aperture, which acts as a perfect absorber, is used.

Lamb has derived a formula for the Q of an aperture, Q_A, and this is

$$\frac{1}{Q_A} = \frac{\lambda A}{8\pi V} \,, \tag{73}$$

where A is the area of the aperture and V is the volume of the box.

The Q of the whole ensemble may now be written down.

$$\frac{1}{Q} = \frac{1}{Q_B} + \frac{1}{Q_V} + \frac{1}{Q_A} \,, \tag{74}$$

where Q_B takes account of all losses (including the losses in oxygen) other than those in the vapor and the aperture. Inserting values, and using $1/\eta$ as the proportionality constant connecting the emf, $\mathcal{E}$, and Q, one then has

$$\frac{1}{\mathcal{E}} = \eta\left(\frac{1}{Q_B} + K\gamma\lambda + \frac{\lambda A}{8\pi V}\right). \tag{75}$$

For constant conditions of humidity, wavelength, and magnetron power output, measurements are now made of the emf $\mathcal{E}_0$, with $A = 0$, and emf $\mathcal{E}_A$, with $A = A$. Using these measured values of emf, equation (75) can be written in the form

$$\frac{\mathcal{E}_A}{\mathcal{E}_0 - \mathcal{E}_A} = \frac{8\pi V}{\lambda A}\left(\frac{1}{Q_B} + K\gamma\lambda\right) \equiv F \,. \tag{76}$$

The humidity is then changed and the measurement repeated until enough points have been obtained to provide a curve of F as a function of ρ, the water vapor density, for constant wavelength.

Since, presumably, γ is the only quantity in this equation which is a function of ρ, and since $\gamma = 0$ for $\rho = 0$, the plot of F against ρ extrapolated to zero humidity will yield a value of Q_B. Consequently, γ is determined as a function of ρ.

Examples of the γ versus ρ curves so obtained are shown in Figure 18 for the wavelengths 0.96, 1.16, 1.28, and 1.69 cm. Data were also taken at the wavelengths 1.06, 1.31, 1.37, and 1.49 cm. These lines are all concave upward with the exception of those at 1.28, 1.31, and 1.37 cm. There is some evidence that the line at 1.31 cm is concave downward, while within experimental error the 1.28- and 1.37-cm lines are straight.

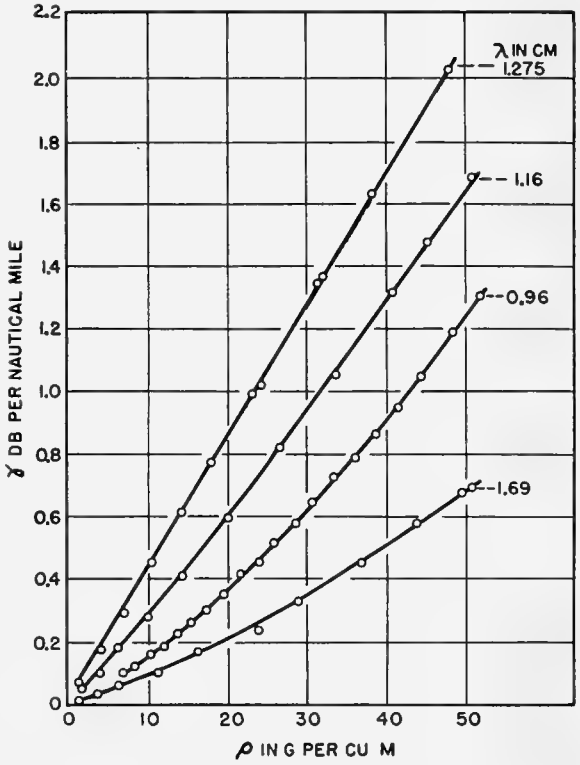

FIGURE 18. Attenuation in water vapor.

The curvature is surprising, since it was believed that γ would be proportional to ρ. The reason for the curvature is not understood, and it is possible that it arises from some systematic experimental error. However, it is difficult to conceive of a systematic error which disappears at resonance.

Because of this curvature, it is not possible to draw a single attenuation curve showing absorption as a function of wavelength for all humidities. Figure 19 shows the variation with wavelength of the attenuation coefficient γ/ρ in decibels per nautical mile per gram

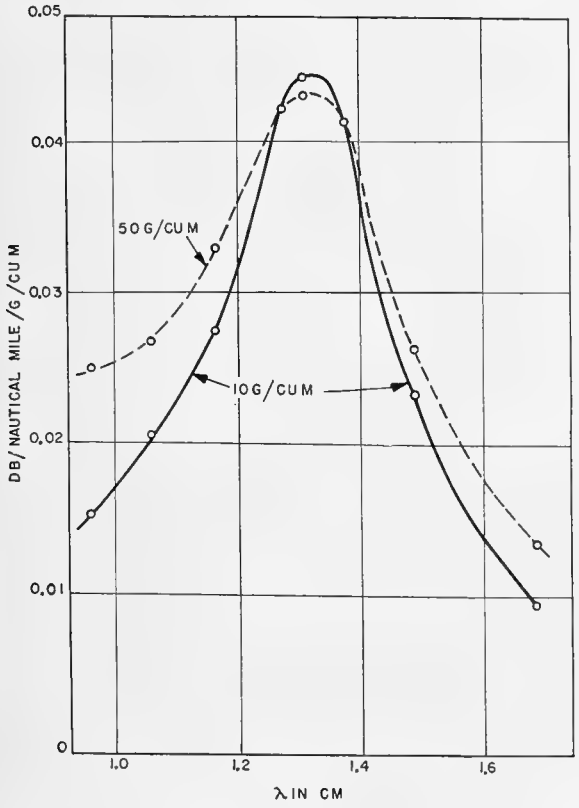

FIGURE 19. Attenuation coefficient, water vapor, 45 C.

of water vapor per cubic meter for humidities of 10 g per cubic meter and of 50 g per cubic meter. It is to be noted that the peak of this curve, at 1.32 cm, is very close to the standard K-band wavelength.

These experimental results are in agreement with other results for the water vapor attenuation at K band. Furthermore, for all practical radar purposes, and within the range of the measurements, they are in agreement with Van Vleck's theory of the absorption of this water vapor line.

DISCUSSION

Comments were made on the great accuracy of the experiment, pointing out that the quantity being measured was extremely small and that other experiments, particularly one made in Florida by measurement of the sky temperature, were leading to substantial agreement with the present findings. The best available data on the performance of K-band radars supported the experimental result obtained and would be of great help in choosing wavelengths for radar and other apparatus in the future.

The good agreement between theory and the experimental result achieved was stressed. Whereas in infrared absorption measurements the results had disagreed with theory by as much as 10 db or more, the discrepancy in these results amounted to a few per cent only. It was noted that from the purely physical standpoint this water vapor line and the 0.5-cm oxygen absorption line were the most carefully investigated lines in the spectrum, aside from some lines in the visible region. The explanation was given that the microwave measurements were much more instructive than the optical ones from the standpoint of the collision broadening theory because the width of the microwave absorption line was comparable to the frequency of the radiation. This results in a shape factor or line form which can be studied in detail. The reported dependence on density presents a difficult problem which is not yet well understood.

The practical importance of the curvature shown in Figure 18 was emphasized. It was pointed out that the effects of a wide range of humidities had been investigated, some very high compared to those ordinarily encountered. In practical work most of the data would be obtained from the low end of the curves of Figure 18, where little ambiguity in numerical values would obtain.

10.4 K-BAND ATTENUATION DUE TO RAINFALL[p]

10.4.1 Introduction

In order to determine the attenuation of 1.25-cm wavelength radiation by rain, controlled radio and meteorological measurements were undertaken in an area providing adequate climatic conditions for the study. It was apparent that the attenuation measurements should be made in an area of maximum precipitation for expediency. Furthermore, the experiment demanded periods of varying rates of rainfall with frequent "clearing" for calibration purposes. Tropical orographic (mountainous) rain seemed to offer the greatest probability of fulfilling these conditions.

A brief reconnaissance of the Hilo, Hawaii, area showed that a site near Kaumana was adequate, having a yearly fall in excess of 250 in., as compared with an annual rainfall of 10.10 in. in the San Diego area. A 1.21 statute mile link was chosen parallel to the mean trade wind vector, i.e., due east-west, and was located on a lava flow of 1881. The lava was covered with saw grass and low brush. The terrain had a gentle slope from the receiver at 2,500 ft to the transmitter at 2,800 ft above mean sea level.

[p]By L. J. Anderson, U. S. Navy Radio and Sound Laboratory.

10.4.2 Rainfall Intensity

Orographic lifting of the unstable moist tropical air caused frequent 2- to 3-day periods of precipitation having a wide range in intensity. On one occasion intensities as high as 125 mm per hour were observed. Due to the light winds associated with orographic precipitation an essentially vertical trajectory of the raindrops was obtained; and, therefore, representative sampling of the rain falling through the radiated energy path was accomplished by placing the gauges directly in line between the transmitter and receiver.

Although the rainfall intensity varied widely both with time and in space, well-coordinated measuring techniques having sufficient coverage detected periods when the rate of fall along the path was uniform. Since such periods of uniformity seldom lasted longer than 60 sec, precise control and timing were vital. Two methods of determining the rate of precipitation were employed. Five Julien Friez tipping-bucket automatic recording rain gauges were evenly dispersed along the path and their signals were recorded on a single Esterline-Angus five-pen recorder at the receiver station. In addition, four rain shelters employing the "funnel and graduate" technique were installed between the automatic gauges as shown in Figure 20. The rain shelters were provided with field phones for receiving instructions as well as simultaneous signals for taking graduate readings and exposing drop size blotters. During operations, signals for graduate readings were given every 30 sec. Blotters for drop size measurements were simultaneously exposed on an average of every 5 min.

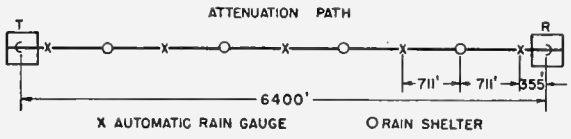

FIGURE 20. Layout of experimental path and apparatus.

10.4.3 Radio Equipment

The equipment used for the attenuation measurements is shown in Figure 21. It was relatively simple and required little attention once the initial warm-up drifts were stabilized. The technique for a satisfactory measurement involved a comprehensive check of the "clear weather" values before and after any one rainfall.

The transmitter was housed in a small elevated shack and the antenna and guide were protected from the rain by a back-sloping shutter flap.

A 2K33 tube, modulated with 800 c, was used as the transmitter. Wave-guide feed was employed on a 2-ft paraboloid antenna (beam width 1.7°). A thermistor with a directional coupler was used as a power monitor.

A 2-ft paraboloid collected energy at the receiving end and fed the receiver through a wave guide. A superheterodyne utilizing a 2K33 local oscillator drove a 30-mc i-f amplifier with 6-mc bandwidth. The second detector output fed an audio amplifier and recorder.

A signal generator was used to check the receiver characteristic. This generator consisted of a 2K33 tube and two flap attenuators. Fixed pads were used on either side of the flap attenuators to provide a flat

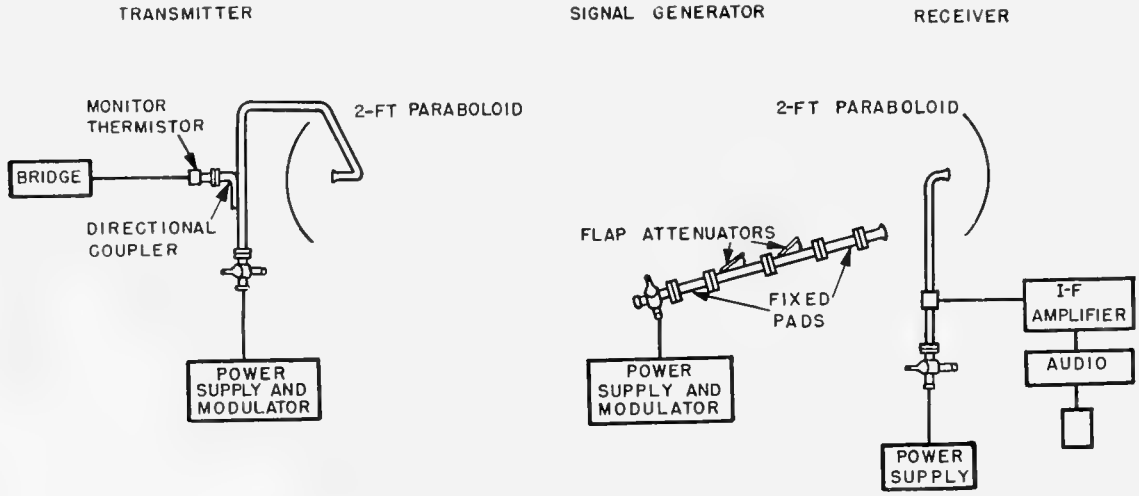

FIGURE 21. Block diagram of K-band attenuation measurement apparatus.

line. The characteristics of the flap attenuators were checked every few hours, using a K-band thermistor. Each flap was calibrated and used over a 12-db range. Resettability was approximately ± 0.1 db. A small nozzle was used to direct the output of the signal generator upon the receiving paraboloid. Calibrations were made before, during, and after rainfalls and were within ± 1.0 db over the 5- and 6-hour measuring periods.

10.4.4

Analysis

The primary attenuation curve of Figure 22, shown with solid dots, was obtained by choosing periods when the rainfall at all stations, including the automatic gauges, was essentially uniform. Six such periods of

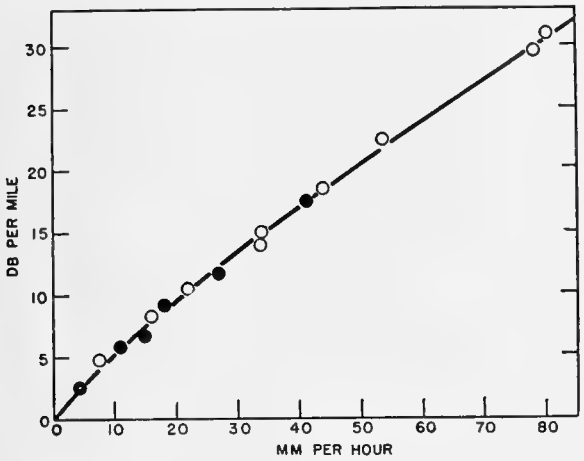

FIGURE 22. Primary attenuation curve of K-band radiation in rain. K-band attenuation versus rainfall intensity. (Note: Decibels per nautical mile.)

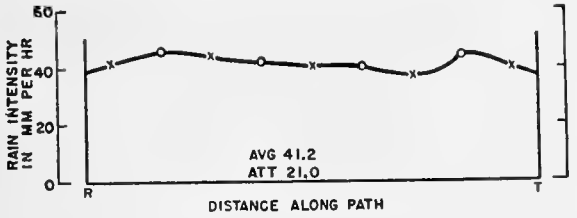

FIGURE 23. Profile of rain intensity along the path. Time 223645.

uniform fall along the path were selected covering the important range of 0 to 41 mm per hour. Figure 23 is a rainfall intensity profile of the highest uniform fall recorded. By Humphreys' classification of rain[q] the intensities covered by the primary curve are more than adequate for normal rates of precipitation encountered in nature.

[q] 1 mm per hour, light rain; 4 mm per hour, moderate rain; 15 mm per hour, heavy rain; 48 mm per hour, excessive rain. See reference 24.

Using the primary attenuation curve thus obtained, it was possible to extend the curve for extremely high rates of fall (cloudbursts) in the following manner. Figure 24 is a rain intensity profile at an interval of

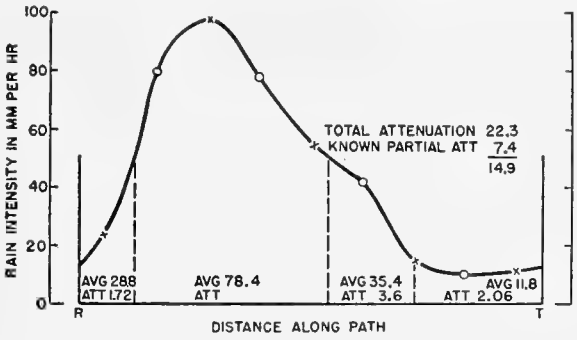

FIGURE 24. Intensity profile during uneven precipitation. Time 171115.

nonuniform rainfall distribution. The area under the curve is divided into sections as shown. These sections cover the portions of the path where the intensity was below 41 mm per hr. Hence with the primary attenuation curve and a planimeter it is possible to assign the contribution that each section makes to the total observed attenuation (assuming that the attenuation in decibels is linear with distance).

After subtracting out the part of the attenuation already known, the high intensity central portion is left to account for the residual attenuation. Dividing the residual attenuation by the fraction of a mile covered by this part of the path and plotting this value against the average intensity in the interval gives a point at 78 mm per hour. As a check on the method, similar profiles were worked up which gave points below 40 mm per hour. These are plotted as open circles, as shown in Figure 22. It will be seen that the open circles agree quite well with the solid ones, and hence considerable confidence in the high intensity points is justified.

Discussion

The total observation time of the experiment was roughly 3 hours, about half of this total time being represented by the figures presented with the paper. It was necessary to employ a large number of precipitation measuring stations along the path in order to obtain an accurate precipitation profile. Some incidental work on drop size was also done. The spread in drop size at a given time was rather large, probably

because of the orographic character of the precipitation, which was made up of drops falling on the average not much more than 1,000 ft, as compared to ordinary rain falling 5,000 to 6,000 ft. The longer period of fall in ordinary rain probably permits a greater number of drops to reach the characteristic sizes.

10.5 ABSORPTION OF MICROWAVES BY THE ATMOSPHERE, BRITISH WORK[r]

The working committee of the Ultra Short Wave Panel has presented a report in which the following questions are treated in detail:

1. The absorption of microwave radiation by oxygen and vapor.

2. The absorption of microwave radiation by water in macroscopic form, for example, rain, clouds, fog.

3. The measurement in the laboratory of dielectric constants and conductivity which have already been described (see Section 9.3).

The work under item (1) consisted chiefly in showing that the attenuation given by Telecommunication Research Establishment radar experiments at Llandudno at a wavelength of 1.25 cm was consistent with the theoretical values given in reference 1. The experimental method consisted of comparing the echoes received on X- and K-band radars from a standard reflector at short range and from land echoes at a large range. Care was taken to insure that the reflecting targets did not reflect an amount of energy which was dependent on frequency. In this way a minimum value for the attenuation on $\lambda = 1.25$ cm was found to be 0.14 db per kilometer. New values based upon revised values of the widths of the various lines of water vapor and oxygen show that almost the whole of this attenuation must be due to absorption by water vapor and further that to obtain an absorption as high as 0.14 db per kilometer the frequency at the important water vapor line must lie close to 1.25 cm.

The work under item (2) has been carried out, in the case of rain, by assuming what seemed a plausible distribution of drop sizes and calculating on this basis the attenuation that would occur at a standard precipitation rate. Then by making a climatological survey, information can be given of the proportion of time during which the attenuation can be expected to exceed a given value for a radar or radio communication set working on a given wavelength at a given location. The calculations for a standard precipitation rate gave the following estimates for the maximum attenuation likely to occur (that is, for the most unfavorable drop size distribution that was thought likely to occur).

S band: 0.003 db per km per mm per hr.
X band: 0.06 db per km per mm per hr.
K band: 0.22 db per km per mm per hr.

The climatological part of the program involves a great deal of statistical work and is not yet complete. The following preliminary results can be given.

At Padang in Sumatra we may expect, twelve times a year, periods of 1 hr when the average attenuation on 1.25 cm will be some 6 to 12 db per kilometer; on 3.0 cm, 2 to 4 db per kilometer; and on 10 cm, 0.1 to 0.2 db per kilometer.

In England only once a year will the average attenuation over a period of one hour reach 1 to 2.5 db per kilometer on 1.25 cm; 0.3 to 0.8 per kilometer on 3.0 cm; and 0.02 to 0.04 db per kilometer on 10.0 cm.

It should be noticed that these attenuation figures are for point-to-point communication and must be doubled in the radar case.

10.6 DIELECTRIC CONSTANT AND LOSS FACTOR OF LIQUID WATER AND THE ATMOSPHERE[s]

In propagation problems the knowledge of the electric properties of the ground, sea, and fresh water, as well as those of the atmospheric gases, are of fundamental importance. Collected here are the available data on these materials. Clearly, the study of the reflection coefficients leads indirectly to the dielectric properties of these materials. Here we will be concerned more with the direct determination of their dielectric constants and loss factors.

10.6.1 Experimental Methods

Reflection-Transmission Method

First we should like to sketch here the basis of the different experimental methods used in the determination of the dielectric properties of materials.

One of these is the reflection-transmission method which was used by Ford[37] in his studies of the properties of the ground. This same method has also been used recently by Saxton[38,39] on water in investigating

[r]By F. Hoyle, Ultra Short Wave Panel, Ministry of Supply, England.

[s]By L. Goldstein, Columbia University Wave Propagation Group.

the temperature dependence of its dielectric properties at 1.25 and 1.58 cm.

If the power transmitted through two thicknesses d_1 and d_2 of the material in question are

$$P_1 = P_0 e^{-\alpha d_1},$$
$$P_2 = P_0 e^{-\alpha d_2},$$

then the absorption coefficient α is given by

$$\alpha = \frac{2.3}{d_2 - d_1} \log_{10} \frac{P_1}{P_2}, \tag{77}$$

where P_0 is the incident power.

The absorption index k in the complex refractive index

$$N = n - jk \tag{78}$$

is related to the absorption coefficient by

$$\alpha = \frac{4\pi k}{\lambda} \tag{79}$$

and hence

$$k = \frac{2.3\lambda}{4\pi d} \log_{10} \frac{P_1}{P_2}, \tag{80}$$

where d stands for $(d_2 - d_1)$. Also

$$N^2 = (n - jk)^2 = \epsilon_r - j\epsilon_i,$$
$$= \epsilon_r - j60\sigma\lambda. \tag{81}$$

ϵ_r is the real part of the dielectric constant, ϵ_i its imaginary part; σ is the conductivity of the substance is mhos per meter; and λ the wavelength in meters. One obtains readily from equation (81)

$$n^2 - k^2 = \epsilon_r$$
$$2nk = \epsilon_i = 60\sigma\lambda. \tag{82}$$

The absorption index k is measured directly by two galvanometer readings proportional to P_1 and P_2. The refractive index n is derived from the reflection coefficient R_N for almost perpendicular incidence, using

$$R_N^2 = \frac{n^2 + k^2 + 1 - 2n}{n^2 + k^2 + 1 + 2n}. \tag{83}$$

Then n and k determine ϵ_r and σ. Saxton claims that in this method at least one quantity, the absorption index, is measured directly while the other, the refractive index, is derived from the measurement of the reflection coefficient.

In the other methods, given later, neither of these quantities is measured directly.

Standing Wave Ratio Method

By limiting the electromagnetic field to the enclosure of a hollow pipe or coaxial line, the energy is completely confined, stray effects are eliminated, and small amounts of any dielectric can be investigated accurately.[40-42] The following gives the theoretical foundation of this "standing wave ratio" method for measuring complex dielectric constants.

1. A transmitter radiates waves of a given frequency into one end of a closed wave guide. These are reflected by the metallic boundary at the other end. Standing waves are set up in the guide, and they can be measured by a probe detector traveling along a slot in the pipe parallel to its axis. The dielectric is inserted at the closed end of the pipe, opposite the transmitter, and fills the pipe up to a height d. Above it the standing wave pattern is measured in air. The real and imaginary parts ϵ_r and ϵ_i of the dielectric constant are calculated from the ratio of the field strengths in node and antinode $E_{\min}/E_{\max}$, and the distance x_0 of the first node from the surface of the dielectric.

The modulus and the argument of the reflection coefficient are obtained from

$$R = \rho\epsilon^{-j\Phi} = \frac{(Z(0)/Z_{01}) - 1}{(Z(0)/Z_{01}) + 1}, \tag{84}$$

where $Z(0)$ is the characteristic impedance of the pipe section filled with the dielectric understudy, Z_{01} is the intrinsic impedance of the air-filled portion of the pipe. By denoting

$$\frac{Z(0)}{Z_{01}} = \tanh \delta = \tanh (\delta_r + j\delta_i), \tag{85}$$

where δ_r and δ_i are, respectively, the real and imaginary part of δ, the reflection coefficient R can be written as

$$R = |R| e^{-j\Phi},$$
$$= \rho e^{-j\Phi}, \tag{86}$$

with

$$\rho = |R| = e^{-2\delta_r}; \arg R = -\pi - 2\delta_i = -\Phi. \tag{87}$$

From the expression of the reflected field strengths one finds that the distance x_0 of the first node from the surface is given by

$$x_0 = \frac{-\delta_i \lambda_1}{2\pi}, \tag{88}$$

where δ_i is connected directly to the phase shift Φ at reflection through equation (87), and λ_1 is the wave-

length in air of the radiation. The measurement of x_0 thus yields δ_i. Similarly, one finds that

$$\tanh \delta_r = | E_{\min} / E_{\max} |. \tag{89}$$

2. *Calculation of dielectric constant and loss factor from terminating impedance.* The intrinsic impedance of the dielectric-filled portion of the guide is found to be

$$Z(0) = Z_{02} \tanh \gamma_2 d, \tag{90}$$

where

$$Z_{02} = \frac{j\omega\mu_2}{\gamma_2}. \tag{91}$$

The subscript 2 refers to the dielectric medium, μ_2 is its permeability and γ_2 is the propagation constant of dielectric-filled section of the guide; for the *TE* waves, Z_{02} is the impedance of the dielectric medium itself. Using equations (90) and (91), one gets

$$\frac{\tanh \gamma_2 d}{\gamma_2 d} = \frac{Z(0)}{Z_{01}} \frac{\mu_1}{d\,\gamma_1\,\mu_2}. \tag{92}$$

The propagation constant γ_2 determines finally the complex dielectric constant ϵ_c through the fundamental relation

$$\gamma_2 = \left[\left(\frac{2\pi}{\lambda_c} \right)^2 - \omega^2 \mu_2 \epsilon_c \right]^{\frac{1}{2}}, \tag{93}$$

where the cutoff wavelength λ_c is determined by the geometry of the guide and the type of wave. In the air-filled section of the guide

$$\gamma_1 = \left[\left(\frac{2\pi}{\lambda_c} \right)^2 - \omega^2 \mu_1 \epsilon_1 \right]^{\frac{1}{2}}. \tag{94}$$

Consequently, from equations (93) and (94), the complex dielectric constant of the material under study becomes

$$\epsilon_c = \epsilon_1 \frac{(1/\lambda_c)^2 - (\gamma_2 / 2\pi)^2}{(1/\lambda_c)^2 + (1/\lambda_1)^2}, \tag{95}$$

where

$$\gamma_1 = j \frac{2\pi}{\lambda_1} \tag{96}$$

for free space. Finally

$$\epsilon_c = \epsilon_1 \left(\frac{\gamma_2}{\gamma_1} \right)^2. \tag{97}$$

The solution of equation (93) can be found from charts. It is claimed that with this method materials with very low dielectric losses can be investigated satisfactorily.

The Resonator Q Method[43]

Here the procedure consists in measuring the change of resonant frequency of a closed cylindrical resonator upon the insertion, along the axis, of a rod of the dielectric material in question. By observing the change of Q value resulting from the insertion of similarly dimensioned specimens of different materials, it is possible to obtain comparative loss tangent values. The relevant theoretical relations are summarized below.

By definition the Q value of a resonator system is given in convenient form by the relation

$$Q = 2\pi \frac{\text{energy stored}}{\text{energy loss per half cycle}}$$

Both the energy stored and the energy loss can be computed from the field distributions within the resonator, and these are given, for a *TM* wave, as

$$H_\theta = A\, J_1 (\gamma\rho), \tag{98}$$

$$E_z = \frac{A\gamma}{\sigma + j\omega\epsilon_r} J_0 (\gamma\rho), \tag{99}$$

where H_θ is the tangential magnetic field strength in amperes per meter. E_z is the axial electric field strength in volts per meter, ρ is the distance of the point in question from the cylinder axis, γ is the propagation constant

$$\gamma^2 = \mu\epsilon_r\omega^2 - j\omega\sigma\mu,$$

ω is the angular frequency, μ the permeability in henrys per meter, and A is a constant determined by the strength of the exciting source. In the formulas (98) and (99) it was assumed that the walls of the resonator are of infinite conductivity so that no electric intensity exists in them. This requires that

$$E_z (\rho = a) = J_0 (\gamma a) = 0, \tag{100}$$

where a denotes the radius of the resonator. This equation has an infinite number of real roots, the lowest being $\gamma a = 2.4048$, and this determines the fundamental resonant frequency and wavelength λ_0. If σ, the conductivity of the dielectric, is neglected in comparison with $\epsilon_r\omega$, the propagation constant becomes

$$\gamma = \omega \sqrt{\mu\epsilon_r} = \frac{2\pi}{\lambda}. \tag{101}$$

ϵ_r is the dielectric constant of the material filling the resonator taken relative to air. Since λ can be meas-

ured, this dielectric constant may be derived from the relation

$$\frac{2\pi a\epsilon_r}{\lambda} = 2.4048$$

or

$$\epsilon_r = 0.146\left(\frac{\lambda}{a}\right)^2 = \left(\frac{\lambda}{\lambda_0}\right)^2. \tag{102}$$

No appreciable error will be committed in using the preceding results for the practical case of dielectrics with low but finite conductivity.

The Q of the filled cylindrical resonator is shown to be

$$Q = \frac{a}{d\left(1 + \frac{a}{2z_0}\right) + a\tan\delta}. \tag{103}$$

Here d is the wave-guide skin depth, $2z_0$ is the axial length of the resonator and $\tan\delta = \epsilon_i/\epsilon_r$ is the loss factor of the dielectric. Consequently

$$\tan\delta = \frac{1}{Q} - \frac{1}{Q_0}, \tag{104}$$

where Q_0 is the Q of the air-filled resonator.

It should be remembered in this connection that the theoretical Q_0 values, in general, are found to be considerably different from the measured ones. This tends to limit the reliability of the method.

After having thus sketched the different methods used in the determination of the complex dielectric constant of substances of importance in wave propagation, we turn now to the presentation of the data.

Liquid Water

Table 17 gives the results obtained recently on liquid water.[22,38,39,44]

Table 17. Temperature variation of the dielectric properties of water. $\lambda = 1.24$ cm.[38,39]

t°C	n	k	ϵ_r	ϵ_i	σ mhos/m
0	4.68	2.73	14.4	25.5	34.3
3	....	....	27*	27*	36.0*
5	5.24	2.89	19.1	30.3	40.7
10	5.74	2.92	24.4	33.5	45.0
15	6.17	2.88	29.8	35.5	47.8
18	....	....	32.1†	39.2†	51.8
20	6.53	2.77	34.9	36.2	48.6
25	6.84	2.63	35*	23*	30.6*
..	....	....	39.8	36.0	51.1
30	7.10	2.48	44.2	35.2	50.0
35	7.30	2.30	48.0	33.6	45.1
40	7.47	2.11	51.3	31.5	42.4
60	....	....	44*	14*	18.6*

*Data from reference 22, at $\lambda = 1.25$ cm.
†Data from reference 44, at $\lambda = 1.26$ cm.

It has been found by Saxton and Lane that the temperature variation of the dielectric constant in the range 0 to 40 C at 1.24 and 1.58 cm can be accounted for with simple theoretical formulas. At any given temperature one single characteristic constant, the "relaxation time," was sufficient to account for the frequency dependence of the complex dielectric constant of water. The formulas in question are the following:

$$\begin{aligned} 2n^2 &= \left(\frac{\epsilon_s^2 + \epsilon_o^2x^2}{1+x^2}\right)^{\frac{1}{2}} + \frac{\epsilon_s + \epsilon_o x^2}{1+x^2}, \\ 2k^2 &= \left(\frac{\epsilon_s^2 + \epsilon_o^2x^2}{1+x^2}\right)^{\frac{1}{2}} - \frac{\epsilon_s + \epsilon_o x^2}{1+x^2}, \end{aligned} \tag{105}$$

or

$$\begin{aligned} \epsilon_r &= n^2 - k^2, \\ &= \frac{\epsilon_s + \epsilon_o x^2}{1+x^2}, \end{aligned} \tag{106}$$

and

$$\epsilon_i = 2nk.$$

Here

$$x = \omega\tau = 2\pi f\tau,$$

with τ denoting the relaxation time, ϵ_s is the static dielectric constant, ϵ_o the optical dielectric constant due to the sum of the electronic and atomic polarizations.

Table 18. Temperature variation of the dielectric properties of water.[38,39] $\lambda = 1.58$ cm.

t°C	n	k	ϵ_r	ϵ_i	σ mhos/m
0	5.24	2.90	19.0	30.4	32.0
5	5.84	2.97	25.3	34.7	36.6
10	6.36	2.91	32.0	37.1	39.2
15	6.77	2.78	38.1	37.6	39.7
20	7.13	2.61	44.0	37.2	39.2
25	7.40	2.41	49.0	35.7	37.6
30	7.59	2.21	52.7	33.5	35.4
35	7.72	2.01	55.5	31.0	32.7
40	7.81	1.80	57.7	28.1	29.7

Considering τ as a parameter to be derived from the experimental data, one finds in Table 19 the relaxation times in the 0 to 40 C temperature range.

Table 19. Relaxation times of water at different temperatures.[38,39]

t°C	$\tau \times 10^{12}$ sec	t°C	$\tau \times 10^{12}$ sec
0	19.0	25	6.8
5	14.6	30	5.9
10	11.85	35	5.2
15	9.6	40	4.5
20	8.1		

TABLE 20. Temperature variation of the dielectric properties of water.[45,46] $\lambda = 10$ cm.

	Refractive index n			Absorption index k					
		Experimental			Experimental				
t°C	Calc	$\lambda = 9.72$ cm	$\lambda = 10$ cm	Calc	$\lambda = 9.72$ cm	$\lambda = 10$ cm	ϵ_r calc	ϵ_i calc	σ mhos/m
0	8.99	8.95	....	1.47	1.35	....	78.66	26.43	4.40
5	9.04	....	....	1.14	....	....	80.42	20.61	3.44
10	9.02	9.00	....	0.90	1.10	....	80.55	16.23	2.70
15	8.96	....	....	0.76	....	....	79.7	13.61	2.27
20	8.88	8.88	8.84	0.63	0.90	0.66	78.46	11.20	1.84
25	8.80	....	....	0.50	....	....	77.20	8.80	1.46
30	8.71	8.75	8.69	0.45	0.73	0.54	75.66	7.84	1.30
35	8.62	....	....	0.40	....	....	74.14	6.89	1.16
40	8.53	8.60	8.56	0.36	0.60	0.40	72.63	6.15	1.02

Table 20 refers to 10-cm waves for which measurements were made in the temperature range 0 to 40 C.[45,46] In one series of measurements the wavelength was 9.72 cm, but this is considered close enough to have the corresponding data included with the 10-cm waves.

The preceding table indicates that the agreement between calculated and measured values of n and k is satisfactory. It is to be noted here that the experimental results on S band were obtained by the standing wave ratio method, those at K band with the reflection-transmission method.

Using equations (105) and (106), the temperature variation of the refractive and absorption index, or real and imaginary parts of the complex dielectric constant, can be computed at any wavelength provided that the relaxation time at the temperature in question is known.

In Tables 21 and 22, the temperature variation of the indices n and k are given. These results were computed with the aid of formulas (105) and (106).

It is thought[38,39] that until more extensive experimental results become available the computed values can be regarded as representing the best information available on the dielectric constant of water in the millimeter and centimeter range. Figure 25 represents the best available information on water at 20 C.

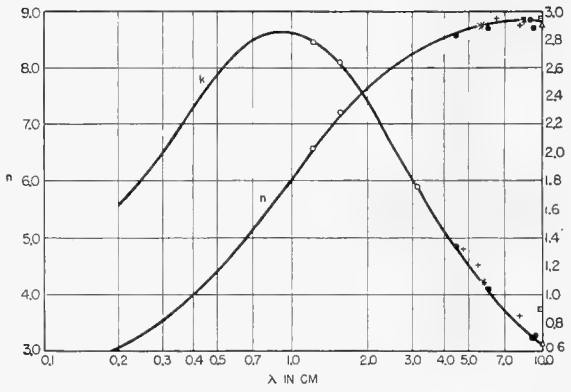

FIGURE 25. Refraction and absorption indices for water.

ICE

A certain number of measurements on the dielectric constants of ice were made in the centimeter wavelength range. The British workers[47] used the resonator Q method at 3 and 9 cm. The latest results on both these wavelengths are collected on the accompanying graph (Figure 26). The temperature range extends from about —50 C to 0 C. The refractive index turns out to be constant in this range. It was found to be equal to 1.75 at 3.01 cm and 1.72 at 9.18 cm. The absorption index increased in this temperature range from about 0.0001 to 0.0010.

TABLE 21. Temperature variation of the dielectric properties of water.[38,39] $\lambda = 0.50$ cm.

t°C	n	k	ϵ_r	ϵ_i	σ mhos/m
0	3.18	1.76	7.01	11.2	37.3
5	3.50	2.03	8.13	14.2	47.3
10	3.80	2.25	9.38	17.1	57.0
15	4.10	2.41	11.0	19.7	65.6
20	4.39	2.54	12.8	22.3	74.3
25	4.67	2.62	14.9	24.4	81.3
30	4.94	2.67	17.3	26.4	88.0
35	5.21	2.69	19.9	28.0	93.3
40	5.47	2.69	22.7	29.4	98.0

TABLE 22. Temperature variation of n, k, ϵ_r, ϵ_i and σ.[38,39] $\lambda = 3.2$ cm.

t°C	n	k	ϵ_r	ϵ_i	σ mhos/m
0	7.10	2.89	42.0	41.1	21.4
5	7.63	2.62	51.3	40.0	20.8
10	8.00	2.33	58.6	37.3	19.4
15	8.22	2.00	63.6	32.9	17.1
20	8.33	1.72	66.4	28.7	14.9
25	8.38	1.50	68.0	25.1	13.1
30	8.39	1.31	68.7	22.0	11.4
35	8.38	1.16	68.9	19.4	10.1
40	8.35	1.02	68.7	17.0	8.85

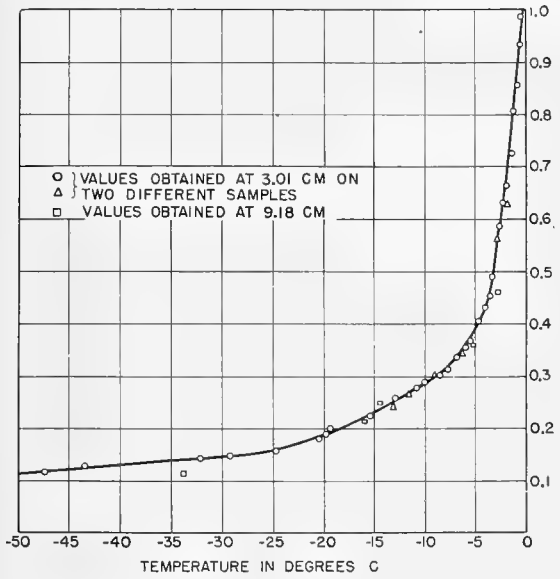

FIGURE 26. Absorption index ($k \times 10^{+3}$) versus temperature for ice.

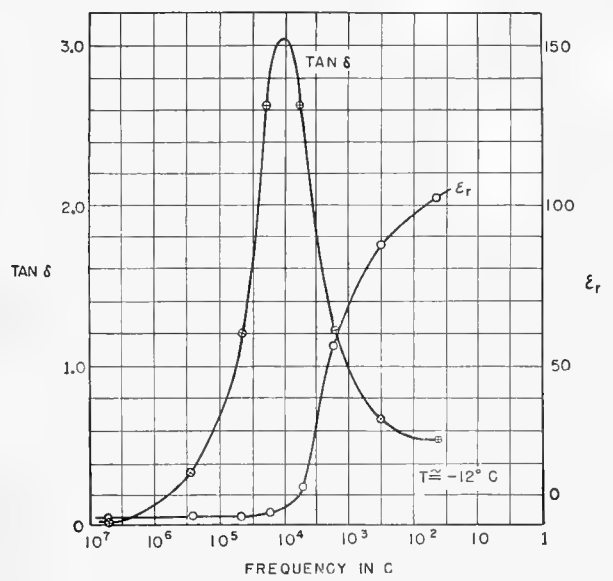

FIGURE 27. Loss factor and dielectric constant of ice.

Younker,[22] using the standing wave ratio method at 1.25 cm, found at about —15 C

$\epsilon_r = 3.3$ and $\epsilon_i = 0.011$, or $\sigma = 0.013$ mhos/m.

These data can be compared with those obtained at 3.01 cm,[47] where

$\epsilon_r = 3.06$ and $\epsilon_i = 0.00080$, $\sigma = 0.00044$ mhos/m.

The difference at these two wavelengths between the conductivities appears much too large and further studies should clear up this discrepancy. The dielectric losses in ice in the centimeter region are, however, very small.

At much lower frequencies the dielectric behavior of ice is given in Figure 27. These data refer to a temperature of —12 C.[47]

Attenuation Due to Water Vapor

In order to determine the attenuation due to water vapor, Saxton endeavored to measure the refractive and absorption indices of water vapor.[48] Using the resonator Q method, he found that by passing from 9 to 3.2 cm the real part of the dielectric constant changes from 1.0056 to 1.0051. According to a general relationship connecting the real and imaginary parts of the complex dielectric constant,[49] the indicated variation of (ϵ_r—1) given by Saxton should be accompanied by a tremendous absorption by water vapor in the microwave region as pointed out by Van Vleck.[49] This is contrary to the data available and rules out the frequency variation of ($\epsilon_r - 1$) given by Saxton. According to Van Vleck, in the microwave region outside of any resonance region, the refraction[(n^2—1), n being the refractive index] or ($\epsilon_r - 1$), must be appreciably constant over the microwave region to account for the absence of any large absorption coefficients.

The conclusion is similar in case of resonance which occurs for both O_2 (0.25 cm and the 0.5-cm. band) and H_2O (—1.30 cm). The refractive index of the atmosphere free of condensation should be constant throughout the microwave region. The refractive index for infinitely long waves or the static dielectric constant can be used here. In the presence of condensation, clouds, fog, and rain, the attenuation is increased considerably, and the refraction or ($\epsilon_r - 1$) might then differ from the static value. But under standard conditions, the refraction of the atmosphere should not change by more than a few parts in a thousand in the microwave region.

10.7 LABORATORY MEASUREMENTS OF DIELECTRIC PROPERTIES[†]

The working committee of Ultra Short Wave Panel has presented a report dealing with the measurement in the laboratory of

1. The dielectric constant and loss angle in superheated steam for wavelengths in the S, X, and K bands.

[†]By F. Hoyle, Ultra Short Wave Panel, Ministry of Supply, England.

2. The dielectric constant and conductivity of bulk water for the K band.

These experiments have been carried out by Saxton. The method adopted on S and X bands in (1) was to allow superheated steam to isue freely through a resonator into the air. The pressure throughout the apparatus was accordingly the atmospheric pressure. The temperature of the steam was measured before entering and after leaving the resonator. The temperature difference between these measurements was no more than 2 C, so it seems clear that no condensation of water droplets could occur within the resonator. A somewhat different technique was employed for X band in that the resonator was replaced by a wave guide. If ϵ is the dielectric constant, then the best representation of the results is obtained by plotting $(\epsilon-1)$ against $1/T$, for each wavelength where T is in degrees absolute. It was found that the results for different values of T fitted very well to a straight line as they should theoretically, but the value of $(\epsilon-1)$ for all values of T was found to be systematically about 10 per cent less than would have been expected on the basis of previous measurements of the dielectric constant of steam at much longer wavelengths. This discrepancy was found on X and K bands. The reason for the discrepancy is not yet understood. It is known, however, that the reduced value of $(\epsilon-1)$ does not arise from strong dispersion occurring in the microwave band since there is no evidence of any abnormal absorption.

The method adopted in (2) was to measure first the attenuation factor of radiation passing through water. This was done by placing a transmitting horn above a large shallow trough and a receiving horn below the trough. The attenuation factor was measured immediately by varying the depth of the water in the trough. Second, the reflection coefficient of electromagnetic waves incident normally on a plane surface of water was measured. These two observations were sufficient to determine the dielectric constant and conductivity of water. The results obtained for a wavelength of 1.58 cm were:

Dielectric constant about 40;

Conductivity about 4.10 esu.[11]

The same values were obtained for both tap water and distilled water, showing that the presence of salts in the water had little effect on the value of the conductivity.

Chapter 11

STORM DETECTION

11.1 STORM DETECTION BY RADAR[a]

THIS SUMMER (1944) a study was made of the meteorological echoes observed on a Canadian microwave S-band early warning radar set at Ottawa. These were correlated with check observations on the weather made by a large number of local observers distributed over the area covered by the set. It was found that observers inside the source area of the echo always reported rain; just outside the echo (1 to 5 miles) there was a half chance of light rain. Atmospheric electrical disturbance was present in less than half the cases checked. Echoes became less frequent at increasing distances from the set but in some cases were seen at 160 miles.

The display system that we have used is a *plan position indicator* [PPI] tube. This tube provides a map of a circular area centered on the location of the set and extending out at choice to 40 or 80 or 160 miles. The last-mentioned setting was the one used most of the time.

11.1.1 Procedure

During the hours of operation a 16-mm motion-picture camera was kept running, taking pictures of the PPI display and a clock alongside, exposing one frame of the film for the duration of each revolution of the array. Thus about four photographs were obtained per minute. At the same time we watched the progress of moving echoes across the screen and made telephone calls to any observers that were available, in the neighborhood of any echo. From the observer the existing state of the weather was determined; his remarks and the exact time were carefully noted.

We checked the echoes and their movement as recorded on the film against the information obtained about the weather from the observers. We also made charts of the echoes, based on the film, at 30-minute intervals.

11.1.2 Weather Information

Facilities of which we availed ourselves for obtaining information were, among others:

1. Ottawa meteorological stations. These stations provided us with as many as three forecasts a day and with weather information generally.

2. Distant meteorological stations. Apart from the Ottawa stations, the nearest weather station, 57 miles away, is at Canton, N. Y. Its reports are included in the teletype sequences that come to us.

3. Unofficial observers, consulted by telephone. Since the official weather stations did not provide the close network that we required, we compiled a list of persons whose location could be closely marked on our map and whom we could consult about existing weather conditions to the extent that an untrained observer would be competent.

11.1.3 Correlations

Our aim was to correlate observed echoes with weather conditions. At first clouds were thought to be possible sources of echoes, and it was thought that fronts might produce some sort of echo quite independently of cloud or precipitation along the front. The earlier part of our work showed that on afternoons with heavy cumulus clouds but with no precipitation there were no weather echoes. On days with scattered showers, however, echoes were observed. Also, the passage of a front did not seem to produce any peculiar sort of echo or any echo that could not be attributed to precipitation along the front.

In analyzing our correlations, we have found it convenient to consider them in two groups. First, there are *correlations with echo,* that is, correlations when the observer was in the vicinity of an echo, although not necessarily right inside the echo. All correlations involving telephone calls to local observers were of this type, for we didn't make such a telephone call unless there was an echo in the vicinity. Second, there are *correlations with weather,* or correlations with weather stations, when we first select an occasion when precipitation is reported (by an official station) and then go looking in our records for an echo to match. Nearly all the precipitation recorded at the weather station during our hours of operation was light, and too light, as it proved, for us to detect it at the distance we were away. Thus there is only a very small number of echoes associated with correlation with weather,

[a] By Col. J. T. Wilson, Director of Operational Research, NDHQ, Canada.

and so very little overlapping between this group and the group of correlations with echo.

11.1.4 Correlations with Echo

Table 1 gives a summary of the results obtained in the form of a comparison of precipitation observed inside and just outside the echoes.

TABLE 1. Precipitation inside and just outside echoes.

	Observer's position relative to echo			
	Inside		Outside (1 to 5 miles)	
	No.	%	No.	%
Cases of no rain	0	0	19	48
Very light rain	6	13	7	17
Light rain	16	33	13	33
Moderate rain	13	27	1	2
Heavy rain	13	27	0	0
Total	48	100	40	100

11.1.5 Correlations with Weather Stations

Correlations with weather stations were notable chiefly for the rain we did not detect. Nearly all the precipitation observed at the station was light and apparently too light to produce echoes effective at such distances. Weather reports on the teletype from Ottawa itself were not correlated with echoes because most meteorological echoes within 10 miles were obscured by permanent echoes and distortion at the center of the PPI. The next closest weather station is at Canton, N. Y., 57 miles from our set. The rainfall for every hour was obtained from a rain gauge at Canton, and in addition some of the teletyped weather reports were received. Rain was reported from Canton on five occasions during our hours of operations. On one of these occasions we had an echo directly over Canton; on three others we had an echo within three miles of Canton; on one occasion we had no echo in the vicinity at all. The details are given in the table. It can be seen that we detected rain falling at a rate of 0.2 in. per hour and failed to detect rain falling at a rate of 0.03 in. per hour.

TABLE 2. Rain at Canton, New York (U. S. Weather Station, 57 miles from set) during analyzed hours of operation.

Case	Rainfall in./hr*	Thunder	Echo
1	0.20	Yes	Overhead
2	0.05	Yes	1 mile away
3	0.3	Yes	2 miles away
4	Trace	No	3 miles away
5	0.03	Yes	No echo

*All rates taken from gauge reading made at hourly intervals.

11.1.6 Résumé of Correlations

Our checks with local observers out to 60 miles from the set revealed the following: Inside the echo there is sure to be rain, with a 0.3 chance that it is moderate or heavy. Just outside (1 to 5 miles) there is never more than light rain, and a half chance of none at all. Further, the chance of an observer in the vicinity of an echo reporting thunder was 0.4. Our checks with weather stations were less relevant, because only two echoes passed over weather stations during the period studied. But from the numerous cases of light rain at these stations that we did not detect, we can say that we cannot detect light rain at 90 miles. By light rain we mean rainfall less than 0.1 in. per hour, and this can just be detected at 50 miles. Further, to judge by one storm that we detected and one we missed at Canton, we can detect 0.2 in. per hour and cannot detect 0.03 in. per hour at 57 miles.

11.1.7 Fraction Detected by Radar of Total Quantity of Rainfall

Starting from the proportion of hours of rain that give an echo, we have used the distribution with rate of rainfall of the hours of rain to give us a value for the minimum rate of rainfall that will give us an echo. Now using a distribution with rate of rainfall of the quantity of rainfall, we can proceed to determine the proportion of the total quantity of rain that was observed by radar. The proportion is quite high: 83 per cent close to the set, 62 per cent at 50 miles.

11.1.8 Comparison with Ryde's Theory

Computations of the echo strength to be expected have been made on the basis of the theory developed by J. G. Ryde of the General Electric Company (British). The experimental results are in satisfactory agreement with theory. (See Section 10.1.)

11.1.9 The Best Frequency for Storm Detection

The sensitivity to rain of the frequencies we have been using is such that with the power available we can obtain satisfactory performance. At higher frequencies the sensitivity, according to theory, is considerably higher, but considerations of absorption made by Ryde would keep us from going to much higher frequencies. Absorption affects us in two different ways. In the case of widespread rain, even of moderate intensity, there is enough absorption between

the set and the echo source to reduce our effective range considerably. Where there is no widespread rain but the rain that we want to see is heavy and concentrated, the absorption of high-frequency radiation by heavy rain can be so great that hardly any of the radiation impinging on the storm makes its way back out to be reflected. We could actually fail to detect a storm in this way, because the storm was too intense. The frequency we are using (S-band) is safe against both these effects, but increasing it by a factor 3 would lead us well into them.

11.1.10 Ultimate Range—Greater Range of a Production Set

The performance of the prototype set we have used has been specified in the previous section by its range for aircraft. The performance of the same design of set, constructed and installed to the final production specification, is known to be better: the range for aircraft is approximately twice as great, and some calculations show that very roughly the range of a production set for storms will be twice that of our prototype set.

The full account of this work is published as: Summer Storm Echoes on Radar MEW, Report No. 18 of the Canadian Army Operational Research Group; 27 Nov., 1944.

11.2 S-BAND RADAR ECHOES FROM SNOW[b]

Since June 1941, the Canadian Army Operational Research Group has been studying the nature and application of S-band radar echoes from storms. During the past winter we studied echoes from snow, obtained on occasions when snow was present and rain definitely was not.

Heavy snow has been detected on five occasions, with maximum ranges varying from 30 to 65 miles. One moderate snowfall which kept all aircraft

[b]By J. S. Marshall, Canadian Army Operational Research Group.

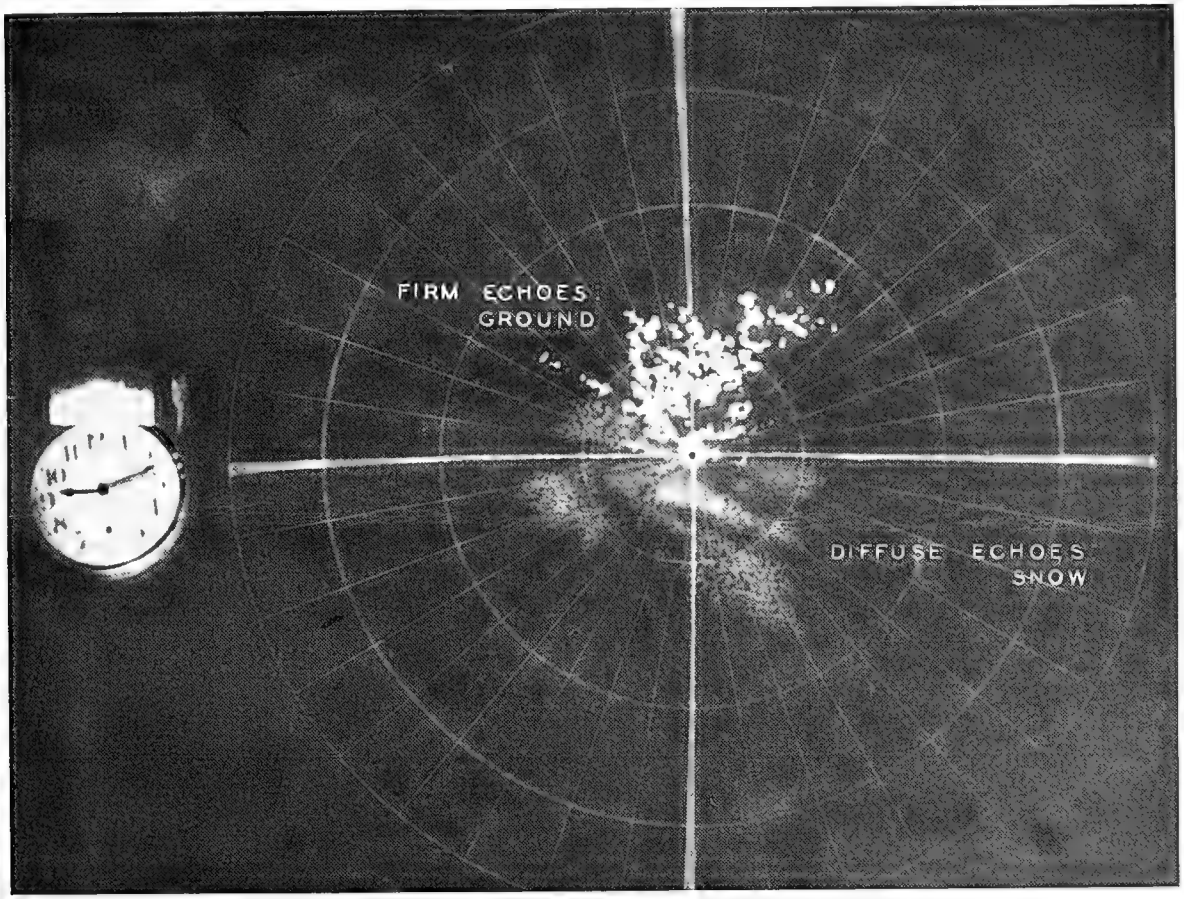

FIGURE 1. Typical S-band PPI display of snow echoes.

grounded was not detected at all, even at the minimum range of 10 miles.

Roughly, rain and snow of the same intensity, expressed in inches of liquid water per hour, produce about the same echo and are detectable to the same range. Further, there seems to be no useful difference in pattern between echoes from the two sources. Figure 1 shows a typical PPI picture of snow echoes made during the course of the study.

Theoretically, this equality is not directly significant; in the case of snow there is a much greater bulk of lighter material, falling more slowly and reflecting less well.

Operationally, there are two reasons why radar storm detection is less useful in winter (in Canada). A given intensity of precipitation in the form of snow, say 0.1 in. of water per hour, is much more hazardous to flying and to ground activities than the same intensity in the form of rain. Further, great intensities of precipitation such as lead to long-range echoes in summer are almost nonexistent in winter in this region; therefore, detection at great ranges is not achieved. Thus S-band radar in summer can detect important storm areas to a radius of about 100 miles; in winter it detects hardly any weather beyond 50 miles and misses some important snow even at 10 to 20 miles.

For the greatest total contribution of radar to flying it is a good thing that echoes from snow are weak. This is important, for while the cumulo-nimbus activity detected in summer must always be avoided by aircraft because of violent air currents, flying in moderate snow can be safe with good blind-flying control. It is fortunate, therefore, that echoes from snow are probably not strong enough to interfere with any radar elements of this control.

This work has been done with the cooperation of the National Research Council of Canada, the Canadian Meteorological Service, and the Royal Canadian Air Force.

Chapter 12

ECHOES AND TARGETS

12.1 FLUCTUATIONS OF RADAR ECHOES[a]

SINCE JUNE, 1943, the Propagation Group of the Radiation Laboratory has had a project under way to investigate the nature and origin of fluctuations from close targets. This work has been done in the microwave region using the mobile S- and X-band sets belonging to the group. Most of the work has been on S band. We have restricted ourselves to targets sufficiently close to the radar that the more usual effects of atmospheric refraction can be neglected. We have not paid much attention to moving targets such as ships or planes, as their echoes are easily accounted for by the changing aspect of the target, propeller modulation, etc.

One of the obvious sources of signal fluctuation is instability in the system. In our case system instability was chiefly due to ripple in the receiver, and sensitivity to changes in line voltage affecting the modulator, receiver, and indicator units. After considerable effort these forms of instability have been reduced but not completely eliminated. The transmitted pulse shows an average fluctuation about the mean of ± 0.1 db with a maximum deviation about 0.5 db. Pulse-to-pulse frequency changes are not greater than 0.1 or 0.2 mc, and frequency modulation inside the pulse is less than 0.2 to 0.3 mc. These figures are for the S-band set, and instability is somewhat greater on X. The r-f signal intensity is measured by comparison with a pulse from a calibrated signal generator. This pulse shows a fluctuation as large as the transmitted pulse, i.e., about ± 0.12 db. It is believed that this apparent change is not in the signal generator but rather in the receiver and indicator units.

Some radar signals show almost as little fluctuation. These are large man-made targets in isolated positions viewed over land. Some examples that we have found are the Provincetown standpipe as viewed from Race Point in Provincetown and the Winthrop standpipe in Boston viewed from Deer Island. In these cases the average pulse to pulse deviation from the mean is ± 0.14 db. Such steady signals are the rare exception. Most echoes show changes that are much larger than can be accounted for by instability in the system tests.

[a]By H. Goldstein, Radiation Laboratory, MIT.

12.1.1 The Interference Concept

When this research was started, it seemed to be a common idea that changes in atmospheric refraction in the path between the target and set could account for the observed variations. We have found little evidence for this belief. If the targets are closer than 10 miles, the effects due to the atmosphere, if there are any, must be small compared to the more important phenomena shown by the echoes. The behavior of the radar echo is determined by the fact that a radar signal is usually not the return from a single target but rather the sum of returns from all targets within the area illuminated by the set. Since the radar beam is coherent, the individual signals must be added in amplitude taking into account the relative phase of the echoes. The total signal is the result of the interference between these component echoes. In the case of the standpipes mentioned above there were intervening hills so that only the top portions of the targets were seen by the radar, but in most other cases there is more than one target present, and the interference between these targets will determine the nature of the total echo.

In the Boston region, we have found one very simple dual target consisting of two radio towers 500 ft high and 60 yd apart in range. Both constructive and destructive interference has been observed in this case.

The changes in the phase between the component signals might be due to several causes. If the index of refraction in the path between the two towers changes, then the optical path length would change. However, the deviation of the index from 1 would have to double in order to produce sufficient phase change. A change in the frequency of the transmitter could also account for the phase change. To produce the observed effect it would have to be greater than ½ mc, which is larger than the frequency instability of the system. Finally, the towers themselves could physically move relative to each other and produce the phase change in a manner similar to that in the Michelson interferometer. To produce a phase change of π the targets need only move $\lambda/4$ relative to each other. At S band this amounts to 1 in. It does not seem unnatural that such tall structures might sway in the wind by even a greater amount. To test this conclusion the signal from these towers

was measured over a period of 4 days. The amount of fluctuation was estimated visually every half hour. These results showed a definite correlation with the speed of the wind. Large fluctuations occurred only with high winds. It was calculated that if the fluctuation had indeed been independent of wind speed the odds against getting the set of readings obtained by these measurements would be 10,000,000 to 1.

12.1.2 Assemblies of Random Scatterers

In a more common type of radar target the entire illuminated area contains a large number of independent targets with random phases. If we represent the signal from each target by a vector showing amplitudes and phase, then the total signal is found by adding up all these vectors. If the phase of the individual vector is changed slightly (for instance, by relative motion) this vector diagram would be rearranged and the total signal changed. Some practical examples are precipitation echoes, where the individual targets are the drops; window, where the echo arises from many strips of tin foil; and sea echo, where the individual targets are probably areas of reflection from the surface of the sea.

The theory of this type of target has been extensively worked out.[1-3] One of the questions that can be answered by the theory is to determine the probability $P(I)$ that a given signal from the target will be of intensity I in range dI. Or equivalently, one can find the fraction of returned pulses having intensity I in range dI. [$P(I)$ has been called the first probability distribution.] The result is simply

$$P(I)\,dI = e^{-I/I_0}\frac{dI}{I_0},$$

where I_0 is the average intensity of the echo. The continuous curve in Figure 1 is a plot of this experimental formula.

The equation for $P(I)$ is independent of the distribution of the individual amplitudes, nor is it required that the individual amplitudes be constant with time, only that the distribution shall be stationary with time. The only other conditions that must be satisfied are that there shall be a large number of scatterers and that they shall be independent of each other with phase random both in space and time. It will be seen from the formula that the most probable signal is always zero. Furthermore the distribution is independent of the number of targets. The rapidity of the fluctuations is determined essentially by the echo changes and the relative velocity of the scatterers. The detailed relation has been worked out between the frequency spectrum of the fluctuations and the velocity distribution of the particles.[3] The frequency of fluctuations should increase linearly with r-f frequency.

In order to investigate experimentally this type of radar signal, it is necessary to get some method of measuring the intensity of the individual pulses. In our case this was obtained by photography of the single sweeps on the A scope. For this purpose a special A scope was used with a blue screen tube operated at 6 kv. Commercial 16-mm movie cameras were used in which the shutter and claw had been removed and to which a high-speed motor drive had been added.

By photographing a calibrated r-f signal generator pulse at the same receiver gain but at different r-f levels, one can obtain a curve for the deflection in centimeters against r-f intensity. By means of this curve the measured deflections from the pulse-to-pulse films can be converted into measurements of r-f intensity. From these experimental data it is possible to compute an experimental first probability distribution.

Figure 1 is an example of such an experimental distribution obtained by measuring a thousand pulses of

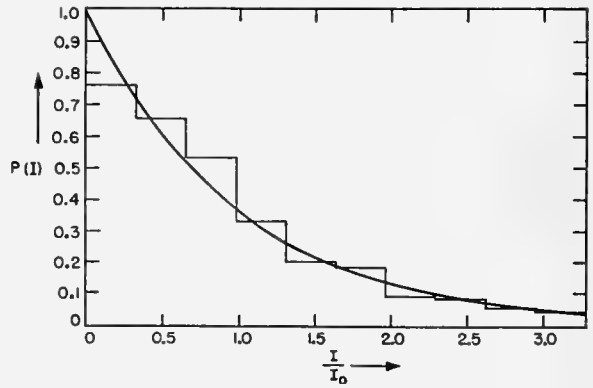

FIGURE 1. The first probability distribution, $P(I)$ of the intensity of cloud echoes. Curve: $P(I) = e^{-I/I_0}$ Histogram: experimental results. Film 90, S band, 1,000 pulses.

precipitation echo on S band. The continuous curve in that figure shows the theoretical formula given above. The agreement is good.

By what is essentially a Fourier analysis of these data, one can also determine the frequency spectrum of the video signal. Figure 2 shows such an experimentally determined frequency spectrum for sea echo on both S and X bands. The spectrum extends to 120 c on X band and about 50 c on S. The ratio be-

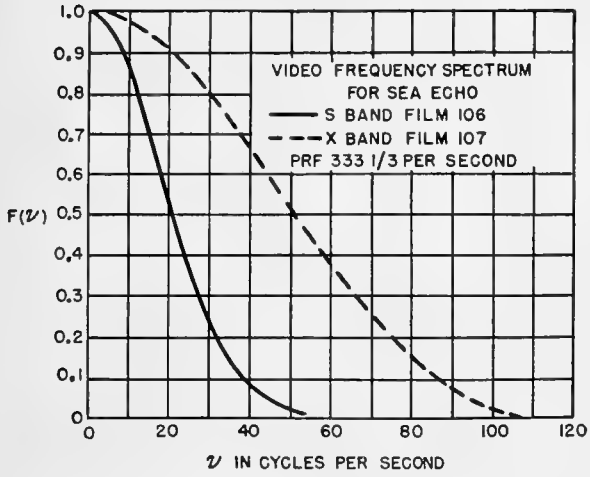

FIGURE 2. Experimentally determined frequency spectrum for sea echo.

tween the width of the spectra is 2.4 compared to 2.88 for the ratio of wavelengths. This discrepancy is probably due to the crudity of the measurements on X band.

12.1.3

Ground Clutter

The ordinary ground clutter consists of echoes from a variety of types of targets: earth, rocks, trees, branches, bushes, leaves, grass. Our present conception is that the fluctuation in ordinary ground clutter arises from the motion of leaves and branches in the wind, changing the phase patterns in a manner somewhat similar to that for random scatterers. There will in addition be a relatively steady signal from fixed objects such as rocks and tree trunks.

We have obtained much qualitative evidence for this picture, but it is difficult to obtain quantitative

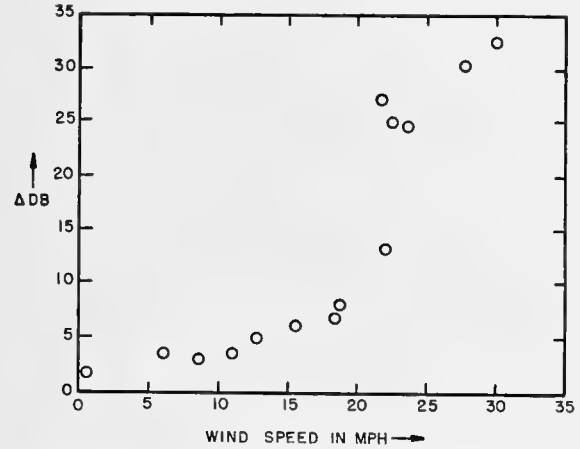

FIGURE 3. Fluctuation in signal from Blue Hills versus wind speed. S band, 10 a.m. April 24, 1944 to 11 a.m. April 25, 1944.

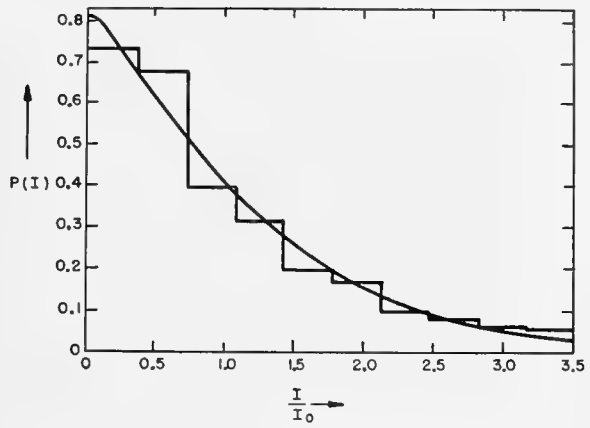

FIGURE 4. First probability distribution, Baker Hill, Maine. Wind speed 25 mph. Curve: theoretical, fixed to random signal = 1 db. I_0 = average intensity. Histogram: experimental results. Film 103, 3,000 pulses, S band.

data because the wind speed at the target is not usually known. Fortunately, in the Boston area the largest ground signal is due to the Great Blue Hills, which is the site of the Blue Hill Observatory. It is thus possible to obtain data on the wind speed at the target. We monitored the signal from Blue Hills for a 24-hr period in April of 1944. Movies were taken of the A scope at regular intervals. During the period of observation the wind speed varied between 30 mph and dead calm. To interpret the data a somewhat crude parameter was defined as a measure of the amount of fluctuation. The change in the signal strength from one frame to the next (0.06 sec) was measured and averaged over 200 frames.

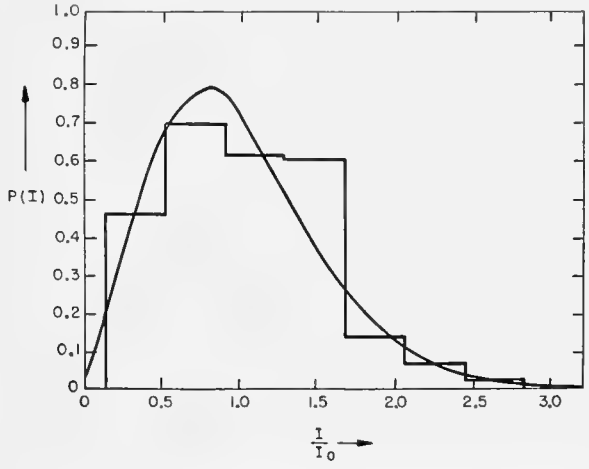

FIGURE 5. First probability distribution, Mt. Penobscot, Maine. Wind speed 10 mph. Curve: theoretical, fixed to random signal = + 7.2 db. I_0 = average intensity. Histogram: experimental results. Film 82 (16 fr per sec), 400 frames, S band.

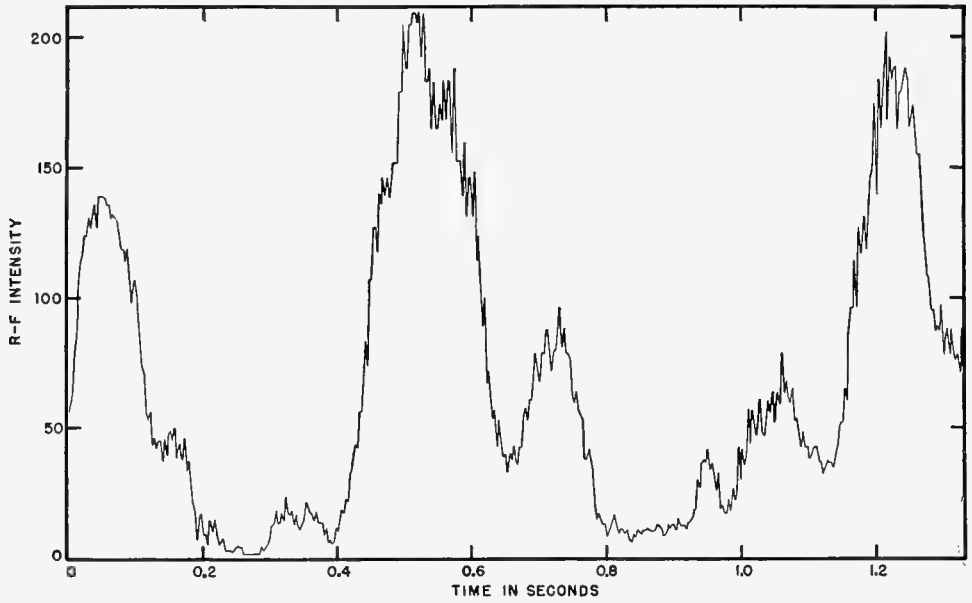

FIGURE 6. Pulse-to-pulse record of the signal from Black Woods, Bar Harbor. Film 87, July 9, 1944. S-band, prf 333⅓ per sec, wind speed 22 mph.

This parameter was then plotted against the wind speed as shown in Figure 3. There is a quite good correlation between the amount of fluctuation as measured by this parameter and the speed of the wind. The fluctuation is of the order of 0.2 db at 0 mph, which is almost as good as our steadiest signals. At the other extreme the fluctuation is about 3.4 db at 30 mph. There appears to be a rather sudden jump in the fluctuation at a wind speed in the neighborhood of 20 mph. This jump has been observed at other seasons of the year and is believed to be rather general. It is significant that the wind speed at which the jump occurs is roughly that at which large branches and small trees begin to move as a whole.

The theoretical description for a simple picture of ground clutter consisting of an assembly of random scatterers (leaves, grass, etc.) plus a fixed signal (rocks, trees, trunks) is not difficult to work out. When the proportion of steady signal is small, the first probability distribution closely resembles that for purely random scatterers. For a large ratio of fixed-to-random signal the amount of fluctuation is greatly reduced, and the first probability distribution tends to a Gaussian curve about the average intensity. This is illustrated in Figures 4 and 5. Figure 4 is a plot of the experimentally determined first probability distribution for a signal from heavily wooded terrain on S band at 25-mph wind speed. This has been fitted by a theoretical curve for a ratio of fixed to random signal of —0.1 db.

Figure 5 shows the distribution for a similar type of terrain but for a wind speed of 10 mph. Here the results are fitted to a curve for a ratio of fixed to random signal of + 5 db. The most probable intensity is no longer at zero, and the amount of fluctuation is considerably reduced.

Figure 6 is a plot of the intensity of some ground clutter at high wind over a period of 1½ seconds as obtained from a pulse-to-pulse film. While the signal changes quite rapidly, it is not nearly so fast as sea return, for example (see Figure 7).

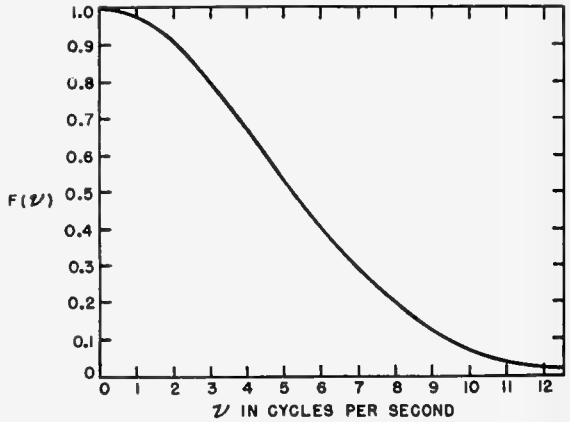

FIGURE 7. Video frequency spectrum for ground clutter, Baker Hill, Maine. Film 103, wind speed 25 mph, prf 333⅓ per sec, wavelength S band.

The frequency spectrum can be obtained from these data as in the previous case. Figure 7 shows the video frequency spectrum obtained under the same conditions as Figure 4 for high winds. The spectrum extends as high as 12 c. Figure 8 is a plot of the frequency spectrum obtained from the same film as in Figure 5. Here at a wind speed of 10 mph the frequency spectrum does not extend beyond 2 c.

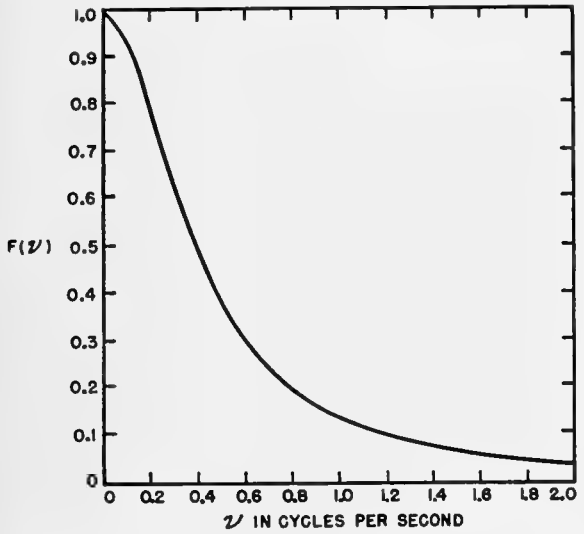

FIGURE 8. Video frequency spectrum for ground clutter. Mt. Penobscot, Mt. Desert Island. Film 82, wind speed 10 mph, wavelength 8 band, prf 333⅓.

12.1.4 Targets Viewed over Water

In addition to the sources of fluctuation described above, echoes from targets viewed over water will change due to the varying reflection from the surface of the sea. Some English investigations have shown that at high angles of incidence the amount of reflection can often change quite rapidly. However, there is another effect due to reflection from the sea surface which is of a much longer period, namely, tidal variations.

Some of our earliest work consisted of monitoring the signal from a number of isolated targets viewed over water over a period of many tidal cycles. It was found that quite a large number of echoes showed a definite correlation with the tide. One very striking example is the case of two standpipes on Strawberry Hill on Nantasket Peninsula, which when viewed from Deer Island in Boston Harbor showed a 15-db variation with tide. Their range is 10,000 yd, and the targets are about 60 ft high. Under these conditions the targets subtend more than two lobes of the interference pattern at S band. Since the effect of the tidal change is to move this lobe structure up and down by 10 ft, it is difficult to believe that a change as large as 15 db could be thus produced. However, one can break up the returned signal into a number of separate signals differing as to whether they suffer two reflections on the surface of the sea or one reflection or go directly to and from the target. While the amplitude of each of these signals does not vary much with tide, their relative phases do, and the total signal can still change considerably in amplitude because of the interference. A similar set of measurements was made on a corner reflector mounted on a small island in Boston Harbor. Here the corner reflector although only 6,000 yd away acts essentially as a point target. The agreement with the theory for a point target is quite good.

Our results emphasize the extreme caution that must be employed in the use of standard targets to monitor radar performance. They are just the type of targets which are normally chosen in the field, and obviously their variations with the tide make them entirely unsuitable for the purpose. It may be possible to find targets whose echoes are sufficiently steady so that they can be used for monitoring. However, they cannot be found without the use of such test equipment as would obviate the need for standard targets.

12.2 THE FREQUENCY DEPENDENCE OF SEA ECHO[b]

As the power and frequency of radar sets continue to increase, and the size of the target to be detected decreases, the presence of sea echo becomes of ever greater operational significance. It acts as a built-in jammer, blanketing and obscuring the desired signals. Despite this growing practical importance the basic phenomena of sea echo have not yet been established. Certainly, the fundamental mechanism responsible for the signal is not yet known. Various conflicting theories have been proposed. It has been suggested that scattering from drops of spray is the cause of the echo. Another hypothesis is that of reflection or diffraction from the large surfaces of the waves themselves. Still other theories have been advanced at one time or another.

Whatever the size of the scatterers, the power received at the radar can be described by a common formula. Consider some particular scatterer, say the

[b]By H. Goldstein, Radiation Laboratory, MIT.

jth one. Then the returned signal from this particular target is

$$P_{rj} = \frac{P_t G^2 \lambda^2}{(4\pi)^3 R^4} \sigma_j,$$

where σ_j is the radar cross section of the jth scatterer, P_t the power transmitted, G the gain, λ the wavelength, and R the range. σ_j differs from the customary cross section in that it incorporates the propagation factor and hence may depend on the height of target and the glancing angle of the incident ray. In considering the time average of the total power received by the radar we can take the scattering to be incoherent. Hence the average radar signal is the sum of P_{rj} over all the j scatterers lying within the area illuminated by the beam width and pulse length:

$$\overline{P}_r = \frac{P_t G^2 \lambda^2}{(4\pi)^3 R^4} \sum_j \sigma_j.$$

It is assumed that the illuminated area is sufficiently large that the sum contains many scatterers and is proportional to the size of the area. In that case this formula can be written

$$\overline{P}_r = \frac{P_t G^2 \lambda^2}{(4\pi)^3} \phi \frac{\tau c}{2} \sigma,$$

where ϕ is the azimuthal beam width, τ the pulse length in seconds, c the speed of light, and σ is defined as the radar cross section of sea echo per unit area of the sea surface and hence is dimensionless. This quantity σ is a function of many parameters: the state of the sea, the glancing angle of the incident beam (and therefore the range), the polarization, and the wavelength. A comprehensive program is under way in the Radiation Laboratory to check the assumptions underlying this formula and to determine the cross section σ as a function of these parameters.

Uhlenbeck has pointed out that the dependence of σ on wavelength should be an especially sensitive function of the scattering mechanism assumed. For drops whose circumference is small compared to the wavelength, the scattering should be of the Rayleigh type, i.e., varying as $1/\lambda^4$. If one takes into account the lobe pattern of the incident field due to reflection on the water surface, the dependence is even faster, possibly as $1/\lambda^8$. On the other hand, if we are dealing with reflection or diffraction from large curved surfaces, then σ should be substantially independent of wavelength or even increase with λ. By measuring σ simultaneously on two or more frequencies, it should be possible to decide between these mechanisms.

Accordingly, such measurements were made in the summer of 1944 at Bar Harbor, using the calibrated S- and X-band mobile radars belonging to the Wave Propagation Group of the Radiation Laboratory. The site elevation was 1,500 ft, and the ranges about 10,000 yd, so that the incident angles were quite small. The constants in the formula for P_r were determined as accurately as possible. In addition, the power, pulse length, and beam width were made comparable in both systems. For relatively stormy sea conditions the ratio of σ on the two wavelengths was found to be:

$$\frac{\sigma_X}{\sigma_S} = +5 \pm 4 \text{ db}$$

for both polarizations. If the Rayleigh $1/\lambda^4$ law holds, the ratio should be +18.5 db, which would seem to exclude spray drops as the scatterers.

One of the difficulties of this type of measurement is to determine the average level of a signal that fluctuates as rapidly as does sea echo. To remove this source of trouble, a device has been developed that reads the average power directly. It might be described as a gated noise meter. With the aid of this instrument we have again begun making measurements of σ on S and X bands, this time from Deer Island in Boston Harbor. The elevation is only 120 ft, and the ranges are correspondingly small.

The results obtained so far do not agree in all respects with the previous data obtained at Bar Harbor. When the sea is fairly calm (Beaufort 3 or less), the ratio of σ_X to σ_S is reproducibly given by:

$$\frac{\sigma_X}{\sigma_S} = +12 \pm 2 \text{ db} \quad \text{horizontal}$$

on horizontal polarization. The scatter is much greater on vertical polarization, and the ratio is much smaller:

$$\frac{\sigma_X}{\sigma_S} \sim +4 \text{ db} \quad \text{vertical.}$$

One set of worth-while measurements has been made with a sea that was considerably rougher (Beaufort 4-5). The ratio was significantly smaller for both polarizations:

$$\frac{\sigma_X}{\sigma_S} = +5 \pm 2 \text{ db} \quad \text{horizontal}$$

$$\frac{\sigma_X}{\sigma_S} = +2 \text{ db} \quad \text{vertical.}$$

At the time these data were obtained the first measurements were made with a calibrated experimental K-band set recently constructed. Only hori-

zontal polarization was available. It was found that

$$\frac{\sigma_K}{\sigma_X} = 3 \text{ to } 5 \text{ db.}$$

Hence under these sea conditions the increase in σ on going from S to X is about the same as when going from X to K.

An interesting by-product of these measurements was the comparison of polarizations, keeping the wavelength the same. This ratio was quite variable, ranging from

$$\frac{\sigma_V}{\sigma_H} = -9 \text{ db} \quad \text{X band}$$

on X band under stormy conditions, to

$$\frac{\sigma_V}{\sigma_H} > +25 \text{ db} \quad \text{S band}$$

on S band with a calm sea. In general the ratio decreases as sea becomes rougher and is almost always less on X than on S band.

It is too early in the investigation to attempt a detailed interpretation of the results. It does seem that scattering from small spray drops is not the sole mechanism, despite the popular observation that sea echo seems to increase rapidly with the appearance of whitecaps. Other evidence also seems to confirm this. Under favorable conditions sea echo appears as discrete signals, moving with the wind, that can be tracked for 15 to 20 sec. This seems longer than one would expect from a breaking wave. On the other hand, reflection from large wave surfaces cannot be the whole story either. This is indicated by the fairly rapid increase of σ with frequency and by the complicated changes with polarization. It is probable that we are dealing with a combination of mechanisms, and it will be a difficult task to unscramble the contribution of each to the total signal.

It should be emphasized that these measurements were taken near the coast, though outside the breakers. Conditions on the high seas might conceivably be quite different.

Discussion

It was stated that individual sea echoes which persist for many seconds cannot be caused either by specular reflection from an inclined water-air interface or by random (Rayleigh) scattering from individual drops of spray. Instead, an aerated surface layer created by a breaking whitecap may persist for many seconds and may be responsible for persistent echoes. Such a layer constitutes an irregular network of air-water interfaces and may give rise to considerable scatter of microwaves. The actual mechanism by which such a layer gives rise to a sea echo is likely to be different at different sea states. If a large area is covered with foam, then in the presence of strong swell the chief return should be expected from a wave crest, and the radar signal would appear to travel slowly on the radar screen as the wave crest progresses.

The author stated that so far no consideration had been given to such involved mechanisms as the one suggested, but added that data already collected might well lead to such an investigation.

It was suggested that several mechanisms, including scattering from droplets, were probably responsible for sea echo in rough weather. Experiments in Britain reported by the British Army Operational Research Group showed that echoes from shell splashes viewed on an S-band gunnery radar could be resolved into two parts. One was from the "boil," a solid wall of water with enclosed air bubbles, which could be readily distinguished from the superimposed response from the larger portion of the splash called the "plume," which is a region of isolated water droplets. Echoes from the droplets in the "plume" region were of many seconds duration, and it seemed likely that an investigation of the frequency dependence of such scatterers would produce useful results.

12.3 THE DEPENDENCE OF SIGNAL THRESHOLD POWER ON RECEIVER PARAMETERS[c]

This paper deals with the effect on the signal threshold power of various parameters in the receiving systems of radar sets, i.e., with the minimum signal power necessary for visibility. Although this is a difficult problem and all the important factors entering it are not known, it is felt that at least qualitatively, and sometimes quantitatively, a fairly good answer can be given at present. First of all it is necessary to define some of the parameters involved in ordinary radar reception. When a signal is reflected from a target the power entering the receiving system may be written in the following form:

$$P_r = \frac{P_t G^2 \lambda^2 \sigma}{(4\pi)^3 R^4}$$

where G, λ, and σ are the antenna gain, radar wave-

[c]By J. L. Lawson, Radiation Laboratory, MIT.

length, and target echoing area or cross section, respectively. P_t is the transmitted power and R the target range. This is, of course, the free space formula. The propagation conditions can be conveniently lumped into a multiplicative factor, which in the following arguments is of little concern. To determine the maximum range capability of the radar set, it is necessary to determine how large P_r must be in order to be detectable. It is then possible to calculate the maximum range capability of the radar set from the above formula, on writing it:

$$R_{\max} = \left(\frac{P_t G^2 \lambda^2 \sigma}{(4\pi)^3 P_{r\,\min}} \right)^{\frac{1}{4}}.$$

It has been common practice to assume that $P_{r\,\min}$, or the signal threshold power, is of the order of magnitude of the noise power in the radar receiver. This is certainly true; it is of the order of magnitude of that noise power but is not generally equal to it. This paper deals with the various factors in the receiving system and display system which affect $P_{r\,\min}$.

A few of the things that affect $P_{r\,\min}$ are

1. The capabilities of the human observer.

2. The properties of the display system on which the signal is presented to the observer.

3. The type of interference which prevents the detection of an extremely small signal.

This interference is not always receiver noise. There are storm cloud echoes and similar interferences, but this discussion will deal only with the case in which receiver noise is the limiting factor.

It is useful to define the signal threshold power. A good deal of work has been done on this question, both theoretical and experimental, and in the course of events a satisfactory criterion has been developed. There is not a defined minimum threshold power above which the signal is always seen and below which it is never seen. One finds experimentally that if the signal power S is plotted against the percentage of cases in which the signal is correctly identified, a "betting curve" is obtained. It takes several times as much signal power to obtain a correlation of 90 per cent as it does to obtain a correlation of 10 per cent. In this paper the signal power which permits a correlation of 90 per cent will be considered the threshhold signal.

Two main types of displays are used in radar sets, the A-scope display and the *plan position indicator* [PPI] or intensity-modulated display. In the A-scope display there is presented a trace in which the apparent range of the target appears as abscissa and the amplitude of the received echo as ordinate. Along the trace the ever present receiver noise appears; where the target is there will be a larger average deflection. In experiments on the A scope an artificial echo of controlled amplitude and range was introduced into the receiving system. This artificial echo was so introduced that it could fall into any one of several fixed range positions. Usually six fixed range positions were used. The observer then attempted to call the position occupied by the signal. "Betting" curves were then drawn and S_{90} (90 per cent signal threshold power) determined. This is the signal power, usually measured in terms of noise power in the receiver. Between zero correlation and 90 per cent correlation a change in signal power of perhaps 5 db is usually required. This is quite a large spread, and it is very difficult to determine S_{90} accurately because of the statistical fluctuations. Ordinarily in running such a curve a single threshold power measurement requires 50 to 100 observations. This laborious and lengthy process of obtaining signal threshold is necessary to remove the subjective element. The results obtained in this way are remarkably constant and consistent among different observers. They do depend on other factors, however. They depend both experimentally and theoretically on the number of range positions, and it becomes necessary to indicate the type of variations which obtain. A "6 position, 90 per cent point" has already been defined for this experiment. This is taken as the standard of reference denoted by 0 db. S_{90} for a "1 position" experiment is +0.8 db experimentally and +1.5 db theoretically. S_{90} for an "N position" experiment is +1.0 db both experimentally and theoretically. S_{90} for the "2 position" experiment is —2 db experimentally and —½ db theoretically. In this last case the experimental improvement is due in part to the statistical difference and in part to the greater ease with which the observer can concentrate on the range positions.

In spite of these variations it is felt that any one of these definitions is representatively good. For convenience the S_{90} for the "6 position" experiment has been chosen, since it gives a sufficient number of positions so that statistical determination of S_{90} can be obtained with reasonable ease. It is possible to make the same correlation trials for the intensity-modulated PPI as for the A scope. The signal is put at any of a number of range positions which are fixed in azi-

muth. Scanning conditions may be included if desired. Some factors which affect the signal threshold power will now be enumerated, and the magnitude of their effects described.

The first such factor is the noise figure of the receiver. In brief, this is simply a multiplicative factor which would go with any of the other determinations made. The noise figure of the receiver specifically measures the amount by which that receiver is noisier than the best theoretical receiver. Ordinarily this noise figure runs to the order of 10 db, which means that the receiver is something like 10 times as noisy as the theoretically perfect receiver. As we are dealing with signal threshold power in terms of the receiver noise power (the latter being a universal parameter) it is only necessary to determine the noise figure of a given receiver in the field to determine what sort of input signal power is necessary.

The second factor affecting the signal threshold is the intermediate frequency or the radio frequency bandwidth B of the receiving system. B represents specifically the narrower of the two. This bandwidth will affect the signal visibility in a way which will be discussed presently. The third quantity is the video bandwidth b of the receiver. At one time it was thought that the video bandwidth and the i-f bandwidth were equivalent, but this is not at all true. Between the i-f and the video systems there is a second detector which is a nonlinear element, which causes frequency conversion to take place. This causes the video bandwidth to have an entirely different action from that of the i-f bandwidth. A third factor is the sweep speed of the scope, denoted by small s. The sweep speed has an important effect which is nearly equivalent to that of video bandwidth. Another parameter is the time interval during which the signal is actually presented to the observer. This quantity will be represented by the letter T and called the signal presentation time. In addition to these there are several other factors connected with contrast effects in the presentation and the scanning variables.

The first four variables mentioned apply to the geometry of the system, and geometrical scaling arguments can be applied to these quantities. One of these variables can thus be eliminated at the start by using not the pulse length τ, but the product $s \times \tau$ as a variable. Similarly, the other variables are $B \times \tau$, $b \times \tau$, and $N \times \tau$. These quantities have a definite physical significance. The sweep speed multiplied by the pulse length is simply the length of the signal on the scope and can be expressed in millimeters if desired. $B \times \tau$ is the i-f bandwidth times the pulse length and turns out to be a simple number. This is a number which will affect the signal visibility curves. Similarly the video bandwidth $b \times \tau$ is another number. The signal power multiplied by the pulse length is simply the energy of the signal per pulse, and so on. These variables are essentially geometrical parameters. The pulse repetition frequency and the signal presentation time are statistical parameters and must be treated in a statistical way as will be shown.

The first geometrical factor to be considered is the i-f bandwidth. The interesting factor is the behavior of signal and noise. Independently, these are known quite well. With respect to noise the power response is proportional to the bandwidth. However, the response to a signal of a particular length, once there has been obtained a bandwidth which is adequate for the transmission of the pulse, will be essentially independent of the bandwidth. When the bandwidth is very narrow the voltage of the output pulse is proportional to the bandwidth of the receiver. A curve can be drawn which is essentially the signal-to-noise power response curve, which for wide bandwidth will be proportional to the signal threshold power, while for narrow bandwidth it will be inversely proportional to the bandwidth. This is exactly the form of curve obtained experimentally. The optimum bandwidth is found to be approximately 1.2 times the reciprocal of the pulse length. The noise power in the receiver is a very poor single criterion as to how small a signal can be seen. For example, with a bandwidth of 1 mc for 1-μsec pulse a signal about 2 db below the noise can be seen. But if the i-f bandwidth is 10 mc for a 1-μsec pulse, a signal is visible 7 db below noise. If the i-f bandwidth is too small, even a signal equal to noise power is invisible. In general, therefore, signal threshold power is rated in decibels above the receiver noise power for a particular value of B (usually $B = 1/\tau$), since this provides a universal scale.

For the video bandwidth the situation is more complicated. A good deal of theoretical work can be done on this problem, but the experimental data do not confirm the theory. The reason is that the video bandwidth is already effectively narrowed by the effect of sweep speed. Video bandwidth effects can be observed when the sweep speed is very fast, where $s \times \tau$ (the pulse length on the scope) is of the order of a millimeter or so. Under these conditions video bandwidth narrowing always reduces the signal visibility and in-

creases the signal threshold power. There is a real difference between the video bandwidth and the i-f bandwidth in the following respect. Decreasing or increasing the i-f bandwidth causes the components of low-frequency noise in the video to change proportionally. Video narrowing, however, does not change the low-frequency video noise components. Therefore, the reduction in signal visibility with video narrowing is less pronounced than with i-f narrowing.

The human eye cannot distinguish between two objects which are closer together than about 1 minute of arc. If the light intensity contrast is limited, two objects cannot be resolved even at a much greater angular separation. When the separation approaches approximately ¼ of a degree, the best visibility will be obtained for the smallest contrast. Thus, the action of the human eye can be regarded as that of a filter which preferentially selects those frequencies having a period of the order of ¼ of a degree on the scope. At normal viewing distances this value of angular separation is of the order of 1 mm linear separation. Since the screen behaves like a linear transformation between the video signal and the light transmitted to the eye, this filter action of the eye is exactly equivalent to a video filter whose maximum pass frequency corresponds to 1 mm divided by the sweep speed s. For most presentations, where the pulse length is considerably shorter than 1 mm on the scope, this effective video narrowing action of the eye is usually much more important than the effect of video bandwidth in the receiver. It is to be noted, however, that video bandwidth effects in the receiver can be observed when the sweep speed is sufficiently fast for proper delineation of the pulse. There is now a considerable amount of experimental evidence to support this rather simple picture of the combined effect of video bandwidth and the resolution properties of the eye.

Because of this property of the eye, if the viewing distance is maintained constant, a large diameter PPI will be more sensitive in the detection of signals than a small one. A magnifying glass will produce an effective increase in sensitivity on the small scope at the expense, however, of a restricted searching area.

The focus on the PPI or A scope also acts like a video narrowing device. If the tube is defocused along the range scale, equivalent video narrowing will take place by an amount which is dependent upon the spot size. However, because of the effect on the human eye a loss in signal visibility will not occur until the defocused spot is larger than approximately 1 mm. Defocusing to this extent is certainly disadvantageous in the ultimate discrimination of two close radar targets, and for this reason good spot focus must be maintained.

In signal detection it is clearly necessary that the average signal deflection voltage be as large as the average noise fluctuation in the absence of signal. This is a purely statistical problem susceptible to theoretical analysis. Calculations show that the quantities which determine signal visibility, apart from the geometrical factors just described, are the total number of sweeps on which the signal is visible and the total number of sweeps on which only noise is visible. It is assumed that for these sweeps integration or averaging takes place. This result is confirmed experimentally with two restrictions. The total number of signal pulses is given by $T \times PRF$ (pulse repetition frequency), and the signal threshold power is found to vary inversely with both PRF and T. While this holds for all values of PRF under investigation (12.5 to 3,200 c) it holds only for a limited region in T (approximately 0.05 to 3 sec). The reason why the integration is not satisfactory outside these limits of T are related to the maximum flicker frequency detectable by the eye. For times shorter than perhaps 0.05 sec additional sweeps containing only noise will be integrated. Likewise, for T greater than 3 sec the eye and brain do not appear to integrate properly all the individual voltages. In other words, the system has incomplete memory. It has been found that the maximum system integration time (usually of the order of 6 sec) can be increased appreciably by operator practice. With a considerable amount of experience a good radar operator can effectively integrate for times as long as ½ min. It is to be noticed that because of this integration in the eye and brain of a radar operator other methods for providing integration, such as P-7 screens or photographic integration, will fail to provide substantial benefit unless their effective integration time exceeds several seconds. This conclusion is borne out experimentally.

In the radar scanning problem the same factors must be considered as have already been discussed, but, in addition, one must investigate factors peculiar to scanning. Among these are the rotation speed of the antenna, the beam width of the set, etc. It has been found, however, that the statisical problem met with in scanning is quite similar to that encountered in the absence of scanning. The complete system integration depends on two factors: the number of pulses intercepted by the radar beam during one traversal of the

target, and scan-to-scan integration. If the scanning rate is sufficiently rapid (faster than 10 rpm) the signal visibility will be independent of the antenna rotation rate. Faster rotation rates intercept a smaller number of pulses for each revolution, but there are a greater number of scan-to-scan integrations which just make up for the deficit. However, below the critical speed of about 10 rpm, scan-to-scan integration will not take place, and the signal threshold power will be proportional to the square root of the antenna rotation rate. This improvement in signal visibility at slower scan rates will continue until the antenna is on the target, during each revolution for approximately 6 sec, whereupon the visibility is essentially that of a "searchlighting" set. Thus the total scanning loss is given by the rather simple formula

$$\text{Loss} = \frac{1}{F_t} ,$$

where F_t is the fraction of time that the system is on target during the scanning procedure. Ordinarily this scanning loss amounts to approximately 10 db in an average radar system, requiring a signal perhaps 10 times as large as the necessary amount for detection while searchlighting. It is important that this formula be used only where scan-to-scan integration takes place.

Discussion

While this paper has specifically been limited to noise considerations, it seemed reasonable to hope that the same general considerations could be applied in determining the visibility of signals in various types of clutter, in particular the simpler types which are echoes from rain and snow. If the mechanisms involved were more thoroughly understood, the fundamentals of the problem would be understood too and could be put together in a coherent form.

The shape of the response curve has been considered by the author and is known to have some effect, but the experimental approach to various shape factors has been rather limited. In the work presented here the response curve of the receivers involved has been that of a so-called double-tuned circuit, whose amplitude response is proportional to

$$\left[1 + \left(\frac{\omega}{\omega_0}\right)^4\right]^{-\frac{1}{2}},$$

where ω is the frequency difference between the frequency under measurement and the center of the band. ω_0 is the ½ bandwidth. The difference between this response curve's performance and that of a multiply narrowed, synchronously tuned, intermediate amplifier, which has Gaussian response, was not observable experimentally. Theoretically also, there is little difference. It is felt that the considerations may not apply in extreme cases of sharp-edged amplifiers or in single single-tuned circuits but that in other cases the same answers do apply.

The question was raised as to the dependence of signal threshold on pulse recurrence rate. In all the other parameters the visibility of the signal is proportional to the signal energy. The author found that for a given average power the visibility is distinctly better if you concentrate more energy into each pulse and separate the pulses by longer intervals. In other words, the threshold is proportional to the energy per pulse but inversely proportional to the square root of the repetition frequency. This settles a disagreement between two groups, one of which believes visibility would be found independent of pulse repetition rate and the other that it depends on average energy. The answer lies between the two views. In this matter of visibility it is interesting to recall that the first successful radar, which was giving ranges up to 25 miles in 1936, had a receiver bandwidth of about 200 kc and a pulse length of 5 μsec, a combination which lies on the peak of the maximum visibility curve. The pulse length on the radar screen was about 3 mm. The curve for optimum visibility peaks at 1 mm and does not decline very rapidly for longer pulses, so that, too, was near the optimum value. The first production radar for use in the fleet had a pulse length of about 3 μsec and a bandwidth of about 300 kc, which is again on the peak of the visibility curve, and its visible pulse was about 2 mm long on the screen. This was of course not entirely accidental but was fortunate, nevertheless. The preproduction model of this radar was built in 1938.

The author discussed the effect of fluctuating signals in scanning as distinct from the steady signals which had been employed in the experiments described. In the case of signal fluctuation, it is necessary first to define the signal amplitude in such a way that analysis is applicable. Employing the average value as a criterion, the visibility of fluctuating signals may actually prove greater than for steady signals. If the peak value of a fluctuating signal is taken as the signal threshold power, the visibility is probably poorer than for a steady echo, but it is felt that the result would

be again essentially independent of the scanning speed, as long as it is high enough to cause pulse-to-pulse and scan-to-scan integration. The limit, however, may occur at 20 rpm instead of 10 rpm.

One variable has been omitted which has proven puzzling. This is the target speed. What really constitutes a scan-to-scan integration? If the target moves the distance of one spot diameter in a scanning period, is it still integrated? It would seem to be so integrated provided the observer is able to perform as an aided tracker, i.e., can appreciate a change in linear motion. If it is not integrated, one would expect to find a difference in signal threshold depending on the target speed, probably in direct proportion to the square root of target speed. Some experiments have been made on simulated echoes of this variety, and there was some indication that targets of higher velocity are definitely harder to see, but this cannot be considered quantitatively established. Signal fluctuation, however, is important, and it is felt that, in general fluctuating targets with cross sections defined on the basis given in the following paper are harder to see by perhaps 2 db but that this estimate is not affected by any arguments about scanning.

There was another inquiry concerning the explanation of the Watson effect observed occasionally at very close ranges when the background noise was so large the normal signal could not be detected. This consisted of an inverted signal smaller in amplitude than the background noise which could be observed to a range of almost 100 yd in sets which had a direct wave extending to 3,000 to 4,000 yd. In these cases the signal, instead of appearing as a small inverted V, showed up as a small upright V, approximately ⅓ the amplitude of the initial noise. This effect had been often reported on short-range targets. The author considered this to be a form of receiver saturation. Another group had been troubled by the same phenomenon and had attributed it to receiver saturation in which there was blocking of the i-f amplifier during a portion of the time.

12.4 RADAR SCATTERING OVER CROSS-SECTION AREA[d]

It is of great interest to determine the cross-section values of aircraft, not only in order to attempt prediction of ranges on these aircraft, but also to make possible the design of radar equipment which will utilize these factors a little better. The instantaneous pattern of reflection properties of an airplane is very complex. It depends upon the frequency, type of aircraft, and certain other factors, such as propeller rotation. The pattern has an extremely complex lobe structure which depends essentially upon the lengths of the plane's structure in terms of wavelength and upon the areas of specular reflection, that is, reflection from fairly large, flat, mirror-like surfaces found in most aircraft, such as the sides, bottoms, or wing surfaces.

It would be possible to define the instantaneous cross-section area as a function of the angle from the airplane, but this kind of thing would be purely academic, since actually the airplane is moving. In the early part of this work an attempt was made to derive a cross-section number which would apply to the actual radar performance on an airplane in flight. The scattering cross section may be calculated from the relation

$$\sigma = \frac{(4\pi)^3 P_r R^4}{P_t G^2 \lambda^2},$$

where the quantities are measured in free space. The symbols are defined in Section 12.3. They are all easily measurable except P_r, the received power. This was measured by injecting into the system, with a signal generator, an artificial echo which was matched to the size of the airplane echo.

In pratice, σ is necessarily a function of time, and for lack of a better criterion the following procedure was adopted. The signal generator reading was continuously matched to the size of the aircraft echo and recorded for successive 3-sec intervals. The signal measured in decibels above receiver noise power was plotted against range. On a logarithmic scale such a plot should be a straight line whose variation is 40 db for a factor 10 in range. This is actually found, provided one draws a line through the average of the 3-sec interval points. From moment to moment the fluctuation is rather high, but nevertheless a good average line can be drawn.

It is now possible to define a cross section by the condition that its value is exceeded in one-half of these 3-sec intervals, and this appears to be an easy operational way of obtaining cross sections. However, this still does not represent what could be called the *average* value for each 3-sec interval. It was found very early that it was very difficult to adjust a signal generator to the average value of the signal. It is much easier to adjust to the top value that has occurred during an interval. The reason for this is that the signal is quite often fuzzy and filled in by propeller modula-

[d]By J. L. Lawson, Radiation Laboratory, MIT

tion. Therefore, the figures represented here are in general the highest values that occur during the 3-sec interval. For this reason we have attempted to see how the value of σ depends upon the interval timing and whether or not it is permissible to put this value into range formulas in the usual way. A rough working model is the following: If these cross-section values are reduced to 60 per cent, they may be used in the range formula presented in the previous paper to obtain the correct operational radar range. The cross section averaged over the lobe structure in the front aspect or tail aspect of a plane would be lower than these values by probably 50 per cent.

Some representative figures are as follows: Fighter aircraft usually vary from 1 to 200 sq ft; medium bombers, B-18, Beaufighter and similar aircraft range from 4 to 600 sq ft; and heavy bombers, B-17, 800 sq ft. The larger bombers such as the B-29 have not been measured but are estimated to be of the order of 1,200 sq ft.

Discussion

To a question regarding the wavelength dependence of aircraft cross sections, the reply was that such a dependence was a function of the structure of the aircraft. Outside surfaces having rounded structures such as wings, wires, and similar members have a cross section which is essentially independent of wavelength and produce random scattering, provided the frequency is high enough. As the frequency is lowered, resonances in the structure of the airplane and differences in the wings may appear. This might possibly cause differences with regard to polarization. At S-band and higher frequencies there seems to be little dependence upon frequency. These figures have been checked at S and X bands with essentially the same results. No sensible dependence on polarization was observed, indicating that at S-band or higher frequencies, this sort of cross-section value will apply.

Ohio State University is conducting an extensive program of cross-section measurements on various types of aircraft for a variety of frequencies up to 500 mc. Measurements are made for all aspects of the aircraft and for both vertical and horizontal polarization. The procedure used is to scale the aircraft down to a convenient model size and to use a correspondingly higher frequency.

The results of these measurements exhibit a confusing lobe structure. In order to give an overall description of the behavior of the cross section, a reasonable procedure must be found for averaging the data. This has been attempted. At 100 mc, the specular reflections are not particularly marked, though the cross section does increase in directions perpendicular to the axis of the aircraft. There is still fairly strong scattering in all directions. At 500 mc the echoes are almost entirely due to specular reflection. The dependence on polarization is stronger at the lower frequencies.

The author commented that simultaneous measurements of average values for different polarizations showed them to be about the same but that instantaneous pulse-to-pulse photographs of a single target with two different polarizations showed them to be quite different at a given instant.

An inquiry was made as to whether any correlation had been made between radar cross section and type and dimensions of aircraft. A report was mentioned which attempted to show that scattering cross section was proportional to wingspread. The results of the author's group did not appear to correlate with wingspread, but the fuselage is important, and both factors must be significant. Experiments had been made with controlled flights in which the aircraft was flown straight toward or away from the radar site. It was believed that, because of normal wind conditions and such factors as yawing in flight, the results obtained represented an average over an angle of about 10° for both front and rear aspects. Some measurements at 45° aspects were made which showed a drop of about 1 or 2 db for most aircraft. Some aircraft showed a difference between average head and average tail aspect of about 1.5 to 1, and the figures previously quoted represented an average between the two aspects. When the aircraft in turning presents a broadside, specular reflection occurs, and this side flash often exceeds the ordinary signal by 100 times or more.

The comment was made that the measurements described seemed to have been made entirely with tracking radars using A-scope presentation. What would be the probable effects of such fluctuations on radars with search type presentation? The author believed that such fluctuations would affect search-type radars when scanning slowly but that no serious effect had been observed at scanning speeds as low as 2 rpm. When the cross-section figures given were used with a 2-db reduction for average values, the predicted ranges were in agreement with the observed ranges even on scanning or search type radars. This is probably not true at certain longer wavelengths for which the lobe structure is such that an aircraft can "ride" a null for an appreciable time interval. At micro wave-

lengths, the lobes are so close together that it becomes practically impossible for an aircraft to remain in a null for an appreciable time.

It was inquired whether drops of more than 2 db were to be expected for other aspects, such as 45 degrees. While a complete series of measurements had not yet been made by the author's group, measurements on three or four aircraft in various aspects had revealed no drops below 2 db. Although the calibration had been carried out entirely with signal generators, standard targets consisting of corner reflectors and spheres had been set up later and produced results in substantial agreement with the theoretically predicted values.

Chapter 13

ANGLE-OF-ARRIVAL EXPERIMENTS

13.1 ANGLE-OF-ARRIVAL MEASUREMENTS IN THE X BAND[a]

THE PURPOSE of this work was to observe the variation in angle of arrival of waves in the X band. No simultaneous air sounding data were taken although general weather observations were made.

The method of measuring the angle of arrival makes use of a very sharp-beamed antenna (Figure 1) mounted so that it may be mechanically tilted back

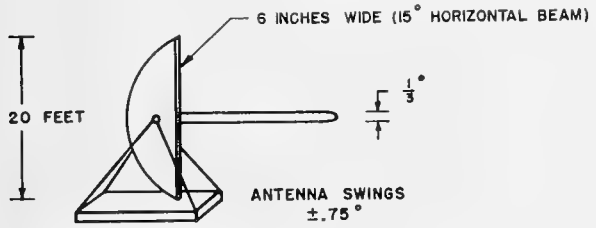

FIGURE 1. Sharp-beamed antenna used for measuring the angle of arrival.

and forth about its center thus sweeping the beam of the antenna through an arc which may be set to include the expected angle of arrival of the incoming signal.

The sharp-beamed antenna has been used to measure the angle of arrival of waves from a distant transmitter over an optical path where both a direct wave and a water-reflected wave are present. If the output

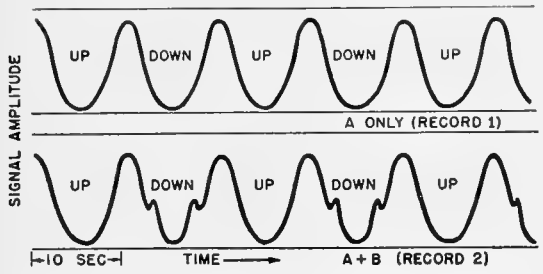

FIGURE 2. Variation in signal intensity during scan. A, direct ray only. B, direct and reflected rays superposed.

of the receiving antenna is fed to a receiver and this receiver is fitted with a recording type output meter, records of the type shown in Figure 2 will be obtained as the antenna scans. Record 1 will be obtained if only a single, direct wave is arriving at an angle corresponding to the mid-point of the antenna swing. The distances between peaks of maximum amplitude along the record will then be equal. A shift in the angle of arrival of the wave would appear on the record as a change in the spacing between the peaks. If two separate waves, direct and reflected, are arriving simultaneously, the record will appear something like record 2.

The actual antenna used for the measurement is a section of a parabolic cylinder arranged so that its beam at the center of swing is pointed directly at the transmitter. This is also the angle at which waves arrive on a normal day. A normal day has been taken as one when the angle of arrival is the same (within the accuracy of the measurements) as that calculated from actual earth geometry and when free space field is received from the direct wave.

The physical position of the antenna may be held to approximately 1/100 degree by the use of a plum-bob line dropped from the top of the 20-ft antenna to the base. Possible errors in reading the records, however, limit the expected relative accuracy to about 1/60 degree. Slight errors in the actual building of the antennas and in the locating of the feed limit the final accuracy to what is believed to be 1/25 degree.

The horizontal angle of arrival is measured with a duplicate antenna turned 90 degrees from the vertical with its flat side toward the ground. The accuracy of measurement is the same as in the vertical plane case.

The entire equipment, including the two scanning antennas, other reference antennas, the receiving equipment, and the receiver building are located on a rotatable platform which is 25 ft in diameter. This equipment, located on top of Beer's Hill, New Jersey, may thus be pointed toward any of several transmitters and comparisons made of the angle of arrival from each transmitter.

Observations during the summer of 1944 have been made on two optical paths shown in Figure 3: (a) A 24.1-mile path partly over land and partly over water between New York City and Beer's Hill, New Jersey. The normal reflecting point for the reflected ray on this path is in the salt water of Raritan Bay; (b) a 12.6-mile path between Beer's Hill and Deal, New Jersey. This path is all over gently rolling land. The

[a]By W. M. Sharpless, Bell Telephone Laboratories.

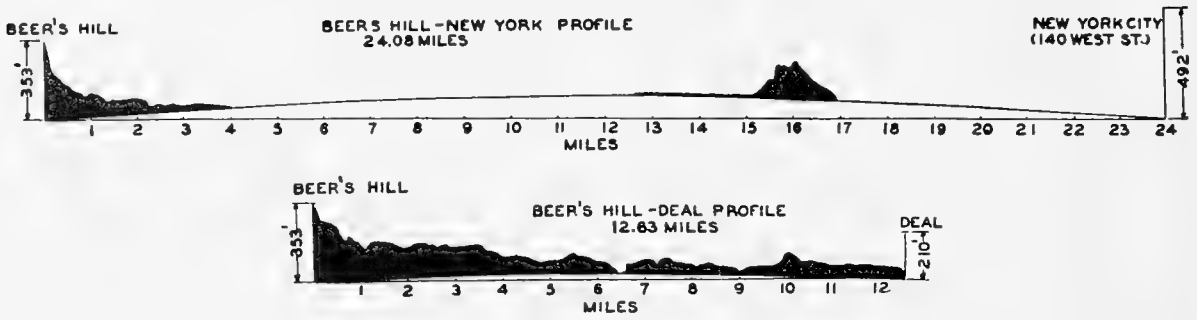

FIGURE 3. Propagation paths, (top) Beer's Hill to New York and (bottom) Beer's Hill to Deal.

transmitters at both Deal and New York radiate waves polarized at 45 degrees so that either vertical or horizontal polarization may be used at the receivers.

Results of angle-of-arrival measurements made during the summer of 1944 indicate that on both the Deal and New York circuits the greatest variation of angle of arrival in the horizontal plane was $\pm 1/10$ degree. Times were found when the angle of arrival remained as much as 1/10 degree east for short periods on the New York circuit, but for the most part the horizontal angle of arrival normally fluctuated $\pm 1/10$ degree from the normal day direction on both the Deal and New York circuits. The maximum variation in the vertical angle of arrival on the direct wave on the New York path has been 0.46 degree above that observed on a normal day, while the reflected wave has come in as low as 0.17 degree below the normal reflected wave. (On a normal day the reflected wave on the New York path should be, by calculations, 0.33 degree lower than the direct wave.)

There does not seem to be any correlation between the variation in angle of arrival on the direct wave and the reflected wave. These variations do not as a rule occur together. At the time when the greatest deviation in the reflected wave was present the direct wave was coming in normally. Also, when the direct wave was up 0.46 degree, it was apparently being trapped, and at that time no reflected wave was received. The greatest spread observed between the direct and reflected wave was 0.75 degree (normal 0.33 degree). At this time the direct wave was 0.35 degree above normal while the reflected wave was 0.07 degree below normal. The near proximity of Staten Island to the path normally taken by the reflected wave on the New York path has probably contributed to complexities of the results obtained on this circuit.

The vertical angle of arrival on the Deal circuit has not varied as greatly as on the New York circuit. The greatest change in angle has been an increase of 0.28 degree in the direct wave angle of arrival. The reflected wave is not of sufficient magnitude to be observed on the Deal circuit.

Height run experiments were conducted to obtain a value for the effective coefficient of reflection for the Deal path. An oscillator was hoisted up and down the 175-ft tower at Deal and the resulting received field recorded at Beer's Hill. The field was found to vary 3.6 db from maximum to minimum (3 maximum values and 2 minimum values) as the oscillator changed height, which indicates an effective coefficient of reflection of 0.2. This means that the received reflected wave is 5 times weaker than the direct or 14 db down. The distance above ground at which the maximum and minimum were obtained were noted on the receiver record, and from these the height of the effective reflection layer was obtained. This height was found to be approximately 100 ft above average ground level.

This experiment is to be repeated when leaves have fallen from the trees to determine if the effective reflection coefficient or the height of the reflecting layer has changed.

Rain has been found to influence the X-band circuits in a manner such as to cause a lowering of the received fields. During very heavy downpours, we have experienced as much as 0.8-db attenuation per mile of path length on both the paths. We have no way of knowing how much rain was falling over an entire path, but the figure of 0.8 db per mile represents the maximum value of rain attenuation so far recorded on our circuits.

Only part-time observations have been made on this project, and the results reported are based on such observations. It is not known, therefore, if more extreme conditions than those reported have existed at times when no observations were being made.

We expect to continue work on propagation and

angle-of-arrival studies through next year. Records made to date are now being studied in detail, and a report will probably be written covering this work.

13.2 METEOROLOGICAL ANALYSIS OF ANGLE-OF-ARRIVAL MEASUREMENTS[b]

13.2.1 Purpose

Recent experiments on propagation in the X band conducted by Bell Telephone Laboratories [BTL] have indicated that the angle of arrival of microwaves may be considerably at variance with that computed on the basis of rectilinear propagation. Deviations as large as 0.46 degree from true bearing[c] were measured during the summer season over a 24-mile path, partly over land and partly over water. The deviations found experimentally exceed considerably the tolerances specified on angle of elevation, azimuth, and height determination in present military characteristics on fire-control radar equipment.

An analysis of propagation from the meteorological point of view has been undertaken to determine whether deviations from rectilinear propagation can be explained by, and predicted from, meteorological data and whether observed extreme deviations can be realized from plausible meteorological stratification. The Bell Laboratories' experimental angle-of-arrival measurements made during the summer of 1944 have been compared with deviations evaluated from meteorological data obtained concurrently by the Signal Corps though not coordinated at the time with these experiments. The current paper is intended to report the results of this study and the procedure utilized in the analysis and, in turn, to establish a framework for interpreting further propagation experiments of this type.

13.2.2 Theory

The equations of propagation can be written in a form such that the angle of departure of the radiation at the transmitter (the direction of the normal to the wave front) and the angle of arrival at the receiver can be written as functions of the meteorological stratification and the constants of the installation (distance between and heights of transmitter and receiver). The solution of the equations of motion is given below by the use of an electromagnetic wave velocity profile obeying a radial power law. The relation of the exponent m in this power law to the excess modified refractive index M is then deduced. The power m in the velocity profile equation is assigned the definition of "meteorological stratification parameter," since it determines the change of modified index of refraction with height.

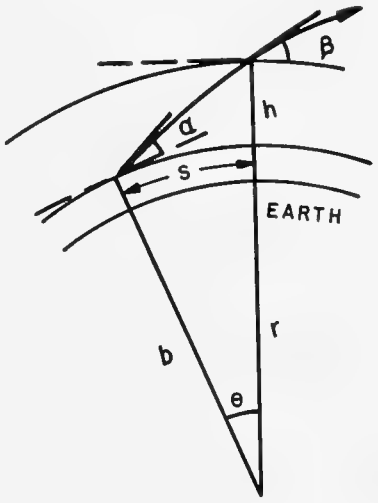

FIGURE 4. Geometry of a ray in the atmosphere.

From Figure 4,

$$d\theta = \frac{dr}{r \tan \beta} = \frac{ds}{b}. \tag{1}$$

Introduce the electromagnetic wave velocity profile

$$\frac{v}{v_0} = \frac{n_0}{n} = \left(\frac{r}{b}\right)^m. \tag{2}$$

Hence,

$$s = \frac{b(\beta - \alpha)}{1 - m} \tag{3}$$

where

$$\cos \beta = \left(\frac{r}{b}\right)^{m-1} \cos \alpha. \tag{4}$$

Snell's law states that

$$\frac{v_0}{b \cos \alpha} = \frac{v}{r \cos \beta}. \tag{5}$$

Then,

$$(1 - m)dr = r \tan \beta d\beta \tag{6}$$

and

$$\frac{ds}{b} = \frac{d\beta}{1 - m}. \tag{7}$$

Now $r = b + h,$

where $h \ll b.$ (8)

[b]By George D. Lukes, Signal Corps Ground Signal Agency.

[c]The term "true bearing" as used in this paper refers to the vertical angle between the horizontal and a line perpendicular to the wave front at the receiving point.

The excess modified refractive index M is given by

$$M \cdot 10^{-6} = \frac{nr}{n_0 b} - 1$$
$$= \left[1 + \left(\frac{h}{b}\right)^{1-m}\right] - 1 \simeq (1-m)\frac{h}{b}. \qquad (9)$$

If now the relation for the distance s is solved simultaneously with the equation stating Snell's law of refraction, we have the angle of arrival α as a function of the excess modified refractive index M, uniquely relating the angular deviation from true bearing to the distribution of modified refractive index required to produce that deviation.

13.2.3 Analysis of the BTL New York-to-Beer's Hill Circuit

The results obtained by Bell Telephone Laboratories, Inc., on measurements of the angle of arrival of microwaves in the X band are contained in two BTL reports.[1,2] The New York-to-Beer's Hill propagation circuit proved to be the more suitable for the meteorological analysis of angle of arrival. On this path the transmitter was located on the New York Telephone building at an elevation of 492 ft above mean sea level; the receiver was erected on top of Beer's Hill at an elevation of 353 ft. The propagation path had a length of 24.08 miles and ran several degrees east of north from Beer's Hill to New York. The bearing from receiver to transmitter on this circuit on the basis of true earth geometry is 0.11 degree below zero elevation angle of Beer's Hill.

During the summer of 1944 a limited number of vertical temperature and humidity soundings were secured by personnel of Wave Propagation Studies, Evans Signal Laboratory, at a 400-ft radar tower in Oakhurst, New Jersey. The location of the tower is shown on the map in Figure 5. The tower stands on a hill 128 ft above mean sea level. The limit of observation is 375 ft above the base of the tower; hence the absolute elevation was 503 ft. It follows that soundings over the height of the tower sample the atmosphere between approximately 11 ft above the transmitter and 225 ft below the receiver.

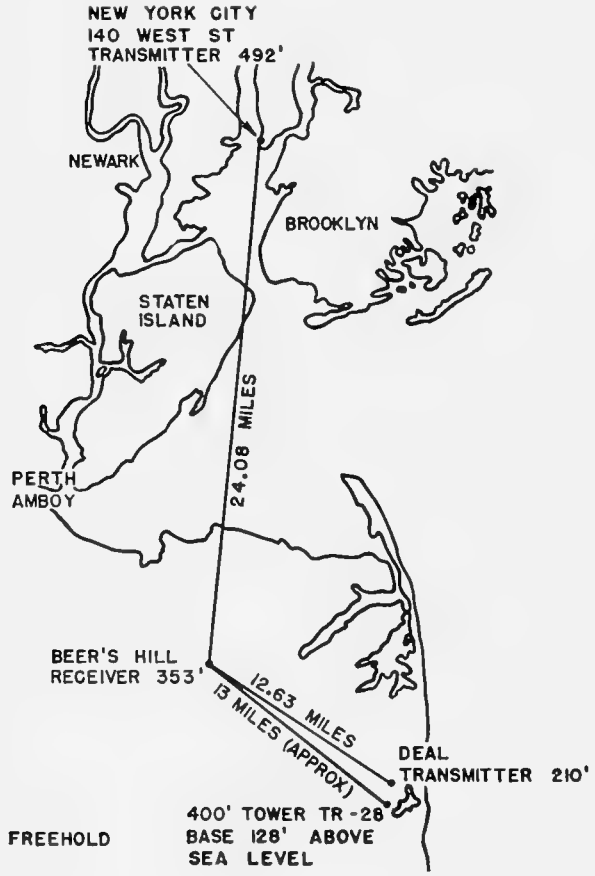

FIGURE 5. Plan view of propagation paths.

13.2.4 The Angle of Arrival Deduced from Type Cases of Atmospheric Stratification

When the path is confined to a layer between receiver and transmitter, there are two limiting paths, as illustrated in Figure 6A: Path A leaving the transmitter at some angle $\beta < 0$ and arriving at the receiver with $\alpha = 0$; Path B leaving the transmitter at an angle $\beta = 0$ and arriving at the receiver with $\alpha > 0$. By applying the equations deduced from theory and expressed by data in Table 1, the necessary and sufficient

TABLE 1

Path	α at receiver (degrees)	β at transmitter (degrees)	Deviation of α and β from true bearing	m
A	0	− 0.125	+ 0.111	0.64
Intervening path	+ 0.0625	− 0.0625	+ 0.1735	1.00
B	+ 0.125	0	+ 0.236	1.36

modified refractive index distributions with height in the layer can be evaluated for the limiting paths A and B and for all intervening paths. Table 2 shows the value of the stratification parameter m required. We therefore conclude that, for a path confined to the layer between transmitter and receiver, the deviation from true bearing must be confined to the interval $+0.111$ to $+0.236°$, and the change in the modified

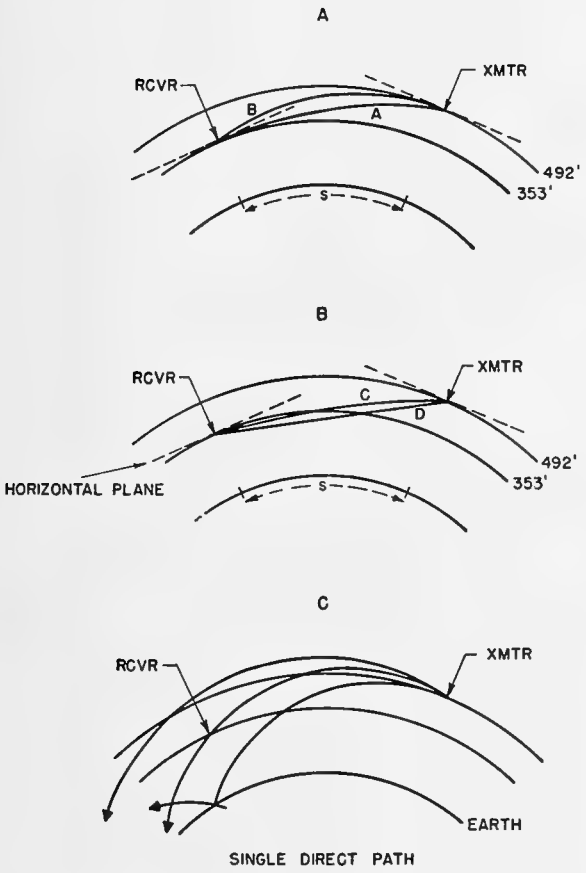

FIGURE 6. Types of vertical variation in ray paths.

refractive index between receiver and transmitter must be in range —2.4 to +2.4 M units. These limits hold for an approximately linear variation of index between receiver and transmitter.

Radiation along paths of type C, which penetrates the layer below the receiver height (see Figure 6B), arrives at the receiver at an angle $\alpha < 0$; therefore, M will of necessity increase by more than 2.4 units from receiver to transmitter. We consider three stratifications producing paths of this category.

1. The so-called "standard" atmosphere utilized for the purposes of representing "normal" propagation by rectilinear rays on an earth distorted to a radius 4/3 that of the true earth. The increase of M is at a rate of 3.6 units per 100 ft.

2. Adiabatic equilibrium for an unsaturated atmospheric layer, representing the condition of a completely stirred or mixed stratum of air. The increase of M is 4.0 units per 100 ft.

3. Rectilinear propagation on a true earth. For this condition there is no variation of electromagnetic velocity with height, and M increases by 4.76 units per 100 ft, equal to the rate of curvature of the earth.

The computed deviations of the angles α and β at the receiver and transmitter, respectively, are given in Table 2. It will be noted that the condition of rectilinear propagation on a true earth produces an angle

TABLE 2

Type of atmospheric stratification	α at receiver (degrees)	β at transmitter (degrees)	Deviation of α and β from true bearing	m
"Standard" atmosphere	− 0.069	− 0.194	+ 0.042	2.44
Adiabatic equilibrium	− 0.083	− 0.208	+ 0.028	0.16
Rectilinear propagation on a true earth	− 0.111	− 0.236	0	0

$\alpha = -0.11°$, which is the true bearing from receiver to transmitter. From the data of Table 1 it follows that a "standard" atmosphere and an atmosphere vertically mixed so as to be in adiabatic equilibrium both provide a variation of modified refractive index with height of a magnitude such that the angle of arrival measured at the Beer's Hill receiver under these conditions is within 0.04° of true geometric bearing. In view of the fact that the instrumental accuracy of the Beer's Hill antenna system is $\pm 0.04°$, it follows further that the differences among these three meteorological stratifications will not be evident in the measurements.

Consider now a case in which the radiation path penetrates the layer above the transmitter. The occurrence of an angle of arrival at the Beer's Hill receiver in excess of 0.236° above true bearing will require a path of propagation rising to some level above the New York City transmitter. The variation of M with height within the layer immediately above the transmitter will be critical in determining the magnitude of the signal received and its angle of arrival. The analysis following is limited to one particular case of this category producing an extreme deviation from true bearing in the angle of arrival.

For the paths shown in Figure 6C, the M distribution between 353 and 492 ft above mean sea level is that computed from the observed meteorological data on the 400-ft tower at 0800 on July 7, 1944. Using only this portion of the actual sounding, the variation of modified index of refraction in the layer immediately above the transmitter has been computed as a

function of the angle α at the receiver. In the case of the angle $\alpha = 0.355°$ (deviation from *true* bearing equal to $+0.466°$), the calculated index at the level of total refraction, which computes as 505 ft, is very closely that observed at the uppermost level of meteorological sounding (503 ft). Thus an angle of arrival deviating by as much as 0.47° from true geometric bearing is entirely possible for the meteorological situation of 0800, July 7, 1944 and for the positions of the New York transmitter and Beer's Hill receiver and could have been predicted from the observed meteorological sounding.

A second significant conclusion can be readily deduced by considering the modified refractive index distributions required in the layer immediately above the transmitter for different values of α. It is apparent that the lapse of modified index required for any of the angles considered in this example is not substantially different among all four angles; the primary requisite for the larger α's is that the lapse continue to greater heights. Thus relatively small fluctuations in the meteorological elements can cause a time change of 0.1° in the angle of arrival measured at the Beer's Hill receiver. Furthermore, a particularly unfavorable combination of small changes in the meteorological elements in this layer may cause the signal at the receiver to fall to a very low level. A similar conclusion is not valid for the case of propagation confined to the layer between transmitter and receiver and the case of path penetration below the receiver, since another slightly different path can always be found along which energy can reach the receiver directly.

A third significant conclusion can be deduced by inspecting the computed deviations from true bearing of the angles at the receiver and the transmitter, as given in Table 3. It will be noted that the deviation from true bearing of the angle of arrival at the receiver is not the same as the deviation from true bearing of the angle of departure at the transmitter. In fact the data of Table 3 indicate that, under the meteorological situation of 0800 on July 7, 1944, the angle of arrival at the receiver would have been $+0.27°$ above true bearing in place of $+0.46°$, were the receiver and transmitter interchanged at the end points of the path. On the other hand, for both cases 1 and 2 treated above, the meteorological stratification was such that the angular deviations from true bearing at both receiver and transmitter were the same. The relations of the angular deviations from true bearing at the end points of the path are summarized in Figure 7.

TABLE 3

α at receiver (degrees)	β at transmitter (degrees)	Deviation from true bearing α	Deviation from true bearing β	m
+ 0.355	+ 0.038	+ 0.466	+ 0.274	1.366
+ 0.372	+ 0.119	+ 0.483	+ 0.354	1.972
+ 0.401	+ 0.190	+ 0.512	+ 0.426	2.436
+ 0.458	+ 0.292	+ 0.569	+ 0.528	3.052

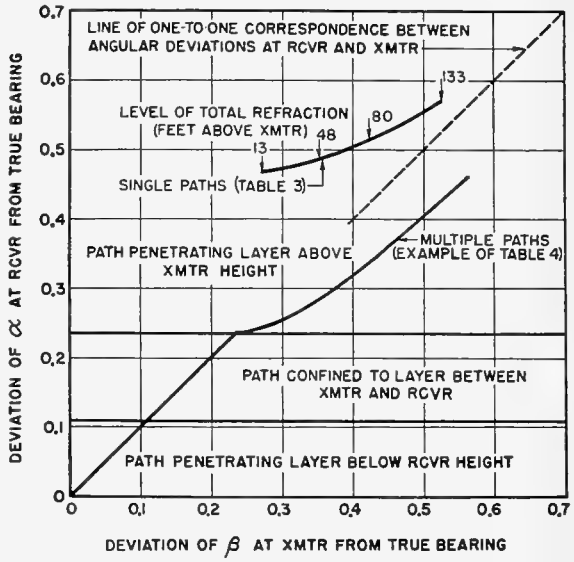

FIGURE 7. Correlation of deviations.

A fourth conclusion can be deduced by considering the curve in Figure 7 based on the computations tabulated in Table 3. It will be recalled that a fluctuation of 0.1° in angle of arrival at the receiver was concluded as possible as a result of relatively small fluctuations in the meteorological elements in the layer immediately above the transmitter. But it should now be noted that fluctuation of angle of departure at the New York transmitter is approximately 0.25° when the Beer's Hill angle of arrival varies approximately 0.1° for the particular meteorological situation of 0800 on July 7, 1944.

It therefore follows, in summary, that the deviation from true bearing measured at the position of the receiver depends not only on the range between transmitter and receiver and on the meteorological conditions but also and equally well on the relative difference in heights of transmitter and receiver and the position in height of the receiver with respect to the transmitter.

13.2.5

Comparison of Computed to Measured Angle of Arrival

The experimental measurements of angle of arrival secured by Bell Telephone Laboratories and the meteorological data obtained on the 400-ft tower in Oakhurst, have been analyzed to determine whether any significant correlations exist between the measured angles of arrival at the Beer's Hill receiver and the angles of arrival computed from meteorological data. A grand synthesis is presented in Figure 8 of all days for which both BTL propagation measurements and Signal Corps tower meteorological soundings were available for comparison. Since simultaneity in radio and meteorological measurements was a rare occurrence, the angle of arrival evaluations from both sources of data are plotted along a time scale (in hours) for each day of the period. The angle evaluations from radio data are represented by circles; angles calculated from the meteorological data are represented by crosses of time length equal to the duration of sampling of the layer between transmitter

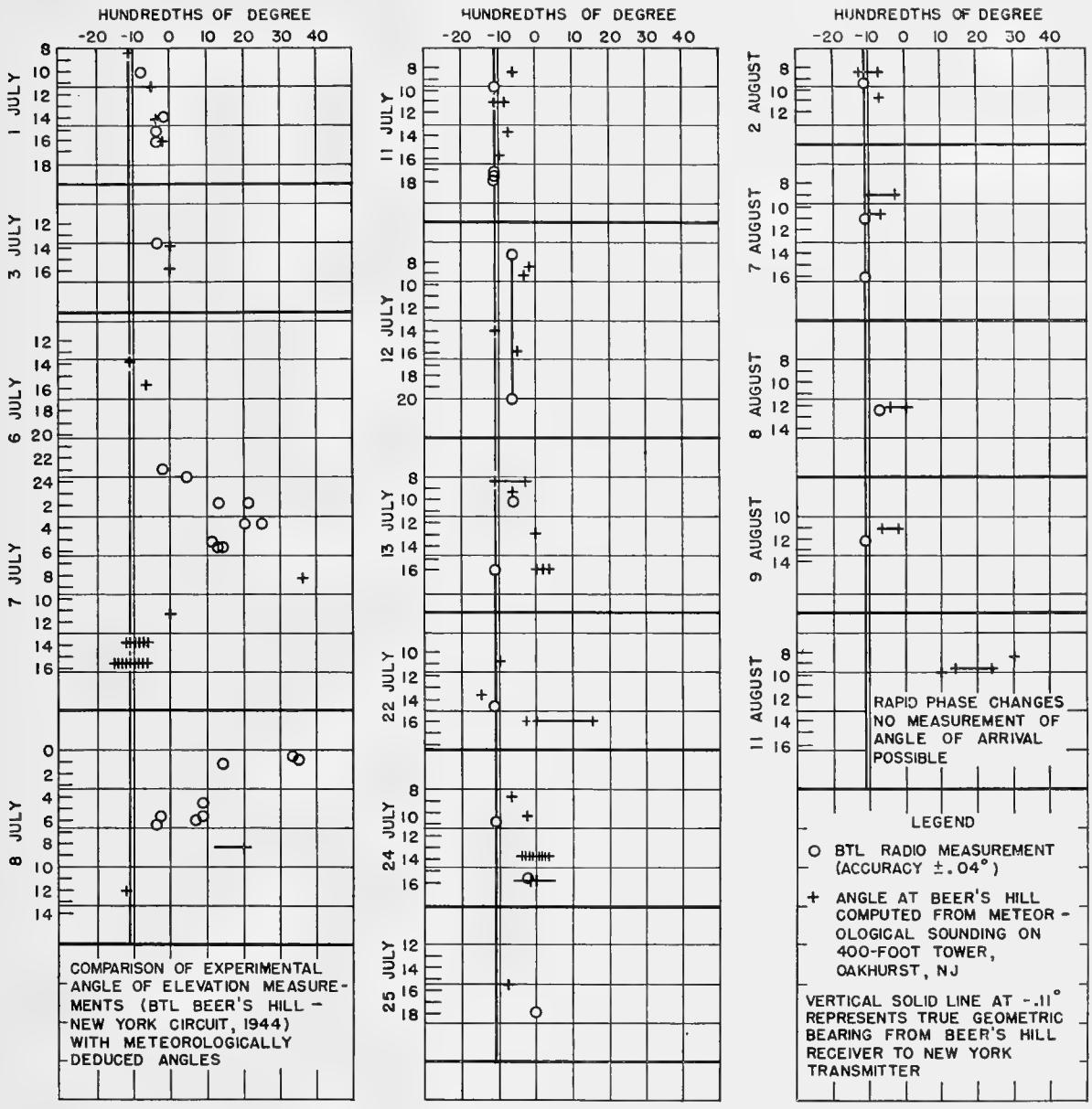

FIGURE 8. Measured versus computed angles of arrival.

and receiver (including both ascent and descent of the tower). Equipment limitations set the accuracy of BTL angle of arrival measurements at $\pm 0.04°$.

It is believed that generalized, overall conclusions for the entire period of comparison can be made as follows:

1. That occasions of true bearing and "near true bearing" (say —0.11 to 0°) could have been predicted from the meteorological data.

2. That the occurrence of extreme deviations from true bearing would have been predicted from meteorological data nearest in time to the radio measurements.

3. That the magnitude of the most extreme measured deviation (0.46°) from true bearing can also be calculated from observed meteorological data, though not simultaneously observed.

13.2.6

Conclusions

The propagation path of microwave radiation can be fairly well specified, given only a knowledge of the temperature and water vapor pressure distribution in the lower atmosphere and the positions in space of transmitter and receiver. The equations of motion of the propagation of the individual wave fronts have been written in a form such that the angles of departure from the transmitter and the angles of arrival at the receiver can be evaluated directly from the meteorological stratification. Application of the theory to certain angle-of-arrival radio propagation experiments conducted by Bell Telephone Laboratories during the summer of 1944 has resulted in the following conclusions:

1. A surprisingly good correlation exists between angles of arrival computed from meteorological and survey data only and the angles of arrival determined experimentally.

2. The extreme deviations (0.46°) from rectilinear propagation measured experimentally by BTL are confirmed as plausible on the basis of observed meteorological stratification.

3. The meteorological analysis indicates that deviations from rectilinear propagation and the fluctuation of the deviations about a mean value are as much a function of position of transmitter and receiver as they are a function of the existing meteorological structure.

It is strongly recommended that low-level meteorological soundings be considered an indispensable part of any experimental angle-of-arrival measurements. The good correlations secured between evaluation of angles of arrival from meteorological data and angles of arrival measured experimentally suggest that deviations from rectilinear propagation can be accounted for by measurable atmospheric conditions and that, further, these deviations can be reasonably well predicted.

BIBLIOGRAPHY[a]

Numbers such as CP-311-M4 indicate that the document listed has been microfilmed and that its title appears in the microfilm index printed in a separate volume. For access to the index volume and to the microfilm, consult the Army or Navy agency listed on the reverse of the half-title page.

Chapter 1

1. *Microwave Transmission over Water and Land under Various Meteorological Conditions*, Pearl J. Rubenstein, I. Katz, L. J. Neelands, and R. M. Mitchell, OEMsr-262, Division 14 Report 547, RL, June 13, 1944. CP-311-M4
2. *Meteorological Equipment for Short Wave Propagation Studies*, Walter M. Elsasser, Report WPG-3, CUDWR, August 1944.
3. *Atmospheric Refraction, A Qualitative Investigation*, Lloyd J. Anderson, F. P. Dane, J. P. Day, R. F. Hopkins, L. G. Trolese, and A. P. D. Stokes, BuShips Problem X4-49CD, Report WP-17, NRSL, Dec. 28, 1944. CP-222-M9

Chapter 2

1. *Transmission of Plane Waves Through a Single Stratum Separating Two Media* (Part II), John B. Smyth, BuShips Problem X4-49CD, Report WP-13, NRSL, June 23, 1944. CP-221-M9
2. *Proceedings of the Institute of Radio Engineers*, R. C. Colwell, **27**, October 1939, pp. 626-634.
3. *Procedure and Charts for Estimating the Low Level Coverage of Shipborne 200-Mc Radars under Conditions of Pronounced Refraction*, F. R. Abbott, Lloyd J. Anderson, F. P. Dane, J. P. Day, R. U. F. Hopkins, John B. Smyth, L. G. Trolese, and A. P. D. Stokes, BuShips Problem X4-49CD, Revised Report WP-11, NRSL, Revised May 10, 1944. CP-202.32-M1
4. *The Mechanical Determination of the Path Difference of Rays Subject to Discontinuities in the Vertical Gradient of Refractive Index*, F. R. Abbott, BuShips Problem X4-49CD, Report WP-10, NRSL, Mar. 10, 1944. CP-222.1-M3
5. *Calibration and Standardization of Land Based Radars by the Use of Small Plane Targets*, F. R. Abbott, BuShips Problem X4-49CD, Report WP-12, NRSL, June 10, 1944. CP-612.5-M1

Chapter 3

1. *New Theoretical Consideration on the Dielectric Properties of the Atmosphere, F. Hoyle, Third Conference on Propagation, Washington, D. C. on November 16-18, 1944*, NDRC CUDWR-WPG, 1945, pp. 26-30. CP-100-M4

Chapter 5

1. *Reviews of Progress of Ultra Short Wave Propagation Work, Part I, The Evaluation of Solutions of the Wave Equation for a Stratified Medium*, D. R. Hartree, OSRD WA-2961-2, Report AC-7017, USWP, Sept. 26, 1944. CP-110-M2
2. *Reviews of Progress of Ultra Short Wave Propagation Work, Part II, Statement of Work in Progress Relevant to Investigations of the Propagation of Radio Waves Through the Troposphere*, R. L. Smith-Rose, OSRD WA-3005-2, Report AC-7018, NPL Report, USWP, Sept. 25, 1944. CP-110-M3
3. *Reviews of Progress of Ultra Short Wave Propagation Work, Part III, Microwave Propagation Research at the Signals Research and Development Establishment*, OSRD 3156-7, Report AC-7019, USWP, Sept. 26, 1944. CP-110-M4
4. *Reviews of Progress of Ultra Short Wave Propagation Work, Part IV, Correlation of Radar Operational Data with Meteorological Conditions*, OSRD WA-3156-8, Report AC-7020, AORG Report, USWP, Sept. 28, 1944. CP-110-M5
5. *Reviews of Progress of Ultra Short Wave Propagation Work, Part V, Progress Report on Forecasting of Radar Conditions*, OSRD 3156-9, Report AC-7021, DMO-USWP, Oct. 2, 1944. CP-110-M6
6. *Reviews of Progress of Ultra Short Wave Propagation Work, Part VI, Vertical Temperature and Humidity Gradients at Rye*, OSRD WA-3156-10, Report AC-7022, DMO-USWP, Oct. 2, 1944. CP-110-M7
7. *Reviews of Progress of Ultra Short Wave Propagation Work, Part VII, The Use of Radar for the Detection of Storms*, OSRD WA-3156-11, Report AC-7023, DMO-USWP, Oct. 2, 1944. CP-110-M8
8. *Reviews of Progress of Ultra Short Wave Propagation Work, Part VIII, Present States of Theoretical Study of Radio Propagation Through the Troposphere by the Mathematics Group, Telecommunications Research Establishment*, OSRD WA-3156-12, Report AC-7024, Oct. 2, 1944. CP-110-M9
9. *Reviews of Progress of Ultra Short Wave Propagation Work, Part IX, Review of Short-Period Experimental Studies of Centimeter Wave Propagation, Carried Out Jointly by Admiralty Signal Establishment, Signals Research and Development Establishment, and General Electric Company*, E. C. S. Megaw, OSRD WA-3156-13, Report AC-7025, USWP, Oct. 16, 1944. CP-110-M10
10. *Reviews of Progress of Ultra Short Wave Propagation Work, Part X, Study of Centimeter Wave Propagation over Cardigan Bay to Mount Snowden*, F. Hoyle, OSRD WA-3157-1, Report AC-7026, USWP, Oct. 14, 1944. CP-110-M11
11. *Reviews of Progress of Ultra Short Wave Propagation Work, Part XI, Study of Reflection Coefficient of the Sea at Centimeter Wavelengths*, F. Hoyle, OSRD WA-3157-2, Report AC-7027, USWP, Oct. 14, 1944. CP-110-M12
12. *Reviews of Progress of Ultra Short Wave Propagation Work, Part XII, Some K-, X-, and S-Band (Llandudno) Trials, General Summary of the Experimental Results Obtained which are Concerned with the Dependence of Radio Propagation on Meteorological Conditions*, OSRD WA-3157-3, Report AC-7028, TRE and RRDE Report, USWP, Oct. 14, 1944. CP-110-M13
13. *Reviews of Progress of Ultra Short Wave Propagation Work, Part XIII, Progress Report on 369 Trials by DNMS*, OSRD WA-3156-1, Report AC-7029, USWP, Oct. 14, 1944. CP-110-M14
14. *Reviews of Progress of Ultra Short Wave Propagation Work, Part XIV, Survey of Progress in the United Kingdom on the Electromagnetic Theory of Tropospheric Propagation*, OSRD

[a] A complete bibliography of CP reports will be found in Volume 1.

WA-3157-4, Report AC-7030, RRDE-USWP, Oct. 16, 1944. CP-110-M15

15. *Reviews of Progress of Ultra Short Wave Propagation Work, Part XV, Study of Meteorological Factors Responsible for the Refractive Structure of the Troposphere,* OSRD WA-3157-5, Report AC-7031, RRDE-USWP, Oct. 16, 1944. CP-110-M16
16. *Centimeter Wave Propagation over Land, Preliminary Study of the Field Strength Records Between March and Sept., 1943,* R. L. Smith-Rose and A. C. Stickland, OSRD WA-1514-6, Report RRB/S-13, DSIR, Nov. 15, 1943. CP-333-M1
17. *Centimeter Propagation over Land, A Study of the Field Strength Records Obtained During the Year 1943-1944,* Report RRB/S-18, NPL-MO DSIR, May 11, 1944. CP-224-M11

Chapter 6

1. *Beitraege zur Physik der Freien Atmosphere,* P. Mildner, 1932, p. 51.
2. *Geophysical Memoirs,* Giblett and others, No. 54.
3. *Proceedings of the Royal Society of London,* O. G. Sutton, 1932, p. 143.
4. *Geophysical Memoirs,* No. 65.
5. *Quarterly Journal of the Royal Meteorological Society,* O. G. Sutton, 1936, p. 125.
6. *Quarterly Journal of the Royal Meteorological Society,* H. V. Sverdrup, 1936, p. 461.
7. *MIT Papers,* Rossby and Montgomery, 1934.
8. *Quarterly Journal of the Royal Meteorological Society,* O. G. Sutton, 1937, p. 105.
9. *Wired Sonde Equipment for High Altitude Soundings,* Lloyd J. Anderson, BuShips Problem X4-49CD, Report WP-16, NRSL, Nov. 17, 1944. CP-341-M2
10. *The Captive Radiosonde and Wired Sonde Techniques for Detailed Low-Level Meteorological Sounding,* Paul A. Anderson, C. L. Barker, K. E. Fitzsimmons, and S. T. Stephenson, OEMsr-728, Research Project PDRC-647, Division 14 Report 192, Report 3, Washington State College, Oct. 4, 1943. CP-341-M1
11. *The Dielectric Constant of Water Vapour and its Effect upon the Propagation of Very Short Waves,* A. C. Stickland, OSRD WA-175-7, Paper RRB/S-2, NPL-DSIR, May 11, 1942. CP-522.12-M2
12. *Lehrbuch der Meteorologie, Funfte Auflage,* J. Hann and R. Suring, 1939.
13. "On Temperature and Humidity Observations Made at Allahabad," S. A. Hill, *Indian Meteorological Memoirs,* **4**, Part 6, 1889.
14. "Ein Beitrag zur Kenntnis der Temperatur und Feuchtigkeitsverhaltnisse in Verschiedener Höhe über dem Erdboden," K. Knoch, *Veröffentlichungen des Königlichen Preussischen, Meteorologischen Institute, Abhandlungen,* **3**, No. 2, 1909.
15. "An Investigation of the Lapse Rate of Temperature in the Lowest Hundred Meters of the Atmosphere," N. K. Johnson and G. S. P. Heywood, *Geophysical Memoirs,* No. 77, 1938.
16. Walter M. Elsasser, NDRC Propagation Memorandum.
17. *Atmospheric Waves, Fluctuations in High Frequency Radio Waves,* L. G. Trolese and John B. Smyth, BuShips Problem X4-49CD, Report WP-18, NRSL, Feb. 1, 1945. CP-225-M1
18. *Dynamic Meteorology,* Bernhard Haurwitz, McGraw-Hill Book Co., 1941.

18a. *Ibid.,* p. 286.

18b. *Ibid.,* p. 288.

19. *Meteorologische Zeitschrift,* Bernhard Haurwitz, 1931.
20. *Monthly Weather Review,* W. C. Jacobs, **65**, No. 9, 1947.
21. "Microbarometric Oscillations at Blue Hill," Bernhard Haurwitz, R. Stone, and C. F. Brooks, *Bulletin of the American Meteorological Society,* **16**, Nos. 6-7, 1935, pp. 153-159.
22. *Wissenschaftliche Ergebnesse der Deutschen Atlantischen Expedition auf dem Forschungs-und Vermessungsschiff, Meteor,* 1925-1927, **15**, Berlin Leipsig, 1933.
23. *Qualitative Survey of Meteorological Factors Affecting Microwave Propagation,* I. Katz and J. M. Austin, OEMsr-262, Division 14 Report 488, RL, June 1, 1944. CP-311-M3
24. "Die Passatinversion," von Ficker, *Veröffentlichungen des Meteorologischen Instituts der Universität, Berlin,* **1**, No. 3, 1936.
25. *Modified Index Distribution Close to the Ocean Surface,* R. B. Montgomery and Robert H. Burgoyne, OEMsr-262, Division 14 Report 651, RL, Feb. 16, 1945. CP-222.2-M1
26. *Results of Low Level Atmospheric Soundings in the Southwest and Central Pacific Ocean Areas,* Paul A. Anderson, K. E. Fitzsimmons, G. M. Grover, and S. T. Stephenson, OEMsr-728, Research Project PDRC-647, NDRC Report 9, Washington State College, Feb. 27, 1945. CP-335-M4
27. *Atlas of Climatic Charts of the Oceans,* W. F. McDonald, U. S. Dept. of Agriculture, Weather Bureau, 1938.
28. *Atmospheric Refraction, A Preliminary Qualitative Investigation,* Lloyd J. Anderson, F. P. Dane, J. P. Day, R. F. Hopkins, L. G. Trolese, and A. P. D. Stokes, BuShips Problem X4-49CD, Report WP-17, NRSL, Dec. 28, 1944. CP-222-M9

Chapter 7

1. *Bureau of Standards Journal of Research,* Diamond, Hinman, F. W. Dunmore, and Lapham. **25**, 1940, p. 328.
2. *Bureau of Standards Journal of Research,* D. N. Craig, **21**, 1938, p. 225.
3. *Bureau of Standards Journal of Research,* F. W. Dunmore, **23**, 1939, p. 702.
4. *Instruments and Methods for Measuring Temperature and Humidity in the Lower Atmosphere,* I. Katz, OEMsr-262, Service Project SC-8, Division 14 Report 487, RL, Apr. 12, 1944. CP-344-M2
5. *The Captive Radiosonde and Wired Sonde Techniques for Detailed Low-Level Meteorological Sounding,* Paul A. Anderson, C. L. Barker, K. E. Fitzsimmons, and S. T. Stephenson, OEMsr-728, Research Project PDRC-647, Division 14 Report 192, Report 3, Washington State College, Oct. 4, 1943. CP-341-M1

5a. *Report of Second Propagation Conference, February 10 to 11, 1944 at the Empire State Building, New York,* OEMsr-1207, CUDWR-WPG, February 1944, p. 38. CP-100-M2

5b. *Notes on Operational Use of Low-Level Meteorological Sounding Equipment,* K. E. Fitzsimmons, S. T. Stephenson, and Robert W. Bauchman, OEMsr-728, Research Project PDRC-647, Report 7, Washington State College, June 15, 1944. CP-342-M2
Operating Instructions for the WSC Low-Level Atmospheric Sounding Equipment, Paul A. Anderson, OEMsr-728,

Research Project PDRC-647, Report 8, Washington State College, July 10, 1944. CP-342-M3

6. *Journal of Scientific Instruments*, P. A. Sheppard, **17**, 1940, p. 218.
7. *A Remote Indicating Cup Anemometer with Magnetic Coupling*, Roscoe G. Dickinson and Douglas L. Kraus, OSRD 3714, NDCrc-137 and OEMsr-861, Service Project CWS-26, NDRC Division 10, CIT, Apr. 10, 1944. Div. 10-301.1-M2
8. *Geophysical Memoirs*, N. K. Johnson, No. 46, 1929.
9. *Propagation and Reflection Characteristics of Radio Waves as Affecting Radar*, W. G. Michels and W. C. Pomeroy, Service Project (M-3) 11a, U.S. Army Air Forces Board, Orlando, Fla., Jan. 31, 1944. CP-531-M1
10. *Balloon Psychrometer for the Measurement of the Relative Humidity of the Atmosphere at Various Heights* (and Addendum), S. M. Doble and S. Inglefield, OSRD II-5-5079(S) and OSRD II-5-5080(S), ICI, Apr. 1, 1943; Addendum Sept. 25, 1943. CP-344-M1
11. *Report of Friez Instrument Division Bendix Aviation Corp.*, to the Bureau of Ships, May 1944. CP-342-M1

Chapter 8

1. *K-Band Rain and Water-Vapor Attenuation over Tokyo*, Arthur E. Bent and E. M. Purcell, Division 14 Report, RL.
2. *Modified Index Distribution Close to the Ocean Surface*, R. B. Montgomery and Robert H. Burgoyne, OEMsr-262, Division 14 Report 651, RL, Feb. 16, 1945. CP-222.2-M1
3. *Determination of a Suitable Method of Forecasting Radar Propagation Variations over Water, Tests Conducted by 26th Weather Region, Orlando, Florida*, J. R. Gerhardt and William E. Gordon, Service Project 4252R000.77, U. S. Army Air Forces, Mar. 10, 1945. CP-425-M1
4. *Tropospheric Propagation and Radio Meteorology*, Report WPG-5, CUDWR-WPG, September 1944.
5. *Preliminary Instruction Manual, Weather Forecasting for Radar Operations*, Report 614, U. S. Army Air Forces, Weather Division, March 1944. CP-410-M4
6. *Variations in Radar Coverage*, Report JANP-101, Joint Communications Board June 1, 1944. CP-202.4-M4 Earlier edition: IRPL T-1, CUDWR-WPG, May 1944. CP-202.5-M1
7. *Tropospheric Weather Factors Likely to Affect Super-refraction of VHF-SHF Radio Propagation as Applied to the Tropical West Pacific*, E. Dillon Smith and R. D. Fletcher, Report RP-1, U. S. Department of Commerce, Weather Bureau, July 1, 1944. CP-424-M1
8. *Nomograms for Computation of Modified Index of Refraction*, Robert H. Burgoyne, OEMsr-262, Division 14 Report 551, RL, Apr. 6, 1945. CP-222.1-M7
9. *Tables for Computing the Modified Index of Refraction M*, E. R. Wicher, Report WPG-8, CUDWR, March 1945.
10. *Elements of Radio Meteorological Forecasting*, H. G. Booker, Report T-1621, Mathematics Group, TRE, Malvern, Feb. 14, 1944. CP-410-M3
11. *World Atlas of Sea Surface Temperatures, Hydrographic Office*, No. 225, 1944.
12. *Atlas of Climatic Charts of the Oceans*, P. W. Kenworthy, U. S. Weather Bureau, 1938.
13. *Monthly Meteorological Charts of the Western Pacific Ocean*, Marine Branch of the Meteorological Office, British Air Ministry, London, England.
14. *Climatic Atlas of Japan and Her Neighboring Countries*, United States Navy Reprint, 1943.
15. *Climatic Atlas for Alaska*, Report 444, Weather Bureau Information Branch, Headquarters Army Air Forces.
16. *Third Conference on Propagation, Washington, D. C.* [on] *November 16 to 18, 1944*, NDRC CUDWR-WPG, 1945, pp. 5-6. CP-100-M4
17. *Effect of Meteorological Conditions at Saipan upon Radar Coverage*, JEIA Survey Report S888, Dec. 5, 1944.
18. *Results of Low Level Atmospheric Soundings in the Southwest and Central Pacific Oceanic Areas*, Paul A. Anderson, K. E. Fitzsimmons, G. M. Grover, and S. T. Stephenson, OEMsr-728, Research Project PDRC-647, Report 9, Washington State College, Feb. 27, 1945. CP-335-M4
19. *Preliminary Instruction Manual of Weather Forecasting for Radar Operations in South West Pacific Areas*, D. F. Martyn and P. Squires, Report RP-220, CSIR-RL, Sept. 4, 1944, p. 46. CP-424-M2
20. *The Air Defense System of the Near Islands*, Thomas J. Carroll, Report OAD-55, U. S. Army Air Forces, Eleventh Air Force, OCSO, Operational Analysis Division, Aug. 30, 1944. CP-202.1-M5
21. *The Coincidence of Temperature Inversions and Non-Standard Radar Propagation and Reflection*, Report JEIA S366.

Chapter 9

1. *Interim Report on Experiments on Ground Reflection at a Wavelength of 9 Cm*, L. H. Ford, RRB/C-101 or JEIA 4899, DSIR, July 7, 1944.
2. *An Experimental Investigation of the Reflection and Absorption of Radiation of 9-Cm Wavelength*, L. H. Ford and R. Oliver, OSRD WA-3386-2, Report RRB/C-107, DSIR, Oct. 27, 1944. CP-532-M2
3. *S-Band Measurements of Reflection Coefficients for Various Types of Earth*, E. M. Sherwood, Report 5220.129, Sperry Gyroscope Company, Oct. 29, 1943. CP-532.1-M1
4. *Centimeter Wave Propagation over Sea within the Optical Range*, H. Archer-Thomson, J. C. Dix, F. Hoyle, E. C. S. Megaw, and M. H. L. Pryce, OSRD W-157-16, Report M-398, ASE, January 1942. CP-532.2-M1
5. *Preliminary Report on the Reflection of 9-Cm Radiation at the Surface of the Sea*, H. Archer-Thomson, N. Brooke, T. Gold, and F. Hoyle, OSRD WA-1131-2, Report M-532, ASE, September 1943. CP-532.2-M2
6. *Preliminary Measurements of 10-Cm Reflection Coefficients of Land and Sea at Small Grazing Angles*, Pearl J. Rubenstein and William T. Fishback, Division 14 Report 478, RL, Dec. 11, 1943. CP-532-M1
7. *Further Measurements of 3- and 10-Cm Reflection Coefficients of Sea Water at Small Grazing Angles*, William T. Fishback and Pearl J. Rubenstein, OEMsr-262, Division 14 Report 568, RL, May 17, 1944. CP-532.2-M4
8. *Ground Reflection Coefficient Experiments on X-Band, Case 20564*, W. M. Sharpless, Report MM-44-160-250, BTL, Dec. 15, 1944. CP-532.1-M3
9. *Scattering*, R. L. Eckersley, OSRD WA-2255-1f, JEIA 3904, Report TR-481, BRL, November 1943. CP-512-M3
10. *Reflection and Scattering*, T. L. Eckersley, OSRD WA-4002-12, Report TR-506, BRL, January 1945. CP-532.2-M5

Chapter 10

1. *The Atmospheric Absorption of Microwaves* (in Third Conference Report of CP), J. H. Van Vleck, Report 175 (43-2), RL, Apr. 27, 1942. Div. 14-121.1-M4 See also Third Conference, Nov. 16-18, 1944. CP-100-M4
2. *Further Theoretical Investigations on the Atmospheric Absorption of Microwaves*, J. H. Van Vleck, OEMsr-262, Service Project AN-25, Division 14 Report 664, RL, Mar. 1, 1945. CP-510-M8
3. *Propagation of K/2 Band Waves*, G. E. Mueller, Report MM-44-160-150, BTL, July 3, 1944. CP-511-M7
4. *The Absorption of One-Half Centimeter Electromagnetic Waves in Oxygen*, E. R. Beringer, OEMsr-262, Service Project AN-25, Division 14 Report 684, RL, Jan. 26, 1945. CP-510-M7
5. *The Absorption of Atmospheric Water-Vapor in the K-Band Region*, R. H. Dicke, R. L. Kyhl, A. B. Vane, and E. R. Beringer, Division 14 Report 1002, RL, Jan. 15, 1946. Div. 14-122.13-M5
6. *An Aerial Investigation of K-Band Radar Performance under Tropical Atmospheric Conditions*, R. S. Bender, A. E. Bent, and J. W. Miller, Division 14 Report 729, RL, Oct. 1, 1945. Div. 14-122.23-M6
7. *Rotational Line Width in the Absorption Spectrum of Atmospheric Water Vapor and Supplement*, Arthur Adel, OEMsr-1361, NDRC Division 14 Report 320, University of Michigan, Oct. 10, 1944; Supplement Feb. 1, 1945. (see also reference 2) CP-510-M6
8. *Annalen der Hydrographie*, M. Diem, Berlin, **70**, 1942, pp. 142-150.
9. *An Investigation on the Number and Size Distribution of Water Particles in Nature*, Josef Mazur, F/Lt. Polish Air Force, OSRD II-5-6306(S), Report MRP-109, Meteorological Research Committee, Great Britain, June 10, 1943. CP-511-M5

10a. *Provincetown Path*, private communication from Donald E. Kerr and G. T. Rado of RL.

10b. *Measurements of the Attenuation of K-Band Waves by Rain*, G. T. Rado, OEMsr-262, Service Project AN-25, Division 14 Report 603, RL, Mar. 7, 1945. CP-511-M10

11. *Interim Report of the U. S. W. Panel Working Committee, Part I, Water in the Atmosphere*, A. C. Best, JEIA 7607, Report AC-7375, MO-USW, Aug. 14, 1944.
12. *Interim Report of the U. S. W. Panel Working Committee, Part III, Attenuation of Centimeter Waves by Rain, Hail, and Clouds*, J. W. Ryde and D. Ryde, JEIA 7607, Report AC-7375, USWP, Report 8516, GEC, Aug. 3, 1944.
13. *Polar Molecules*, P. Debye, The Chemical Catalogue Co., New York, 1929.
14. *Summer Storm Echoes on Radar MEW*, J. S. Marshall, R. C. Langille, William M. Palmer, R. A. Rodgers, G. P. Adamson, and F. F. Knowles, Report 18, CAORG, Nov. 27, 1944. CP-621.1-M2
15. *The Effect of Clutter Fluctuations on MTI*, H. Goldstein, Division 14 Report 700, RL, Dec. 27, 1945. Div. 14-263.1-M4
16. *Annalen der Physik*, G. Mie, **25**, 1908, p.377.
17. *Echo Intensities and Attenuation Due to Clouds, Rain, Hail, Sand, and Duststorms at Centimeter Wavelengths*, J. W. Ryde, OSRD WA-81-25, Report 7831, GEC, Oct. 13, 1941. CP-511-M1
18. *Electromagnetic Theory*, J. A. Stratton, McGraw-Hill Book Co., 1941.

18a. *Ibid.*, pp. 563-573.

18b. *Ibid.*, pp. 554-560.

19. *The Theory of Sound*, Lord Rayleigh, McMillan and Co., Ltd., London, 1940.
20. *On Light Scattering by Spheres, Parts I and II*, Leon Brillouin, OEMsr-1007, AMG-C 100 and 132, AMP 87.1 and 87.2, December 1943 and April 1944. AMP-202-M2, M3
21. *Preliminary Report on the Dielectric Properties of Water in the K-Band*, C. H. Collie, CL Misc. 25, CVD Report, May 1944.
22. *Properties of Ordinary Water-Substance*, N. E. Dorsey, American Chemical Society Monograph Series, Reinhold Publishing Corp., New York, pp. 350-373.
23. *Dielectric Properties of Water and Ice at K-Band*, E. L. Younker, OEMsr-262, Service Project AN-25, Division 14 Report 644, RL, Dec. 4, 1944. CP-522.1-M2
24. *H. G. Houghton's data reproduced in: Aeronautical Meteorology*, G. F. Taylor, Pitman Publishing Corp., New York-Chicago, 1943.
25. *Physics of the Air*, W. J. Humphreys, McGraw-Hill Book Co., 1940.

26a. *Third Conference on Propagation, Washington, D. C.* [on] *November 16 to 18, 1944*, E. Dillon Smith, NDRC CUDWR-WPG, 1945. CP-100-M4

26b. J. O. Laws and D. O. Parsons, National Research Council, *Transactions of the American Geophysical Union*, Part II 1943, p. 452.

27. *The Effect of Rain upon the Propagation of 1-Cm Electro-Magnetic Waves, Case 2209S*, S. D. Robertson, Report MM-42-160-87, BTL, Aug. 1, 1942. CP-511-M2
28. *Absorption of 1-Cm Radiation by Rain*, M. G. Adam, R. A. Hull, and C. Hurst, Misc. Report 3, CVD-CL.
29. *K-Band Radar Transmission, A Preliminary Report of Tests Made Near Atlantic Highlands, N. J. between December 1943 and April 1944*, G. C. Southworth, A. P. King, and S. D. Robertson, Report MM-44-160-115, BTL, May 19, 1944. CP-202.2-M1
30. *The Effect of Rain on the Propagation of Microwaves, Case 2209S*, A. P. King and S. D. Robertson, Report MM-42-160-93, BTL, Aug. 26, 1942. CP-511-M3
31. *Calibration and Operational Tests of AN/CPS-1 (MEW)*, Army Air Forces Board Project (M-3)-9, Mar. 30, 1944.
32. *Radar Echoes from Atmospheric Phenomena*, A. E. Bent, Division 14 Report 173(42-2), RL, Mar. 13, 1943. CP-621.1-M1
33. A. E. Bent, RL, unpublished report, Feb. 29, 1944.
34. *Radar Echoes from Clouds of Water Droplets*, F. Hoyle, Report AC-7930, USW 128, Mar. 16, 1945.
35. A. J. F. Siegert, RL unpublished, 1943.
36. *Interim Report of the U.S.W. Panel Working Committee, Part II, The Attenuation of Centimeter Waves by Atmospheric Gases*, J. M. Hough, JEIA 7607, Report AC-7375, USW, July, 1944.
37. *Interim Report on Experiments on Ground Reflection at a Wavelength of 9 Cm*, L. H. Ford, JEIA 4899, Report RRB/C-101, DSIR, July 7, 1944.
38. *The Dielectric Properties of Water in the Temperature Range 0° C to 40° C for Wavelengths of 1.24 Cm and 1.58 Cm*, J. A. Saxton and J. A. Lane, JEIA 9811, Report RRB/C-116, DSIR, Mar. 7, 1945.
39. *The Anomalous Dispersion of Water at Very High Radio Frequencies in the Temperature Range 0° C to 40° C,*

J. A.Saxton, JEIA 9812, Report RRB/C-118, NPL-DSIR, Apr. 6, 1945. CP-522.11-M3

40. *A New Method for Measuring Dielectric Constant and Loss in the Range of Centimeter Waves*, S. Roberts and Arthur R. von Hippel; *Wave Guides with Dielectric Sections*, L. J. Chu, Report 102, MIT, March 1941. CP-521-M1
41. *The Measurement of Dielectric Constant and Loss with Standing Waves in Coaxial Wave Guides*, Arthur R. von Hippel, D. G. Jelatis, and W. B. Westphal, OEMsr-191, NDRC Division 14 Report 142, Laboratory for Insulation Research, MIT, April 1943. CP-521-M4
42. *Auxiliary Equipment for the MIT Coax Instrument and Its Use*, Arthur R. von Hippel, D. G. Jelatis, W. B. Westphal, M. G. Haugen, and R. E. Charles, OEMsr-191, NDRC Division 14 Report 210, Laboratory for Insulation Research, MIT, Nov. 1, 1943. Div. 14-131.2-M1
43. T. A. Taylor and Willis Jackson, Ministry of Supply, CPR Report 30.
44. "The Dielectric Dispersion and Absorption of Water and Some Organic Liquids," W. P. Connor and C. P. Smyth, *Journal American Chemical Society*, **65**, 1943, pp. 382-389.
45. *Progress Report on Ultra High Frequency Dielectrics*, Arthur R. von Hippel, OEMsr-191, NDRC Division 14 Report 121, Laboratory for Insulation Research, MIT, January 1943. CP-521-M2
46. R. Dunsmuir and J. Lamb, Ministry of Supply, 287/Gen/35, DSR Report 61, Department of Scientific Research, Mar. 5, 1945.

47a. *The Dielectric Constant and Absorption Coefficient of Water Vapour for Wavelengths of 9 Cm and 3.2 Cm, Frequencies 3,330 and 9,350 Mc/s*, J. A. Saxton, Paper RRB/S-11, NPL-DSIR, June 14, 1943. CP-522.12-M3

47b. *The Dielectric Constant and Absorption Coefficient of Water Vapour for Radiation of Wavelength 1.6 Cm, Frequency 18,800 Mc/s*, J. A. Saxton, Report RRB/S-17, NPL-DSIR, Apr. 22, 1944.

48. *The Relation between Absorption and the Frequency Dependence of Refraction* (Fourth Conference), J. H. Van Vleck, Division 14 Report 735, RL, May 26, 1945. Div. 14-122.24-M4

Chapter 12

1. *Possible Measurement of Radar Echoes by Use of Model Targets*, S. A. Goudsmit and P. R. Weiss, Division 14 Report 196 (43-24), RL, Mar. 4, 1943. Div. 14-122.113-M5
2. *The Theory of Random Processes*, G. E. Uhlenbeck, Division 14 Report 454, RL, Oct. 15, 1943. Div. 14-125-M7
3. *On the Fluctuations in Signals Returned by Many Independently Moving Scatterers*, A. J. F. Siegert, Division 14 Report 465, RL, Nov. 12, 1943. Div. 14-122.113-M7

Chapter 13

1. *Measurements of the Angle of Arrival of Microwaves in the X-Band, Case 20564*, W. M. Sharpless, Report MM-44-160-249, BTL, Nov. 7, 1944.
2. *Ground Reflection Coefficient Experiments on X-Band, Case 20564*, W. M. Sharpless, Report MM-44-160-250, BTL, Dec. 15, 1944. CP-532.1-M3

COMMITTEE ON PROPAGATION

Chairman

CHAS. R. BURROWS

Members

H. H. BEVERAGE
T. J. CARROLL
J. H. DELLINGER
MARTIN KATZIN
D. E. KERR
J. A. STRATTON

Consultants

S. S. ATTWOOD
C. E. BUELL
J. A. STRATTON

Technical Aides

(Listed in the order they served.)

A. F. MURRAY
S. W. THOMAS
R. J. HEARON

Contract No.	*Contractor*	*Subject*
OEMsr-1207	Columbia University New York City, New York	Correlation, analysis and integration of data on radio and radar propagation.
OEMsr-728	State College of Washington Pullman, Washington	Develop meteorological equipment and conduct meteorological soundings in the Southwest Pacific and correlate it with radio propagation data.
OEMsr-1497	Humble Oil & Refining Company Houston, Texas	Development and construction of microwave field strength measuring sets.
OEMsr-1496	University of Texas Austin, Texas	Development of equipment for and making measurements of time and space deviations in radio wave propagation.
OEMsr-1502	Jam Handy Organization, Inc. Detroit, Michigan	Preparation of a General Outline of Training Material and the preparation of manuals, films and other training aids for use in instructing technical and other personnel in radio-weather and radio propagation.

The Committee on Propagation did all of its work under Project Control SOS-9, which was originally set up through the request of the Combined Chiefs of Staff following recommendations submitted by the Combined Meteorological Committee:

1. That the Committee on Propagation of the National Defense Research Committee be requested to act as a coordinating agency for all meteorological information associated with short wave propagation;

2. That the Committee on Propagation be requested to forward periodically to the CMC a list of all reports and papers dealing with the meteorological aspects on short wave propagation which have been received or transmitted by that Committee.

Later the Combined Meteorological Committee in its 37th meeting on Tuesday, February 22, 1944, agreed that the National Defense Research Committee (NDRC) Committee on Propagation be recognized as the supervising committee on all basic research being done in the United States on the related problems of radar propagation and weather, in addition it shall be the recognized channel whereby international exchange of papers of the two related sciences will be effected.

The Joint Communications Board therefore approved the following policy, which was concurred in by NDRC and by the Joint Meteorological Committee:

1. The NDRC Propagation Committee and its associated working groups will initiate and exercise technical supervision over such tests and investigations as they deem necessary to ascertain the nature of the above-mentioned propagation anomalies in the VHF, UHF, and SHF bands, to devise the most practicable methods to determine the occurrence and characteristics of these anomalies from appropriate meteorological forecasts, with a view to improving the interim solutions offered by the Joint Wave Propagation Committee of the JCB.

2. The Army and Navy will furnish by direct coordination between them the basic staff guidance for such tests and investigations. They will accomplish this by determining:

a. The specific forms in which basic prediction data shall be presented, and

b. The method of use required for operational forecast of propagation anomalies in the VHF, UHF, and SHF bands.

3. When the NDRC requires the cooperation of the operating units of the Army and Navy in conducting such tests and investigations as it deems necessary and this cooperation is of such an extent and nature that it cannot be furnished by informal coordination, it will be requested through the Joint Wave Propagation Committee of the JCB. Such requests will be initiated by the NDRC representative on the Wave Propagation Committee and recommended to the Joint Communications Board by the Joint Wave Propagation Committee for consideration.

4. The Joint Wave Propagation Committee will be responsible for devising and furnishing immediately, interim operational forecasting guides based upon information already available.

On April 3, the Coordinator of Research and Development requested that the Army Project SOS-9 be made a joint Army-Navy project. Project No. AN-16 was assigned to this.

On May 23, 1944, the Chief Signal Officer requested that under Project AN-16 the following work be inaugurated:

Project AC 230.04 "Wave Propagation Study of Line-of-Sight Communication and Navigation."

INDEX

The subject indexes of all STR volumes are combined in a master index printed in a separate volume. For access to the index volume consult the Army or Navy Agency listed on the reverse of the half-title page.